Ioan Sporea
Roxana Șirli

Alina Popescu
Dana Stoian

TEXTBOOK OF ELASTOGRAPHY

Editura „VICTOR BABEȘ”
Timișoara, 2024

„Victor Babeş" Publishing House
Eftimie Murgu Square 2, room 316, 300041 Timişoara
Tel./ Fax 0256 495 210
e-mail: *evb@umft.ro*
www.umft.ro/editura

General Director: Prof. dr. Sorin Ursoniu

HIPPOCRATE Collection

Collection Coordinator: Prof. dr. Andrei Motoc

Scientific Referent: Prof. dr. Florică Bîrsăștеanu

CNCSIS number: 324

ISBN 978-606-786-416-8

The authors of the book:

Editors

1. **Prof. Ioan Sporea[1], [2], [3]**
   - Senior Consultant in Gastroenterology and Internal Medicine, MD, PhD, Member of the Academy of Medical Sciences Romania, Vice-President of the World Federation for Ultrasound in Medicine and Biology (WFUMB), Director of the WFUMB Center of Education (CoE) Romania.
2. **Prof. Roxana Șirli[1], [3], [4], [5]**
   - Senior Consultant in Gastroenterology and Internal Medicine, MD, PhD, Corresponding Member of the Academy of Medical Sciences, Member of the WFUMB Center of Education (CoE) Romania.
3. **Prof. Alina Popescu[1], [3], [4], [5]**
   - Senior Consultant in Gastroenterology and Internal Medicine, MD, PhD, Member of the WFUMB Center of Education (CoE) Romania.
4. **Prof. Dana Stoian[1], [6], [7]**
   - Senior Consultant in Endocrinology, MD, PhD, Member of the WFUMB Center of Education (CoE) Romania.

Contributors

1. **Prof. Mirela Dănilă[1], [3], [4], [5]**
   - Senior Consultant in Gastroenterology, MD, PhD.
2. **Lecturer Corina Pienar[8], [9]**
   - Senior Consultant in Pediatrics, Specialist in Pediatric Gastroenterology, MD, PhD.
3. **Assist. Prof. Felix Bende[1], [3], [4], [5]**
   - Senior Consultant in Gastroenterology, MD, PhD.
4. **Assist. Prof. Renata Bende[1], [3], [4]**
   - Specialist in Gastroenterology, MD, PhD.
5. **Assist. Prof. Ana-Maria Ghiuchici[1], [3], [4]**
   - Specialist in Gastroenterology, MD, PhD.
6. **Assist. Prof. Raluca Lupusoru[3], [10]**
   - Specialist in Gastroenterology, MD, PhD.
7. **Assist. Prof. Ruxandra Mare[1], [3], [4], [5]**
   - Specialist in Gastroenterology, MD, PhD.
8. **Assist. Prof. Bogdan Miuțescu[1], [3], [4], [5]**
   - Senior Consultant in Gastroenterology, MD, PhD.
9. **Assist. Prof. Tudor Moga[1], [3], [4], [5]**
   - Senior Consultant in Gastroenterology, MD, PhD.

10. **Assist. Prof. Camelia Nica[1], [3], [4]**
    - Specialist in Gastroenterology, MD, PhD.
11. **Assist. Prof. Alexandru Popa[1], [3], [4]**
    - Specialist in Gastroenterology, MD, PhD.
12. **Dr. Victor Băldea[3], [11]**
    - Specialist in Gastroenterology, MD, PhD.
13. **Prof. Adrian Săftoiu[12]**
    - Senior Consultant in Gastroenterology and Internal Medicine, MD, PhD, Full Member of the Academy of Medical Sciences.
14. **Assoc. Prof. Angela Peltec[13]**
    - Gastroenterologist, Senior Ultrasound Specialist, MD, PhD, Member of the Liver Transplant Team in the Republic of Moldova.
15. **Assist. Prof. Andreea Borlea[1], [6]**
    - Specialist in Endocrinology, MD, PhD.
16. **Dr. Laura Tăban[14]**
    - Specialist in Endocrinology, MD, PhD.
17. **Prof. Flaviu Bob[1], [15], [16]**
    - Senior Consultant in Nephrology, MD, PhD.
18. **Prof. Sorin M. Dudea[17]**
    - Senior Consultant in Radiology and Medical Imaging, MD, PhD.
19. **Assoc. Prof. Anca Ciurea[18]**
    - Senior Consultant in Radiology and Medical Imaging, MD, PhD.
20. **Assoc. Prof. Carolina Solomon[18]**
    - Senior Consultant in Radiology and Medical Imaging, MD, PhD.
21. **Prof. Daniela Fodor[19]**
    - Senior Consultant in Rheumatology and Internal Medicine, MD, PhD.
22. **Lecturer Oana Șerban[19]**
    - Specialist in Internal Medicine, MD, PhD.
23. **Assist. Prof. Maria Bădărăniță[19]**
    - Specialist in Rheumatology, MD, PhD.
24. **Assist. Prof. Mihaela Pelea[19]**
    - Specialist in Internal Medicine, PhD Candidate.
25. **Dr. Vasile Simon[17]**
    - Specialist in Urology, PhD Candidate.
26. **Prof. Paul S. Sidhu[20]**
    - BSc MBBS MRCP FRCR DTM&H, Professor of Imaging Sciences and Consultant Radiologist.
27. **Senior Lecturer Cheng Fang[20]**
    - MBBS FRCR, Consultant Radiologist.
28. **Dr. Nuran Seneviratne[21]**
    - MBBS FRCR, Specialist Registrar.

Affiliations

1. World Federation for Ultrasound in Medicine and Biology (WFUMB) Center of Education (CoE) Romania.
2. "Victor Babeș" University of Medicine and Pharmacy Timișoara, Romania.
3. Advanced Hepatology Research Center, Academy of Medical Sciences, Romania.
4. Advanced Gastroenterology and Hepatology Research Center, University Clinic of Gastroenterology, University of Medicine and Pharmacy "Victor Babeș".
5. Gastroenterology Clinic, "Pius Brinzeu" County Emergency Clinical Hospital, Timișoara, Romania.
6. Endocrinology Clinic, University of Medicine and Pharmacy "Victor Babeș", Timișoara, Romania.
7. Endocrinology Outpatient Clinic, "Pius Brinzeu" County Emergency Clinical Hospital, Timișoara, Romania.
8. University Pediatric Clinic II, University of Medicine and Pharmacy "Victor Babeș", Timișoara, Romania.
9. Pediatric Clinic 2, "Pius Brinzeu" County Emergency Clinical Hospital, Timișoara, Romania.
10. Center for Modeling Biological Systems and Data Analysis, Department III: Functional Sciences, Medical Informatics and Biostatistics, University of Medicine and Pharmacy "Victor Babeș", Timișoara, Romania.
11. Laurus Medical, Deva, Romania.
12. Elias University Emergency Hospital, University of Medicine and Pharmacy "Carol Davila", Bucharest, Romania.
13. Gastroenterology Department, Internal Medicine Department, University of Medicine and Pharmacy "Nicolae Testemițanu", Chișinău, Republic of Moldova.
14. Endocrinology Unit, Luxembourg Hospital Center, Luxembourg.
15. University Clinic of Nephrology, Molecular Research Center in Nephrology, University of Medicine and Pharmacy "Victor Babeș", Timișoara, Romania.
16. Vascular Pathology, University of Medicine and Pharmacy "Victor Babeș", Timișoara, Romania.
17. Nephrology Clinic, "Pius Brinzeu" County Emergency Clinical Hospital, Timișoara, Romania.
18. University of Medicine and Pharmacy "Iuliu Hațieganu", Cluj-Napoca, Romania.
19. Department of Radiology - Medical Imaging, University of Medicine and Pharmacy "Iuliu Hațieganu", Cluj-Napoca, Romania.
20. Medical Clinic II, University of Medicine and Pharmacy "Iuliu Hațieganu", Cluj-Napoca, Romania.
21. Department of Imaging Sciences, School of Biomedical Engineering and Imaging Sciences, Faculty of Life Sciences and Medicine, King's College London.
22. Department of Radiology, King's College Hospital, London, United Kingdom.
23. Department of Radiology, King's College Hospital, Denmark Hill, London, United Kingdom.

CONTENT

FOREWORD

In the context of remarkable advances in technologies with medical applications and of concerns for prioritizing non-invasive diagnostic methods, elastography has gained a well-deserved place.

Simplifying to the extreme, elastography replaces the sense of touch (with limited sensitivity, uneven individual accuracy, and inability to approach a large number of organs and tissues), with a standardized method, of high sensitivity and specificity, which allows the evaluation of the elasticity of organs and tissues inaccessible to clinical examination, having a wide practical applicability.

The development of the method was explosive, both in terms of the techniques used and the fields of application. Numerous technical variants are currently available, developed in correlation with the type of application. Strain elastography, which measures the longitudinal deformation of tissues when applying an external stimulus, is especially applicable in the evaluation of breast, prostate, and thyroid tumors. Shear wave elastography, which measures the speed of displacement of shear waves generated in the tissue by an external stimulus, has multiple applications in hepatology, both in diffuse liver diseases, including steatotic liver (MASLD), and liver tumors, but also in pancreatic, breast, thyroid, prostate, testicular, renal, musculoskeletal pathologies.

The medical industry has quickly adapted to the beneficiaries' requirements and has managed in a short time to develop elastography modules, included in both medium-class and state-of-the-art ultrasound systems, which has led to increased accessibility to this examination method, thus making it possible to quickly assess patients in ultrasound offices. Although MRI elastography has a higher value, it is limited by its still low accessibility.

It is also remarkable that the authors open a window into the future, looking at the role of artificial intelligence in elastography.

The "**Textbook of Elastography**" appears at the initiative and under the coordination of the ultrasound school in Timișoara, a structure unanimously recognized and appreciated at national, European and world level, recognition validated by the presence of its members in European and world management structures. It responds to an acute need of the medical world to have access to exhaustive informative material, with scientific, didactic, and educational value in this dynamic field, addressing a wide range of practitioners who use this method.

Prof. dr. Mircea Grigorescu

Honorary member of the Romanian Academy

Chapter 1. Introduction

Ioan Sporea, Roxana Șirli, Dana Stoian, Alina Popescu

Why would a Textbook on Elastography be needed at this time? The answer is given by the practical need for information in a relatively new field of medicine. For over 2000 years, physical palpation was considered to be the golden standard to evaluate an organ's elasticity (stiffness). However, in the last 20 years, with the development of clinical elastography, things have started to change. If, at first, there was a reluctance or distrust regarding elastography, in recent years, more and more practitioners from various medical fields have been using this method and enjoyed its results.

At first, elastography was mainly used for liver assessment, by means of Vibration-Controlled Transient Elastography. Later, the development of other elastographic techniques (such as Acoustic Radiation Force Impulse and Strain Elastography) led to the use of this method in many other fields of medicine. Currently, elastographic evaluation is used for the diagnosis of soft tissue tumors, such as breast, thyroid, parathyroid, lymph nodes or in dermatology, for cervical or prostate lesions, as well as for the evaluation of musculoskeletal lesions. At present, all major ultrasound companies have implemented elastography modules in their new prototypes, and the number of users of the method is constantly increasing.

The publication more than 10 years ago of the European (EFSUMB) or World (WFUMB) elastography guidelines, which have been permanently updated, has made the best scientific information available, and the use of elastography in clinical practice, more and more frequent. The technique of performing elastography is relatively simple to learn, but the confounding factors must be well known and applied in practice, in order to avoid erroneous results.

The publication of a Textbook on Elastography aims to disseminate this method as much as possible in our geographical area and to be available to all interested specialties. From this point of view, Romania was among the countries that made a major contribution to the development of elastography, through published research, dissemination workshops and the development of national guidelines.

We have tried to include in this Textbook those areas of medicine where elastography is of great clinical utility, inviting authors with great experience to write the respective chapters. The book should remain open to the future, as new research and development may enable the use of elastography in other medical fields as well.

Finally, the question may arise whether elastography can replace clinical medicine and palpation? Probably not, because elastography data will have to be integrated in a clinical context, in which the anamnesis, clinical and biological examination data are indispensably linked, but elastography certainly complement and refine the others in order to obtain early

and correct diagnoses, and to begin appropriate therapy. In the coming years, Artificial Intelligence will also contribute to the integration of elastography in diagnosis, and the first steps are already being taken.

We hope that this Textbook on Elastography will be a useful and pleasant book to read, allowing a wide use of this new medical method, in parallel with the continuous development of elastography equipment.

The authors

Chapter 2. History of elastography

Roxana Șirli, Camelia Nica

Elasticity is an intrinsic property of all substances, implicitly tissues, to deform when an external stimulus is applied. The more elastic a tissue is, the more it will deform, and the stiffer it is (less elastic), the less it will deform when applying a stimulus of similar intensity. Palpation, an indispensable element in clinical examination, is the oldest method of assessing tissue elasticity, as it is known that some diseases (malignant tumors, accumulation of fibrotic tissue) lead to an increase in tissue stiffness, while others (inflammation, edema) lead to a stiffness decrease.

Elastography is a medical imaging technique that measures tissue stiffness (elasticity), the terms elasticity – stiffness having the value of antonyms. Elastography has proven to be valuable in the diagnosis and monitoring of multiple medical conditions, especially in the field of chronic liver diseases, but also in breast, thyroid, prostate, vascular pathology, etc.

The mathematical formula for calculating elasticity has been established since the fifteenth century – Hooke's law (1678) (1). This is applicable to solid structures, whose deformation is linear. Tissue elasticity differs from that of solids, since it is a visco-elastic medium, being influenced by factors other than the stimulus' intensity, such as the direction of the stimuli application and the visco-elastic properties of the tissue. However, a fairly accurate approximation of the tissues' elastic properties can be made using elastic moduli (1), as will be explained in the chapter on the technical principles of elastography.

Starting from the relationship between the elastic properties of tissues and certain diseases, the concept of elastography was developed, an imaging method that measures tissue elasticity/stiffness. The measurement of tissue deformation induced by an external stimulus can be done either parallel to the direction of stimulus application (strain elastography) or perpendicular to the direction of stimulus, by assessing the speed of the shear waves generated by the stimulus into the tissue (shear-wave elastography).

The first studies on the elasticity of viscoelastic substances date back to 1951 (2), when a mathematical model was developed that estimated the behavior of a sphere oscillating in a viscoelastic medium. Subsequently, using a strobe, members of the same group measured the speed of thigh surface deformation, generated by the vibration of a piston applied to the skin (3). This research was the basis for the development of elastographic methods used to assess living tissues elasticity, based on either nuclear magnetic resonance or on ultrasound.

1. Ultrasound-based elastography

a) Strain Elastography (SE)

One of the first applications *of strain elastography (SE)* was described by Eisensher et al. in 1983, who used M-mode ultrasound to track low-frequency (1.5 Hz) vibration-induced tissue dislocation in breast and liver tissue, thus managing to differentiate benign tumors from malignant ones (4).

At the beginning of the 90s, SE techniques were developed, incorporated into common ultrasound systems, in which the stimulus used for tissue deformation was light manual compression with the transducer, the longitudinal tissue dislocation (parallel to the direction of application of the stimulus) being estimated using gray scale ultrasound (B-ultrasound mode) (5). The first clinical applications of SE were developed by the team led by BB Golberg in the mid-90s, for the evaluation of breast nodules (6). Subsequent studies in the early 2000s demonstrated the value of SE for increasing the accuracy of the BIRADS classification (7), as well as for differentiating benign from malignant nodules, using either the Tsukuba score (8) or the ratio of the lesion size measured by elastography vs. by gray scale ultrasound (B mode) (9).

Since the mid-2000s, SE has also proven useful for the localization and characterization of prostate nodules (10), as well as for guiding prostate puncture for the diagnosis of prostate cancer (11). In the same period, SE began to be used for the evaluation of thyroid nodules (12,13), proving its usefulness in differentiating benign vs. malignant ones.

Foreign elastography has limited value for the evaluation of the liver, due to the low penetrance of the deformation stimulus and the fact that the elastogram generated does not allow numerical results to be obtained, being only a quantitative method.

Modern ultrasound machines use heartbeat and respiratory movements as a stimulus for tissue deformation (14). Other strain elastography techniques use an acoustic impulse as a stimulus for tissue deformation (14).

b) Shear-wave elastography (SWE)

As mentioned above, shear-wave elastography (SWE) is based on measuring the speed of shear waves generated into tissues by a stimulus, perpendicular to the direction of application of the stimulus. Depending on the way the tissue is stimulated, and the method used to measure the shear waves speed, SWE techniques have been classified as follows (14):

- Vibration Controlled Transient Elastography (VCTE), originally known as Transient Elastography (TE), in which the stimulus is a mechanical impulse generated by a vibrator
- SWE techniques based on ARFI (Acoustic Radiation Force Impulse), in which the stimulus is an acoustic pulse generated by the transducer

Vibration Controlled Transient Elastography (VCTE)

In the early 2000s, Laurent Sandrin and his team developed the technique of transient elastography, building a device called FibroScan™ (Echosens, Paris, France) (15). A special transducer, mounted on the shaft of a vibrator, measures the speed of the shear waves generated into the liver by the mechanical impulse generated by the vibrator. The value measured in m/s is automatically converted, using the Young modulus, to kiloPascals (kPa), considered indicative of liver stiffness. VCTE represented a real revolution for the non-invasive evaluation of liver fibrosis, being currently one of the reference methods for the evaluation of chronic liver diseases (16-19).

One of the biggest obstacles in achieving correct measurements of liver stiffness by VCTE proved to be obesity (20), in the severely obese, with a body mass index above 40 kg/m^2, the failure rate of the measurements being 88% (21). In order to avoid this shortcoming, the XL probe was developed in 2010, with a central frequency of 2.5 MHz (22), thus with better penetrance than the usual probe – the M probe, whose central frequency is 3.5 MHz. Using the XL probe, valid results can be obtained in more than 60-80 % of patients with failed measurements with the M probe (22, 23). During the same period, the S probe also became available for pediatric use (24).

Over the years, numerous studies have been published regarding the usefulness of VCTE for assessing the severity of liver fibrosis in chronic liver diseases, the value of this method being confirmed by meta-analyses, both in mixed cohorts of patients (25-28) and in specific pathologies, such as chronic viral hepatitis (29-33); alcohol-induced liver disease (34.35); metabolic dysfunction associated steatotic liver disease - MASLD (36,37); but also in rarer diseases such as cholestatic liver diseases (38,39); alpha-1 antitrypsin deficiency (40); liver damage in cystic fibrosis (41,42); autoimmune liver disease (43). Moreover, VCTE has also proven its usefulness as a predictor of portal hypertension (44-47), as a predictor of hepatic mortality (48), but also of hepatocellular carcinoma occurrence (49,50).

In 2011, Horia Ștefănescu published the first study that evaluated the performance of VCTE in the spleen for the prediction of esophageal varices (51). In this study, special software was used, which expands the measurement range, opening up a new perspective in the use of VCTE.

Taking into account the high prevalence of steatotic liver disease, and its association with fibrosis, the manufacturers of FibroScan device have developed an application dedicated to quantifying steatosis, ***Controlled Attenuation Parameter*** (CAP), implemented in the same apparatus, both on the M probe, from 2010 (52) and on the XL probe, from 2015 (53).

When VCTE started to be used, there was great interest on establishing cut-off values for differentiating the stages of histological fibrosis. However, in recent years, considering the new concept in hepatology of compensated advanced chronic liver disease (cACLD), as well as the overlapping cut-off values for mild stages of fibrosis, emphasis is placed on the diagnosis of advanced stages of fibrosis and clinically significant portal hypertension. This pragmatic

approach was introduced by the Society of American Radiologists, who proposed in 2020 the "rule of 5" regarding the evaluation by VCTE of patients with chronic viral hepatitis or MASLD, namely (54): liver stiffness (LS) ≤5 kPa - high probability of normal liver (without fibrosis); LS <10 kPa in the absence of significant clinical signs excludes compensated advanced chronic liver disease (cACLD), i.e. stages F3-F4; LS values between 10 and 15 kPa are suggestive of cACLD, but require additional testing for confirmation; >15 kPa LS values are highly suggestive of cACLD; LS values ≥20-25 kPa confirm clinically significant portal hypertension.

This approach is also mentioned in the Baveno VII consensus (55), which also includes platelet counts as a criterion in determining the need for endoscopic screening of esophageal varices in patients with LS values between 20-25 kPa.

SWE techniques based on ARFI (Acoustic Radiation Force Impulse)

As mentioned above, in all ARFI-based SWE techniques, the stimulus that causes tissue deformation is an acoustic impulse centered at a certain depth, which generates shear waves that move away from the application area. Depending on the technique for measuring the velocity of these shear waves, the ARFI-based SWE techniques are (14):

- ***point SWE (p-SWE)*** in which the acoustic impulse is centered onto a point and the speed of the shear waves is measured in a region of interest, expressed in m/s that can be converted to kPa.
- ***2D-SWE and 3D-SWE***, in which tissue stimulation is performed at several points by acoustic impulses and the measurement of shear waves velocity is done in a larger area. This type of elastography became possible due to technical advances in ultrasound, the evaluation result being not only a numerical value (expressed either in m/s or in kPa), but also an elastogram, a color-coded image superimposed on the gray scale ultrasound image.

The ARFI technique was introduced in 1998 by Sarvazyan et al. (56), who used for the first time an acoustic pulse to produce tissue deformation (shear waves), the propagation speed of which was measured using ultrasonography. The major advantage of this technique is that no other device is required (as in the case of FibroScan™), as long as the ARFI pulse and the B-mode ultrasound used to measure shear waves velocity are integrated into the same transducer. In the early 2000s, papers on the in vitro and in vivo applications of ARFI technique began to be published (57, 58).

In 2007, the first commercial application of the p-SWE technique, Virtual Touch quantification - VTQ™ was developed by Siemens. This was followed by the publication of numerous papers validating this method as compared to liver biopsy, but also to VCTE (59-61). Currently, VTQ is included in international guidelines as a method to assess liver fibrosis (17-19,54). Later, p-SWE became available on other platforms, perhaps the most documented being the Philips' ElastPQ™ technique (62-64).

Technological development has made it possible for tissue stimulation to no longer be done by ARFI at a single point, as in p-SWE, but at several points in rapid succession. Measurement of shear waves velocity generated by multiple ARFI pulses could be achieved by ultrasonography transducers with a very high scan rate (on the order of 10 images/s). This technology was proposed in 2004 (65) and was the basis for the development of 2D-SWE real-time elastography, being integrated into Supersonic Imagine's Aixplorer™ system. The clinical applications of this technology refer to liver fibrosis assessment (66-68), breast nodules (69), thyroid and prostate pathology, etc.

Later, 2D-SWE became available on other platforms such as General Electric, Samsung, Cannon, Toshiba, the technologies used to generate the acoustic pulse and to measure the shear waves velocity being different, from manufacturer to manufacturer.

In the following years, multiple clinical validation studies of 2D-SWE methods followed, compared to both biopsy and other elastographic methods, for the evaluation of liver fibrosis, of thyroid, breast, prostate pathology, etc. They demonstrated that 2D-SWE elastographic techniques are valuable methods, with good feasibility, being now included in international guidelines (17, 19, 54).

2. MRI Elastography

The concept of MRI elastography was developed in 1991-1995 by a team led by Dr. Richard Ehman, who used nuclear magnetic resonance assessment of tissue dislocation induced in tissues by a low-frequency vibrator (70,71). They started from the idea that the shear waves generated into the tissue by a stimulus with a fixed frequency will have a different wavelength, depending on the tissue stiffness. The advantage of MRI elastography is that it evaluates a large volume of tissue (especially valid in the case of the liver, where an elastogram of the entire liver is obtained). The first results on the differentiation of normal liver from fibrotic liver were published in 2004 (72).

The early 2000s saw significant advances in MRI technology, including the development of more sophisticated vibration sources and algorithms for processing shear wave images into elastograms. This period also marked the validation of MRI elastography in different clinical situations, especially for the evaluation of fibrosis in chronic liver diseases (73, 74), which has been demonstrated by several meta-analyses (75-77). Currently, MRI elastography is considered the most accurate non-invasive method of staging liver fibrosis, being accepted by international guidelines as an alternative to liver biopsy (17, 78).

Other clinical applications of MRI elastography are neurological diseases (79, 80), breast tumor pathology (81, 82), in musculoskeletal pathology, etc.

In conclusion, in the last 30 years, elastography based on either ultrasound or MRI has proven its usefulness for the non-invasive evaluation of liver fibrosis, of breast, thyroid, prostate tumoral pathology, of musculoskeletal pathology, etc. It is an extremely dynamic field, new technologies constantly opening new paths for the non-invasive evaluation of various pathologies.

Bibliography

1. Ormachea J, Parker KJ. Elastography imaging: the 30 year perspective. Phys Med Biol. 2020; 65(24).
2. HL O. Field and Impedance of an Oscillating Sphere in a Viscoelastic Medium with an Application to Biophysics. J Acoust Soc Am. 1951; 23:707–14.
3. Gierke HE, Oestreicher HL, Franke EK, Parrack HO, Wittern WW. Physics of vibrations in living tissues. J Appl Physiol. 1952; 4(12):886-900.
4. Eisensher A S-TE, Pelletier G and Jacquemard G. Rhythmic ultrasound palpation-echosismography. J Radiol. 1983; 64:225–61.
5. Ophir J, Cespedes I, Ponnekanti H, Yazdi Y, Li X. Elastography: a quantitative method for imaging the elasticity of biological tissues. Ultrasound Imaging. 1991; 13(2):111-34.
6. Shankar PM, Molthen R, Narayanan VM, Reid JM, Genis V, Forsberg F, et al. Studies on the use of non-Rayleigh statistics for ultrasonic tissue characterization. Ultrasound Med Biol. 1996; 22(7):873-82.
7. Tan SM, Teh HS, Mancer JF, Poh WT. Improving B mode ultrasound evaluation of breast lesions with real-time ultrasound elastography--a clinical approach. Breast. 2008; 17(3):252-7.
8. Itoh A, Ueno E, Tohno E, Kamma H, Takahashi H, Shiina T, et al. Breast disease: clinical application of US elastography for diagnosis. Radiology. 2006; 239(2):341-50.
9. Barr RG, Destounis S, Lackey LB, 2nd, Svensson WE, Balleyguier C, Smith C. Evaluation of breast lesions using sonographic elasticity imaging: a multicenter trial. J Ultrasound Med. 2012; 31(2):281-7.
10. Taylor LS, Porter BC, Nadasdy G, di Sant'Agnese PA, Pasternack D, Wu Z, et al. Three-dimensional registration of prostate images from histology and ultrasound. Ultrasound Med Biol. 2004; 30(2):161-8.
11. König K, Scheipers U, Pesavento A, Lorenz A, Ermert H, Senge T. Initial experiences with real-time elastography guided biopsies of the prostate. J Urol. 2005; 174(1):115-7.
12. Rago T, Di Coscio G, Basolo F, Scutari M, Elisei R, Berti P, et al. Combined clinical, thyroid ultrasound and cytological features help to predict thyroid malignancy in follicular and Hupsilonrthle cell thyroid lesions: results from a series of 505 consecutive patients. Clin Endocrinol (Oxf). 2007; 66(1):13-20.
13. Cantisani V, Lodise P, Di Rocco G, Grazhdani H, Giannotti D, Patrizi G, et al. Diagnostic accuracy and interobserver agreement of Quasistatic Ultrasound Elastography in the diagnosis of thyroid nodules. Ultraschall Med. 2015; 36(2):162-7.
14. Shiina T, Nightingale KR, Palmeri ML, Hall TJ, Bamber JC, Barr RG, et al. WFUMB guidelines and recommendations for clinical use of ultrasound elastography: Part 1: basic principles and terminology. Ultrasound Med Biol. 2015; 41(5):1126-47.
15. Sandrin L, Fourquet B, Hasquenoph JM, Yon S, Fournier C, Mal F, et al. Transient elastography: a new noninvasive method for assessment of hepatic fibrosis. Ultrasound Med Biol. 2003; 29(12):1705-13.
16. European Association for Study of L. Asociación Latinoamericana para el Estudio del H. EASL-ALEH Clinical Practice Guidelines: Non-invasive tests for evaluation of liver disease severity and prognosis. J Hepatol. 2015; 63(1):237-64.
17. European Association for the Study of the Liver. Electronic address eee, Clinical Practice Guideline P, Chair, representative EGB, Panel m. EASL Clinical Practice Guidelines on non-invasive tests for evaluation of liver disease severity and prognosis - 2021 update. J Hepatol. 2021; 75(3):659-89.

18. Ferraioli G, Filice C, Castera L, Choi BI, Sporea I, Wilson SR, et al. WFUMB guidelines and recommendations for clinical use of ultrasound elastography: Part 3: liver. Ultrasound Med Biol. 2015; 41(5):1161-79.
19. Ferraioli G, Wong VW, Castera L, Berzigotti A, Sporea I, Dietrich CF, et al. Liver Ultrasound Elastography: An Update to the World Federation for Ultrasound in Medicine and Biology Guidelines and Recommendations. Ultrasound Med Biol. 2018; 44(12):2419-40.
20. Foucher J, Castera L, Bernard PH, Adhoute X, Laharie D, Bertet J, et al. Prevalence and factors associated with failure of liver stiffness measurement using FibroScan in a prospective study of 2114 examinations. Eur J Gastroenterol Hepatol. 2006; 18(4):411-2.
21. Roulot D, Czernichow S, Le Clesiau H, Costes JL, Vergnaud AC, Beaugrand M. Liver stiffness values in apparently healthy subjects: influence of gender and metabolic syndrome. J Hepatol. 2008; 48(4):606-13.
22. de Ledinghen V, Vergniol J, Foucher J, El-Hajbi F, Merrouche W, Rigalleau V. Feasibility of liver transient elastography with FibroScan using a new probe for obese patients. Liver Int. 2010; 30(7):1043-8.
23. Sporea I, Sirli R, Mare R, Popescu A, Ivascu SC. Feasibility of Transient Elastography with M and XL probes in real life. Med Ultrasound. 2016; 18(1):7-10.
24. de Ledinghen V, Le Bail B, Rebouissoux L, Fournier C, Foucher J, Miette V, et al. Liver stiffness measurement in children using FibroScan: feasibility study and comparison with Fibrotest, aspartate transaminase to platelets ratio index, and liver biopsy. J Pediatr Gastroenterol Nutr. 2007; 45(4):443-50.
25. Friedrich-Rust M, Ong MF, Martens S, Sarrazin C, Bojunga J, Zeuzem S, Herrmann E. Performance of transient elastography for the staging of liver fibrosis: a meta-analysis. Gastroenterology. 2008; 134(4):960-74.
26. Stebbing J, Farouk L, Panos G, Anderson M, Jiao LR, Mandalia S, et al. A meta-analysis of transient elastography for the detection of hepatic fibrosis. J Clin Gastroenterol. 2010; 44(3):214-9.
27. Talwalkar JA, Kurtz DM, Schoenleber SJ, West CP, Montori VM. Ultrasound-based transient elastography for the detection of hepatic fibrosis: systematic review and meta-analysis. Clin Gastroenterol Hepatol. 2007; 5(10):1214-20.
28. Tsochatzis EA, Gurusamy KS, Ntaoula S, Cholongitas E, Davidson BR, Burroughs AK. Elastography for the diagnosis of severity of fibrosis in chronic liver disease: a meta-analysis of diagnostic accuracy. J Hepatol. 2011; 54(4):650-9.
29. Houot M, Ngo Y, Munteanu M, Marque S, Poynard T. Systematic review with meta-analysis: direct comparisons of biomarkers for the diagnosis of fibrosis in chronic hepatitis C and B. Aliment Pharmacol Ther. 2016; 43(1):16-29.
30. Li Y, Huang YS, Wang ZZ, Yang ZR, Sun F, Zhan SY, et al. Systematic review with meta-analysis: the diagnostic accuracy of transient elastography for the staging of liver fibrosis in patients with chronic hepatitis B. Aliment Pharmacol Ther. 2016; 43(4):458-69.
31. Xu X, Su Y, Song R, Sheng Y, Ai W, Wu X, Liu H. Performance of transient elastography assessing fibrosis of single hepatitis B virus infection: a systematic review and meta-analysis of a diagnostic test. Hepatol Int. 2015; 9(4):558-66.

32. Erman A, Sathya A, Nam A, Bielecki JM, Feld JJ, Thein HH, et al. Estimating chronic hepatitis C prognosis using transient elastography-based liver stiffness: A systematic review and meta-analysis. J Viral Hepat. 2018; 25(5):502-13.
33. Qi X, An M, Wu T, Jiang D, Peng M, Wang W, et al. Transient Elastography for Significant Liver Fibrosis and Cirrhosis in Chronic Hepatitis B: A Meta-Analysis. Can J Gastroenterol Hepatol. 2018;2018:3406789.
34. Pavlov CS, Casazza G, Nikolova D, Tsochatzis E, Gluud C. Systematic review with meta-analysis: diagnostic accuracy of transient elastography for staging of fibrosis in people with alcoholic liver disease. Pharmacol Ther Food. 2016; 43(5):575-85.
35. Nguyen-Khac E, Thiele M, Voican C, Nahon P, Moreno C, Boursier J, et al. Non-invasive diagnosis of liver fibrosis in patients with alcohol-related liver disease by transient elastography: an individual patient data meta-analysis. Lancet Gastroenterol Hepatol. 2018; 3(9):614-25.
36. Hashemi SA, Alavian SM, Gholami-Fesharaki M. Assessment of transient elastography (FibroScan) for diagnosis of fibrosis in non-alcoholic fatty liver disease: A systematic review and meta-analysis. Caspian J Intern Med. 2016; 7(4):242-52.
37. Mozes FE, Lee JA, Selvaraj EA, Jayaswal ANA, Trauner M, J Fellow, et al. Diagnostic accuracy of non-invasive tests for advanced fibrosis in patients with NAFLD: an individual patient data meta-analysis. Gut. 2022; 71(5):1006-19.
38. Manzo-Francisco LA, Aquino-Matus J, Vidana-Perez D, Uribe M, Chavez-Tapia N. Systematic review and meta-analysis: Transient elastography compared to liver biopsy for staging of liver fibrosis in primary biliary cholangitis. Ann Hepatol. 2023; 28(4):101107.
39. Marcos Carrasco N, Lopez Jerez A, Garrido E, Garcia Gonzalez M. Estimation of liver fibrosis using elastography in cholestatic diseases: systematic review and meta-analysis. Rev Esp Enferm Dig. 2023.
40. Huang DQ, Chan KE, Tan C, Zeng RW, Koh B, Ong EYH, et al. Meta-analysis: Prevalence of significant or advanced fibrosis in adults with alpha-1-antitrypsin deficiency. Pharmacol Ther Food. 2023; 58(2):152-8.
41. Martonosi AR, Soos A, Rumbus Z, Hegyi P, Izsak V, Pazmany P, et al. Non-invasive Diagnostic Tests in Cystic Fibrosis-Related Liver Disease: A Diagnostic Test Accuracy Network Meta-Analysis. Front Med (Lausanne). 2021;8:598382.
42. Lam S, Nettel-Aguirre A, Van Biervliet S, Roeb E, Sadler MD, Friedrich-Rust M, et al. Transient Elastography in the Evaluation of Cystic Fibrosis-Associated Liver Disease: Systematic Review and Meta-analysis. J Can Assoc Gastroenterol. 2019; 2(2):71-80.
43. Chen H, Shen Y, Wu SD, Zhu Q, Weng CZ, Zhang J, et al. Diagnostic role of transient elastography in patients with autoimmune liver diseases: A systematic review and meta-analysis. World J Gastroenterol. 2023; 29(39):5503-25.
44. Cheng F, Cao H, Liu J, Jiang L, Han H, Zhang Y, Guo D. Meta-analysis of the accuracy of transient elastography in measuring liver stiffness to diagnose esophageal varices in cirrhosis. Medicine (Baltimore). 2018; 97(28):E11368.
45. You MW, Kim KW, Pyo J, Huh J, Kim HJ, Lee SJ, Park SH. A Meta-analysis for the Diagnostic Performance of Transient Elastography for Clinically Significant Portal Hypertension. Ultrasound Med Biol. 2017; 43(1):59-68.
46. Kim G, Kim MY, Baik SK. Transient elastography versus hepatic venous pressure gradient for diagnosing portal hypertension: a systematic review and meta-analysis. Clin Mol Hepatol. 2017; 23(1):34-41.

47. Shi KQ, Fan YC, Pan ZZ, Lin XF, Liu WY, Chen YP, Zheng MH. Transient elastography: a meta-analysis of diagnostic accuracy in evaluation of portal hypertension in chronic liver disease. Liver Int. 2013; 33(1):62-71.
48. Wang J, Li J, Zhou Q, Zhang D, Bi Q, Wu Y, Huang W. Liver stiffness measurement predicted liver-related events and all-cause mortality: A systematic review and nonlinear dose-response meta-analysis. Common hepatol. 2018; 2(4):467-76.
49. Kim DY, Song KJ, Kim SU, Yoo EJ, Park JY, Ahn SH, Han KH. Transient elastography-based risk estimation of hepatitis B virus-related occurrence of hepatocellular carcinoma: development and validation of a predictive model. Onco Targets Ther. 2013;6:1463-9.
50. Masuzaki R, Tateishi R, Yoshida H, Goto E, Sato T, Ohki T, et al. Prospective risk assessment for hepatocellular carcinoma development in patients with chronic hepatitis C by transient elastography. Hepatology. 2009; 49(6):1954-61.
51. Stefanescu H, Grigorescu M, Lupsor M, Procopet B, Maniu A, Badea R. Spleen stiffness measurement using Fibroscan for the noninvasive assessment of esophageal varices in liver cirrhosis patients. J Gastroenterol Hepatol. 2011; 26(1):164-70.
52. Sasso M, Beaugrand M, de Ledinghen V, Douvin C, Marcellin P, Poupon R, et al. Controlled attenuation parameter (CAP): a novel VCTE guided ultrasonic attenuation measurement for the evaluation of hepatic steatosis: preliminary study and validation in a cohort of patients with chronic liver disease from various causes. Ultrasound Med Biol. 2010; 36(11):1825-35.
53. Sasso M, Audiere S, Kemgang A, Gaouar F, Corpechot C, Chazouilleres O, et al. Liver Steatosis Assessed by Controlled Attenuation Parameter (CAP) Measured with the XL Probe of the FibroScan: A Pilot Study Assessing Diagnostic Accuracy. Ultrasound Med Biol. 2016; 42(1):92-103.
54. Barr RG, Wilson SR, Rubens D, Garcia-Tsao G, Ferraioli G. Update to the Society of Radiologists in Ultrasound Liver Elastography Consensus Statement. Radiology. 2020; 296(2):263-74.
55. de Franchis R, Bosch J, Garcia-Tsao G, Reiberger T, Ripoll C, Baveno VIIF. Baveno VII - Renewing consensus in portal hypertension. J Hepatol. 2022; 76(4):959-74.
56. Sarvazyan AP, Rudenko OV, Swanson SD, Fowlkes JB, Emelianov SY. Shear wave elasticity imaging: a new ultrasonic technology of medical diagnostics. Ultrasound Med Biol. 1998; 24(9):1419-35.
57. Nightingale K, McAleavey S, Trahey G. Shear-wave generation using acoustic radiation force: in vivo and ex vivo results. Ultrasound Med Biol. 2003; 29(12):1715-23.
58. Nightingale K, so MS, Nightingale R, Trahey G. Acoustic radiation force impulse imaging: in vivo demonstration of clinical feasibility. Ultrasound Med Biol. 2002; 28(2):227-35.
59. Bota S, Herkner H, Sporea I, Salzl P, Sirli R, Neghina AM, Peck-Radosavljevic M. Meta-analysis: ARFI elastography versus transient elastography for the evaluation of liver fibrosis. Liver Int. 2013; 33(8):1138-47.
60. Friedrich-Rust M, Nierhoff J, Lupsor M, Sporea I, Fierbinteanu-Braticevici C, Strobel D, et al. Performance of Acoustic Radiation Force Impulse imaging for the staging of liver fibrosis: a pooled meta-analysis. J Viral Hepat. 2012; 19(2):E212-9.
61. Sporea I, Sirli RL, Deleanu A, Popescu A, Focsa M, Danila M, Tudora A. Acoustic radiation force impulse elastography as compared to transient elastography and liver biopsy in patients with chronic hepatopathies. Ultraschall Med. 2011; 32 Suppl 1:S46-52.

62. Ling W, Lu Q, Quan J, Ma L, Luo Y. Assessment of impact factors on shear wave based liver stiffness measurement. Eur J Radiol. 2013; 82(2):335-41.
63. Sporea I, Bota S, Gradinaru-Tascau O, Sirli R, Popescu A. Comparative study between two point Shear Wave Elastographic techniques: Acoustic Radiation Force Impulse (ARFI) elastography and ElastPQ. Med Ultrasound. 2014; 16(4):309-14.
64. Ma JJ, Ding H, Mao F, Sun HC, Xu C, Wang WP. Assessment of liver fibrosis with elastography point quantification technique in chronic hepatitis B virus patients: a comparison with liver pathological results. J Gastroenterol Hepatol. 2014; 29(4):814-9.
65. Bercoff J, Tanter M, Fink M. Supersonic shear imaging: a new technique for soft tissue elasticity mapping. IEEE Trans Ultrasonic Ferroelectr Freq Control. 2004; 51(4):396-409.
66. Bota S, Paternostro R, Etschmaier A, Schwarzer R, Salzl P, Mandorfer M, et al. Performance of 2-D shear wave elastography in liver fibrosis assessment compared with serologic tests and transient elastography in clinical routine. Ultrasound Med Biol. 2015; 41(9):2340-9.
67. Ferraioli G, Tinelli C, Dal Bello B, Zicchetti M, Filice G, Filice C, Liver Fibrosis Study G. Accuracy of real-time shear wave elastography for assessing liver fibrosis in chronic hepatitis C: a pilot study. Hepatology. 2012; 56(6):2125-33.
68. Herrmann E, de Ledinghen V, Cassinotto C, Chu WC, Leung VY, Ferraioli G, et al. Assessment of biopsy-proven liver fibrosis by two-dimensional shear wave elastography: An individual patient data-based meta-analysis. Hepatology. 2018; 67(1):260-72.
69. Evans A, Whelehan P, Thomson K, McLean D, Brauer K, Purdie C, et al. Quantitative shear wave ultrasound elastography: initial experience in solid breast masses. Breast Cancer Res. 2010; 12(6):R104.
70. Fowlkes JB, Emelianov SY, Pipe JG, Skovoroda AR, Carson PL, Adler RS, Sarvazyan AP. Magnetic-resonance imaging techniques for detection of elasticity variation. Med Phys. 1995; 22(11 Pt 1):1771-8.
71. Muthupillai R, Lomas DJ, Rossman PJ, Greenleaf JF, Manduca A, Ehman RL. Magnetic resonance elastography by direct visualization of propagating acoustic strain waves. Science. 1995; 269(5232):1854-7.
72. Dresner MA FJ, Ehman RL. MR elastography of in vivo human liver 11:. Proc Intl Soc Mag Reason Med 2004;11:502.
73. Yin M, Talwalkar JA, Glaser KJ, Manduca A, Grimm RC, Rossman PJ, et al. Assessment of hepatic fibrosis with magnetic resonance elastography. Clin Gastroenterol Hepatol. 2007; 5(10):1207-13 e2.
74. Yin M, Woollard J, Wang X, Torres VE, Harris PC, Ward CJ, et al. Quantitative assessment of hepatic fibrosis in an animal model with magnetic resonance elastography. Magn Reson Med. 2007; 58(2):346-53.
75. Kim YS, Jang YN, Song JS. Comparison of gradient-recalled echo and spin-echo echo-planar imaging MR elastography in staging liver fibrosis: a meta-analysis. Eur Radiol. 2018; 28(4):1709-18.
76. Singh S, Venkatesh SK, Loomba R, Wang Z, Sirlin C, Chen J, et al. Magnetic resonance elastography for staging liver fibrosis in non-alcoholic fatty liver disease: a diagnostic accuracy systematic review and individual participant data pooled analysis. Eur Radiol. 2016; 26(5):1431-40.

77. Singh S, Venkatesh SK, Wang Z, Miller FH, Motosugi U, Low RN, et al. Diagnostic performance of magnetic resonance elastography in staging liver fibrosis: a systematic review and meta-analysis of individual participant data. Clin Gastroenterol Hepatol. 2015; 13(3):440-51 e6.
78. Lim JK, Flamm SL, Singh S, Falck-Ytter YT, Clinical Guidelines Committee of the American Gastroenterological A. American Gastroenterological Association Institute Guideline on the Role of Elastography in the Evaluation of Liver Fibrosis. Gastroenterology. 2017; 152(6):1536-43.
79. Murphy MC, Huston J, 3rd, Ehman RL. MR elastography of the brain and its application in neurological diseases. Neuroimaging. 2019;187:176-83.
80. Pepin KM, McGee KP. Quantifying Tumor Stiffness With Magnetic Resonance Elastography: The Role of Mechanical Properties for Detection, Characterization, and Treatment Stratification in Oncology. Top Magn Reson Imaging. 2018; 27(5):353-62.
81. McKnight AL, Kugel JL, Rossman PJ, Manduca A, Hartmann LC, Ehman RL. MR elastography of breast cancer: preliminary results. AJR Am J Roentgenol. 2002; 178(6):1411-7.
82. Plewes DB, Bishop J, Samani A, Sciarretta J. Visualization and quantification of breast cancer biomechanical properties with magnetic resonance elastography. Phys Med Biol. 2000; 45(6):1591-610.

Chapter 3. History of Elastography Guidelines

Ioan Sporea

When discussing practice guidelines in medicine, the first question is why they are necessary. Specifically, why do we need guidelines in the field of elastography? Practice guidelines are essential for educating physicians on the latest advancements and their application in practice. Periodic updates of these guidelines allow for the continuous improvement and incorporation of recent research and publications. Guidelines are typically published by professional societies at various levels (national, European, or global) and reflect their perspectives on different areas of activity. These parallel guidelines often highlight differences in approaches and views at continental or national levels, influenced by varying levels of resources and pathological characteristics.

In the relatively new field of elastography, changes occur frequently, and new technical developments necessitate more frequent updates of these guidelines. A proper use of elastography in practice requires staying informed about the latest research and publications. Practitioners are encouraged to study these new guidelines to stay up to date with the latest developments and their practical applications.

We will review the elastography guidelines produced by various scientific societies, from the earliest guidelines to the most recent ones (some of which are still being published). Fortunately, I have been part of the working groups for many of these guidelines, developed through careful study of emerging publications, academic debates among experienced individuals, and the formulation of recommendations based on Oxford levels of evidence.

The first elastography guideline was published in 2013 by the European Federation of Societies for Ultrasound in Medicine and Biology (EFSUMB). Structured in two parts (the first covering physical principles and technology, and the second covering clinical applications) (1,2), this guideline was the first in the literature to review the basics of elastography.

Also in 2013, the Japanese Society of Ultrasound published its elastography guideline. Published in multiple parts, it first presented the physical principles and terminology, followed by hepatic applications of the technique (3,4). Unlike the EFSUMB guideline, the Japanese guideline recommended the use of strain elastography for hepatic evaluation, whereas the European version did not. Subsequently, the Japanese Society of Ultrasound proposed two more guidelines related to the elastographic evaluation of the breast and pancreas (5,6).

In 2014, the Romanian guideline for hepatic elastography was published (7). This guideline, which appeared relatively early, reflects the development of elastography (primarily hepatic) in Romania. Strong research centers in elastography (mainly hepatic, using impulse elastography and later ARFI technology) from Cluj and Timișoara, with numerous primary publications, allowed the accumulated experience to be shared in this Romanian guideline. This guideline begins with the physical principles of elastography and types of

elastography (SWE - Shear Wave Elastography and SE - Strain Elastography), followed by indications for hepatic elastography, the types of pathologies where hepatic elastography is used, and publications supporting the recommendations made. Finally, it includes references to the use of hepatic elastography in diagnosing circumscribed hepatic lesions.

The American Society of Radiologists in Ultrasound (SRU) published its guideline on the elastographic evaluation of the liver in the following year (8).

In 2015, three guidelines from the World Federation for Ultrasound in Medicine and Biology (WFUMB) were published (9,10,11). The first of these guidelines discusses terminology related to elastography and the basic principles of the method. The second guideline is for breast elastography, and the third is for hepatic elastography. The significant merit of these three guidelines is that they brought together the leading researchers and experts worldwide under the WFUMB umbrella in this new field. These guidelines allowed for a relative unification of the method globally. In 2017, the WFUMB guidelines on thyroid (12) and prostate (13) elastography were published.

After this period, hepatology societies began to get involved in developing liver elastography guidelines. In 2015, the European Association for the Study of the Liver (EASL), along with the Latin American Society, published a guideline on non-invasive liver evaluation (14), in which hepatic elastography plays a central role. Two years later, the American Gastroenterological Association (AGA) published its guideline on the elastographic evaluation of the liver (15).

Given the dynamic nature of elastographic methods, where the number of publications each year is high, as well as the emergence of numerous meta-analyses, the need arose for renewing and updating such guidelines after their first edition. Thus, the first renewed elastography guideline was from EFSUMB (16). This guideline also makes several recommendations for using hepatic elastography in clinical practice. Again, the European priority in renewing the hepatic elastography guideline comes from the extensive experience accumulated in European centers and the publications by European authors with considerable expertise in this field. Also, in 2017, the EFSUMB guideline for non-hepatic applications (17) was published.

In 2018, the World Federation for Ultrasound in Medicine and Biology (WFUMB) updated its guideline (18), incorporating new information related to elastographic methods for liver evaluation. The recommendations made, based on levels of scientific evidence, are helpful for practitioners. In 2020, an updated hepatic guideline from the American Society of Radiologists in Ultrasound (SRU) was published (19), introducing an important rule, the “Rule of 4,” which aims to standardize ARFI technique cut-offs for liver evaluation.

In 2021, EASL updated its guideline for the non-invasive evaluation of liver fibrosis (20). In parallel with these guidelines related to liver fibrosis evaluation, two guidelines for assessing portal hypertension were published, in 2015 (Baveno 6) and 2022 (Baveno 7) (21, 22). In these two guidelines, which represent consensus on portal hypertension, the “Rule of 5” is introduced for Impulse Elastography (VCTE), simplifying the use of cut-off values for

different grades of fibrosis and the risk of portal hypertension in patients with compensated advanced chronic liver disease (cACLD).

The most recent renewed guideline is from the World Federation for Ultrasound in Medicine and Biology (WFUMB) (23), updating information related to the elastographic evaluation of liver fibrosis and portal hypertension, providing several practical recommendations. This guideline also includes information on quantifying hepatic steatosis using ultrasound methods (24).

We have attempted to review the main guidelines published by various professional associations, initially focusing on general use guidelines and later on those for evaluating hepatic fibrosis (and subsequently hepatic steatosis). The continuous emergence of updated guideline versions demonstrates the dynamic nature of this method, with numerous valuable publications appearing annually.

Reviewing these guidelines aims to provide readers with these bibliographic materials, which can be consulted for a precise understanding of their recommendations. The continuous renewal of good practice guidelines and the physicians' knowledge of them allows for the correct use of the method, ensuring accurate clinical implementation.

References

1. Bamber J, Cosgrove D, Dietrich CF, Fromageau J, Bojunga J, Calliada F et al. EFSUMB guidelines and recommendations on the clinical use of ultrasound elastography. Part 1: Basic principles and technology. Ultraschall Med. 2013 Apr;34(2):169-84.
2. Cosgrove D, Piscaglia F, Bamber J, Bojunga J, Correas JM, Gilja OH, et al EFSUMB guidelines and recommendations on the clinical use of ultrasound elastography. Part 2: Clinical applications. Ultraschall Med. 2013 Jun;34(3):238-53.
3. Shiina T. JSUM ultrasound elastography practice guidelines: basics and terminology. J Med Ultrason (2001). 2013 Oct;40(4):309-23.
4. Kudo M, Shiina T, Moriyasu F, Iijima H, Tateishi R, Yada N, et al. JSUM ultrasound elastography practice guidelines: liver. J Med Ultrason (2001). 2013 Oct;40(4):325-57
5. Nakashima K, Shiina T, Sakurai M, Enokido K, Endo T, Tsunoda H, et al. JSUM ultrasound elastography practice guidelines: breast. J Med Ultrason (2001). 2013 Oct;40(4):359-91
6. Hirooka Y, Kuwahara T, Irisawa A, Itokawa F, Uchida H, Sasahira N, et al. JSUM ultrasound elastography practice guidelines: pancreas. J Med Ultrason (2001). 2015 Apr;42(2):151-74.
7. Sporea I, Bota S, Săftoiu A, Şirli R, Gradinăru-Taşcău O, Popescu A et al. Romanian national guidelines and practical recommendations on liver elastography. Med Ultrason. 2014 Jun;16(2):123-38.
8. Barr RG, Ferraioli G, Palmeri ML, Goodman ZD, Garcia-Tsao G, Rubin J, et al. Elastography Assessment of Liver Fibrosis: Society of Radiologists in Ultrasound Consensus Conference Statement. Radiology. 2015 Sep;276(3):845-61.
9. Shiina T, Nightingale KR, Palmeri ML, Hall TJ, Bamber JC, Barr RG, et al. WFUMB guidelines and recommendations for clinical use of ultrasound elastography: Part 1: basic principles and terminology. Ultrasound Med Biol. 2015 May;41(5):1126-1147.

10. Barr RG, Nakashima K, Amy D, Cosgrove D, Farrokh A, Schafer F, et al. WFUMB guidelines and recommendations for clinical use of ultrasound elastography: Part 2: breast. Ultrasound Med Biol. 2015 May;41(5):1148-1160.
11. Ferraioli G, Filice C, Castera L, Choi BI, Sporea I, Wilson SR, etal. WFUMB guidelines and recommendations for clinical use of ultrasound elastography: Part 3: liver. Ultrasound Med Biol. 2015 May;41(5):1161-1179
12. Cosgrove D, Barr R, Bojunga J et al. WFUMB Guidelines and Recommendations on the Clinical Use of Ultrasound Elastography: Part 4. Thyroid. Ultrasound Med Biol. 2017 Jan;43(1):4-26.
13. Barr RG, Cosgrove D, Brock M et al. WFUMB Guidelines and Recommendations on the Clinical Use of Ultrasound Elastography: Part 5. Prostate. Ultrasound Med Biol. 2017 Jan;43(1):27-48.
14. European Association for Study of Liver; Asociacion Latinoamericana para el Estudio del Higado. EASL-ALEH Clinical Practice Guidelines: Non-invasive tests for evaluation of liver disease severity and prognosis. J Hepatol. 2015 Jul;63(1):237-64.
15. Lim JK, Flamm SL, Singh S, Falck-Ytter YT; Clinical Guidelines Committee of the American Gastroenterological Association. American Gastroenterological Association Institute Guideline on the Role of Elastography in the Evaluation of Liver Fibrosis. Gastroenterology. 2017 May;152(6):1536-1543.
16. Dietrich CF, Bamber J, Berzigotti A, Bota S, Cantisani V, Castera L, et al. EFSUMB Guidelines and Recommendations on the Clinical Use of Liver Ultrasound Elastography, Update 2017 (Long Version). Ultraschall Med. 2017 Aug;38(4):e16-e47.
17. Săftoiu A, Gilja OH, Sidhu PS et al.The EFSUMB Guidelines and Recommendations for the Clinical Practice of Elastography in Non-Hepatic Applications: Update 2018. Ultraschall Med. 2019 Aug;40(4):425-453.
18. Ferraioli G, Wong VW, Castera L, Berzigotti A, Sporea I, Dietrich CF, et al. Liver Ultrasound Elastography: An Update to the World Federation for Ultrasound in Medicine and Biology Guidelines and Recommendations. Ultrasound Med Biol. 2018 Dec;44(12):2419-2440.
19. Barr RG, Wilson SR, Rubens D, Garcia-Tsao G, Ferraioli G. Update to the Society of Radiologists in Ultrasound Liver Elastography Consensus Statement. Radiology. 2020 Aug;296(2):263-274.
20. European Association for the Study of the Liver. EASL Clinical Practice Guidelines on non-invasive tests for evaluation of liver disease severity and prognosis - 2021 update. J Hepatol. 2021 Sep;75(3):659-689.
21. de Franchis R; Baveno VI Faculty. Expanding consensus in portal hypertension: Report of the Baveno VI Consensus Workshop: Stratifying risk and individualizing care for portal hypertension. J Hepatol. 2015 Sep;63(3):743-52.
22. de Franchis R, Bosch J, Garcia-Tsao G, Reiberger T, Ripoll C; Baveno VII Faculty. Baveno VII - Renewing consensus in portal hypertension. J Hepatol. 2022 Apr;76(4):959-974.
23. Ferraioli G, Barr RG, Berzigotti A, Sporea I, Wong VWS, Reiberger T, et al. WFUMB Guideline/Guidance on Liver Multiparametric Ultrasound. Part 1: Update to 2018 Guidelines on Liver Ultrasound Elastography. Ultrasound Med Biol 2024 Aug;50(8):1071-1087
24. Ferraioli G, Barr RG, Berzigotti A, Sporea I, Wong VWS, Reiberger T et al. WFUMB Guidelines/Guidance on Liver Multiparametric Ultrasound. Part 2: Guidance on Liver Fat Quantification. . Ultrasound Med Biol 2024 Aug;50(8):1088-1098.

Chapter 4. Principles of elastographic techniques

Felix Bende, Tudor Moga, Roxana Şirli

Elastography assesses the elasticity of tissues, representing the tendency of a tissue to resist deformation under the action of an applied force or to return to its original shape after the removal of that force. Elastography is a form of remote sensing that measures and shows the biomechanical characteristics of a tissue resisting shear deformation. A force can be applied widely across the surface of the body or at a single point, which results in shear deformation. This force can be generated naturally by physiological movement applied to the body's surface by vibration, or it can be concentrated at specific depths using an ultrasonic transducer to create a force of acoustic radiation (1,2).

Ultrasound is used in all ultrasound-based elastography techniques to quantify tissue shear deformations produced by an applied force. Both dynamic and quasi-static forces can be used. Quantitative imaging of tissue characteristics is not possible with quasi-static pressures. Tissue properties can be quantified thanks to dynamic forces. These include force impulses generated by acoustic radiation at specific depths or mechanical impulses generated at the body's surface.

According to EFSUMB (European Federation of Ultrasound in Medicine and Biology) guidelines (3), elastography techniques can be classified according to how tissue deformation data are displayed. Three options are available:

a. Display displacement without additional processing. This kind of displacement is employed in acoustic radiation force impulse imaging (ARFI imaging), where the presented image is scaled between bright (soft tissue) and dark (hard tissue), and it allows for a quantitative measurement (units of µm). Liver elastography does not employ this method.

b. Display of tissue deformation or strain rate, which is calculated from the spatial gradient of the displacement or velocity. This type of displacement works according to Hooke's law, which states that $E=\sigma / \varepsilon$, where stress is the force applied per unit area and strain is the change in tissue length divided by its original length. If the stress (unknown in the strain modulus) is assumed to be the same for all image locations, a strain image can be thought of as the inverse of the Young's modulus map. Distortion is a quantitative measurement (%) and the image brightness is usually scaled between bright (soft) and dark (hard).

c. Display of shear wave velocity, which is calculated by measuring the arrival time of a shear wave at various locations in the tissue. This is only possible when the force is applied dynamically. The shear wave velocity can be displayed in units of m/s. Alternatively, it can be converted to either Young's modulus E or shear modulus G, which are expressed in units of kilopascals (kPa). These elastography techniques are called shear wave elastography (SWE) and include vibration controlled transient elastography (VCTE), point shear wave elastography (pSWE) and multidimensional shear wave elastography (2D-SWE and 3D-SWE) (Fig. 4.1).

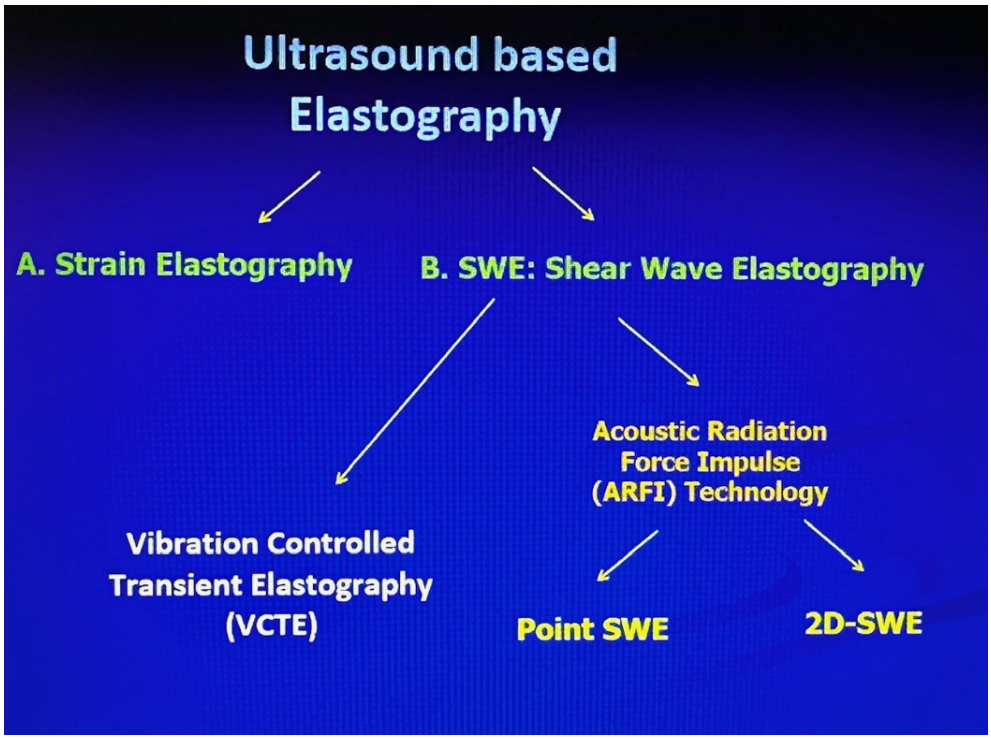

Fig. 4.1. Classification of elastographic techniques

For liver applications, elastography methods that display shear wave velocity are most commonly used in practice, followed by strain and displacement imaging (for liver lesions), which are used less frequently. Elastography methods integrated into clinical practice for the liver are described in Table I.

Table 4.1. Elastography methods used for the liver.

Deformation/displacement techniques	Shear wave elastography techniques
1. Strain elastography	1. Vibration Controlled Transient Elastography – VCTE (Impulsive Elastography) 2. Point shear wave elastography (Point Shear Wave Elastography) – pSWE 3. Multidimensional shear wave elastography (2D Shear Wave Elastography and 3D Shear Wave Elastography)

1. Strain elastography

Strain elastography is the most widely implemented elastography method on commercial systems, however, it is the least used technique for liver applications. The force used in strain elastography is either produced with the ultrasound probe or due to internal physiological motion. Axial displacement images are computed using radiofrequency echo correlation tracking or Doppler processing, which converts axial displacement images to strain images [2,4]. Manual pressure stimulation measures elasticity in superficial tissues. A disadvantage of this excitation method is that manual stress is not effectively transmitted to the deeper tissues. Excitation from natural physiological movement, such as heart rate and breathing, is another mechanism for generating tissue stress. Deep organs such as the liver or kidney can be evaluated with this method [2,4].

Strain elastography is a semi-quantitative method for analyzing the elastic properties of tissues, which has not demonstrated high accuracy in liver applications.

2. Shear Wave Elastography (SWE)

a) Vibration Controlled Transient Elastography – VCTE

VCTE was designed to measure liver elasticity only. It uses an automatic piston, which is also a disk-shaped ultrasound transducer, that applies a low-frequency (50 Hz) mechanical push to the body surface with a controlled applied force (5). A transient shear wave is created that propagates through the tissue. The velocity of shear wave propagation is proportional to tissue stiffness, which increases with liver fibrosis (6). VCTE measures tissue stiffness over a region of tissue 1 cm in diameter and 4 cm in length, which is 100 times larger than that assessed with liver biopsy. The transient deformation of the shear wave is propagated at a constant speed for 4 cm and measured by a straight line automatically displayed in a displacement ultrasound M-mode shown in the result (Figure 4.2) (3). If the pulse is not successfully transmitted and recorded, the software does not provide a reading. Transient elastography is marketed under the trade name FibroScan®. Stiffness values are given in kPa. Controlled Attenuation Parameter (CAP) is a technology that quantifies hepatic steatosis by measuring the loss of energy as the sound wave passes through the medium. Total attenuation at 3.5MHz is expressed in dB/m and steatosis is estimated using the same radiofrequency data as elastography at the same location where stiffness is measured (7). A schematic representation of the basic principle of VCTE is shown in Figure 4.3.

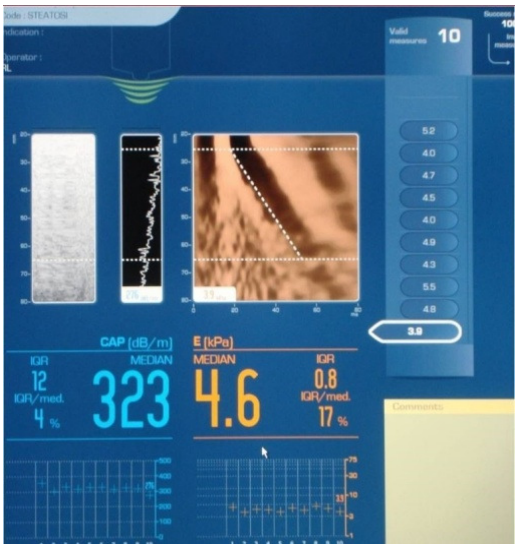

Fig. 4.2 Vibration Controlled Transient Elastography (VCTE) and controlled attenuation parameter (CAP) with the Fibroscan® device. Sample display showing the M-echo scan on the left, the single-line amplitude A-scan in the middle, and the displacement M-mode after a vibration-controlled surface pulse on the right. Numerical values for CAP are shown on the left (db/m) and for VCTE on the right (kPa).

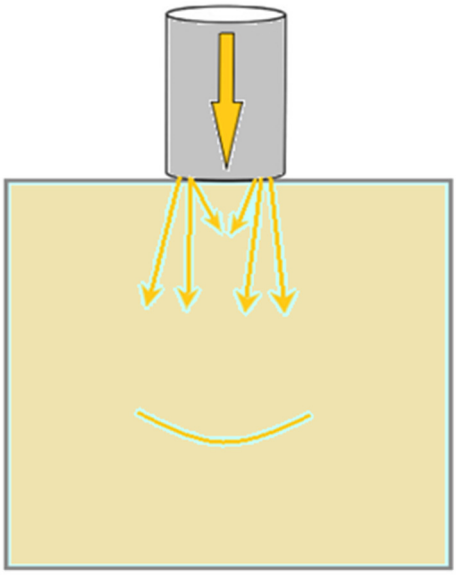

Fig. 4.3. Schematic representation of the principle of transient elastography. A mechanically induced pulse at the tissue surface with an A-mode transducer produces an axial shear wave pulse. The shear wave velocity measured is proportional to the fibrosis.

b) Point Shear Wave Elastography – pSWE

Applying an acoustic radiation force impulse (ARFI) at a controlled depth within a tissue generates a shear wave that propagates away from the axis and focal point of the thrust beam (Figure 4.4). The average propagation speed from the focal point positioned at the lateral boundary of a measurement region of interest (ROI) to another opposite lateral boundary of the ROI can be measured by detecting its arrival time at that point (2). Ultrasonography is used

to guide ROI placement, however, no elasticity images are produced (Figure 4.5). First introduced by the Siemens company, pSWE is available on various commercial systems from different vendors (e.g. Canon, Samsung, Hitachi, Esaote, etc.). Results can be expressed in either m/s or kPa.

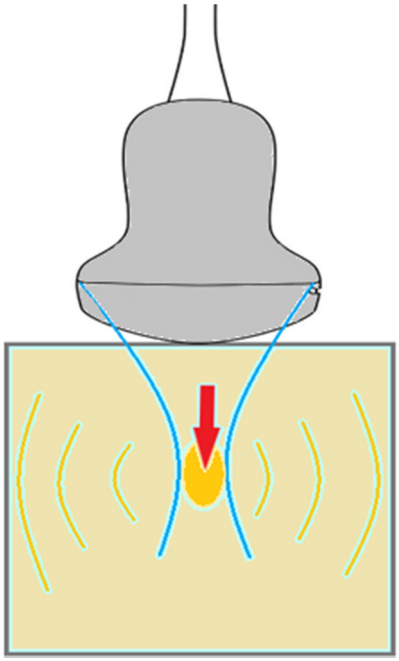

Figure 4.4. Schematic representation of the pSWE principle. An ultrasound-induced focused radiation force impulse is produced at a controlled depth generating a lateral shear wave in a region of interest (ROI). The measured shear wave velocity represents the stiffness of the tissue.

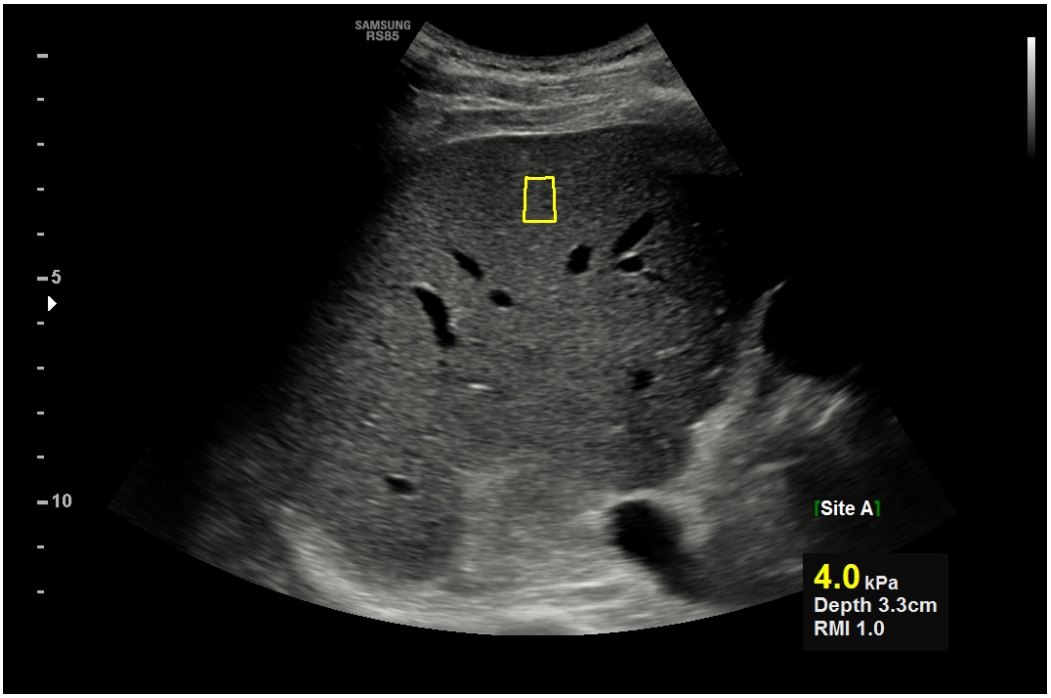

Figure 4.5. pSWE elastography implemented on the Samsung system. A region of interest (ROI) is placed 1-2 cm below the liver capsule. Liver stiffness measurement is shown in kPa.

c) Two-dimensional shear wave elastography (2D-SWE)

This method creates several locations of tissue displacement using the force impulse of acoustic radiation (Figure 4.6). Quantitative shear wave velocity images can be created by arranging the ARFI focus at multiple consecutive sites and measuring the shear wave velocity and arrival time at each (1,2). This results in the display of a sizable quantitative color-coded elasticity map, or elastogram, which can be shown independently side by side or overlaid over the B-mode image (Figure 6). By enclosing smaller ROIs (area of measurement) inside the elastogram, one can receive a quantitative measurement in addition to the visual impression of the elastogram on a color scale. A measurement's mean and standard deviation are typically shown, either as Young's modulus in kPa or as the shear wave propagation velocity in m/s (Figure 4.7).

Numerous ultrasound systems, including SuperSonic Imagine, GE Healthcare, Canon, Philips, Siemens, and Mindray, support this technique.

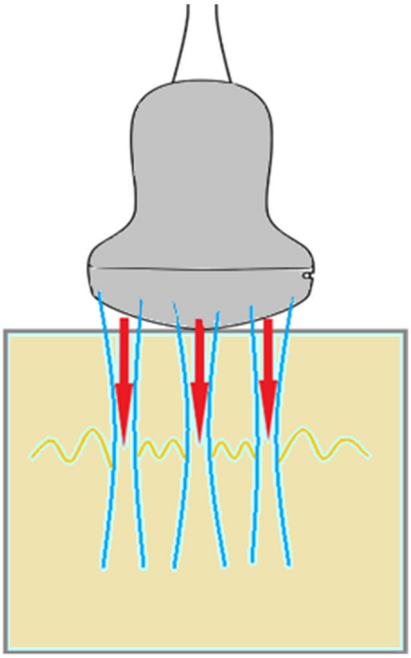

Figure 4.6. Schematic representation of the principle of 2D shear wave elastography (2D-SWE). Multiple ultrasound-induced ARFI lines create transverse shear waves that produce quantitative images of their velocity.

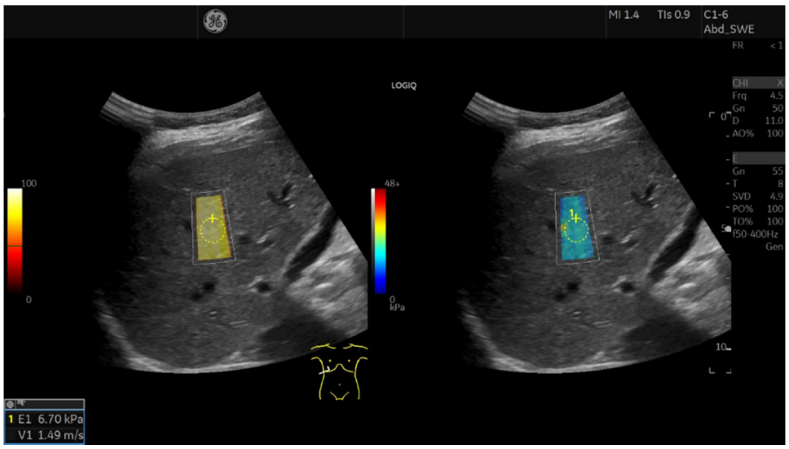

Figure 4.7. 2D Shear Wave Elastography (2D-SWE) implemented by General Electric. The elastogram, which is superimposed on the B-mode image, is placed 1-2 cm below the liver capsule (right image). A circular ROI is placed inside the elastogram for liver stiffness measurements. A quality color-coded map (pictured left) may be available to guide placement of measurements. The result is expressed in kPa and m/s.

References

1. Bamber J, Cosgrove D, Dietrich CF, Fromageau J, Bojunga J, et al. EFSUMB guidelines and recommendations on the clinical use of ultrasound elastography. Part 1: Basic principles and technology. Ultraschall Med. 2013 Apr;34(2):169-84.
2. Shiina T, Nightingale KR, Palmeri ML, Hall TJ, Bamber JC, et al. WFUMB guidelines and recommendations for clinical use of ultrasound elastography: Part 1: basic principles and terminology. Ultrasound Med Biol. 2015 May;41(5):1126-47.
3. Dietrich CF, Bamber J, Berzigotti A, Bota S, Cantisani V, et al. EFSUMB Guidelines and Recommendations on the Clinical Use of Liver Ultrasound Elastography, Update 2017 (Long Version). Ultraschall Med. 2017 Aug;38(4):e16-e47. English. doi: 10.1055/s-0043-103952. Epub 2017 Apr 13. Erratum in: Ultraschall Med. 2017 Aug;38(4):e48.
4. Sigrist RMS, Liau J, Kaffas AE, Chammas MC, Willmann JK. Ultrasound Elastography: Review of Techniques and Clinical Applications. Theranostics. 2017 Mar 7;7(5):1303-1329.
5. Sandrin L, Tanter M, Gennisson JL, Catheline S, Fink M. Shear elasticity probe for soft tissues with 1-D transient elastography. IEEE Trans Ultrason Ferroelectr Freq Control. 2002 Apr;49(4):436-46.
6. Srinivasa Babu A, Wells ML, Teytelboym OM, Mackey JE, Miller FH, Yeh BM, Ehman RL, Venkatesh SK. Elastography in Chronic Liver Disease: Modalities, Techniques, Limitations, and Future Directions. Radiographics. 2016 Nov-Dec;36(7):1987-2006.
7. Sasso M, Beaugrand M, de Ledinghen V, Douvin C, Marcellin P, Poupon R, Sandrin L, Miette V. Controlled attenuation parameter (CAP): a novel VCTE™ guided ultrasonic attenuation measurement for the evaluation of hepatic steatosis: preliminary study and validation in a cohort of patients with chronic liver disease from various causes. Ultrasound Med Biol. 2010 Nov;36(11):1825-35.

Chapter 5. Liver Elastography

5.1. Diffuse Hepatopathies

5.1.a. Examination Techniques and Confounding Factors in Liver Elastography

Felix Bende, Tudor Moga

1. Elastographic Examination Technique

All elastographic methods follow an evaluation technique that allows a good visualization and approach to the liver parenchyma. Patients will be positioned supine with the right arm in maximum abduction to widen the intercostal spaces thus providing a better view of the right liver lobe. Measurements from the left lobe of the liver are not recommended due to higher values and significant variability. Minimal training is required to be able to perform measurements of liver fibrosis, and the acquisition itself will usually take less than 5 minutes. Patients must be fasting (at least 2 hours) and not exerting themselves for at least 10 minutes before the assessment. At the time of ultrasound scanning of the liver, large vessels, artefacts and deep inspiratory movements should be avoided, both in A-mode Vibration Controlled Transient Elastography (VCTE) and in B-mode imaging (pSWE and 2D-SWE) (1- 4). To improve contact, a common ultrasound gel is used as the interface between the probe and the patient's skin.

For the VCTE technique (FibroScan®, Echosens), the transducer is placed between the right intercostal spaces (spaces 9-11) to facilitate pulse penetration at least 4 cm deep into the liver parenchyma. The device provides an A-mode image that will help the examiner choose the best section of the liver. The VCTE probe will transmit a mechanical impulse to the liver through a special (cylinder-shaped) piston that will apply a controlled force and thus generate shear waves. The probe is able to detect the speed of propagation of shear waves in the liver, reflecting the stiffness (hardness) of the liver. Measurements are expressed in kiloPascals (kPa) with a range of 1.5 kPa to 75 kPa. If the system detects errors in the acquisition process, it will automatically remove the measurement. At the end of the examination, the median of 10 measurements is displayed together with the quality parameters (interquartile range – IQR and success rate – SR). Although an IQR/median ratio ≤ 30% and a success rate ≥ 60% were initially recommended as quality criteria, currently only an IQR/median ratio ≤ 30% is sufficient to qualify the assessment as valid (1-4).

For more accurate measurements, manufacturers have developed several probes (M, XL and S) that are recommended to overcome the error factors given by obesity and variations in chest circumference (4). Boursier et al. (5) examined the learning curve and interobserver reproducibility of liver stiffness measurement (LSM) using VCTE elastography. The study found that novice examiners can obtain reliable LSM results with minimal training, indicating an

insignificant learning curve. The success rate of LSM is expected to increase with experience. Other studies have shown that at least 100 measurements are needed as training to obtain valid results and 500 for expert level (6, 7). It is also a reproducible method with excellent intra- and interobserver agreement (8).

pSWE elastography is a different method from VCTE, being integrated into an ultrasonographic system that evaluates liver fibrosis by non-invasive means. The "acoustic pulse" generated by the probe will generate shear waves that propagate in the liver parenchyma. Being an ultrasound-assisted method, ultrasonographic experience plays an important role in the successful performance of the technique, the reproducibility of the method being excellent (4, 8).

Using this technique, ascites is not a barrier to measuring liver stiffness (hardness). The probe, as in VCTE, should be placed in the right intercostal spaces to visualize liver tissue, avoiding large vessels or other structures. Next, the region of interest (ROI) should be placed at depths between 1 and 6 cm below the liver capsule, ideally 1-2 cm (9). Special attention should be paid to respiratory movements and cardiac cycles, patients should hold their breath for several seconds during the acquisition, and the operator should choose a correct distance from the heart when selecting the examination section and ROI.

Ten valid measurements are recommended and the result (median of measurements) is displayed in m/s or kPa. Quality parameters such as IQR/M and standard deviation (SD) are used to optimize method performance (10, 11). The most important quality parameter common to all pSWE technologies is the IQR/median ratio, which should be ≤ 30% if results are expressed in kPa (2, 10). The WFUMB guideline is more restrictive and states that, if the results are expressed in m/s, the IQR/median ratio must be ≤ 10% (2).

2D-SWE elastography is a real-time visualization technique based on ultrasound. As in the other methods, 2D-SWE uses a section through the right liver lobe, with the avoidance of large vessels and other structures, which require a stable image to make the acquisition. Patients must hold their breath for a few seconds so that the machine can track and measure the speed of propagation of the shear waves generated by the acoustic pulse in the region of interest. The speed of shear wave travel is displayed via a color-coded map, so the technique provides both quantitative and qualitative assessments of tissue stiffness. The region of interest, where the elastogram overlaps the gray-scale image, should be positioned at least 1-2 cm below the liver capsule, but no deeper than 7 cm in the liver parenchyma (12). A smaller measurement area is selected in the region of interest, the size of which can be selected by the operator, the results will be expressed as mean value and standard deviation, in kPa or in m/s.

The biggest advantage that 2D-SWE offers is that it evaluates a larger area of the liver parenchyma (up to 10 cm^2). Typically, stiffer (harder) tissue will be represented in red and softer tissue in blue. The operator should obtain as many "loops" of elastograms as possible in which in post-processing the region of interest will be selected for the acquisition of liver

stiffness measurements in the most homogeneous elastogram (13). Minimal training in abdominal ultrasonography (> 300 examinations) is required to be able to obtain good elastograms (14). IQR/M ratio and measurement depth < 5–6 cm are recommended as quality factors (10, 15). The median of at least three measurements should be used when performing liver stiffness measurements, but the examiner can choose between 3 and 15 measurements (16-18). Even though it is a reproducible method (19), inter- and intraobserver agreement in patients may be slightly inferior to pSWE (20, 21).

Real-time strain elastography, offered by the Hitachi system (HI-RTE) (22), uses a conventional ultrasound transducer that has the SE module built into it. A good ultrasound window is needed for the SE system to work properly, so a good ultrasound image is mandatory. The probe will generate longitudinal tissue deformation by mild tissue compression and thereby produce a real-time elasticity image by superimposing a color map on the B-mode image (23, 24). It has all the advantages of B-mode imaging and the approach to the examination will be the same as for the rest of the techniques, with the patient in supine position, with the right arm in maximum abduction with a short stop of breathing at the time of acquisition, ascites and increased BMI not being contraindications for this method.

The method is mainly used as a qualitative assessment. Results will be displayed as blue for stiffer tissue and red for soft tissue. Several methods have been developed to quantitatively assess tissue stiffness, such as elastic ratio, elastic index, elasticity score, and liver fibrosis index, but without proven consistency. The examiner must have ultrasound skills, and special training is required to set the region of interest and adjust the probe for a homogeneous compression/relaxation index (4, 25). Even though experience plays a role in SE, studies have shown that SE has good to very good intra- and inter-observer variability and is a reproducible method (26, 27).

2. Confounding Factors in Ultrasound-based Elastography

When measuring liver stiffness (hardness) using ultrasound-based elastography, we must recognize several factors that may influence the results. Some of these are related to a physiological state, others are related to pathology. Hepatic inflammation with a threshold of AST and/or ALT values > 5 times the normal value, liver congestion, cholestasis, acute hepatitis and infiltrative liver disease are known to increase liver stiffness (4). It is also known that food intake and physical activity can falsely increase liver stiffness, so a minimum of two hours of fasting and ten minutes of rest before the examination is recommended (4, 28, 29). The error factors associated with liver elastography, depending on the method, are represented in Fig.5.1.

For VCTE, BMI appeared to be the main factor influencing results (30), therefore a new probe, XL (2.5 MHz), dedicated to overweight and obese patients (BMI>28 Kg/m2) was produced with good results in clinical practice (31, 32).

In addition to BMI, VCTE results may be influenced by elevated transaminases (33), cholestasis (34), hepatic congestion (35), infiltrative liver disease, dietary intake (36, 37), and alcohol consumption. VCTE does not provide valid measurements in patients with ascites, another disadvantage being the lack of B-mode imaging, which prevents visualization of the liver, making it more difficult to avoid possible vascular or tumor structures (7, 38).

The study by Kettaneh et al. (39) evaluate the efficacy of VCTE in a cohort of 935 patients with Hepatitis C Virus (HCV). In this study, it was found that the success rate of VCTE measurements decreases with age and is lower in obese patients. However, the experience of the operator, especially those with more than 50 examinations, significantly improves the success rate. The performance of VCTE for the diagnosis of cirrhosis was consistent regardless of the number of valid measurements and operator skills, suggesting that, even with minimal training, VCTE provides reliable diagnostic performance for the diagnosis of cirrhosis.

The pSWE technique uses B-mode ultrasound to visualize an appropriate liver section where the acquisition is to be made, thus making the method more dependent on the ultrasonographic image selection by the operator (8). Region of interest and right lobe depths vs. left are aspects that can influence the results (40, 41). Increased BMI, moderate/severe steatosis (42, 43), elevated transaminases, congestive liver, cholestasis, as well as dietary intake influence liver stiffness measurements. The examination must be done in a fasting state or at least 3-4 hours after the last meal (44-46).

The 2D-SWE technique is an ultrasound-based method that allows for the real-time visualization of the visco-elastic properties of tissues. It is an operator-dependent method, with experience playing an important role in obtaining reliable results (14), from the study by Leung et al. (47), however, we find that 3 to 5 valid measurements can be obtained in 90-98.9% of the examined cases. Even though the method overcomes some of the previous limitations, results may be influenced in patients with large amount of ascites, poor sonographic window, obesity (BMI > 30 kg/m2), inability to stop breathing, abdominal wall thickness (≥25 mm), steatosis, waist circumference (≥ 102 cm), and recent dietary intake (4, 37, 48, 49).

The strain elastography method is an operator-dependent method, with the ultrasound window being a prerequisite for a correct acquisition. We know from the study of Bilgen et al. (50) that when we use a convex transducer, extra care must be taken because the region immediately in front of the transducer could be under greater stress than the lateral portions of the sector. In this case, reducing the size of the ROI sector for elastography will improve the uniformity of the deformation image. It is essential to avoid placing the region of interest (ROI) near large blood vessels during elastography, as blood circulation can create an artificial displacement effect or an apparent 'soft' area in the elastogram. For the correct evaluation of liver fibrosis, it is recommended to position the ROI more than 1 cm below the liver capsule to avoid the area of reduced tension (colored in blue) that is found under the capsule (25). Experience also plays an important role. The method is not widely used in daily practice because of its inconsistency (1, 2, 4, 24, 51).

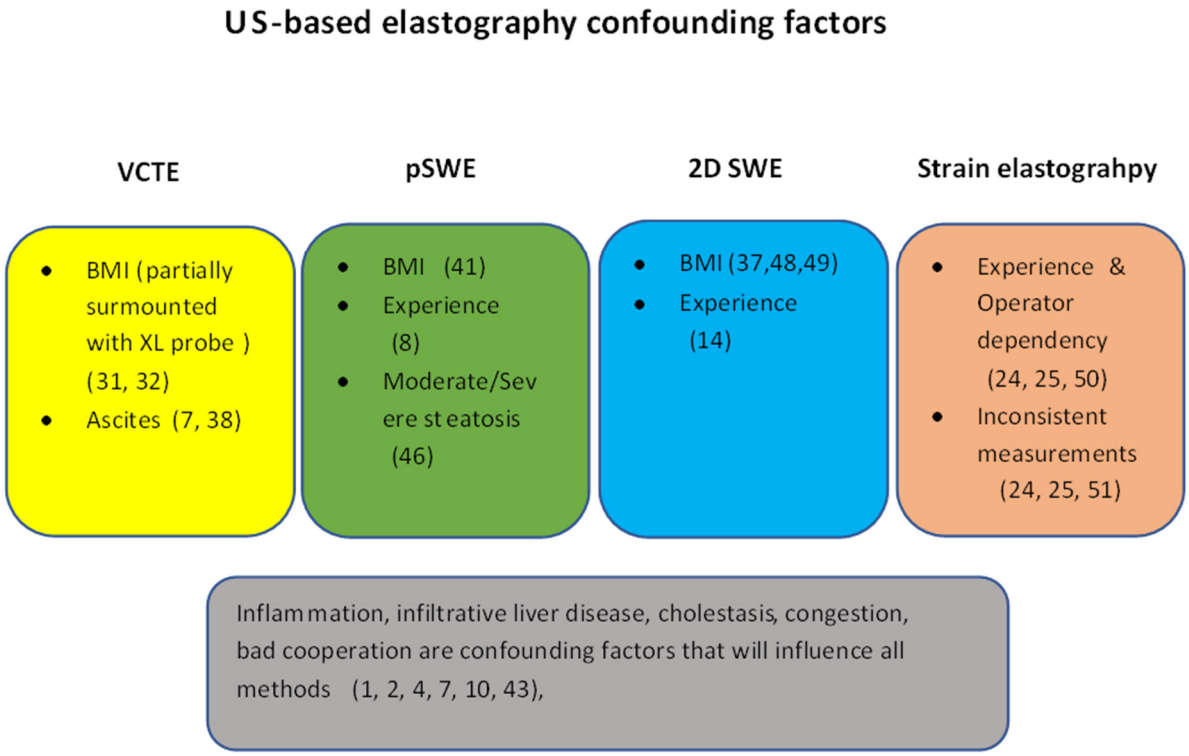

Fig. 5.1. Confounding factors associated in ultrasound-based elastography

References

1. Ferraioli G, Filice C, Castera L, Choi BI, Sporea I, Wilson SR, et al. WFUMB guidelines and recommendations for clinical use of ultrasound elastography: Part 3: liver. Ultrasound Med Biol. 2015;41(5):1161-79.
2. Ferraioli G, Wong VW, Castera L, Berzigotti A, Sporea I, Dietrich CF, et al. Liver Ultrasound Elastography: An Update to the World Federation for Ultrasound in Medicine and Biology Guidelines and Recommendations. Ultrasound Med Biol. 2018;44(12):2419-40.
3. Beaugrand M. [Fibroscan: instructions for use]. Gastroenterol Clin Biol. 2006;30(4):513-4.
4. Cosgrove D, Piscaglia F, Bamber J, Bojunga J, Correas JM, Gilja OH, et al. EFSUMB guidelines and recommendations on the clinical use of ultrasound elastography. Part 2: Clinical applications. Ultraschall Med. 2013;34(3):238-53.
5. Boursier J, Konate A, Guilluy M, Gorea G, Sawadogo A, Quemener E, et al. Learning curve and interobserver reproducibility evaluation of liver stiffness measurement by transient elastography. Eur J Gastroenterol Hepatol. 2008;20(7):693-701.
6. Armstrong MJ, Corbett C, Hodson J, Marwah N, Parker R, Houlihan DD, et al. Operator training requirements and diagnostic accuracy of Fibroscan in routine clinical practice. Postgrad Med J. 2013;89(1058):685-92.
7. Castéra L, Foucher J, Bernard PH, Carvalho F, Allaix D, Merrouche W, et al. Pitfalls of liver stiffness measurement: a 5-year prospective study of 13,369 examinations. Hepatology. 2010;51(3):828-35.

8. Simona Bota IS. Acoustic Radiation Force Impulse Elastography, Hepatic Elastography Using Ultrasound Waves Bentham Science Publisher; 2012.
9. Sporea I, Sirli RL, Deleanu A, Popescu A, Focsa M, Danila M, et al. Acoustic radiation force impulse elastography as compared to transient elastography and liver biopsy in patients with chronic hepatopathies. Ultraschall Med. 2011;32 Suppl 1:S46-52.
10. Dietrich CF, Bamber J, Berzigotti A, Bota S, Cantisani V, Castera L, et al. EFSUMB Guidelines and Recommendations on the Clinical Use of Liver Ultrasound Elastography, Update 2017 (Long Version). Ultraschall Med. 2017;38(4):e16-e47.
11. Ioan Sporea RȘ. Transient Elastography (TE), Hepatic Elastography Using Ultrasound Waves: Bentham Science Publisher; 2012.
12. Wang CZ, Zheng J, Huang ZP, Xiao Y, Song D, Zeng J, et al. Influence of measurement depth on the stiffness assessment of healthy liver with real-time shear wave elastography. Ultrasound Med Biol. 2014;40(3):461-9.
13. Ioan Sporea RȘ. "Hepatic Elastography Using Ultrasound Waves ": Bentham Science Publishers. ; 2012.
14. Grădinaru-Taşcău O, Sporea I, Bota S, Jurchiş A, Popescu A, Popescu M, et al. Does experience play a role in the ability to perform liver stiffness measurements by means of supersonic shear imaging (SSI)? Med Ultrason. 2013;15(3):180-3.
15. Colombo S, Buonocore M, Del Poggio A, Jamoletti C, Elia S, Mattiello M, et al. Head-to-head comparison of transient elastography (TE), real-time tissue elastography (RTE), and acoustic radiation force impulse (ARFI) imaging in the diagnosis of liver fibrosis. J Gastroenterol. 2012;47(4):461-9.
16. Ferraioli G, Tinelli C, Dal Bello B, Zicchetti M, Filice G, Filice C. Accuracy of real-time shear wave elastography for assessing liver fibrosis in chronic hepatitis C: a pilot study. Hepatology. 2012;56(6):2125-33.
17. Sporea I, Grădinaru-Taşcău O, Bota S, Popescu A, Şirli R, Jurchiş A, et al. How many measurements are needed for liver stiffness assessment by 2D-Shear Wave Elastography (2D-SWE) and which value should be used: the mean or median? Med Ultrason. 2013;15(4):268-72.
18. Huang ZP, Zhang XL, Zeng J, Zheng J, Wang P, Zheng RQ. Study of detection times for liver stiffness evaluation by shear wave elastography. World J Gastroenterol. 2014;20(28):9578-84.
19. Moga TV, Stepan AM, Pienar C, Bende F, Popescu A, Șirli R, et al. Intra- and Inter-Observer Reproducibility of a 2-D Shear Wave Elastography Technique and the Impact of Ultrasound Experience in Achieving Reliable Data. Ultrasound Med Biol. 2018;44(8):1627-37.
20. Woo H, Lee JY, Yoon JH, Kim W, Cho B, Choi BI. Comparison of the Reliability of Acoustic Radiation Force Impulse Imaging and Supersonic Shear Imaging in Measurement of Liver Stiffness. Radiology. 2015;277(3):881-6.
21. Alina Popescu FB, Ioan Sporea. . 2D-ShearWaves Elastography (2D-SWE), Hepatic Elastography Using Ultrasound Waves. 2016. Bentham Science Publisher; [88].
22. Friedrich-Rust M, Ong MF, Herrmann E, Dries V, Samaras P, Zeuzem S, et al. Real-time elastography for noninvasive assessment of liver fibrosis in chronic viral hepatitis. AJR Am J Roentgenol. 2007;188(3):758-64.
23. Frey H. [Realtime elastography. A new ultrasound procedure for the reconstruction of tissue elasticity]. Radiologe. 2003;43(10):850-5.

24. Larisa Săndulescu IS, Alina Popescu. . Real-Time Strain Elastography (HI-RTE), Hepatic Elastography Using Ultrasound Waves Revised Edition of Volume 1 (2016) 2016. Bentham Science Publisher.
25. Dietrich CF, Barr RG, Farrokh A, Dighe M, Hocke M, Jenssen C, et al. Strain Elastography - How To Do It? Ultrasound Int Open. 2017;3(4):E137-e49.
26. Gheonea DI, Săftoiu A, Ciurea T, Gorunescu F, Iordache S, Popescu GL, et al. Real-time sono-elastography in the diagnosis of diffuse liver diseases. World J Gastroenterol. 2010;16(14):1720-6.
27. Koizumi Y, Hirooka M, Kisaka Y, Konishi I, Abe M, Murakami H, et al. Liver fibrosis in patients with chronic hepatitis C: noninvasive diagnosis by means of real-time tissue elastography--establishment of the method for measurement. Radiology. 2011;258(2):610-7.
28. Arena U, Lupsor Platon M, Stasi C, Moscarella S, Assarat A, Bedogni G, et al. Liver stiffness is influenced by a standardized meal in patients with chronic hepatitis C virus at different stages of fibrotic evolution. Hepatology. 2013;58(1):65-72.
29. Gersak MM, Sorantin E, Windhaber J, Dudea SM, Riccabona M. The influence of acute physical effort on liver stiffness estimation using Virtual Touch Quantification (VTQ). Preliminary results. Med Ultrason. 2016;18(2):151-6.
30. Foucher J, Castéra L, Bernard PH, Adhoute X, Laharie D, Bertet J, et al. Prevalence and factors associated with failure of liver stiffness measurement using FibroScan in a prospective study of 2114 examinations. Eur J Gastroenterol Hepatol. 2006;18(4):411-2.
31. Myers RP, Pomier-Layrargues G, Kirsch R, Pollett A, Duarte-Rojo A, Wong D, et al. Feasibility and diagnostic performance of the FibroScan XL probe for liver stiffness measurement in overweight and obese patients. Hepatology. 2012;55(1):199-208.
32. Sporea I, Şirli R, Mare R, Popescu A, Ivașcu SC. Feasibility of Transient Elastography with M and XL probes in real life. Med Ultrason. 2016;18(1):7-10.
33. Viganò M, Massironi S, Lampertico P, Iavarone M, Paggi S, Pozzi R, et al. Transient elastography assessment of the liver stiffness dynamics during acute hepatitis B. Eur J Gastroenterol Hepatol. 2010;22(2):180-4.
34. Millonig G, Reimann FM, Friedrich S, Fonouni H, Mehrabi A, Büchler MW, et al. Extrahepatic cholestasis increases liver stiffness (FibroScan) irrespective of fibrosis. Hepatology. 2008;48(5):1718-23.
35. Millonig G, Friedrich S, Adolf S, Fonouni H, Golriz M, Mehrabi A, et al. Liver stiffness is directly influenced by central venous pressure. J Hepatol. 2010;52(2):206-10.
36. Mederacke I, Wursthorn K, Kirschner J, Rifai K, Manns MP, Wedemeyer H, et al. Food intake increases liver stiffness in patients with chronic or resolved hepatitis C virus infection. Liver Int. 2009;29(10):1500-6.
37. Yoon JH, Lee JM, Han JK, Choi BI. Shear wave elastography for liver stiffness measurement in clinical sonographic examinations: evaluation of intraobserver reproducibility, technical failure, and unreliable stiffness measurements. J Ultrasound Med. 2014;33(3):437-47.
38. Sporea I, Şirli R. Hepatic Elastography Using Ultrasound Waves; Revised Edition of Volume 1: Bentham Science Publishers 2016.

39. Kettaneh A, Marcellin P, Douvin C, Poupon R, Ziol M, Beaugrand M, et al. Features associated with success rate and performance of FibroScan measurements for the diagnosis of cirrhosis in HCV patients: a prospective study of 935 patients. J Hepatol. 2007;46(4):628-34.
40. D'Onofrio M, Gallotti A, Mucelli RP. Tissue quantification with acoustic radiation force impulse imaging: Measurement repeatability and normal values in the healthy liver. AJR Am J Roentgenol. 2010;195(1):132-6.
41. Liao LY, Kuo KL, Chiang HS, Lin CZ, Lin YP, Lin CL. Acoustic radiation force impulse elastography of the liver in healthy patients: test location, reference range and influence of gender and body mass index. Ultrasound Med Biol. 2015;41(3):698-704.
42. Sporea I, Sirli RL, Deleanu A, Popescu A, Focsa M, Danila M, et al. Acoustic Radiation Force Impulse Elastography as Compared to Transient Elastography and Liver Biopsy in Patients with Chronic Hepatopathies. Ultraschall Med. 2011;32(S 01):46-52.
43. Ferraioli G, Wong VW-S, Castera L, Berzigotti A, Sporea I, Dietrich CF, et al. Liver Ultrasound Elastography: An Update to the World Federation for Ultrasound in Medicine and Biology Guidelines and Recommendations. Ultrasound in Medicine & Biology. 2018;44(12):2419-40.
44. Goertz RS, Egger C, Neurath MF, Strobel D. Impact of food intake, ultrasound transducer, breathing maneuvers and body position on acoustic radiation force impulse (ARFI) elastometry of the liver. Ultraschall Med. 2012;33(4):380-5.
45. Bota S, Sporea I, Peck-Radosavljevic M, Sirli R, Tanaka H, Iijima H, et al. The influence of aminotransferase levels on liver stiffness assessed by Acoustic Radiation Force Impulse Elastography: a retrospective multicentre study. Dig Liver Dis. 2013;45(9):762-8.
46. Bota S, Sporea I, Sirli R, Popescu A, Dănilă M, Sendroiu M. Factors that influence the correlation of acoustic radiation force impulse (ARFI), elastography with liver fibrosis. Med Ultrason. 2011;13(2):135-40.
47. Leung VY, Shen J, Wong VW, Abrigo J, Wong GL, Chim AM, et al. Quantitative elastography of liver fibrosis and spleen stiffness in chronic hepatitis B carriers: comparison of shear-wave elastography and transient elastography with liver biopsy correlation. Radiology. 2013;269(3):910-8.
48. Staugaard B, Christensen PB, Mössner B, Hansen JF, Madsen BS, Søholm J, et al. Feasibility of transient elastography versus real-time two-dimensional shear wave elastography in difficult-to-scan patients. Scand J Gastroenterol. 2016;51(11):1354-9.
49. Cassinotto C, Lapuyade B, Mouries A, Hiriart JB, Vergniol J, Gaye D, et al. Non-invasive assessment of liver fibrosis with impulse elastography: comparison of Supersonic Shear Imaging with ARFI and FibroScan®. J Hepatol. 2014;61(3):550-7.
50. Bilgen M, Insana MF. Error analysis in acoustic elastography. II. Strain estimation and SNR analysis. J Acoust Soc Am. 1997;101(2):1147-54.
51. Morikawa H, Fukuda K, Kobayashi S, Fujii H, Iwai S, Enomoto M, et al. Real-time tissue elastography as a tool for the noninvasive assessment of liver stiffness in patients with chronic hepatitis C. J Gastroenterol. 2011;46(3):350-8.

5.1.b. Fibrosis Assessment by VCTE, pSWE and 2D-SWE

Roxana Sirli, Ruxandra Mare, Alina Popescu

The evaluation of liver fibrosis in chronic liver diseases of various etiologies is one of the most intensively studied and used clinical applications of elastography. Strain elastography, even if it was the first to appear on the market, has not confirmed its usefulness in everyday practice. Shear-wave elastography is the one used in daily clinical activity, as you will see below.

5.1.b.1. Fibrosis Assessment by VCTE

Vibration Controlled Transient Elastography (VCTE), originally known as Transient Elastography (TE), is the most established elastographic method used for fibrosis staging in chronic liver diseases. As shown in previous chapters, the method was developed in the early 2000s (1). Liver stiffness (LS) is measured with the FibroScan™ device (EchoSens, Paris, France) (Fig.5.2.). A special transducer, mounted on the shaft of a vibrator, measures the velocity of shear waves generated into the liver by the mechanical impulse of the vibrator. The value measured in m/s is automatically converted using the Young modulus into kiloPascals (kPa), which is considered indicative of liver stiffness. As previously described, 10 LS measurements are required for a correct assessment, the device automatically calculating their median value and IQR, which must be lower than 30% for the obtained value to be considered interpretable (1-7).

Fig. 5.2. FibroScan device with M and XL probes. Measurement in an individual without fibrosis (LS 4.9 kPa - in yellow) and without steatosis (CAP 272 dB/m - in blue)

A. Evaluation by VCTE in Individuals with Normal Liver

Since the method was introduced, multiple studies have been conducted that have evaluated subjects without liver damage. One of the first studies published was the one conducted by Roulot et al. on a group of 429 apparently healthy consecutive subjects, the mean LS value being 5.49±1.59 kPa (8). In another large study, on 445 patients, the mean LS value was 5.1±1.19 kPa (9). Two other large studies with more than 600 patients revealed slightly lower mean values, of 4.4 kPa (10, 11). In a personal study of 152 subjects, the mean LS value in normal individuals was 4.8±1.3 kPa (12).

Factors influencing LS values in healthy subjects were also evaluated. The first factor taken into account was the patients' gender. Most studies have shown that the values are higher in men than in women (8-10, 12).

Based on the already demonstrated fact that liver fibrosis progresses more rapidly in elderly subjects (13), another factor considered was whether the LS values measured by VCTE in healthy subjects are influenced by the subjects' age. In a study conducted in our clinic, although we found small differences in mean LS values between age groups, they did not reach statistical significance, nor could an upward trend in relation to age be highlighted (12). Similar results were observed in the Roulot study (8), as well as in two other smaller studies (14, 15). However, in another large study, a negative correlation between age and LS was observed in 530 patients ($r=-0.168$, $p<0.001$). For those aged ≤25, 26-35, 36-45, 46-55 and >55 years, the mean LS values were 4.2, 4.3, 4.0, 3.8 and 3.4 kPa ($p = 0.001$), respectively (16). In a paediatric population of 240 children, the LS value was significantly age-dependent, with median values being 4.40, 4.73 and 5.1 kPa in children aged 0-5, 6-11, and 12-18 years ($p = 0.001$), respectively (17).

It is known that in overweight and obese patients it is more difficult to obtain valid measurements by VCTE. The same is true for subjects without liver pathology. Hence the idea of seeing whether the body mass index (BMI) influences the LS values measured by VCTE. In the Roulot study, LS values were significantly higher in subjects with BMI≥30kg/m^2. In the Kumar study, LS was also higher in subjects with higher BMI (normal, overweight and obese subjects: 4.10±0.75, 5.08±0.66 and 6.05±1.28kPa, respectively; $p<0.001$) (9). Another large study demonstrated that LS values in individuals with BMI <18.5 kg/m^2 were comparable to those of obese subjects, being significantly higher than in normal-weight subjects (6.05 ± 1.78 kPa. and 6.60 ± 1.21 kPa versus 5.51 ± 1.59 kPa, $p = 0.016$ and 0.349 respectively (18).

In a study including individual data from 16,082 subjects without chronic liver disease, with normal transaminases values (≤ 33 IU in men and ≤ 25 IU in women), the mean LS value in non-obese individuals was 4.68 kPa, with values increasing in patients with liver steatosis by ultrasound (5.42 kPa), with diabetes mellitus (5.56 kPa), with steatosis and diabetes (5.94 kPa). In obese individuals, the values were significantly higher: 5.6 kPa (in those without steatosis or diabetes), 5.71 kPa in those with steatosis by ultrasound, 6.34 kPa in those with diabetes, 6.49 kPa in those with steatosis and diabetes (19).

In conclusion, considering all these data, what do the guidelines say? The EFSUMB (European Federation of Societies for Ultrasound in Medicine and Biology) guidelines state that LS values measured by VCTE in normal liver range between 4.5-5.5 kPa, these values being sufficient to exclude significant liver fibrosis in the absence of significant clinical and biological signs (20). According to the Guidelines of the American Society of Radiologists, LS values ≤ 5kPa by VCTE exclude the presence of fibrosis in patients with chronic viral hepatitis or with metabolic dysfunction-associated steatosis (MASLD) (21).

B. Evaluation by VCTE in Patients with Chronic Hepatitis C

The first published studies regarding the value of VCTE for predicting liver fibrosis severity included patients with chronic hepatitis caused by hepatitis C virus (HCV). These studies tried to find cut-off LS values by VCTE that would differentiate between the stages of fibrosis diagnosed by liver biopsy. The conclusion was that VCTE is not precise enough to differentiate between close stages of fibrosis (in particular F0, F1, F2 Metavir) but it is sufficient to differentiate the absence of fibrosis and mild fibrosis (F0 and F1) from significant fibrosis (F2), which was essential for the treatment decision at the time. VCTE also had excellent predictive value for the diagnosis of HCV-induced cirrhosis.

In a French multicenter study coordinated by Beaugrand (22), which included 494 patients with chronic HCV hepatitis, evaluated by liver biopsy and VCTE, a significant correlation was found between fibrosis severity and LS ($r = 0.57$, $p<0.001$). This study calculated cut-off values to differentiate fibrosis stages. Thus, the value of 7.5 kPa differentiated F0-1 from F2-4 with sensitivity (Se) of 67%, specificity (Sp) of 87%, positive predictive value (PPV) of 86% and negative predictive value (NPV) of 68%, with a diagnostic accuracy of 76% (22).

In a study by our group that included 407 naïve patients with chronic HCV hepatitis, we found a significant direct correlation of LS measurements with fibrosis severity: Spearman $r=0.605$, $P<0.0001$. For a cut-off value of 6.8 kPa, LS had a sensitivity of 58.9% and a specificity of 89.1% (AUROC 0.760) for predicting significant fibrosis (at least F2 Metavir), while for a cut-off value of 12.6 kPa, the sensitivity was 92.1%, specificity 91.6% (AUROC 0.953) for the prediction of cirrhosis (23). Other studies have established cut-off values that differentiate F0-1 from F2-4 ranging from 6.8-7.3 kPa (23-25).

Over the years, countless studies have been published on the value of VCTE for the discrimination of fibrosis stages, which have been summarized in several meta-analyses (26-29). In the Friedrich-Rust meta-analysis, based on 50 studies, the mean AUROC for the prediction of significant fibrosis (F2) was 0.84, at a suggested cut-off value of 7.6 kPa (26). In the Tsochatzis meta-analysis, the cut-off value calculated for F≥2 Metavir was also 7.6 kPa, with 0.78 Cumulative Se and 0.89 Cumulative Sp (29).

The conclusion would be that, in viremic patients with HCV, if the LS is greater than 6.8–7.6 kPa (22-24, 26, 28), there is a high probability that the liver biopsy will reveal

significant fibrosis (F2-F4), the patient requiring antiviral therapy according to the guidelines valid at the time, when only patients with at least significant fibrosis had a firm indication for treatment. Currently, taking into account the excellent efficacy of interferon-free treatment regimens exceeding 95-96%, their minimal adverse effects, all patients with active HCV infection should be treated, regardless of the stage of fibrosis (30, 31).

For the presence of cirrhosis, the predictive value of VCTE is much better, the AUROCs calculated in different studies exceeding 0.95 (26, 27). A meta-analysis published in 2016, that included 24 papers estimated a Se of 84%, with a Sp of 90%, with AUROC 0.95 for the prediction of cirrhosis in patients with chronic HCV hepatitis (32). The suggested cut-off value for the diagnosis of HCV liver cirrhosis was 12.5-15 kPa (24, 29).

Another question that arose was whether VCTE could be useful for *tracking antiviral treatment outcomes*. In a study published in 2011, Hezode et al. prospectively evaluated 91 patients with HCV chronic hepatitis during pegInterferon and Ribavirin therapy (33) using VCTE. LS was assessed at weeks 4, 12, 24, at the end of treatment and at 12 and 24 weeks after treatment. A significant decrease in LS during therapy, which continued after treatment, was only observed in patients who achieved a sustained virologic response (SVR). The median decrease in VCTE values from baseline at the end of follow-up was -3.4 kPa, compared to -1.8 kPa in patients who did not achieve SVR (33). Similar results have been observed in other studies, in patients treated with both interferon-based regimens and patients treated with direct antiviral agents (34-37). However, the decrease in LS values at the end of treatment, as well as at short intervals after the end of treatment (12, 24 weeks) cannot be attributed to a regression of fibrosis, most likely to be caused by a decrease in inflammation (38). Long-term follow-up of LS values showed significant decreases in VCTE values in those with SVR, more intense immediately after therapy, slower in years of surveillance, more important in patients with liver cirrhosis and clinically significant portal hypertension (CSPH) (36, 39, 40).

The question that arises is whether we can interrupt the surveillance of cirrhotic patients with SVR regarding the occurrence of CSPH and hepatocarcinoma. The Baveno VI and VII criteria state that patients with VCTE values ≤ 20 kPa and platelet count ≥150 × 10^9/L have a <5% risk of having esophageal varices with a high risk of bleeding (41). According to a recent study, if after SVR the LS values by VCTE fall below 12 kPa, in patients with normal platelet counts, the risk of developing CSPH is excluded with a Se of 99.2% (42). Thus, if the Baveno VI/VII criteria are met after SVR, patients may no longer need screening endoscopy.

However, regardless of the decrease in LS values, patients with severe fibrosis and cirrhosis should undergo the hepatocarcinoma screening program (5, 20).

The value of VCTE to predict complications of cirrhosis in patients with chronic HCV hepatitis, especially CSPH, will be discussed in a separate chapter.

C. Evaluation by VCTE in Patients with Chronic Hepatitis B

Initial studies of cut-off values for predicting different stages of fibrosis had conflicting results in patients with chronic hepatitis B, with variations in cut-off values for the same stage of fibrosis, particularly when compared to those in patients with chronic hepatitis C. In one of the first larger studies published, a prospective study by Marcellin et al. including 202 patients with chronic HBV hepatitis, the AUROCs for F≥2, F≥3 and F=4 were 0.81, 0.93 and 0.93, respectively. The optimal cut-off values were 7.2 and 11.0 kPa for F≥2 and F=4, respectively, by maximizing the sum of sensitivity and specificity, and 7.2 and 18.2 kPa by maximizing diagnostic accuracy (43).

Comparative studies of the VCTE value for predicting fibrosis severity in patients with chronic hepatitis B vs. chronic hepatitis C have shown similar performance (44, 45). However, a significant dependence of cut-off values on serum transaminase values was highlighted in patients with flares of chronic HBV hepatitis (46-48). Consequently, LS measurements by VCTE must be interpreted in a biochemical context; Otherwise, there is a risk of overestimating the severity of fibrosis. This is also why evaluation by VCTE is not recommended in acute hepatitis or during flares of chronic hepatitis B (3, 5, 20).

To minimize the risk of overestimation of fibrosis during flares, Chan et al. calculated the LS cut-off values by VCTE for different stages of fibrosis taking into account aminotransferase levels (49). In this study, the LS cut-off value for F3 was 9 kPa in patients with normal ALT and 12 kPa in patients with ALT greater than 5 times the upper limit of normal. The cut-off values for cirrhosis were 12 kPa in patients with normal ALT and 13.4 kPa in those with elevated ALT (49).

The Tsochatzis meta-analysis evaluated the predictive value of LS assessed by VCTE also in patients with chronic hepatitis B. The calculated cut-off value for F≥2 Metavir was 7 kPa (range 6.9–7.2, lower than in HCV patients), with Se of 0.84 and Sp of 0.78 (29). The Chon meta-analysis included 2772 patients with HBV chronic hepatitis, the mean AUROC for the diagnosis of significant fibrosis (F2), severe fibrosis (F3), and cirrhosis (F4) were 0.859, 0.887, and 0.929, respectively. The calculated cut-off values were 7.9 kPa for F2 (Se 74.3% and Sp 78.3%), 8.8 kPa for F3 (Se 74.0% and Sp 63.8%), while for F4 it was 11.7 kPa (Se 84.6% and Sp 81.5%) (50).

In 2015, two more meta-analyses were published on the performance of VCTE in staging fibrosis in HBV patients. Xu meta-analysis showed that there are significant differences in performance in European vs. Asian populations, the AUROC for F≥2 and F4 diagnosis were 0.803 and 0.905 vs. 0.871 and 0.914, respectively (51). In the Li meta-analysis, which included 4386 HBV patients, the corresponding AUROCs for F≥2, F≥3, and F=4 was 0.88, 0.91, and 0.93, respectively (52).

Given all these data, VCTE has become an established method for staging fibrosis in chronic hepatitis B in patients with normal ALT (2, 3, 5, 20), with even better performance than serological tests (2). This is important because patients with chronic HBV hepatitis with significant fibrosis should receive antiviral treatment regardless of transaminase levels (53, 54).

Regarding the evolution of LS values in patients with chronic HBV hepatitis under antiviral treatment, several studies have shown a significant stiffness decrease during treatment (55-59). The decrease was more significant in the first 2-3 years of treatment, after which the values remained relatively stable (58, 59). However, as in patients with chronic HCV hepatitis, the decrease in LS values in cirrhotic patients following effective antiviral treatment should not influence the hepatocarcinoma screening program (5, 20). With regard to CSPH, the Baveno VI/VII criteria should also be applied to patients with chronic HBV hepatitis (60).

A special category of patients are those with *chronic HBeAg negative HBV infection* (previously known as HBsAg inactive carriers; patients HBsAg positive, HBeAg negative, with HBV-DNA viral load < 2000 IU/ml and normal ALT level). Significant fibrosis and even cirrhosis may be present in these patients, albeit in a small percentage of cases. In a study by our group, the mean values of LS by VCTE in chronic HBV AgHBe negative infection was 5.6±2.1kPa, significantly higher than in normal subjects (4.8 ± 1.2 kPa, p = 0.0002). In patients with undetectable viral load, the mean LS was 4.9 ± 1.2 kPa, significantly lower than in those with detectable DNA (< 2000 IU/ml) (6.7 ± 2.7 kPa, p < 0.001) (61). International guidelines state that VCTE can be used to exclude significant fibrosis and diagnose cirrhosis in these patients (5, 20).

The value of VCTE to predict complications of cirrhosis in patients with chronic hepatitis B, especially CSPH, will be discussed in a separate chapter.

D. Evaluation by VCTE in Patients with Hepatic Steatosis Associated with Metabolic Dysfunction (MASLD)

Metabolic dysfunction associated steatotic liver disease (MASLD), previously classified as non-alcoholic fatty liver disease (NAFLD), is currently the leading cause of chronic liver disease worldwide. MASLD affects more than 60% of people who are overweight/obese or have type 2 diabetes (62, 63). This category of patients is at risk of liver fibrosis which can progress to cirrhosis as a consequence of associated steatohepatitis (MASH, formerly known as non-alcoholic steatohepatitis - NASH). Considering the large number of patients with MASLD, it was very important to find a non-invasive method to assess fibrosis severity, since it is the most important prognostic factor in these patients (64).

Even from the beginning, VCTE was used to evaluate patients with MASLD (NAFLD) and a significant correlation has been observed between the LS values by VCTE and the severity of histological fibrosis (65), even though in obese patients (a large part of patients with MASLD) it was more difficult to obtain valid measurements, an obstacle largely overcome by the development of the XL probe.

One of the discussions in patients with MASLD is to what extent the presence of steatosis influences LS values. Wong et al. evaluated VCTE as a predictor of fibrosis and cirrhosis in patients with MASLD and factors associated with VCTE discordance with histology in 246 consecutive patients (48). LS was not affected by hepatic steatosis, necroinflammation

or body mass index. Discordance of at least two stages between VCTE and histology was observed in 33 (13.4%) patients. By multivariate analysis, biopsy fragment length less than 20 mm and F0-2 disease were associated with discordance (48). In a Romanian study, multivariate analysis demonstrated that the only factor that independently influenced the LS values by VCTE in patients with MASH was the severity of fibrosis (66).

In terms of predicting fibrosis severity, in the Wong study, the VCTE AUROCs for F≥3 and F4 were 0.93 and 0.95, respectively. At a cut-off value of 7,9 kPa, Se, Sp, PPV and NPV for F≥3 were 91%, 75%, 52% and 97% respectively (67). In a meta-analysis published in 2014, including 856 patients with MASLD, assessed with the M probe, VCTE had good accuracy for the diagnosis of F≥3 (Se 85%; Sp 82%) and F4 (Se 92%; Sp, 92%), but only moderate accuracy for F≥2 (Se 79%; Sp 75%) (68).

Over the years, numerous studies have been published trying to generate a screening algorithm for these patients, to identify those with significant/severe fibrosis, using serological markers, with or without elastographic methods. A recent meta-analysis included individual data from 5735 patients from 37 studies, assessed by liver biopsy and a sequential combination of FIB-4 (cut-off <1.3; ≥2.67), followed by LS measurements by VCTE (cut-off <8.0; ≥10.0 kPa) to exclude or confirm advanced fibrosis (69). This combination of non-invasive tests had a Se and Sp of 66% and 86% respectively for the diagnosis of severe fibrosis. For the diagnosis of cirrhosis, FIB-4 (cut-off <1.3; ≥3.48) followed by VCTE (cut-off <8.0; ≥20.0 kPa) to exclude severe fibrosis and to confirm cirrhosis had a Se of 38%, with a Sp of 90% (69).

Another recent meta-analysis including over 11,000 patients with MASLD evaluated by biopsy and VCTE, highlighted AUROC curves of 0.82, 0.85, and 0.89 respectively for the diagnosis of F≥2, F≥3, and F4, respectively. The cut-offs ranged from 3.8 to 10.2 kPa for F≥2, 6.8 to 12.9 kPa for F≥3, and 6.9 to 19.9 kPa for F4 (70).

The American Gastroenterology Association (AGA) guidelines suggest 12 kPa for confirming severe fibrosis (71). With regard to the prognosis of MASLD, the guidelines of the European Association for the Study of the Liver (EASL) suggest that repetitive assessment by VCTE at 1-3 years intervals, depending on the clinical and biological scenario, would be useful for the prognosis of patients (3), a recommendation also supported by the AGA guideline (71).

In patients with MASLD, it is also important to quantify steatosis. Details on this topic can be found in the dedicated chapter. We will only mention that the manufacturers of FibroScan™ have developed an application dedicated to the quantification of steatosis, ***Controlled Attenuation Parameter*** (CAP), implemented in the same device, both on the M probe (72) and on the XL probe (73).

The predictive value of VCTE to for cirrhosis complications in patients with MASLD, especially CSPH, will be discussed in a separate chapter.

E. Evaluation by VCTE in Patients with Alcohol-related Liver Disease (ALD)

ALD is one of the most important causes of chronic liver disease, accounting for about 50% of the etiology of cirrhosis in Europe (74). Unfortunately, these patients are diagnosed in most cases late, in the cirrhotic stage, although the risk factor is clear and they come into contact with the medical system, at least at the level of primary medicine. This is why it would be important to find non-invasive screening tests to diagnose ALD in the precirrhotic stage, when abstinence from alcohol would significantly improve the prognosis.

Regarding VCTE assessment of patients with ALD, it should be taken into account that in most of these patients, inflammation coexists with fibrosis and steatosis, and can influence the results of LS measurements. Initial studies reported higher cut-off values for the diagnosis of cirrhosis in ALD than in those with viral hepatitis: 19.5 kPa in the Nguyen-Khac et al study (75) and 22.6 kPa in the Nahon study (76). However, ALT values were high in patients in these cohorts, but were not considered.

In a study conducted by Mueller et al (77), 50 patients undergoing a rehab program were included in the training cohort, were evaluated by VCTE at admission and after transaminase normalization, the mean interval being 5.3 days. A significant decrease in LS was observed in most patients, which correlated best with the decrease in AST. No significant changes in LS were observed below AST levels of 100 U/L. In the study cohort that included 101 patients with histologically confirmed alcohol-induced steatohepatitis (ASH), if LS was measured by VCTE in patients with AST ≤ 100 U/L at the time of evaluation vs. at admission, the AUROC for the detection of cirrhosis improved from 0.921 to 0.945, while the specificity increased from 80% to 90%, to a sensitivity of 96%. A similar AUROC curve was obtained for F3 fibrosis if measurements were limited to patients with AST <50 U/L. The conclusion of this study was that delaying evaluation by VCTE in patients with ALD until AST decreases to <100 U/ml (under abstinence conditions, significantly improves diagnostic accuracy (77).

These results have also been confirmed by other studies which concluded that increased transaminase values correlate with increased VCTE values, and that the resolution of liver inflammation (evidenced by AST normalization) parallels the decrease in LS after a period of 1-8 weeks of abstinence (78-81). In a study in which VCTE was assessed compared to liver biopsy in patients with ALD, it was found that in patients with advanced fibrosis, mean LS values by VCTE decreased from 21.5 kPa at baseline to 11.4 kPa after two months of abstinence, with mean AST values decreasing from 70 U/L to 30 U/L over the same period (80). Another study found a steep increase in LS in ALD patients with advanced fibrosis when AST levels exceeded 70 U/L (81).

As regards the effect of alcohol abuse per se on LS values assessed by VCTE, it does not appear to result in falsely elevated LS values, as long as transaminases are not highly elevated (82). Also, several studies have shown that low LS values by VCTE exclude advanced fibrosis in patients with ALD, regardless of concomitant alcohol abuse and the presence of histological steatohepatitis (80, 83, 84).

In a meta-analysis published in 2015 (85), due to the wide variability in the results of the included studies, cut-off values could not be calculated to discriminate fibrosis stages in patients with ALD. However, this meta-analysis suggests that VCTE can be used to exclude severe fibrosis and cirrhosis using cut-off values of 9.5 and 12.5 kPa, respectively, but with caution, taking into account the risk of overestimation in patients who continue alcohol consumption (85).

A meta-analysis published in 2018, including individual data from 1026 patients with ALD found that the cut-off values of VCTE for fibrosis staging are strongly influenced by AST and bilirubin levels (cut-off values for AST>75 U/L and bilirubin >0.94 mg dl) (86). The cut-off values calculated for VCTE were 7 kPa (AUROC 0.83) for F≥1; 9 kPa (AUROC 0.86) for F≥2; 12.1 kPa (AUROC 0.90) for F≥3 and 18.6 kPa (AUROC 0.91) for F=4 (86).

The predictive value of VCTE for cirrhosis complications in patients with ALD, especially CSPH, will be discussed in a separate chapter.

F. Evaluation by VCTE in Patients with Cholestatic Hepatopathies (Primary Biliary Cholangitis – PBC and Primary Sclerosing Cholangitis – PSC)

The first study on the value of LS measurement by VCTE in patients with cholestatic liver diseases (***PBC and PSC***) was published in 2006 (87). In this study, LS was correlated with both fibrosis (Spearman r = 0.84, P<0.0001) and histological activity (r=0.79, P<0.0001). These correlations were maintained when patients with PBC and PSC were analyzed separately. The AUROC curves were 0.92 for F≥2, 0.95 for F≥3 and 0.96 for F=4, the calculated cut-off values being 7.3, 9.8 and 17.3 kPa, respectively (87).

In another study published in 2008 in 80 patients with ***PBC,*** LS measured by VCTE was significantly correlated with histological fibrosis stage, with AUROCs being 0.89 for F>2 and 0.96 for F=4 (88). A study published in 2012 by Corpechot calculated cut-off values of LS by VCTE of 7.1 kPa for F≥ 1, 8.8 kPa for F≥ 2, 10.7 kPa for F3 and 16.9 kPa for F4, the performance of VCTE being better than that of biochemical markers (89).

An international multicenter study published by Corpechot's team in 2022, which included 3,985 patients with PBC, found that each additional kPa of LS increases the risk rate of poor outcome by 1.040 times, thus establishing that LS is an independent prognostic factor for PBC (90). The cut-off values of 8 kPa and 15 kPa effectively classified patients into low, medium and high-risk groups (90), respectively. A recently published meta-analysis from 2023 showed that LS assessed by VCTE not only correlates with the presence of fibrosis but is also an important indicator for prognosis (91).

Regarding ***PSC***, the same team led by Copechot conducted a study that included 73 patients with PSC evaluated by liver biopsy and VCTE. The cut-off values calculated for ≥F1, ≥F2, ≥F3 and F4 were 7.4 kPa, 8.6 kPa, 9.6 kPa and 14.4 kPa (92) respectively. Another important conclusion of this study was that baseline LS values as well as their growth rate were strongly and independently correlated with patients' prognosis.

G. Evaluation by VCTE in Patients with Autoimmune Hepatitis

Autoimmune hepatitis (HAI) is characterized by episodes of major cytolysis that result in progression to fibrosis and cirrhosis. Liver biopsy is essential for diagnosis and prognosis (93), but in recent years non-invasive staging methods have also been evaluated. It is a known fact that inflammation (with its indirect sign of major cytolysis) is one of the factors that lead to the overestimation of fibrosis by VCTE (2, 5, 20). Consequently, the results of VCTE at the time of diagnosis correlate with the histological degree of inflammation rather than with the stage of fibrosis (94). However, if the assessment is made after at least 6 months of successful immunosuppressive therapy, VCTE is accurate enough to diagnose cirrhosis and differentiate advanced stages of fibrosis (F3, F4) from less severe stages (F0-F2) (94). The calculated cut-off values were 5.8 kPa for F≥2, 10.5 kPa for F≥3 and 16 kPa for F≥4 (94). The decrease in LS values correlates with biochemical remission, fibrosis regression and favorable prognosis (95).

H. New Concepts in VCTE

If at the beginning there was emphasis on establishing threshold values by VCTE for differentiating the stages of histological fibrosis, in recent years, taking into account the new concept in hepatology of compensated advanced chronic liver disease (cACLD), as well as the overlapping of the measured values for mild stages of fibrosis, emphasis is placed on the diagnosis of advanced stages of fibrosis and clinically significant portal hypertension. This pragmatic approach was introduced by the Society of American Radiologists, which proposed in 2020 the "rule of 5" regarding the evaluation by VCTE of patients with chronic viral liver diseases or MAFLD, namely (21): liver stiffness (LS) ≤ 5 kPa - high probability of normal liver (without fibrosis); LS < 10 kPa in the absence of significant clinical signs excludes compensated advanced chronic liver disease (cACLD), i.e. stages F3-F4; values between 10 and 15 kPa are suggestive of cACLD, but require additional testing for confirmation; values > 15 kPa are highly suggestive of cACLD; values ≥ 20-25 kPa confirm clinically significant portal hypertension.

This approach is also continued in the Baveno VII consensus (41), which also includes platelet counts as a criterion in determining the need for endoscopic screening of esophageal varices in patients with LS values between 20-25 kPa.

5.1.b.2. Evaluation of Fibrosis by Point Shear-wave Elastography (pSWE)

pSWE elastography uses ARFI technology, which is integrated into multiple ultrasound systems, thus allowing the quantification of liver stiffness (LS) during a standard ultrasound. The measurements are made in an area of the parenchyma in the right hepatic lobe devoid of large vessels, by placing a region of interest (ROI) whose size is predetermined by the manufacturer (4, 20). The first pSWE elastographic techniques were Virtual Touch Tissue Quantification (VTQ)® (Siemens Healthcare, Erlangen, Germany) (Fig. 5.3) followed by

Elastography Point Quantification (ElastPQ)® (Philips Healthcare, The Netherlands) (Fig. 5.4). Many other manufacturers have created this technique in recent years (Hitachi Ltd, Japan; Esaote, Italy; Samsung Medison, South Korea) (Fig.5.5). Regardless of the type of system used, 10 measurements are required for an accurate assessment of liver stiffness, with the device automatically calculating the median and interquartile range (IQR), and the median/IQR ratio must be below 30% for the value to be considered interpretable (20, 96). The measured values are expressed either in m/s or in kPa, most systems being able to convert according to the operator's decision (4, 20, 96). The WFUMB guideline is more restrictive and states that if the result is expressed in m/s, the median/IQR ratio must be below 10% (4).

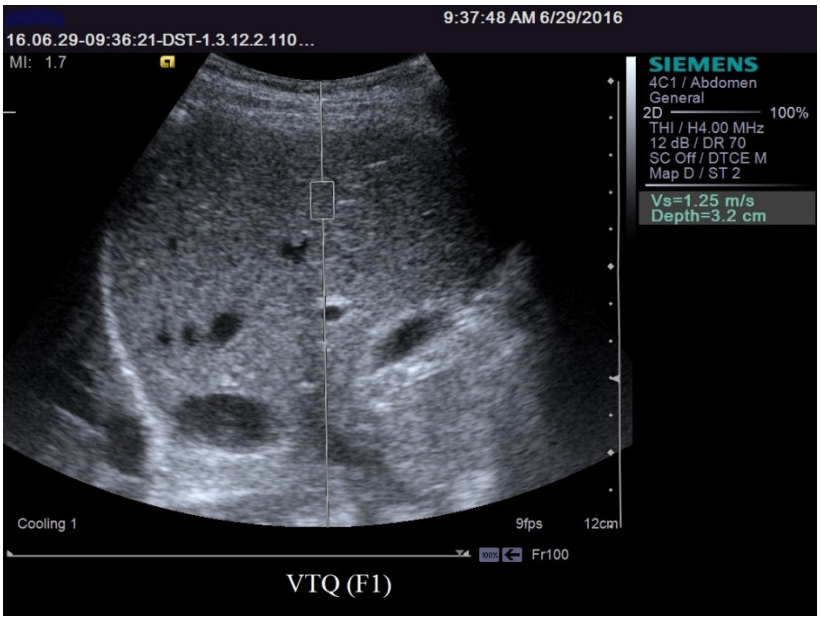

Fig. 5.3. Measurements of liver stiffness using VTQ in a subject with mild fibrosis. The region of interest is placed in the liver parenchyma 3.2 cm below the liver capsule, avoiding large vessels.

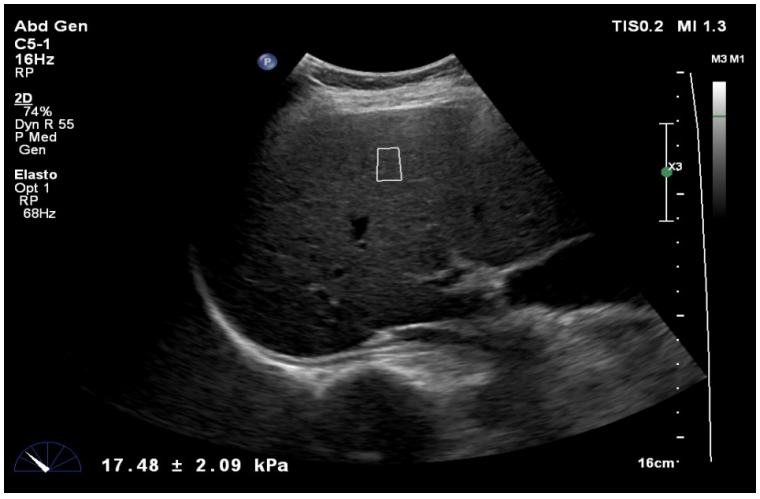

Fig. 5.4. Measurements of liver stiffness using ElastPQ in a patient with cirrhosis. The region of interest is placed 1-2 cm below the liver capsule, avoiding large vessels. The mean value and standard deviation are displayed on the screen.

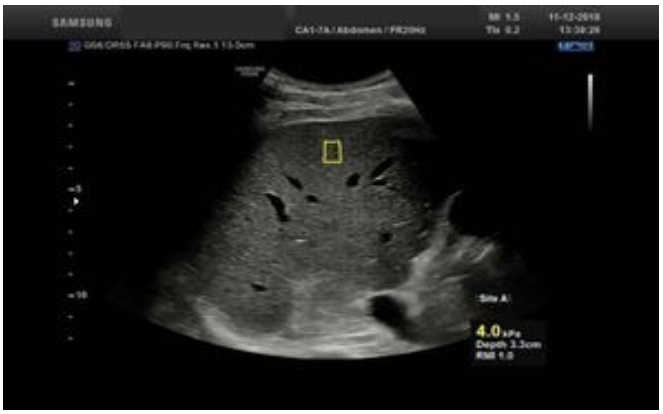

Fig. 5.5. Measurements of liver stiffness using pSWE elastography in a patient without fibrosis (Samsung Medison, South Korea). The region of interest is placed 3.3 cm below the liver capsule, avoiding large vessels. The median (kPa), depth of the region of interest, and RMI (Reliability Measurement Index) are displayed on the screen.

Regardless of the system used, current guidelines recommend the use of first line VCTE or pSWE or 2D-SWE elastography to assess the severity of liver stiffness in patients with chronic viral hepatitis. These elastographic methods have good accuracy in excluding cirrhosis in patients with chronic viral hepatitis C and in identifying patients with viral liver cirrhosis B (2, 4, 20, 96).

A. Evaluation by pSWE in Individuals with Normal Liver

Before starting the evaluation of LS in patients with chronic liver diseases, we need to know the values in healthy subjects. In the literature there are numerous studies that have determined the reference values of pSWE elastography in healthy subjects, especially using the VTQ technique. The mean values vary between 1.07 and 1.19 m/s, and are not influenced by age, sex and body mass index (97-101). On the other hand, the values are influenced by the place where the examination is performed, i.e. at the level of the left hepatic lobe, values are higher than at the level of the right hepatic lobe (98). Regarding ElastPQ, the values in healthy subjects are 1.08 ± 0.12 m/s (equivalent to 3.5 ± 0.04 kPa) (102-104), but one study found higher values in men than in women, significantly higher values at the end of exhalation compared to the end of inspiration, and the smallest variations in LS were obtained in segment V of the right hepatic lobe (103).

B. Evaluation by pSWE in Patients with Chronic Hepatitis C Virus

In the literature, there are a number of publications on the performance of VTQ elastography for the evaluation of fibrosis in patients with chronic HCV hepatitis, using liver biopsy as a reference method (Table 5.I).

Table 5.I Performance of VTQ in the evaluation of liver stiffness in patients with chronic hepatitis C virus (HCV)

Study	Number of patients (n)	F ≥ 2		F=4	
		Reference value (m/s)	AUROC	Reference value (m/s)	AUROC
Friedrich-Rust et al. (105)	n=64	1.35	0.86	1.75	0.95
Lupșor et al. (106)	n=112	1.34	0.851	2	0.945
Sporea et al. (107)	n=274	1.21	0.893	1.82	0.937
Sporea et al. (108)	n=914	1.33	0.792	1.55	0.842
Rizzo et al. (109)	n=139	1.3	0.86	2	0.89
Chen et al. (110)	n=127	1.55	0.847	1.98	0.831
Li et al. (111)	n=128	1.53	0.775	1.79	0.792
Joo et al. (112)	n=101	1.335	0.853	1.665	0.828
Ragazo et al. (113)	n=107	1.22	0.67	2.37	0.96
Hsu et al. (114)	n=63	1.225	0.786	1.710	0.937
Ueda et al. (115)	n=108	1.26	0.93	1.94	0.86

According to the EFSUMB guidelines, VTQ values of 1.21–1.34 m/s predict significant fibrosis (F ≥ 2) (AUROC 0.85–0.89), while values between 1.55 and 2 m/s (AUROC 0.89–0.93) predict cirrhosis (20). The same guideline recommends the use of pSWE mainly VTQ as a first-line assessment for predicting the severity of liver fibrosis in patients with chronic viral hepatitis HCV, this elastographic method having a very good accuracy in excluding the diagnosis of cirrhosis.

Data on the ElastPQ value for the assessment of liver fibrosis severity in chronic HCV hepatitis are limited. Few studies have evaluated cohorts of HCV patients using biopsy as a reference method. In a pilot study, the diagnostic performance (AUROC) for predicting significant fibrosis (F≥2) was 0.80 and for predicting cirrhosis 0.95 (102). Similar diagnostic performance, with AUROC 0.831 for F≥2 and 0.954 for advanced fibrosis (F=4) was obtained in a study published in 2017 using liver biopsy as a reference method (116). Other studies evaluated the diagnostic performance of ElastPQ using VCTE as a reference method. Diagnostic performance (AUROC) ranged from 0.92 to 0.96 for the diagnosis of significant fibrosis and from 0.83 to 0.95 for the diagnosis of cirrhosis (117, 118).

As in VCTE, LS values decrease in patients with sustained viral response (SVR) after antiviral treatment (119, 120). In a prospective study involving 336 patients, including 121 patients with SVR, the diagnostic performance was 0.818 for the diagnosis of significant fibrosis (≥F2) and 0.981 for the diagnosis of cirrhosis (F4), respectively, and the cut-off values were 1.26 m/s for ≥F2 and 1.49 m/s for F4 (120). In another study, this time involving 644 patients, of whom 80.9% were assessed by liver biopsy at the start of treatment and in 19.1% at 3 years after SVR was obtained, decreases in median LS were observed in the postSVR group, even though biopsy-assessed liver fibrosis did not change (119).

The predictive value of pSWE for complications of cirrhosis in patients with chronic HCV hepatitis, especially CSPH, will be discussed in a separate chapter.

C. Evaluation by pSWE in Patients with Chronic Hepatitis B Virus

Using liver biopsy as a reference method, published studies have shown a diagnostic accuracy of VTQ comparable to that of VCTE in chronic viral HBV liver diseases (121-123). The diagnostic accuracy (AUROC) in these studies ranged from 0.75 for the diagnosis of F≥2 to 0.764 for VTQ and from 0.81 to 0.83 for VCTE, and for the diagnosis of cirrhosis (F=4), AUROC values ranged from 0.825 to 0.97 for VTQ and from 0.799 to 0.93 for VCTE (122, 123).

Our group (124) evaluated the value of VTQ elastography compared to liver biopsy in 160 patients: 53 with chronic hepatitis B and 107 with chronic hepatitis C. The percentage of patients with indeterminable or invalid measurements was similar for VTQ and VCTE: 8.8% versus 10.9% (p=0.66). The mean LS values assessed by VTQ were similar for the same stage of histological fibrosis in patients with chronic hepatitis B and C. In patients with chronic hepatitis B, VTQ and VCTE elastography could not differentiate between patients without fibrosis (F0, Metavir) and mild fibrosis (F1, Metavir) respectively those with at least moderate fibrosis (F≥2, Metavir), but had a good value for differentiating between patients with or without severe fibrosis (F≥3, Metavir) and especially between non-cirrhotic patients and patients with cirrhosis (F=4, Metavir) (124).

Already published meta-analyses have confirmed the good predictive value of VTQ in various chronic liver diseases, with AUROC curves for F≥2 of 0.84-0.87 and for F4 of 0.91-0.93 (125, 126).

The usefulness of ElastPQ in the diagnosis of chronic HBV liver disease has been evaluated in a small number of studies compared to VTQ, but with good results. Published studies have demonstrated an excellent diagnostic performance of ElastPQ in the diagnosis of significant fibrosis (AUROC 0.94-0.95) and a very good one in the diagnosis of cirrhosis (AUROC 0.88-0.89) (127, 128).

In this context, the EFSUMB guidelines state that pSWE-type elastography, as demonstrated with VTQ, is useful in patients with chronic HBV hepatitis to identify those with cirrhosis (20).

D. Evaluation by pSWE in Patients with Hepatic Steatosis Associated with Metabolic Dysfunction (MASLD)

In 2023, a new nomenclature was adopted that replaced the terminology of NAFLD (non-alcoholic fatty liver disease) in MASLD (hepatic steatosis associated with metabolic dysfunction (129). Yoneda et al. (130) evaluated 54 patients with MASLD by liver biopsy, VCTE and VTQ. In this study, the best cut-off value for the diagnosis of severe fibrosis (F≥3) was 1.77 m/s (AUROC=0.973, with 100% Se, 91% Sp) and 1.9 m/s (AUROC=0.976, with 100% Se, 96% Sp) for the diagnosis of cirrhosis (F4). Two other studies that evaluated the diagnostic performance of VTQ using liver biopsy as a reference method showed that the diagnostic accuracy of VTQ expressed by ROC curves for F≥3 ranges from 0.71 to 0.944 and for F4 from 0.74 to 0.984 (131, 132).

According to a meta-analysis published in 2015 involving 723 patients, the accuracy of VTQ in the diagnosis of F≥2 is only moderate (AUROC – 0.898, Se – 80.2%, Sp – 85.2%) (133). Another meta-analysis published in 2018, including 982 patients with MASLD evaluated by biopsy and pSWE, showed AUROC curves of 0.86, 0.94, and 0.95, respectively, for the diagnosis of F≥2, F≥3, and F4 respectively (134).

A recent meta-analysis (70) evaluating the diagnostic accuracy of several types of elastographic methods, including pSWE, concluded that the diagnostic performance of pSWE in advanced fibrosis and cirrhosis expressed by AUROC curves is good (0.89 and 0.90 respectively).

Regarding the diagnostic performance of ElastPQ in MASLD, the evidence is limited. A European multicentre study showed that the values obtained by ElastPQ correlate with those obtained by VCTE (135). ElastPQ can reliably exclude fibrosis at a cut-off value <6.0 kPa (<1.41 m/s, AUROC 0.940) and indicate a high risk of advanced fibrosis at a cut-off value ≥10.4 kPa (≥1.86 m/s, AUROC: 0.949) (135). Another study evaluating the diagnostic performance of ElastPQ showed an excellent correlation with VCTE (Spearman r = 0.80, p<0.001), which was better for mild/moderate stages of fibrosis (136). In the subgroup of patients with histology available, ElastPQ showed diagnostic accuracy similar to VCTE in staging liver fibrosis (AUROC values of 0.84, 0.83, 0.86 and 0.95, for F ≥ 1, F ≥ 2, F ≥ 3 respectively F = 4) (136).

In view of all these data, the EFSUMB guidelines conclude that pSWE represented in particular by VTQ can be used to exclude cirrhosis in patients with MASLD (20).

E. Evaluation by pSWE in Patients with Alcohol-related Liver Disease (ALD)

Chronic alcohol abuse is a major public health problem worldwide. Alcoholic liver disease (ALD) is one of the most common complications and a leading cause of alcohol-related death, due to cirrhosis of the liver and its complications. Three histological lesions characterize ALD: steatosis, steatohepatitis and fibrosis. There are different stages of fibrosis, the most

severe of which is cirrhosis. In ALD it is important to know the stage of fibrosis to guide management decisions and estimate the prognosis.

In a study involving 112 subjects with ALD assessed by VTQ and liver biopsy (137), VTQ was significantly correlated with histologically quantified fibrosis ($r = 0.685$, $P < 0.001$). The diagnostic accuracy expressed using the AUROC curves was 0.846 for F≥2, 0.875 F≥3, and 0.893 for F=4. The optimal cut-off values were 1.33 m/s for F≥2, 1.40 m/s for F≥3, and 1.65 m/s for F=4 in patients with high ALT values. In patients with normal ALT values, the cut-off values were 1.24 m/s for F≥2, 1.27 m/s for F≥3, and 1.41 m/s for F = 4 (137).

Another study evaluated the diagnostic performance of VTQ in 83 patients with ALD. The cut-off values of the calculated VTQ were 1.63 m/s (AUROC 0.87) for F≥2; 1.84 m/s (AUROC 0.86) for F≥3; and 1.94 m/s (AUROC 0.89) for F=4 (138).

The predictive value of pSWE for complications of cirrhosis in patients with ALD, especially CSPH, will be discussed in a separate chapter.

F. Evaluation by pSWE in Patients with Cholestatic Liver Diseases (Primary Biliary Cholangitis – PBC and Primary Sclerosing Cholangitis – PSC)

The pSWE value in cholestatic liver disease requires further study due to the small number of patients enrolled in existing studies (139). Thus, in a study with 126 subjects with PBC, the diagnostic performance of VTQ was good for the Child-Pugh A class (AUROC – 0.852) and excellent for the Chid Pugh C class (AUROC – 0.936) (139).

In a study involving 152 subjects with PSC, the LS values obtained by ElastPQ highly correlated with the values obtained by VCTE ($p < 0.001$, Spearman 0.93; Lin 0.86) (140). Also, ElastPQ had a good diagnostic performance for fibrosis staging (AUROC 0.96, 0.97, 0.97 and 0.99 for F≥1, F≥2, F≥3 respectively, F=4). The best cut-off value to suggest compensated advanced chronic liver disease (cACLD) was 11.3 kPa, and to exclude cACLD, the cut-off value was ≤ 8kPa (140).

G. Evaluation by pSWE in Patients with Autoimmune Hepatitis

Studies on the diagnostic utility of pSWE in autoimmune hepatitis are limited. In a study involving 49 subjects with autoimmune hepatitis, ElastPQ showed moderate diagnostic accuracy to detect significant fibrosis (cut-off 4.47 kPa, AUROC 0.70), and cirrhosis (cut-off 9.28 kPa, AUROC 0.75) (141).

H. New Concepts in pSWE

Cut-off values differ for fibrosis staging between ultrasound systems produced by different providers, however, the Society of American Radiologists has attempted a unification of these values, suggesting the "rule of four" (5, 9, 13, 17 kPa) for ARFI techniques, valid in

chronic liver diseases of viral etiology and MASLD (21). This provider-neutral rule actually mirrors the 'rule of 5' used for the staging of liver fibrosis by VCTE, proposed at the Baveno VI consensus conference (142, 143). Thus, LS of 5 kPa (1.3 m/sec) or less has a high probability of being normal, LS less than 9 kPa (1.7 m/sec), in the absence of other known clinical signs, excludes compensated advanced liver disease (cACLD), and values between 9 kPa (1.7 m/sec) and 13 kPa (2.1 m/sec) suggest cACLD, but additional tests are required for confirmation. Values higher than 13 kPa (2.1 m/sec) are highly suggestive of cACLD, and LS higher than 17 kPa (2.4 m/sec) is suggestive of CSPH (21).

In conclusion, pSWE is an easy-to-perform elastographic technique, integrated into a common ultrasound machine, with performance similar to VCTE to predict the severity of fibrosis in patients with liver diseases of various etiologies, the performance increasing with the severity of fibrosis.

5.1.b.3. Evaluation of Fibrosis by 2D-SWE

2D-SWE elastography is the latest non-invasive technique developed for the evaluation of LS considered as a marker of fibrosis, the ARFI (Acoustic Radiation Force Impulse) technique being used in this situation to interrogate the tissue at several points (5, 144). The technique displays a qualitative color-coded elasticity map (elastogram), usually superimposed on the conventional B-mode ultrasound image, and it additionally allows for quantitative measurement by placing a smaller region of interest (ROI) inside the color map. The result of a measurement is usually displayed as the mean and standard deviation, either in m/s or kPa. This technique is available on several ultrasound systems including: Aixplorer (Supersonic Imagine – Hologic), General Electric Healthcare, Canon, Philips, Siemens, Samsung, Mindray and others (Fig.5.6, Fig.5.7). Although the systems are different, the principle of the technique is similar, and the results obtained are comparative, as will be seen from the data presented, having the additional advantage of the possibility of combined use with other ultrasound applications, in a multiparametric evaluation of patients with liver diseases.

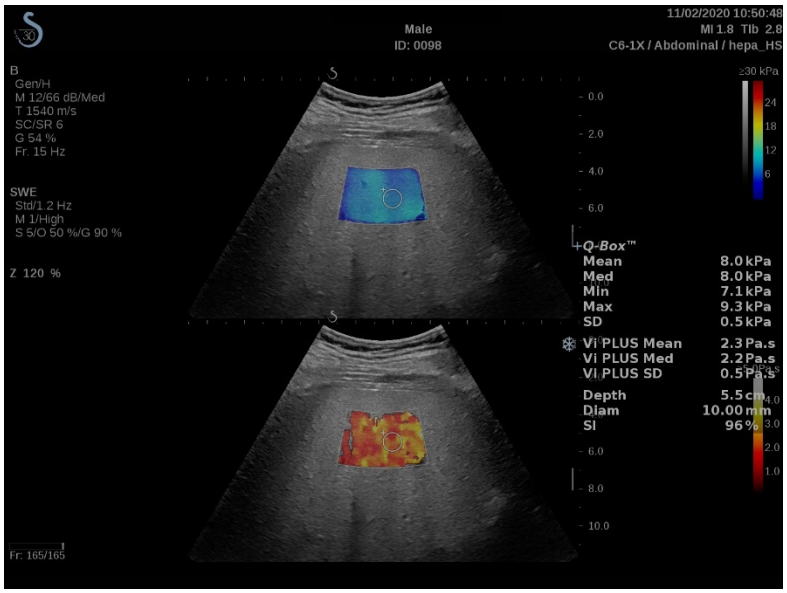

Fig. 5.6. Evaluation of liver fibrosis using 2D-SWE.SSI elastography (Aixplorer®, Supersonic Imagine/Hologic), upper image. In the lower image, the assessment of viscosity (Vi.Plus) as a marker of inflammation.

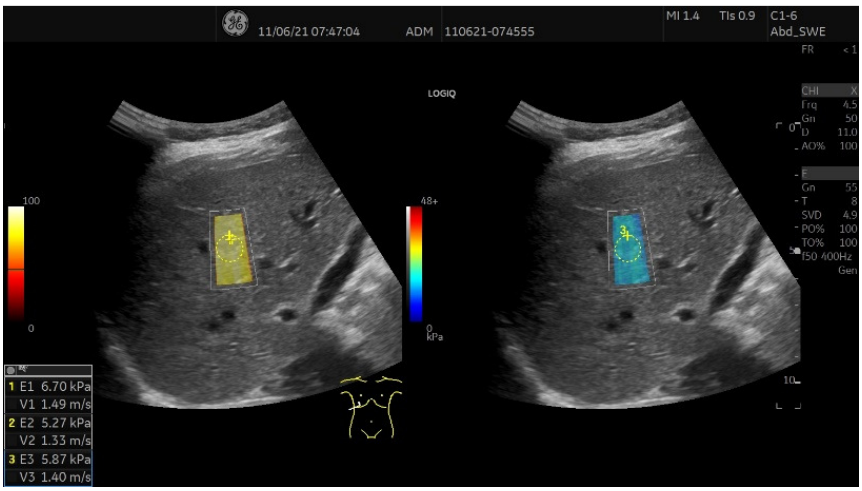

Fig. 5.7. Evaluation of liver fibrosis using 2D-SWE.GE elastography, the right image. In the left image, the reliability map.

A. 2D-SWE Assessment in Individuals with Normal Liver

The first ultrasound system to implement a 2D-SWE technique was Aixplorer™ (Supersonic Image – Hologic). The mean liver stiffness (LS) value in healthy volunteers using this system ranged from 2.6 kPa to 6.2 kPa in one study (145), being 6 ± 1.4 kPa (median 5.7 kPa) in another publication (146), the latter showing higher values in males than females (6.6 ± 1.5 kPa vs. 5.7 ± 1.3 kPa, p=0.01). These values are also close to those obtained by our group using another 2D-SWE (General Electric) technique, where the average LS values obtained by 2D-SWE.GE were 5.1 ± 1.3 kPa, significantly higher than those obtained by VCTE (4.3 ± 0.9 kPa, $p < 0.0001$) and again significantly higher in males than females, 5.9 ± 1.2 kPa compared to 4.7 ± 1.2 kPa ($p = 0.0005$) (147).

B. Evaluation by 2D-SWE in Patients with C Virus Chronic Hepatitis

The first studies to evaluate liver fibrosis using 2D-SWE techniques included patients with chronic HCV liver disease, and also used the technique incorporated in Aixplorer™, showing very good results compared to liver biopsy or VCTE.

Thus, in one of the first studies, Bavu et al. (148) included 133 patients with chronic HCV infection and compared the accuracy of 2D-SWE with VCTE and liver biopsy. The study showed a good correlation between the histological stage of fibrosis and the evaluation of LS using 2D-SWE and VCTE ($p<0.0001$), the AUROC values for the different stages of fibrosis for 2D-SWE being higher compared to those for VCTE: 0.948 for F≥2, 0.962 for F≥3 and 0.968 for F=4, vs. AUROC for VCTE for F≥2, F≥3, F4: 0.846, 0.857 and 0.940 respectively. Data published later in another study, using the same technique, proved that 2D-SWE is a good and reliable method for the evaluation of LS in patients with chronic HCV hepatitis, the best cut-off values for different stages of fibrosis being: F≥2: 7.1 kPa (AUROC=0.92), F≥3: 8.7 kPa (AUROC=0.98) and F4: 10.4 kPa (AUROC=0.98) (149).

More recent studies have followed the evaluation of patients with chronic HCV hepatitis using other 2D-SWE techniques, showing similar results. Thus, a study of our team (150) compared two methods of 2D-SWE, 2D-SWE.SSI (Aixplorer™) and 2D-SWE.GE (General Electric), using VCTE as a reference method. The study group included 208 consecutive patients with chronic HCV infection, in whom LS was evaluated in the same session using the two 2D-SWE techniques. LS values obtained with 2D-SWE.GE correlated better with VCTE than 2D-SWE.SSI ($r=0.75$, $p<0.0001$ vs. $r=0.57$, $p<0.0001$, z-test $p=0.0012$), but no significant differences between AUROC values for 2D-SWE.GE and 2D-SWE.SSI in the identification of fibrosis F≥2 (0.97 vs. 0.96, $p = 0.5650$), F≥3 (0.97 vs. 0.95, $p = 0.2935$) or F = 4 (0.97 vs. 0.96, $p = 0.6914$) were found.

2D-SWE.GE technique (LOGIQ E9 GE Medical Systems, Wisconsin, USA) was also used in a study involving 103 patients with chronic HBV and HCV liver diseases, the reference method being liver biopsy (151). The authors demonstrated a statistically significant positive correlation between LS values and the degree of liver fibrosis for both etiologies (Spearman correlation coefficient = 0.76 and 0.83 for HBV and HCV, respectively) ($p = 0.0001$), and the cut-off values of LS were also comparable for the two etiologies: F≥1: 5.92 kPa, F≥2: 7.69 kPa, F≥3: 8.97 kPa, F=4: 12.15 kPa in HBV; and F≥1: 6.09 kPa, F≥2: 7.81 kPa, F≥3: 9.0 kPa, F= 4: 12.47 kPa in HCV patients.

A newer 2D-SWE technique was also used by Villani et al. (152) in a study enrolling 178 patients with chronic HCV hepatitis. The 2D-SWE technique existing in the EPIQ 7 US system (Philips Healthcare, The Netherlands) - ElastQ - was evaluated using VCTE as a reference standard, the cut-off values obtained for the diagnosis of fibrosis ≥F2, ≥F3 and F4 being 8.15 (AUROC=0.899), 10.31 (AUROC=0.900) and 12.65 kPa (AUROC=0.899) (152), respectively.

C. Evaluation by 2D-SWE in Patients with B Virus Chronic Hepatitis

In case of chronic HBV viral liver diseases, the initial data were also obtained with the 2D-SWE technique incorporated by Supersonic Imagine in Aixplorer. Data from the initial studies of LS assessment using 2D-SWE in patients with chronic HBV hepatitis showed cut-off values and accuracy almost similar to those in HCV patients: F≥1: 6.5 kPa (AUROC=0.86), F≥2: 7.1 kPa (AUROC=0.88), F≥3: 7.9 kPa (AUROC=0.93), and F4: 10.1 kPa (AUROC=0.98) (153).

In another study (154) that enrolled 303 patients with chronic HBV hepatitis, in which the first 202 patients were the initial cohort and the next 101 patients the validation cohort, the AUROC curves for significant fibrosis, severe fibrosis, and cirrhosis were all greater than 0.90. Using the cut-off values generated from the index cohort, in the validation cohort 2D-SWE had a negative predictive value (NPV) of 82.6% for significant fibrosis, 95.1% for severe fibrosis, and 97.4% for cirrhosis. The positive predictive values (PPVs) were 83.6%, 65.0% and 60.0% for F≥2, F≥3 and F4, respectively, demonstrating that the method has the highest accuracy in excluding the diagnosis of cirrhosis (154).

A more recent study evaluated 602 patients with chronic HBV liver diseases using the 2D-SWE ElastQ technique and liver biopsy as a reference method. The LS values obtained by 2D-SWE showed a strong correlation with the fibrosis stage (r=0.71, P<0.001), the optimal cut-off values for different degrees of fibrosis being: F≥1 5.72 kPa (Se 78%, Sp 70%), F≥3 6.85 kPa (Se 77%, Sp 86%), F≥3 7.43 kPa (Se 80%, Sp 86%), F4 8.03 kPa (Se 81%, Sp 73%) respectively.

D. Evaluation by 2D-SWE in Patients With Metabolic Dysfunction-Associated Steatotic Liver Disease (MASLD)

One of the first studies comparing 2D-SWE, VCTE, and pSWE (VTQ) with liver biopsy in 291 patients with MASLD (155), showed similar good accuracy for all three techniques, slightly better for 2D-SWE: AUROC for 2D-SWE, VCTE, and VTQ were 0.86, 0.82, and 0.77 for diagnosing ≥F2; 0.89, 0.86, and 0.84 for ≥F3; and 0.88, 0.87 and 0.84 for F4 respectively. The cut-off values for 2D-SWE and VCTE for predicting different stages of fibrosis with a Se ≥90% were very close: 6.3/6.2 kPa for ≥F2, 8.3/8.2 kPa for ≥F3 and 10.5/9.5 kPa for F4 (155).

In a study conducted by our group (156), which included 204 consecutive adult patients with MASLD, liver fibrosis was evaluated by the 2D-SWE technique incorporated into the Aixplorer™ MACH 30 System: ShearWave Elastography (2D-SWE.PLUS), using VCTE as a reference method. The study showed a strong correlation between the LS values obtained with 2D-SWE.PLUS and VCTE (r = 0.89), with the best cut-off value for 2D-SWE.PLUS for the presence of significant fibrosis (F≥2) of 7 kPa (156).

Similar results have been demonstrated with other equipment incorporating 2D-SWE techniques. Thus, in a study involving 232 patients (164 in the MASLD group and 68 in the healthy control group) assessed by 2D-SWE (Canon) and VCTE, respectively, the authors demonstrated a significant correlation between 2D-SWE and VTCE (r=0.71, p < 0.0001) (157).

The MASLD-specific cut-off values of LS for 2D-SWE were: for F≥2: 7.9 kPa (AUROC=0.91); F≥3: 10 kPa (AUROC = 0.92); and F=4: 11.4 kPa (AUROC = 0.95).

In a more recent study (158) involving 104 patients with MASLD assessed by VCTE and 2D-SWE, with liver biopsy as the reference method, the correlation between the histological grade of liver fibrosis and LS values was significantly stronger for 2D-SWE compared to VCTE (Spearman correlation coefficient of 0.71 vs. 0.51, z=2.21, p=0.027). Inflammatory activity was an independent predictor of LS by VCTE, but not by 2D-SWE.

Similar to all elastographic techniques, 2D-SWE has better accuracy for diagnosing severe stages of fibrosis. In a study involving 552 patients with MASLD who had their LS assessed by 2D-SWE and VCTE in the same session (159), the median LS was 5.5 (2.8-75) kPa for VCTE and 6.2 (3.7-46.2) kPa for 2D-SWE. LS by VCTE and 2D-SWE were correlated regardless of the presence of obesity ($r= 0.774$; $p < 0.001$; $r= 0.774$; $p < 0.001$; $r= 0.75$; $p < 0.001$ at BMI <25, 25-30 and ≥30 kg/^{m2} respectively), or by the degree of hepatic steatosis ($r = 0.63$; $p < 0.001$ and $r = 0.743$; $p < 0.001$ in mild steatosis, and moderate/severe, respectively). The correlation between the two methods was strong in patients with at least severe fibrosis ($r=0.84$; $p < 0.001$) or cirrhosis ($r=0.658$; $p < 0.001$), with excellent 2D-SWE accuracy of 98.8 and 99.8% in diagnosing severe fibrosis and liver cirrhosis using VCTE as a reference method (159).

One of the questions related to elastographic techniques regards their feasibility. From this point of view, patients with MASLD are difficult patients, frequently obese, and for 2D-SWE techniques, the role of experience in increasing the feasibility and accuracy of measurements has been demonstrated (160). However, in a study involving 90 morbidly obese patients proposed for bariatric surgery, for whom LS was assessed by 2D-SWE 14 days prior to a liver biopsy performed during bariatric surgery, the feasibility of the technique was 97.3% (161). In the univariate analysis, 2D-SWE values were correlated with BMI, waist circumference, NAFLD activity score (NAS), and steatosis, while these components did not affect LS in the multivariate analysis.

Another advantage offered by 2D-SWE techniques comes from the fact that they are incorporated into ultrasound machines, which allow for a complex multiparametric evaluation, especially for patients with fatty liver, but not only. The emergence of liver fat load assessment software, and their incorporation together with elastographic techniques in top ultrasound equipments and then also in mid-range ultrasound machines, makes a complex evaluation of patients with MASLD very easy. In a prospective study involving 120 patients evaluated by liver biopsy for suspected MASLD, the diagnostic performance of the measurements of dispersion slope [(m/sec)/kHz], attenuation coefficient [dB/cm/MHz] and shear wave velocity (in m/s) was evaluated using 2D-SWE elastography for the assessment of inflammation, steatosis and fibrosis in the non-invasive diagnosis of MASLD (162). The dispersion slope allowed for the identification of lobular inflammation, with an AUROC of 0.95 for a degree of inflammation ≥A1 (mild), 0.81 for a degree of inflammation ≥A2 (moderate) and 0.85 for a degree of inflammation A3 (severe). The attenuation coefficient allowed for the

identification of steatosis, with an AUROC of 0.88 for the grade of steatosis ≥S1 (mild), 0.86 for the grade of steatosis ≥S2 (moderate) and 0.79 for the grade of steatosis equal to S3 (severe). 2D-SWE allowed the identification of fibrosis, with an AUROC of 0.79 for the fibrosis stage ≥F1 (portal fibrosis), 0.88 for stage ≥F2 fibrosis (periportal fibrosis), 0.90 for the fibrosis stage ≥F3 (septal fibrosis) and 0.95 for the F4 fibrosis stage (cirrhosis). The combination of the 3 parameters showed an AUROC of 0.81 for the diagnosis of MASH.

The performance of elastographic techniques for staging liver fibrosis in MASLD/NAFLD was evaluated in a recent meta-analysis that included 53 studies with VCTE (11,701 patients), 12 studies with pSWE (1,312 patients) and only 4 studies with 2D-SWE (502 patients), the reference method being liver biopsy (70). The Summary Area Under the Curve (sAUC) for 2D-SWE was similar to that of the other elastographic techniques: sAUC for the diagnosis of significant fibrosis - 0.75, for advanced fibrosis 0.72, and for cirrhosis 0.88.

E. 2D-SWE Assessment in Patients with Alcohol-related Liver Disease (ALD)

Although the ethanolic etiology for chronic liver diseases is one of the most common in clinical practice, dedicated studies for the non-invasive evaluation of liver fibrosis in these patients are relatively limited for all types of elastography techniques, and especially for 2D-SWE techniques. Data on the performance of this technique for the evaluation of ALD patients from studies published on a cohort of 289 patients, with a 23% prevalence of advanced fibrosis (82, 84), showed AUROC values of 0.88, 0.97 and 0.97 for the diagnosis of significant fibrosis (≥F2), advanced fibrosis (≥F3) and liver cirrhosis, with a much higher cut-off value for advanced fibrosis than for other etiologies: 16.4 kPa (Se - 90% and Sp - 96%).

In another recent study involving 462 patients with cACLD of ethanolic etiology, followed for an average period of 49 months, the prognostic accuracy for events related to liver pathology was evaluated for several non-invasive methods of evaluation, using liver biopsy as an initial reference (163). The prognostic accuracy for 2D-SWE was comparable to that of VCTE, with a C-statistics coefficient of 0.87 (vs. 0.876 for VCTE) for predicting liver-related events over 4.1 years of follow-up. The event rate was 5% for 2D-SWE values <10 kPa, 15% for 10.0-16.4 kPa, and 64% for >16.4 kPa. Episodes of binge drinking during follow-up increased the risk of hepatic pathology-related events, except for patients in low-risk groups (163).

F. Evaluation by 2D-SWE in Patients with Cholestatic Hepatopathies (Primary Biliary Cholangitis – PBC and Primary Sclerosing Cholangitis – PSC)

The existing data in the literature regarding the role of elastographic techniques in cholestatic pathologies are not very numerous, and those related to 2D-SWE are even fewer. However, data collected retrospectively for 157 patients with ***PBC*** showed a good performance of the technique for the evaluation of liver fibrosis in this etiology as well. The AUROC values for LS measured by 2D-SWE for significant fibrosis, severe fibrosis, and cirrhosis

were 0.88, 0.97, and 0.99, respectively. The cut-off values for 2D-SWE for the discrimination of significant fibrosis, severe fibrosis and liver cirrhosis were 10.7 kPa, 12.2 kPa and 14.1 kPa, respectively, with the diagnostic accuracy of 2D-SWE for staging liver fibrosis of 73.9% (164).

And in the case of ***PSC,*** a study that included 66 patients assessed using VCTE, pSWE, and 2D-SWE, showed a moderate correlation for 2D-SWE with pSWE and VCTE, with a tendency to underestimate LS for 2D-SWE (165).

G. Evaluation by 2D-SWE in Patients with Autoimmune Hepatitis

The presence of significant cytolysis in active forms of autoimmune hepatitis is a disadvantage for elastographic techniques, which are influenced by high transaminase values. For this etiology, the existing data in the literature are relatively limited. In a study involving 63 patients with autoimmune hepatitis in whom liver biopsy was the reference method, the cut-off values for LS for the detection of liver cirrhosis by 2D-SWE were 16.1 kPa (AUROC 0.93) (166).

H. 2D-SWE Assessment in Mixed Cohorts

In a Romanian study that included patients with chronic liver diseases with various etiologies evaluated with 2D-SWE Aixplorer™, and which used VCTE as a reference method, the cut-off values for predicting different degrees of fibrosis were similar to the data published by other authors: F≥1: 7.1 kPa (AUROC=0.825), F≥2: 7.8 kPa (AUROC= 0.859), F≥3: 8 kPa (AUROC=0.897) and for F=4: 11.5 kPa (AUROC=0.914) (167). Similar results were obtained by our group on a subsequent cohort of 133 patients with chronic liver diseases, evaluated by 2D-SWE PLUS (Aixplorer™ Mach 30 Supersonic Imagine, Aix-en-Provence, France), VCTE being the reference method, the calculated correlation between LS measurements by 2D-SWE. PLUS and VCTE being excellent ($r=0.92$, $p < 0.0001$), and the cut-off values comparable to the previous ones: F≥2 6.8 kPa; F≥3, 8.4 kPa; and for F4, 11 kPa (168).

The very good accuracy of 2D-SWE was also demonstrated in a study comparing 2D-SWE, VCTE and VTQ in 349 consecutive patients with chronic liver diseases of different etiologies, using liver biopsy as a reference method (169). Thus, 2D-SWE performed better than VCTE and VTQ: AUROC values for 2D-SWE, VCTE, and VTQ were 0.89, 0.86, and 0.84 for the diagnosis of mild fibrosis; 0.88, 0.84 and 0.81 for the diagnosis of significant fibrosis; 0.93, 0.87 and 0.89, for the diagnosis of severe fibrosis; 0.93, 0.90 and 0.90 for the diagnosis of liver cirrhosis, respectively (169).

Studies using other types of 2D-SWE techniques have shown the same good accuracy for assessing liver fibrosis, especially in advanced fibrosis. Thus, a study that included 54 healthy subjects and 174 patients with chronic liver diseases, evaluated using 2D-SWE.GE (LOGIQ E9; GE Healthcare), the reference method being liver biopsy, showed a strong positive correlation of LS with the fibrosis stage ($rho = 0.628$; $p > 0.001$). AUROC values were 0.724 for

mild fibrosis (F≥1), 0.857 for moderate fibrosis (F≥2), 0.946 for severe fibrosis (F≥3) and 0.935 for cirrhosis (F4) (170).

Similar results were obtained by our team on a group of 179 patients with or without chronic liver diseases, in whom LS was evaluated in the same session by VCTE (FibroScan, EchoSens) and 2D-SWE.GE (LOGIQ S8; GE Healthcare), with a good correlation between the LS values obtained by the two methods ($r = 0.72$, $P < 0.0001$). The cut-off values for 2D-SWE.GE were as follows: for F≥2 - 6.9 kPa (AUROC 0.93; Se 85.8%; Sp 90.2%), for F≥3 - 8.2 kPa (AUROC, 0.93; 87.5%; Sp 86.8%) and for F4 9.3 kPa (AUROC, 0.91; Se 85.7%; Sp 81.2%) (171).

Another study (172) involving 640 patients with chronic liver disease assessed by 2D-SWE (Canon) and VCTE as a reference method showed a significantly strong correlation between the two techniques ($r = 0.932$, $p < 0.001$). The good accuracy of the technique (2D-SWE Canon Aplio i800) was proved also by another study using liver biopsy as a reference method. The cut-off values obtained for significant, severe fibrosis and liver cirrhosis were 6.5 (AUROC 85.2%), 9.8 (AUROC 86.8%) and 13.1 kPa (AUROC 95.6%) (173).

In the same session, our group evaluated a 115 patients mixed cohort, by VCTE (FibroScan, EchoSens) (reference method), and pSWE and 2D-SWE (Samsung-Medison RS85). The cut-off values obtained for 2D-SWE were quite close: F≥2 LS >6.1 kPa (AUROC=0.93), F4 LS>7.6 kPa (AUROC=0.98), with a strong correlation between the LS values obtained by VCTE and 2D-SWE (r=0.85) (174).

The status of 2D-SWE as a feasible and very accurate technique was reinforced by the results of meta-analyses that included studies in the literature using this type of techniques. Thus, in one of the first meta-analyses, based on individual data from a mixed cohort (175), which included 1,340 patients and compared 2D-SWE with liver biopsy, the overall performance of 2D-SWE was good to excellent in HCV, HBV and MASLD patients with AUROC values of 86.3%, 91.6%, 85.9% for the diagnosis of significant fibrosis and 96.1%, 97.1% and 95.5% for diagnosing liver cirrhosis, respectively. The cut-off value for predicting significant fibrosis in all patients was 7.1 kPa, while for the diagnosis of liver cirrhosis it was 13.5 kPa in HCV and MASLD patients and 11.5 kPa in HBV patients (175).

Another meta-analysis, published relatively quickly after the introduction of the techniques on the market (176), assessed the accuracy of 2D-SWE for the diagnosis of different stages of fibrosis. The included studies reported Se, SP, PPV and NPV of 2D-SWE for the diagnosis of liver fibrosis. The meta-analysis included 13 articles, 2303 patients, and the Se and Sp 2D-SWE obtained for the diagnosis of different stages of liver fibrosis were as follows: ≥F1 0.76 ($p<0.001$), 0.92 ($p<0.001$); ≥F2 0.84 ($p = 0.35$), 0.83 ($p<0.001$); ≥F3 0.89 ($p = 0.56$), 0.86 ($p<0.001$); F4 0.89 ($p = 0.24$), 0.88 ($p<0.001$), respectively.

Moreover, regardless of the type of cohort studied, similar to the other elastographic techniques, 2D-SWE has a better accuracy the higher the degree of fibrosis is, which makes it a feasible technique for both the diagnosis and exclusion of liver cirrhosis (4, 20).

I. New Concepts in 2D-SWE

As with VCTE and pSWE, the initial studies focused on differentiating individual stages of fibrosis. The more modern concept is to diagnose severe fibrosis/cirrhosis, as this is the one with the greatest prognostic impact. As we mentioned in relation to pSWE, the cut-off values also differ in the case of 2D-SWE depending on the system and technology used. The American Society of Radiologists has attempted a unification of these values, suggesting the "rule of four" (5, 9, 13, 17 kPa) for ARFI techniques, valid in chronic liver diseases of viral etiology and MASLD (21). This provider-neutral rule actually mirrors the 'rule of 5' used for the staging of liver fibrosis by VCTE, proposed at the Baveno VI consensus conference (142, 143). Thus, LS of 5 kPa (1.3 m/sec) or less has a high probability of being normal, LS less than 9 kPa (1.7 m/sec), in the absence of other known clinical signs, excludes compensated advanced liver disease (cACLD), and values between 9 kPa (1.7 m/sec) and 13 kPa (2.1 m/sec) suggest cACLD, but additional tests are required for confirmation. Values higher than 13 kPa (2.1 m/sec) are highly suggestive of cACLD, and LS higher than 17 kPa (2.4 m/sec) is suggestive of CSPH (21).

In conclusion, elastographic techniques, whether we are talking about VCTE, pSWE or 2D-SWE, are a particularly useful tool in assessing the severity of liver fibrosis, and their first-line use in the evaluation of patients with chronic liver diseases is recommended. The performance is very good for the diagnosis of advanced stages of fibrosis, but also for the prediction of their complications, as will be seen below. In addition, if pSWE and 2D-SWE were previously available only on top-of-the-line systems, they are now also available in mid-range systems, which are much cheaper and available.

References

1. Sandrin L, Fourquet B, Hasquenoph JM, Yon S, Fournier C, Mal F, et al. Transient elastography: a new noninvasive method for assessment of hepatic fibrosis. Ultrasound Med Biol. 2003; 29(12):1705-13.
2. European Association for Study of L. Asociación Latinoamericana para el Estudio del H. EASL-ALEH Clinical Practice Guidelines: Non-invasive tests for evaluation of liver disease severity and prognosis. J Hepatol. 2015; 63(1):237-64.
3. European Association for the Study of the Liver. Electronic address eee, Clinical Practice Guideline P, Chair, representative EGB, Panel m. EASL Clinical Practice Guidelines on non-invasive tests for evaluation of liver disease severity and prognosis - 2021 update. J Hepatol. 2021; 75(3):659-89.
4. Ferraioli G, Filice C, Castera L, Choi BI, Sporea I, Wilson SR, et al. WFUMB guidelines and recommendations for clinical use of ultrasound elastography: Part 3: liver. Ultrasound Med Biol. 2015; 41(5):1161-79.
5. Ferraioli G, Wong VW, Castera L, Berzigotti A, Sporea I, Dietrich CF, et al. Liver Ultrasound Elastography: An Update to the World Federation for Ultrasound in Medicine and Biology Guidelines and Recommendations. Ultrasound Med Biol. 2018; 44(12):2419-40.

6. Shiina T, Nightingale KR, Palmeri ML, Hall TJ, Bamber JC, Barr RG, et al. WFUMB guidelines and recommendations for clinical use of ultrasound elastography: Part 1: basic principles and terminology. Ultrasound Med Biol. 2015; 41(5):1126-47.
7. Cosgrove D, Piscaglia F, Bamber J, Bojunga J, Correas JM, Gilja OH, et al. EFSUMB guidelines and recommendations on the clinical use of ultrasound elastography. Part 2: Clinical applications. Ultraschall Med. 2013; 34(3):238-53.
8. Roulot D, Czernichow S, Le Clesiau H, Costes JL, Vergnaud AC, Beaugrand M. Liver stiffness values in apparently healthy subjects: influence of gender and metabolic syndrome. J Hepatol. 2008; 48(4):606-13.
9. Kumar M, Sharma P, Garg H, Kumar R, Bhatia V, Sarin SK. Transient elastographic evaluation in adult subjects without overt liver disease: influence of alanine aminotransferase levels. J Gastroenterol Hepatol. 2011; 26(8):1318-25.
10. Colombo S, Belloli L, Zaccanelli M, Badia E, Jamoletti C, Buonocore M, Del Poggio P. Normal liver stiffness and its determinants in healthy blood donors. Dig Liver Dis. 2011; 43(3):231-6.
11. Wong GL, Chan HL, Choi PC, Chan AW, Lo AO, Chim AM, Wong VW. Association between anthropometric parameters and measurements of liver stiffness by transient elastography. Clin Gastroenterol Hepatol. 2013; 11(3):295-302 e1-3.
12. Sirli R, Sporea I, Tudora A, Deleanu A, Popescu A. Transient elastographic evaluation of subjects without known hepatic pathology: does age change the liver stiffness? J Gastrogut Liver Dis. 2009; 18(1):57-60.
13. Poynard T, Mathurin P, Lai CL, Guyader D, Poupon R, Tainturier MH, et al. A comparison of fibrosis progression in chronic liver diseases. J Hepatol. 2003; 38(3):257-65.
14. Alsebaey A, Allam N, Alswat K, Waked I. Normal liver stiffness: A study in living donors with normal liver histology. World J Hepatol. 2015; 7(8):1149-53.
15. Corpechot C, El Naggar A, Poupon R. Gender and liver: is the liver stiffness weaker in weaker sex? Hepatology. 2006; 44(2):513-4.
16. Fung J, Lee CK, Chan M, Seto WK, Wong DK, Lai CL, Yuen MF. Defining normal liver stiffness range in a normal healthy Chinese population without liver disease. PLoS One. 2013; 8(12):e85067.
17. Engelmann G, Gebhardt C, Wenning D, Wuhl E, Hoffmann GF, Selmi B, et al. Feasibility study and control values of transient elastography in healthy children. Eur J Pediatr. 2012; 171(2):353-60.
18. Das K, Sarkar R, Ahmed SM, Mridha AR, Mukherjee PS, Das K, et al. "Normal" liver stiffness measure (LSM) values are higher in both lean and obese individuals: a population-based study from a developing country. Hepatology. 2012; 55(2):584-93.
19. Bazerbachi F, Haffar S, Wang Z, Cabezas J, Arias-Loste MT, Crespo J, et al. Range of Normal Liver Stiffness and Factors Associated With Increased Stiffness Measurements in Apparently Healthy Individuals. Clin Gastroenterol Hepatol. 2019; 17(1):54-64 e1.
20. Dietrich CF, Bamber J, Berzigotti A, Bota S, Cantisani V, Castera L, et al. EFSUMB Guidelines and Recommendations on the Clinical Use of Liver Ultrasound Elastography, Update 2017 (Long Version). Ultraschall Med. 2017; 38(4):e48.
21. Barr RG, Wilson SR, Rubens D, Garcia-Tsao G, Ferraioli G. Update to the Society of Radiologists in Ultrasound Liver Elastography Consensus Statement. Radiology. 2020; 296(2):263-74.

22. Ziol M MP, Douvin C, de Ledinghen V, Poupon R, Beaugrand M Liver stiffness cut off values in HCV patients: validation and comparison in an independent population. Hepatology. 2006; 44(4):269A-70A.
23. Sporea I, Sirli R, Deleanu A, Tudora A, Curescu M, Cornianu M, Lazar D. Comparison of the liver stiffness measurement by transient elastography with the liver biopsy. World J Gastroenterol. 2008; 14(42):6513-7.
24. Castera L, Vergniol J, Foucher J, Le Bail B, Chanteloup E, Haaser M, et al. Prospective comparison of transient elastography, Fibrotest, APRI, and liver biopsy for the assessment of fibrosis in chronic hepatitis C. Gastroenterology. 2005; 128(2):343-50.
25. Ziol M, Handra-Luca A, Kettaneh A, Christidis C, Mal F, Kazemi F, et al. Noninvasive assessment of liver fibrosis by measurement of stiffness in patients with chronic hepatitis C. Hepatology. 2005; 41(1):48-54.
26. Friedrich-Rust M, Ong MF, Martens S, Sarrazin C, Bojunga J, Zeuzem S, Herrmann E. Performance of transient elastography for the staging of liver fibrosis: a meta-analysis. Gastroenterology. 2008; 134(4):960-74.
27. Shaheen AA, Wan AF, Myers RP. FibroTest and FibroScan for the prediction of hepatitis C-related fibrosis: a systematic review of diagnostic test accuracy. I have J Gastroenterol. 2007; 102(11):2589-600.
28. Talwalkar JA, Kurtz DM, Schoenleber SJ, West CP, Montori VM. Ultrasound-based transient elastography for the detection of hepatic fibrosis: systematic review and meta-analysis. Clin Gastroenterol Hepatol. 2007; 5(10):1214-20.
29. Tsochatzis EA, Gurusamy KS, Ntaoula S, Cholongitas E, Davidson BR, Burroughs AK. Elastography for the diagnosis of severity of fibrosis in chronic liver disease: a meta-analysis of diagnostic accuracy. J Hepatol. 2011; 54(4):650-9.
30. Bhattacharya D, Aronsohn A, Price J, Lo Re V, Panel A-IHG. Hepatitis C Guidance 2023 Update: AASLD-IDSA Recommendations for Testing, Managing, and Treating Hepatitis C Virus Infection. Clin Infect Dis. 2023.
31. European Association for the Study of the Liver. Electronic address eee, Clinical Practice Guidelines Panel C, representative EGB, Panel m. EASL recommendations on treatment of hepatitis C: Final update of the series(☆). J Hepatol. 2020; 73(5):1170-218.
32. Ying HY, Lu LG, Jing DD, Ni XS. Accuracy of transient elastography in the assessment of chronic hepatitis C-related liver cirrhosis. Clin Invest Med. 2016; 39(5):E150-E60.
33. Hezode C, Castera L, Roudot-Thoraval F, Bouvier-Alias M, Rosa I, Roulot D, et al. Liver stiffness diminishes with antiviral response in chronic hepatitis C. Aliment Pharmacol Ther. 2011; 34(6):656-63.
34. Dolmazashvili E, Abutidze A, Chkhartishvili N, Karchava M, Sharvadze L, Tsertsvadze T. Regression of liver fibrosis over a 24-week period after completing direct-acting antiviral therapy in patients with chronic hepatitis C receiving care within the national hepatitis C elimination program in Georgia: results of hepatology clinic HEPA experience. Eur J Gastroenterol Hepatol. 2017; 29(11):1223-30.
35. Lledó GM, Carrasco I, Benitez-Gutierrez LM, Arias A, Royuela A, Requena S, et al. Regression of liver fibrosis after curing chronic hepatitis C with oral antivirals in patients with and without HIV coinfection. AIDS. 2018; 32(16):2347-52.
36. Pietsch V, Deterding K, Attia D, Ringe KI, Heidrich B, Cornberg M, et al. Long-term changes in liver elasticity in hepatitis C virus-infected patients with sustained virologic response after treatment with direct-acting antivirals. United European Gastroenterol J. 2018; 6(8):1188-98.

37. Sporea I, Lupusoru R, Mare R, Popescu A, Gheorghe L, Iacob S, Sirli R. Dynamics of liver stiffness values by means of transient elastography in patients with HCV liver cirrhosis undergoing interferon free treatment. J Gastrogut Liver Dis. 2017; 26(2):145-50.
38. Liang X, Xie Q, Tan D, Ning Q, Niu J, Bai X, et al. Interpretation of liver stiffness measurement-based approach for the monitoring of hepatitis B patients with antiviral therapy: A 2-year prospective study. J Viral Hepat. 2018; 25(3):296-305.
39. Knop V, Hoppe D, Welzel T, Vermehren J, Herrmann E, Vermehren A, et al. Regression of fibrosis and portal hypertension in HCV-associated cirrhosis and sustained virologic response after interferon-free antiviral therapy. J Viral Hepat. 2016; 23(12):994-1002.
40. Ogasawara N, Kobayashi M, Akuta N, Kominami Y, Fujiyama S, Kawamura Y, et al. Serial changes in liver stiffness and controlled attenuation parameter following direct-acting antiviral therapy against hepatitis C virus genotype 1b. J Med Virol. 2018; 90(2):313-9.
41. de Franchis R, Bosch J, Garcia-Tsao G, Reiberger T, Ripoll C, Baveno VIIF. Baveno VII - Renewing consensus in portal hypertension. J Hepatol. 2022; 76(4):959-74.
42. Semmler G, Lens S, Meyer EL, Baiges A, Alvardo-Tapias E, Llop E, et al. Non-invasive tests for clinically significant portal hypertension after HCV cure. J Hepatol. 2022; 77(6):1573-85.
43. Marcellin P, Ziol M, Bedossa P, Douvin C, Poupon R, de Ledinghen V, Beaugrand M. Non-invasive assessment of liver fibrosis by stiffness measurement in patients with chronic hepatitis B. Liver Int. 2009; 29(2):242-7.
44. Cardoso AC, Carvalho-Filho RJ, Stern C, Dipumpo A, Giuily N, Ripault MP, et al. Direct comparison of diagnostic performance of transient elastography in patients with chronic hepatitis B and chronic hepatitis C. Liver Int. 2012; 32(4):612-21.
45. Sporea I, Sirli R, Deleanu A, Tudora A, Popescu A, Curescu M, Bota S. Liver stiffness measurements in patients with HBV vs HCV chronic hepatitis: a comparative study. World J Gastroenterol. 2010; 16(38):4832-7.
46. Cho HJ, Seo YS, Lee KG, Hyun JJ, An H, Keum B, et al. Serum aminotransferase levels instead of etiology affects the accuracy of transient elastography in chronic viral hepatitis patients. J Gastroenterol Hepatol. 2011; 26(3):492-500.
47. Vigano M, Massironi S, Lampertico P, Iavarone M, Paggi S, Pozzi R, et al. Transient elastography assessment of the liver stiffness dynamics during acute hepatitis B. Eur J Gastroenterol Hepatol. 2010; 22(2):180-4.
48. Wong GL, Wong VW, Choi PC, Chan AW, Chim AM, Yiu KK, et al. Increased liver stiffness measurement by transient elastography in severe acute exacerbation of chronic hepatitis B. J Gastroenterol Hepatol. 2009; 24(6):1002-7.
49. Chan HL, Wong GL, Choi PC, Chan AW, Chim AM, Yiu KK, et al. Alanine aminotransferase-based algorithms of liver stiffness measurement by transient elastography (Fibroscan) for liver fibrosis in chronic hepatitis B. J Viral Hepat. 2009; 16(1):36-44.
50. Chon YE, Choi EH, Song KJ, Park JY, Kim DY, Han KH, et al. Performance of transient elastography for the staging of liver fibrosis in patients with chronic hepatitis B: a meta-analysis. PLoS One. 2012; 7(9):E44930.
51. Xu X, Su Y, Song R, Sheng Y, Ai W, Wu X, Liu H. Performance of transient elastography assessing fibrosis of single hepatitis B virus infection: a systematic review and meta-analysis of a diagnostic test. Hepatol Int. 2015; 9(4):558-66.

52. Li Y, Huang YS, Wang ZZ, Yang ZR, Sun F, Zhan SY, et al. Systematic review with meta-analysis: the diagnostic accuracy of transient elastography for the staging of liver fibrosis in patients with chronic hepatitis B. Aliment Pharmacol Ther. 2016; 43(4):458-69.
53. European Association for the Study of the Liver. Electronic address eee, European Association for the Study of the L. EASL 2017 Clinical Practice Guidelines on the management of hepatitis B virus infection. J Hepatol. 2017; 67(2):370-98.
54. Terrault NA, Lok ASF, McMahon BJ, Chang KM, Hwang JP, Jonas MM, et al. Update on prevention, diagnosis, and treatment of chronic hepatitis B: AASLD 2018 hepatitis B guidance. Hepatology. 2018; 67(4):1560-99.
55. Enomoto M, Mori M, Ogawa T, Fujii H, Kobayashi S, Iwai S, et al. Usefulness of transient elastography for assessment of liver fibrosis in chronic hepatitis B: Regression of liver stiffness during entecavir therapy. Hepatol Res. 2010; 40(9):853-61.
56. Jang W, Yu SI, Sinn LS, Park SH, Park H, Park JY, et al. Longitudinal change of liver stiffness by transient elestography in chronic hepatitis B patients treated with nucleos(t)ide analogue. Clin Res Hepatol Gastroenterol. 2014; 38(2):195-200.
57. Kuo YH, Lu SN, Chen CH, Chang KC, Hung CH, Tai WC, et al. The changes of liver stiffness and its associated factors for chronic hepatitis B patients with entecavir therapy. PLoS One. 2014; 9(3):E93160.
58. Ogawa E, Furusyo N, Murata M, Ohnishi H, Toyoda K, Taniai H, et al. Longitudinal assessment of liver stiffness by transient elastography for chronic hepatitis B patients treated with nucleoside analog. Hepatol Res. 2011; 41(12):1178-88.
59. Lazar A, Sporea I, Popa A, Lupusoru R, Gherhardt D, Mare R, et al. Dynamic Changes in Liver Stiffness in Patients with Chronic Hepatitis B Undergoing Antiviral Therapy. Diagnostics (Basel). 2022; 12(11).
60. Zhang X, Song J, Zhang Y, Wen B, Dai L, Xi R, et al. Baveno VII algorithm outperformed other models in ruling out high-risk varices in individuals with HBV-related cirrhosis. J Hepatol. 2023; 78(3):574-83.
61. Sporea I, Nicolita D, Sirli R, Deleanu A, Tudora A, Bota S. Assessment of noninvasive liver stiffness in inactive HBsAg carriers by transient elastography: Fibroscan in inactive HBsAg carriers. Hepat Mon. 2011; 11(3):182-5.
62. Liu J, Ayada I, Zhang X, Wang L, Li Y, Wen T, et al. Estimating Global Prevalence of Metabolic Dysfunction-Associated Fatty Liver Disease in Overweight or Obese Adults. Clin Gastroenterol Hepatol. 2022; 20(3):E573-E82.
63. Quek J, Chan KE, Wong ZY, Tan C, Tan B, Lim WH, et al. Global prevalence of non-alcoholic fatty liver disease and non-alcoholic steatohepatitis in the overweight and obese population: a systematic review and meta-analysis. Lancet Gastroenterol Hepatol. 2023; 8(1):20-30.
64. Sanyal AJ, Van Natta ML, Clark J, Neuschwander-Tetri BA, Diehl A, Dasarathy S, et al. Prospective Study of Outcomes in Adults with Nonalcoholic Fatty Liver Disease. N Engl J Med. 2021; 385(17):1559-69.
65. Abenavoli L, Beaugrand M. Transient elastography in non-alcoholic fatty liver disease. Ann Hepatol. 2012; 11(2):172-8.
66. Lupsor M, Badea R, Stefanescu H, Grigorescu M, Serban A, Radu C, et al. Performance of unidimensional transient elastography in staging non-alcoholic steatohepatitis. J Gastrogut Liver Dis. 2010; 19(1):53-60.

67. Wong VW, Vergniol J, Wong GL, Foucher J, Chan HL, Le Bail B, et al. Diagnosis of fibrosis and cirrhosis using liver stiffness measurement in nonalcoholic fatty liver disease. Hepatology. 2010; 51(2):454-62.
68. Kwok R, Tse YK, Wong GL, Ha Y, Lee AU, Ngu MC, et al. Systematic review with meta-analysis: non-invasive assessment of non-alcoholic fatty liver disease--the role of transient elastography and plasma cytokeratin-18 fragments. Pharmacol Ther Food. 2014; 39(3):254-69.
69. Mozes FE, Lee JA, Selvaraj EA, Jayaswal ANA, Trauner M, J Fellow, et al. Diagnostic accuracy of non-invasive tests for advanced fibrosis in patients with NAFLD: an individual patient data meta-analysis. Gut. 2022; 71(5):1006-19.
70. Selvaraj EA, Mozes FE, Jayaswal ANA, Zafarmand MH, Vali Y, Lee JA, et al. Diagnostic accuracy of elastography and magnetic resonance imaging in patients with NAFLD: A systematic review and meta-analysis. J Hepatol. 2021; 75(4):770-85.
71. Wattacheril JJ, Abdelmalek MF, Lim JK, Sanyal AJ. AGA Clinical Practice Update on the Role of Noninvasive Biomarkers in the Evaluation and Management of Nonalcoholic Fatty Liver Disease: Expert Review. Gastroenterology. 2023; 165(4):1080-8.
72. Sasso M, Beaugrand M, de Ledinghen V, Douvin C, Marcellin P, Poupon R, et al. Controlled attenuation parameter (CAP): a novel VCTE guided ultrasonic attenuation measurement for the evaluation of hepatic steatosis: preliminary study and validation in a cohort of patients with chronic liver disease from various causes. Ultrasound Med Biol. 2010; 36(11):1825-35.
73. Sasso M, Audiere S, Kemgang A, Gaouar F, Corpechot C, Chazouilleres O, et al. Liver Steatosis Assessed by Controlled Attenuation Parameter (CAP) Measured with the XL Probe of the FibroScan: A Pilot Study Assessing Diagnostic Accuracy. Ultrasound Med Biol. 2016; 42(1):92-103.
74. Huang DQ, Mathurin P, Cortez-Pinto H, Loomba R. Global epidemiology of alcohol-associated cirrhosis and HCC: trends, projections and risk factors. Nat Rev Gastroenterol Hepatol. 2023; 20(1):37-49.
75. Nguyen-Khac E, Chatelain D, Tramier B, Decrombecque C, Robert B, Joly JP, et al. Assessment of asymptomatic liver fibrosis in alcoholic patients using fibroscan: prospective comparison with seven non-invasive laboratory tests. Pharmacol Ther Food. 2008; 28(10):1188-98.
76. Nahon P, Kettaneh A, Tengher-Barna I, Ziol M, de Ledinghen V, Douvin C, et al. Assessment of liver fibrosis using transient elastography in patients with alcoholic liver disease. J Hepatol. 2008; 49(6):1062-8.
77. Mueller S, Millonig G, Sarovska L, Friedrich S, Reimann FM, Pritsch M, et al. Increased liver stiffness in alcoholic liver disease: differentiating fibrosis from steatohepatitis. World J Gastroenterol. 2010; 16(8):966-72.
78. Gelsi E, Dainese R, Truchi R, Marine-Barjoan E, Anty R, Autuori M, et al. Effect of detoxification on liver stiffness assessed by Fibroscan(R) in alcoholic patients. Alcohol Clin Exp Res. 2011; 35(3):566-70.
79. Girard M, Carrier P, Loustaud-Ratti V, Nubukpo P. BDNF levels and liver stiffness in subjects with alcohol use disorder: Evaluation after alcohol withdrawal. Am J Drug Alcohol Abuse. 2021; 47(2):191-8.

80. Legros L, Bardou-Jacquet E, Turlin B, Michalak S, Hamonic S, Le Gruyer A, et al. Transient Elastography Accurately Screens for Compensated Advanced Chronic Liver Disease in Patients With Ongoing or Recent Alcohol Withdrawal. Clin Gastroenterol Hepatol. 2022; 20(7):1542-52 e6.
81. Mueller S, Englert S, Seitz HK, Badea RI, Erhardt A, Bozaari B, et al. Inflammation-adapted liver stiffness values for improved fibrosis staging in patients with hepatitis C virus and alcoholic liver disease. Liver Int. 2015; 35(12):2514-21.
82. Thiele M, Detlefsen S, Sevelsted Moller L, Madsen BS, Fuglsang Hansen J, Fialla AD, et al. Transient and 2-Dimensional Shear-Wave Elastography Provide Comparable Assessment of Alcoholic Liver Fibrosis and Cirrhosis. Gastroenterology. 2016; 150(1):123-33.
83. Salavrakos M, Piessevaux H, Komuta M, Lanthier N, Starkel P. Fibroscan Reliably Rules Out Advanced Liver Fibrosis and Significant Portal Hypertension in Alcoholic Patients. J Clin Gastroenterol. 2019; 53(10):772-8.
84. Thiele M, Madsen BS, Hansen JF, Detlefsen S, Antonsen S, Krag A. Accuracy of the Enhanced Liver Fibrosis Test vs FibroTest, Elastography, and Indirect Markers in Detection of Advanced Fibrosis in Patients With Alcoholic Liver Disease. Gastroenterology. 2018; 154(5):1369-79.
85. Pavlov CS, Casazza G, Nikolova D, Tsochatzis E, Burroughs AK, Ivashkin VT, Gluud C. Transient elastography for diagnosis of stages of hepatic fibrosis and cirrhosis in people with alcoholic liver disease. Cochrane Database Syst Rev. 2015; 1(1):CD010542.
86. Nguyen-Khac E, Thiele M, Voican C, Nahon P, Moreno C, Boursier J, et al. Non-invasive diagnosis of liver fibrosis in patients with alcohol-related liver disease by transient elastography: an individual patient data meta-analysis. Lancet Gastroenterol Hepatol. 2018; 3(9):614-25.
87. Corpechot C, El Naggar A, Poujol-Robert A, Ziol M, Wendum D, Chazouilleres O, et al. Assessment of biliary fibrosis by transient elastography in patients with PBC and PSC. Hepatology. 2006; 43(5):1118-24.
88. Gómez-Dominguez E, Mendoza J, Garcia-Buey L, Trapero M, Gisbert JP, Jones EA, Moreno-Otero R. Transient elastography to assess hepatic fibrosis in primary biliary cirrhosis. Pharmacol Ther Food. 2008; 27(5):441-7.
89. Corpechot C, Carrat F, Poujol-Robert A, Gaouar F, Wendum D, Chazouilleres O, Poupon R. Noninvasive elastography-based assessment of liver fibrosis progression and prognosis in primary biliary cirrhosis. Hepatology. 2012; 56(1):198-208.
90. Corpechot C, Carrat F, Gaouar F, Chau F, Hirschfield G, Gulamhusein A, et al. Liver stiffness measurement by vibration-controlled transient elastography improves outcome prediction in primary biliary cholangitis. J Hepatol. 2022; 77(6):1545-53.
91. Manzo-Francisco LA, Aquino-Matus J, Vidana-Perez D, Uribe M, Chavez-Tapia N. Systematic review and meta-analysis: Transient elastography compared to liver biopsy for staging of liver fibrosis in primary biliary cholangitis. Ann Hepatol. 2023; 28(4):101107.
92. Corpechot C, Gaouar F, El Naggar A, Kemgang A, Wendum D, Poupon R, et al. Baseline values and changes in liver stiffness measured by transient elastography are associated with severity of fibrosis and outcomes of patients with primary sclerosing cholangitis. Gastroenterology. 2014; 146(4):970-9; Quiz E15-6.

93. Mack CL, Adams D, Assis DN, Kerkar N, Manns MP, Mayo MJ, et al. Diagnosis and Management of Autoimmune Hepatitis in Adults and Children: 2019 Practice Guidance and Guidelines From the American Association for the Study of Liver Diseases. Hepatology. 2020; 72(2):671-722.
94. Hartl J, Denzer U, Ehlken H, Zenouzi R, Peiseler M, Sebode M, et al. Transient elastography in autoimmune hepatitis: Timing determines the impact of inflammation and fibrosis. J Hepatol. 2016; 65(4):769-75.
95. Hartl J, Ehlken H, Sebode M, Peiseler M, Krech T, Zenouzi R, et al. Usefulness of biochemical remission and transient elastography in monitoring disease course in autoimmune hepatitis. J Hepatol. 2018; 68(4):754-63.
96. Sporea I, Bota S, Saftoiu A, Sirli R, Gradinaru-Tascau O, Popescu A, et al. Romanian national guidelines and practical recommendations on liver elastography. Med Ultrasound. 2014; 16(2):123-38.
97. Goertz RS, Amann K, Heide R, Bernatik T, Neurath MF, Strobel D. An abdominal and thyroid status with Acoustic Radiation Force Impulse Elastometry--a feasibility study: Acoustic Radiation Force Impulse Elastometry of human organs. Eur J Radiol. 2011; 80(3):E226-30.
98. Karlas T, Pfrepper C, Wiegand J, Wittekind C, Neuschulz M, Mossner J, et al. Acoustic radiation force impulse imaging (ARFI) for non-invasive detection of liver fibrosis: examination standards and evaluation of interlobe differences in healthy subjects and chronic liver disease. Scand J Gastroenterol. 2011; 46(12):1458-67.
99. Madhok R, Tapasvi C, Prasad U, Gupta AK, Aggarwal A. Acoustic radiation force impulse imaging of the liver: measurement of the normal mean values of the shearing wave velocity in a healthy liver. J Clin Diagn Res. 2013; 7(1):39-42.
100. Popescu A, Sporea I, Sirli R, Bota S, Focsa M, Danila M, et al. The mean values of liver stiffness assessed by Acoustic Radiation Force Impulse elastography in normal subjects. Med Ultrasound. 2011; 13(1):33-7.
101. Son CY, Kim SU, Han WK, Choi GH, Park H, Yang SC, et al. Normal liver elasticity values using acoustic radiation force impulse imaging: a prospective study in healthy living liver and kidney donors. J Gastroenterol Hepatol. 2012; 27(1):130-6.
102. Ferraioli G, Tinelli C, Lissandrin R, Zicchetti M, Dal Bello B, Filice G, Filice C. Point shear wave elastography method for assessing liver stiffness. World J Gastroenterol. 2014; 20(16):4787-96.
103. Ling W, Lu Q, Quan J, Ma L, Luo Y. Assessment of impact factors on shear wave based liver stiffness measurement. Eur J Radiol. 2013; 82(2):335-41.
104. Sporea I, Bota S, Gradinaru-Tascau O, Sirli R, Popescu A. Comparative study between two point Shear Wave Elastographic techniques: Acoustic Radiation Force Impulse (ARFI) elastography and ElastPQ. Med Ultrasound. 2014; 16(4):309-14.
105. Friedrich-Rust M, Wunder K, Kriener S, Sotoudeh F, Richter S, Bojunga J, et al. Liver fibrosis in viral hepatitis: noninvasive assessment with acoustic radiation force impulse imaging versus transient elastography. Radiology. 2009; 252(2):595-604.
106. Lupsor M, Badea R, Stefanescu H, Sparchez Z, Branda H, Serban A, Maniu A. Performance of a new elastographic method (ARFI technology) compared to unidimensional transient elastography in the noninvasive assessment of chronic hepatitis C. Preliminary results. J Gastrogut Liver Dis. 2009; 18(3):303-10.

107. Sporea I, Sirli R, Bota S, Fierbinteanu-Braticevici C, Petrisor A, Badea R, et al. Is ARFI elastography reliable for predicting fibrosis severity in chronic HCV hepatitis? World J Radiol. 2011; 3(7):188-93.
108. Sporea I, Bota S, Peck-Radosavljevic M, Sirli R, Tanaka H, Iijima H, et al. Acoustic Radiation Force Impulse elastography for fibrosis evaluation in patients with chronic hepatitis C: an international multicenter study. Eur J Radiol. 2012; 81(12):4112-8.
109. Rizzo L, Calvaruso V, Cacopardo B, Alessi N, Attanasio M, Petta S, et al. Comparison of transient elastography and acoustic radiation force impulse for non-invasive staging of liver fibrosis in patients with chronic hepatitis C. Am J Gastroenterol. 2011; 106(12):2112-20.
110. Chen SH, Li YF, Lai HC, Kao JT, Peng CY, Chuang PH, et al. Effects of patient factors on noninvasive liver stiffness measurement using acoustic radiation force impulse elastography in patients with chronic hepatitis C. BMC Gastroenterol. 2012;12:105.
111. Li SM, Li GX, Fu DM, Wang Y, Dang LQ. Liver fibrosis evaluation by ARFI and APRI in chronic hepatitis C. World J Gastroenterol. 2014; 20(28):9528-33.
112. Joo SK, Kim JH, Oh S, Kim BG, Lee KL, Kim HY, et al. Prospective Comparison of Noninvasive Fibrosis Assessment to Predict Advanced Fibrosis or Cirrhosis in Asian Patients With Hepatitis C. J Clin Gastroenterol. 2015; 49(8):697-704.
113. Ragazzo TG, Paranaguá-Vezozzo D, Lima FR, de Campos Mazo DF, Pessoa MG, Oliveira CP, et al. Accuracy of transient elastography-FibroScan(R), acoustic radiation force impulse (ARFI) imaging, the enhanced liver fibrosis (ELF) test, APRI, and the FIB-4 index compared with liver biopsy in patients with chronic hepatitis C. Clinics (São Paulo). 2017; 72(9):516-25.
114. Hsu TH, Tsui PH, Yu WT, Huang SF, Tai J, Wan YL, Tai DI. Cutoff Values of Acoustic Radiation Force Impulse Two-Location Measurements in Different Etiologies of Liver Fibrosis. J Med Ultrasound. 2019; 27(3):130-4.
115. Ueda N, Kawaoka T, Imamura M, Aikata H, Nakahara T, Murakami E, et al. Liver fibrosis assessments using FibroScan, virtual-touch tissue quantification, the FIB-4 index, and mac-2 binding protein glycosylation isomer levels compared with pathological findings of liver resection specimens in patients with hepatitis C infection. BMC Gastroenterol. 2020; 20(1):314.
116. Conti F, Serra C, Vukotic R, Fiorini E, Felicani C, Mazzotta E, et al. Accuracy of elastography point quantification and steatosis influence on assessing liver fibrosis in patients with chronic hepatitis C. Liver Int. 2017; 37(2):187-95.
117. Baldea V, Sporea I, Lupusoru R, Bende F, Mare R, Popescu A, Sirli R. Comparative Study Between the Diagnostic Performance of Point and 2-D Shear-Wave Elastography for the Non-invasive Assessment of Liver Fibrosis in Patients With Chronic Hepatitis C Using Transient Elastography as Reference. Ultrasound Med Biol. 2020; 46(11):2979-88.
118. Mare R, Sporea I, Lupusoru R, Sirli R, Popescu A, Danila M, Pienar C. The value of ElastPQ for the evaluation of liver stiffness in patients with B and C chronic hepatopathies. Ultrasonics. 2017;77:144-51.
119. Chen SH, Lai HC, Chiang IP, Su WP, Lin CH, Kao JT, et al. Performance of Acoustic Radiation Force Impulse Elastography for Staging Liver Fibrosis in Patients With Chronic Hepatitis C After Viral Eradication. Clin Infect Dis. 2020; 70(1):114-22.
120. Tachi Y, Hirai T, Kojima Y, Miyata A, Ohara K, Ishizu Y, et al. Liver stiffness measurement using acoustic radiation force impulse elastography in hepatitis C virus-infected patients with a sustained virological response. Pharmacol Ther Food. 2016; 44(4):346-55.

121. Dong DR, Hao MN, Li C, Peng Z, Liu X, Wang GP, Ma AL. Acoustic radiation force impulse elastography, FibroScan(R), Forns' index and their combination in the assessment of liver fibrosis in patients with chronic hepatitis B, and the impact of inflammatory activity and steatosis on these diagnostic methods. Mol Med Rep. 2015; 11(6):4174-82.
122. Friedrich-Rust M, Buggisch P, de Knegt RJ, Dries V, Shi Y, Matschenz K, et al. Acoustic radiation force impulse imaging for non-invasive assessment of liver fibrosis in chronic hepatitis B. J Viral Hepat. 2013; 20(4):240-7.
123. Zhang D, Chen M, Wang R, Liu Y, Zhang D, Liu L, Zhou G. Comparison of acoustic radiation force impulse imaging and transient elastography for non-invasive assessment of liver fibrosis in patients with chronic hepatitis B. Ultrasound Med Biol. 2015; 41(1):7-14.
124. Sporea I, Sirli R, Bota S, Popescu A, Sendroiu M, Jurchis A. Comparative study concerning the value of acoustic radiation force impulse elastography (ARFI) in comparison with transient elastography (TE) for the assessment of liver fibrosis in patients with chronic hepatitis B and C. Ultrasound Med Biol. 2012; 38(8):1310-6.
125. Friedrich-Rust M, Nierhoff J, Lupsor M, Sporea I, Fierbinteanu-Braticevici C, Strobel D, et al. Performance of Acoustic Radiation Force Impulse imaging for the staging of liver fibrosis: a pooled meta-analysis. J Viral Hepat. 2012; 19(2):E212-9.
126. Nierhoff J, Chavez Ortiz AA, Herrmann E, Zeuzem S, Friedrich-Rust M. The efficiency of acoustic radiation force impulse imaging for the staging of liver fibrosis: a meta-analysis. Eur Radiol. 2013; 23(11):3040-53.
127. Lu Q, Lu C, Li J, Ling W, Qi X, He D, et al. Stiffness Value and Serum Biomarkers in Liver Fibrosis Staging: Study in Large Surgical Specimens in Patients with Chronic Hepatitis B. Radiology. 2016; 280(1):290-9.
128. Ma JJ, Ding H, Mao F, Sun HC, Xu C, Wang WP. Assessment of liver fibrosis with elastography point quantification technique in chronic hepatitis B virus patients: a comparison with liver pathological results. J Gastroenterol Hepatol. 2014; 29(4):814-9.
129. Rinella ME, Neuschwander-Tetri BA, Siddiqui MS, Abdelmalek MF, Caldwell S, Barb D, et al. AASLD Practice Guidance on the clinical assessment and management of nonalcoholic fatty liver disease. Hepatology. 2023; 77(5):1797-835.
130. Yoneda M, Suzuki K, Kato S, Fujita K, Nozaki Y, Hosono K, et al. Nonalcoholic fatty liver disease: US-based acoustic radiation force impulse elastography. Radiology. 2010; 256(2):640-7.
131. Fierbinteanu Braticevici C, Sporea I, Panaitescu E, Tribus L. Value of acoustic radiation force impulse imaging elastography for non-invasive evaluation of patients with nonalcoholic fatty liver disease. Ultrasound Med Biol. 2013; 39(11):1942-50.
132. Friedrich-Rust M, Romen D, Vermehren J, Kriener S, Sadet D, Herrmann E, et al. Acoustic radiation force impulse-imaging and transient elastography for non-invasive assessment of liver fibrosis and steatosis in NAFLD. Eur J Radiol. 2012; 81(3):E325-31.
133. Liu H, Fu J, Hong R, Liu L, Li F. Acoustic Radiation Force Impulse Elastography for the Non-Invasive Evaluation of Hepatic Fibrosis in Non-Alcoholic Fatty Liver Disease Patients: A Systematic Review & Meta-Analysis. PLoS One. 2015; 10(7):E0127782.
134. Jiang W, Huang S, Teng H, Wang P, Wu M, Zhou X, Ran H. Diagnostic accuracy of point shear wave elastography and transient elastography for staging hepatic fibrosis in patients with non-alcoholic fatty liver disease: a meta-analysis. BMJ Open. 2018; 8(8):E021787.

135. Bauer DJ, Matic V, Mare R, Maiocchi L, Chromy D, Mullner-Bucsics T, et al. Point Shear Wave Elastography by ElastPQ for Fibrosis Screening in Patients with NAFLD: A Prospective, Multicenter Comparison to Vibration-Controlled Elastography. Ultraschall Med. 2023; 44(2):169-78.
136. Roccarina D, Iogna Prat L, Pallini G, Guerrero Misas M, Buzzetti E, Saffioti F, et al. Comparison of point-shear wave elastography (ElastPQ) and transient elastography (FibroScan) for liver fibrosis staging in patients with non-alcoholic fatty liver disease. Liver Int. 2022; 42(10):2195-203.
137. Zhang D, Li P, Chen M, Liu L, Liu Y, Zhao Y, Wang R. Non-invasive assessment of liver fibrosis in patients with alcoholic liver disease using acoustic radiation force impulse elastography. Abdom Imaging. 2015; 40(4):723-9.
138. Kiani A, Brun V, Laine F, Turlin B, Morcet J, Michalak S, et al. Acoustic radiation force impulse imaging for assessing liver fibrosis in alcoholic liver disease. World J Gastroenterol. 2016; 22(20):4926-35.
139. Zhang HC, Hu RF, Zhu T, Tong L, Zhang QQ. Primary biliary cirrhosis degree assessment by acoustic radiation force impulse imaging and hepatic fibrosis indicators. World J Gastroenterol. 2016; 22(22):5276-84.
140. Roccarina D, Saffioti F, Rosselli M, Marshall A, Pinzani M, Thorburn D. Utility of ElastPQ point-shear wave elastography in the work-up of patients with primary sclerosing cholangitis. JHEP Rep. 2023; 5(11):100873.
141. Park DW, Lee YJ, Chang W, Park JH, Lee KH, Kim YH, et al. Diagnostic performance of a point shear wave elastography (pSWE) for hepatic fibrosis in patients with autoimmune liver disease. PLoS One. 2019; 14(3):E0212771.
142. Augustin S, Pons M, Maurice JB, Bureau C, Stefanescu H, Ney M, et al. Expanding the Baveno VI criteria for the screening of varices in patients with compensated advanced chronic liver disease. Hepatology. 2017; 66(6):1980-8.
143. by Franchis R, Baveno VIF. Expanding consensus in portal hypertension: Report of the Baveno VI Consensus Workshop: Stratifying risk and individualizing care for portal hypertension. J Hepatol. 2015; 63(3):743-52.
144. Dietrich CF, Bamber J, Berzigotti A, Bota S, Cantisani V, Castera L, et al. EFSUMB Guidelines and Recommendations on the Clinical Use of Liver Ultrasound Elastography, Update 2017 (Long Version). Ultraschall Med. 2017; 38(4):e16-e47.
145. Suh CH, Kim SY, Kim KW, Lim YS, Lee SJ, Lee MG, et al. Determination of normal hepatic elasticity by using real-time shear-wave elastography. Radiology. 2014; 271(3):895-900.
146. Sirli R, Bota S, Sporea I, Jurchis A, Popescu A, Gradinaru-Tascau O, Szilaski M. Liver stiffness measurements by means of supersonic shear imaging in patients without known liver pathology. Ultrasound Med Biol. 2013; 39(8):1362-7.
147. Bende F, Mulabecirovic A, Sporea I, Popescu A, Sirli R, Gilja OH, et al. Assessing Liver Stiffness by 2-D Shear Wave Elastography in a Healthy Cohort. Ultrasound Med Biol. 2018; 44(2):332-41.
148. Bavu E, Gennisson JL, Couade M, Bercoff J, Mallet V, Fink M, et al. Noninvasive in vivo liver fibrosis evaluation using supersonic shear imaging: a clinical study on 113 hepatitis C virus patients. Ultrasound Med Biol. 2011; 37(9):1361-73.
149. Ferraioli G, Tinelli C, Dal Bello B, Zicchetti M, Filice G, Filice C, Liver Fibrosis Study G. Accuracy of real-time shear wave elastography for assessing liver fibrosis in chronic hepatitis C: a pilot study. Hepatology. 2012; 56(6):2125-33.

150. Baldea V, Bende F, Popescu A, Sirli R, Sporea I. Comparative study between two 2D-Shear Waves Elastography techniques for the non-invasive assessment of liver fibrosis in patients with chronic hepatitis C virus (HCV) infection. Med Ultrasound. 2021; 23(3):257-64.
151. Aksakal M, Oktar SO, Sendur HN, Esendagli G, Ozenirler S, Cindoruk M, Hizel K. Diagnostic performance of 2D shear wave elastography in predicting liver fibrosis in patients with chronic hepatitis B and C: a histopathological correlation study. Abdom Radiol (NY). 2021; 46(7):3238-44.
152. Villani R, Cavallone F, Romano AD, Bellanti F, Serviddio G. Two-Dimensional Shear Wave Elastography versus Transient Elastography: A Non-Invasive Comparison for the Assessment of Liver Fibrosis in Patients with Chronic Hepatitis C. Diagnostics (Basel). 2020; 10(5).
153. Leung VY, Shen J, Wong VW, Abrigo J, Wong GL, Chim AM, et al. Quantitative elastography of liver fibrosis and spleen stiffness in chronic hepatitis B carriers: comparison of shear-wave elastography and transient elastography with liver biopsy correlation. Radiology. 2013; 269(3):910-8.
154. Zeng J, Liu GJ, Huang ZP, Zheng J, Wu T, Zheng RQ, Lu MD. Diagnostic accuracy of two-dimensional shear wave elastography for the non-invasive staging of hepatic fibrosis in chronic hepatitis B: a cohort study with internal validation. Eur Radiol. 2014; 24(10):2572-81.
155. Cassinotto C, Boursier J, de Ledinghen V, Lebigot J, Lapuyade B, Cales P, et al. Liver stiffness in nonalcoholic fatty liver disease: A comparison of supersonic shear imaging, FibroScan, and ARFI with liver biopsy. Hepatology. 2016; 63(6):1817-27.
156. Popa A, Bende F, Sirli R, Popescu A, Baldea V, Lupusoru R, et al. Quantification of Liver Fibrosis, Steatosis, and Viscosity Using Multiparametric Ultrasound in Patients with Non-Alcoholic Liver Disease: A "Real-Life" Cohort Study. Diagnostics (Basel). 2021; 11(5).
157. Podrug K, Sporea I, Lupusoru R, Pastrovic F, Mustapic S, Baldea V, et al. Diagnostic Performance of 2-D Shear-Wave Elastography with Propagation Maps and Attenuation Imaging in Patients with Non-Alcoholic Fatty Liver Disease. Ultrasound Med Biol. 2021; 47(8):2128-37.
158. Mendoza YP, Rodrigues SG, Delgado MG, Murgia G, Lange NF, Schropp J, et al. Inflammatory activity affects the accuracy of liver stiffness measurement by transient elastography but not by two-dimensional shear wave elastography in non-alcoholic fatty liver disease. Liver Int. 2022; 42(1):102-11.
159. Karagiannakis DS, Markakis G, Lakiotaki D, Cholongitas E, Vlachogiannakos J, Papatheodoridis G. Comparing 2D-shear wave to transient elastography for the evaluation of liver fibrosis in nonalcoholic fatty liver disease. Eur J Gastroenterol Hepatol. 2022; 34(9):961-6.
160. Gradinaru-Tascau O, Sporea I, Bota S, Jurchis A, Popescu A, Popescu M, et al. Does experience play a role in the ability to perform liver stiffness measurements by means of supersonic shear imaging (SSI)? Med Ultrasound. 2013; 15(3):180-3.
161. Jamialahmadi T, Nematy M, Jangjoo A, Goshayeshi L, Rezvani R, Ghaffarzadegan K, et al. Measurement of Liver Stiffness with 2D-Shear Wave Elastography (2D-SWE) in Bariatric Surgery Candidates Reveals Acceptable Diagnostic Yield Compared to Liver Biopsy. Obes Surg. 2019; 29(8):2585-92.

162. Sugimoto K, Moriyasu F, Oshiro H, Takeuchi H, Abe M, Yoshimasu Y, et al. The Role of Multiparametric US of the Liver for the Evaluation of Nonalcoholic Steatohepatitis. Radiology. 2020; 296(3):532-40.
163. Rasmussen DN, Thiele M, Johansen S, Kjaergaard M, Lindvig KP, Israelsen M, et al. Prognostic performance of 7 biomarkers compared to liver biopsy in early alcohol-related liver disease. J Hepatol. 2021; 75(5):1017-25.
164. Yan Y, Xing X, Lu Q, Wang X, Luo X, Yang L. Assessment of biopsy proven liver fibrosis by two-dimensional shear wave elastography in patients with primary biliary cholangitis. Dig Liver Dis. 2020; 52(5):555-60.
165. Mjelle AB, Fossdal G, Gilja OH, Vesterhus M. Liver Elastography in Primary Sclerosing Cholangitis Patients Using Three Different Scanner Systems. Ultrasound Med Biol. 2020; 46(8):1854-64.
166. Janik MK, Kruk B, Szczepankiewicz B, Kostrzewa K, Raszeja-Wyszomirska J, Gornicka B, et al. Measurement of liver and spleen stiffness as complementary methods for assessment of liver fibrosis in autoimmune hepatitis. Liver Int. 2021; 41(2):348-56.
167. Sporea I, Bota S, Gradinaru-Tascau O, Sirli R, Popescu A, Jurchis A. Which are the cut-off values of 2D-Shear Wave Elastography (2D-SWE) liver stiffness measurements predicting different stages of liver fibrosis, considering Transient Elastography (TE) as the reference method? Eur J Radiol. 2014; 83(3):E118-22.
168. Popa A, Sirli R, Popescu A, Baldea V, Lupusoru R, Bende F, et al. Ultrasound-Based Quantification of Fibrosis and Steatosis with a New Software Considering Transient Elastography as Reference in Patients with Chronic Liver Diseases. Ultrasound Med Biol. 2021; 47(7):1692-703.
169. Cassinotto C, Lapuyade B, Mouries A, Hiriart JB, Vergniol J, Gaye D, et al. Non-invasive assessment of liver fibrosis with impulse elastography: comparison of Supersonic Shear Imaging with ARFI and FibroScan(R). J Hepatol. 2014; 61(3):550-7.
170. Serra C, Grasso V, Conti F, Felicani C, Mazzotta E, Lenzi M, et al. A New Two-Dimensional Shear Wave Elastography for Noninvasive Assessment of Liver Fibrosis in Healthy Subjects and in Patients with Chronic Liver Disease. Ultraschall Med. 2018; 39(4):432-9.
171. Bende F, Sporea I, Sirli R, Nistorescu S, Fofiu R, Baldea V, Popescu A. The Performance of a 2-Dimensional Shear-Wave Elastography Technique for Predicting Different Stages of Liver Fibrosis Using Transient Elastography as the Control Method. Ultrasound Q. 2020; 37(2):97-104.
172. Ronot M, Ferraioli G, Muller HP, Friedrich-Rust M, Filice C, Vilgrain V, et al. Comparison of liver stiffness measurements by a 2D-shear wave technique and transient elastography: results from a European prospective multi-centre study. Eur Radiol. 2021; 31(3):1578-87.
173. Kovatsch A, Honcharova-Biletska H, Segna D, Steigmiller K, Blumel S, Deibel RA, et al. Performance of two-dimensional shear wave elastography and transient elastography compared to liver biopsy for staging of liver fibrosis. Eur J Clin Invest. 2023; 53(7):E13980.
174. Foncea CG, Popescu A, Lupusoru R, Fofiu R, Sirli R, Danila M, Sporea I. Comparative study between pSWE and 2D-SWE techniques integrated in the same ultrasound machine, with Transient Elastography as the reference method. Med Ultrasound. 2020; 22(1):13-9.

175. Herrmann E, de Ledinghen V, Cassinotto C, Chu WC, Leung VY, Ferraioli G, et al. Assessment of biopsy-proven liver fibrosis by two-dimensional shear wave elastography: An individual patient data-based meta-analysis. Hepatology. 2018; 67(1):260-72.
176. Jiang T, Tian G, Zhao Q, Kong D, Cheng C, Zhong L, Li L. Diagnostic Accuracy of 2D-Shear Wave Elastography for Liver Fibrosis Severity: A Meta-Analysis. PLoS One. 2016; 11(6):E0157219.

5.1.c. Comparative Studies between Elastographic Techniques

Ioan Sporea, Victor Bâldea

Given the multiple possibilities for elastographic evaluation of the liver—Vibration Controlled Transient Elastography (VCTE), initially known as Transient Elastography (TE), point Shear Wave Elastography (pSWE), 2D Shear Wave Elastography (2D-SWE), and also Magnetic Resonance Elastography (MRE)—the reader is interested in comparing the performance of various methods in order to choose the optimal technique for the non-invasive assessment of liver fibrosis in current practice. Here, we will attempt a comparative analysis between the elastographic methods available on the market.

1. Comparison between the Performance of pSWE Techniques in Staging Liver Fibrosis

Most studies evaluating the performance of pSWE methods, especially VTQ® (Virtual Touch Quantification) (Siemens), have been conducted on patients with chronic liver disease of mixed etiology, with chronic viral hepatitis being the most prevalent liver disease (1-9). These studies have shown a superior performance of VTQ in identifying patients with cirrhosis (AUROC values: 0.81-0.99) than with significant fibrosis (AUROC values: 0.77-0.94). Moreover, numerous meta-analyses have shown that VTQ has a better performance in the diagnosis of cirrhosis than of various stages of liver fibrosis (3,4).

According to the EFSUMB clinical practice guidelines, VTQ can be used as a first-line method for assessing the severity of liver fibrosis in patients with chronic hepatitis C virus (HCV) infection, with the best performance in excluding cirrhosis (1). In line with the same guidelines, the best cut-off values of VTQ for predicting significant fibrosis (F≥2) ranged between 1.21-1.34 m/s (AUROC = 0.85-0.89), and for predicting cirrhosis (F = 4) they ranged between 1.55 and 2 m/s (AUROC = 0.89-0.93) (1).

Regarding ElastPQ (Philips), data is available for patients with chronic liver diseases of mixed etiology. In a study comparing the diagnostic performance of ElastPQ and VCTE, the latter being considered the reference method, the calculated AUROC values for significant fibrosis (F≥2), severe fibrosis (F≥3), and cirrhosis (F = 4) were 0.94, 0.97, and 0.97, respectively (10). In another study which used liver biopsy as the reference method, ElastPQ showed good accuracy in identifying each stage of liver fibrosis. ElastPQ showed similar performance compared to VCTE in the diagnosis of liver cirrhosis (AUROC = 0.834 and 0.879, respectively) (11).

In terms of ElastPQ for patients with NAFLD, a study by Bauer demonstrated that ElastPQ is an accurate method for diagnosing fibrosis and cirrhosis, with a good level of agreement with VCTE for staging fibrosis in these patients. The optimal cut-off values for classifying significant fibrosis and cirrhosis (F≥2) (F=4) were 7.5 kPa and 10.1 kPa, respectively (12).

Many manufacturers like Esaote, Samsung, Mindray, or Hitachi (Fujifilm) have implemented pSWE techniques in their ultrasound machines. In a study which enrolled 196 consecutive liver transplant patients, pSWE using QElaXto embedded on the MyLab Eight platform by Esaote was used for the non-invasive assessment of liver fibrosis using VCTE as the reference method (13). Excellent agreement was found between paired measurements by QElaXto pSWE and VCTE (CCC = 0.91). The performance of QElaXto pSWE for diagnosing clinically significant fibrosis (F2-F3) and cirrhosis (F4) was evaluated using AUROC curves. The optimal cut-off value for F2-F3 and F=4 was >6.7 kPa (AUROC=0.90) and >11.6 kPa (AUROC=0.99), respectively (13).

In another study that included 115 patients with chronic liver diseases of mixed etiology, the performance of pSWE implemented on the Samsung platform was compared to VCTE for the non-invasive assessment of liver fibrosis (14). The results of this study have shown strong correlations between measurements obtained using pSWE and VCTE (r = 0.90). AUROC curve analysis was used to evaluate the performance of Samsung pSWE for diagnosing significant fibrosis and cirrhosis (F≥2, respectively F=4). The optimal cut-off value for significant fibrosis was >5.9 kPa (AUROC=0.95), and for cirrhosis it was >8 kPa (AUROC=0.98) (14).

In another study which enrolled 445 individuals, the performance of a pSWE technique implemented on the Hitachi Ascendus system (SWM) was analyzed. When assessing the diagnostic performance of SWM, ROC curve analysis was used with a specificity or sensitivity >90% in order to exclude F≥2 and F=4 (15). The optimal cut-off values for confirming ("rule-in") and excluding ("rule-out") F≥2 were 6.78 kPa (Se: 76.9%, Sp: 90.3%) and 5.55 kPa (Se: 90.6%, Sp: 72.2%), respectively. The optimal cut-off values for confirming and excluding F=4 were 9.15 kPa (Se: 83.3%, Sp: 90.1%) and 8.41 kPa (Se: 90.6%, Sp: 82.2%), respectively (15).

These results from published articles indicate that pSWE methods have good diagnostic accuracy in identifying patients with significant fibrosis and excellent diagnostic accuracy for advanced fibrosis and cirrhosis, and are similar to those obtained in the meta-analysis conducted by Bota et al., where VCTE and VTQ were found to have nearly identical performance in the diagnosis of significant fibrosis and cirrhosis (16). However, some studies have found that VCTE may have better performance for diagnosing significant fibrosis than VTQ (9, 17,18).

2. Comparison between the Performance of 2D-SWE Techniques in Staging Liver Fibrosis

Many published studies evaluating 2D-SWE technology for assessing liver fibrosis, implemented on different ultrasound systems, have shown a good correlation with liver histology or VCTE (19-22).

In a study by Cassinotto et al., which enrolled 349 consecutive patients with various chronic liver diseases who underwent liver biopsy, 2D-SWE.SSI (Aixplorer®, Supersonic Imagine), pSWE (VTQ®, Siemens), and VCTE (FibroScan®, Echosens) were compared (19). The AUROC of 2D-SWE.SSI for diagnosing mild, significant, severe fibrosis, and cirrhosis was 0.89,

0.88, and 0.93, respectively. There was a good correlation between all methods and histological fibrosis scores. 2D-SWE.SSI had better accuracy compared to VCTE for diagnosing severe fibrosis (F≥3) (p = 0.0016) and better accuracy than VTQ for diagnosing significant fibrosis (F≥2) (p = 0.0003). In the same study, which also included an analysis of 294 patients with MASLD confirmed by liver biopsy, the performance of VCTE, VTQ, and 2D-SWE.SSI in diagnosing significant, severe fibrosis, and cirrhosis in this patient category was compared. In this study, 2D-SWE.SSI had AUROC values of 0.86, 0.89, and 0.88 for diagnosing significant fibrosis, severe fibrosis, and cirrhosis. Additionally, pairwise comparisons of AUROC values between 2D-SWE.SSI, VCTE, and VTQ were performed on 231 patients, and 2D-SWE.SSI showed similar diagnostic performance in identifying significant fibrosis, severe fibrosis, and cirrhosis (all p values = 0.5), while the difference between the correlation coefficients of VCTE and 2D-SWE.SSI was not significant (r2 = 0.67 vs. 0.72, p = 0.1).

In a more recent study that enrolled 115 consecutive patients with chronic liver disease, the diagnostic performance of a 2D-SWE technique with a propagation map (Canon) was evaluated for the non-invasive assessment of liver fibrosis and compared with VCTE (23). This study found a moderate correlation between 2D-SWE and VCTE in diagnosing liver fibrosis (r = 0.511), with good ICC concordance between operators with different experience levels (ICC = 0.878). However, 2D-SWE demonstrated good reliability in predicting significant fibrosis and cirrhosis (AUROC = 0.777, at a cut-off value >1.78 m/s and AUROC = 0.935 at a cut-off value >2.24 m/s, respectively).

More recently, in a prospective multicentric study conducted in Europe, the diagnostic performance of a 2D-SWE technique with a propagation map (Canon) was used in the non-invasive evaluation of liver fibrosis and compared with VCTE (24). This study showed that the average liver stiffness values obtained using 2D-SWE were significantly lower compared to VCTE, especially for more advanced fibrosis (9.1 ± 6.1 kPa vs. 10.1 ± 9.4 kPa, paired t-test: p <0.001), but were significantly correlated (Pearson r = 0.932, p <0.001, ICC 0.850) (21,24). Additionally, the performance of 2D-SWE for diagnosing significant fibrosis (F≥2), severe fibrosis (F≥3), and cirrhosis (F4) based on AUROC analysis was: 0.935, 0.954, and 0.973, respectively, with optimal cut-off values ≥7.40 kPa, ≥7.95 kPa, and ≥10.50 kPa, results which confirm the good performance of 2D-SWE with a propagation map for the non-invasive assessment of liver fibrosis (4,25).

In a study on 199 consecutive patients with alcohol-induced liver disease (ALD), all patients were evaluated for liver fibrosis by 2D-SWE.SSI, liver biopsy, and VCTE. The optimal cut-off values of 2D-SWE.SSI for diagnosing significant fibrosis and cirrhosis were 10.2 kPa (AUC = 0.94) and 16.4 kPa (AUC = 0.95), respectively, with better performance in excluding cirrhosis (26).

In a cohort of 66 patients with primary sclerosing cholangitis (PSC), the performance of 2D-SWE.GE (2D-SWE implemented on a General Electric ultrasound) was compared to that of VCTE and pSWE in the non-invasive assessment of liver fibrosis (27). The ability of 2D-SWE.GE to discriminate between mild and advanced fibrosis (F3-F4), as defined by VCTE, was

good (AUROC=0.85), with an optimal cut-off value of 7.8 kPa (Se=76.9%, Sp=88.2%). Moreover, moderate to excellent correlations were found between 2D-SWE.GE, pSWE, and VCTE LSM values.

In a study by Gargovich et al., which included 253 patients with chronic liver disease, the diagnostic performance of a pSWE method (X+pSWE, X-CUBE 90, Alpinion Medical Systems Co) was compared with 2D-SWE.SSI (Aixplorer, Supersonic Imagine) as the reference method (28). A very good correlation was found between X+pSWE and 2D-SWE.SSI ($r2 = 0.94$; $p < 0.001$), with mean liver stiffness values for X+pSWE being 0.24 kPa lower than those obtained with 2D-SWE.SSI. The AUROCs for X+pSWE for staging significant fibrosis (F2), severe fibrosis (F3), and cirrhosis (F4) using 2D-SWE.SSI as the reference method were 0.96, 0.98, and 0.99, respectively. The best cut-off values for diagnosing fibrosis ≥F2, ≥F3, and F4 were: 6.9, 8.5, and 12 kPa for X+pSWE. According to histological classification, X+pSWE correctly identified 93 out of 113 patients (82%) for F ≥ 2 and 101 out of 113 patients (89%) for F ≥ 3, using the mentioned cut-off values.

In a study comparing pSWE with 2D-SWE incorporated into the same ultrasound system (Philips) (29), using liver biopsy as the reference method, in a cohort of 87 patients, it was found that measurements not meeting quality criteria were rarer with 2D-SWE (1.1%) than with pSWE (9.2%)($p<0.001$) and that the AUROC of the 2D-SWE technique was significantly better for diagnosing significant fibrosis (0.965 vs 0.872, $p=0.022$) and cirrhosis (0.994 vs 0.886, $p=0.042$) than the pSWE technique.

Several publications from our group refer to comparative clinical studies between various elastographic methods. In one such study (30), a pSWE technique (ElastPQ) was compared with 2D-SWE.GE for the non-invasive evaluation of patients with chronic hepatitis C, considering VCTE as the reference method. First, this study found no significant differences in feasibility between the methods (VCTE, ElastPQ, and 2D-SWE.GE) ($p=0.507$), then a good correlation was found between pSWE and 2D-SWE ($r=0.78$), but the mean values obtained by pSWE were significantly higher than those obtained using 2D-SWE. At the same time, the study showed that pairwise comparison found no significant differences in performance for staging F ≥ 2 ($p = 0.89$), F ≥ 3 ($p = 0.76$), and F = 4 ($p = 0.86$) between pSWE and 2D-SWE, in patients with chronic viral hepatitis C.

In another study, considering liver biopsy as the reference method, in a cohort of 157 patients with chronic viral hepatitis (80 HBV cases and 77 HCV cases), the performance of VCTE was compared with pSWE (VTQ) (31). The two methods were strongly linearly correlated (Spearman $p=0.826$; $p<0.001$). Regarding AUROCs, VCTE and VTQ had similar predictive values (F≥1 Metavir score: AUROC VCTE = 0.876, AUROC VTQ = 0.832, $p = 0.358$; for F≥2 Metavir: AUROC VCTE = 0.826, AUROC VTQ = 0.862, $p = 0.313$; for F≥3 Metavir: AUROC VCTE = 0.907, AUROC VTQ = 0.880, $p = 0.434$, and for F = 4 Metavir: AUROC VCTE = 0.981, AUROC VTQ = 0.974, $p = 0.423$). Based on these published data, we can state that the diagnostic performance of pSWE and VCTE in evaluating patients with chronic viral hepatitis is similar.

All the data presented above lead to the conclusion that all SWE techniques have similar performances in clinical practice and also similar feasibility. The decision to use them depends on the users. For ARFI methods (pSWE and 2D-SWE), an advantage is that they are available as modules included in standard ultrasound machines (so the examination can start with a standard liver evaluation, and the elastographic evaluation site can be chosen while avoiding vascular structures and possible liver lesions), and they can also assess patients with ascites (who cannot be examined by VCTE).

With the emergence of Magnetic Resonance Elastography (MRE), it is increasingly used, especially in the United States. Although the method is more costly, it has the advantage of investigating the entire liver with high accuracy, can be performed without major difficulties, and can be done on obese patients. Several meta-analyses have evaluated the accuracy of MRE for liver fibrosis staging. For instance, in a meta-analysis by Singh and colleagues (34) comparing this technique with liver biopsy in a cohort of 697 patients with chronic liver diseases of various etiologies, the AUROC curves calculated for fibrosis stages of F≥1, F≥2, F≥3, and F=4 were 0.84, 0.88, 0.93, and 0.92, respectively, with the performance being independent of body mass index or liver disease etiology. A few years later, another meta-analysis (35) assessed the value of MRE for fibrosis staging in patients with metabolic associated fatty liver disease (MAFLD) compared to liver biopsy in a cohort of 910 patients, showing AUROC curves of 0.89, 0.93, 0.93, and 0.95 for the above-mentioned fibrosis stages. Both meta-analyses, whether with various liver diseases or MAFLD patients, demonstrated that MRE has very good accuracy, regardless of the fibrosis stage, but which increases with fibrosis severity.

Given the proven high accuracy of MRE from biopsy studies or meta-analyses, many studies have tried to compare ultrasound-based elastography methods with this technique. For example, a meta-analysis comparing VCTE with MRE in 230 patients with MAFLD with liver biopsy calculated AUROCs for F≥1, F≥2, F≥3, and F=4 of 0.82 vs. 0.87 (p=0.04), 0.87 vs. 0.92 (p=0.03), 0.84 vs. 0.93 (p=0.001), and 0.84 vs. 0.94 (p=0.005) (36). The meta-analysis concluded that MRE has significantly higher diagnostic accuracy compared to VCTE in this patient category.

Another study compared VCTE, pSWE, and MRE in a group of 100 patients with chronic liver diseases of various etiologies, all having undergone liver biopsy (37). Feasibility and reliable values were achieved in 92%, 79%, and 91% of cases, and the accuracy of the methods for fibrosis staging was 0.89, 0.90, and 0.94, respectively, with the conclusion that MRE is the most sensitive method for diagnosing fibrosis. In a study comparing MRE with 2D-SWE (38) in a group of 888 patients with liver biopsy, it indicated an almost perfect correlation between the two methods (0.8231; 95% CI, 0.8006 - 0.8432; P<0.001), leading to the conclusion that the methods may be interchangeable.

Lately, there has been increasing interest in evaluating patients with Metabolic Dysfunction Associated Steatotic Liver Disease (MASLD) due to the very high prevalence of this pathology in the population of developed countries. Multiple comparative studies between non-invasive methods for assessing fibrosis in these patients have been published.

In three studies comparing liver biopsy with VCTE, 2D-SWE, and MRE, the three methods showed comparable results in patients with fatty liver. For example, in a study by Furlan and colleagues (39) involving 62 patients with a BMI of 35 kg/m2 (severe obesity), the pairwise comparison of methods with liver biopsy revealed similar accuracy for significant fibrosis (2D-SWE vs. MRE, p = 0.431; 2D-SWE vs. VCTE, p = 0.317; and MRE vs. VCTE, p = 0.052) and for severe fibrosis (2D-SWE vs. MRE, p = 0.348; 2D-SWE vs. VCTE, p = 0.293; and MRE vs. VCTE, p = 0.059). The study concluded that all three methods have similar and very good accuracy for at least moderate fibrosis. In another study by Imajo et al. (40), comparing VCTE, 2D-SWE, and MRE in 231 MASLD patients with biopsy, the AUROC curves for the three methods did not significantly differ for F1, F2, and F3 but were superior for F=4 in MRE vs. VCTE. This study showed that the distance from the liver capsule to the skin and the IQR/median value were correlated with the accuracy of assessments by 2D-SWE. Lastly, in a third study (41) comparing MRE with 2D-SWE in 100 patients with the same pathology and undergoing liver biopsy, with a BMI of 31.6 kg/m2 (obese patients), there was a significant difference between methods for F1, F2 (in favor of MRE) but not for F3 and F4, where the AUROCs were 0.95 vs. 0.85 and 0.92 vs. 0.91, respectively. The study concluded that SWE and MRE do not significantly differ in performance for severe fibrosis and cirrhosis diagnosis.

Similar comparisons have been made in several published meta-analyses. In one meta-analysis (42), where biological scores (FIB-4, BARD, NAFLD Fibrosis Score) were compared with VCTE, SWE, and MRE in a cohort of 13,046 patients, AUROC curves of 0.88 and 0.85 were calculated for VCTE with M and XL probes, 0.95 for SWE, and 0.96 for MRE (these values were significantly higher than biological scores), concluding that elastographic methods outperform biological scores and that SWE and MRE have the highest accuracy among elastographic methods. In another meta-analysis (43), analyzing 30 studies comparing VCTE, ARFI methods, and MRE, AUROC curves of 0.82 were found for VCTE, 0.90 for ARFI technology, and 0.93 for MRE. In a recent meta-analysis (44) comparing VCTE with pSWE, 2D-SWE, and MRE in a cohort of 14,609 patients with fatty liver (from 82 studies), AUROC curves for significant fibrosis were 0.83 for VCTE, 0.86 for pSWE, 0.75 for 2D-SWE, and 0.91 for MRE. For severe fibrosis diagnosis, the AUROCs were 0.85, 0.89, 0.72, and 0.92, and for liver cirrhosis, the AUROCs were 0.89, 0.90, 0.88, and 0.90. The meta-analysis concluded that all these elastographic methods have a good practical value for evaluating severe fibrosis and cirrhosis.

After reviewing several comparative studies and meta-analyses, all demonstrating good to very good accuracy of elastographic methods for diagnosing significant fibrosis, severe fibrosis, and cirrhosis, we can conclude that elastographic methods can be confidently used in the non-invasive evaluation of fibrosis in patients with chronic liver diseases of various etiologies. The choice of elastographic technique used in different centres depends on the technical capabilities of the unit, the experience of the elastography centre, and the preference of the performing physician. With the introduction of the new concept of compensated advanced liver disease (cACLD) in the Baveno Consensus 6 (and maintained in Baveno Consensus 7) (45,46), several important fibrosis cut-offs are present in clinical practice, such as the "Rule of 5" for VCTE and the "Rule of 4" for ARFI methods (45,46).

References

1. Dietrich C, Bamber J, Berzigotti A, Bota S, Cantisani V, Castera L, et al. EFSUMB guidelines and recommendations on the clinical use of liver ultrasound elastography, update 2017 (long version). Ultraschall in der Medizin - European Journal of Ultrasound. 2017 Apr 13;38(04).
2. Bota S, Sporea I, Peck-Radosavljevic M, Sirli R, Tanaka H, Iijima H, et al. The influence of aminotransferase levels on liver stiffness assessed by acoustic radiation force impulse elastography: A retrospective multicentre study. Digestive and Liver Disease. 2013 Sept;45(9):762–8.
3. Friedrich-Rust M, Nierhoff J, Lupsor M, Sporea I, Fierbinteanu-Braticevici C, Strobel D, et al. Performance of acoustic radiation force impulse imaging for the staging of liver fibrosis: A pooled meta-analysis. Journal of Viral Hepatitis. 2011 Oct 30;19(2).
4. Nierhoff J, Chávez Ortiz AA, Herrmann E, Zeuzem S, Friedrich-Rust M. The efficiency of acoustic radiation force impulse imaging for the staging of liver fibrosis: A meta-analysis. European Radiology. 2013 Jun 26;23(11):3040–53.
5. Hu X, Qiu L, Liu D, Qian L. Acoustic radiation force impulse (ARFI) elastography for non‐invasive evaluation of hepatic fibrosis in chronic hepatitis B and C patients: A systematic review and meta-analysis. Medical Ultrasonography. 2017 Jan 31;19(1):23.
6. Friedrich-Rust M, Wunder K, Kriener S, Sotoudeh F, Richter S, Bojunga J, et al. Liver fibrosis in viral hepatitis: Noninvasive assessment with acoustic radiation force impulse imaging versus transient elastography. Radiology. 2009 Aug;252(2):595–604.
7. Goertz R, Zopf Y, Jugl V, Heide R, Janson C, Strobel D, et al. Measurement of liver elasticity with acoustic radiation force impulse (ARFI) technology: An alternative noninvasive method for staging liver fibrosis in viral hepatitis. Ultraschall in der Medizin - European Journal of Ultrasound. 2010 Mar 19;31(02):151–5.
8. Rifai K, Cornberg J, Mederacke I, Bahr MJ, Wedemeyer H, Malinski P, et al. Clinical feasibility of liver elastography by Acoustic Radiation Force Impulse Imaging (ARFI). Digestive and Liver Disease. 2011 Jun;43(6):491–7.
9. Sporea I, Sirli R, Deleanu A, Popescu A, Focsa M, Danila M, et al. Acoustic radiation force impulse elastography as compared to transient elastography and liver biopsy in patients with chronic hepatopathies. Ultraschall in der Medizin - European Journal of Ultrasound. 2010 Jul 5;32(S 01):46–52.
10. Mare R, Sporea I, Lupuşoru R, Şirli R, Popescu A, Danila M, et al. The value of elastpq for the evaluation of liver stiffness in patients with B and C chronic hepatopathies. Ultrasonics. 2017 May;77:144–51.
11. Lee JE, Shin KS, Cho J-S, You SK, Min JH, Kim K-H, et al. Non-invasive assessment of liver fibrosis with ELASTPQ: Comparison with transient elastography and serologic fibrosis marker tests, and correlation with liver pathology results. Ultrasound in Medicine & Biology. 2017 Nov;43(11):2515–21.
12. Bauer D, Bucsics T, Chromy D, Simbrunner B, Jachs M, Schwabl P, et al. Point shear wave elastography by ELASTPQ accurately stages hepatic fibrosis in patients with NAFLD: A prospective, multicentric study. Zeitschrift für Gastroenterologie. 2019 May;
13. Valente G, Rinaldi L, Moggio G, Piai G. Point shear wave elastography and vibration controlled transient elastography for estimating liver fibrosis in a cohort of liver transplant patients. Eur Rev Med Pharmacol Sci. 2020 Oct;24(13):7357–65.

14. Foncea CG, Popescu A, Lupusoru R, Fofiu R, Sirli R, Danila M, et al. Comparative study between pSWE and 2D-SWE techniques integrated in the same ultrasound machine, with transient elastography as the reference method. Medical Ultrasonography. 2020 Feb 24;1(1):13.
15. Ferraioli G, Maiocchi L, Lissandrin R, Tinelli C, De Silvestri A, Filice C. Ruling-in and ruling-out significant fibrosis and cirrhosis in patients with chronic hepatitis C using a shear wave measurement method. Journal of Gastrointestinal and Liver Diseases. 2017 Jun 1;26(2):139–43.
16. Bota S, Herkner H, Sporea I, Salzl P, Sirli R, Neghina AM, et al. Meta-analysis: arfi elastography versus transient elastography for the evaluation of liver fibrosis. Liver International. 2013 Jul 16;33(8):1138–47.
17. Rizzo L, Calvaruso V, Cacopardo B, Alessi N, Attanasio M, Petta S, et al. Comparison of transient elastography and acoustic radiation force impulse for non-invasive staging of liver fibrosis in patients with chronic hepatitis C. American Journal of Gastroenterology. 2011 Dec;106(12):2112–20.
18. Ragazzo TG, Paranagua-Vezozzo D, Lima FR, de Campos Mazo DF, Pessoa MG, Oliveira CP, et al. Accuracy of transient elastography-fibroscan®, Acoustic Radiation Force Impulse (ARFI) imaging, the Enhanced Liver Fibrosis (ELF) test, APRI, and the FIB-4 index compared with liver biopsy in patients with chronic hepatitis C. Clinics. 2017;72(9):516–25.
19. Cassinotto C, Lapuyade B, Mouries A, Hiriart J-B, Vergniol J, Gaye D, et al. Non-invasive assessment of liver fibrosis with impulse elastography: Comparison of supersonic shear imaging with ARFI and FibroScan®. Journal of Hepatology. 2014 Sept;61(3):550–7.
20. Herrmann E, de Lédinghen V, Cassinotto C, Chu WC -W., Leung VY -F., Ferraioli G, et al. Assessment of biopsy-proven liver fibrosis by two-dimensional shear wave elastography: An individual patient data-based meta-analysis. Hepatology. 2017 Nov 15;67(1):260–72.
21. Bende F, Sporea I, Sirli R, Popescu A, Mare R, Miutescu B, et al. Performance of 2D-swe.ge for predicting different stages of liver fibrosis, using transient elastography as the reference method. Medical Ultrasonography. 2017 Apr 22;19(2):143.
22. Gao Y, Zheng J, Liang P, Tong M, Wang J, Wu C, et al. Liver fibrosis with two-dimensional us shear-wave elastography in participants with chronic hepatitis B: A prospective multicenter study. Radiology. 2018 Nov;289(2):407–15.
23. Lee ES, Lee JB, Park HR, Yoo J, Choi JI, Lee HW, et al. Shear wave liver elastography with a propagation map: Diagnostic Performance and inter-observer correlation for hepatic fibrosis in chronic hepatitis. Ultrasound in Medicine & Biology. 2017 Jul;43(7):1355–63.
24. Ronot M, Ferraioli G, Müller H-P, Friedrich-Rust M, Filice C, Vilgrain V, et al. Comparison of liver stiffness measurements by a 2D-shear wave technique and transient elastography: Results from a European Prospective multi-centre study. European Radiology. 2020 Sept 9;31(3):1578–87.
25. Sporea I, Bâldea V, Lupușoru R, Bende F, Mare R, Lazăr A, et al. Quantification of steatosis and fibrosis using a new system implemented in an ultrasound machine. Medical Ultrasonography. 2020 Sept 5;22(3):265.

26. Thiele M, Detlefsen S, Sevelsted Møller L, Madsen BS, Fuglsang Hansen J, Fialla AD, et al. Transient and 2-dimensional shear-wave elastography provide comparable assessment of alcoholic liver fibrosis and cirrhosis. Gastroenterology. 2016 Jan;150(1):123–33.
27. Mjelle AB, Fossdal G, Gilja OH, Vesterhus M. Liver elastography in primary sclerosing cholangitis patients using three different scanner systems. Ultrasound in Medicine & Biology. 2020 Aug;46(8):1854–64.
28. Garcovich M, Paratore M, Riccardi L, Zocco MA, Ainora ME, Mingrone G, et al. Correlation between a new point-shear wave elastography device (x+pswe) with liver histology and 2D-SWE (SSI) for liver stiffness quantification in chronic liver disease. Diagnostics. 2023 May 15;13(10):1743.
29. Lee SM, Ha HI, Lee IJ, Lee K, Lee JW, Park JW, et al. Comparison between two-dimensional and point shear wave elastography techniques in evaluating liver fibrosis using histological staging as the reference standard: A prospective pilot study. Diagnostics. 2023 May 7;13(9):1646.
30. Bâldea V, Sporea I, Lupușoru R, Bende F, Mare R, Popescu A, et al. Comparative study between the diagnostic performance of Point and 2-D shear-wave elastography for the non-invasive assessment of liver fibrosis in patients with chronic hepatitis C using transient elastography as reference. Ultrasound in Medicine & Biology. 2020 Nov;46(11):2979–88.
31. Bâldea V, Sporea I, Tudor A, Popescu A, Bende F, Șirli R. Virtual touch quantification using acoustic radiation force impulse imaging technology versus transient elastography for the noninvasive assessment of liver fibrosis in patients with chronic hepatitis B or C using liver biopsy as the gold standard. Journal of Gastrointestinal and Liver Diseases. 2020 Jun 3;29(2):181–90.
32. Bâldea V, Bende F, Popescu A, Șirli R, Sporea I. Comparative study between two 2D-shear waves elastography techniques for the non-invasive assessment of liver fibrosis in patients with chronic hepatitis C virus (HCV) infection. Medical Ultrasonography. 2021 Aug 11;23(3):257-264
33. Sporea I, Mare R, Lupusoru R, Popescu A, Danila M, Bende F, et al. Comparative study between four ultrasound shear waves elastographic methods for liver fibrosis assessment. Medical Ultrasonography. 2018 Aug 30;20(3):265.
34. Singh S, Venkatesh SK, Wang Z, Miller FH, Motosugi U, Low RN, et al. Diagnostic performance of Magnetic Resonance Elastography in staging liver fibrosis: A systematic review and meta-analysis of individual participant data. Clinical Gastroenterology and Hepatology. 2015 Mar;13(3). 440-451.e6
35. Liang Y, Li D. Magnetic resonance elastography in staging liver fibrosis in non-alcoholic fatty liver disease: A pooled analysis of the diagnostic accuracy. BMC Gastroenterology. 2020 Apr 6;20(1).89
36. Hsu C, Caussy C, Imajo K, Chen J, Singh S, Kaulback K, et al. Magnetic resonance vs transient elastography analysis of patients with nonalcoholic fatty liver disease: A systematic review and pooled analysis of individual participants. Clinical Gastroenterology and Hepatology. 2019 Mar;17(4). 630-637.e8.
37. Lefebvre T, Wartelle-Bladou C, Wong P, Sebastiani G, Giard J-M, Castel H, et al. Prospective comparison of transient, point shear wave, and magnetic resonance elastography for staging liver fibrosis. European Radiology. 2019 Jul 5;29(12):6477–88.

38. Ichikawa H, Yasuda E, Kumada T, Takeshima K, Ogawa S, Tsunekawa A, et al. Intra-individual comparison of liver stiffness measurements by magnetic resonance elastography and two-dimensional shear-wave elastography in 888 patients. Ultrasonography. 2023 Jan 1;42(1):65–77.
39. Furlan A, Tublin ME, Yu L, Chopra KB, Lippello A, Behari J. Comparison of 2D shear wave elastography, transient elastography, and mr elastography for the diagnosis of fibrosis in patients with nonalcoholic fatty liver disease. American Journal of Roentgenology. 2020 Jan;214(1). W20-W26
40. Imajo K, Honda Y, Kobayashi T, Nagai K, Ozaki A, Iwaki M, et al. Direct comparison of US and Mr Elastography for staging liver fibrosis in patients with nonalcoholic fatty liver disease. Clinical Gastroenterology and Hepatology. 2022 Apr;20(4). 908-917.e11
41. Zhang YN, Fowler KJ, Boehringer AS, Montes V, Schlein AN, Covarrubias Y, et al. Comparative diagnostic performance of ultrasound shear wave elastography and magnetic resonance elastography for classifying fibrosis stage in adults with biopsy-proven nonalcoholic fatty liver disease. European Radiology. 2021 Dec 2;32(4):2457–69.
42. Xiao G, Zhu S, Xiao X, Yan L, Yang J, Wu G. Comparison of laboratory tests, ultrasound, or magnetic resonance elastography to detect fibrosis in patients with nonalcoholic fatty liver disease: A meta-analysis. Hepatology. 2017 Sept 26;66(5):1486–501.
43. Besutti G, Valenti L, Ligabue G, Bassi MC, Pattacini P, Guaraldi G, et al. Accuracy of imaging methods for steatohepatitis diagnosis in non-alcoholic fatty liver disease patients: A systematic review. Liver International. 2019 May 8;39(8):1521–34.
44. Selvaraj EA, Mózes FE, Jayaswal AN, Zafarmand MH, Vali Y, Lee JA, et al. Diagnostic accuracy of elastography and magnetic resonance imaging in patients with NAFLD: A systematic review and meta-analysis. Journal of Hepatology. 2021 Oct;75(4):770–85.
45. de Franchis R. Expanding consensus in portal hypertension. Journal of Hepatology. 2015 Sept;63(3):743–52.
46. de Franchis R, Bosch J, Garcia-Tsao G, Reiberger T, Ripoll C, Abraldes JG, et al. Baveno VII – renewing consensus in portal hypertension. Journal of Hepatology. 2022 Apr;76(4):959–74.

5.1.d. Evaluation of Hepatic Steatosis

Ioan Sporea, Raluca Lupușoru

To define fatty liver, it is necessary to highlight the presence of fat loading in the liver. A loading of more than 5% of hepatocytes with fat defines fatty liver. The interest in evaluating liver fat also resides in the fact that hepatic steatosis is a factor leading to liver inflammation, an essential factor for subsequent secondary liver fibrosis (1).

The best practical non-invasive method for proving fatty liver loading is imaging methods. These can be ultrasonography, computed tomography, and nuclear magnetic resonance (NMR), respectively. Discussing each, ultrasonography is inexpensive and within the reach of many physicians, easy to perform or repeat. At the same time, ultrasound is increasingly used nowadays as a "Point of Care" method (POCUS), that is, it is performed in the consulting room, immediately after the clinical evaluation, a doctor in a clinical specialty (and not by imagist, as it happens in Anglo-Saxon countries). As an imaging alternative, computed tomography primarily has the disadvantage of irradiation, and MRI has the disadvantage of high cost and less accessibility.

The prevalence of fatty liver (hepatic steatosis) associated with metabolic dysfunction (MASLD - Metabolic dysfunction associated steatotic liver disease) is high globally, reaching up to 30% of the adult population (2) and is constantly increasing. At the same time, in certain categories of patients, such as those with type 2 diabetes, it reaches over 50% of individuals (3,4). Other categories of patients such as those with obesity or metabolic syndrome frequently have this associated pathology. Hence the need for the evaluation of this huge cohort of individuals to be done with the simplest, cheapest, and most accessible diagnostic means.

Non-alcoholic fatty liver was for a long time NAFLD (Non-Alcoholic Fatty Liver Disease), which relatively recently (2020) was changed to MAFLD (Metabolic Dysfunction Associated Fatty Liver Disease) (5) so that in 2023 it will be renamed ***MASLD*** (Metabolic Dysfunction Associated Steatotic Liver Disease) (6).

So, considering the huge number of individuals with fatty liver (over 2.5 billion people worldwide), distributed in countries with different economic conditions, we consider that a cheap and accessible means of diagnosis such as ultrasound is of great use to screen the population at risk for this pathology.

Using abdominal ultrasound, with two simple ultrasonic semiology signs, such as increased ultrasound brightness with posterior attenuation (Fig. 5.7.) and respectively the increase of the hepato-renal index (Fig. 5.8.), a good practical value is obtained for a diagnosis of hepatic steatosis. According to the intensity of these two signs, steatosis can be assessed semi-quantitatively as mild, moderate, and severe respectively (Fig 1,2). Various steatosis assessment scores have been proposed, the best-known of which is the Hamaguchi score (7).

This score is based on 4 ultrasound signs: increased hepatic ultrasound brightness, posterior attenuation, increased hepatorenal index, and obliteration of intrahepatic vessels and their narrowing, respectively.

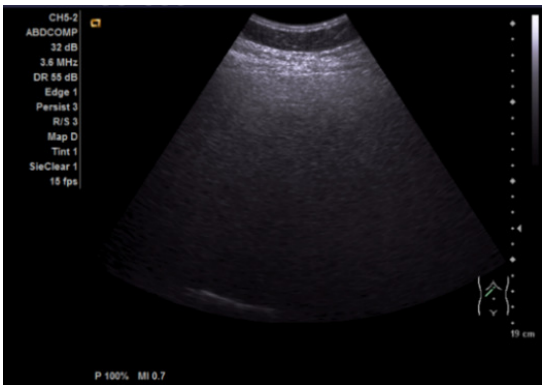

Fig.5.7 Ultrasonographic bright liver with attenuation

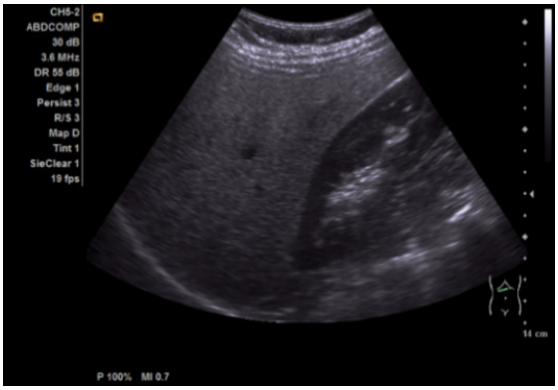

Fig. 5.8. Increased hepato-renal index

Liver ultrasound can estimate the severity of fatty liver load with relative accuracy, as demonstrated by two published studies and a meta-analysis. Thus, Palmentieri (8), who compared "ultrasound glow" with liver biopsy in a cohort of 235 patients, found this ultrasound sign in 67% of patients with hepatic steatosis of any degree and respectively in 89% of patients with severe steatosis. In the subgroup of patients with severe hepatic steatosis, ultrasound had a sensitivity of 91% with a specificity of 93%.

In another published study, Mathiesen (9), who also compared liver ultrasound with biopsy, in a group of 165 patients, demonstrated that among those with increased ultrasound brightness, 86.7% have at least moderate histological liver steatosis. In this study, for the detection of steatosis, liver ultrasound has a sensitivity of 90%, a specificity of 82%, a positive predictive value of 87%, and a negative predictive value also of 87%.

But perhaps the most convincing example of the value of liver ultrasound for the diagnosis of fatty liver is Hernaez's meta-analysis (10). Thus, analyzing 4,720 patients from 49 studies, the author compared ultrasound with liver biopsy and found that ultrasonography has a sensitivity of 84.8% (95% CI: 79.5-88.9%), with a specificity of 93.6% (95% CI: 87.2-97.0%) for the detection of moderate and severe hepatic steatosis (those with clinical relevance).

Some older or newer studies have shown that by using computer-assisted diagnosis (Computer Assisted CAD Diagnosis) (10) or, more recently, Artificial Intelligence (AI) (11), the sensitivity of ultrasound in the diagnosis of fatty liver can be increased (12, 13, 14).

Liver ultrasound being very widely spread in clinical practice, but also easy to perform and accessible everywhere, it also has the role of a "point of care" method for the semi-quantitative detection of the fat load of the liver, and the latest EASL Guide (European Association for the Study of the Liver) (15) believe that liver ultrasound will be the first-line method for the diagnosis of hepatic steatosis in clinical practice, regardless of all known limitations.

After reviewing these data regarding the value of transabdominal ultrasound in the diagnosis of fatty liver, the question can be raised as to whether we still need other more powerful ultrasound methods. And the answer is certainly positive because we want more objective, numerical methods for evaluating hepatic steatosis. One of the criticisms of conventional liver ultrasound in quantifying liver fat load is the interobserver (but also intraobserver) variability for this method (16,17).

This is where the idea of objective, numerical methods to quantify liver fat load came from. The first method introduced for the numerical quantification of liver fat load was the ***CAP module (Controlled Attenuation Parameter)*** integrated in FibroScan® (Echosens, Paris, France). Introduced in 2010, this module allows for the measurement of the attenuation of the ultrasound beam, which is directly proportional to the fat content of the liver. This measurement is performed simultaneously with the determination of liver hardness (stiffness) as a marker of fibrosis, which increases the value of the method for examining patients with fatty liver. CAP results are expressed in decibels/meter (dB/m) and range from 100 to 400 dB/m (18). If initially, this CAP module existed only for the M probe, later it was also integrated into the XL probe (for overweight and obese patients), increasing the feasibility of the method (Fig.5.9. and Fig.5.10). At the same time, several studies have demonstrated that for CAP the same cut-offs can be used for various degrees of steatosis, regardless of whether we use the M or XL probe (19,20).

Fig. 5.9 and Fig. 5.10. The FibroScan device, with the two probes M and XL and with the fibrosis (stiffness) module (the result in yellow on the screen) and CAP (the result in blue).

Over time, many publications have attempted to establish the accuracy of CAP for assessing liver fat load. Studies have compared this method with liver biopsy or more recently with MRI evaluation (PDFF - proton density fat fractions). The results are satisfactory for clinical practice, usually being between 80-90%. Thus, the CAP AUROC for the detection of

steatosis was between 0.823 (95% CI: 0.809-0.837) and respectively 0.865 (95% CI: 0.850-0.880), in a clinical trial and respectively in a meta-analysis, which used liver biopsy for comparison.

In another meta-analysis (23), the AUROC for CAP was 0.85 (95% CI: 0.81–0.88) for mild steatosis, 0.88 (95% CI: 0.85 -0.91) for moderate steatosis and 0.87 (95% CI: 0.84-0.90) for severe steatosis, respectively. All these studies were performed on patients with diffuse chronic liver diseases of various etiologies (usually including many chronic viral hepatitis).

Over the years, in the nearly 15 years of CAP use, multiple publications have appeared, each proposing their own cut-offs. These cut-offs are summarized in Table 5.I.

Table 5.I. CAP values in the most representative publications

Study	Comparative method	No. of patients	Cut-off values for each degree of steatosis (dB/m)		
			S≥1	S≥2	S≥3
Bao et al. (24)	MRI-PDFF	159		310	328
Baumeler et al. (25)	Liver biopsy	224	258.5	282.5	307.54
Chan et al. (26)	Liver biopsy	105	263	281	283
By Ledinghen et al. (27)	Liver biopsy	112	215	252	296
By Ledinghen et al. (28)	Liver biopsy	261	-	310	311
Eddowes et al. (20)	Liver biopsy	88	302	331	337
Ferraioli et al. (29)	Liver biopsy	114	219	296	
Gu et al. (30)	Liver biopsy	1183/3295/2835	273.5	288.5	309
Imajo et al. (31)	Liver biopsy	142	236	279	302
Kamali et al. (32)	Liver biopsy	77	237	259	291
Karlas et al. (33)	Liver biopsy	2735	248	268	280
Lupsor-Platon et al. (34)	Liver biopsy	201	226	285	194
Mikolasevic et al. (35)	Liver biopsy	179	304	311	345
Myers et al. (36)	Liver biopsy	153	283		
Naveau et al. (37)	Liver biopsy	123	298	303	326
Oeda et al. (38)	Liver biopsy	137	-	264	289
Park et al. (39)	Liver biopsy	104	261	305	312
Park et al. (40)	Liver biopsy	104	261	-	-

Petroff et al. (41)	Liver biopsy	2346	294	310	331
Sasso et al. (42)	Liver biopsy	615	222	233	290
Shalimar et al. (43)	Liver biopsy	219	285	331	348
Siddiqui et al. (44)	Liver biopsy	393	285	311	306
Somda et al. (45)	Liver biopsy	249	255	288	297
Steinmann et al. (46)	Liver biopsy	433	288		
Thiele et al. (47)	Liver biopsy	269	290	328	339
Trowell et al. (48)	Liver biopsy	217	278	301	
Zeng et al. (49)	Liver biopsy	173	244		
Zenovia et al. (50)	Liver biopsy	204	245	273.5	333

However, the most relevant studies for practice are probably those that establish the cut-offs for CAP in patients with fatty liver (MASLD). In this category of patients, the numerical quantification of the fat load is the most important clinically, for diagnosis and supervision. From this point of view, we consider the publication by Eddowes (20), who used liver biopsy to stratify patients, to be the most relevant. In this meta-analysis, a cut-off of 302 dB/m for mild steatosis, 331 dB/m for moderate steatosis, and 337 dB/m for severe steatosis was calculated (S1, S2, and S3). In Petroff's publication (41), cut-offs of 294 dB/m for mild steatosis, 310 dB/m for moderate steatosis, and 331 dB/m for severe steatosis were calculated (S1, S2, and S3). Based on this biopsy study in patients with MASLD and for the simplicity of memorizing the values, we propose to use in practice the cut-offs of 290 dB/m, 310 dB/m, and 330 dB/m (for S1, S2, and S3) at patients with MASLD.

Along with FibroScan, in recent years a similar system for quantifying fibrosis and steatosis has been developed, namely FibroTouch (iLivTouch) (Fig.5.11 and Fig.5.12), which uses the UAP module to quantify steatosis (Ultrasound Attenuation Parameter). The advantage of this system would be that it uses a single probe (and not M and XL respectively as in FibroScan) and that it allows for the ultrasound visualization of the liver, to establish the correct region to evaluate. Published studies for this system showed AUROCs for UAP of 0.88, 0.93, and 0.88 for mild, moderate, and severe steatosis and established cut-offs of 244, 269, and 296 dB/m for S1, S2 and S3 respectively (51). Other cut-offs can be found in Table 5.II. An advantage of this system would be that, more recently, it also evaluates inflammation, which is essential in differentiating simple hepatic steatosis from steatohepatitis (MASH - metabolic associated steatohepatitis) (52).

Fig. 5.11. and Fig. 5.12. iLivTOUCH (FibroTouch) with two forms of presentation, the fixed and the mobile version. Note the included ultrasound probe and the unique fibrosis/steatosis assessment probe.

Table 5.II. UAP values in the most representative publications

Study	Comparative method	No. of patients	Cut-off values for each degree of steatosis (dB/m)		
			S≥1	S≥2	S≥3
Deng et al. (53)	Liver biopsy	254	230.6	246.9	261.1
Hou et al. (54)	Standard ultrasound	3770	257.2	286.2	315
Mu et al. (55)	MRI-PDFF	275	259	274	295
Qiao et al. (56)	Liver biopsy	130	276	288	293
Qu et al. (52)	Liver biopsy	237	244	269	296
Yu et al. (57)	CAP	85	278	305	307
Zhu et al. (58)	Liver biopsy	497	295	314	324

Ultrasonographic quantification techniques of steatosis (Quantitative Ultrasound = QUS) have been increasingly developed. These modules are included in most modern ultrasound machines and allow for a quantification of the fat load of the liver with good precision. The physical principle behind these modules is represented by the measurement of the posterior attenuation of the ultrasound beam, the measurement of the "scatter" of the ultrasound beam ("backscatter") and respectively the measurement of the speed of ultrasound in the liver (" Speed of Sound"). Various ultrasound companies use one of these

techniques, or a combination thereof, to assess liver fat load. Usually, the evaluation technique is easy, quickly performed (under 5 minutes for all determinations), with high reproducibility and feasibility, and does not require most special system conditions (such as fasting condition or respiratory arrest during the evaluation, as in the determination of liver fibrosis). Generally, 10 determinations are made, and the device calculates the median of these values. The values are expressed in decibels/meter (dB/m) as in CAP, or dB/cm/MHz (Fig. 5.13-Fig. 5.28).

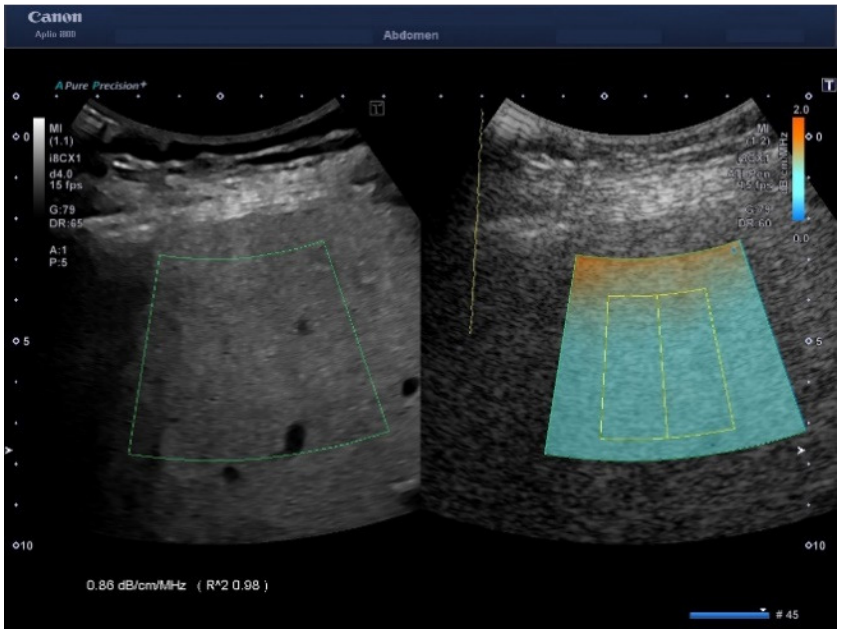

Fig. 5.13. Canon's ATI assessment with severe steatosis

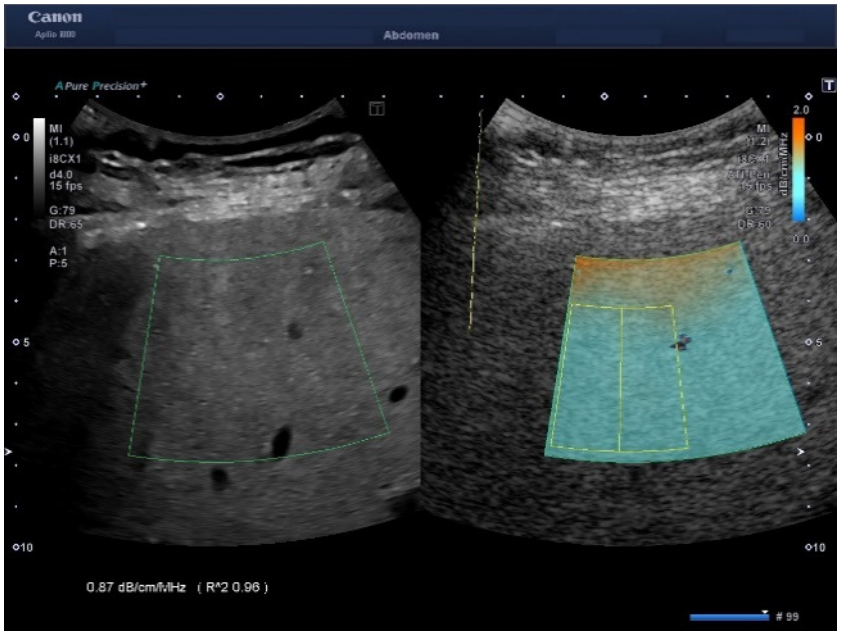

Fig.5.14. Canon's ATI evaluation with severe steatosis

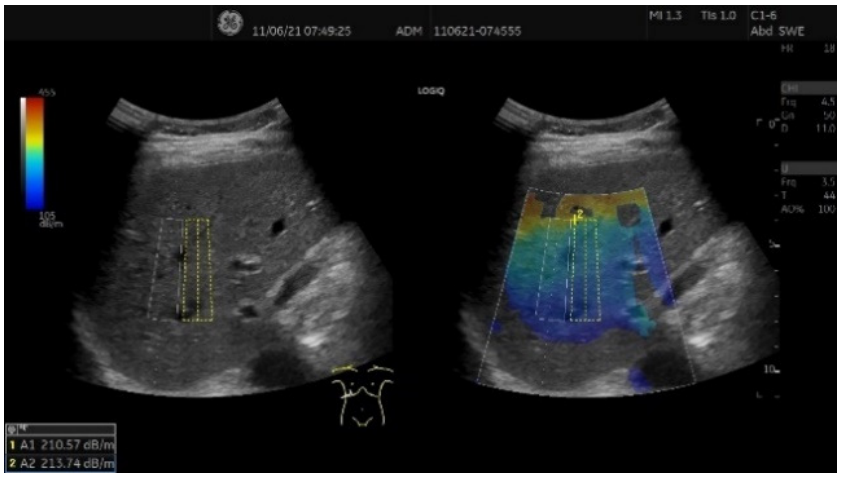

Fig.5.15. Normal UGAP, measured in dB /m (GE)

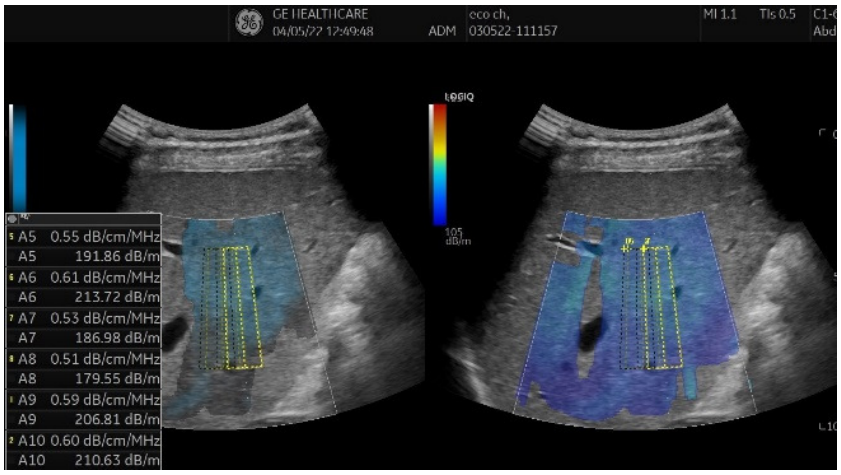

Fig. 5.16. Normal UGAP, measured in dB/cm/MHz (GE)

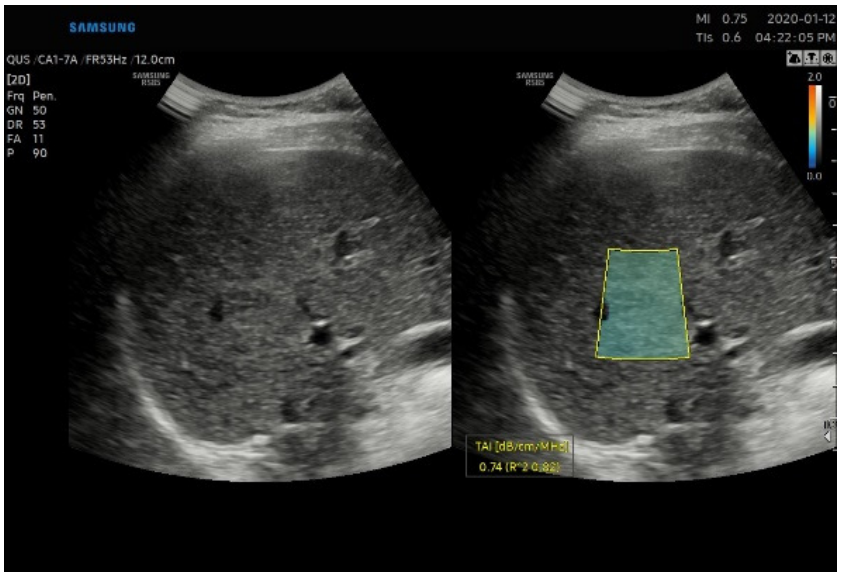

Fig. 5.17. TAI with normal values (Samsung)

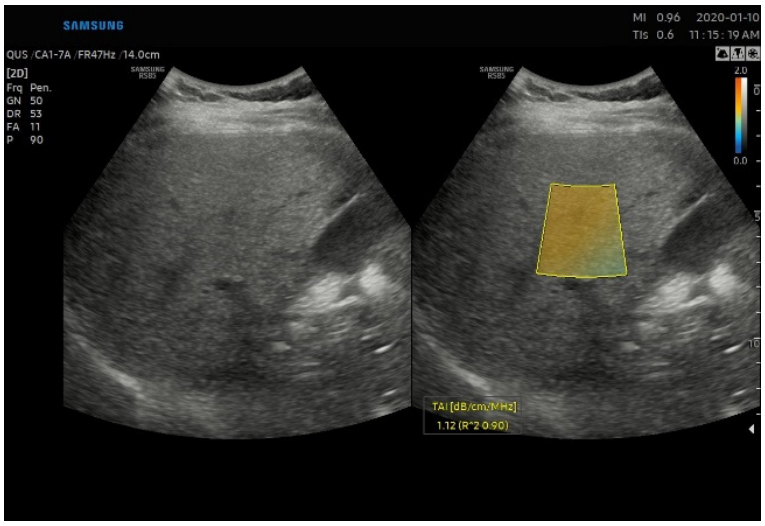

Fig. 5.18. TAI with severe steatosis (Samsung)

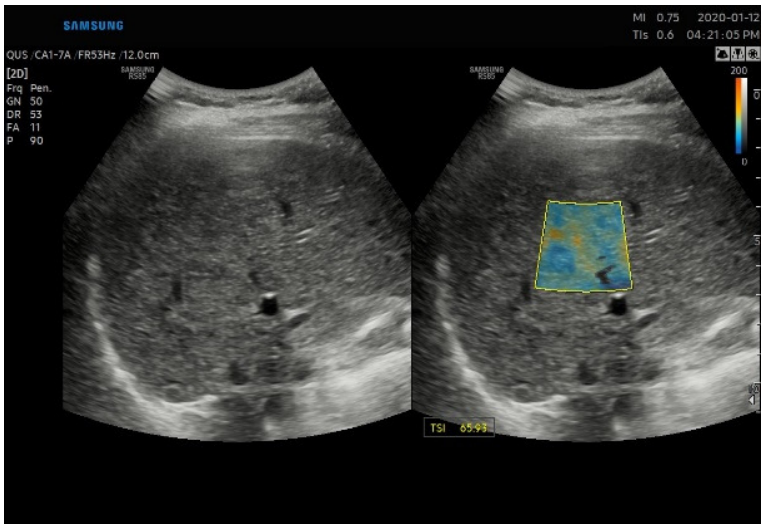

Fig. 5.19. TSI with normal values (Samsung)

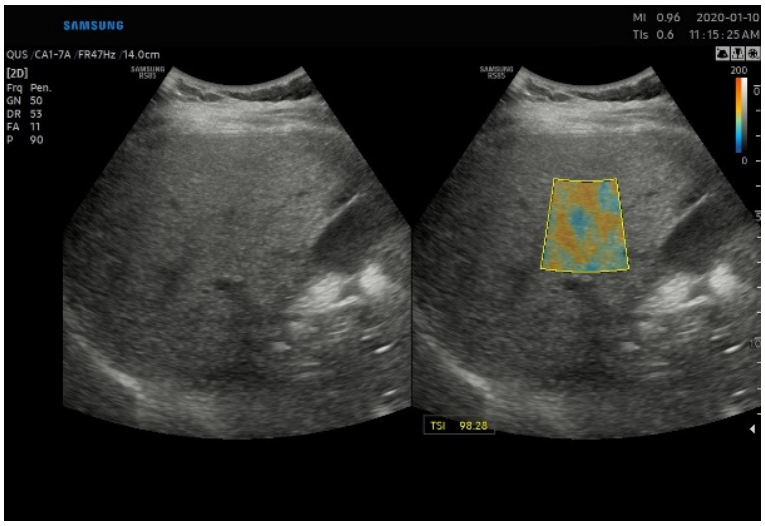

Fig. 5.20. TSI with severe steatosis (Samsung)

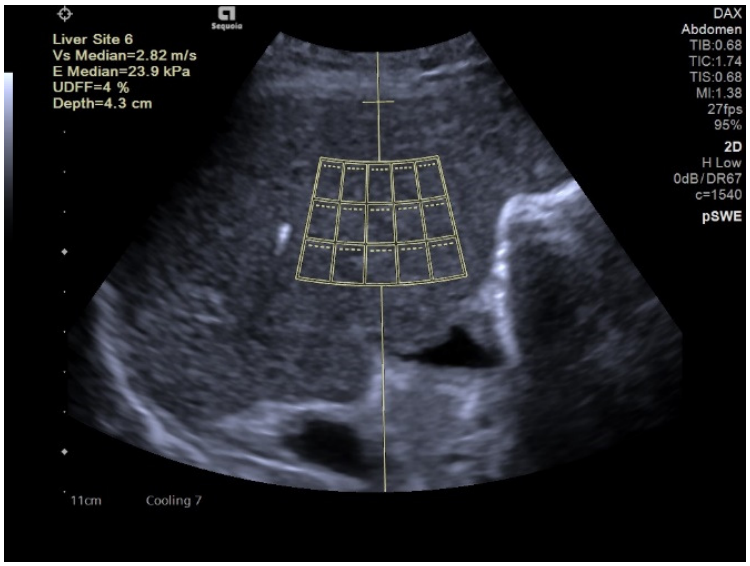

Fig. 5.21. Normal UDFF (4%) (Siemens)

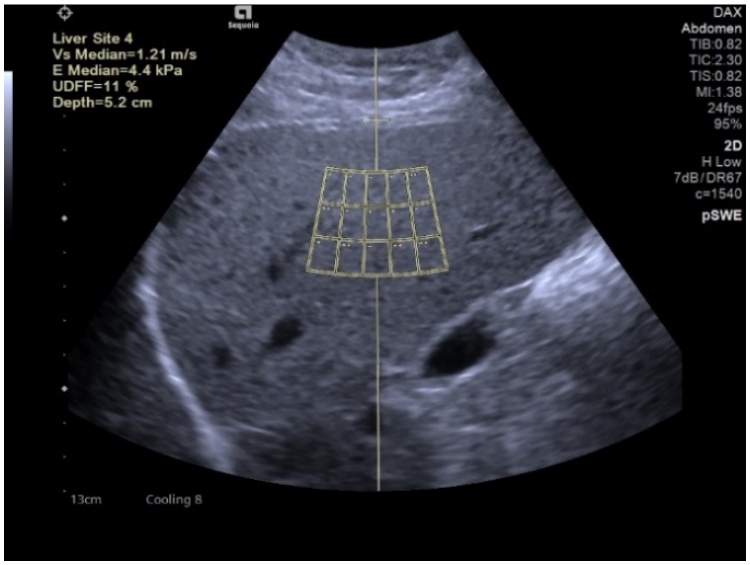

Fig. 5.22. UDFF with moderate steatosis (11%) Siemens

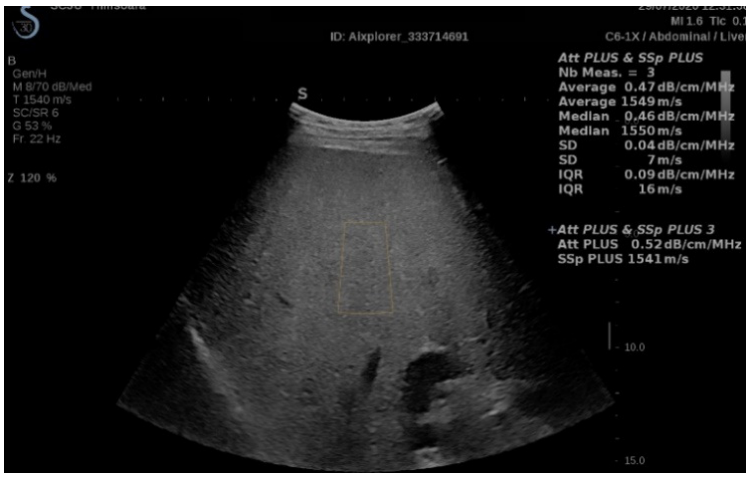

Fig. 5.23. Aixplorer Rating (Hologic)

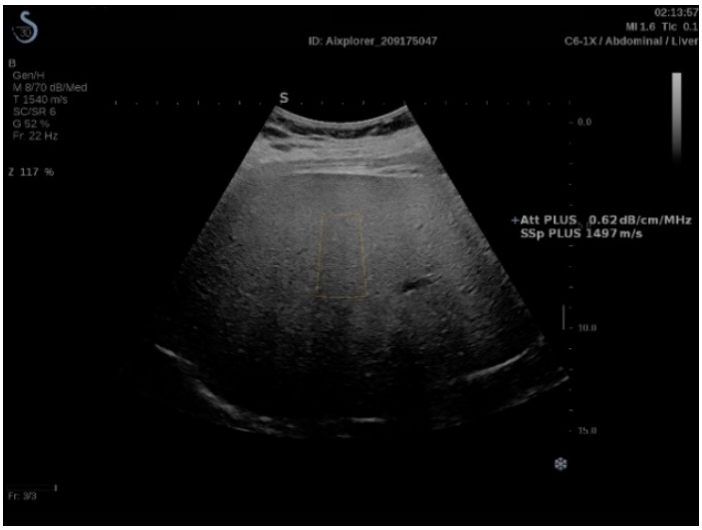

Fig. 5.24. Aixplorer (Hologic)- severe steatosis

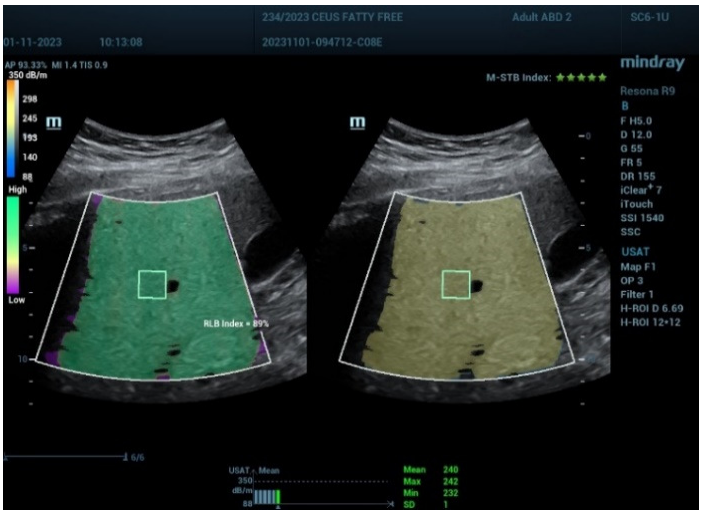

Fig. 5.25. Mindray System with RLB Index (Quality of acquisition)

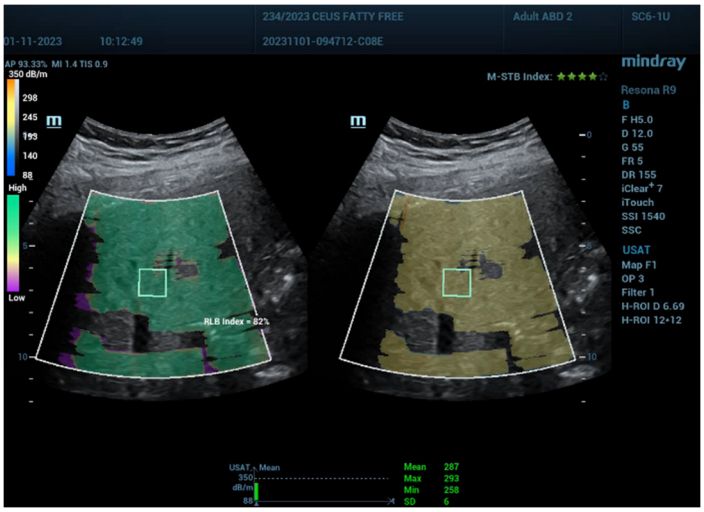

Fig. 5.26. Mindray system with USAT quantification

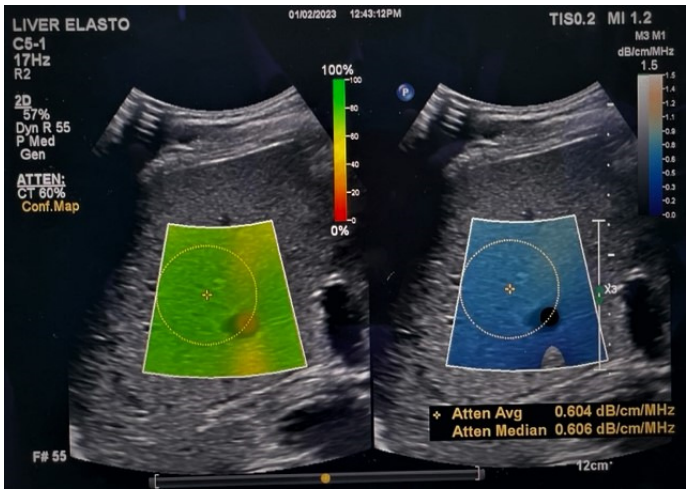

Fig. 5.27. Philips steatosis quantification system

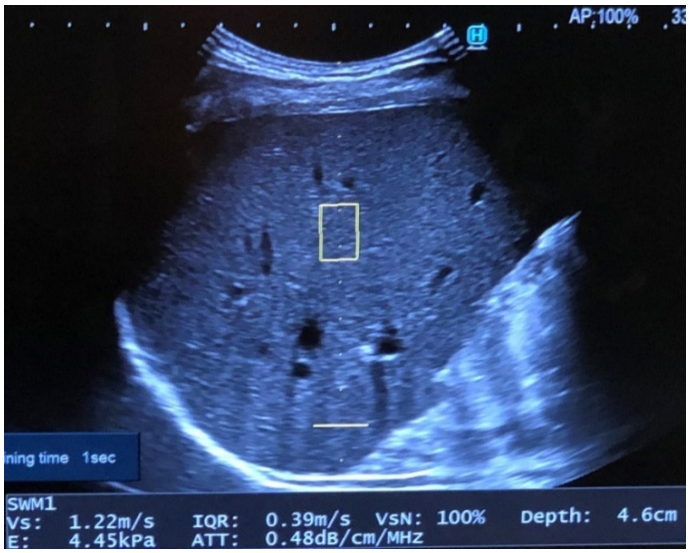

Fig. 5.28. ATT from Hitachi/ Fujifilm

All QUS images shown above show a simple way to quantify steatosis. Usually, an area is selected, away from the liver capsule, where the evaluation area is placed, and the system performs an analysis of the region, using either back attenuation, or "backscatter", or measuring the speed of sound (or a combination thereof), to assess the severity of steatosis. The first publications on the value of these steatosis quantification systems appeared more than 5 years ago and demonstrated very high accuracy, several of them comparing the method with FibroScan's CAP, demonstrating its superiority.

We would like to present only a few published studies on QUS to prove the practical value of these methods. Thus, the Canon system (***Attenuation Image)*** with the **ATI module** was compared with the PDFF method (from MRI) in a cohort of 15 healthy volunteers and 114 subjects with fatty liver and showed that between ATI and PDFF there is a good correlation (r=0.81), better than between PDFF and CAP (r=0.65) (59). A study by Bae, using liver biopsy as the reference method for assessing steatosis, in a group of 108 patients, calculated AUROC

curves ranging from 0.84 to 0.93, depending on the severity of steatosis (60). Another study by Tada used liver biopsy for comparison in a cohort of 148 patients and calculated AUROC curves of 0.85, 0.91, and 0.91 for mild, moderate, and severe steatosis, respectively (S1, S2, and S3). In patients with non-alcoholic fatty liver, the diagnostic value of ATI was 0.77, 0.88, and 0.86, respectively, for mild, moderate, and severe steatosis (61). In another recently published study (62), where ATI was compared with liver biopsy in a group of 76 patients, it was shown that ATI values increase with the severity of steatosis (0.60, 0.65, 0.83, and 0.90 dB/cm/MHz for S0, S1, S2, and S3). In this study, the AUROC of ATI to diagnose any degree of steatosis (S1-S3) was 0.85, and, for the diagnosis of at least moderate steatosis (S2-S3), it was 0.91. The above results plus others studied with ATI can be found in Table 5.III.

Table 5.III. Performance of ATI in the diagnosis of fatty LIVER

Study	No. of patients	Comparative method	Cut-off values for each degree of steatosis (dB/cm/MHz)			AUROCs		
			S≥1	S≥2	S≥3	S≥1	S≥2	S≥3
Bae et al. (60)	108	Liver biopsy	0.63-0.74			0.84-0.92		
Tada et al. (61)	148	Liver biopsy				0.85	0.91	0.91
	76	Liver biopsy	0.65	0.83	0.90			
Bao et al. (24)	159	MRI-PDFF	0.69		328			
Seo et al. (63)	105	Liver biopsy				0.93	0.94	0.87
Zhu et al. (64)	130	MRI-PDFF						
Ferraioli et al. (65)	72	MRI-PDFF	0.69			0.90		
Hsu et al. (66)	28	Liver biopsy				0.97	0.99	0.97
Kim et al. (67)	70	CAP	0.66					
Burgio et al. (68)	191 187	Liver biopsy MRI-PDFF				0.86 0.92	0.71 0.79	
Jang et al. (69)	57	Liver biopsy				0.80		
Bae et al. (70)	120	MRI-PDFF						0.88-0.94

Mindray developed the **USAT technique** (***Ultrasound Attenuation Analysis)*** which is also based on the attenuation coefficient. This technique automatically avoids structures that could affect the measurements, analyzing the values in the region of interest, the result being expressed as a median thereof. In one of the publications on this technique, 326 subjects with or without chronic liver diseases were analyzed, comparing USAT with CAP, with a Pearson coefficient, r=0.78 between methods, and the cut-offs for the three degrees of steatosis (S1,

S2, and S3) were 0.62, 0.66, and 0.72 dB/cm/MHz (71). Another recent study that compared all USAT with CAP, in 212 patients, showed a correlation with CAP of r=0.67, and the cut-offs for the various degrees of steatosis were 0.59, 0.73, and 0.87 dB/cm/MHz (72).

Several articles have been published regarding the quantification of steatosis by **UGAP (*Ultrasound-Guided Attenuation Parameter)*** from General Electric. Thus, in a study by Fujiwara (73), using liver biopsy as a reference method in patients with chronic liver disease, the calculated AUROCs for UGAP were 0.900, 0.953, and 0.959 in patients with S1, S2, and respectively S3. The median UGAP attenuation coefficient was 0.485, 0.560, 0.660, and 0.720 dB/cm/MHz in patients with S0, S1, S2, and S3, respectively. Compared with liver biopsy, this study showed significantly better results for UGAP compared to CAP. In another study comparing UGAP with PDFF (MRI) in a cohort of 126 patients with chronic liver disease, the correlation coefficient between PDFF and UGAP was 0.746 ($p<0.001$) and the AUROC for UGAP was 0.922, 0.874 and 0.892 for S1, S2 and S3, respectively (74).

A more recently published article, a Japanese multicentre study (75), compared PDFF with UGAP in a cohort of 1010 patients, found a correlation between the two methods of 0.768, and the AUROC for S1, S2, and S3 for UGAP was 0.91, 0.91 and 0.89, respectively. In a publication by our group (76), in a cohort of 179 subjects, in which UGAP was compared with CAP, UGAP values increased with the severity of steatosis (obtained by CAP), from S0: 198.3±25 .7 dB/m, at S1: 216.86±26.3 dB/m, at S2: 237.79±26.3 dB/m and respectively S3: 270.8±31.62 dB/m ($p< 0.001$). A good positive correlation was found between CAP and UGAP ($r=0.73$, $p<0.0001$). Ogino et al (77) compared UGAP and with PDFF (MRI) methods for 84 patients having a steatosis score ≥1, ≥2, and ≥3 (AUROC = 0.94, 0.95, and 0.88) and a correlation of r=0.88. The results are summarized in Table 5. IV.

Table 5.IV UGAP performance in the diagnosis of fatty LIVER

Study	No. of patients	Comparative Methods	Median values for each degree of steatosis (dB/m)			AUROCs		
			S≥1	S≥2	S≥3	S≥1	S≥2	S≥3
Fujiwara et al. (73)	163	Liver biopsy				0.90	0.95	0.95
Tada et al. (74)	136	MRI-PDFF				0.92	0.87	0.89
Imajo et al. (75)	1010	MRI-PDFF				0.91	0.91	0.89
Bende et al. (76)	179	CAP	216.8±26.3	237.7±26.3	270.8±31.6			
Ogino et al. (77)	84	Liver biopsy				0.94	0.94	0.88

As early as 2018, the first articles were published regarding the quantification of steatosis using the Hitachi (currently Fujifilm) system. The quantification module called **ATT** was used in a multicentre prospective study in a cohort of 351 patients with chronic liver diseases, being compared with a liver biopsy performed in the same session. The mean attenuation coefficient values for S0, S1, S2, and S3 were 0.55, 0.63, 0.69, and 0.85 dB/cm/MHz, and the attenuation coefficient was significantly correlated with the degree of histological fat loading (r=0.50, p<0.001). In this study, the AUROC for S1, S2, and S3 was 0.79, 0.87, and 0.96 (78).

To quantify fat loading, the module proposed by Samsung evaluates two parameters - **TAI** (***Tissue Attenuation Imaging)*** which aims to attenuate the ultrasound beam and **TSI** (***Tissue Scatter-distribution Imaging)*** which follows the dispersion of the ultrasound beam, along with the use of the hepato-renal index. One of the studies performed on this device compared these techniques with PDFF (MRI), in a cohort of 120 subjects with suspected fatty liver (79) and obtained a significant correlation between the methods of 0.659 for TAI and 0.727 for TSI, respectively (p<0.001 for both). For PDFF values of ≥5% and ≥10% fat loading, the AUROC for TAI was 0.861 and 0.835, and for TSI, the AUROC was higher, at 0.964 and 0.935. In another study conducted on 123 patients which compared this Samsung module with CAP, taking PDFF as the reference method (80), the AUROC curve calculated for the Samsung module was superior to assessments by CAP, 0.92 versus 0.79 (p = 0.03). Another study compared ATI, TAI, TSI, and CAP with PDFF, concluding that ATI and TAI correlated better than CAP with PDFF (r=0.58, r=0.71, r=0, 48), but instead, the areas under the ROC curve (AUROC) were similar between the methods: ATI - 0.88, TAI - 0.86, TSI - 0.87 and CAP - 0.86 (83).

More recently, Samsung has implemented the **USFF system (*UltraSound Fat Fraction)***, which, using artificial intelligence (convolutional neural network - CNN), quantifies the fat load in percentages (55). In a study of 173 patients comparing PDFF with USFF, a Pearson correlation of 0.86 was obtained between methods, and the AUROC for more than mild steatosis for USFF was 0.97 (superior AUROC- for TAI or TSI).

UDFF (*Ultrasound Density Fat Fraction*) from the Siemens company has the advantage of quantifying the fatty liver load in percentage (%). This system has the advantage that it is not necessary to memorize cut-offs for clinical practice. Although the experience with this system is quite new, two relevant articles have been published. Thus, in a cohort of 101 patients with suspected fatty liver in whom PDFF was performed, and in 90 of them liver biopsy, using posterior attenuation and dispersion for ultrasonic quantification of steatosis, a Pearson correlation coefficient of r=0 was found, 87 between UDFF and PDFF (84). In patients with PDFF values greater than 5% and 10%, respectively, the AUROC for UDFF was 0.97 and 0.95. In another study published in 2022 (57) that compared UDFF with PDFF in 56 subjects, a positive correlation between methods of 0.82 was found. The AUROC of UDFF was 90% for more than mild steatosis (F2, F3), and UDFF values greater than 5% had a sensitivity of 94.1% and a specificity of 63.6% for at least mild steatosis compared to PDFF.

For the Aixplorer system (Hologic) which uses the **speed of sound** evaluation in the liver**,** but also posterior attenuation, there are several publications. One compared PDFF with ultrasound speed (sound speed estimation - SSE) in the liver in 100 subjects (50 for the training cohort and 50 for the validation cohort) (85). In this study, several cut-off values for sound speed were calculated: 1.570 ± 0.026 mm/μs for S0, 1.568 ± 0.023 mm/μs for S1, 1.521 ± 0.031 for S2, and 1.514 ± 0.019 mm/μs for S3 respectively ($p<0.01$). Regarding the correlation of SSE with PDFF, it was 0.73 in the training cohort and 0.76 in the validation cohort, respectively.

In a study by our group, using the Aixplorer MACH 30 (86), in a cohort of 238 patients with fatty liver, this system was compared with CAP. Two parameters were used to quantify steatosis, sound speed (Sound Speed Plane- wave UltraSound - SSp.PLUS) and attenuation respectively (Attenuation Plane- wave UltraSound - Att. PLUS), and the CAP method was used as the reference method. The feasibility of both methods was over 95%, and sound speed correlated better than attenuation for quantifying hepatic steatosis (0.74 versus 0.45). The cut-off value obtained for SSp.PLUS for significant steatosis was 1524 m/s.

We have tried to review some of the publications related to the quantification of steatosis, using ultrasound devices on the market. There are other steatosis quantification modules implemented in other ultrasound systems, but not all have relevant publications to highlight their performance. Some newer, less well-known systems also allow steatosis to be quantified. Moreover, the ENDRA system should be mentioned that uses the TAEUS modality (Thermo Acoustic Enhanced Ultrasound) for the assessment of fatty liver load, it being approved for use in Europe and the United States.

For a long time, liver biopsy has been considered the ideal comparison method for non-invasive steatosis evaluation methods, however, in recent years, with the appearance of studies and several meta-analyses, **PDFF** (***Proton Density Fat Fraction)*** made with the help of MRI has become the new reference method for comparison. This is due to the significant decrease in the number of liver biopsies performed in the world, but also to the need for comparative studies to be published as quickly as possible (and performing a significant number of biopsies would greatly delay publication). A meta-analysis published in 2019 (87) comparing liver biopsy with PDFF-MRI found for this method an AUROC of 0.98, 0.91, and 0.90 for mild, moderate, and severe steatosis, respectively (S1, S2, and S3).

Several comparative studies between various non-invasive steatosis evaluation techniques have been conducted, which have attempted to demonstrate the practical value of each. Thus, in a study on 105 patients in which the reference method was PDFF (88), the evaluation of the speed of sound (SSE), then of the attenuation coefficient, of the hepato-renal index (all from MACH 30 Aixplorer) was performed in the same session, and respectively CAP. The AUROC for these methods was 0.73, 0.82, 0.79, and 0.91, respectively, and this study concluded that the hepatorenal index (a very simple index) appears to be the most useful. Another comparative study used histology from liver resection for comparison and preoperatively evaluated the liver by standard ultrasonography, ATI, CAP, CT, and PDFF in a group of 120 patients. For the detection of at least mild histological steatosis, the AUROC for

PDFF, CAP, CT, ATI, and standard ultrasound were: 0.946, 0.807, 0.829, 0.892, and 0.761, respectively. In pairwise comparison, there were no significant differences between methods, except for standard ultrasound, but for severe steatosis, all methods had good diagnostic value, with no significant differences (70).

Under these conditions, we believe that we currently have numerous imaging methods for evaluating the severity of hepatic steatosis in clinical practice, in patients with MASLD. But there are some comments to be made. Thus, computed tomography is irradiating and therefore not recommended, and MRI is less available and expensive. Therefore, ultrasound-based methods remain the the most cost-effective repetitive methods. QUS-type steatosis quantification methods, implemented in modern ultrasound machines, have the advantage of being able to be performed immediately after the standard ultrasound evaluation, have good feasibility, are quick to perform, repetitive, and with very good accuracy, becoming POCUS methods ("Point of Care" US). In addition, these QUS methods have started to be implemented in mid-range ultrasound machines, which makes them more and more accessible to a growing category of doctors.

References

1. Mooli RGR, Ramakrishnan SK. Liver Steatosis is a Driving Factor of Inflammation. Cell. Mol Gastroenterol Hepatol. 2022;13(4):1267-1270.
2. Younossi ZM, Golabi P, Paik JM, Henry A, Van Dongen C, Henry L. The global epidemiology of nonalcoholic fatty liver disease (NAFLD) and nonalcoholic steatohepatitis (NASH): a systematic review. Hepatology 2023, 77, 1335–1347,
3. Younossi Z, Golabi P, de Avila L, Paik J, Srishord M, et al. The global epidemiology of NAFLD and NASH in patients with type 2 diabetes: A systematic review and meta-analysis. J. Hepatol. 2019, 71, 793–801,
4. En Li Cho E, Ang CZ, Quek J, Fu CE, Lim LKE, et al. Global prevalence of non-alcoholic fatty liver disease in type 2 diabetes mellitus: an updated systematic review and meta-analysis. Gut 2023, 72, 2138–2148,
5. Eslam M, Sanyal A, George J. MAFLD: A Consensus-Driven Proposed Nomenclature for Metabolic Associated Fatty Liver Disease. Gastroenterology 2020, 158, 1999-2014.e1,.
6. Rinella M , Lazarus J, Ratziu V, Francque S, Sanyal A et al. A multisociety Delphi consensus statement on new fatty liver disease nomenclature. Hepatology 2023, 78, 1966–1986,.
7. Hamaguchi M, Kojima T, Itoh Y, Harano Y, Fujii K et al. The severity of ultrasonographic findings in nonalcoholic fatty liver disease reflects the metabolic syndrome and visceral fat accumulation. I have. J. Gastroenterol. 2007, 102, 2708–2715,
8. Palmentieri B, de Sio I, La Mura V, Masarone M, Vecchione R, et al. The role of bright liver echo pattern on ultrasound B-mode examination in the diagnosis of liver steatosis . Digestive and Liver Disease . 2006;38(7):485-489.
9. Mathiesen UL, Franzén LE, Aselius H, Resjö M, Jacobsson L, et al. Increased liver echogenicity at ultrasound examination reflected degree of steatosis but not of fibrosis in asymptomatic patients with mild / moderate liver abnormalities transaminases . Digestive and Liver Disease . 2002;34(7):516-522.

10. Hernaez R, Lazo M, Bonekamp S, Kamel I, Brancati F et al Diagnostic accuracy and reliability of ultrasonography for the detection of fatty liver: a meta-analysis. Hepatology 2011, 54, 1082–1090.
11. Mihăilescu DM, Gui V, Toma CI, Popescu A, Sporea I. Computer aided diagnosis method for steatosis rating in ultrasound images using random forests . Medical Ultrasonography . 2013;15(3):184-190.
12. Gaber A, Youness HA, Hamdy A, Abdelaal HM, Hassan AM. Automatic classification of fatty liver disease based on supervised learning and genetic algorithm , Applied Sciences 2022;12(1):521.
13. Rhyou SY, Yoo JC. Cascaded deep learning neural network for automated liver steatosis diagnosis using ultrasound images , Sensors 2021; 21 (16) :620
14. Constantinescu EC, Udristoiu AL, Udristoiu SC, Iacob AV, Gruionu LG, et al. Transfer learning with pretrained deep convolutional neural networks for the automatic assessment of liver steatosis in ultrasound images . Med. Ultrasound 2021; 23 (2): 135-139
15. Byra M, Styczynski G, Szmigielski C, Kalinowski P, Michałowski Ł, et al. Transfer learning with deep convolutional neural network for liver steatosis assessment in ultrasound images . International Journal of Computer Assisted Radiology and Surgery . 2018;13(12):1895-1903.
16. European Association for the Study of the Liver . Clinical Practice Guideline Panel; Chair : EASL Governing Board representatives : Panel members . EASL clinical practice guidelines on noninvasive tests for evaluation of liver disease severity and forecast – 2021 update. Journal of Hepatology . 2021;75(3):659-689.
17. Cengiz M , Sentürk S, Cetin B, Bayrak AH, Bilek SU. Sonography assessment of fatty liver : intraobserver and interobserver variability . Int J Clin Exp Med 2014; 7 : 5453-5460
18. Strauss S , Gavish E, Gottlieb P, Katsnelson L. Interobserver and intraobserver variability in the sonographic assessment of fatty liver AJR Am J Roentgenol 2007; 189 : W320-W323
19. Ferraioli, G. Quantitative assessment of liver steatosis using ultrasound controlled attenuation parameter (Echosens). J. Med. Ultrasound. 2021, 48, 489–495,
20. Eddowes PJ, Sasso M, Allison M, Tsochatzis E, Anstee QM, et al. Accuracy of FibroScan Controlled Attenuation Parameter and Liver Stiffness Measurement in Assessing Steatosis and Fibrosis in Patients With Nonalcoholic Fatty Liver Disease. Gastroenterology 2019, May;156(6):1717-1730.
21. Chan WK, Nik Mustapha NR, Mahadeva S, Wong VW-S, Cheng JY-K, Wong GL-H. Can the same controlled attenuation parameter cut-offs be used for M and XL probes for diagnosing hepatic steatosis? J. Gastroenterol. Hepatol. 2018, 33, 1787–1794.
22. Lupșor-Platon M, Feier D, Stefănescu H, Tamaș A, Botan E, et al. Diagnostic accuracy of controlled attenuation parameter measured by transient elastography for the non-invasive assessment of liver steatosis: A prospective study. J. Gastrointest. Liver Dis. 2015, 24, 35–42.
23. Karlas T, Petroff D, Sasso M, Fan JG, Mi YQ, et al. Individual patient data meta-analysis of controlled attenuation parameter (CAP) technology for assessing steatosis. J. Hepatol. 2017, 66, 1022–1030.

24. Bao J, Lv Y, Wang K, Wang Q, Chen Y, Dong Y, Zhu Y, Wang W. A Comparative Study of Ultrasound Attenuation Imaging, Controlled Attenuation Parameters, and Magnetic Resonance Spectroscopy for the Detection of Hepatic Steatosis. J Ultrasound Med. 2023 Jul;42(7):1481-1489.
25. Baumeler S, Jochum W, Neuweiler J, Bergamin J, and Semela D, "Controlled attenuation parameter for the assessment of liver steatosis in comparison with liver histology: a single- center real life experience," Swiss Medical Weekly, vol. 149, Article ID w20077, 2019.
26. Chan WK, Nik Mustapha NR, Mahadeva S. Controlled attenuation parameter for the detection and quantification of hepatic steatosis in nonalcoholic fatty liver disease. J Gastroenterol Hepatol. 2014;29(7):1470-6.
27. de Lédinghen V, Wong GL, Vergniol J, Chan HL, Hiriart JB, Chan AW, et al. Controlled attenuation parameter for the diagnosis of steatosis in non-alcoholic fatty liver disease. J Gastroenterol Hepatol. 2016 Apr;31(4):848-55.
28. De Ledinghen V, Vergniol J, Foucher J, Merrouche W, and Bail B, "Non-invasive diagnosis of liver steatosis using controlled attenuation parameter (CAP) and transient elastography," Liver International, vol. 32, no. 6, pp. 911–918, 2012.
29. Ferraioli G, Tinelli C, Lissandrin R, Zicchetti M, Dal Bello B, Filice G, Filice C. Controlled attenuation parameter for evaluating liver steatosis in chronic viral hepatitis. World J Gastroenterol. 2014 Jun 7;20(21):6626-31.
30. Gu Q, Cen L, Lai J, Zhang Z, Pan J, Zhao F, et al. A meta-analysis on the diagnostic performance of magnetic resonance imaging and transient elastography in nonalcoholic fatty liver disease. Eur J Clin Invest. 2021 Feb;51(2):e 13446.
31. Imajo K, Kessoku T, Honda Y, Tomeno W, Ogawa Y, Mawatari H, et al. Magnetic Resonance Imaging More Accurately Classifies Steatosis and Fibrosis in Patients With Nonalcoholic Fatty Liver Disease Than Transient Elastography. Gastroenterology. 2016 Mar;150(3):626-637.e7.
32. Kamali L, Adibi A, Ebrahimian S, Jafari F, Sharifi M. Diagnostic Performance of Ultrasonography in Detecting Fatty Liver Disease in Comparison with Fibroscan in People Suspected of Fatty Liver. Adv Biomed Res. 2019 Nov 27;8:69 .
33. Karlas T, Petroff D, Sasso M, Fan JG, Mi YQ, de Lédinghen Vet al. Individual patient data meta-analysis of controlled attenuation parameter (CAP) technology for assessing steatosis. J Hepatol. 2017 May;66(5):1022-1030.
34. Lupșor -Platon M, Feier D, Stefănescu H, Tamas A, Botan E, Sparchez Z, Maniu A, Badea R. Diagnostic accuracy of controlled attenuation parameter measured by transient elastography for the non-invasive assessment of liver steatosis: a prospective study. J Gastrointestinal Liver Dis. 2015 Mar;24(1):35-42.
35. Mikolasevic I, Domislovic V, Klapan M, Juric T, Lukic A, Krznaric-Zrnic I, et al. Accuracy of Controlled Attenuation Parameter and Liver Stiffness Measurement in Patients with Non-alcoholic Fatty Liver Disease. Ultrasound Med Biol. 2021 Mar;47(3):428-437.
36. Myers, RP, Pollett, A., Kirsch, R., Pomier- Layrargues , G., Beaton, M., Levstik , M., et al. Controlled Attenuation Parameter (CAP): A noninvasive method for the detection of hepatic steatosis based on transient elastography. Liver International, 2012 , 32 (6), 902-910.

37. Naveau S, Voican CS, Lebrun A, Gaillard M, Lamouri K, Njiké-Nakseu M, et al. Controlled attenuation parameter for diagnosing steatosis in bariatric surgery candidates with suspected nonalcoholic fatty liver disease. Eur J Gastroenterol Hepatol. 2017 Sep;29(9):1022-1030.
38. Oeda S, Takahashi H, Imajo K, Seko Y, Ogawa Y, Moriguchi M, et al. Accuracy of liver stiffness measurement and controlled attenuation parameter using FibroScan ® M/XL probes to diagnose liver fibrosis and steatosis in patients with nonalcoholic fatty liver disease: a multicenter prospective study. J Gastroenterol. 2020 Apr;55(4):428-440.
39. Park CC, Nguyen P, Hernandez C, Bettencourt R, Ramirez K, Fortney L, et al. Magnetic Resonance Elastography vs Transient Elastography in Detection of Fibrosis and Noninvasive Measurement of Steatosis in Patients With Biopsy-Proven Nonalcoholic Fatty Liver Disease. Gastroenterology. 2017 Feb;152(3):598-607.e2.
40. Park CC, Nguyen P, Hernandez C, Bettencourt R, Ramirez K, Fortney L, et al. Magnetic Resonance Elastography vs Transient Elastography in Detection of Fibrosis and Noninvasive Measurement of Steatosis in Patients With Biopsy-Proven Nonalcoholic Fatty Liver Disease. Gastroenterology. 2017 Feb;152(3):598-607.e2.
41. Petroff D, Blank V, Newsome PN, Shalimar, Voican CS, Thiele M, et al. Assessment of hepatic steatosis by controlled attenuation parameter using the M and XL probes: an individual patient data meta-analysis. Lancet Gastroenterol Hepatol. 2021 Mar;6(3):185-198.
42. Sasso M, Tengher -Barna I, Ziol M, Miette V, Fournier C, Sandrin L, et al. Novel controlled attenuation parameter for noninvasive assessment of steatosis using Fibroscan (®): validation in chronic hepatitis C. J Viral Hepat . 2012 Apr;19(4):244-53.
43. Shalimar, Kumar R, Rout G, Kumar R, Yadav R, Das P, Aggarwal S, et al. Body mass index-based controlled attenuation parameter cut-offs for assessment of hepatic steatosis in non-alcoholic fatty liver disease. Indian J Gastroenterol. 2020 Feb;39(1):32-41.
44. Siddiqui MS, Vuppalanchi R, Van Natta ML, Hallinan E, Kowdley KV, Abdelmalek M, et. Al. NASH Clinical Research Network. Vibration-Controlled Transient Elastography to Assess Fibrosis and Steatosis in Patients With Nonalcoholic Fatty Liver Disease. Clin Gastroenterol Hepatol. 2019 Jan;17(1):156-163.e2.
45. Somda S, Lebrun A, Tranchart H, Lamouri K, Prevot S, Njike- Nakseu M, et al. Adaptation of controlled attenuation parameter (CAP) measurement depth in morbidly obese patients addressed for bariatric surgery. PLoS One. 2019 May 24;14(5):e 0217093.
46. Steinmann S, Hartl J, Weidemann S, Füssel K, Kroll C, Sebode M, Lohse AW, Schramm C. Accuracy of controlled attenuation parameter measurement for the detection of steatosis in autoimmune liver diseases. JHEP Rep. 2023 Aug 29;5(12):100898.
47. Thiele M, Rausch V, Fluhr G, Kjærgaard M, Piecha F, Mueller J, et al. Controlled attenuation parameter and alcoholic hepatic steatosis: Diagnostic accuracy and role of alcohol detoxification. J Hepatol. 2018 May;68(5):1025-1032.
48. Trowell J, Alukal J, Zhang T, Liu L, Maheshwari A, Yoo HY, Thuluvath PJ. How Good Are Controlled Attenuation Parameter Scores from Fibroscan to Assess Steatosis, NASH, and Fibrosis? Dig Dis Sci. 2021 Apr;66(4):1297-1305.

49. Zeng Q, Song Z, Zhao Y, Wu J, Wang L, Ye H, et al. Controlled attenuation parameter by vibration-controlled transient elastography for steatosis assessment in members of the public undergoing regular health checkups with reference to magnetic resonance imaging-based proton density fat fraction. Hepatol Res. 2020 May;50(5):578-587.
50. Zenovia S, Stanciu C, Sfarti C, Singeap AM, Cojocariu C, Girleanu I, et al. Vibration-Controlled Transient Elastography and Controlled Attenuation Parameter for the Diagnosis of Liver Steatosis and Fibrosis in Patients with Nonalcoholic Fatty Liver Disease. Diagnostics (Basel). 2021 Apr 27;11(5):787.
51. Shi KQ, Tang JZ, Zhu XL, Ying Li DW, Gao J, et al. Controlled attenuation parameter for the detection of steatosis severity in chronic liver disease: A meta-analysis of diagnostic accuracy. J. Gastroenterol. Hepatol. 2014, 29, 1149–1158.
52. Qu Y, Song YY, Chen CW, Fu QC, Shi JP, Xu Y, et al. Diagnostic Performance of FibroTouch Ultrasound Attenuation Parameter and Liver Stiffness Measurement in Assessing Hepatic Steatosis and Fibrosis in Patients With Nonalcoholic Fatty Liver Disease. Clin. Transl. Gastroenterol. 2021, 12, e00323,
53. Deng H, Wang CL, Lai J, Yu SL, Xie DY, Gao ZL. Noninvasive Diagnosis of Hepatic Steatosis Using Fat Attenuation Parameter Measured by FibroTouch and a New Algorithm in CHB Patients. Liver Mon. 2016 Jul 24;16(9):e 40263.
54. Hou MM, Yuan XW, Wang YQ, Zhang Y, Zhang SY, Yu SH, Nan YM. [Applied research of ultrasound attenuation parameter in the diagnosis of metabolic dysfunction-associated fatty liver disease]. Zhonghua Gan Zang Bing Za Zhi. 2022 Mar 20;30(3):290-296. Chinese.
55. Mu R, Xia YC, Zhu KY, Lu JY, Luo Q, Zhang L, et al. Diagnostic value of FibroTouch in identifying hepatic steatosis in NAFLD with MRI-PDFF as the reference standard. J Dig Dis. 2023 Dec;24(12):691-701.
56. Qiao J, Zhao W, Du JH, Zhang SY, Wang RQ, Nan YM. [Analysis of the clinical value of ultrasound attenuation parameters in evaluating liver steatosis degree in patients with chronic liver disease]. Zhonghua Gan Zang Bing Za Zhi. 2020 Oct 20;28(10):876-881.
57. Yu H, Liu H, Zhang J, Jia G, Yang L, Zhang Q, et al. Accuracy of FibroTouch in assessing liver steatosis and fibrosis in patients with metabolic-associated fatty liver disease combined with type 2 diabetes mellitus. Ann Palliat Med. 2021 Sep;10(9):9702-9714.
58. Zhu SH, Zheng KI, Hu DS, Gao F, Rios RS, Li G, et al. Optimal thresholds for ultrasound attenuation parameter in the evaluation of hepatic steatosis severity: evidence from a cohort of patients with biopsy-proven fatty liver disease. Eur J Gastroenterol Hepatol. 2021 Mar 1;33(3):430-435.
59. Ferraioli, G.; Maiocchi, L.; Raciti, MV; Tinelli, C.; De Silvestri, A.; Nichetti, M.; et al. Detection of Liver Steatosis With a Novel Ultrasound-Based Technique: A Pilot Study Using MRI-Derived Proton Density Fat Fraction as the Gold Standard. Clin. Transl. Gastroenterol. 2019, 10, e00081.
60. Bae, JS; Lee, DH; Lee, JY; Kim, H.; Yu, SJ; Lee, JH; et al. Assessment of hepatic steatosis by using attenuation imaging: a quantitative, easy-to-perform ultrasound technique. Eur. The radio. 2019, 29, 6499–6507.
61. Tada T, Iijima H, Kobayashi N, Yoshida M, Nishimura T, Kumada T, et al. Usefulness of Attenuation Imaging with an Ultrasound Scanner for the Evaluation of Hepatic Steatosis. Ultrasound Med Biol. 2019 Oct;45(10):2679-2687.

62. Welman CJ, Saunders J, Zelesco M, Abbott S, Boardman G, Ayonrinde OT. Hepatic steatosis: Ultrasound assessment using attenuation imaging (ATI) with liver biopsy correlation. J Med Imaging Radiation Oncol. 2023 Feb;67(1):45-53.
63. Seo JW, Kim YR, Jang JK, Kim SY, Cho YY, Lee ES, Lee DH. Transient elastography with controlled attenuation parameter versus two-dimensional shear wave elastography with attenuation imaging for the evaluation of hepatic steatosis and fibrosis in NAFLD. Ultrasonography. 2023 Jul;42(3):421-431.
64. Zhu Y, Yin H, Zhou D, Zhao Q, Wang K, Fan Y, Chen K, Han H, Xu H. A prospective comparison of three ultrasound-based techniques in quantitative diagnosis of hepatic steatosis in NAFLD. Abdomen Radiol (NY). 2024 Jan;49(1):81-92.
65. Ferraioli G, Maiocchi L, Savietto G, Tinelli C, Nichetti M, Rondanelli M, et al. Performance of the Attenuation Imaging Technology in the Detection of Liver Steatosis. J Ultrasound Med. 2021 Jul;40(7):1325-1332.
66. Hsu PK, Wu LS, Yen HH, Huang HP, Chen YY, Su PY, Su WW. Attenuation Imaging with Ultrasound as a Novel Evaluation Method for Liver Steatosis. J Clin Med. 2021 Mar 2;10(5):965.
67. Kim PH, Cho YA, Yoon HM, Bak B, Lee JS, Jung AY, Oh SH, Kim KM. Accuracy of attenuation imaging in the assessment of pediatric hepatic steatosis: correlation with the controlled attenuation parameter. Ultrasonography. 2022 Oct;41(4):761-769.
68. Dioguardi Burgio M, Castera L, Oufighou M, Rautou PE, Paradis V, Bedossa P, et al. QUID – NASH Investigators. Prospective Comparison of Attenuation Imaging and Controlled Attenuation Parameter for Liver Steatosis Diagnosis in Patients With Nonalcoholic Fatty Liver Disease and Type 2 Diabetes. Clin Gastroenterol Hepatol. 2023 Dec 10:S 1542-3565(23)00999-0.
69. Jang JK, Kim SY, Yoo IW, Cho YB, Kang HJ, Lee DH. Diagnostic performance of ultrasound attenuation imaging for assessing low-grade hepatic steatosis. than EUR The radio . 2022 Mar;32(3):2070-2077.
70. Bae JS, Lee DH, Suh KS, Kim H, Lee KB, Lee JY, Han JK. Noninvasive assessment of hepatic steatosis using a pathological reference standard: comparison of CT, MRI, and US-based techniques. Ultrasonography 2022 Apr;41(2):344-354.
71. Jiang M, Zhang X, Wu X, Xu Z, Pan J, He H, Luo Y, Chen J. The diagnostic value of novel ultrasound attenuation analysis in detecting liver steatosis identified by the controlled attenuation parameter: a diagnostic accuracy study. Ann Transl Med. 2023 Jan 31;11(2):38.
72. Wang M, Tang S, Li G, Huang Z, Mo S, Yang K, Chen J, Du B, Xu J, Ding Z, Dong F. Comparative study of ultrasound attenuation analysis and controlled attenuation parameter in the diagnosis and grading of liver steatosis in non-alcoholic fatty liver disease patients. BMC Gastroenterol. 2024 Feb 23;24(1):81
73. Fujiwara, Y.; Kuroda, H.; Abe, T.; Ishida, K.; Oguri, T.; Noguchi, S.; et al. The B-Mode Image-Guided Ultrasound Attenuation Parameter Accurately Detects Hepatic Steatosis in Chronic Liver Disease. Ultrasound Med. Biol. 2018, 44, 2223–2232.
74. Tada T , Kumada T Toyoda H , Kobayashi N , Son Y Ogres T Kamiyama N. Utility of Attenuation Coefficient Measurement Using an Ultrasound-Guided Attenuation Parameter for Evaluation of Hepatic Steatosis: Comparison With MRI-Determined Proton Density Fat Fraction. AJR Am J Roentgenol . 2019 Feb;212(2):332-341.

75. Imajo, K.; Toyoda, H.; Yasuda, S.; Suzuki, Y.; Sugimoto, K.; Kuroda, H.; et al. Utility of Ultrasound-Guided Attenuation Parameter for Grading Steatosis With Reference to MRI-PDFF in a Large Cohort. Clin. Gastroenterol. Hepatol. off Clin. Practically. J. Am. Gastroenterol. Assoc. 2022, 20, 2533-2541.e7.
76. Bende F, Sporea I, Sirli R, Baldea V, Lazar A, Lupușoru R, Fofiu R, Popescu A UGAP for the quantification of liver steatosis using CAP as the reference method. Med Ultrasound 2021; 23(1): 7-14
77. Ogino Y, Wakui N, Nagai H, Igarashi Y. The ultrasound-guided attenuation parameter is useful in quantification of hepatic steatosis in non-alcoholic fatty liver disease. JGH Open. 2021 Jul 16;5(8):947-952.
78. Tamaki N, Koizumi Y, Hirooka M, Yada N, Takada H, Nakashima O, Kudo M, Hiasa Y, Izumi N. Novel quantitative assessment system of liver steatosis using a newly developed attenuation measurement method. Hepatol Res. 2018 Sep;48(10):821-828.
79. Jeon, SK; Lee, JM; Joo, I.; Park, SJ Quantitative Ultrasound Radiofrequency Data Analysis for the Assessment of Hepatic Steatosis in Nonalcoholic Fatty Liver Disease Using Magnetic Resonance Imaging Proton Density Fat Fraction as the Reference Standard. Korean J. Radiol. 2021, 22, 1077–1086.
80. Jung, J.; Han, A.; Madamba, E.; Bettencourt, R.; Loomba, RR; Boehringer, AS; et al. Direct Comparison of Quantitative US versus Controlled Attenuation Parameter for Liver Fat Assessment Using MRI Proton Density Fat Fraction as the Reference Standard in Patients Suspected of Having NAFLD. Radiology 2022, 304, 75–82.
81. Jeon SK, Lee JM, Joo I, Yoon JH, Lee G. Two-dimensional Convolutional Neural Network Using Quantitative US for Noninvasive Assessment of Hepatic Steatosis in NAFLD. Radiology. 2023 Apr;307(1):e 221510.
82. Labyed Y, Milkowski A. Novel Method for Ultrasound-Derived Fat Fraction Using an Integrated Phantom. J Ultrasound Med. 2020 Dec;39(12):2427-2438.
83. Jeon SK, Lee JM, Cho SJ, Byun YH, Jee JH, Kang M. Development and validation of multivariable quantitative ultrasound for diagnosing hepatic steatosis. Science Rep. 2023 Sep 14;13(1):15235.
84. Dillman JR, Thapaliya S, Tkach JA, Trout AT. Quantification of Hepatic Steatosis by Ultrasound: Prospective Comparison With MRI Proton Density Fat Fraction as Reference Standard. AJR Am J Roentgenol . 2022 Nov;219(5):784-791.
85. Dioguardi Burgio M, Imbault M, Ronot M, Faccinetto A, Van Beers BE, Rautou PE, Castera L, Gennisson JL, Tanter M, Vilgrain V. Ultrasonic Adaptive Sound Speed Estimation for the Diagnosis and Quantification of Hepatic Steatosis: A Pilot Study. Ultrasound Med. 2019 Dec;40(6):722-733. English.
86. Popa A, Bende F, Şirli R, Popescu A, Bâldea V, Lupușoru R, et al. Quantification of Liver Fibrosis, Steatosis, and Viscosity Using Multiparametric Ultrasound in Patients with Non-Alcoholic Liver Disease : A "Real-Life" Cohort Study. Diagnostics (Basel). 2021 Apr 26;11(5):783.
87. Gu J , Liu S , Du S , Zhang Q , Xiao J , Dong Q , Xin Y . Diagnostic value of MRI-PDFF for hepatic steatosis in patients with non-alcoholic fatty liver disease: a meta-analysis. than EUR The radio . 2019 Jul;29(7):3564-3573.
88. Collin R, Magnin B, Gaillard C, Nicolas C, Abergel A, Buchard B. Prospective study comparing hepatic steatosis assessment by magnetic resonance imaging and four ultrasound methods in 105 successive patients. World J Gastroenterol. 2023 Jun 14;29(22):3548-3560.

5.1.e. Elastography in Portal Hypertension

Alina Popescu, Renata Bende

Portal hypertension (PH) is one of the most feared complications of liver cirrhosis and is diagnosed when the hepatic venous-portal gradient (HVPG) has a value greater than 5 mm Hg. Clinically significant portal hypertension (CSPH) is defined at values of HVPG> 10 mmHg (1).

Regardless of the etiology, liver cirrhosis is the most common cause of PH. In this case, the increase in pressure is due to structural changes in liver architecture that lead to distortion of the vascular bed. In addition to the structural component that contributes about 70% to the increase in portal pressure, there is also a dynamic component determined by the contraction of smooth muscle in the vascular walls and the activation of Ito stellate cells, a component that is responsible for 30% of the intrahepatic resistance of portal flow. Increased resistance to portal flow, along with compensatory mechanisms of increased splanchnic blood flow and hyperdynamic circulation maintain and worsen PH (2, 3).

The development of CSPH represents a crucial step in the natural history of patients with compensated advanced chronic liver disease (cACLD) and is accompanied by the occurrence of complications associated with PH, such as ascites or esophageal varices (EV). Variceal rupture occurs when the parietal tension exceeds the limit of wall elasticity, and generally occurs at a value of HVPG> 12 mmHg (4).

Taking these aspects into account, the assessment of PH status is recommended for all patients with advanced chronic liver disease, at the time of diagnosis, both for therapeutic management and for prognosis.

5.1.e.1. Diagnosis of Portal Hypertension. Invasive Techniques

Hepatic Venous Gradient (HVPG) Measurement

The measurement of HPVG is the method of choice for diagnosing PH and establishing its severity. However, it is an invasive method that involves catheterization with a balloon catheter of one of the hepatic veins, under ultrasound guidance, using the right jugular vein (or femoral vein, or antecubital vein) as an approach (5).

HVPG is calculated by subtracting free liver venous pressure (FHVP) from blocked liver venous pressure (WHVP) (HVPG = WHVP-FHVP). The median of three measures is considered the most accurate value for HVPG (6).

Based on these findings, HVPG is recommended for all patients with advanced chronic liver disease at the time of diagnosis for risk and prognosis assessment (7, 8). Moreover, HVPG

seems to be the ideal tool to assess the response to therapy of patients with CSPH, with the target being an HVPG value <12 mmHg, or a decrease of at least 20% compared to baseline (8, 9). Failure to meet these targets is the best independent predictor of bleeding or rebleeding (10), with a 2 to 4 times higher relative risk for non-responders to non-selective beta-blockers (11).

Despite its excellent diagnostic and prognostic value, HVPG is an invasive procedure, has low availability, increased costs, and is more difficult for patients to accept (12).

Upper Digestive Endoscopy

Upper digestive endoscopy is the method of choice for the objective diagnosis of esophageal and gastric varices and portal-hypertensive gastropathy. Although this is an invasive method, it is the only method that allows for the evaluation of specific characteristics of esophageal or gastric varices (their size, the presence of bleeding stigmas) that are directly associated with the risk of variceal bleeding (13).

However, given the high rate of endoscopies performed in patients with advanced chronic liver disease in whom varices at high risk of bleeding (HRV) are not detected, the cost-effectiveness of extensive screening is controversial.

The Baveno VI consensus (12) proposes the use of non-invasive methods as initial screening in order to stratify the risk, identifying with very good accuracy patients at low risk of having esophageal or gastric varices, which patients can avoid endoscopic screening.

5.1.e.2. Diagnosis of Portal Hypertension. Non-invasive Techniques

In recent years, the arsenal of tools available for PH assessment has been enriched by the introduction of numerous non-invasive markers, thus complementing traditional and invasive methods. Given the limited availability and invasiveness of these conventional techniques, there is a growing need for new, non-invasive and easily reproducible methods, especially in patients with newly diagnosed cACLD.

In such cases, initial screening with non-invasive markers is preferable, to determine the optimal time to perform endoscopy or other invasive procedures.

The arsenal of non-invasive techniques for predicting PH includes biological tests, biological scores or multiparametric scores, imaging techniques (B-mode ultrasound, Doppler ultrasound, computed tomography (CT), CT angiography, magnetic resonance imaging, MRI angiography, ultrasound-based elastography techniques, MRI elastography), up to prediction models based on artificial intelligence (13).

Among these, ultrasound-based elastography techniques have been intensively studied in recent years for the non-invasive evaluation of the mechanical properties of tissues,

providing quality and quantity information regarding the elastic properties of the interrogated tissue.

The interest in ultrasound-based elastography techniques lies in their many advantages: they are widely available, easily reproducible, cost-effective, and very well accepted by patients (14).

Although initially developed for non-invasive staging of fibrosis in chronic liver diseases, numerous studies have analyzed the performance of these methods for the non-invasive evaluation of PH by measuring liver and splenic stiffness, with promising results (15-23).

According to international guidelines (24, 25), elastography techniques can be classified into: strain elastography (mainly used for breast, thyroid and prostate) and shear wave elastography (SWE). The SWE technique uses an external pulse that generates shear waves inside the examined organ, and the speed of these waves is measured by ultrasound, being indicative of tissue stiffness (rigidity), in the case of the liver as a marker of fibrosis severity.

Depending on the type of external pulse applied and the technique for measuring the speed of the shear waves, SWE elastography is subdivided into: Vibration Controlled Transient Elastography (VCTE); Point SWE (pSWE), which uses Acoustic Radiation Force Impulse (ARFI) technology as a stimulus, and the speed of the shear waves is measured at a certain point; and real-time elastography, which includes 2D-SWE and 3D-SWE (also uses ARFI technology as a stimulus, and the speed of the shear waves is measured in an area of interest and at the same time a color elastogram is generated) (24, 25). It should be noted that the cut-off values proposed for different stages of fibrosis are system-specific.

5.1.e.3. Ultrasound-based Elastography Techniques. Hepatic Elastography.

Vibration Controlled Transient Elastography (VCTE)

It is the first elastography technique introduced for the evaluation of liver fibrosis, having the richest scientific support so far. The basic principle of VCTE is that the speed of wave propagation through a homogeneous tissue is directly proportional to its elasticity, which is correlated with the amount of liver fibrosis (26). The VCTE has a transducer that produces low-frequency (50 Hz) and low-amplitude vibrations, consequently generating shear waves that propagate to the liver. Their propagation rate is directly proportional to the stiffness of the tissue assessed (27). VCTE is a quantitative elastography technique, so the result is represented by a numerical value expressed in kilopascals (kPa). The values obtained are between 1.5 and 75 kPa, and normal values are considered to be below 5 kPa (29-31).

Numerous studies have demonstrated correlations between liver stiffness (LS) and the presence of EV (32, 33, 34-38), as well as between LS values and their severity/size

(32,35,37,39), therefore, the attention of subsequent research has been directed towards confirming LS as a predictor of PH.

Thus, one of the first and most important studies carried out regarding the LS value as a predictor of PH, concluded that a cut-off value of 13.6 kPa of LS predicted the presence of HVPG ≥10 mmHg with excellent accuracy (AUC-0.99, Se-97%), while for the prediction of HVPG≥12 mmHg, AUC was 0.92, with Se-94%, for a cut-off value of 17.6 kPa. These results confirmed that LS correlates very well with HVPG up to values of 10 mmHg, values above which the worsening of PH is more dependent on the increase in splanchnic flow, than on the flow resistance determined by LS (33), results later confirmed by another study in which LS predicted the presence of HVPG ≥10 mmHg with an AUC-0.945 (at a cut-off value of 21 kPa) (39).

A meta-analysis, carried out on 18 studies, concluded that LS assessed by VCTE has a very good accuracy in detecting CSPH (AUC-0.93). Subsequently, another meta-analysis showed a very good correlation between LSand HVPG, having a good diagnostic and predictive performance for the detection of CSPH (40). Furthermore, the Baveno VI consensus suggested that if the LS assessed with VCTE is <20 kPa and platelet count is >150x 10^9/L, upper digestive endoscopy could be avoided in patients with advanced liver disease, as the likelihood of having esophageal varices at high risk of bleeding is very low (<5%) when these criteria are met simultaneously (12).

On the other hand, the total number of endoscopies avoided by using these criteria was found to be relatively low, so, in another study published in 2017 (41), the Baveno VI criteria were extended and validated in additional cohorts. 499 patients with cACLD of various etiologies were evaluated to study the performance of different platelet and LS cut-off values to identify patients at very low risk (<5%) of having EV with high risk of bleeding (HRV). The newly established criteria (platelet count >110 $\times^{10.9}$ cells/L and LS<25 kPa) were validated in two additional cohorts in London (309 patients) and Barcelona (117 patients). Using these criteria, 40% of screening endoscopies could have been avoided (versus 21% with the Baveno VI criteria) with a 1.6% risk of missing HRV.

However, in the latest versions of the EASL and AASLD guidelines, a clear recommendation has not been made regarding the ideal LS cut-off value (20 or 25 kPa) to predict the risk of clinical decompensation.

In light of these inconsistencies, a meta-analysis that included 30 studies to assess the accuracy of the Baveno VI criteria (LS<20 kPa and platelet count >150 x 10^9) and the Extended Baveno criteria (LS<25 kPa and platelet count >110 x 109 cells/L) to identify HRV in patients with cACLD were published in 2019 (42), concluding that these criteria are very sensitive but not very specific for identifying patients with HRV.

More recently, the Baveno VII consensus (43) reiterates the idea that non-invasive tests are accurate enough to identify CSPH. Thus, LS≤15 kPa and a platelet value >150x109/L exclude CSPH (Se and NPV >90%) in patients with cACLD.

In patients with cACLD of viral and/or ethanolic etiology, as well as in non-obese patients (BMI <30 kg/m2) with MASH, LS≥25 kPa is sufficient to predict CSPH (Sp and PPV >90%). In this category of patients, using the previous model, the risk of CSPH can be predicted with very good accuracy. Thus, patients with LS between 20-25 kPa and a platelet value <150x109 /L or LS between 15-20 kPa and a platelet value <110x10^9 /L, have a 60% risk of having CSPH.

Shear-wave Elastography Techniques Using ARFI Technology.

Point Shear-wave Elastography (pSWE)

Point shear-waves elastography is an elastography technique based on ARFI technology, integrated into standard ultrasound systems, enabling direct visualization of the evaluated parenchyma. These methods allow for querying a specific region of the parenchyma with the help of a region of interest (ROI), which has a predetermined size depending on the ultrasonographic system. The most studied types of pSWE elastography were: Virtual Touch Tissue Quantification® (VTQ) implemented on Siemens systems and the ElastPQ® technique implemented by Philips. Subsequently, other manufacturers also implemented pSWE on their systems: Samsung, Hitachi and Esaote (44, 45).

Studies have shown that pSWE (VTQ) is a reliable technique for predicting liver cirrhosis even when liver biopsy has been used as a reference method. For cut-off values between 1.55 and 2 m/s, the AUC was 0.89-0.93 (46, 47-50). Several meta-analyses confirmed that pSWE is a useful method for the diagnosis of liver cirrhosis, with mean diagnostic accuracy values of 0.93 (51) and 0.91 (52), respectively, values similar to those obtained for VCTE (51, 53).

A study evaluating the performance of another pSWE technique (ElastPQ) for the diagnosis of liver cirrhosis demonstrated a good correlation between LS values and fibrosis stage (r=0.61) (54).

Regarding the LS performance evaluated with pSWE implemented on another ultrasound system (Samsung-Medison RS85), a very good diagnostic performance was also detected (AUC-0.95 for significant fibrosis and AUC-0.98 for cirrhosis) (55).

For the evaluation of PH, the most studied pSWE technique is VTQ, but the results are inhomogeneous between studies. One of the first studies carried out detected a cut-off value for the prediction of large esophageal varices of 2.25 m/s (AUC-0.596), results that are similar to those found in another study in which the AUC for the prediction of HRV was 0.58 (56).

Better results were obtained in a study that showed a good correlation (r=0.646; p < 0.001) between VTQ and HVPG measurements, with an AUC of 0.85 for the CSPH prediction (57).

In a South Korean study (58), LS assessed with VTQ had an AUC of 0.76 (cut-off value - 2.08 m/s) and 0.78 (cut-off value - 1.9 m/s), for the detection of esophageal varices of any grade and those at increased risk of bleeding, respectively.

Regarding the LS value assessed with the ElastPQ technique, for the prediction of PH, studies are more limited. A recent study showed that LS assessed with ElastPQ was positively and significantly correlated with portal pressure ($r = 0.482$, $p < 0.001$) (59).

Real-time Shear-waves Elastography (2D-SWE and 3D-SWE)

Real-time shear-wave (2D-SWE) elastography is an elastography technique based on ARFI technology, implemented on different ultrasound systems, which enables the real-time capture of the propagation speed of shear waves.

The advantage of this technique is that the elasticity of the interrogated tissue is displayed using a color-coded image superimposed on a B-mode image and, at the same time, a quantitative estimation of LS in a given region can be performed, the results being expressed in kPa or m/s (60). Studies have shown that for good feasibility, it is necessary to obtain a quality image in B mode, as well as to have an experienced operator (61,62).

Initially, the 2D-SWE technique was developed by Supersonic Imagine (France) (2D-SWE. SSI) and incorporated into the Aixplorer® system. Eventually, other companies developed similar techniques: General Electric (2D-SWE.GE), Canon, Philips (ElastQ), Samsung etc. (60).

Several studies have shown good accuracy of the 2D SWE.SSI technique for the prediction of significant fibrosis and liver cirrhosis in patients with cACLD of different etiologies (63, 64-67), however revealing very different cut-off values, depending on the etiology.

As for 2D-SWE.GE, less data is available. A study of 331 subjects (68) concluded that this technique has very good diagnostic accuracy for significant fibrosis (AUC-0.95) and cirrhosis (AUC-0.96), respectively. Similar results were obtained in an Italian study (69) that used liver biopsy as a reference method.

A recent study evaluated LS performance with a 2D-SWE technique from Samsung and established a cut-off value of 7.6 kPa (AUC-0.98) for the prediction of liver cirrhosis (55). Using ElastQ, Villani et al. (70) obtained an LS cut-off value of 12.65 kPa for the prediction of cirrhosis (AUC-0.89).

Regarding the LS performance assessed by 2D-SWE techniques for PH prediction, most of the published studies used the 2D-SWE.SSI technique.

Kim et al. (22) found a significant correlation between HVPG and LS values in patients with CSPH ($r=0.574$; $p<0.001$). For an LS cut-off value of 15.2 kPa, the AUC for the CSPH prediction was 0.819 (95% CI, 0.725–0.892). In another study (20), for an LS cut-off value of 15.4 kPa, the AUC for the CSPH prediction was 0.948.

A meta-analysis on 2D-SWE.SSI performance to identify CSPH was performed on 519 patients from seven centers. At a cut-off value of LS<14 kPa, CSPH was excluded with an accuracy of 85% (sAUC-0.88), while LS≥32 kPa was able to make a positive prediction of CSPH with an accuracy of 55% (sAUC—0.83). The authors concluded that LS values below 14 kPa can be used to exclude CSPH, however, LS values could not predict the presence of EV at increased risk of bleeding (71).

Fewer studies are available on the performance of 2D-SWE.GE for PH prediction. In a study in which LS was determined with the 2D-SWE.GE technique (72) a very good correlation between LS and HVPG was proven (r=0.704; p <0.0001). For a cut-off value of 11.3 kPa for LS, the performance to detect CSPH was very good (AUC-0.91).

Given the inconsistency of the results obtained regarding the cut-off values of LS, for both pSWE and 2D-SWE techniques, within the Liver Elasography Consensus of the American Society of Radiologists, a neutral approach called the "rule of four" (5, 9, 13, 17 kPa) was proposed. This approach has been established for viral etiologies and MASLD and can be interpreted as follows: LS≤5 kPa (1.3 m/sec) indicates, with a very high probability, a normal subject from the point of view of LS; LS≤9 kPa (1.7 m/sec), in the absence of clinical signs, excludes cACLD; values between 9 kPa (1.7 m/sec) and 13 kPa (2.1 m/sec) suggest cACLD, but require further testing for confirmation, and LS≥13 kPa (2.1 m/sec) is highly suggestive of cACLD. If LS≥17 kPa (2.4 m/sec), CSPH is likely (73).

5.1.e.4. Ultrasound-based Elastography Techniques. Splenic Elastography

The spleen is considered an important regulatory factor in order to maintain adequate portal hepatic flow. Splenomegaly in subjects with portal hypertension occurs through the interaction of several factors, both through congestion of the spleen and through hyperplasia and hyperactivation of splenic lymphoid tissue. Also, accelerating the processes of angiogenesis and fibrogenesis plays an important role. This process of accelerated fibrogenesis leads to increased spleen stiffness (hardness), which is why the assessment of spleen stiffness (SS) as a non-invasive marker for predicting portal hypertension and CSPH has attracted increasing interest (74). SS was evaluated by different ultrasound-based elastography techniques, both by VCTE and by ARFI (pSWE and 2D-SWE) techniques (24, 25, 75, 76).

Vibration Controlled Transient Elastography (VCTE)

In recent years, numerous studies have been oriented toward the evaluation of SS and its correlation with portal hypertension. Studies have demonstrated a definite and reproducible correlation between SS values measured with VCTE and the presence of PH. One of the first studies to evaluate SS (77) concluded that SS values are significantly elevated in patients with liver cirrhosis. Subsequently, another study proved that an SS with values greater than 46.4 kPa can predict the presence of esophageal varices in patients with liver cirrhosis,

with a diagnostic accuracy of 80.5% (AUC-0.78) (78). Also, using a prediction model that included both LS (≥ 19 kPa) and SS (≥ 55 kPa), the prediction accuracy increased to 88.5%.

Another prediction model, which combined SS with Baveno VI criteria, was useful to exclude the presence of HRV (79). Using this multiparametric model, a higher number of endoscopies could be avoided compared to using the Baveno VI criteria alone. The study was conducted on 498 patients and established a cut-off value ≤46 kPa to exclude the presence of HRV. Using this cut-off value or the Baveno VI criteria, 35.8% and 21.7% of the validation batch subjects, respectively, could have avoided upper digestive endoscopy with an HRV loss rate of less than 2% in both cases. When the two parameters were used simultaneously in a prediction model, an additional 22.5% of endoscopies could have been avoided, thus increasing the final percentage to 43.8%, with a very good prediction performance and an HRV failure rate below 5% (79).

Another important study evaluating the performance of SS measured with VCTE for PH prediction, was published by Colechia et al. (23) and concluded that SS is a useful non-invasive marker for predicting the presence of EV and CSPH. The AUC value for the EV prediction was 0.94 and 0.95 for the prediction of HVPG≥12 mm Hg. A more recent study published by Wang et al. (80) reiterates the results of previous studies that SS is a non-invasive marker with very good EV prediction accuracy. The study included 102 subjects with liver cirrhosis in whom SS was assessed using VCTE elastography. For a cut-off value of 45.5 kPa, SS had AUC-0.98 for the prediction of esophageal varices at increased risk of bleeding and AUC-0.92 for the prediction of variceal bleeding.

Most of the studies evaluating SS were performed using FibroScan® (RS@50 Hz), which allowed SS to be measured up to a maximum of 75 kPa, which may have underestimated the severity of EV. Finally, EchoSens has developed a new variant of FibroScan® (SSM@100 Hz) with a specific module for spleen assessment. After the emergence of this new variant of FibroScan® (SSM@100 Hz), in a study comparing the two techniques, valid SS measurements were obtained in a significantly higher proportion of patients using this technique compared to the previous technique (92.5% vs. 76.0%, p <0.001) (81).

The Baveno VII Consensus specifies that SS measured with VCTE can be used in patients with cACLD of viral etiology to exclude or confirm the presence of CSPH, using the following cut-off values: SS<21 kPa and SS>50 kPa, respectively. However, these cut-off values require additional validation (43).

Another important note regarding SS is that in patients who are not candidates for non-selective beta-blocker therapy and who, according to Baveno VI criteria, should undergo upper digestive endoscopy, they can avoid endoscopy, having a low risk of HRV, if SS ≤40 kPa (43).

Shear-wave Elastography Techniques Using ARFI Technology

Point Shear-wave Elastography (pSWE)

Multiple studies have evaluated SS performance determined with pSWE elastography techniques as a predictive marker of PH. Among the pSWE elastography techniques, the most studied and validated technique for the evaluation of SS is the VTQ technique.

In a study published by Rifai et al. (82), SS assessed with VTQ was found to be lower than LS for PH detection (AUC 0.68 vs. 0.90). Another study published by Vermehren et al. (83), proved that in the multivariate analysis, there was a stronger association between SS assessed with VTQ and PH, compared to LS, even though the prediction accuracy of the two markers was similar. Bota et al. (84) concluded that the SS assessed with VTQ had a very good predictive value for liver cirrhosis, but could not predict the presence and severity of EV. The same author formulated a multiparametric prediction model. In the univariate analysis, LS and SS assessed with VTQ, as well as the presence of ascites were independent predictors of HRV. Combining these parameters into a prediction score, this author obtained an HRV detection accuracy of 69.6% (AUC=0.72) (56).

Although data on the superiority of SS compared to LS are inconsistent in studies, in a meta-analysis that included 16 studies, it was concluded that SS has a superior predictive accuracy for PH. (85). Takuma et al. (86) used VTQ for the assessment of SS. The AUC for the prediction of HRV was between 0.92-0.94, depending on the etiology. Another study concluded that SS assessed with VTQ can predict the presence of HRV with an AUC of 0.97 (87).

There is not as much data on SS evaluation as other elastography techniques. A more recent study, conducted on 107 subjects in whom SS was determined with another pSWE technique (ElastPQ) using HVPG as a reference method, demonstrated a significant correlation between SS and portal pressure values ($r=0.489$, $p<0.001$). A diagnostic algorithm using SS<20kPa and a platelet count $\geq 150 \times 10^9$ /L was able to exclude CSPH with 92.9% accuracy (59).

Real-time Shear-waves Elastography (2D-SWE and 3D-SWE)

There are a smaller number of studies that have evaluated SS performance queried with a 2D-SWE technique as a predictor of portal hypertension. A study in 77 subjects in which SS was determined using 2D-SWE.SSI concluded that SS<35.8 kPa excluded the presence of HRV (AUC-0.85, NPV-91.3%) (88). In a study on a larger number of subjects, SS had very good predictive accuracy for predicting esophageal varices, regardless of grade (AUC-0.8) and HRV (AUC-0.78), respectively (89).

An interesting approach to predict CSPH by means of 2D-SWE.SSI was proposed by Jansen et al. (90), who formulated a sequential algorithm using LS and SS. The study included 158 patients with liver cirrhosis who also had measurements of HVPG.

First, LS was evaluated, if LS>38 kPa, 36/39 patients were correctly classified with CSPH. If LS<38 kPa, the next step was to measure SS. If LS<38 kPa and SS<27.9 kPa, 32/40 patients were correctly classified as having CSPH, and in the case of LS<38 kPa, but SS>27.9 kPa, 35/37 patients were correctly classified with CSPH. This algorithm had a sensitivity of 89.2% and a specificity of 91.4% for the diagnosis of CSPH (90).

Also a 2D-SWE technique, this time implemented on another ultrasound system (General Electric), was used to evaluate the performance of SS in HRV prediction and compared this technique with a pSWE technique (VTQ). Optimal cut-off value of SS assessed with 2D-SWE.GE for the HRV prediction was 13.2 kPa (AUC–0.84), while for the VTQ it was 2.91 m/s (AUC–0.90), with no significant difference in performance between the two techniques (p = 0.1606) (91).

Several meta-analyses have been published regarding the usefulness of SS in PH prediction and concluded that there is a good correlation between SS and HVPG (r=0.72) (92), with SS having good accuracy in HRV detection as well (93).

5.1.e.5. Nuclear Magnetic Resonance Elastography (MRI-Elastography)

A number of meta-analyses have been published regarding the accuracy of MRI elastography for the prediction of liver fibrosis, proving an accuracy of over 90% for the prediction of advanced fibrosis and cirrhosis (94–96).

In addition to its very good predictive value, MRI elastography has a number of notable advantages: it enables the evaluation of the entire liver parenchyma, the quantification of hepatic steatosis, and the identification of focal liver lesions. In addition, obesity does not influence the feasibility and accuracy of the method (97). The most important limitations, however, are related to increased costs and limited availability.

A preliminary study, conducted on 34 patients, evaluated the LS value determined by MRI-elastography for PH prediction, using HVPG as a reference method. LS values were weak, but significantly correlated with HVPG values (r = 0.478, p = 0.016). However, the accuracy of LS for predicting PH (AUC-0.809) and CSPH (0.742), respectively, was very good (98).

The SS determined by MRI-elastography was evaluated together with LS for the prediction of EV. SS values were significantly higher in EV patients, and in multivariate regression analysis, SS was an independent predictor for the presence of EV. In contrast, no association was detected between LS values and the presence of EV. For a cut-off value of 9.53 a SS, the predictive accuracy for EV was very good (AUC-0.853, Se-84.4% and Sp- 73.7%) (99).

These results were confirmed by two other studies (100, 101). More recently, in a meta-analysis that included 14 studies, SS and LS were assessed as predictors of PH. The summarized and adjusted values of Se, Sp and AUC were 83%, 80% and 0.88 respectively for LS, while for SS they were 79%, 90% and 0.92 respectively (102). The conclusion of this meta-

analysis was that SS is slightly more specific and has a higher accuracy compared to LS for PH prediction.

***In conclusion*,** Elastography, whether hepatic, splenic, ultrasound-based, or MRI is a useful tool for stratifying the risk of portal hypertension in patients with advanced liver disease. The Baveno VI and Baveno VII Consensus, as well as the American Radiologists' Consensus, state this.

References

1. Procopet B, Berzigotti A. Diagnosis of cirrhosis and portal hypertension: imaging, noninvasive markers of fibrosis and liver biopsy. Gastroenterol Rep (Oxf). 2017 May; 5(2): 79–89.
2. Iwakiri Y. Pathophysiology of Portal Hypertension. Clin Liver Dis. 2014 May; 18(2): 281–291.
3. García-Pagán J.C, Gracia-Sancho J, Bosch J. Functional aspects on the pathophysiology of portal hypertension in cirrhosis. J Hepatol 2012 Aug; 57(2):458-61.
4. Dib N, Oberti F, Calès P. Current management of the complications of portal hypertension: variceal bleeding and ascites. CMAJ. 2006 May 9; 174(10): 1433–1443.
5. Perello A, Escorsell A, Bru C, Gilabert R, Moitinho E, Garcia-Pagan JC, , J Bosch. Wedged hepatic venous pressure adequately reflects portal pressure in hepatitis C virus-related cirrhosis. Hepatology. 1999; 30(6):1393-1397
6. Bosch J, Abraldes JG, Berzigotti A, Garcia-Pagan JC. The clinical use of HVPG measurements in chronic liver disease. Nature Reviews. Gastroenterology & Hepatology. 2009; 6(10):573-582
7. Groszmann RJ, Garcia-Tsao G, Bosch J, Grace ND, Burroughs AK, Planas R, Escorsell A, Garcia-Pagan JC, Patch D, Matloff DS. Beta-blockers to prevent gastroesophageal varices in patients with cirrhosis. N Engl J Med. 2005; 353:2254– 2261.
8. Ripoll C, Groszmann R, Garcia-Tsao G, Grace N, Burroughs A, Planas R, Escorsell A, Garcia-Pagan JC, Makuch R, Patch D. Hepatic venous pressure gradient predicts clinical decompensation in patients with compensated cirrhosis. Gastroenterology. 2007; 133:481–488.
9. Garcia-Tsao G, Groszmann RJ, Fisher RL, Conn HO, Atterbury CE, Glickman M. Portal pressure, presence of gastroesophageal varices and variceal bleeding. Hepatology 1985; 5:419–424.
10. Boyer TD, Haskal JZ, American Association for the Study of Liver Diseases practice guidelines. The role of transjugular intrahepatic portosystemic shunt creation in the management of portal hypertension. Journal of Vascular and Interventional Radiology 2005, vol. 16, no. 5, pp. 615–629.
11. Boyer TS, Z. J. Haskal, and American Association for the Study of Liver Diseases. The role of transjugular intrahepatic portosystemic shunt (TIPS) in the management of portal hypertension: update. Hepatology 2010, vol. 51, no. 1, pp. 306–306.
12. De Franchis R, Baveno T. Faculty. Expanding consensus in portal hypertension: report of the Baveno VI consensus workshop: stratifying risk and individualizing care for portal hypertension. J Hepatol. 2015; 63(3): 743-752.

13. Ravaioli F, Montagnani M , Lisotti A , Festi D , Mazzella G,Azzaroli F. Noninvasive Assessment of Portal Hypertension in Advanced Chronic Liver Disease: An Update. Gastroenterol Res Pract 2018 Jun 7; 2018:4202091
14. Sigrist R, Liau J, Ahmed El Kaffas, Chammas M.C., Willmann J.K. Ultrasound Elastography: Review of Techniques and Clinical Applications. Theranostics 2017; 7(5): 1303–1329.
15. Carrión JA, Navasa M, Bosch J, Bruguera M, Gilabert R, Forns X. Transient elastography for diagnosis of advanced fbrosis and portal hypertension in patients with 99 hepatitis C recurrence after liver transplantation. Liver Transpl. 2006; 12(12): 1791- 1798.
16. Karagiannakis DS, Voulgaris T, Siakavellas SI, Papatheodoridis GV, Vlachogiannakos J. Evaluation of portal hypertension in the cirrhotic patient: hepatic vein pressure and beyond. Scand J Gastroenterol. 2018; 53(10-11):1153-1164.
17. Castera L, Pinzani M, Bosch J. Non invasive evaluation of portal hypertension using transient elastography. J Hepatol. 2012; 56(3): 696-703.
18. Lemoine M, Katsahian S, Ziol M, Nahon P, Ganne-Carrie N, Kazemi F, GrandoLemaire V, Trinchet JC, Beaugrand M. Liver stifness measurement as a predictive tool of clinically signifcant portal hypertension in patients with compensated hepatitis C virus or alcoholrelated cirrhosis. Pharmacol Ther Food. 2008; 28(9): 1102-1110.
19. Yu JB, Xiong H, Yuan XC, Zhou AY. Liver Stiffness Detected by Shear Wave Elastography Predicts Esophageal Varices in Cirrhotic Patients. Ultrasound Q. 2019.
20. Procopet B, Berzigotti A, Abraldes JG, Turon F, Hernandez-Gea V, García-Pagán JC, Bosch J. Real-time shear-wave elastography: applicability, reliability and accuracy for clinically significant portal hypertension. J Hepatol. 2015; 62(5): 1068-1075.
21. Elkrief L, Rautou PE, Ronot M, Lambert S, Dioguardi Burgio M, Francoz C, Plessier A, Durand F, Valla D, Lebrec D, Vilgrain V, Castéra L. Prospective comparison of spleen and liver stiffness by using shear-wave and transient elastography for detection of portal hypertension in cirrhosis. Radiology 2015; 275(2): 589-598.
22. Kim TY, Jeong WK, Sohn JH, Kim J, Kim MY, Kim Y. Evaluation of portal hypertension by real-time shear wave elastography in cirrhotic patients. Liver Int. 2015; 35(11): 2416-2424.
23. Colecchia A, Montrone L, Scaioli E, Bacchi-Reggiani ML, Colli A, Casazza G, Schiumerini R, Turco L, Di Biase AR, Mazzella G, Marzi L, Arena U, Pinzani M, Festi D. Measurement of spleen stiffness to evaluate portal hypertension and the presence of esophageal varices in patients with HCV-related cirrhosis. Gastroenterology 2012; 143(3): 646-654.
24. Bamber J, Cosgrove D, Dietrich CF, Fromageau J, Bojunga J, Calliada F, Cantisani V, Correas JM, D'Onofrio M, Drakonaki EE, Fink M, Friedrich-Rust M, Gilja OH, Havre RF, Jenssen C, Klauser AS, Ohlinger R, Saftoiu A, Schaefer F, Sporea I, Piscaglia F. EFSUMB guidelines and recommendations on the clinical use of ultrasound elastography. Part 1: Basic principles and technology. Ultraschall in der Medizin—European Journal of Ultrasound 2013; 34(2):169-184
25. Shiina T, Nightingale KR, Palmeri ML, Hall TJ, Bamber JC, Barr RG, Castera L, Choi BI, Chou YH, Cosgrove D, Dietrich CF, Ding H, Amy D, Farrokh A, Ferraioli G, Filice C, Friedrich-Rust M, Nakashima K, Schafer F, Sporea I, Suzuki S, Wilson S, Kudo M.WFUMB guidelines and recommendations for clinical use of ultrasound elastography: Part 1: Basic principles and terminology. Ultrasound in Medicine & Biology 2015; 41(5):1126-1147

26. Yeh WC, Li PC, Jeng YM, Hsu HC, Kuo PL, Li ML, Hsu HC, Kuo PL, Li ML, Yang PM, Lee PH. Elastic modulus measurements of human liver and correlation with pathology. Ultrasound Med Biol. 2002; 28:467–474.
27. Castera L, Forns X, Alberti A. Non-invasive evaluation of liver fibrosis using transient elastography. J Hepatol 2008; 48:835–847.
28. Roulot D, Czernichow S, Le Clesiau H, Costes JL, Vergnaud AC, Beaugrand M. Liver stiffness values in apparently healthy subjects: influence of gender and metabolic syndrome. J Hepatol 2008; 48:606–613.
29. Kim SU, Choi GH, Han WK, Kim BK, Park JY, Kim DY, Choi JS, Yang SC, Choi EH, Ahn SH, Han KH, Chon CY. What are true normal' liver stiffness values using FibroScan?: a prospective study inhealthy living liver and kidney donors in South Korea. Liver Int. 2010; 30:268–274.
30. Colombo S, Belloli L, Zaccanelli M, Badia E, Jamoletti C, Buonocore M, Del Poggio P. Normal liver stiffness and its determinants in healthy blood donors. Dig Liver Dis 2011; 43:231–236.
31. Das K, Sarkar R, Ahmed SM, Mridha AR, Mukherjee PS, Das K, Dhali GK, Santra A, Chowdhury A. Normal'' liver stiffness measure (LSM) values are higher in both lean and obese individuals: a population-based study from a developing country. Hepatology 2012; 55:584–593.
32. Castera L, Bail B.L, Roudot-Thoraval F, Bernard PH, Foucher J, Merrouche W, Couzigou P, de Lédinghen V. Early detection in routine clinical practice of cirrhosis and oesophageal varices in chronic hepatitis C: comparison of transient elastography (FibroScan) with standard laboratory tests and non-invasive scores. Journal of Hepatology 2009, vol. 50, no. 1, pp. 59–68.
33. Vizzutti F, Arena U, Romanelli RG, Rega L, Foschi M, Colagrande S, Petrarca A, Moscarella S, Belli G, Zignego AL, Marra F, Laffi G, Pinzani M. Liver stiffness measurement predicts severe portal hypertension in patients with HCV-related cirrhosis. Hepatology 2007; 45:1290–1297.
34. Reiberger T, Ferlitsch A, Payer BA, Pinter M, Homoncik M, Peck-Radosavljevic M. Non-selective β-blockers improve the correlation of liver stiffness and portal pressure in advanced cirrhosis. J Gastroenterol. 2012; 47:561–568
35. Kazemi F, Kettaneh A, N'kontchou G, Pinto E, Ganne-Carrie N, Trinchet JC, Beaugrand M. Liver stiffness measurement selects patients with cirrhosis at risk of bearing large oesophageal varices. J Hepatol. 2006, 45, pp. 230-23
36. Pineda JA, Recio E, Camacho A, Macías J, Almodóvar C, González-Serrano M, Merino D, Tellez F, Ríos MJ, Rivero A; Andalusian Viral Hepatitis Group (HEPAVIR) of the Andalusian Society of Infectious Diseases (SAEI). Liver stiffness as a predictor of esophageal varices requiring therapy in HIV/hepatitis C virus-coinfected patients with cirrhosis. J Acquir Immune Defic Syndr.2009, 51, pp. 445-449
37. Pritchett S., Cardenas A., Manning D., Curry M., Afdhal N.H.The optimal cut-off for predicting large oesophageal varices using transient elastography is disease specific. J Viral Hepat.2018, 18, pp. e75-e80
38. Malik R, Lai M, Sadiq A, Farnan R, Mehta S, Nasser I, Challies T, Schuppan D, Afdhal N. Comparison of transient elastography, serum markers and clinical signs for the diagnosis of compensated cirrhosis. J Gastroenterol Hepatol.2010, 25, pp. 1562-1568

39. Bureau C, Metivier S, Peron JM, Selves J, Robic MA, Gourraud PA, Rouquet O, Dupuis E, Alric L, Vinel JP. Transient elastography accurately predicts presence of significant portal hypertension in patients with chronic liver disease. Food Pharmacol Ther 2008; 27:1261–1268.
40. Shi KQ, Fan YC, Pan ZZ, Lin XF, Liu WY, Chen YP, Zheng MH. Transient elastography: a meta-analysis of diagnostic accuracy in evaluation of portal hypertension in chronic liver disease. Liver, Int., 2013, Jan; 33(1):62-71.
41. Augustin S, Pons M, Maurice JB, Bureau C, Stefanescu H, Ney M, et al. Expanding the Baveno VI criteria for the screening of varices in patients with compensated advanced chronic liver disease. Hepatology. 2017 Dec; 66(6):1980-1988.
42. Stafylidou M, Paschos P, Katsoula A, Malandris K, Ioakim K, Bekiari E, et al. Performance of Baveno VI and Expanded Baveno VI Criteria for Excluding High-Risk Varices in Patients With Chronic Liver Diseases: A Systematic Review and Meta-analysis. Clin Gastroenterol Hepatol. 2019 Aug; 17(9):1744-1755.E11.
43. de Franchis R, Bosch J, Garcia-Tsao G, Reiberger T, Ripoll C; Baveno VII Faculty. Baveno VII - Renewing consensus in portal hypertension. J Hepatol. 2022 Apr; 76(4):959-974. doi:10.1016/j.jhep.2021.12.022. Epub 2021 Dec 30. Erratum in: J Hepatol. 2022 Apr 14.
44. Şirli R, Sporea I, Popescu A, Dănilă M. Ultrasound-based elastography for the diagnosis of portal hypertension in cirrhotics. World J Gastroenterol. 2015 Nov 7; 21(41): 11542–11551.
45. Dietrich CF, Bamber J, Berzigotti A, Bota S, Cantisani V, Castera L, et al. EFSUMB Guidelines and Recommendations on the Clinical Use of Liver Ultrasound Elastography, Update 2017 (Long Version). Ultraschall Med. 2017; 38(4): e48.
46. Lupsor M, Badea R, Stefanescu H, Sparchez Z, Branda H, Serban A, Maniu A. Performance of a new elastographic method (ARFI technology) compared to unidimensional transient elastography in the noninvasive assessment of chronic 106 hepatitis C. preliminary results. Journal of Gastrointestinal and Liver Diseases. 2009; 18(3):303-310
47. Friedrich-Rust M, Wunder K, Kriener S, Sotoudeh F, Richter S, Bojunga J, et al. Liver fibrosis in viral hepatitis: noninvasive assessment with acoustic radiation force impulse imaging versus transient elastography. Radiology 2009; 252: 595-604.
48. Sporea I, Sirli R, Bota S, Fierbinţeanu-Braticevici C, Petrişor A, Badea R, et al. Is ARFI elastography reliable for predicting fibrosis severity in chronic HCV hepatitis? World J Radiol. 2011; 3:188–193 168.
49. Sporea I, Badea R, Sirli R, Lupsor M, Popescu A, Danila M, Focsa M, Deleanu A. How efficient is acoustic radiation force impulse elastography for the evaluation of liver stiffness? Hepat Mon. 2011; 11:532–538
50. Rizzo L, Calvaruso V, Cacopardo B, Alessi N, Attanasio M, Petta S, et al. Comparison of transient elastography and acoustic radiation force impulse for noninvasive staging of liver fibrosis in patients with chronic hepatitis C. Am J Gastroenterol. 2011; 106:2112–2120.
51. Friedrich-Rust M, Nierhoff J, Lupsor M, Sporea I, Fierbinteanu-Braticevici C, Strobel D, et al. Performance of Acoustic Radiation Force Impulse imaging for the staging of liver fibrosis: a pooled meta-analysis. J Viral Hepat. 2012; 19:E212–E219
52. Nierhoff J, Chávez Ortiz AA, Herrmann E, Zeuzem S, Friedrich-Rust M. The efficiency of acoustic radiation force impulse imaging for the staging of liver fibrosis: a metaanalysis. Eur Radiol. 2013; 23:3040–3053 108

53. Bota S, Herkner H, Sporea I, Salzl P, Sirli R, Neghina AM, Peck-Radosavljevic M. Meta-analysis: ARFI elastography versus transient elastography for the evaluation of liver fibrosis. Liver Int. 2013; 33:1138–1147
54. Ferraioli G, Tinelli C, Lissandrin R, Zicchetti M, Dal Bello B, Filice G, Filice C. Point shear wave elastography method for assessing liver stiffness. World Journal of Gastroenterology. 2014; 20(16):4787-4796
55. Foncea C.G., Popescu A., Lupusoru R., Fofiu R., Sirli R., Danila M, Sporea I. Comparative study between pSWE and 2D-SWE techniques integrated in the same ultrasound machine, with Transient Elastography as the reference method. Med Ultrason 2020, Mar 1; 22(1):13-19.
56. Bota S, Sporea I, Sirli R, Focsa M, Popescu A, Danila M, Foreigner M. Can ARFI elastography predict the presence of significant esophageal varices in newly diagnosed cirrhotic patients? Annals of Hepatology. 2012; 11(4):519-525
57. Salzl P, Reiberger T, Ferlitsch M, Payer BA, Schwengerer B, Trauner M, Peck Radosavljevic M, Ferlitsch A. Evaluation of portal hypertension and varices by acoustic radiation force impulse imaging of the liver compared to transient elastography and AST to platelet ratio index. Ultraschall Med 2014;35:528-533.
58. Park Y, Kim SU, Park SY, Kim BK, Park JY, Kim DY, et al. A novel model to predictesophageal varices in patients with compensated cirrhosis using acoustic radiation force impulse elastography. PLoS One 2015; 10:E0121009.
59. Bucsics T., Grasl B., Schwabl P., Mandorfer M, Dmitrieva J., Peck-Radosavljevic M., et al. The novel point shear-wave elastography method ElastPQ® is accurate for non-invasive evaluation of liver fibrosis and portal hypertension. Zeitschrift für Gastroenterologie 2017; 55(05):E28-E56
60. Popescu A, Şirli R, Sporea I. Ultrasound elastography.2D-Shear wave elastography for liver fibrosis evaluation chapter, March 2020, ISBN: 978-1-78985-710-8, print ISBN: 978-1-78985-709-2, eBook (PDF) ISBN: 978-1-83880-015-4
61. Grădinaru-Taşcău O, Sporea I, Bota S, Jurchiş A, Popescu A, Popescu M, Şirli R, Szilaski M.. Does experience play a role in the ability to perform liver stiffness measurements by means of supersonic shear imaging (SSI)? Medical Ultrasonography 2013; 15:180-183 185.
62. Ferraioli G, Tinelli C, Dal Bello B, Zicchetti M, Filice G, Filice C; Liver Fibrosis Study Group. Accuracy of real-time shear wave elastography for assessing liver fibrosis in chronic hepatitis C: A pilot study. Hepatology 2012; 56:2125-2133
63. Lupșor-Platon M, Badea R, Gersak M, Maniu A, Rusu I, Suciu A, et al. Noninvasive assessment of liver diseases using 2D shear wave Elastography. Journal of Gastrointestinal and Liver Diseases. 2016; 25(4):525-532
64. Sporea I, Bota S, Gradinaru-Taşcău O, Sirli R, Popescu A, Jurchiş A. Which are the cut-off values of 2D-shear wave Elastography (2D-SWE) liver stiffness measurements predicting different stages of liver fibrosis, considering transient Elastography (VCTE) as the reference method? European Journal of Radiology 2014; 83:E118-E122
65. Jeong JY, Kim TY, Sohn JH, Kim Y, Jeong WK, Oh YH, Yoo KS. Real time shear wave elastography in chronic liver diseases: Accuracy for predicting liver fibrosis, in comparison with serum markers. World Journal of Gastroenterology 2014; 20:13920-13929

66. Deffieux T, Gennisson JL, Bousquet L, Corouge M, Cosconea S, Amroun D, et al. Investigating liver stiffness and viscosity for fibrosis, steatosis and activity staging using shear wave elastography. Journal of Hepatology 2015; 62:317-324
67. Cassinotto C, Boursier J, de Lédinghen V, Lebigot J, Lapuyade B, Cales P, et al. Liver stiffness in nonalcoholic fatty liver disease: A comparison of supersonic shear imaging, FibroScan, and ARFI with liver biopsy. Hepatology 2016; 63:1817-1827
68. Bende F, Sporea I, Sirli R, Popescu A, Mare R, Miutescu B, et al. Performance of 2D-SWE. GE for predicting different stages of liver fibrosis, using Transient Elastography as the reference method. Med Ultrason 2017 Apr 22; 19(2):143-149.
69. Serra C, Grasso V, Conti F, Felicani C, Mazzotta E, Lenzi M, Verucchi G, D'errico A, Andreone P. A new two-dimensional shear wave Elastography for noninvasive assessment of liver fibrosis in healthy subjects and in patients with chronic liver disease. Ultraschall in der Medizin. 2018; 39:432-439
70. Villani R., Cavallone F., Davide Romano A., Bellanti F., Serviddio G. Two-Dimensional Shear Wave Elastography versus Transient Elastography: A Non-Invasive Comparison for the Assessment of Liver Fibrosis in Patients with Chronic Hepatitis C. Diagnostics (Basel). 2020 May; 10(5): 313.
71. Thiele M, Hugger MB, Kim Y, Rautou PE, Elkrief L, Jansen C, et al. 2D shear wave liver elastography by Aixplorer to detect portal hypertension in cirrhosis: An individual patient data meta-analysis. Liver International 2020; 40(6):1435-1446
72. Ștefănescu H., Rusu C., Lupsor-Platon M., Nicoară Farcau O., Fischer P, Grigoras C, et al. Liver Stiffness Assessed by Ultrasound Shear Wave Elastography from General Electric Accurately Predicts Clinically Significant Portal Hypertension in Patients with Advanced Chronic Liver Disease. Ultraschall Med. 2020 Oct; 41(5):526-533.
73. Barr RG, Wilson SR, Rubens D, Garcia-Tsao G, Ferraioli G. Update to the society of radiologists in ultrasound liver Elastography consensus statement. Radiology. 2020; 296(2):263-274
74. Bolognesi M, Merkel C, Sacerdoti D, Nava V, Gatta A. Role of spleen enlargement in cirrhosis with portal hypertension. Dig Liver Dis. 2002 Feb; 34(2):144-50.
75. Ferraioli G, Wong VW, Castera L, Berzigotti A, Sporea I, Dietrich CF, et al. Liver ultrasound elastography: An update to the world federation for ultrasound in medicine and biology guidelines and recommendations. Ultrasound in Medicine & Biology. 2018; 44(12):2419-2440
76. Saftoiu A, Gilja OH, Sidhu PS, Dietrich CF, Cantisani V, Amy D, et al. The EFSUMB guidelines and recommendations for the clinical practice of elastography in non-hepatic applications: Update 2018. Ultraschall in der Medizin—European Journal of Ultrasound 2019; 40(4):425-453
77. Stefanescu H, Lupsor M, Grigorescu M, Procopet B, Maniu A, Badea R. Transient elastography of the spleen as non-invasive assessment of portal hypertension in liver cirrhosis patients. Poster abstract nr 63, Proceedings of EASL Monothematic Conference Portal Hypertension: Advances in Knowledge, Evaluation and Management, Budapest, 2009, p. 130
78. Stefanescu H, Grigorescu M, Lupsor M, Procopet B, Maniu A, Badea R. Spleen stiffness measurement using Fibroscan for the noninvasive assessment of esophageal varices in liver cirrhosis patients. J Gastroenterol Hepatol. 2011; 26(1):164-170.

79. Colecchia A, Ravaioli F, Marasco G, Colli A, Dajti E, Di Biase AR, et al. A combined model based on spleen stiffness measurement and Baveno VI criteria to rule out high-risk varices in advanced chronic liver disease. J Hepatol. 2018 Aug; 69(2):308-317.
80. Wang X.K., Wang P., Zhang Y., Sheng-Lin Q., Chi K.; Wang G.C. A study on spleen transient elastography in predicting the degree of esophageal varices and bleeding. Medicine (Baltimore) 2019 Mar; 98(9):E14615.
81. Stefanescu H, Marasco G, Calès P, Fraquelli M, Rosselli M, Ganne-Carriè N, et al. A novel spleen-dedicated stiffness measurement by FibroScan® Improves the screening of high-risk oesophageal varices. Liver Int. 2020 Jan; 40(1):175-185.
82. Rifai K, Cornberg J, Bahr M, Mederacke I, Potthoff A, Wedemeyer H, Manns M, Gebel M. ARFI elastography of the spleen is inferior to liver elastography for the detection of portal hypertension. Ultraschall in der Medizin 2011; 32(Suppl 2):E24-E30
83. Vermehren J, Polta A, Zimmermann O, Herrmann E, Poynard T, Hofmann WP, et al. Comparison of acoustic radiation force impulse imaging with transient elastography for the detection of complications in patients with cirrhosis. Liver Int. 2012; 32:852–858.
84. Bota S, Sporea I , Şirli R , Popescu A , Dănilă M , Şendroiu M, Focşa M. Spleen assessment by Acoustic Radiation Force Impulse Elastography (ARFI) for prediction of liver cirrhosis and portal hypertension. Med Ultrason 2010; 12(3):213-7
85. Ma X, Wang L, Wu H, Feng Y, Han X, Bu H, Zhu Q. Spleen Stiffness Is Superior to Liver Stiffness for Predicting Esophageal Varices in Chronic Liver Disease: A Meta Analysis. PLoS One. 2016; 11(11):E0165786. Published 2016 Nov 9. doi:10.1371/journal.pone.0165786
86. Takuma Y, Nouso K, Morimoto Y, Tomokuni J, Sahara A, Toshikuni N, et al. Measurement of spleen stiffness by acoustic radiation force impulse imaging identifies cirrhotic patients with esophageal varices. Gastroenterology 2013; 144(1):92-101.e2
87. Fierbinteanu-Braticevici C, Tribus L, Peagu R, Petrisor A, Baicus C, Cretoiu D, Pasternak A, Oprea G, Purcareanu A, Moldoveanu AC. Spleen Stiffness as Predictor of Esophageal Varices in Cirrhosis of Different Etiologies. Ski Rep. 2019; 9(1):16190.
88. Karagiannakis DS, Voulgaris T, Koureta E, Chloupi E, Papatheodoridis GV, Vlachogiannakos J. Role of Spleen Stiffness Measurement by 2D-Shear Wave Elastography in Ruling Out the Presence of High-Risk Varices in Cirrhotic Patients. Thu Dis Sci. 2019 Sep; 64(9):2653-2660.
89. Cassinotto C, Charrie A, Mouries A, Lapuyade B, Hiriart JB, Vergniol J, et al. Liver and spleen elastography using supersonic shear imaging for the non-invasive diagnosis of cirrhosis severity and oesophageal varices. Digestive and Liver Disease. 2015; 47(8):695-701
90. Jansen C, Bogs C, Verlinden W, Thiele M, Möller P, Görtzen J, et al. Shear-wave elastography of the liver and spleen identifies clinically significant portal hypertension: A prospective multicentre study. Liver Int. 2016; 37:396- 405.
91. Fofiu R, Bende F, Popescu A, Şirli R, Lupușoru R, Ghiuchici AM, Sporea I. Spleen and Liver Stiffness for Predicting High-Risk Varices in Patients with Compensated Liver Cirrhosis. Ultrasound Med Biol. 2021 Jan; 47(1):76-83.
92. Song J, Huang J, Huang H, Liu S, Luo Y. Performance of spleen stiffness measurement in prediction of clinical significant portal hypertension: A meta-analysis. Clin Res Hepatol Gastroenterol. 2018 Jun; 42(3):216-226.

93. Singh S, Eaton JE, Murad MH, Tanaka H, Iijima H, Talwalkar JA. Accuracy of spleen stiffness measurement in detection of esophageal varices in patients with chronic liver disease: Systematic review and meta-analysis. Clinical Gastroenterology and Hepatology 2014; 12(6):935-45E4
94. Wang QB, Zhu H, Liu HL, Zhang B. Performance of magnetic resonance elastography and diffusion-weighted imaging for the staging of hepatic fibrosis: A meta-analysis. Hepatology 2012; 56(1):239-247
95. Singh S, Venkatesh SK, Wang Z, Miller FH, Motosugi U, Low RN, et al. Diagnostic performance of magnetic resonance elastography in staging liver fibrosis: a systematic review and meta-analysis of individual participant data. Clin Gastroenterol Hepatol. 2015 Mar; 13(3):440-451.e6.
96. Friedrich-Rust M, Poynard T, Castera L. Critical comparison of elastography methods to assess chronic liver disease. Nature Reviews Gastroenterology & Hepatology 2016; 13(7):402-411
97. European Association for the Study of the Liver. EASL clinical practice guidelines on non-invasive tests for evaluation of liver disease severity and prognosis. Journal of Hepatology 2021; 75(3):659-689
98. Wagner M, Hectors S, Bane O, Gordic S, Kennedy P, Besa C, Schiano TD, Thung S, Fischman A, Taouli B. Noninvasive prediction of portal pressure with MR elastography and DCE-MRI of the liver and spleen: Preliminary results. J Magn Reson Imaging 2018 Oct; 48(4):1091-1103.
99. Jhang ZE, Wu KL, Chen CB, Chen YL, Lin PY, Chou CT. Diagnostic value of spleen stiffness by magnetic resonance elastography for prediction of esophageal varices in cirrhotic patients. Abdominal Radiology (NY) 2021; 46(2):526-533
100. Abe H, Midorikawa Y, Matsumoto N, Moriyama M, Shibutani K, Okada M, et al. Prediction of esophageal varices by liver and spleen MR elastography. Eur Radiol. 2019 Dec; 29(12):6611-6619.
101. Hoffman RH, Ayoola A, Nickel D, Han F, Chandarana H, Babb J, Shanbhogue KP. MR elastography, T1 and T2 relaxometry of liver: role in noninvasive assessment of liver function and portal hypertension. Abdom Radiol (NY) 2020 Sep; 45(9):2680-2687.
102. Singh R, Wilson MP, Katlariwala P, Murad MH, McInnes MDF, Low G. Accuracy of liver and spleen stiffness on magnetic resonance elastography for detecting portal hypertension: A systematic review and meta-analysis. European Journal of Gastroenterology & Hepatology 2021; 32(2):237-245

5.1.f. Multiparametric Ultrasound Evaluation of Fatty Liver Disease

Alexandru Popa, Ioan Sporea

Chronic liver diseases (CLD) represent a significant public health issue worldwide, being a major cause of mortality and morbidity. The etiological factors of CLD are multiple and vary from one geographical region to another. Metabolic Dysfunction Associated Steatotic Liver Disease (MASLD), hepatitis B virus (HBV), hepatitis C virus (HCV), and alcohol-associated liver disease (ALD) are the most widespread etiologies of CLD. Considering the high rates of sustained virological response in HCV-infected patients after an 8–12-week treatment with direct-acting antivirals (DAAs) and the improved management of HBV-infected patients using nucleotide/nucleoside analogs, hepatologists' attention has increasingly shifted towards MASLD (1). Hepatic steatosis is among the leading factors responsible for chronic liver disease (2). Evaluating the prevalence of fatty liver in the general population, a recent epidemiological study by Younossi Z et al. indicates that approximately 30% of the global general population is affected by this condition (3). According to the study, Europe has the lowest prevalence of this pathology at 25%, while South America has a prevalence of 44%, and South Asia 34%. These figures represent an increase compared to previous studies, which reported prevalences of 30.4% in South America and 23.7% in Europe (4). Regarding the terminology for fatty liver, the term NAFLD (Non-Alcoholic Fatty Liver Disease) was used for a long time. Recently, this term was modified to MAFLD (Metabolic Dysfunction Associated Fatty Liver Disease), as proposed by Eslam M in 2020 (5). However, in 2023, a group of experts decided to change the nomenclature to MASLD (Metabolic Dysfunction Associated Steatotic Liver Disease), as detailed in the consensus on the new nomenclature published by Rinella (6).

Liver injury, regardless of etiology, triggers a sequence of inflammatory events that lead to a chronic inflammatory status. Chronic inflammation is an active process responsible for the development of fibrosis, ultimately inducing irreversible alteration of the hepatic architecture (liver cirrhosis), with the potential for hepatocellular carcinoma (HCC) occurrence (7–10). Since it marks a critical point in the evolution of CLD, liver fibrosis is considered one of the most important prognostic parameters. Hepatic steatosis is also an important prognostic factor linked with the progression of CLD. Additionally, the need for quantification and monitoring of hepatic fat load in a non-invasive manner has increased with the rapid rise in obesity prevalence and the introduction of new potential therapies for this pathology.

Until 15-20 years ago, liver biopsy was the only method for determining the presence of liver fibrosis, steatosis, and inflammation. Although it remains the "golden standard" for confirming CLD, liver biopsy is an invasive procedure with well-known disadvantages, such as its potential risks, high costs, sampling errors that can lead to the underestimation of liver lesion severity, and inter- and intra-operator variability in histological evaluations among pathologists (11).

In the last 20 years, significant progress has been made in the non-invasive evaluation of patients with CLD. Several ultrasound-based elastographic techniques have been developed to assess the physical properties of liver tissue to evaluate CLD severity. At present, the physical characteristics of tissues can be assessed through ultrasound-based elastography, which analyzes tissue responses to mechanical or acoustic energy generated by external stimuli. Non-invasive ultrasound techniques for measuring liver stiffness (LS) via elastography have become increasingly accessible. One of the first and most validated elastographic methods was vibration-controlled transient elastography (VCTE), followed by other techniques such as point shear wave elastography (pSWE) and two-dimensional shear wave elastography (2D-SWE).

Conventional techniques, such as standard abdominal ultrasound, can detect diffuse fat accumulation in the liver. The typical signs of hepatic steatosis are hyperechogenicity and posterior attenuation of the ultrasound signal. These indicators have led to the development of several quantitative ultrasound-based techniques for evaluating hepatic steatosis: attenuation coefficient, backscatter coefficient, acoustic structure quantification, and sound speed quantification.

However, besides liver fibrosis, numerous other factors influence liver stiffness. Among these, probably the most important and difficult to assess is necroinflammation. Given that these conditions frequently coexist, it is essential to evaluate whether increased liver stiffness can be attributed to fibrosis or inflammation. Shear wave dispersion is an ultrasound-based method that can be used as an indirect marker of liver viscosity. According to preliminary studies, this method could be useful for determining inflammation.

In the context of the alarming rise in the incidence of metabolic diseases, it becomes essential to identify and manage MASLD early in at-risk patients. The risk factors for MASLD, such as obesity, type 2 diabetes (T2DM), and metabolic syndrome, are well defined. Thus, we face a major challenge: how to detect this pathology efficiently, quickly, and cost-effectively among at-risk populations? In this context, the emergence of new technologies offers us the possibility to use multiparametric ultrasound (MPUS) evaluation as a solution.

What does MPUS entail? ***MPUS (Multiparametric Ultrasound)*** is an advanced ultrasound method that enables detailed tissue analysis using different ultrasonographic parameters, all integrated into the same ultrasound device. For patients with chronic diffuse liver diseases, such as MASLD, MPUS provides important data about the hepatic structure's appearance in standard ultrasound, as well as allowing for the quantitative determination of steatosis, fibrosis, and more recently, the evaluation of hepatic inflammation. This method ensures a rapid and non-invasive evaluation, which can be performed immediately after the patient's clinical evaluation, right in the medical office (“point-of-care”), being particularly useful in the diagnosis and management of chronic liver diseases. Therefore, we propose the use of ultrasound as the primary method for identifying and evaluating hepatic fat load due to its cost-effectiveness and easy applicability. Once hepatic steatosis is identified by MPUS,

we aim to quantify it, evaluate liver stiffness as an indicator of fibrosis, and finally, analyze hepatic inflammation.

5.1.f.1. Standard Abdominal Ultrasound

B-mode (gray scale) ultrasound of the liver is the classic method used to examine the morphology of the liver and other abdominal organs. This technique provides information about the shape, size, contour, and structure of the hepatic parenchyma, as well as the presence of focal lesions. It also allows the evaluation of hepatic vascularization (vessel diameter, permeability, presence of solid intraluminal lesions, and thromboses) and the biliary tree (bile duct dilation).

In diffuse liver diseases, ultrasound allows for the assessment of disease stage, including the identification of morphological characteristics of cirrhosis, such as the heterogeneous appearance of the hepatic parenchyma's echostructure, nodular or irregular surface, changes in hepatic vascularization, and caudate lobe hypertrophy. The clinical context plays an essential role in interpreting ultrasound results. It is important to note that ultrasound has low sensitivity and high specificity for cirrhosis in patients with chronic liver disease, meaning that the absence of typical morphological features does not exclude the presence of cirrhosis, while their presence is very specific in this clinical context. Additionally, ultrasound examination of other abdominal organs can provide valuable additional information for a comprehensive evaluation of diffuse liver diseases. Spleen size, the presence of ascitic fluid, and secondary changes to portal hypertension (increased portal vein diameter and development of porto-systemic collateral pathways) can be detected, contributing to a detailed overall assessment. Ultrasound is also recommended as a screening tool for HCC in patients with liver cirrhosis.

Over time, standard ultrasound has been recognized as an accessible, rapid, inexpensive, and efficient method for evaluating hepatic steatosis. Ultrasound changes appear when 15-20% of hepatocytes are infiltrated with fat, and simple signs such as the "bright liver" with "posterior attenuation" of ultrasound waves or an increased "hepato-renal contrast index" facilitate the semi-quantitative assessment of fatty infiltration in the liver (Fig.5.29) (12). Hepatic steatosis can be subjectively divided on ultrasound into mild, moderate, or severe, based on the severity of the mentioned signs. Although these ultrasonographic signs are simple and somewhat subjective, numerous studies have demonstrated their significant value in assessing the severity of hepatic steatosis. In a comprehensive meta-analysis by Hernaez R et al., which included 49 studies and 4,720 subjects, ultrasound was compared with liver biopsy. Ultrasound demonstrated a sensitivity of 84.8% (95% CI: 79.5-88.9%) for identifying moderate to severe steatosis, and a specificity of 93.6% (95% CI: 87.2-97.0%) (13).

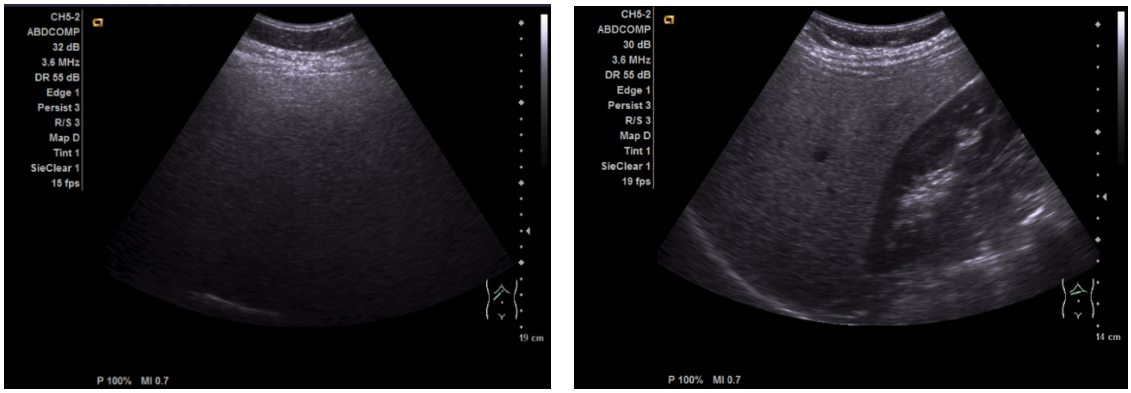

Fig. 5.29. Ultrasonographic Aspects of Hepatic Steatosis

Posterior attenuation (left image) and increased hepato-renal index (right image).

In conclusion, abdominal ultrasound proves to be an indispensable tool in liver evaluation. However, certain limitations of this method must be recognized, such as its subjective nature of assessment, variability in interpretations between different operators, differences in quality between ultrasound equipment, and challenges in monitoring the progression or regression of conditions over time. In this context, the development and integration of quantitative ultrasound-based techniques that offer a multiparametric hepatic analysis represent a crucial step. These emerging technologies extend the capabilities of standard ultrasound, providing a broader and more objective perspective on liver evaluation.

5.1.f.2. Evaluation of Hepatic Steatosis Using Ultrasound-Based Techniques

Semi-Quantitative Techniques for Steatosis Quantification

Three semi-quantitative scores have been developed to meet the need for more precise evaluations of hepatic steatosis: the hepato-renal index, Hamaguchi score, and US-FLI index.

The hepato-renal index (HRI) is determined by comparing the brightness ratio between the liver and the renal cortex. This process requires selecting two regions of interest (ROI): one in segment VI of the liver and another in the cortex of the upper pole of the right kidney. The mean brightness of these ROIs is measured based on numerical values assigned to the pixels on the gray scale, which are then used to calculate the index. Certain ultrasound devices are equipped with software that can automatically compute this index (Fig. 5.30).

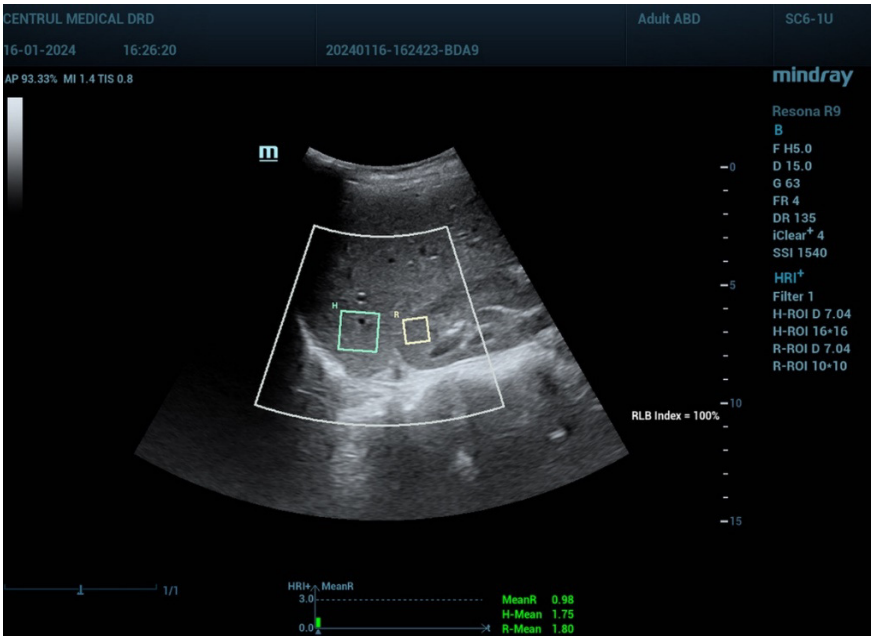

Fig. 5.30. Illustration of a Technique for Quantifying the Hepato-Renal Index (HRI)

Other authors have utilized specialized software to analyze images in JPEG format or conducted histogram analyses on DICOM images. Webb et al. used liver biopsy as the control method in a study of 111 patients with CLD and proposed HRI cut-off values of 1.49 (AUROC 0.99) for S1, 1.86 (AUROC 0.96) for S2, and 2.23 (AUROC 0.96) for S3 (14). Petzold defined an HRI cut-off value of 1.46 for ≥S1, with a sensitivity of 42.7% and a specificity of 90.7% (AUROC 0.680) in a cohort of 157 patients with chronic liver diseases (15). In a retrospective study published by Johnson, which included 267 patients who underwent liver ultrasound and biopsy, it was showed that an HRI ≥ 1.4 corresponds to a PPV >95% for hepatic steatosis ≥ 10%, while an HRI ≤ 1.17 has a PPV >95% for hepatic steatosis ≤ 5% (16). Stahlschmidt demonstrated that HRI is not suitable for estimating hepatic steatosis in patients with advanced liver fibrosis due to the substitution of fat with fibrosis in the progression of MASLD (17). In a group of 34 patients with suspected hepatic steatosis and advanced liver fibrosis, a weak correlation ($r = 0.33$; $p = 0.058$) between HRI and the control method was observed. Similarly, HRI should not be used in patients with chronic kidney disease, as they may have increased renal cortex echogenicity due to the accumulation of fibrotic tissue at this level. Although several authors have proven the effectiveness of HRI in quantifying hepatic steatosis, the validation of this index by large clinical studies is still lacking (18).

In 2007, Hamaguchi presented a score based on 4 ultrasonographic parameters to improve the evaluation of hepatic steatosis: hepato-renal contrast (contrast between the hepatic parenchyma and the right renal parenchyma), hepatic brightness, posterior attenuation (attenuation of the ultrasonographic signal in the deep hepatic segments and reduced diaphragm visualization), and vessel blurring (blurring of hepatic vessel margins and lumen narrowing). A score higher than 2 indicates the presence of steatosis, while a value greater than 4 indicates moderate-severe steatosis. The Hamaguchi score demonstrated a

sensitivity and specificity of 91.7% and 100%, respectively, with an AUROC of 0.98 in detecting hepatic steatosis, using biopsy as the reference method. In another study, the Hamaguchi score was validated for detecting steatosis in 167 patients with and without MASLD, showing 82% and 100% sensitivity and specificity, with an AUROC of 0.94 compared to CAP as the reference technique (12, 19).

Similar to the Hamaguchi score, the Ultrasound Fatty Liver Index (US-FLI) is based on several ultrasonographic factors, comprising liver/kidney contrast, attenuation, vessel visualization, gallbladder wall visualization, diaphragm visualization, and whether fatty-free areas are present or absent. When the score is greater than 2, the presence of steatosis is identified. In a study published by Ballestri, which included 352 biopsied patients with chronic liver diseases, the following cut-off values for US-FLI were established: ≥ 2 for mild steatosis (AUROC 0.934), ≥ 3 for moderate steatosis (AUROC 0.958), and ≥ 5 for severe steatosis (AUROC 0.954) with sensitivities greater than 86% and specificities over 87% (18, 20, 21). A recent article compared US-FLI with CAP in 96 patients with MASLD and revealed that a US-FLI ≥ 6 had a positive predictive value (PPV) of 94% for steatosis >S2, while a US-FLI ≤ 3 had a negative predictive value (NPV) of 100% for steatosis >S2, with good discrimination capacity between different grades of steatosis (AUROC scores of 0.88 for S1 and 0.90 for S2) (22).

Quantitative Techniques for Steatosis Quantification

The limitations of standard ultrasound and semi-quantitative techniques have led to the development and integration of quantitative ultrasound-based techniques. These offer a multiparametric analysis of hepatic pathology. Quantitative methods have established links between the physical characteristics of hepatic tissue (lipid droplets in hepatocytes have different impedance characteristics) and data obtained from the analysis of ultrasound propagation in tissue (attenuation coefficient and backscatter coefficient) (23). The attenuation coefficient quantifies the energy loss of ultrasound as it traverses the liver, while the backscatter coefficient quantifies the energy of the ultrasound returned by the liver. These emerging technologies extend the capabilities of standard ultrasound, providing a broader and more objective perspective on liver evaluation.

Controlled Attenuation Parameter (CAP) - VCTE (Vibration-Controlled Transient Elastography)

The advent of the FibroScan® device (Echosens, Paris, France) has enabled the quantification of steatosis through the CAP (Controlled Attenuation Parameter) module, used in conjunction with VCTE for stiffness assessment (Fig. 5.31). The CAP software, integrated into the FibroScan device since 2010, measures the attenuation of the ultrasound beam, which is directly related to the fat content in the liver. Results are reported in decibels per meter (dB/m), ranging from 100 to 400 dB/m, providing a quantitative assessment of hepatic steatosis (24).

Fig. 5.31. FibroScan with CAP (CAP values are in light blue), with M and XL probes

Numerous studies and meta-analyses have evaluated the efficacy of the CAP method, particularly in comparison with liver biopsy. The AUROCs for CAP in quantifying hepatic fat infiltration ranged from 0.823 (95% CI: 0.809-0.837) to 0.865 (95% CI: 0.850-0.880) (25, 26). Additionally, a meta-analysis by Shi, which included data from 11 patient cohorts, reported that the AUROCs for CAP were 0.85 (95% CI: 0.81-0.88) for mild steatosis ≥ S1, 0.88 (95% CI: 0.85-0.91) for moderate steatosis ≥ S2, and 0.87 (95% CI: 0.84-0.90) for severe steatosis S3 (27).

The cut-off values for assessing the severity of hepatic steatosis vary according to etiology and authors. The reported cut-off values for detecting hepatic steatosis range from 222 dB/m in patients with chronic hepatitis C to 294 dB/m in patients with MASLD (28, 29). In MASLD, and the most reliable cut-off values were proposed by Eddowes and established using liver biopsy as the control method: for S1 (mild) – 294 dB/m, for S2 (moderate) – 310 dB/m, and for S3 (severe) – 331 dB/m. For ease of memorization, these can be approximated to 290 dB/m, 310 dB/m, and 330 dB/m, respectively (30). Therefore, it has been proposed that cut-off values be specific to the etiology of liver pathology.

CAP can be measured using either the M probe or the XL probe, the latter being particularly useful for overweight and obese patients. This raises an important question: should different cut-off values be applied for these two probes? A study by Chan (31), which used liver biopsy as the reference method and included 180 patients with hepatic steatosis evaluated using both M and XL probes, found that the same CAP cut-off values can be applied for both probes in assessing the degree of hepatic steatosis. These results were corroborated by data from another study by Eddowes (30), which obtained similar results. Under these conditions, it is considered that the same CAP cut-off values can be used for the same degree of steatosis, regardless of the probe.

Steatosis quantification can also be performed using the FibroTouch (iLivTouch) system, which uses the Ultrasound Attenuation Parameter (UAP) (Fig. 5.32). In a prospective study including 237 patients evaluated by FibroTouch and liver biopsy, the FibroTouch examination success rate was 96.5%. The AUROCs of UAP for diagnosing steatosis ≥ S1, ≥ S2, and S3 were 0.88, 0.93, and 0.88, respectively, and cut-off values were 244, 269, and 296 dB/m. The advantage of the FibroTouch system is that it uses a single probe for all patients, and the system benefits from a standard ultrasound probe, allowing for an ultrasound evaluation of the liver before quantitative assessment. Like the FibroScan, the system has the capability to evaluate steatosis and liver stiffness (and more recently hepatic inflammation) (32).

Fig. 5.32. The iLivTouch (FibroTouch) System with Ultrasound and Elastography Probe

Quantification of Steatosis (Quantitative Ultrasound QUS)

In recent years, the field of ultrasound has seen the development of new software tools integrated into various ultrasound machines. These quantitative techniques—Quantitative Ultrasound (QUS)—enable precise evaluation of ultrasound beam attenuation, backscatter coefficient, and sound speed in hepatic tissue, serving as markers for identifying fat accumulation in the liver (Fig. 5.33). Several ultrasound manufacturers go further by combining these parameters to provide a detailed quantitative measurement of steatosis.

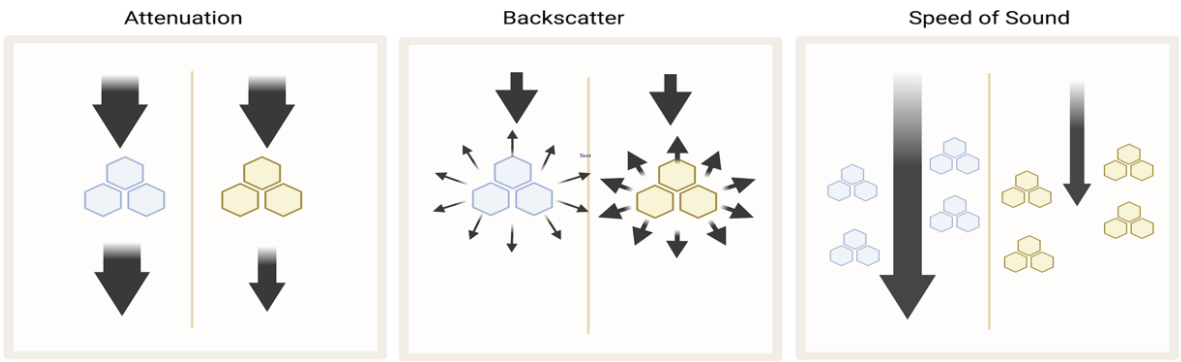

Fig. 5.33. Quantitative Ultrasound (QUS) Parameters for Steatosis Evaluation

These new techniques are extremely simple, requiring only a few seconds to be performed, and a major advantage is that they are practical, immediately applicable methods ("point of care"). When a patient presents for an abdominal ultrasound, and hepatic steatosis is identified in a standard ultrasound, a QUS evaluation can be performed on the spot, providing an objective measurement of steatosis. This method is particularly valuable in monitoring the patient's progression, allowing for the comparison of results obtained in successive evaluations with the initial ones.

Attenuation

Regarding attenuation analysis, advanced technologies have been developed to measure the attenuation of ultrasound beams. These include Attenuation (ATT) from Fujifilm, Ultrasound Attenuation Parameter (UAP) from FibroTouch, Ultrasound-Guided Attenuation Parameter (UGAP) from General Electric, Attenuation Imaging (ATI) from Canon, Tissue Attenuation Imaging (TAI) from Samsung, Attenuation Coefficient (AC) from Siemens, and Liver Fat Quantification (LFQ) from Philips. These technologies represent a significant step forward in diagnosing and evaluating hepatic steatosis, having been recently introduced to the market (32-38). Unlike CAP, these techniques integrated into ultrasound devices allow for B-mode guidance for determining the measurement area.

The validation of various QUS techniques has been carried out through studies using liver biopsy as the golden standard or, for some of them, MRI-PDFF (Proton Density Fat Fraction from MRI). The encouraging performances obtained by many such systems make QUS an extremely attractive option for both the initial evaluation of patients with MASLD and their long-term monitoring.

Using UGAP from GE Healthcare, the attenuation coefficient is determined in a region of interest with a length of 65 mm and placed at least 20 mm underneath the liver capsule (Fig. 5.34). In a study published by Fujiwara (2018), which included 163 patients and intended

to assess UGAP's performance for quantifying hepatic fat load using liver biopsy as a control method, excellent AUROCs for UGAP were obtained for identifying grades S1, S2, and S3, at 0.900, 0.953, and 0.959, respectively. The mean UGAP values for patients with steatosis grades S0, S1, S2, and S3 were 0.48, 0.56, 0.66, and 0.72, respectively (39). In another study published on UGAP, conducted on a cohort of 1,010 patients with chronic liver diseases, examined by MRI-PDFF and UGAP in 6 hepatology centers in Japan, a significant correlation between UGAP values and MRI-PDFF results was observed (intraclass correlation coefficient being 0.768). The AUROCs for differentiating steatosis levels ≥ 1 (MRI-PDFF >5.2%), ≥ 2 (MRI-PDFF > 11.3%), and 3 (MRI-PDFF >17.1%) were 0.91 (CI 95%, 0.891–0.928), 0.91 (CI 95%, 0.894–0.929), and 0.89 (CI 95%, 0.873–0.916) respectively (40). In 2019, Tada conducted a study involving 126 patients, utilizing MRI-PDFF as the reference standard for detecting and grading hepatic steatosis. There was a high correlation of r = 0.75 between PDFF and UGAP. The AUROCs of UGAP for steatosis grades S ≥ 1, S ≥ 2, and S = 3 were 0.92, 0.87, and 0.89, respectively (35).

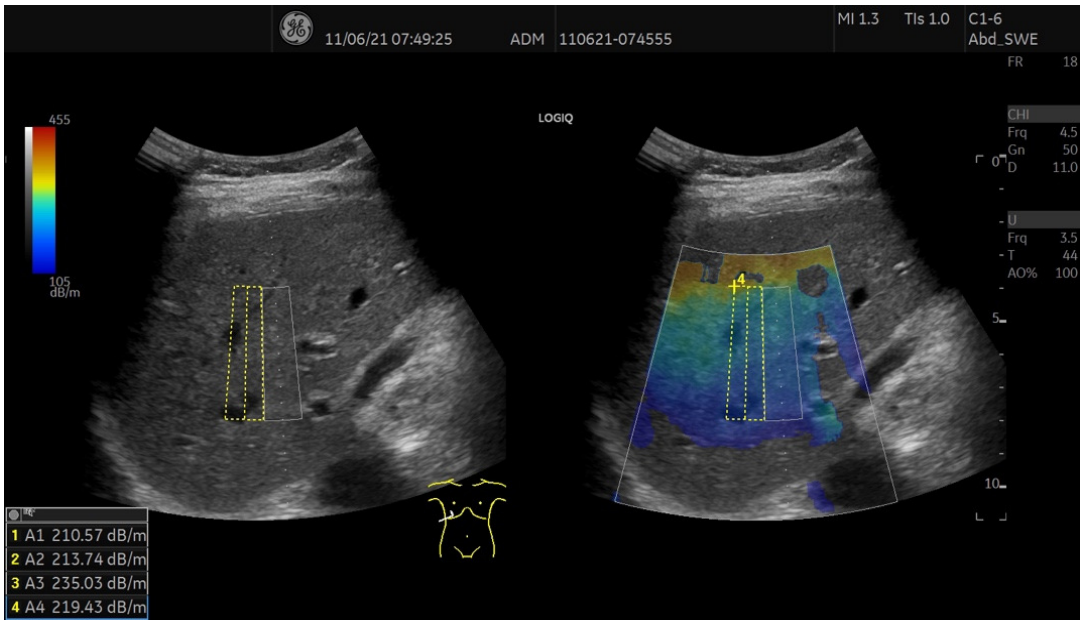

Fig.5.34. UGAP (Ultrasound-Guided Attenuation Parameter) developed by General Electric™

Using the ATT (attenuation measurement function) technology from Hitachi/Fujifilm (Tokyo, Japan), the measurement area is visualized in real-time without requiring additional tools. In B-mode ultrasound, multiple ultrasound waves at various frequencies are used for measurements. Therefore, ATT identifies hepatic steatosis by analyzing the variations in attenuation of the ultrasound signal. The ATT technique was analyzed in a prospective study by Tamaki, which included 351 patients with chronic liver diseases and used liver biopsy as the control method. Results showed a moderate correlation between ATT and liver biopsy (r = 0.50), and AUROC values for diagnosing S ≥ 1, S ≥ 2, and S ≥ 3 were 0.79, 0.87, and 0.96, respectively (41).

Using a color-coded map, ATI from Canon (Japan) measures and displays attenuation in real-time over an extensive area. The attenuation coefficient is expressed in decibels per centimeter per Megahertz (dB/cm/MHz). An automatic filter excludes blood vessels and other artifacts from the analysis, thus improving the accuracy of the measurements (Fig. 5.35) (18).

In a study conducted by Ferraioli, which included 129 participants, ATI was compared with MRI-PDFF. There was excellent inter-observer and intra-observer agreement, with ICCs ranging from 0.91 to 0.98. ATI demonstrated a strong correlation with MRI-PDFF, at 0.81, with an AUROC of 0.91 for identifying steatosis with grade S > 0 and 0.95 for S > 1. The cut-off values for ATI were 0.63 dB/cm/MHz for detecting steatosis S > 0 and 0.72 dB/cm/MHz for S > 1 (33). In another study by Bae, which used liver histology as the reference standard in a group of 108 subjects, the reported AUROC values for this method ranged between 0.84 and 0.93 (34).

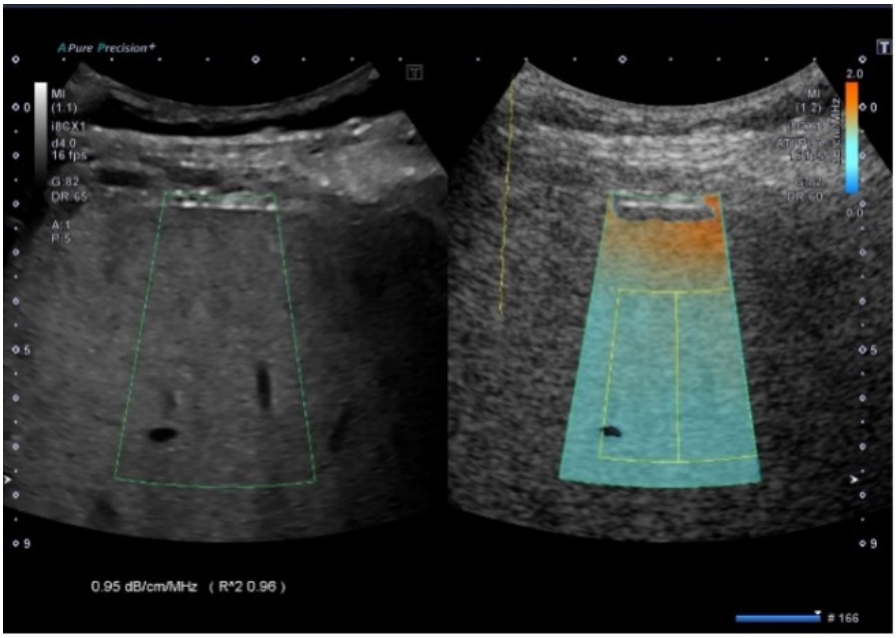

Fig.5.35. ATI (Attenuation Imaging) developed by Canon™

The Tissue Attenuation Imaging (TAI) technique from Samsung quantifies attenuation based on changes in the central frequency under optimal transmission and reception conditions. It is part of Samsung's advanced solution for liver fat load analysis, which includes other tools for assessing hepatic steatosis and fibrosis (Fig. 5.36).

Jeon's study revealed a significant correlation between TAI and MRI-PDFF ($r = 0.65$, $p < 0.001$). The AUROCs for TAI in detecting hepatic fat content of ≥ 5% and ≥ 10% were 0.86 (95% CI: 0.78-0.91) and 0.83 (95% CI: 0.75-0.89), respectively (42).

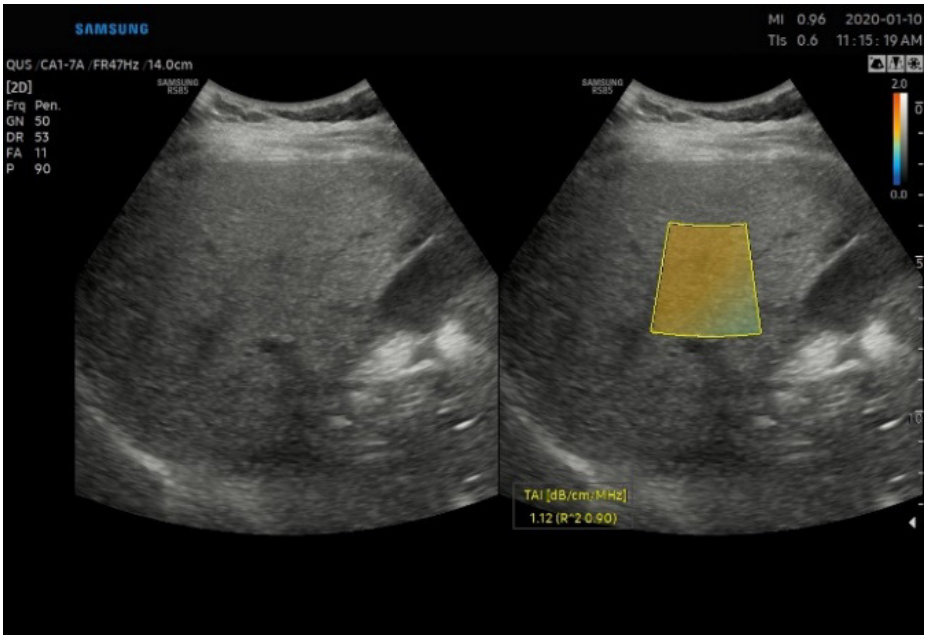

Fig. 5.36. TAI (Tissue Attenuation Imaging) developed by Samsung™

Other ultrasound-based approaches have also been developed to evaluate hepatic steatosis by analyzing multiple acoustic parameters, such as the backscatter coefficient (BSC), speckle statistics, or sound speed.

Backscatter Coefficient (BSC)

The backscatter coefficient (BSC) is a quantitative method that assesses the amount of ultrasound energy reflected by tissue during an ultrasound examination. BSC refers to the echogenicity or "brightness" of the tissue as measured by conventional ultrasound. In standard ultrasound, echogenicity intensifies with the presence of fat in the liver, and BSC also increases with fat infiltration in the liver (43). Recent studies have highlighted a significant correlation between BSC and the degree of hepatic steatosis determined by biopsy ($r = 0.67$) or by MRI-PDFF ($r = 0.72$). Additionally, BSC has demonstrated remarkable diagnostic accuracy for hepatic steatosis, with AUROCs for $S \geq 1$, $S \geq 2$, and $S \geq 3$ of 0.95, 0.85, and 0.83, respectively (44, 45).

Siemens Medical Solutions (USA) introduced the concept of Ultrasound-Derived Fat Fraction (UDFF), a methodology that integrates attenuation quantification with BSC (Fig. 5.37). According to Labyed's study, a strong correlation was found between values obtained by UDFF and MRI-PDFF (0.87). Furthermore, in the context of diagnosing hepatic steatosis, defined by an MRI-PDFF of over 5% and 10%, UDFF recorded AUROCs of 0.97 and 0.95, respectively (23).

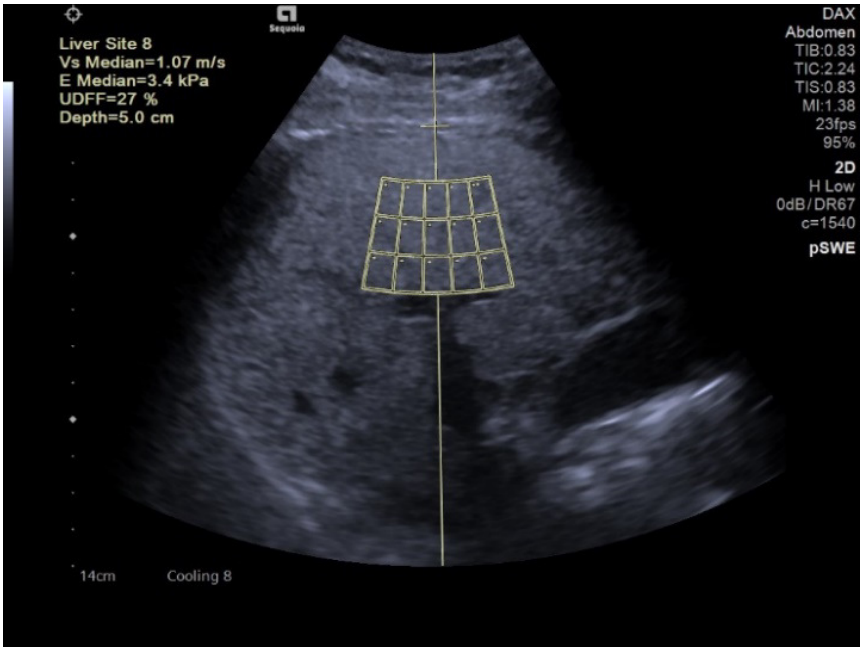

Fig. 5.37. UDFF (Ultrasound Derived Fat Fraction) developed by Siemens™.

Backscatter (Ultrasound Envelope Statistic Parametric Imaging)

Speckle patterns (pixel models) can be observed in ultrasound imaging. As microstructures in tissue scatter ultrasound, generating the speckle pattern, speckle statistics can be used to describe the scattering characteristics of the tissue. The Nakagami distribution and Acoustic Structure Quantification (ASQ) have been most intensively investigated for evaluating tissue properties.

Tissue Scatter Distribution Imaging (TSI)

Developed by Samsung, TSI is a technique based on the Nakagami distribution and has been recently introduced (Fig. 5.38). The technique demonstrated a significant correlation with MRI-PDFF results ($r = 0.68$, $p < 0.001$) in evaluating hepatic steatosis in patients with NAFLD. Regarding diagnostic performance, TSI had AUROC values of 0.87 for detecting hepatic fat content of ≥5% and 0.86 for content of ≥10%. Inter-observer analysis showed moderate reproducibility for TSI (ICC = 0.73), indicating some variability between different operators (46). In conclusion, TSI represents a promising technique for the non-invasive evaluation of hepatic steatosis.

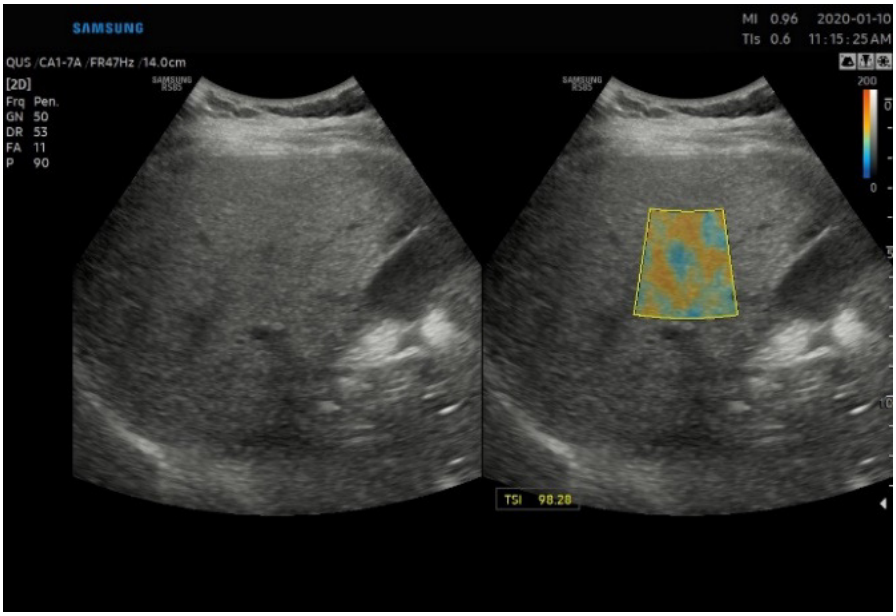

Fig. 5.38. TSI (Tissue Scatter distribution Imaging) developed by Samsung™

Acoustic Structure Quantification (ASQ)

The Acoustic Structure Quantification (ASQ) technique by Canon Medical Systems evaluates the difference between theoretical and actual tissue distributions, providing a non-invasive method for estimating the degree of hepatic steatosis (43). Karlas conducted a cohort study comparing ASQ with magnetic resonance spectroscopy (MRS), identifying a negative correlation between the focal disturbance ratio (FD ratio) and MRS (Spearman $r = -0.43$, $p = 0.004$) (47). In a prospective study involving 36 patients suspected of hepatic steatosis, a similar negative correlation was observed between FD ratio and MRS (Spearman $r = -0.43$, $p = 0.004$) (48). In Son's 2016 study, ASQ demonstrated excellent diagnostic performance in detecting hepatic steatosis over 10% (AUROC = 0.96) (49). Additionally, Keller's study highlighted a significant correlation between ASQ and the degree of hepatic steatosis established through histological examination ($r = -0.55$, $p < 0.0001$), but no correlation was found between histologically determined fibrosis stage and ASQ (50). These findings underscore ASQ's value as an effective non-invasive tool for evaluating hepatic steatosis.

Speed of Sound

In the presence of hepatic steatosis, a decrease in the speed of sound propagation through the hepatic parenchyma has been observed (51). In a study aimed at evaluating this principle, Imbault analyzed an ultrasound technique (SSE) capable of estimating the speed of sound in the liver. Validation on artificial anatomical models demonstrated the method's accuracy, and a preliminary clinical study (on 17 patients) showed a high correlation between SSE results and fat fraction determined by MRI, as well as biopsy results, highlighting this technique's potential in non-invasive diagnosis of hepatic steatosis (52). In a study published by Dioguardi Burgio, MRI-PDFF was used as the control method to test this technique's ability

to detect hepatic steatosis. With a speed of sound cut-off value of 1.537 mm/s, steatosis could be detected with a sensitivity of 80% and a specificity of 85.7% (S1-S3). There was also a strong correlation between SSE and MRI-PDFF of 0.73 (53).

A study dedicated to the Sound Speed Plane-wave UltraSound (SSp PLUS) technique (Fig. 5.39) revealed a strong correlation between this technique and the reference method used for steatosis evaluation, with a correlation coefficient of $r = 0.70$ ($p < 0.0001$). This suggests the effectiveness of SSp PLUS in identifying and determining the degree of hepatic steatosis. The optimal cut-off value established for SSp PLUS in predicting hepatic steatosis is 1.537 m/s. However, additional evidence is needed to confirm that measuring the speed of sound is a useful tool in evaluating hepatic steatosis (37).

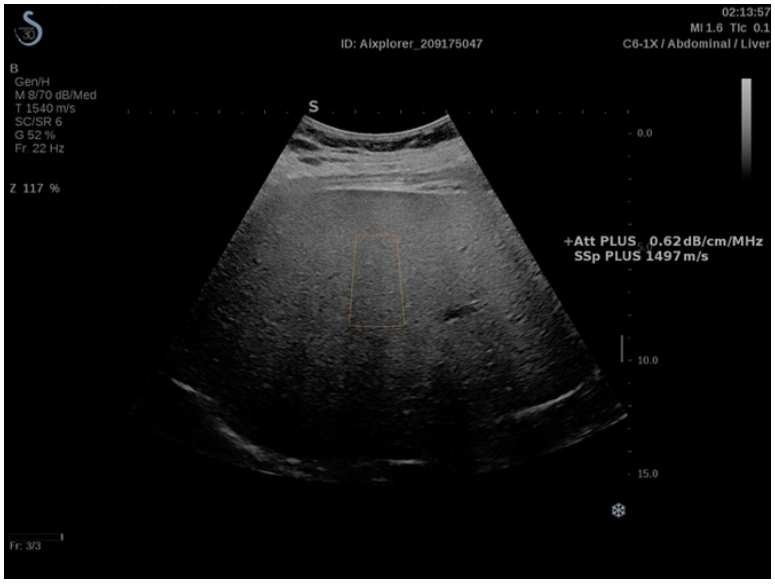

Fig. 5.39. Speed of Sound (Att Plus & SSp Plus) developed by Aixplorer (Hologic™)

Techniques for quantifying steatosis through ultrasonography provide a numerical and objective indicator of liver fat load. This allows for access to previous evaluations of patients undergoing follow-up visits to assess changes in the degree of hepatic steatosis, which is useful for monitoring the impact of clinical and therapeutic interventions. Furthermore, given that hepatic steatosis can negatively affect patient prognosis, quantifying liver fat gains significant clinical importance. For example, severe steatosis can accelerate disease progression to MASH (metabolic-associated steatohepatitis) or liver fibrosis (54). Patients requiring hepatic resections are more prone to postoperative complications and have an increased risk of death if they have hepatic steatosis. Compared to patients without steatosis, those with steatosis >20% have a significantly higher risk of postoperative complications, and those with steatosis >30% have an increased risk of postoperative mortality (55).

It is important to emphasize that even simple steatosis can lead to an unfavorable prognosis. A study conducted on a national cohort in Sweden from 1966-2017, which included

10,568 patients, showed that simple steatosis, MASH without fibrosis, non-cirrhotic fibrosis, and cirrhosis are associated with a significantly higher risk of mortality compared to the control group. Total mortality in the cohorts with simple steatosis, MASH without fibrosis, fibrosis, and cirrhosis was 2.5%, 3.0%, 3.5%, and 7.0% per year, respectively, while mortality among the control group was 1.69% per year (56).

A study by Izumi highlighted that in patients with chronic hepatitis C, a CAP value ≤ 221 dB/m is associated with a higher risk of HCC (57). In another cross-sectional study, which included 130 patients with HCC and 54 with chronic hepatitis C, it was observed that the CAP value in the chronic hepatitis C group was significantly higher than in the HCC group (259.96 dB/m vs. 209.57 dB/m, $p < 0.001$) (58). J. Oh et al. demonstrated that patients with HBV and advanced chronic liver disease (cACLD), identified by measuring liver stiffness (>10 kPa), have an increased risk of HCC when CAP values are below 222 dB/m. Patients with higher CAP values showed a reduced risk of HCC compared to those with lower values. However, in patients without cACLD, no significant difference in the risk of HCC was observed based on CAP value (59).

In conclusion, the quantification of steatosis in the context of chronic liver diseases represents a valuable diagnostic strategy, contributing to the efficient monitoring of disease progression and the optimization of therapeutic management.

5.1.f.3. Evaluation of Liver Fibrosis Using Ultrasound-Based Techniques

After assessing hepatic steatosis through standard ultrasound and quantifying it using QUS, patients with significant steatosis can immediately have their liver stiffness evaluated using MPUS. Liver stiffness serves as a marker for liver fibrosis, and its assessment is essential for all patients with chronic liver diseases, indicating the risk of future liver morbidity and, consequently, establishing the need for therapy, monitoring, and follow-up. However, certain factors can influence the accuracy of measurements, such as whether the examination is performed fasting or postprandial, elevated aminotransferase levels, the presence of extrahepatic cholestasis, or right heart failure. Therefore, we believe this measurement should be performed by qualified personnel familiar with the patient's history, ensuring that the results are correctly interpreted in the appropriate clinical context.

In the past, the performance of liver stiffness as a predictor of fibrosis severity was evaluated by direct comparison with liver biopsy results, following different stages of fibrosis, usually classified according to the METAVIR score (F1, F2, F3, F4). However, more recently, this differentiation method has been abandoned in favor of a new terminology introducing the term cACLD (compensated Advanced Chronic Liver Disease), as presented in the Baveno VI consensus (60). The main advantage of this revised terminology is that it shifts the focus from the need to distinguish between absent or mild fibrosis (F0 and F1), instead emphasizing the importance of differentiating between significant fibrosis, advanced fibrosis, and cirrhosis. This modernized approach improves risk stratification and personalized care for patients,

emphasizing disease stages that present a higher risk of unfavorable progression and complications.

In clinical practice, ultrasound-based elastographic methods used to evaluate liver stiffness are Shear Wave Elastography (SWE) methods, as described in the EFSUMB guidelines (61). These methods are divided into VCTE, which applies a short-duration mechanical impulse on the skin surface at a low frequency with a specific force, and ARFI techniques, where the probe itself generates the ultrasonic acoustic stimulus. ARFI techniques are further subdivided into pSWE and 2D-SWE. Results for VCTE are expressed in kilopascals (kPa), while for ARFI, they can be expressed in meters per second (m/s) or kPa.

Studies demonstrate high feasibility, generally over 90%, for all ultrasound elastographic methods. In the case of VCTE, two different probes must be used: the M probe and the XL probe (the latter for overweight and obese individuals). Another disadvantage of VCTE is that it cannot be used in the presence of ascites, and the probes need to be calibrated periodically, which involves additional costs. For all elastographic techniques, there are qualitative parameters, and perhaps the most important is the IQR/median (interquartile range), which should be below 30%. For 2D-SWE acquisition, qualitative criteria are implemented in each system, showing the acquisition quality. Currently, all ultrasound equipment manufacturers on the market integrate elastographic SWE modules into their equipment, some having not only pSWE or 2D-SWE but both (such as Samsung, Mindray, and others). What is the advantage of having two elastographic modules in the system? For example, when applying a method like 2D-SWE encounters difficulties in acquiring information, either due to not meeting qualitative parameters or technical infeasibility, resorting to pSWE can overcome these obstacles, and the patient can leave with a valid result.

VCTE (Vibration-Controlled Transient Elastography)

The principle of VCTE is used by both FibroScan and FibroTouch equipment, as shown in the images presented earlier. Comparative studies, such as the one conducted by Xu (62), have indicated similar results between these two systems. In a prospective study on a cohort of 435 patients with chronic liver diseases who underwent liver biopsy (32), the AUROC for FibroTouch was comparable to that of FibroScan in diagnosing significant fibrosis, severe fibrosis, or cirrhosis. There was a strong correlation ($r = 0.85$, $p < 0.001$) between values obtained with FibroTouch and FibroScan for liver stiffness. Moreover, no significant differences were found between FibroTouch and FibroScan in terms of sensitivity, specificity, negative predictive value, positive predictive value, and overall accuracy.

Numerous publications and meta-analyses have suggested different cut-off values for measuring liver stiffness using VCTE (FibroScan), considering various disease etiologies. More recently, however, the Baveno VI consensus, followed by Baveno VII, supported the so-called "Rule of 5" - a simplified approach for classifying stiffness values (Fig. 5.40) (60, 63).

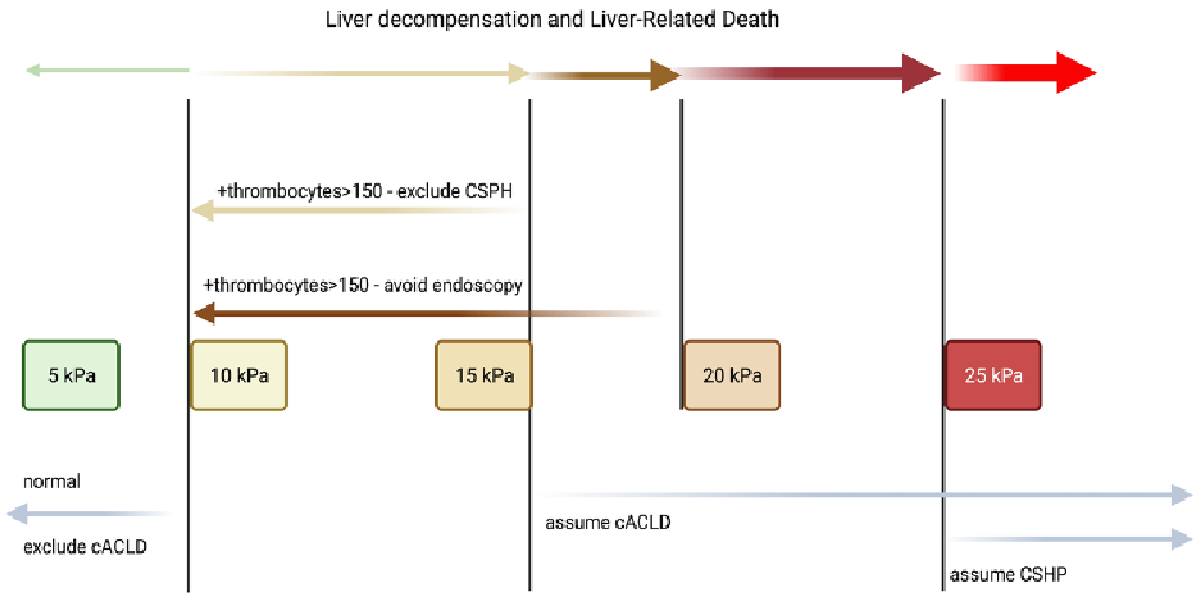

Fig. 5.40. Liver Stiffness Measurement Scale ("Rule of 5" - adapted from the Baveno VII consensus).

The "Rule of 5" provides a simple and user-friendly framework for clinical practice: less than 5 kPa indicates a normal liver; a value below 10 kPa excludes the presence of cACLD; a value above 15 kPa suggests the presence of cACLD; and values over 25 kPa denote the presence of clinically significant portal hypertension (CSPH). In clinical practice, these guidelines allow for the efficient use of elastography for various purposes, such as assessing fibrosis and determining cACLD or significant portal hypertension. Using the FibroScan system, CAP is used to stratify the severity of steatosis, while VCTE quickly confirms or excludes significant fibrosis in a very short time.

ARFI (Acoustic Radiation Force Impulse) Techniques

Due to their integration into standard ultrasound systems, ARFI methods can be performed immediately after routine abdominal ultrasound. Additionally, ultrasound machines are equipped with other functionalities such as Doppler evaluation, quantification of hepatic steatosis, and liver stiffness. Furthermore, when a focal liver lesion is identified, contrast-enhanced ultrasound (CEUS) can be performed immediately for characterization. This comprehensive approach, available with a single ultrasound device, provides an efficient multiparametric evaluation (MPUS). Regarding ARFI methods, all of them are based on the same principle; the probe is used to induce acoustic impulses into the liver tissue. The following images present examples of pSWE and 2D-SWE techniques (Fig. 5.41 - Fig. 5.47).

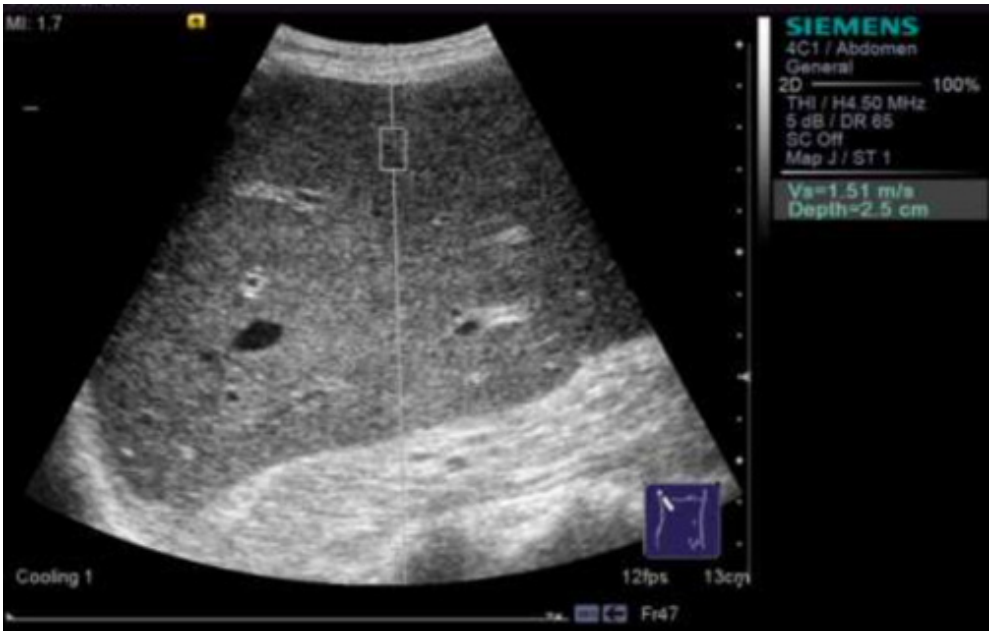

Fig. 5.41. pSWE-VTQ developed by Siemens™

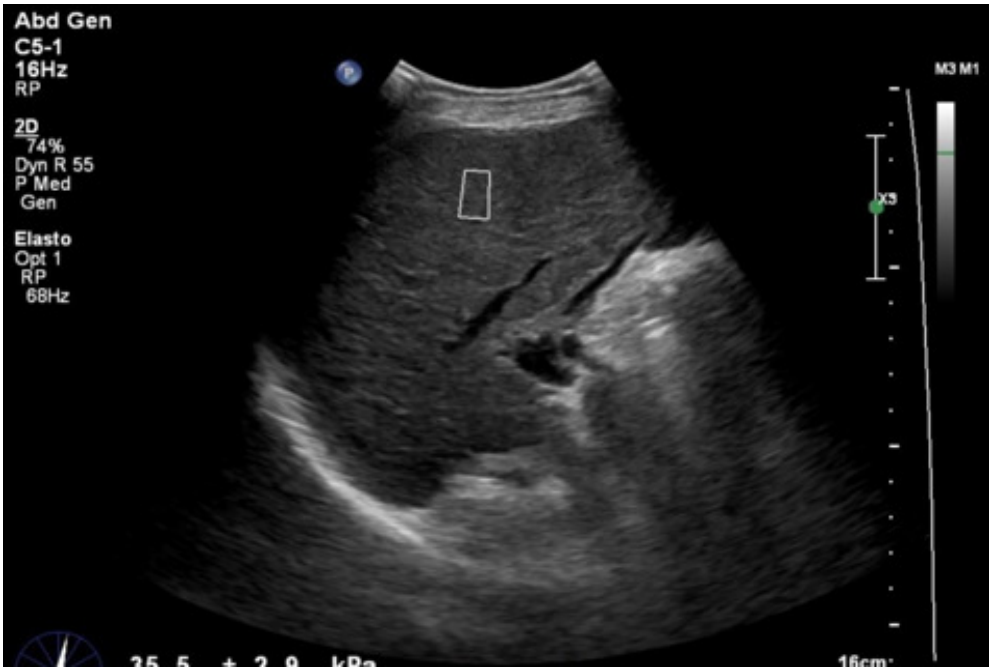

Fig. 5.42. pSWE-ElastPQ developed by Philips™

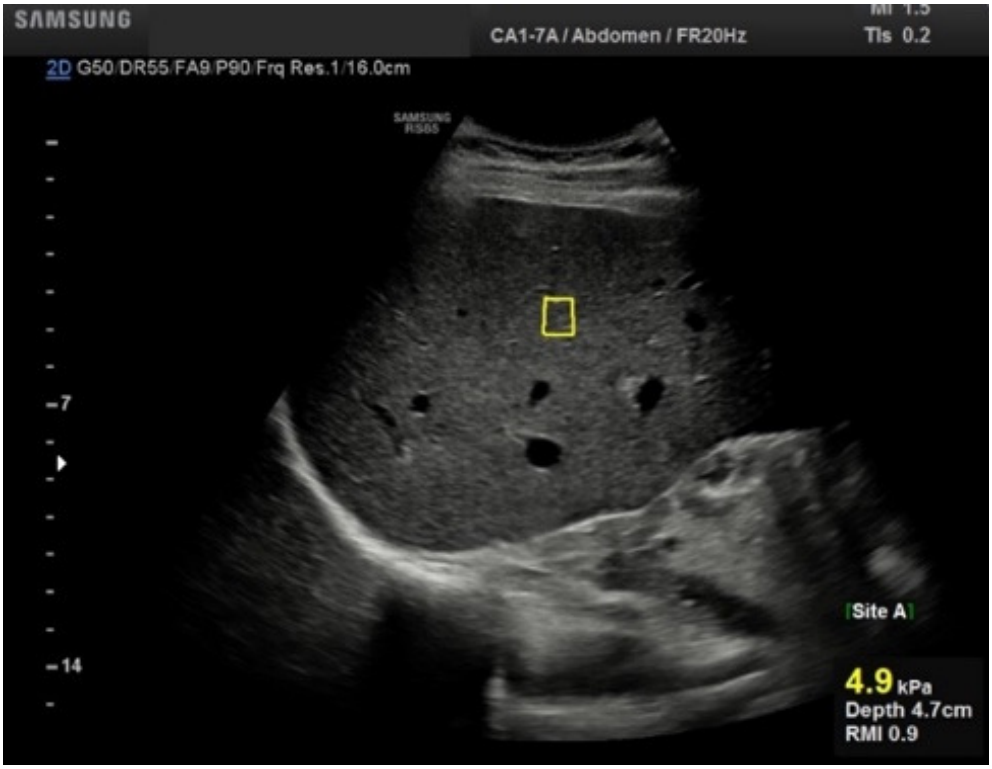

Fig. 5.43. pSWE developed by Samsung™

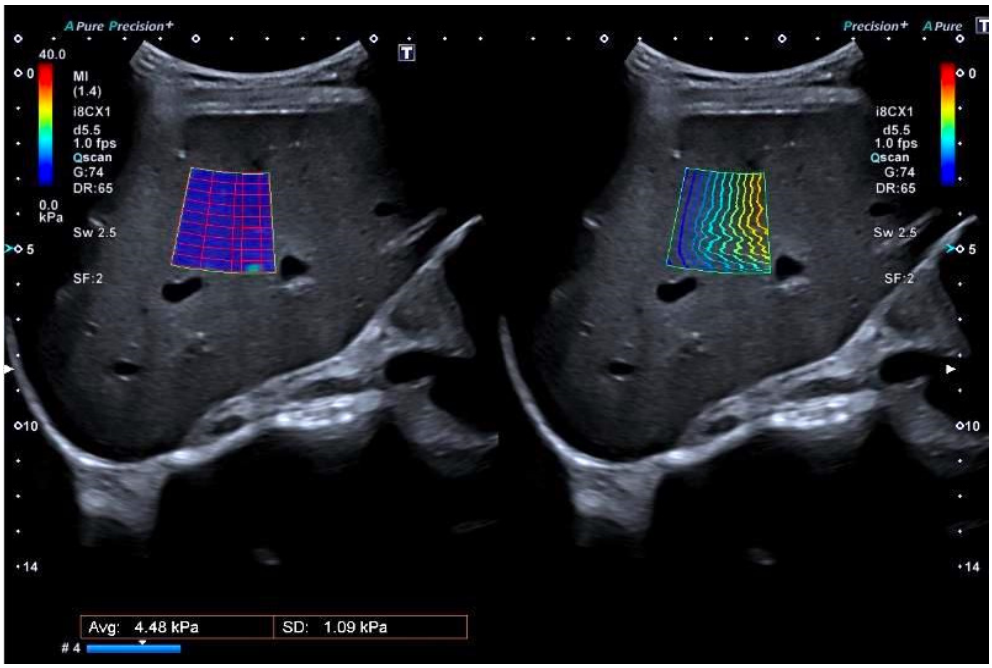

Fig. 5.44. 2D-SWE developed by Canon™

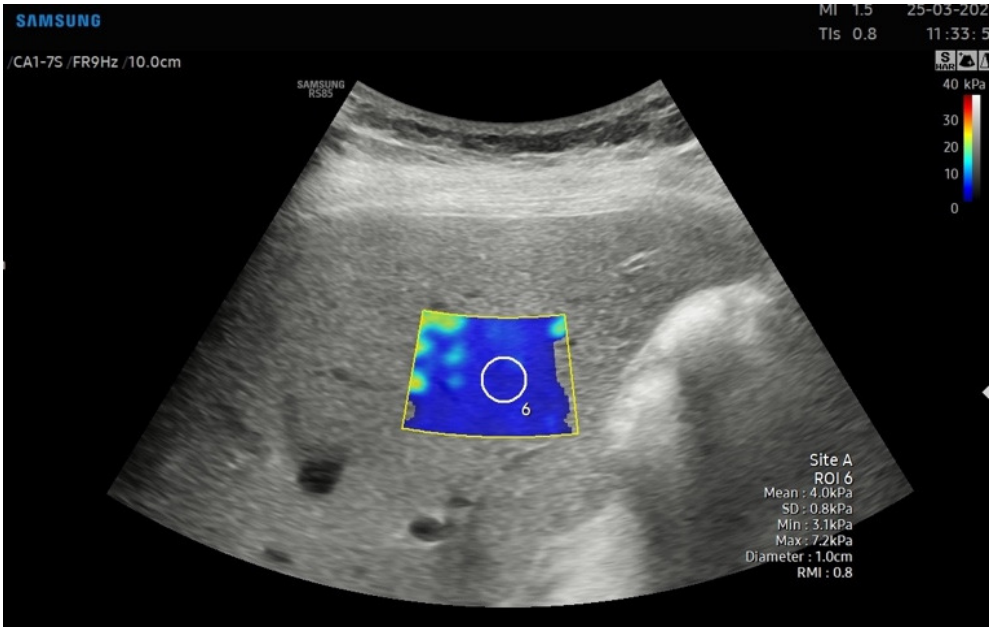

Fig. 5.45. 2D-SWE developed by Samsung™

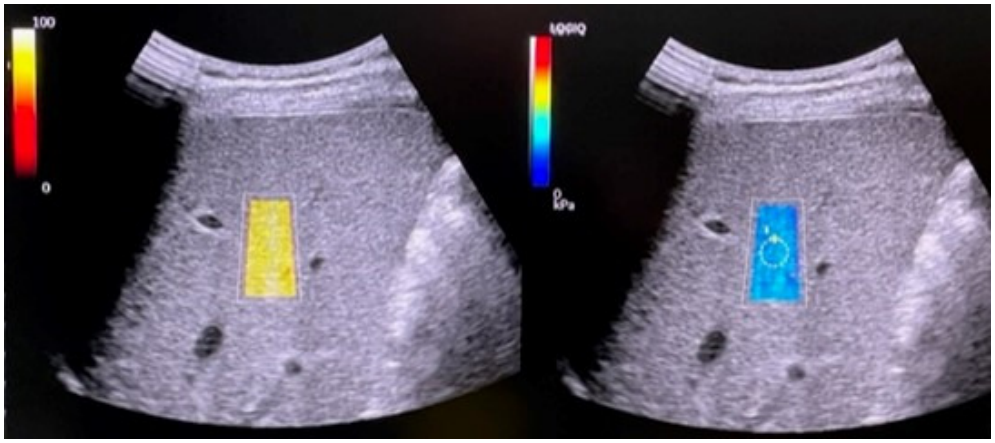

Fig. 5.46. 2D-SWE developed by General Electric™

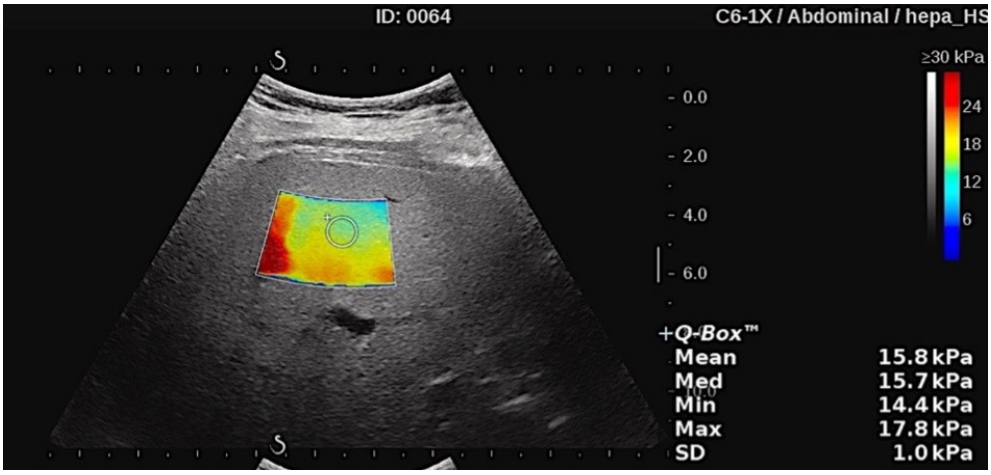

Fig. 5.47. 2D-SWE developed by Hologic™(Aixplorer)

Technically, SWE-ARFI methods are easy to perform. The patient lies on their back with the right arm in maximum abduction, similar to the positioning for VCTE. The transducer is placed in an intercostal space to capture the clearest possible image of the hepatic parenchyma. In pSWE elastography, a small measurement "box" of 10 by 5 mm is placed 1-2 cm below the liver capsule, ensuring optimal selection of the liver section and avoiding blood vessels. The patient is then asked to hold their breath in a neutral position, and the acquisition is performed. Five to ten measurements are taken, with the median value displayed afterward. For 2D-SWE, which provides both a qualitative assessment displayed as a color-coded map and a quantitative, numerical one, a larger "box" of approximately 3 by 2 cm is positioned similarly, at a distance below the liver capsule. Multiple loops are recorded, and the ROI (region of interest) is placed in each frame for evaluation. Three to five 2D-SWE measurements are sufficient, and the system calculates and displays the median value of the measurements (note, the median, not the mean, is used) (61).

In the past, each company developing a new ARFI technique proposed its own cut-off values for evaluating liver fibrosis, making their application in practice quite difficult (memorizing many values, each specific to an ultrasound company). In 2020, Barr proposed a simplified algorithm known as the "Rule of 4," facilitating easier application in clinical practice (64). Recommendations for interpreting liver stiffness values obtained with ARFI techniques in patients with viral hepatitis and NAFLD are as follows:

- A stiffness value <5 kPa (1.3 m/s) suggests a high likelihood that the liver is normal.
- A value < 9 kPa (1.7 m/s), in the absence of other known clinical signs, indicates that cACLD is unlikely. If known clinical signs are present, further tests may be necessary for confirmation.
- A value between 9 and 13 kPa (1.7-2.1 m/s) indicates possible cACLD but requires additional tests for confirmation.
- A value > 13 kPa (2.1 m/s) confirms cACLD (compensated advanced chronic liver disease).
- A value > 17 kPa (2.4 m/s) suggests the presence of clinically significant portal hypertension (CSPH).

Numerous prospective studies and meta-analyses (most using liver biopsy as the reference standard) have demonstrated the practical utility of SWE methods in evaluating liver stiffness as a marker of fibrosis. These studies reveal that the performance of these methods, expressed through AUROC curves, tends to increase in parallel with the severity of fibrosis, frequently exceeding 90% for cases of liver cirrhosis (65-69). Comparative studies between various SWE methods have demonstrated their equivalent practical value in evaluating liver fibrosis (70-75).

The latest EASL guidelines regarding non-invasive tests for evaluating liver fibrosis highlight the advantages and disadvantages of different methods (Table 5.VI) (76). These

guidelines provide a comprehensive overview of several technologies, VCTE, pSWE, 2D-SWE, and magnetic resonance elastography (MRE).

Table 5.VI. Advantages and disadvantages of different non-invasive tests

Serum markers			**Transient Elastography**	**pSWE**	**2D-SWE**	**MRE**
Advantages	Non-patented -good reproducibility -high applicability -no cost and wide availability -well validated -can be performed in the outpatient clinic -validated prognostic value	Patented -good reproducibility -high applicability -can be performed in the outpatient clinic -validated prognostic value	-most widely used and validated technique -point-of-care (bedside, easy to learn, rapid) -quality criteria well defined -good reproducibility -high performance for cirrhosis -prognostic value in compensated cirrhosis well validated	-can be performed with regular ultrasound device -ROI smaller than TE and location chosen by the operator -higher applicability than TE -equivalent performance that of TE for advanced fibrosis and cirrhosis -prognostic value in cirrhosis -high applicability for spleen stiffness measurement	-can be performed with regular ultrasound device -large ROI that can be adjusted in size and location chosen by the operator -measures liver stiffness in real time -good applicability - high performance for the diagnosis of advanced fibrosis and cirrhosis - prognostic value in cirrhosis	-can be implemented on a regular MRI machine -examination of the whole liver -higher applicability than TE (ascites and obesity) -high performance for the earlier fibrosis stage and for diagnosis of cirrhosis
Disadvantages	-non-liver specific -performance not as good as TE and patented serum markers -false positive results with FIB4 and NFS in case of age>65yrs	-cost -non-liver specific -performance not as good as TE for cirrhosis -false positive results in case of extrahepatic inflammatory conditions, profibrotic, extrahepatic conditions and other (Gilbert syndrome, hemolysis)	-requires a dedicated device -ROI cannot be chosen -lower applicability than serum markers -false positive in case of acute hepatitis, extrahepatic cholestasis, liver congestion, food intake, excessive alcohol intake.	- false positive in case of acute hepatitis, extrahepatic cholestasis, liver congestion, food intake, excessive alcohol intake.	-false positive in case of acute hepatitis, extrahepatic cholestasis, liver congestion, food intake, excessive alcohol intake.	-not applicable in case of iron overload -requires an MRI facility -time consuming -costly -not clear data on prognostic value

5.1.f.4. Evaluation of Hepatic Inflammation Using Ultrasound-Based Techniques

Given that biological soft tissues are hydrated, they are viscoelastic rather than purely elastic. SWE are shear waves that propagate laterally, moving away from the deformation stimulus, which can be an acoustic impulse in ARFI techniques (pSWE and 2D-SWE) or a mechanical impulse in VCTE. The characteristics of shear waves (SWE) (such as speed, attenuation, and dispersion) are closely correlated with the properties of the propagation medium. Viscosity and elasticity are the two parameters that most influence SWE properties. One of the major limitations of most SWE methods is that they only calculate elasticity, using a linear elastic model and ignoring the dispersion effect, which characterizes tissue viscosity (77).

Several studies have revealed that liver stiffness significantly decreases in patients with alcoholic liver disease (ALD) after withdrawal, while fibrosis stages assessed using liver biopsy remain largely unchanged (78). Liver stiffness also decreases in patients with chronic hepatitis C after sustained viral response following interferon or direct-acting antiviral therapy. A similar pattern was observed in patients with HBV initiated on antiviral therapy (79). These results suggest that, in addition to fibrosis, inflammation is a major contributor to stiffness. Therefore, when evaluating elastography results, it is critical to distinguish between the inflammatory and fibrotic components.

Ultrasound manufacturers have developed techniques that evaluate the slope of the shear-wave dispersion curve, identified as being associated with tissue viscosity, thus providing biomechanical information regarding necroinflammation. A study published by Sugimoto (2018) demonstrated that SWE is more effective than viscosity for predicting fibrosis grade and that viscosity is more useful than SWE for predicting necroinflammation grade. Consequently, the slope of the dispersion curve, which reflects viscosity, may offer additional pathophysiological insights into CLD (80, 81).

Determining the degree of inflammation is essential in several specific pathological conditions. Firstly, due to significant variations in prognosis, it is important to distinguish between simple hepatic steatosis and steatohepatitis (MASH) in patients with MASLD. Liver biopsy is the ideal technique to distinguish this, but MASLD affects over 30% of the population in developed countries, making it impractical to evaluate all these patients by this invasive procedure. Several biological markers have been analyzed in this regard, but it has been established that biological tests alone (such as transaminases or Cytokeratin 18) are insufficient to predict the presence of inflammation.

Regarding the VCTE system using iLivTouch, a study by Gao, which included a cohort of 259 individuals with biopsy-confirmed MASLD, explored an innovative QUS method to identify inflammation (MASH). This score demonstrated a promising ability to discriminate MASH, with an AUROC of 0.798 (95% CI 0.731-0.865, p = 0.755) in the training set and 0.816 (95% CI 0.725-0.906; p = 0.397) in the validation set (82).

A prospective study conducted by Sugimoto on a group of 111 patients who underwent liver biopsy for suspected MASLD investigated the role of shear-wave dispersion slope (SWDS) using the Aplio i800 (Canon, Japan) in diagnosing steatohepatitis. The study results indicated that SWDS increases significantly with the degree of inflammation. Using a cut-off value of 8.5 m/s/kHz, SWDS demonstrated very high accuracy in identifying the presence of lobular inflammation ≥1, with an AUROC of 0.95. It also showed good ability to distinguish inflammation grades ≥2 and equal to 3, with AUROCs of 0.81 and 0.85, respectively. Interestingly, when combining shear-wave speed, attenuation coefficient, and SWDS into a regression model, the overall AUROC for diagnosing MASH was higher than the AUROC of each parameter alone (0.81 vs. 0.76, 0.71, and 0.70 for SWDS, attenuation coefficient, and shear-wave speed, respectively). Additionally, both SWDS and attenuation coefficient were significantly influenced by lobular inflammation and steatosis grade, while fibrosis was significantly influenced by shear-wave speed (83).

A study conducted by Lee evaluated the effectiveness of a multiparametric approach using attenuation imaging, 2D-SWE, and SWDS in detecting steatosis, fibrosis, and inflammation in patients with biopsy-proven MASLD. The results of this study, which included 102 patients with MASLD, showed that the attenuation coefficient was associated with steatosis grade ($p<0.01$), identifying patients with steatosis grades ≥S1, ≥S2, and ≥S3 with AUROC values of 0.93, 0.88, and 0.83, respectively. Liver stiffness was correlated with fibrosis stage ($p<0.01$), and lobular inflammatory activity was identified as the only factor associated with SWDS ($p<0.01$), detecting inflammation grades I≥1, I≥2, and I=3 with AUROC values of 0.89, 0.85, and 0.78, respectively. A risk score system was developed to detect steatohepatitis based on the attenuation coefficient and SWDS, identifying patients with steatohepatitis with an AUROC of 0.93, which was significantly higher than that of other parameters ($p<0.05$) except for SWDS (AUROC 0.89; $p=0.18$) (84).

A multicenter study conducted by Jang (2022) evaluated the utility of MPUS in assessing hepatic steatosis, inflammation, and fibrosis in a cohort of 132 patients. Participants were evaluated using the attenuation coefficient (AC) from ATI, liver stiffness assessed by 2D-SWE, and the slope of the dispersion curve (DS). The authors developed a risk scoring system by combining these parameters. This score demonstrated high diagnostic performance for detecting MASH, with an AUROC of 0.94 (95% CI: 0.89 to 0.98, $p < 0.05$) (85).

Another system used to evaluate hepatic inflammation is the Viscosity Plane-Wave UltraSound (Vi.PLUS) technology (Hologic Aixplorer system) (Fig. 5.48). In a cohort of 204 subjects who did not undergo liver biopsy, data analysis revealed that Vi.PLUS values correlated with body mass index (BMI) and liver stiffness measurements obtained using the ultrasound system, but not with transaminase values (86, 87). The same system was used in a recent study published by Minciună et al., where data showed that Vi.PLUS results weakly correlated with GOT ($r=0.33$, $p<0.001$) but did not correlate with GPT values. No differences were observed in mean viscosity values between patients with GOT ≥100 U/l and those with lower levels (2.3 vs. 2.1, $p>0.05$). In the study group, viscosity moderately correlated with VCTE

values (r=0.679, p<0.001) and with other non-invasive markers of liver fibrosis, including FIB-4, APRI, and e-LIFT (r=0.486, r=0.437, r=0.473, p<0.001). However, viscosity weakly correlated with CAP values (r=0.209, p=0.004) (88). However, neither of the last two studies used liver biopsy as a control method, so no firm conclusions can be drawn.

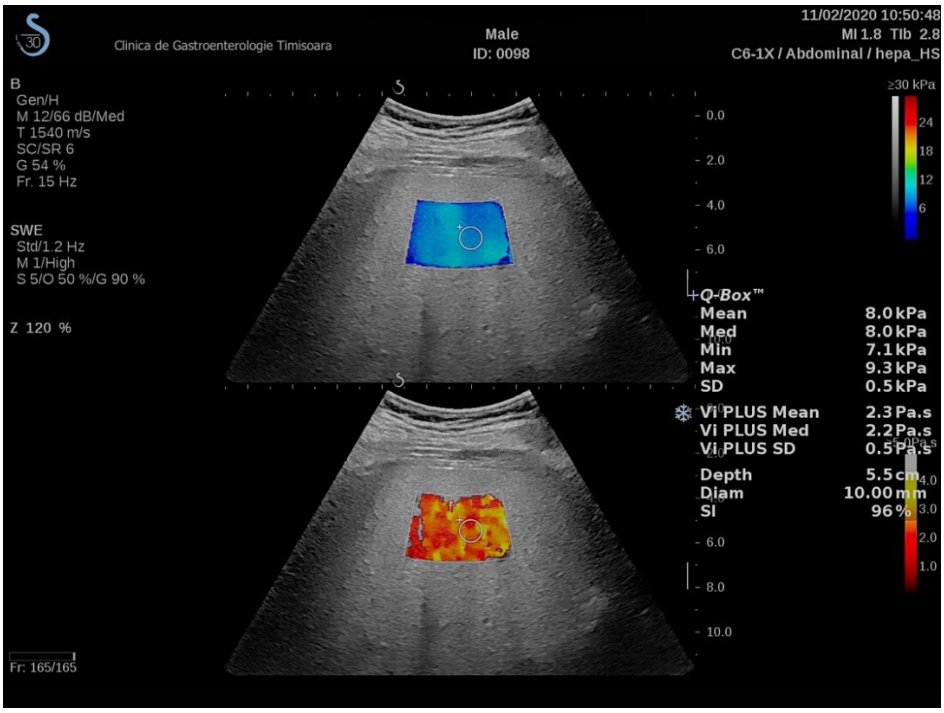

Fig.5.48. Vi.Plus developed by Hologic™(Aixplorer)

The number of studies evaluating the capability of these non-invasive techniques to assess hepatic inflammation is still limited, and their role is not yet fully established. Future studies using liver biopsy as the reference method are necessary to clarify this aspect.

In summary, the advantages of simultaneously assessing fibrosis and steatosis, along with the accessibility, affordability, absence of radiation, repeatability, and high patient acceptance, suggest that this multiparametric approach (MPUS) is well-suited for evaluating at-risk patients. During the initial patient encounter, a comprehensive multiparametric assessment of hepatic features—including structure, fibrosis, steatosis, and inflammation—can be achieved within minutes. The continued development and integration of these multiparametric techniques into routine clinical practice will provide significant benefits not only to hepatologists but also to general practitioners and any physician conducting abdominal ultrasound examinations.

References

1. Moon AM, Singal AG, Tapper EB. Contemporary Epidemiology of Chronic Liver Disease and Cirrhosis. Clin Gastroenterol Hepatol. 2020 Nov 1;18(12):2650–66.
2. Estes C, Anstee QM, Arias-Loste MT, Bantel H, Bellentani S, Caballeria J, et al. Modeling NAFLD disease burden in China, France, Germany, Italy, Japan, Spain, United Kingdom, and United States for the period 2016-2030. J Hepatol. 2018 Oct;69(4):896–904.
3. Younossi ZM, Golabi P, Paik JM, Henry A, Van Dongen C, Henry L. The global epidemiology of nonalcoholic fatty liver disease (NAFLD) and nonalcoholic steatohepatitis (NASH): a systematic review. Hepatology. 2023 Apr;77(4):1335–47.
4. Younossi ZM, Koenig AB, Abdelatif D, Fazel Y, Henry L, Wymer M. Global epidemiology of nonalcoholic fatty liver disease—Meta-analytic assessment of prevalence, incidence, and outcomes. Hepatology. 2016;64(1):73–84.
5. Eslam M, Sanyal AJ, George J. MAFLD: A Consensus-Driven Proposed Nomenclature for Metabolic Associated Fatty Liver Disease. Gastroenterology. 2020 May;158(7):1999-2014.e1.
6. Rinella ME, Lazarus J V, Ratziu V, Francque SM, Sanyal AJ, Kanwal F, et al. A multisociety Delphi consensus statement on new fatty liver disease nomenclature. Hepatology. 2023 Dec;78(6):1966–86.
7. Pinzani M. Pathophysiology of Liver Fibrosis. Dig Dis. 2015;33(4):492–7.
8. Böttcher K, Pinzani M. Pathophysiology of liver fibrosis and the methodological barriers to the development of anti-fibrogenic agents. Adv Drug Deliv Rev. 2017;121:3–8.
9. Bataller R, Brenner DA. Liver fibrosis. J Clin Invest. 2005 Feb;115(2):209–18.
10. Thorgeirsson SS, Grisham JW. Molecular pathogenesis of human hepatocellular carcinoma. Nat Genet. 2002 Aug;31(4):339–46.
11. Bedossa P, Carrat F. Liver biopsy: The best, not the gold standard. J Hepatol. 2009 Jan;50(1):1–3.
12. Hamaguchi M, Kojima T, Itoh Y, Harano Y, Fujii K, Nakajima T, et al. The severity of ultrasonographic findings in nonalcoholic fatty liver disease reflects the metabolic syndrome and visceral fat accumulation. Am J Gastroenterol. 2007 Dec;102(12):2708–15.
13. Hernaez R, Lazo M, Bonekamp S, Kamel I, Brancati FL, Guallar E, et al. Diagnostic accuracy and reliability of ultrasonography for the detection of fatty liver: a meta-analysis. Hepatology. 2011 Sep;54(3):1082–90.
14. Webb M, Yeshua H, Zelber-Sagi S, Santo E, Brazowski E, Halpern Z, et al. Diagnostic value of a computerized hepatorenal index for sonographic quantification of liver steatosis. AJR Am J Roentgenol. 2009 Apr;192(4):909–14.
15. Petzold G, Lasser J, Rühl J, Bremer SCB, Knoop RF, Ellenrieder V, et al. Diagnostic accuracy of B-Mode ultrasound and Hepatorenal Index for graduation of hepatic steatosis in patients with chronic liver disease. PLoS One. 2020;15(5):e0231044.
16. Johnson SI, Fort D, Shortt KJ, Therapondos G, Galliano GE, Nguyen T, et al. Ultrasound Stratification of Hepatic Steatosis Using Hepatorenal Index. Diagnostics (Basel, Switzerland). 2021 Aug;11(8).
17. Stahlschmidt FL, Tafarel JR, Menini-Stahlschmidt CM, Baena CP. Hepatorenal index for grading liver steatosis with concomitant fibrosis. PLoS One. 2021;16(2):e0246837.
18. Ferraioli G, Soares Monteiro LB. Ultrasound-based techniques for the diagnosis of liver steatosis. World J Gastroenterol. 2019 Oct;25(40):6053–62.

19. Kozłowska-Petriczko K, Wunsch E, Petriczko J, Syn WK, Milkiewicz P. Diagnostic Accuracy of Non-Imaging and Ultrasound-Based Assessment of Hepatic Steatosis Using Controlled Attenuation Parameter (CAP) as Reference. J Clin Med. 2021 Apr;10(7).
20. Ballestri S, Nascimbeni F, Baldelli E, Marrazzo A, Romagnoli D, Targher G, et al. Ultrasonographic fatty liver indicator detects mild steatosis and correlates with metabolic/histological parameters in various liver diseases. Metabolism. 2017;72:57–65.
21. Ferraioli G, Berzigotti A, Barr RG, Choi BI, Cui XW, Dong Y, et al. Quantification of Liver Fat Content with Ultrasound: A WFUMB Position Paper. Ultrasound Med Biol. 2021;47(10):2803–20.
22. Xavier SA, Monteiro SO, Arieira CM, Castro FD, Magalhães JT, Leite SM, et al. US-FLI score - Is it possible to predict the steatosis grade with an ultrasonographic score? Mol Genet Metab. 2021 Mar;132(3):204–9.
23. Labyed Y, Milkowski A. Novel Method for Ultrasound-Derived Fat Fraction Using an Integrated Phantom. J Ultrasound Med [Internet]. 2020 Dec 1;39(12):2427–38.
24. Ferraioli G. Quantitative assessment of liver steatosis using ultrasound controlled attenuation parameter (Echosens). J Med Ultrason. 2021;48(4):489–95.
25. Lupsor-Platon M, Feier D, Stefănescu H, Tamas A, Botan E, Sparchez Z, et al. Diagnostic accuracy of controlled attenuation parameter measured by transient elastography for the non-invasive assessment of liver steatosis: A prospective study. J Gastrointest Liver Dis. 2015;24(1):35–42.
26. Karlas T, Petroff D, Sasso M, Fan JG, Mi YQ, de Lédinghen V, et al. Individual patient data meta-analysis of controlled attenuation parameter (CAP) technology for assessing steatosis. J Hepatol. 2017;66(5):1022–30.
27. Shi KQ, Tang JZ, Zhu XL, Ying L, Li DW, Gao J, et al. Controlled attenuation parameter for the detection of steatosis severity in chronic liver disease: A meta-analysis of diagnostic accuracy. J Gastroenterol Hepatol. 2014 Jun 1;29(6):1149–58.
28. Sasso M, Tengher-Barna I, Ziol M, Miette V, Fournier C, Sandrin L, et al. Novel controlled attenuation parameter for noninvasive assessment of steatosis using Fibroscan®: Validation in chronic hepatitis C. J Viral Hepat. 2012;19(4):244–53.
29. Petroff D, Blank V, Newsome PN, Shalimar, Voican CS, Thiele M, et al. Assessment of hepatic steatosis by controlled attenuation parameter using the M and XL probes: an individual patient data meta-analysis. Lancet Gastroenterol Hepatol. 2021;6(3): 185-19
30. Eddowes PJ, Sasso M, Allison M, Tsochatzis E, Anstee QM, Sheridan D, et al. Accuracy of FibroScan Controlled Attenuation Parameter and Liver Stiffness Measurement in Assessing Steatosis and Fibrosis in Patients With Nonalcoholic Fatty Liver Disease. Gastroenterology. 2019; May;156(6):1717-1730
31. Chan WK, Nik Mustapha NR, Mahadeva S, Wong VWS, Cheng JYK, Wong GLH. Can the same controlled attenuation parameter cut-offs be used for M and XL probes for diagnosing hepatic steatosis? J Gastroenterol Hepatol. 2018 Oct;33(10):1787–94.
32. Qu Y, Song YY, Chen CW, Fu QC, Shi JP, Xu Y, et al. Diagnostic Performance of FibroTouch Ultrasound Attenuation Parameter and Liver Stiffness Measurement in Assessing Hepatic Steatosis and Fibrosis in Patients With Nonalcoholic Fatty Liver Disease. Clin Transl Gastroenterol. 2021 Apr;12(4):e00323.

33. Ferraioli G, Maiocchi L, Raciti MV, Tinelli C, De Silvestri A, Nichetti M, et al. Detection of Liver Steatosis With a Novel Ultrasound-Based Technique: A Pilot Study Using MRI-Derived Proton Density Fat Fraction as the Gold Standard. Clin Transl Gastroenterol. 2019;10(10):e00081.
34. Bae JS, Lee DH, Lee JY, Kim H, Yu SJ, Lee JH, et al. Assessment of hepatic steatosis by using attenuation imaging: a quantitative, easy-to-perform ultrasound technique. Eur Radiol. 2019;29(12):6499–507.
35. Tada T, Kumada T, Toyoda H, Kobayashi N, Sone Y, Oguri T, et al. Utility of attenuation coefficient measurement using an ultrasound-guided attenuation parameter for evaluation of hepatic steatosis: Comparison with MRI-Determined proton density fat fraction. Am J Roentgenol. 2019;212(2):332–41.
36. Bende F, Sporea I, Sirli R, Baldea V, Lazar A, Lupușoru R, et al. Ultrasound-Guided Attenuation Parameter (UGAP) for the quantification of liver steatosis using the Controlled Attenuation Parameter (CAP) as the reference method. Med Ultrason. 2021;23(1):7–14.
37. Popa A, Șirli R, Popescu A, Bâldea V, Lupușoru R, Bende F, et al. Ultrasound-Based Quantification of Fibrosis and Steatosis with a New Software Considering Transient Elastography as Reference in Patients with Chronic Liver Diseases. Ultrasound Med Biol. 2021 Jul;47(7):1692-1703
38. Serra JT, Mueller J, Teng H, Elshaarawy O, Mueller S. Prospective Comparison of Transient Elastography Using Two Different Devices: Performance of FibroScan and FibroTouch. Hepat Med. 2020;12:41–8.
39. Fujiwara Y, Kuroda H, Abe T, Ishida K, Oguri T, Noguchi S, et al. The B-Mode Image-Guided Ultrasound Attenuation Parameter Accurately Detects Hepatic Steatosis in Chronic Liver Disease. Ultrasound Med Biol. 2018;44(11):2223–32.
40. Imajo K, Toyoda H, Yasuda S, Suzuki Y, Sugimoto K, Kuroda H, et al. Utility of Ultrasound-Guided Attenuation Parameter for Grading Steatosis With Reference to MRI-PDFF in a Large Cohort. Clin Gastroenterol Hepatol Off Clin Pract J Am Gastroenterol Assoc. 2022 Nov;20(11):2533-2541.e7.
41. Tamaki N, Koizumi Y, Hirooka M, Yada N, Takada H, Nakashima O, et al. Novel quantitative assessment system of liver steatosis using a newly developed attenuation measurement method. Hepatol Res. 2018;48(10):821–8.
42. Jeon SK, Lee JM, Joo I, Park SJ. Quantitative Ultrasound Radiofrequency Data Analysis for the Assessment of Hepatic Steatosis in Nonalcoholic Fatty Liver Disease Using Magnetic Resonance Imaging Proton Density Fat Fraction as the Reference Standard. Korean J Radiol. 2021 Jul;22(7):1077–86.
43. Park J, Lee JM, Lee G, Jeon SK, Joo I. Quantitative Evaluation of Hepatic Steatosis Using Advanced Imaging Techniques: Focusing on New Quantitative Ultrasound Techniques. Korean J Radiol. 2022 Jan;23(1):13–29.
44. Lu ZF, Zagzebski JA, Lee FT. Ultrasound backscatter and attenuation in human liver with diffuse disease. Ultrasound Med Biol. 1999 Sep;25(7):1047–54.
45. Paige JS, Bernstein GS, Heba E, Costa EAC, Fereirra M, Wolfson T, et al. A Pilot Comparative Study of Quantitative Ultrasound, Conventional Ultrasound, and MRI for Predicting Histology-Determined Steatosis Grade in Adult Nonalcoholic Fatty Liver Disease. AJR Am J Roentgenol. 2017 May;208(5):W168–77.

46. Rónaszéki AD, Budai BK, Csongrády B, Stollmayer R, Hagymási K, Werling K, et al. Tissue attenuation imaging and tissue scatter imaging for quantitative ultrasound evaluation of hepatic steatosis. Medicine (Baltimore). 2022 Aug;101(33):e29708.
47. Karlas T, Berger J, Garnov N, Lindner F, Busse H, Linder N, et al. Estimating steatosis and fibrosis: Comparison of acoustic structure quantification with established techniques. World J Gastroenterol. 2015 Apr;21(16):4894–902.
48. Lee DH, Lee JY, Park MS, Han JK. Non-invasive monitoring of hepatic steatosis via acoustic structure quantification of ultrasonography with MR spectroscopy as the reference standard. Ultrason (Seoul, Korea). 2020 Jan;39(1):70–8.
49. Son JY, Lee JY, Yi NJ, Lee KW, Suh KS, Kim KG, et al. Hepatic Steatosis: Assessment with Acoustic Structure Quantification of US Imaging. Radiology. 2016 Jan;278(1):257–64.
50. Keller J, Kaltenbach TEM, Haenle MM, Oeztuerk S, Graeter T, Mason RA, et al. Comparison of Acoustic Structure Quantification (ASQ), shearwave elastography and histology in patients with diffuse hepatopathies. BMC Med Imaging. 2015 Dec;15:58.
51. Suzuki K, Hayashi N, Sasaki Y, Kono M, Kasahara A, Fusamoto H, et al. Dependence of ultrasonic attenuation of liver on pathologic fat and fibrosis: Examination with experimental fatty liver and liver fibrosis models. Ultrasound Med Biol. 1992;18(8):657–66.
52. Imbault M, Faccinetto A, Osmanski BF, Tissier A, Deffieux T, Gennisson JL, et al. Robust sound speed estimation for ultrasound-based hepatic steatosis assessment. Phys Med Biol. 2017;62(9):3582–98.
53. Dioguardi Burgio M, Imbault M, Ronot M, Faccinetto A, Van Beers BE, Rautou PE, et al. Ultrasonic Adaptive Sound Speed Estimation for the Diagnosis and Quantification of Hepatic Steatosis: A Pilot Study. Ultraschall der Medizin. 2019;40(6):722–33.
54. Suliman I, Abdelgelil N, Kassamali F, Hassanein TI. The Effects of Hepatic Steatosis on the Natural History of HBV Infection. Clin Liver Dis. 2019;23(3):433–50.
55. Spitzer AL, Lao OB, Dick AAS, Bakthavatsalam R, Halldorson JB, Yeh MM, et al. The biopsied donor liver: Incorporating macrosteatosis into high-risk donor assessment. Liver Transplant. 2010;16(7):874–84.
56. Simon TG, Roelstraete B, Sharma R, Khalili H, Hagström H, Ludvigsson JF. Cancer Risk in Patients With Biopsy-Confirmed Nonalcoholic Fatty Liver Disease: A Population-Based Cohort Study. Hepatology. 2021 Nov;74(5):2410–23.
57. Izumi T, Sho T, Morikawa K, Shigesawa T, Suzuki K, Nakamura A, et al. Assessing the risk of hepatocellular carcinoma by combining liver stiffness and the controlled attenuation parameter. Hepatol Res. 2019 Oct 1;49(10):1207–17.
58. Abdelaziz AO, Shousha HI, Said EM, Soliman ZA, Shehata AA, Nabil MM, et al. Evaluation of liver steatosis, measured by controlled attenuation parameter, in patients with hepatitis C-induced advanced liver fibrosis and hepatocellular carcinoma. Eur J Gastroenterol Hepatol 2018;30(11): 1384-1388
59. Oh JH, Lee HW, Sinn DH, Park JY, Kim BK, Kim SU, et al. Controlled attenuation parameter value and the risk of hepatocellular carcinoma in chronic hepatitis B patients under antiviral therapy. Hepatol Int. 2021 Aug;15(4):892–900.
60. de Franchis R. Expanding consensus in portal hypertension: Report of the Baveno VI Consensus Workshop: Stratifying risk and individualizing care for portal hypertension. J Hepatol. 2015 Sep;63(3):743–52.

61. Dietrich CF, Bamber J, Berzigotti A, Bota S, Cantisani V, Castera L, et al. EFSUMB Guidelines and Recommendations on the Clinical Use of Liver Ultrasound Elastography, Update 2017 (Long Version). Ultraschall Med. 2017 Aug;38(4):e48.
62. Xu X, Su Y, Song R, Sheng Y, Ai W, Wu X, et al. Performance of transient elastography assessing fibrosis of single hepatitis B virus infection: a systematic review and meta-analysis of a diagnostic test. Hepatol Int. 2015 Oct;9(4):558–66.
63. de Franchis R, Bosch J, Garcia-Tsao G, Reiberger T, Ripoll C. Baveno VII - Renewing consensus in portal hypertension. J Hepatol. 2022 Apr;76(4):959–74.
64. Barr RG, Wilson SR, Rubens D, Garcia-Tsao G, Ferraioli G. Update to the Society of Radiologists in Ultrasound Liver Elastography Consensus Statement. Radiology. 2020 Aug;296(2):263–74.
65. Friedrich-Rust M, Ong MF, Martens S, Sarrazin C, Bojunga J, Zeuzem S, et al. Performance of Transient Elastography for the Staging of Liver Fibrosis: A Meta-Analysis. Gastroenterology. 2008 Apr;134(4):960-74.
66. Tsochatzis EA, Gurusamy KS, Ntaoula S, Cholongitas E, Davidson BR, Burroughs AK. Elastography for the diagnosis of severity of fibrosis in chronic liver disease: A meta-analysis of diagnostic accuracy. J Hepatol. 2011;54(4):650–9.
67. Herrmann E, de Lédinghen V, Cassinotto C, Chu WCW, Leung VYF, Ferraioli G, et al. Assessment of biopsy-proven liver fibrosis by two-dimensional shear wave elastography: An individual patient data-based meta-analysis. Hepatology. 2018;67(1):260–72.
68. Feng JC, Li J, Wu XW, Peng XY. Diagnostic accuracy of supersonic shear imaging for staging of liver fibrosis: A meta-analysis. J Ultrasound Med. 2016;35(2):329–39.
69. Jiang TNA, Tian G, Zhao Q, Kong D, Cheng C, Zhong L, et al. Diagnostic accuracy of 2D-shear wave elastography for liver fibrosis severity: A meta-analysis. PLoS One. 2016;11(6):e0157219.
70. Cassinotto C, Boursier J, de Lédinghen V, Lebigot J, Lapuyade B, Cales P, et al. Liver stiffness in nonalcoholic fatty liver disease: A comparison of supersonic shear imaging, FibroScan, and ARFI with liver biopsy. Hepatology. 2016;63(6):1817–27.
71. Lefebvre T, Wartelle-Bladou C, Wong P, Sebastiani G, Giard JM, Castel H, et al. Prospective comparison of transient, point shear wave, and magnetic resonance elastography for staging liver fibrosis. Eur Radiol. 2019 Dec;29(12):6477–88.
72. Xiao G, Zhu S, Xiao X, Yan L, Yang J, Wu G. Comparison of laboratory tests, ultrasound, or magnetic resonance elastography to detect fibrosis in patients with nonalcoholic fatty liver disease: A meta-analysis. Hepatology. 2017 Nov;66(5):1486–501.
73. Furlan A, Tublin ME, Yu L, Chopra KB, Lippello A, Behari J. Comparison of 2D Shear Wave Elastography, Transient Elastography, and MR Elastography for the Diagnosis of Fibrosis in Patients With Nonalcoholic Fatty Liver Disease. AJR Am J Roentgenol. 2020 Jan;214(1):W20–6.
74. Selvaraj EA, Mózes FE, Jayaswal ANA, Zafarmand MH, Vali Y, Lee JA, et al. Diagnostic accuracy of elastography and magnetic resonance imaging in patients with NAFLD: A systematic review and meta-analysis. J Hepatol. 2021 Oct;75(4):770–85.
75. Imajo K, Honda Y, Kobayashi T, Nagai K, Ozaki A, Iwaki M, et al. Direct Comparison of US and MR Elastography for Staging Liver Fibrosis in Patients With Nonalcoholic Fatty Liver Disease. Clin Gastroenterol Hepatol Off Clin Pract J Am Gastroenterol Assoc. 2022 Apr;20(4):908-917.e11.

76. Berzigotti A, Tsochatzis E, Boursier J, Castera L, Cazzagon N, Friedrich-Rust M, et al. EASL Clinical Practice Guidelines on non-invasive tests for evaluation of liver disease severity and prognosis – 2021 update. J Hepatol. 2021 Sep 1;75(3):659–89.
77. Chen S, Sanchez W, Callstrom MR, Gorman B, Lewis JT, Sanderson SO, et al. Assessment of liver viscoelasticity by using shear waves induced by ultrasound radiation force. Radiology. 2013 Mar;266(3):964–70.
78. Mueller S, Millonig G, Sarovska L, Friedrich S, Reimann FM, Pritsch M, et al. Increased liver stiffness in alcoholic liver disease: Differentiating fibrosis from steatohepatitis. World J Gastroenterol. 2010;16(8):966–72.
79. Lim SG, Cho SW, Lee YC, Jeon SJ, Lee MH, Cho YJ, et al. Changes in liver stiffness measurement during antiviral therapy in patients with chronic hepatitis B. Hepatogastroenterology. 2011;58(106):539–45.
80. Sugimoto K, Moriyasu F, Oshiro H, Yoshimasu Y, Takeuchi H, Kasai Y, et al. Value of Viscosity and Viscoelasticity Measurement in Patients with NAFLD Using Shear Wave Ultrasound Elastography. Kanzo. 2018 Jul 20;59:370–3.
81. Sugimoto K, Moriyasu F, Oshiro H, Takeuchi H, Yoshimasu Y, Kasai Y, et al. Clinical utilization of shear wave dispersion imaging in diffuse liver disease. Ultrason (Seoul, Korea). 2020 Jan;39(1):3–10.
82. Gao F, He Q, Li G, Huang OY, Tang LJ, Wang XD, et al. A novel quantitative ultrasound technique for identifying non-alcoholic steatohepatitis. Liver Int. 2022 Jan 1;42(1):80–91.
83. Sugimoto K, Moriyasu F, Oshiro H, Takeuchi H, Abe M, Yoshimasu Y, et al. The Role of Multiparametric US of the Liver for the Evaluation of Nonalcoholic Steatohepatitis. Radiology. 2020 Jun 23;296(3):532–40.
84. Lee DH, Cho EJ, Bae JS, Lee JY, Yu SJ, Kim H, et al. Accuracy of Two-Dimensional Shear Wave Elastography and Attenuation Imaging for Evaluation of Patients With Nonalcoholic Steatohepatitis. Clin Gastroenterol Hepatol Off Clin Pract J Am Gastroenterol Assoc. 2021 Apr;19(4):797-805.e7.
85. Jang JK, Lee ES, Seo JW, Kim YR, Kim SY, Cho YY, et al. Two-dimensional Shear-Wave Elastography and US Attenuation Imaging for Nonalcoholic Steatohepatitis Diagnosis: A Cross-sectional, Multicenter Study. Radiology. 2022 Oct;305(1):118–26.
86. Popa A, Sporea I, Bende F, Popescu A, Fofiu R, Borlea A, et al. The Non-Invasive Ultrasound-Based Assessment of Liver Viscosity in a Healthy Cohort. Diagnostics. 2022 Jun 13;12(6):1451.
87. Popa A, Bende F, Șirli R, Popescu A, Bâldea V, Lupușoru R, et al. Quantification of Liver Fibrosis, Steatosis, and Viscosity Using Multiparametric Ultrasound in Patients with Non-Alcoholic Liver Disease: A “Real-Life” Cohort Study. Diagnostics. 2021;11(5):783.
88. Minciuna I, Taru M, Fodor A, Nicoara Farcau O, Fischer P, Radu C, et al. Multiparametric ultrasound evaluation of liver fibrosis, steatosis, and viscosity in patients with chronic liver disease. Med Ultrason. 2024 Jun 21;26(2):117-124

5.1.g. Elastographic Screening in Fatty Liver Disease

Ioan Sporea, Ruxandra Mare, Camelia Nica

The prevalence of NAFLD (Non-alcoholic Fatty Liver Disease) and NASH (non-alcoholic steatohepatitis) is increasing worldwide, in parallel with the increasing prevalence of obesity and comorbid metabolic diseases (1,2). The prevalence of NAFLD in adults has been estimated to be 25%–30% in the general population (3–5) and varies by race/ethnicity and geographic region. The prevalence of NASH in the general population is difficult to determine with certainty, due to the need to highlight inflammation, obtained only by liver biopsy. However, NASH has been identified in 14% of asymptomatic patients screened for colon cancer (6). On the other hand, the prevalence of NAFLD and NASH in patients with type 2 diabetes (DM2) is 65% and 32%, respectively, according to a meta-analysis published in 2023 (7). Of these, 35% had significant fibrosis (F2-F4), and 15% had severe fibrosis (F3-F4) (7).

In this context, screening in high-risk populations, such as those with T2DM, obesity with metabolic complications, a family history of cirrhosis but also those with significant alcohol consumption, can identify those with asymptomatic but clinically significant fibrosis (8). Early identification of these at-risk patients enables interventions that can prevent future liver complications.

In 2023, a new nomenclature was adopted to replace the terminology of NAFLD (8). Non-alcoholic fatty liver disease (NAFLD) has become Metabolic Dysfunction Associated Steatotic Liver Disease (MASLD). MASLD includes patients who have hepatic steatosis and have at least one of the five cardiometabolic risk factors (Table 1). At the same time, a new category, in addition to pure MASLD, called MetALD, has been defined, to describe those with MASLD who consume higher amounts of alcohol per week (maximum of 140 g/week and 210 g/week for women and men, respectively). Metabolic dysfunction-associated steatohepatitis (MASH) is the replacement term for NASH.

Table 1. Cardiometabolic criteria in adults*

1. **BMI** ≥25 kg/m2 or waist circumference >94 in men or > 80 cm in women or ethnic adjustment
2. **Fasting blood glucose** ≥ 5.6 mmol/L (100 mg/dl) or 2 hours postprandial glycemic values ≥ 7.8 mmol/L (≥140 mg/dl) or Hb A1c ≥ 5.7% (39 mmol/L) or DZ2 or under treatment for DZ2
3. **Blood pressure** ≥ 130/85 mmHg or antihypertensive treatment
4. **Serum triglycerides** ≥ 1.70 mmol/L (150 mg/dL) or lipid-lowering treatment
5. **HDL cholesterol** ≤ 1.0 mmol/L (≤40 mg/dL) in men and 1.3 mmol/L (≤50 mg/dl) in women or lipid-lowering treatment

*At least 1 in 5

Under these conditions, the screening of the population at risk for MASLD is an imperative of current medicine, which is also intended to be preventive. The following questions arise: **Which** population needs to be screened? **Who** performs the screening? **What** are the methods used for screening?

1. Which population needs to be screened?

Screening in the general population is not cost-effective, while screening of at-risk populations (subjects with DM, dyslipidemia, obesity, metabolic syndrome) is feasible and recommended by international guidelines (9,10). Liver fibrosis seems to be the main factor influencing the long-term survival of these patients.

In this context, we ask ourselves when we should start screening people at risk? Some papers are in favor of starting screening as soon as possible. In a recent meta-analysis in diabetic patients, it was found that 5.2% of patients with type 1 diabetes (DM1) and 19.8% of patients with type 2 diabetes (DM2) have elevated liver stiffness values, suggestive of significant or advanced liver fibrosis (F2-F4) (11). According to this study, the highest risk of severe fibrosis is found in male, obese, older patients with DM2. Another study showed that in a cohort of patients with DM2, 60% of patients had severe steatosis and 20% of them had advanced fibrosis (12). Factors associated with advanced fibrosis were body mass index, waist circumference, increased AST levels, increased HbA1c, and elevated CAP (Controled Attenuation Parameter at Fibroscan) values. Younossi (13) estimated that 25% of the world's adult population has MASLD, resulting in a huge screening cohort. Using artificial intelligence (AI) algorithms, we can define more precisely the population that needs to be examined first, having a higher risk (14). Such an algorithm has recently been evaluated in terms of the general population, trying to identify patients who are at high risk of developing severe liver disease. The chronic liver disease (CLivD) risk prediction score was developed and validated, based on age, gender, alcohol consumption, waist-to-hip ratio, presence of diabetes, and smoking history, with or without the inclusion of the liver enzyme gamma-glutamyltransferase (15).

2. Who can perform the screening?

Screening for MASLD can be initiated at baseline level, by the general practitioner, by means of simple and inexpensive biological tests, such as the FIB4 index (16). This score, based on the following formula: age (years) x AST (U/L)/ [platelets (109/ L) x ALT1/2 (U/L), can be the first step in making the decision to refer the patient to the specialist. However, published data agree that biological tests are inferior to imaging techniques in assessing fibrosis severity (17). A study published in 2022 (18) highlighted that both FIB-4 and non-alcoholic fatty liver fibrosis (NFS) scores are suboptimal for screening purposes, due to a high risk of overdiagnosis and a not insignificant percentage of false-negative results, especially in patients with risk factors (obesity, diabetes, alcohol) to develop chronic liver disease. Measurement of abdominal

circumference has emerged as a potential first step in identifying patients at risk for liver fibrosis in the general population (18).

Considering that patients at risk for MASLD represent a very clear cohort (obese, patients with type 2 diabetes, dyslipidemia patients or those with metabolic syndrome), any doctor, regardless of the specialty (internal medicine, diabetology, but also other specialties) can send them all for imaging evaluation, by standard ultrasound, quantification of steatosis and elastography. These methods can quickly detect and quantify steatosis, they can also assess liver stiffness as a marker of fibrosis, and, with modern systems, the viscoelastic properties of the liver can be assessed for a final diagnosis of MASLD.

The imaging evaluation of fatty liver is done in some countries by the radiologist (the only one who uses imaging techniques, including ultrasound), or in some countries, such as Germany, Italy, Romania or Japan, ultrasound is used intensively by the gastroenterologist/ hepatologist, thus this screening is performed by the clinician. We believe that the screening of fatty liver by the clinician has certain advantages, such as the evaluation in the consultation room (point of care) and a therapeutic attitude, immediate if deemed necessary.

3. What are the methods used in screening?

3.1. The first step in the diagnosis of MASLD is to show *the presence of fatty liver* disease (as a mandatory element to define fatty liver).

Conventional ultrasound is considered the first-line method for diagnosing steatosis in clinical practice, despite its well-known limitations (steatosis is visible on ultrasound only if it is in a proportion of more than 20% of hepatocytes, there is interoperative variability, and accuracy is reduced in patients with obesity) (17). Currently, MRI-PDFF (PDFF=proton density fat fraction) is considered to be the most accurate non-invasive method for detecting and quantifying steatosis. However, it is not recommended as a first line tool, given its cost and limited availability. It is therefore more suitable for clinical trials and not for population screening (17). In a meta-analysis published in 2011, in which ultrasound was compared with liver biopsy in 4720 subjects, the sensitivity of ultrasound was 84.8% (95% CI: 79.5-88.9%) for diagnosing moderate and severe steatosis, with a specificity of 93.6% (95% CI: 87.2-97.0) (19). The results of this meta-analysis allow us to affirm that, in everyday practice, standard ultrasound can be a good method of screening fatty liver, as a first step in discovering cases that require further evaluation. The use of this simple technique, available in many outpatient clinics (at least in some geographical areas), makes it very useful. Although it is a semi-quantitative method, it can determine the referral of patients with steatosis to a liver fibrosis assessment center. The use of simple ultrasound signs, such as increased "ultrasound brightness", "posterior attenuation" or increased hepatorenal index, allow for a fairly accurate assessment of the presence of hepatic steatosis, at least for moderate and severe steatosis (with clinical significance).

In recent years, ultrasound methods for quantitative quantification of fatty infiltration of the liver have emerged. The most used and the best-known is the Controlled Attenuation Parameter (CAP= Controled Attenuation Parameter), an application developed by the manufacturers of FibroScan® (EchoSens, Paris, France), an initial device dedicated to the evaluation of fibrosis by means of Vibration-Controlled Transient Elastography. (Vibration Controled Transient Elastography=VCTE). VCTE measures the speed of shear waves generated inside the liver by an external mechanical impulse. Several probes are available, depending on the body weight of the patients: M for those of normal weight, XL for obese and S for children and adolescents. CAP assesses the severity of fatty liver disease by measuring the attenuation of ultrasound beams as they pass through the liver and is available on both M and XL probes. The results are expressed in decibels per meter (dB/m), ranging from 100 to 400 dB/m (20,21).

CAP is a promising technique for rapid and standardized detection of steatosis. Although there are no well-defined reference values, values above 275 dB/mm can be used to diagnose steatosis as it has shown a sensitivity (Se) and a positive predictive value (PPV) of over 90% (17).

In recent years, techniques for the quantitative assessment (QUS) of steatosis have been implemented in ultrasound scanners from several providers. These techniques use ultrasound attenuation or reverse scattering (backscattering), thus allowing for an accurate, fast and objective assessment of hepatic steatosis. Such modules are implemented on the Canon system (Attenuation Imaging - ATI), General Electric (Ultrasound-Guided Attenuation Parameter - UGAP), Samsung (Tissue Attenuation Imaging - TAI and Tissue Scatter distribution Imaging - TSI), Siemens (Ultrasound Derived Fat Fraction - UDFF), Fujifilm/Hitachi (Attenuation Coefficient - ATT), on Hologic/Aixplorer (Attenuation PLUS - Att PLUS and Sound Speed PLUS - SSp PLUS), or Mindray (USFF)(see chapter on Ultrasonic Evaluation of Steatosis hepatic).

These methods of quantifying steatosis are promising, they are introduced in ultrasound machines that are used in daily practice, and certain ultrasound companies have started to implement them in their middle-class systems (therefore, they will become more and more accessible)! What would be the advantages of these QUS systems? If the signs of hepatic steatosis are detected through ultrasound screening, then instead of a subjective, semi-quantitative assessment, a quantitative evaluation is carried out. As there are certain cut-offs for each ultrasound system, the severity of steatosis can be assessed, and later, when the patient is reassessed, the numerical values can be compared.

3.2. **Liver fibrosis** is the main prognostic factor for patients with MASLD, and an independent risk factor for both adverse and extrahepatic hepatic events, as well as for hepatic and overall mortality.

One-dimensional transient elastography (VCTE-FibroScan®) was the first ultrasound-based elastographic method used to assess the severity of fibrosis, and numerous studies that considered liver biopsy as a reference method confirmed its value. The accuracy of VCTE for

assessing fibrosis ranges from 0.80 to 0.95, increasing with fibrosis severity and being greater than 90% for predicting the presence of liver cirrhosis (22, 23).

The reference values of VCTE vary with the etiology of the liver disease (24). It has also been suggested that different reference values should be used for the M and XL probes, since in the same individual, liver stiffness values obtained by the XL probe are approximately 1.5 kPa lower than those obtained with the M probe (25). However, when the right probe is used in a particular patient (XL probe in patients with > 25 mm skin-liver capsule distance (SCD) and M probe in patients with SCD < 25 mm), there is no significant difference in liver stiffness values for the same stage of fibrosis (26). Currently, there is no agreement in clinical practice on the reference values for the exclusion of advanced fibrosis, although 8 kPa is the most validated threshold, with a predictive negative value of over 90% (27). In contrast, VCTE values > 12 kPa define advanced fibrosis, according to a recent meta-analysis (28).

The development of ultrasound-based techniques in recent years has led to the implementation of elastographic modules in medium and high-class ultrasound scanners. In these cases, unlike VCTE, shear waves are generated in the liver tissue by an acoustic impulse generated by the transducer (Acoustic Radiation Force Impulse – ARFI technology). The speed of the shear waves is measured either at a point (point Shear-Waves Elastography - pSWE) (Fig.1,2) or over a larger area, also generating a color-coded elastogram (Shear-Waves Two-Dimensional Elastography - 2D-SWE) (Fig.3)(24) .

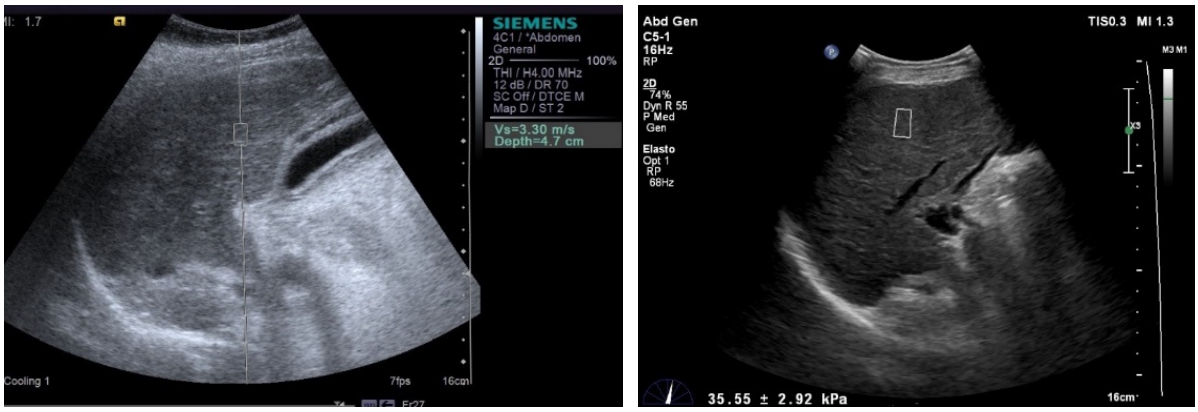

Fig.1 and Fig.2 pSWE: Severe fibrosis (F4)- quantified by Virtual Touch Quantification (VTQ) and ElastPQ

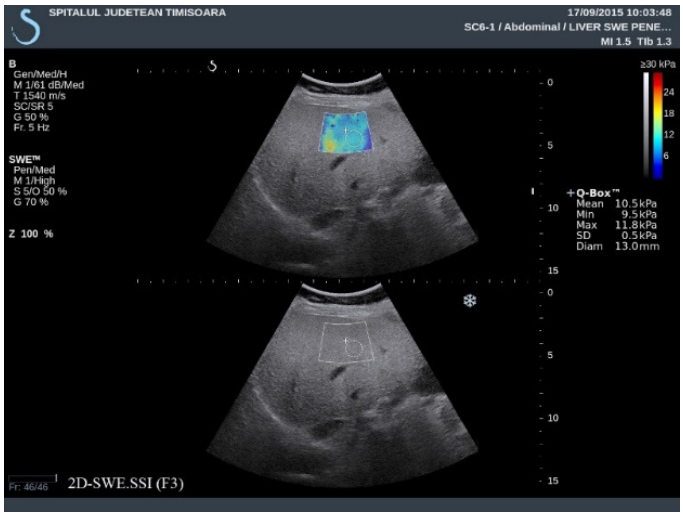

Fig. 3. Severe fibrosis assessed by the Hologic/Aixplorer system

Two recent meta-analyses indicate that both point elastography (pSWE) and two-dimensional 2D-SWE have the same performance in identifying advanced fibrosis as VCTE (29, 30).

After presenting the data related to the evaluation of steatosis and fibrosis based on ultrasound, we can conclude that, in current clinical practice, these methods are sensitive and specific enough to be used. They are useful for an initial diagnosis, but also for the follow-up ("follow-up") of these patients.

It is necessary and important that this screening should start as soon as possible (31, 32), and probably with certain categories of patients who are monitored anyway (patients with DM2), then moving on to metabolic patients.

If we look at the WHO (World Health Organization) criteria regarding screening (which have to offer high validity and confidence, to be accepted by patients and to have a positive balance between results and cost), then ultrasonography (together with the quantification of steatosis and fibrosis) is probably an important method for screening fatty liver in at-risk populations (representing the "one stop shop") (33). The accuracy of the evaluation of steatosis and fibrosis ranges between 80-95%, the repetitive evaluation, a not very high maintenance cost of the device and the availability of medium-class ultrasound systems that can make all these evaluations, make it very attractive for practice. What other positive prospects are there? Small, portable, wireless systems for the evaluation of liver fibrosis ("Palm-Sized Wireless Transient Elastography System with Real-Time B-Mode Ultrasound Imaging Guidance") (34) have appeared! The use of such equipment called Liverscan (Hong Kong, China), in a cohort of 121 patients, in which the system was compared with VCTE and 2D-SWE, demonstrated a very high correlation with the first one (r = 0.975) and a strong agreement with the other one (mean difference of -0.77 kPa). They will allow a greater number of doctors to use ultrasound systems for the detection of fibrosis and the start of mass screening soon.

A very important element for a screening is its cost-effectiveness. In a study by Canadian group (35), the cost-effectiveness of non-invasive screening in the general population versus in the at-risk population (T2DM and/or obese) was analyzed, using VCTE and VTQ (a pSWE method) for the detection of advanced fibrosis (≥ F3) in these populations. The conclusion of the study was that annual screening in patients at risk is cost-effective. The same results were obtained by other groups (36).

In conclusion, screening for liver fibrosis in the at-risk population using ultrasound-based methods is feasible, simple to perform and cost-effective. It is necessary to start such a screening program as soon as possible, in order to prevent the progression of fibrosis in those at risk.

References

1. Estes C, Razavi H, Loomba R, Younossi Z, Sanyal AJ. Modeling the epidemic of nonalcoholic fatty liver disease demonstrates an exponential increase in burden of disease. Hepatology. 2018; 67:123–33.
2. Le P, Chaitoff A, Rothberg MB, McCullough A, Gupta NM, Alkhouri N. Population-based trends in prevalence of non-alcoholic fatty liver disease in US adults with type 2 diabetes. Clin Gastroenterol Hepatol. 2019; 17:2377–78.
3. Browning JD, Szczepaniak LS, Dobbins R, Nuremberg P, Horton JD, Cohen JC, et al. Prevalence of hepatic steatosis in an urban population in the United States: impact of ethnicity. Hepatology. 2004; 40:1387–95.
4. Younossi ZM, Koenig AB, Abdelatif D, Fazel Y, Henry L, Wymer M. Global epidemiology of nonalcoholic fatty liver disease—meta-analytic assessment of prevalence, incidence, and outcomes. Hepatology. 2016; 64:73–84.
5. Le MH, Devaki P, Ha NB, Jun DW, Te HS, Cheung RC, et al. Prevalence of non-alcoholic fatty liver disease and risk factors for advanced fibrosis and mortality in the United States. PLoS One. 2017; 12:e0173499.
6. Harrison SA, Gawrieh S, Roberts K, Lisanti CJ, Schwope RB, Cebe KM, et al. Prospective evaluation of the prevalence of non-alcoholic fatty liver disease and steatohepatitis in a large middle-aged US cohort. J Hepatol. 2021; 75:284–91.
7. En Li Cho E, Ang CZ, Quek J, Fu CE, Lim LKE, Heng ZEQ, et al. Global prevalence of non-alcoholic fatty liver disease in type 2 diabetes mellitus: an updated systematic review and meta-analysis. Gut. 2023 Nov; 72(11):2138-2148.
8. Rinella ME, Neuschwander-Tetri BA, Siddiqui MS, Abdelmalek MF, Caldwell S, Barb D, Kleiner DE, Loomba R. AASLD Practice Guidance on the clinical assessment and management of nonalcoholic fatty liver disease. Hepatology. 2023 May 1; 77(5):1797-1835.
9. American Diabetes Association Professional Practice Committee 4. Comprehensive Medical Evaluation and Assessment of Comorbidities: Standards of Medical Care in Diabetes—2022. Diabetes Care 2021, 45, S46–S59.
10. EASL–EASD–EASO Clinical Practice Guidelines for the Management of Non-Alcoholic Fatty Liver Disease. J. Hepatol. 2016, 64,1388–1402.

11. Ciardullo S, Perseghin G. Prevalence of elevated liver stiffness in patients with type 1 and type 2 diabetes: A systematic review and meta-analysis. Diabetes Res Clin Pract. 2022; 190:109981
12. Sporea I, Mare R, Popescu A, Nistorescu S, Baldea V, Sirli R, et al. Screening for Liver Fibrosis and Steatosis in a Large Cohort of Patients with Type 2 Diabetes Using Vibration Controlled Transient Elastography and Controlled Attenuation Parameter in a Single-Center Real-Life Experience. J Clin Med. 2020; 9(4).
13. Younossi ZM, Blissett D, Blissett R, Henry L, Stepanova M, Younossi Y, et al. The economic and clinical burden of nonalcoholic fatty liver disease in the United States and Europe. Hepatology. 2016; 64(5):1577-86.
14. Shafiha R, Bahcivanci B, Gkoutos GV, Acharjee A. Machine Learning-Based Identification of Potentially Novel Non-Alcoholic Fatty Liver Disease Biomarkers. Biomedicines. 2021; 9(11).
15. Aberg F, Luukkonen PK, But A, Salomaa V, Britton A, Petersen KM, et al. Development and validation of a model to predict incident chronic liver disease in the general population: The CLivD score. J Hepatol. 2022; 77(2):302-11.
16. Shah, A.G.; Lydecker, A.; Murray, K.; Tetri, B.N.; Contos, M.J.; Sanyal, A.J. Nash Clinical Research Network Comparison of Noninvasive Markers of Fibrosis in Patients with Nonalcoholic Fatty Liver Disease. Clin. Gastroenterol. Hepatol. 2009, 7, 1104–1112
17. European Association for the Study of the Liver. EASL Clinical Practice Guidelines on non-invasive tests for evaluation of liver disease severity and prognosis - 2021 update. J Hepatol. 2021 Sep; 75(3):659-689.
18. Graupera I, Thiele M, Serra-Burriel M, Caballeria L, Roulot D, Wong GL, et al. Investigators of the LiverScreen Consortium. Low Accuracy of FIB-4 and NAFLD Fibrosis Scores for Screening for Liver Fibrosis in the Population. Clin Gastroenterol Hepatol. 2022 Nov; 20(11):2567-2576.e6.
19. Hernaez R, Lazo M, Bonekamp S, Kamel I, Brancati FL, Guallar E, et al. Diagnostic accuracy and reliability of ultrasonography for the detection of fatty liver: a meta-analysis. Hepatology. 2011; 54(3):1082-90
20. Sasso M, Beaugrand M, de Ledinghen V, Douvin C, Marcellin P, Poupon R, et al. Controlled attenuation parameter (CAP): a novel VCTE guided ultrasonic attenuation measurement for the evaluation of hepatic steatosis: preliminary study and validation in a cohort of patients with chronic liver disease from various causes. Ultrasound Med Biol. 2010; 36(11):1825-35.
21. de Ledinghen V, Vergniol J, Capdepont M, Chermak F, Hiriart JB, Cassinotto C, et al. Controlled attenuation parameter (CAP) for the diagnosis of steatosis: a prospective study of 5323 examinations. J Hepatol. 2014; 60(5):1026-31
22. Talwalkar JA, Kurtz DM, Schoenleber SJ, West CP, Montori VM. Ultrasound-based transient elastography for the detection of hepatic fibrosis: systematic review and meta-analysis. Clin Gastroenterol Hepatol. 2007; 5(10):1214-20.
23. Friedrich-Rust M, Ong MF, Martens S, Sarrazin C, Bojunga J, Zeuzem S, et al. Performance of transient elastography for the staging of liver fibrosis: a meta-analysis. Gastroenterology. 2008; 134(4):960-74.
24. Ferraioli G, Wong VW, Castera L, Berzigotti A, Sporea I, Dietrich CF, et al. Liver Ultrasound Elastography: An Update to the World Federation for Ultrasound in Medicine and Biology Guidelines and Recommendations. Ultrasound Med Biol. 2018; 44(12):2419-40.

25. Wong GL, Vergniol J, Lo P, Wai-Sun Wong V, Foucher J, Le Bail B, et al. Non-invasive assessment of liver fibrosis with transient elastography (FibroScan(R)): applying the cut-offs of M probe to XL probe. Ann Hepatol. 2013; 12(4):570-80.
26. Berger A, Shili S, Zuberbuhler F, Hiriart JB, Lannes A, Chermak F, et al. Liver Stiffness Measurement With FibroScan: Use the Right Probe in the Right Conditions! Clin Transl Gastroenterol. 2019; 10(4):e00023
27. Castera L, Friedrich-Rust M, Loomba R. Noninvasiveassessmentof liver disease in patients with nonalcoholic fatty liver disease. Gastroenterology2019;156.1264-1281.e1264.
28. Papatheodoridi M, Hiriart JB, Lupsor-Platon M, Bronte F, Boursier J, ElshaarawyO,etal. Refining the BavenoVI elastography criteria for the definition of compensated advanced chronic liver disease. J Hepatol 2021May; 74(5):1109–1116.
29. Jiang W, Huang S, Teng H, Wang P, Wu M, Zhou X, Ran H. Diagnostic accuracy of point shear wave elastography and transient elastography for staging hepatic fibrosis in patients with non-alcoholic fatty liver disease: a meta-analysis. BMJ Open. 2018 Aug 23; 8(8):e021787.
30. Herrmann E, de Ledinghen V, Cassinotto C, Chu WC, Leung VY, Ferraioli G, et al. Assessment of biopsy-proven liver fibrosis by two-dimensional shear wave elastography: An individual patient data-based meta-analysis. Hepatology. 2018; 67(1):260-72
31. Ginès P, Graupera I, Lammert F, Angeli P, Caballeria L, Krag A, et al. Screening for liver fibrosis in the general population: a call for action. Lancet Gastroenterol Hepatol. 2016 Nov; 1(3):256-260. doi: 10.1016/S2468-1253(16)30081-4. Epub 2016 Oct 12. PMID: 28404098
32. Sporea I, Sirli R. Nonalcoholic Fatty Liver Disease and the Need for Action. J Gastrointestin Liver Dis. 2020 Jun 3; 29(2):139-141.
33. Sporea I. Ultrasound: "one stop shop" in hepatology. Med Ultrason. 2016 Jun; 18(2):143-144.
34. Huang ZH, Wang LK, Cai SY, Chen HX, Zhou Y, et al. Palm-Sized Wireless Transient Elastography System with Real-Time B-Mode Ultrasound Imaging Guidance: Toward Point-of-Care Liver Fibrosis Assessment. Diagnostics (Basel). 2024 Jan 15; 14(2):189.
35. Zhang E, Wartelle-Bladou C, Lepanto L, Lachaine J, Cloutier G, Tang A. Cost-utility analysis of nonalcoholic steatohepatitis screening. Eur Radiol. 2015 Nov; 25(11):3282-94.
36. Phisalprapa P, Supakankunti S, Charatcharoenwitthaya P, Apisarnthanarak P, Charoensak A, Washirasaksiri C, Srivanichakorn W, Chaiyakunapruk N. Cost-effectiveness analysis of ultrasonography screening for nonalcoholic fatty liver disease in metabolic syndrome patients. Medicine (Baltimore). 2017 Apr; 96(17):e6585.

5.2. Ultrasound-based Elastography of Solid Focal Liver Lesions

Ana-Maria Ghiuchici, Mirela Dănilă

1. Introduction

Standard abdominal ultrasonography (US) is the most commonly used imaging technique for liver evaluation due to several advantages, including non-invasiveness, accessibility, safety, integrated clinical information, and cost-effectiveness. Focal liver lesions (FLL) are often detected incidentally during routine abdominal US (1-3). Distinguishing between benign and malignant lesions can be challenging due to similar sonographic features and the heterogeneity of tumor types and subtypes (2). Superior contrast-enhanced imaging methods (CT/MRI with contrast) and/or liver biopsy are often necessary for a definitive diagnosis. However, these techniques have potential complications or contraindications, with additional limitations related to increased costs and prolonged waiting lists due to limited accessibility.

Continuous advances in US and access to new techniques implemented in most modern ultrasound machines (Doppler ultrasound, contrast-enhanced ultrasound - CEUS, elastography, 3-D or 4-D ultrasound, fusion techniques) have significantly improved the characterization of FLLs. Furthermore, it allows for a comprehensive assessment of diffuse and focal liver pathology, making it accessible to physicians in clinical practice (4, 5).

Ultrasound-based elastography is a non-invasive imaging technique, easy to perform, repeatable, and can be added to a standard ultrasound examination. Most available elastographic methods are integrated into modern US systems (6). US based elastography is widely used for liver stiffness assessment as a non-invasive marker of fibrosis, which is important for the management of patients with diffuse liver disease. Clinical applications for liver elastography include diagnosis of clinically significant portal hypertension, prognostic assessment in patients with chronic diffuse liver disease, and characterization of hepatic tumors (7-11).

Supplementing a standard US and CEUS examination with elastographic evaluation provides additional information regarding tissue stiffness of the liver parenchyma and FLLs in a quantifiable manner, considered by some authors as a virtual biopsy (12). The multiple associated advantages and the validated performance of liver fibrosis assessment have led to the expanding clinical applicability of US elastography. Thus, several studies have investigated the role of different elastographic techniques in the characterization and discrimination of tumor nature. The role of US elastography for FLL diagnosis, including hepatocellular carcinoma (HCC) is not established (13, 14). Recent advances in US elastography for FLL evaluation are presented in this chapter.

2. Ultrasound-based Elastography for the Evaluation of Focal Liver Lesions

Currently, liver cancer is the sixth most common cancer and the fourth leading cause of cancer death worldwide, with HCC accounting for more than 90% of primary malignant liver tumors (15, 16). The clinical interest in excluding malignancy of liver tumors is the early diagnosis of liver cancer and optimization of therapeutic intervention, with a positive impact on the prognosis of these patients.

Considering that malignant transformation can modify tissue structure/composition, elastography could be useful for the detection, evaluation of elasticity differences, and in predicting FLLs nature (17, 18). These aspects are supported by the fact that elastographic evaluation is based on the elastic properties of the tissue under analysis, namely, the ability to recover its shape and dimensions after the application of an external deformation force (14, 20). Technically, elastographic assessment involves applying an external force to the region of interest and evaluating the generated response, stiff tissues with low elasticity will deform less than soft tissues. Thus, it is possible to obtain a qualitative and quantitative assessment of the elasticity difference between normal and pathological tissues.

FLL elastographic evaluation should be performed and interpreted with knowledge of the clinical context and history of the patient (chronic liver disease, history of neoplasms, medications, comorbidities, infections) (19). The importance of assessing liver fibrosis arises from the increased incidence of different tumor types in well-defined clinical contexts (for example, HCC develops in a cirrhotic liver in more than 90% of cases) (16).

Several elastographic methods have been developed, most of which have been integrated into high-performance ultrasound scanners, except transient elastography performed with the FibroScan (EchoSens, Paris, France). These methods are non-invasive, painless, repetitive, fast, and can be performed during a standard US examination.

EFSUMB (European Federation of Societies for Ultrasound in Medicine and Biology) and WFUMB (World Federation for Ultrasound in Medicine and Biology) have developed several elastography guidelines classifying elastographic methods and presenting the clinical applications, advantages, and limitations of these techniques (6, 13-14). According to the EFSUMB and WFUMB guidelines, elastographic methods can be classified as follows:

1. Strain elastography (SE)

2. Shear wave elastography (SWE):

    (a) Transient Elastography-TE (FibroScan);

    (b) Point Shear Wave Elastography - pSWE (Acoustic Radiation Force Impulse Quantification (ARFI technique): VTQ (Siemens), Elast PQ(Philips), Samsung, Hitachi, Mindray, others)

    c) Real-Time Shear Wave Elastography - 2D SWE (Aixplorer, General Electric, Canon, Samsung, Samsung, Philips, Siemens, others).

Both qualitative methods (SE) and quantitative methods (SWE) are useful for assessing tissue stiffness. The measurement of the minimum deformations in the tissue under interrogation induced by mechanical compression or a forced acoustic impulse represents the basic principle of these methods.

Strain Elastography for the Evaluation of Solid Focal Liver Lesions

SE (quasi-static elastography) is a qualitative technique that enables the measurement of the physical displacement of tissue parallel to the normal applied tension. The applied stress can be induced mechanically (actively via compression with a US transducer or passively via physiological movements) or US-induced using focused ultrasound beams- ARFI imaging (6, 17).

SE provides information about the relative stiffness value between different tissue types. Among the limitations regarding SE techniques for FLL evaluation are high interobserver variability, and the difficulty in applying it to patients with ascites or deep lesion localization (6, 17, 21).

Although SE is not a commonly used method for liver evaluation, some studies have shown its usefulness in characterizing tumors as soft or hard. Additionally, histograms can be obtained and the ratio between the tumor stiffness and the liver parenchyma ("strain ratio") can be calculated (22-24).

In a recent prospective study (22), the usefulness of SE in characterizing solid FLLs was evaluated. The study analyzed qualitative (deformation pattern, type of elasticity of FHC) and semi-quantitative (strain ratio, hardness percentage, and histogram) measurements of 38 FLLs. A statistically significant difference ($p<0.001$) was observed between the median values of the three parameters measured for benign tumors (1.02; 12%; 47) compared to malignant tumors (1.66; 65%; 20.5). Additionally, the values of these parameters were significantly different between hepatic hemangioma (HH), focal nodular hyperplasia (FNH), and liver metastases (LM) ($p<0.05$). The cut-off values of 1.2, 45, and 30 for strain ratio, hardness percentage, and histogram showed an AUROC of 0.88, 0.89, and 0.86, respectively. The study suggests the usefulness of SE for differentiating benign from malignant liver formations, especially LM, with good diagnostic performance.

In a study conducted by Onur et al. (23), stiffness differences between benign and malignant FLLs were reported by analysing the strain index value, representing the ratio between liver and tumor stiffness. Malignant lesions had an increased strain index compared to benign FLLs (strain index 2.82 ± 1.82 vs 1.45 ± 1.28, $p < .0001$). However, the significant overlap in the strain index values of benign and malignant solid FLLs limits the clinical utility of this technique.

Similarly, another study (24) showed a significant difference in the stiffness SE ratio (strain ratio) between benign and malignant FLLs (1.08 ± 0.40 vs 4.14 ± 1.25). The study

proposed a cut-off value of1.7 for FLL differential diagnosis with a Se 100%, Sp 93.10%, PPV 97.40%, and NPV 100.

In a study comparing the diagnostic accuracy of IO-SE with IO-CEUS for FLL differentiation, the authors concluded that IO-CEUS can be useful for the localization and characterization before surgical resection. On the other hand, IO-SE provided accurate characterization for only a limited number of lesions. IO-SE presented Se 70.5%, Sp 60%, PPV 94%, and NPV 18.75 with 69% accuracy (25).

In conclusion, SE evaluation of solid FLLs provides information about the tumoral relative stiffness compared to the surrounding liver parenchyma. Therefore, liver fibrosis can limit the accuracy of FLL evaluation using SE. Overlaps between malignant and benign FLL stiffness values should also be considered. Currently, the EFSUMB and WFUMB elastography guidelines do not recommend the use of this technique in clinical practice for the diagnosis of solid FLL [6, 14].

Shear Wave Elastography for the Evaluation of Solid Focal Liver Lesions

SWE methods are based on the ARFI technique, shear waves are generated using the US transducer for US-integrated techniques. Transient elastography involves a controlled external mechanical excitation using a piston that is integrated with an ultrasonic transducer to monitor the pulse of shear waves that are generated by the punch. These methods can provide quantitative information about tissue stiffness by measuring shear wave velocity (SWV), results being expressed in meters per second (m/sec), or by converting Young's modulus to kiloPascal (kPa) (6, 14, 26).

The main SWE methods used in clinical practice are transient elastography (TE), pointSWE, which evaluates tissue stiffness at a single point (pSWE), and 2D-SWE or 3D-SWE, with multidimensional tissue evaluation.

SWE methods have been validated for liver fibrosis evaluation and can be used as complementary methods for breast, thyroid gland, prostate, gastrointestinal tract, or lymph node tumor stiffness assessment (6, 14, 27-28). TE is the most widely used method for assessing liver fibrosis. This method is not feasible for liver tumor evaluation because the measurements are not under direct US guidance in B mode. It is possible to evaluate large tumors in the right liver lobe with the risk of incorrect determinations.

The SWE evaluation of FLLs is performed under US control (except for the Fibroscan), making it possible to precisely choose the region of interest (ROI) in the liver parenchyma and at the tumor level, while avoiding the vessels or liver capsule that can influence the results of the elastographic determinations. Using the SWE elastography module available in the US machine during a standard examination, we can obtain information about the tumor and the surrounding liver parenchyma stiffness.

pointSWE Evaluation of Solid Focal Liver Lesions

Based on the ARFI technique, pSWE methods are available in various US devices (VTQ (Siemens), Elast PQ (Philips), Samsung, Hitachi, etc.) and allow non-invasive, real-time evaluation of tissue stiffness, being the most studied elastographic methods for the characterization and differential diagnosis of FLLs.

From a technical point of view, during the US examination in B mode, the operator will access the elastography module and select, under US guidance, the ROI to be evaluated at the level of the liver parenchyma or FLL. The ROI box will be placed, avoiding large vessels or the liver capsule, followed by the generation of the acoustic impulse and the recording shear wave speed propagation which is dependent on the stiffness of the analyzed tissue. The results are displayed on the monitor, respectively the SWV expressed in m/s and the ROI depth evaluated, as in the example in Figure 5.2.1. The measuring box can be placed at a maximum depth of 8 cm from the skin surface. "X.XX" results (undetermined values) may occur in FLLs with marked heterogeneity, predominantly fluid content, or due to the deep localization of the lesion (Figure 5.2.2).

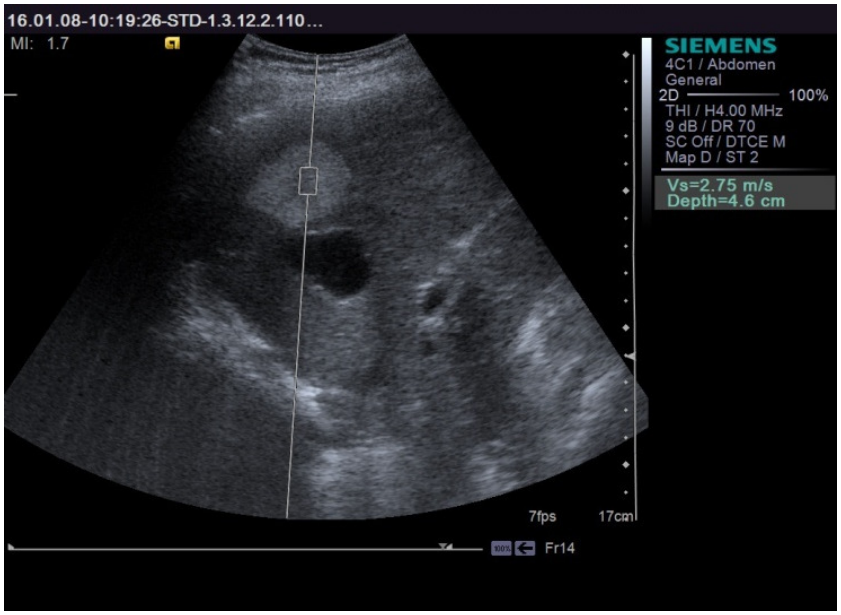

Figure 5.2.1. pSWE measurement in a hepatic hemangioma with central thrombosis using VTQ - Acuson S2000™ (Siemens AG, Erlangen, Germania); thrombosis was evidenced by a previous CEUS examination. The results are displayed on the monitor, Vs (velocity speed) = 2.75 m/s and ROI depth = 5.5 cm.

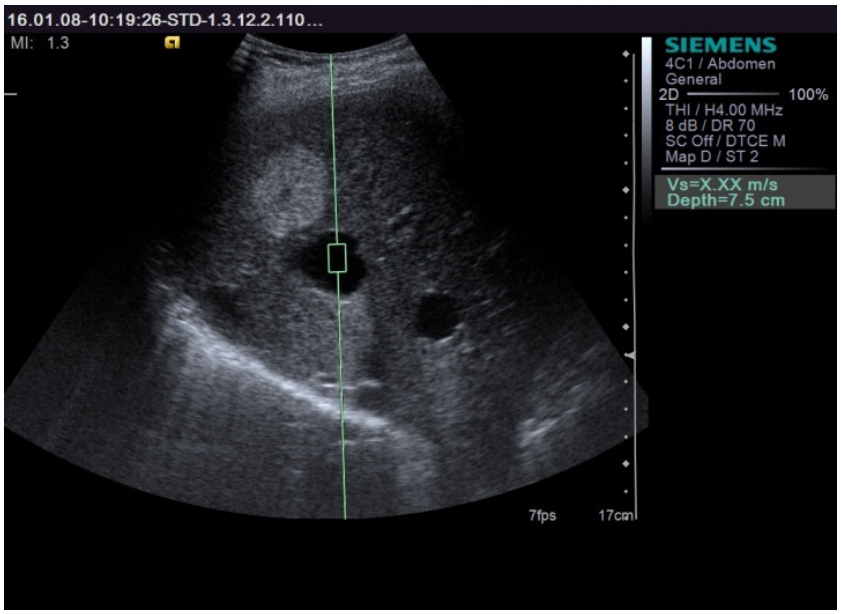

Figure 5.2.2. pSWE measurement in a simple liver cyst using VTQ - Acuson S2000TM (Siemens AG, Erlangen, Germania); "X.XX" result (undetermined values), Vs (velocity speed) = X.XX m/s and ROI depth = 7.5 cm.

Several recent studies and meta-analyses have shown promising results regarding the performance of pSWE in discriminating and characterizing benign and malignant liver tumor formations.

The meta-analysis published in 2017 by Jiao et al. (29) included 9 prospective studies and 1,046 FLLs, out of which 679 were malignant lesions. The results demonstrated a combined Se and Sp of pSWE in discriminating the tumoral nature of 82.2% (95% CI: 73.4-88.5) and 80.2% (95% CI: 73.3-85.7), respectively. The results showed a positive likelihood ratio of 4.159 (95% CI: 2.899-5.966) and a negative likelihood ratio of 0.222 (95% CI: 0.140-0.352) of pSWE for differentiating malignant vs. benign liver lesions, respectively.

The most recent meta-analysis (30) included 1894 FLLs analyzed by SWE, comprising 12 pSWE and 3 2D-SWE studies. The results revealed an overall Se and Sp for the identification of malignant FLLs of 0.82 (95% CI: 0.77-0.86) and 0.82 (95% CI: 0.76-0.87), respectively, with AUROC of 0.89 (95% CI: 0.86-0.91). The study also assessed the accuracy of the SWV ratio in differentiating benign and malignant lesions. Combined SE, Sp, PLR, and NLR of the SWV ratio (FLL to surrounding liver parenchyma) for differentiation of tumor nature were 0.72 (95% CI: 0.59-0.83), 0.82 (95% CI: 0.43-0.97), 4.08 (95% CI: 0.88-18.89), and 0.33 (95% CI: 0.19-0.60), respectively. The Fagan graph demonstrated that the SWE assessment is effective for liver tumor differentiation: 82% probability of malignancy following a positive measurement, and the probability was reduced to 18% when a negative measurement occurred.

The results of both meta-analyses suggest that complementary SWE assessment may be useful for the non-invasive differentiation of FLLs.

Several published studies on FLL characterization using pSWE have reported overlapping results. Some studies have shown higher SWV values in malignant tumors (31),

while others have found similar SWV values in benign and malignant tumors (32-35). The different findings can be explained by the degree of vascularization and the accumulation of fibrous tissue at the tumor level (31).

Malignant FLLs are generally stiffer than benign lesions, with some studies reporting the following decreasing order of stiffness: MH> HCC >HFN>HH (19, 31, 36-37).

In the context of a cirrhotic liver, HCC nodules may have decreased stiffness compared to the surrounding liver parenchyma or other malignant liver tumors (LM and intrahepatic cholangiocarcinoma -ICC) (38-40), with reported SWV values ranging from 2.16 ± 0.75 m/s [41] to 3.07 ± 0.89 m/s in Guo's study (42). HCC stiffness can correlate with the degree of vascularization and histological differentiation (43). In a study (44) involving 99 patients with confirmed HCC through histopathology, pSWE examination showed significantly higher stiffness values in patients with hypervascular HCC and poor histological differentiation compared to hypovascular ($P<0.03$) and moderately or well-differentiated ($P<0.01$) nodules.

MH and ICC have variable stiffness values on pSWE assessment, often characterized as hard lesions compared to other tumor types or the surrounding liver parenchyma.

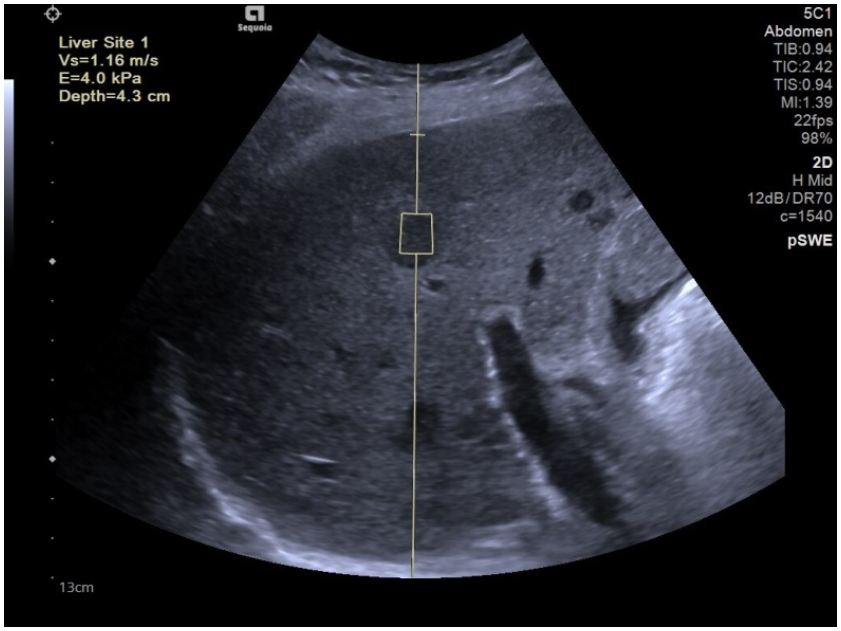

Figure 5.2.3. pSWE measurement in a liver metastasis using VTQ - Acuson SequoiaTM (Siemens AG, Erlangen, Germania). The results are displayed on the monitor, Vs (velocity speed) = 1.56 m/s and ROI depth = 4.6 cm.

Tables 5.2.I-II summarizes the results of studies (35, 37-48) on pSWE elastographic characterization of the most common types of benign (HH, FNH, HA) and malignant (HCC, ICC, LM) liver tumors encountered in clinical practice.

Table 5.2.I. Benign solid FLLs; pSWE mean values (m/s)

Author/Year	Hepatic hemangioma	Focal nodular hyperplasia	Hepatic Adenoma
Heide/2010 (35)	2.36 ± 0.77	3.11 ± 0.93	2.23 ±0.97
Davies/2011 (46)	1.35 ± 0.38	-	-
Yu/2011 (34)	1.75 ± 0.80	2.18 ± 0.84	1.79 ±0.14
Gallotti/2012 (40)	2.30 ± 0.95	2.75 ± 0.95	1.25 ±0.37
Park/2013 (47)	1.83 ± 0.62	0.97 ± 0.48	-
Kim/2013 (39)	1.80 ± 0.57	-	-
Zhang/2014 (33)	1.33 ± 0.38	1.90 ± 0.45	-
Guo/2015 (42)	1.48 ± 0.70	2.30 ± 1.18	-
Goya/2015 (45)	2.32 ± 0.93	2.76 ± 0.47	1.72 ± 0.85
Dong/2017 (32)	1.5 (0.79-2.61)	1.35 (0.69-2.94)	-
Akdogan/2018 (38)	2.15 ± 0.73	3.22 ± 0.18	-
Galati/2019 (48)	1.34 ± 0.91	-	-

Table 5.2.II. Malign solid FLLs; pSWE mean values (m/s)

Author/Year	Hepatocellular carcinoma	Liver metastases	Intrahepatic cholangiocarcinoma
Heide/2010 (35)	2.63 ± 1.09	2.88 ± 1.16	3.78±1.73
Davies/2011 (46)	-	4.23 ± 0.59	-
Yu/2011 (34)	2.49 ± 1.07	2.73 ± 0.89	-
Gallotti/2012 (40)	2.17 ± 0.85	2.87 ± 1.13	-
Park/2013 (47)	2.48 ± 0.84	2.35 ± 1.18	1.65 ± 1.43
Kim/2013 (39)	2.66 ± 0.94	2.82 ± 0.96 3.70 ± 0.61	3.27 ± 0.67
Zhang/2014 (33)	2.59 ± 0.91	3.20 ± 0.62	3.74 ± 0.54
Guo/2015 (42)	3.07 ± 0.89	2.74 ± 1.06	3.44 ± 1.18
Goya/2015 (45)	3.39 ± 0.56	1.64 ± 0.45	1.80 ± 0.63
Dong/2017 (32)	2.63 (1.84-5.68)	2.78 (1.02-3.15)	2.42 (1.99-3.31)
Akdogan/2018 (38)	2.75 ± 0.53	3.59 ± 0.51	-
Galati/2019 (48)	2.47 ± 1.42	3.29 ± 1.23	-
Ghiuchici/2021 (41)	2.16 ± 0.75	-	-

The results presented in the tables above reflect significant heterogeneity of stiffness within the same tumor type but also overlaps of pSWE values between malignant and benign liver lesions, which is why EFSUMB/WFUMB have not validated the use of elastographic methods for the differential diagnosis of FLLs in clinical practice.

2D-SWE Evaluation of Solid Liver Lesions

2D-SWE is a quantitative elastographic technique, integrated into ultrasound systems and can be performed during the standard US examination session. Compared to pSWE, it allows for the real-time visualization of a color-coded elastogram superimposed on a B-mode image. The ROI box has a variable size that can be adjusted by the operator. Figures 5.2.4-6 show examples of 2D-SWE assessment for different FLLs.

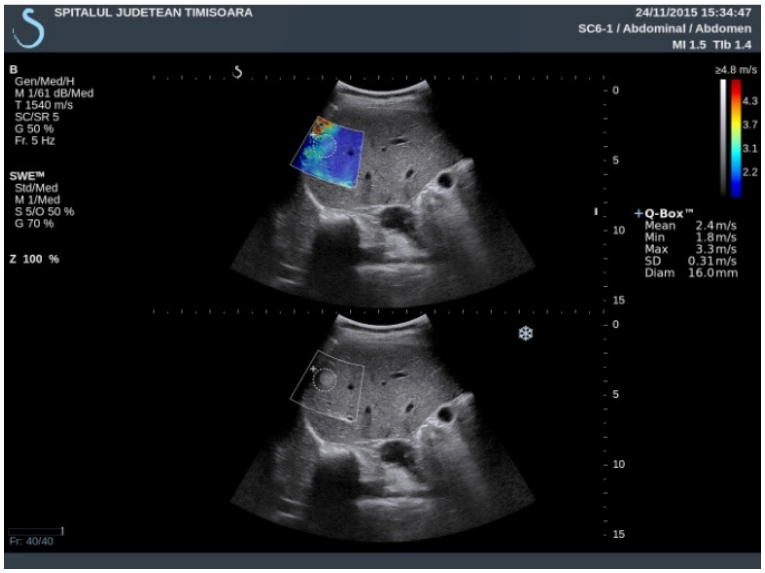

Figure 5.2.4. 2D-SWE evaluation of a hepatic hemangioma using SSI–SuperSonic imagine from Aixplorer US system.

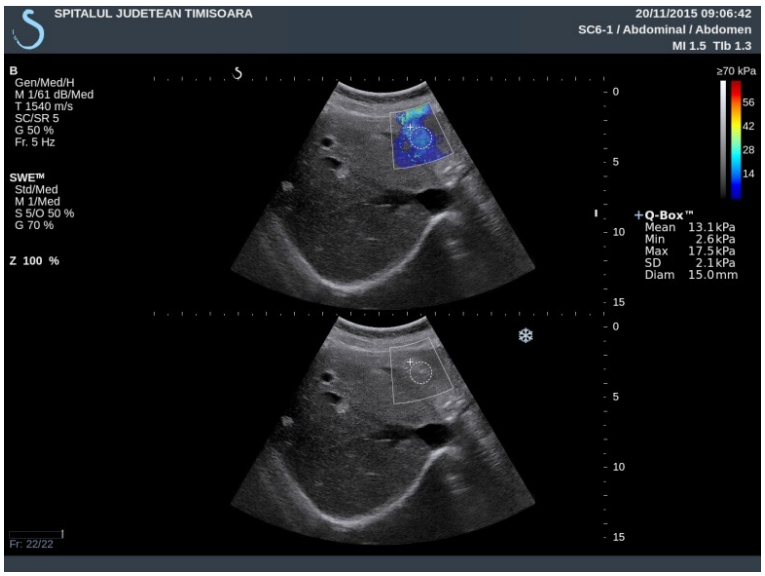

Figure 5.2.5. 2D-SWE evaluation of a liver metastasis using SSI–SuperSonic imagine from Aixplorer US system.

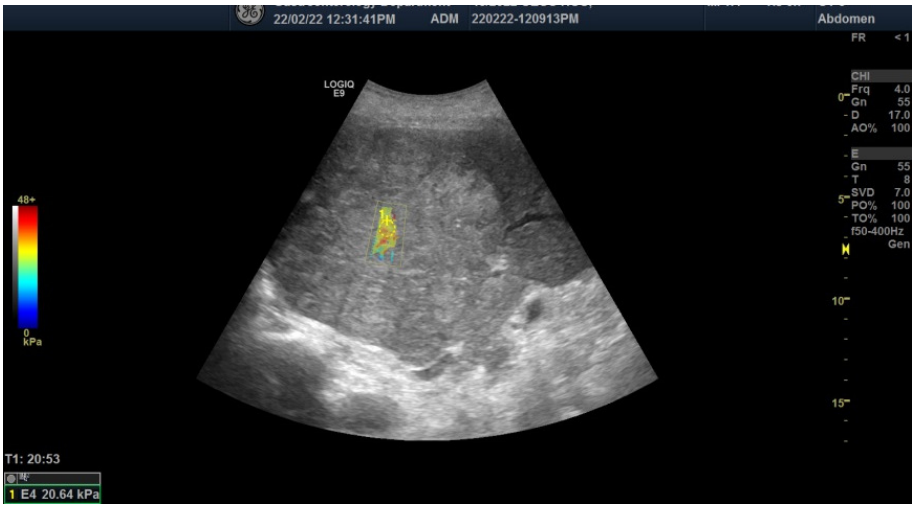

Figure 5.2.6. 2D-SWE evaluation of a hepatocellular carcinoma using 2D-SWE.GE from Logiq E9 General Electric US system.

The Liver Elastography Malignancy Prediction score (LEMP) developed by Grgurevic et al. (49) using RT-2D-SWE elastography allowed for the correct differentiation of benign and malignant FLLs in 96% of patients. The best cut-off value for predicting malignancy was 22.4 kPa with Se 83%, Sp 86%, PPV 91.5%, and NPV 73%. These results suggest the usefulness of 2D-SWE for FLL characterization and differentiation. In contrast, two other studies (50, 51) that evaluated the utility of 2D-SWE for FLL characterization did not find significant differences between malignant and benign FLL stiffness. However, both studies showed that HFN was significantly stiffer than HA.

The evaluation of HCC nodules using 2D-SWE revealed an increased stiffness variability ranging from 19.6 kPa to 44.8 kPa (range 15.8 kPa-97 kPa) (50,52). Factors influencing elastographic determinations include tumor size, ROI positioning, degree of liver fibrosis, etc.

In the prospective study conducted by Gerber (52), malignant FLLs were significantly stiffer than benign lesions ($p<0.0001$). ICCs were stiffer than HCC and LM ($p=0.033$ and $p=0.0079$). The median for 2D-SWE values corresponding to the stiffness of benign FLLs was 16.4 (2.1-71.9) kPa, and for malignant ones 36 (4.1-142.9) kPa.

Limitations of Elastography for FLL Evaluation

Lesions, patients, or technique characteristics can limit the accuracy of elastography for the characterization of FLL.

SWE measurements can be influenced by tumor size, position, and heterogeneity. Patient-related limitations involve poor ultrasound image acquisition, narrow intercostal spaces, obesity, lack of patient cooperation, or inability to hold breath. The overlap of SWE values between malignant and benign lesions can lead to diagnostic confusion. Additionally, there is no consensus on the required number of elastographic measurements in FLL (6, 13, 43).

Despite these limitations, elastography remains a simple, non-invasive, and rapid diagnostic tool for stiffness assessment of FLL and surrounding liver parenchyma.

In conclusion, studies on the performance of elastographic methods for FLL characterization have contradictory and heterogeneous results. The WFUMB [14] and EFSUMB [6] guidelines do not recommend the use of elastography in clinical practice for the diagnosis or discrimination of FLL.

References

1. Gore RM, Pickhardt PJ, Mortele KJ, Fishman EK, Horowitz JM, Fimmel CJ, et. al. Management of Incidental Liver Lesions on CT: A White Paper of the ACR Incidental Findings Committee. J Am Coll Radiol. 2017 Nov;14(11):1429-1437.
2. Dietrich CF, Sharma M, Gibson RN, Schreiber-Dietrich D, Jenssen C. Fortuitously discovered liver lesions. World J Gastroenterol. 2013;19(21):3173-3188.
3. Kaltenbach TE-M, Engler P, Kratzer W, Oeztuerk S, Seufferlein T, et al. Prevalence of benign focal liver lesions ultrasound investigation of 45,319 hospital patients. Abdom Radiol (NY). 2016;41(1):25-32.
4. Sporea I, Sandulescu DL, Sirli R, Popescu A, Danila M, Sparchez Z, et al. Contrast-Enhanced Ultrasound for the Characterization of Malignant versus Benign Focal Liver Lesions in a Prospective Multicenter Experience - The SRUMB Study. J Gastrointestin Liver Dis. 2019;28:191-196.
5. Bartolotta TV, Taibbi A, Randazzo A, Gagliardo C. New frontiers in liver ultrasound: From mono to multi parametricity. World J Gastrointest Oncol. 2021 Oct 15;13(10):1302-1316
6. Dietrich CF, Bamber J, Berzigotti A, Bota S, Cantisani V, Castera L, et al. EFSUMB Guidelines and Recommendations on the Clinical Use of Liver Ultrasound Elastography, Update 2017 (Long Version). Ultraschall Med. 2017;38(4):e16-e47.
7. Lupsor-Platon M, Serban T, Silion AI, Tirpe A, Florea M. Hepatocellular Carcinoma and Non-Alcoholic Fatty Liver Disease: A Step Forward for Better Evaluation Using Ultrasound Elastography. Cancers (Basel). 2020 Sep 28;12(10):2778.
8. Grgurevic I, Tjesic Drinkovic I, Pinzani M. Multiparametric ultrasound in liver diseases: an overview for the practising clinician. Postgrad Med J. 2019 Aug;95(1126):425-432.
9. Fofiu R, Bende F, Popescu A, Şirli R, Lupușoru R, Ghiuchici AM, et al. Spleen and Liver Stiffness for Predicting High-Risk Varices in Patients with Compensated Liver Cirrhosis. Ultrasound Med Biol. 2021;47(1):76-83.
10. Gerber L, Fitting D, Srikantharajah K, Weiler N, Kyriakidou G, Bojunga J, et al. Evaluation of 2D- Shear Wave Elastography for Characterisation of Focal Liver Lesions. J Gastrointestin Liver Dis. 2017;26(3):283-290.
11. Ronot M, Di Renzo S, Gregoli B, Duran R, Castera L, Van Beers BE, et al. Characterization of fortuitously discovered focal liver lesions: additional information provided by shearwave elastography. Eur Radiol. 2015 Feb;25(2):346-58.
12. Martelletti C, Armandi A, Caviglia GP, Saracco GM, Pellicano R. Elastography for characterization of focal liver lesions: current evidence and future perspectives. Gastroenterol (Torino). 2021;67(2):196-208

13. Ferraioli G, Filice C, Castera L, Choi BI, Sporea I, Wilson SR, et al. WFUMB guidelines and recommendations for clinical use of ultrasound elastography: Part 3: Liver. Ultrasound Med. Biol. 2015;41(5):1161-1179.
14. Ferraioli G, Wong VW, Castera L, Berzigotti A, Sporea I, Dietrich CF, et al. Liver Ultrasound Elastography: An Update to the World Federation for Ultrasound inMedicine and Biology Guidelines and Recommendations. Ultrasound Med Biol 2018;44(12): 2419-2440.
15. Bray F, Ferlay J, Soerjomataram I, Siegel RL, Torre LA, Jemal A. Global cancer statistics 2018: GLOBOCAN estimates of incidence and mortality worldwide for 36 cancers in 185 countries. CA Cancer J Clin 2018;68:394–424.
16. European Association for the Study of the Liver. Electronic address eee, European Association for the Study of the L. EASLClinical Practice Guidelines: Management of hepatocellular carcinoma. J. Hepatol. 2018, 69, 182–236.
17. Shiina T, Nightingale KR, Palmeri ML, Hall TJ, Bamber JC, Barr RG, et al. WFUMB guidelines and recommendations for clinical use of ultrasound elastography: Part 1: basic princi¬ples and terminology. Ultrasound Med Biol 2015; 41(5):1126-1147.
18. Yeh WC, Li PC, Jeng YM, Hsu HC, Kuo PL, Li ML, et al. Elastic modulus measurements of human liver and correlation with pathology. Ultrasound Med Biol. 2002;28(4):467-474.
19. Berzigotti A, Ferraioli G, Bota S, Gilja OH, Dietrich CF. Novel ultrasound-based methods to assess liver disease: The game has just begun. Dig Liver Dis. 2018 Feb;50(2):107-112.
20. Srinivasa Babu A, Wells ML, Teytelboym OM, Mackey JE, Miller FH, Yeh BM, et al. Elastography in Chronic Liver Disease: Modalities, Techniques, Limitations, and Future Directions. Radiographics. 2016;36(7):1987-2006.
21. Rus G, Faris IH, Torres J, Callejas A, Melchor J. Why Are Viscosity and Nonlinearity Bound to Make an Impact in Clinical Elastographic Diagnosis? Sensors (Basel). 2020 Apr 22;20(8):2379.
22. Cesario V, Accogli E, Domanico A, Di Lascio FM, Napoleone L, Gasbarrini A, et al. Percutaneous real-time sonoelastography as a non-invasive tool for the characterization of solid focal liver lesions: A prospective study. Dig Liver Dis. 2016 Feb;48(2):182-8.
23. Onur MR, Poyraz AK, Ucak EE, Bozgeyik Z, Özercan IH, Ogur E. Semiquantitative strain elastography of liver masses. J Ultrasound Med. 2012 Jul;31(7):1061-7.
24. Emara DM, El Shafei MM, El-Gendi A, Yousif AA. Is ultrasound elastography adding value in diagnosis of focal he¬patic lesions? Our experience in a single-center study. Egypt J Radiol Nucl Med 50, 103 (2019).
25. Jung EM, Platz Batista da Silva N, Jung W, Farkas S, Stroszczynski C, Rennert J. Is Strain Elastography (IO-SE) Sufficient for Characterization of Liver Lesions before Surgical Resection--Or Is Contrast Enhanced Ultrasound (CEUS) Necessary?. PLoS One. 2015;10(6):e0123737. Published 2015 Jun 26.
26. Sigrist RMS, Liau J, Kaffas AE, Chammas MC, Willmann JK. Ultrasound Elastography: Review of Techniques and Clinical Applications. Theranostics. 2017;7(5):1303-1329. doi:10.7150/thno.18650.
27. Săftoiu A, Gilja OH, Sidhu PS, Dietrich CF, Cantisani V, Amy D, et al. The EFSUMB Guidelines and Recommendations for the Clinical Practice of Elastography in Non-Hepatic Applications: Update 2018. Ultraschall Med 2019;40:425–53.

28. European Association for the Study of the Liver. Electronic address: easloffice@easloffice.eu; Clinical Practice Guideline Panel; Chair:; EASL Governing Board representative:; Panel members:. EASL Clinical Practice Guidelines on non-invasive tests for evaluation of liver disease severity and prognosis - 2021 update. J Hepatol. 2021;75(3):659-689.
29. Jiao Y, Dong F, Wang H, Zhang L, Xu J, Zheng J, et al. Shear wave elastography imaging for detecting malignant lesions of the liver: a systematic review and pooled meta-analysis. Med Ultrason. 2017;19(1):16-22.
30. Hu X, Huang X, Chen H, Zhang T, Hou J, Song A, et al. Diagnostic effect of shear wave elastography imaging for differentiation of malignant liver lesions: a meta-analysis. BMC Gastroenterol. 2019;19(1):60.
31. Wu, JP, Shu R, Zhao YZ, Ma GL, Xue W, He QJ, et al. Comparison of contrast-enhanced ultrasonography with virtual touch tissue quantification in the evaluation of focal liver lesions. J Clin Ultrasound. 2016;44(6):347-353.
32. Dong Y, Wang WP, Xu Y, Cao J, Mao F, Dietrich CF. Point shear wave speed measurement in differentiating benign and malignant focal liver lesions. Med Ultrason. 2017;19(3):259-264.
33. Zhang P, Zhou P, Tian SM, Qian Y, Li JL, Li RZ. Diagnostic performance of contrast-enhanced sonography and acoustic radiation force impulse imaging in solid liver lesions. J Ultrasound Med. 2014;33(2):205-214.
34. Yu H, Wilson SR. Differentiation of benign from malignant liver masses with Acoustic Radiation Force Impulse technique. Ultrasound Q. 2011;27(4):217-223.
35. Heide R, Strobel D, Bernatik T, Goertz RS. Characterization of focal liver lesions (FLL) with acoustic radiation force impulse (ARFI) elastometry. Ultraschall Med. 2010;31(4):405-409.
36. Ying L, Lin X, Xie ZL, Tang FY, Hu YP, Shi KQ. Clinical utility of acoustic radiation force impulse imaging for identification of malignant liver lesions: a meta-analysis. Eur Radiol. 2012;22(12):2798-2805.
37. Hasab Allah M, Salama RM, Marie MS, Mandur AA, Omar H. Utility of point shear wave elastography in characterisation of focal liver lesions. Expert Rev Gastroenterol Hepatol. 2018;12(2):201-207.
38. Akdoğan E, Yılmaz FG. The role of acoustic radiation force impulse elastography in the differentiation of benign and malignant focal liver masses [published correction appears in Turk J Gastroenterol. 2018 Oct;29(6):722]. Turk J Gastroenterol. 2018;29(4):456-463.
39. Kim JE, Lee JY, Bae KS, Han JK, Choi BI. Acoustic radiation force impulse elastography for focal hepatic tumors: usefulness for differentiating hemangiomas from malignant tumors. Korean J Radiol. 2013;14(5):743-753.
40. Gallotti A, D'Onofrio M, Romanini L, Cantisani V, Pozzi Mucelli R. Acoustic Radiation Force Impulse (ARFI) ultrasound imaging of solid focal liver lesions. Eur J Radiol. 2012;81(3):451-455.
41. Ghiuchici AM, Sporea I, Dănilă M, Șirli R, Moga T, Bende F, et al. Is There a Place for Elastography in the Diagnosis of Hepatocellular Carcinoma?. J Clin Med. 2021;10(8):1710. Published 2021 Apr 15.
42. Guo LH, Wang SJ, Xu HX, Sun LP, Zhang YF, Xu JM, et al. Differentiation of benign and malignant focal liver lesions: value of virtual touch tissue quantification of acoustic radiation force impulse elastography. Med Oncol. 2015;32(3):68.

43. Dong Y, Koch J, Alhyari A, Safai Zadeh E, Görg C, Wang WP, et al. Ultrasound Elastography for Characterization of Focal Liver Lesions. Z Gastroenterol. 2023 Apr;61(4):399-410.
44. Ling W, Lu Q, Lu C, Quan J, Ma L, Li J, et al. Effects of vascularity and differentiation of hepatocellular carcinoma on tumor and liver stiffness: in vivo and in vitro studies. UltrasoundMed Biol 2014;40:739–46.
45. Goya C, Hamidi C, Yavuz A, Hattapoglu S, Uslukaya O, Cetincakmak MG, Teke M, Urakci Z. The Role of Acoustic Radiation Force Impulse Elastography in the Differentiation of Infectious and Neoplastic Liver Lesions. Ultrason Imaging. 2015 Oct;37(4):312-22.
46. Davies G, Koenen M. Acoustic radiation force impulse elastography in distinguishing hepatic haemangiomata from metastases: preliminary observations. Br J Radiol. 2011 Oct;84(1006):939-43.
47. Park H, Park JY, Kim DY, Ahn SH, Chon CY, Han KH, Kim SU. Characterization of focal liver masses using acoustic radiation force impulse elastography. World J Gastroenterol. 2013 Jan 14;19(2):219-26.
48. Galati G, De Vincentis A, Gallo P, Guidi A, Vespasiani-Gentilucci U, Picardi A. Diagnostic value of Virtual Touch Quantification (VTQ®) for differentiation of hemangiomas from malignant focal liver lesions. Med Ultrason. 2019;21(4):371-376.
49. Grgurevic I, Bokun T, Salkic NN, Brkljacic B, Vukelić-Markovic M, Stoos-Veic T, et al. Liver elastography malignancy prediction score for noninvasive characterization of focal liver lesions. Liver Int. 2018;38(6):1055-1063. doi:10.1111/liv.13611
50. Ronot M, Di Renzo S, Gregoli B, Duran R, Castera L, Van Beers BE, et al. Characterization of fortuitously discovered focal liver lesions: additional information provided by shearwave elastography. Eur Radiol. 2015;25(2):346-358.
51. Guibal A, Boularan C, Bruce M, Vallin M, Pilleul F, Walter T, et al. Evaluation of shearwave elastography for the characterisation of focal liver lesions on ultrasound. Eur Radiol. 2013;23(4):1138-1149.
52. Gerber L, Fitting D, Srikantharajah K, Weiler N, Kyriakidou G, Bojunga J, et al. Evaluation of 2D- Shear Wave Elastography for Characterisation of Focal Liver Lesions. J Gastrointestin Liver Dis. 2017;26(3):283-290.

5.2.a. Multiparametric Ultrasound Evaluation in Focal Liver Lesions

Alina Popescu, Roxana Șirli, Tudor Moga

Ultrasound is an extremely widespread diagnostic method, being an accessible, non-invasive, and non-irradiating technique, which complements the clinical evaluation of patients. Conventional ultrasound examination modes, grayscale mode (B-mode) and Doppler mode, are considered as first-line options for imaging diagnosis in many specialties. Advances in ultrasound technology have introduced a variety of new functions, increasing the versatility and effectiveness of ultrasound examination. Thus, the new ultrasound machines have the ability to evaluate the degree of fibrosis by elastographic methods (Fig. 5.58). Moreover, with the introduction of contrast agents in contrast-enhanced ultrasound or CEUS (Fig. 5.59.), the paradigm of the indication for ultrasound evaluation has changed especially for focal liver lesions. By using contrast in ultrasound, a wide range of features has been implemented in ultrasound machines, allowing quantitative analysis of organ perfusion in terms of time and intensity (time-intensity curve) and parametric imaging analysis (1-3).

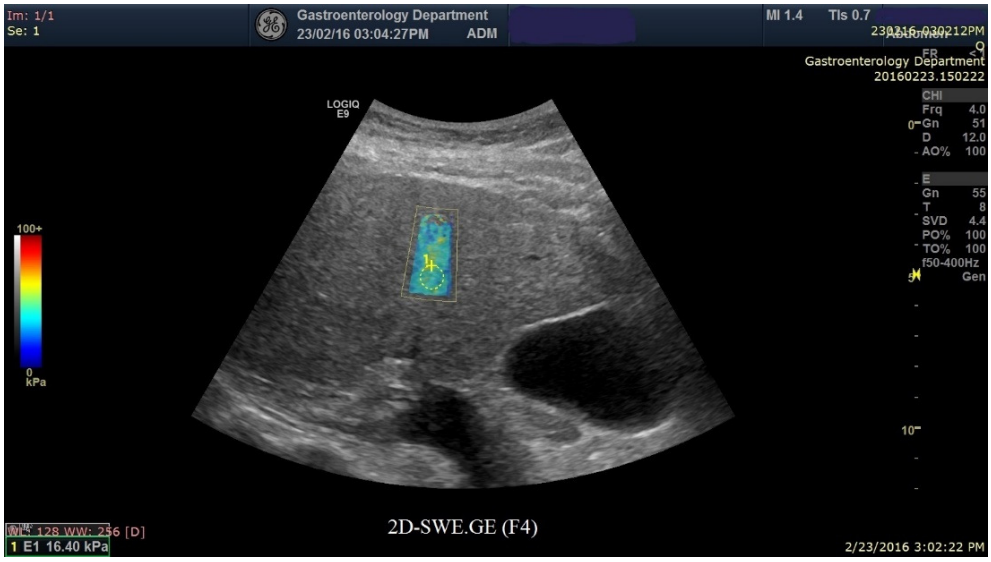

Fig. 5.58. Highlights of a cirrhotic liver evaluated by the 2D-SWE.GE technique, LOGIQ E9 system (GE Healthcare, Chalfont St Giles, United Kingdom) (version 2.0), where the color-coded map indicates a reddish-yellow color, signifying the presence of significant fibrosis.

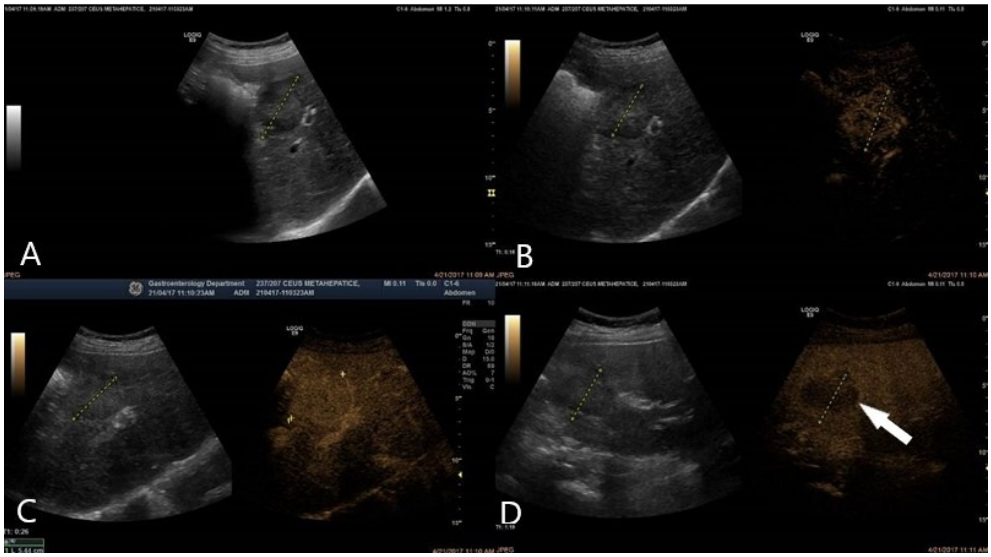

Fig. 5.59. In these images, a malignant liver lesion (marked by the dotted line) as illustrated in B-mode (box A) was assessed by CEUS. The CEUS assessment is illustrated in frames B–D, representing the vascular times: B- arterial phase; C- portal phase and D- late phase (Arrow representing the wash-out phenomenon). (1)

Focal liver lesions (FLLs) are often detected in daily practice during routine abdominal ultrasounds. The new features implemented in newer ultrasound machines allow the examiner to gain a better understanding of the structural and functional changes of the lesions. Therefore, the role of ultrasound examination is to evaluate functional changes by analyzing vascularization by both quantitative (Fig. 5.60) and qualitative (Fig. 5.61.) means, and structural changes by measuring the stiffness of both the liver and the focal liver lesion as can be seen in Fig. 5.62. (4, 5).

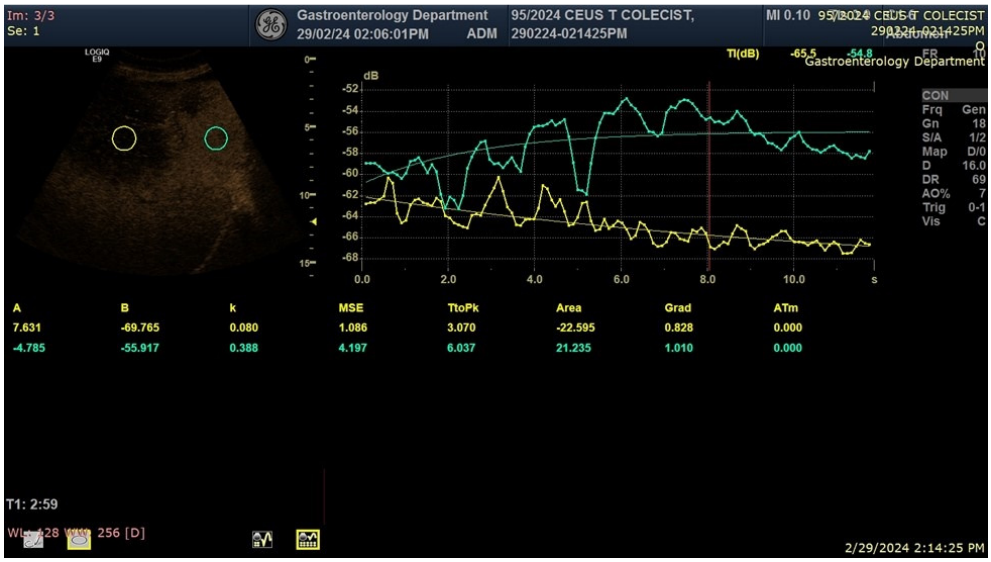

Fig. 5.60. In this figure, a malignant lesion was evaluated, and the time-intensity curve (TIC) analysis was applied in the wash-out format. On the right side of the image are represented the graphs of the intensity variations as well as the parameters analyzed in the preselected regions of interest (yellow circle; blue circle) (6)

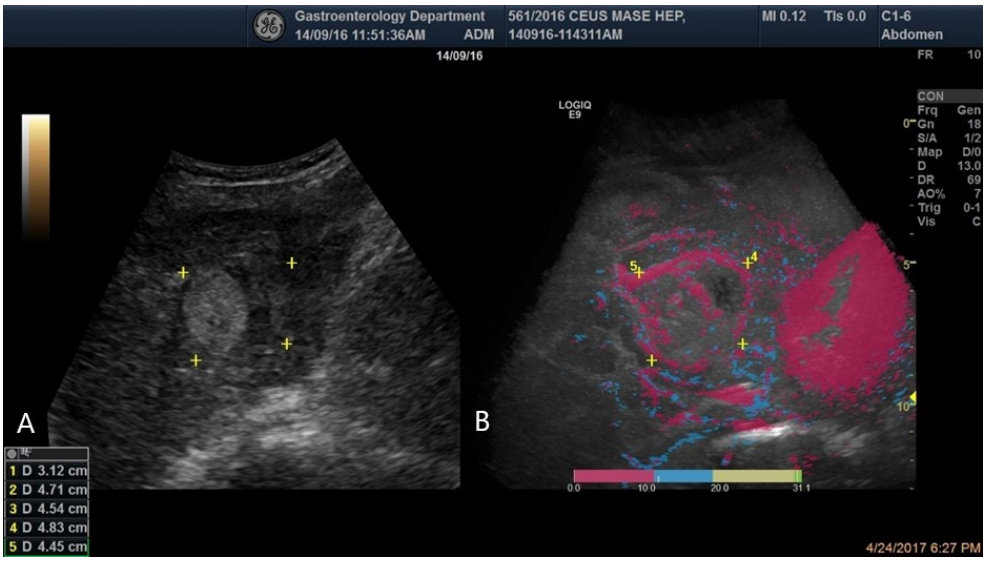

Fig. 5.61. The arterial phase of CEUS is illustrated in (A). In frame (B), parametric imaging has been applied, thus better documenting contrast arrival time by using color coding (7).

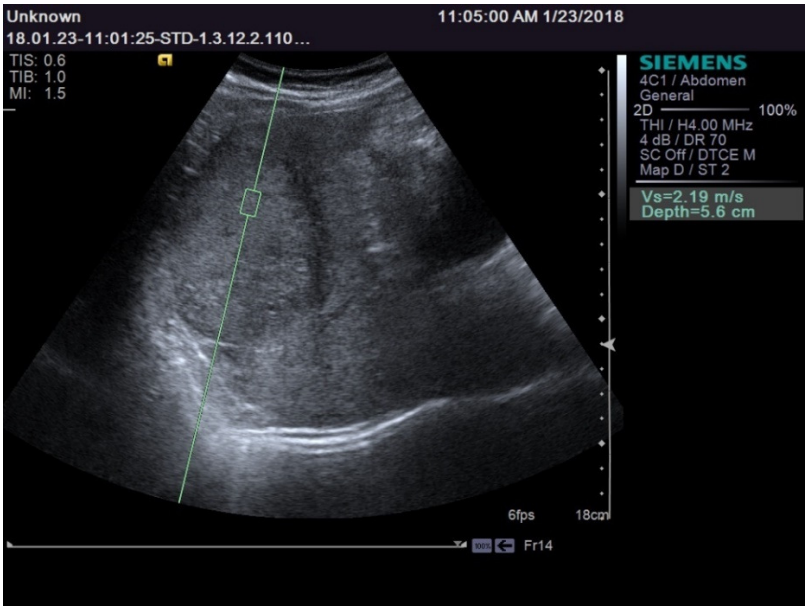

Figure 5.62. It reveals a VTQ (Virtual Touch Quantification) measurement, performed with a Siemens Acuson S2000™ (Erlangen, Germany) system in a focal liver lesion (hepatocellular carcinoma).

The new imaging options offer a broader perspective on the structures examined and have led to the creation of a concept called "multiparametric ultrasound" (MPUS) (8, 9), a concept already used in the literature for the evaluation of other pathologies. MPUS is successfully used to evaluate parathyroid lesions, thyroid nodules (10), prostate cancer (11), breast lesions (12) and in the evaluation of chronic kidney disease (13). All these new features have propelled ultrasonographic evaluation to the level of other contrast imaging techniques that, not long ago, were considered superior to ultrasonography. Of all the organs, the liver

was probably the most privileged from this point of view and, in the context of the evaluation of focal liver lesions, the concept of MPUS brings considerable advantages. Thus, given the amount of information that ultrasound can provide, the time required to perform a complete examination with all these new applications is increasing, which is why the ultrasound evaluation could be changed to multiparametric evaluation (8, 14, 15).

Several approaches have been proposed regarding multiparametric ultrasound examination in focal liver lesions. In a study published in 2020 (16), the use of contrast vector imaging (CVI) combined with CEUS ultrasonography at a high frame rate for the characterization of focal liver lesions was analyzed, highlighting its feasibility and potential benefits. The results demonstrated CVI's ability to provide quantitative and multiparametric information, improving diagnostic accuracy for differentiating between hepatocellular carcinoma (HCC) and non-HCC tumors. The study represents a promising approach to improve the characterization and implicitly the diagnosis of lesions, reducing, at least theoretically, the need for more invasive diagnostic methods.

A different approach (17) proposes to reassess inconclusive focal liver lesions using MPUS analysis together with a binary decision tree classifier (BDTC) after the initial analysis at CEUS. The study showed that, by applying this concept, 78% of the lesions could be classified as malignant, with the type of lesion being determined in 28% of the cases. This approach demonstrates the potential of MPUS combined with BDTC in improving the accuracy of the diagnosis of focal liver lesions.

In the study by Ainora et al. (18), a multiparametric dynamic ultrasound (D-CEUS) approach is developed to differentiate between hepatocellular carcinoma (HCC) and intrahepatic cholangiocarcinoma (ICC), with the aim of improving the accuracy of non-invasive diagnosis. The study proposes the integration of liver stiffness measurements and CEUS-standardized parameters, developing a score to improve the differentiation of the two entities. The study reveals significant differences in blood perfusion parameters and tissue stiffness between HCC and ICC, suggesting the potential of this multiparametric approach to reduce the need for liver biopsies in certain patient groups.

Multiparametric ultrasound (MPUS) is a significant advance in the diagnosis of focal liver damage, providing a non-invasive and radiation-free alternative that is based on advanced technologies, including elastography and contrast enhanced ultrasonography. These techniques allow for quantitative and qualitative evaluations of tissue vascularization and stiffness, improving the ability to differentiate between different types of liver damage. Recent studies highlight the potential of MPUS to reduce reliance on biopsies by providing accurate characterization of lesions, taking a step forward in the accurate and minimally invasive diagnosis of liver lesions.

References

1. Dietrich CF, Nolsøe CP, Barr RG, Berzigotti A, Burns PN, Cantisani V, et al. Guidelines and Good Clinical Practice Recommendations for Contrast-Enhanced Ultrasound (CEUS) in the Liver-Update 2020 WFUMB in Cooperation with EFSUMB, AFSUMB, AIUM, and FLAUS. Ultrasound Med Biol. 2020; 46(10):2579-604.
2. Sporea I, Badea R, Brisc C, Ioanițescu S, Moga T, Popescu A, et al. Romanian National Guidelines on Contrast Enhanced Ultrasound in clinical practice. Med Ultrasound. 2017; 19(4):401-15.
3. Dietrich CF, Averkiou MA, Correas JM, Lassau N, Leen E, Piscaglia F. An EFSUMB introduction into Dynamic Contrast-Enhanced Ultrasound (DCE-US) for quantification of tumour perfusion. Ultraschall Med. 2012; 33(4):344-51.
4. Ghiuchici A-M, Sporea I, Dănilă M, Șirli R, Moga T, Bende F, Popescu A. Is There a Place for Elastography in the Diagnosis of Hepatocellular Carcinoma? Journal of Clinical Medicine. 2021; 10(8):1710.
5. Lupușoru R, Sporea I, Rațiu I, Lungeanu D, Popescu A, Dănilă M, et al. Contrast-Enhanced Ultrasonography with Arrival Time Parametric Imaging as a Non-Invasive Diagnostic Tool for Liver Cirrhosis. Diagnostics (Basel). 2022; 12(12).
6. Ultrasound Lab. GE Healthcare Time Intensity Curve Manual. Available online: https://www.logiqportal.net
7. LOGIQ™ XDclear™ Family Parametric Analysis. Available online: https://www.gehealthcare.com/products/logiq-xdclear-family (accessed on 15 July 2021).
8. Sidhu PS. Multiparametric ultrasound (MPUS) imaging: terminology describing the many aspects of ultrasonography. Ultraschall in der Medizin-European Journal of Ultrasound. 2015; 36(04):315-7.
9. Popescu A. Multiparametric ultrasound (MPUS) or "the many faces" of ultrasonography. Medical Ultrasonography. 2019; 21(4):369-70.
10. Cantisani V, D'Andrea V, Biancari F, Medvedyeva O, Di Segni M, Olive M, et al. Prospective evaluation of multiparametric ultrasound and quantitative elastosonography in the differential diagnosis of benign and malignant thyroid nodules: preliminary experience. Eur J Radiol. 2012; 81(10):2678-83.
11. Kierans AS, Taneja SS, Rosenkrantz AB. Implementation of Multi-parametric Prostate MRI in Clinical Practice. Curr Urol Rep. 2015; 16(8):56.
12. Kapetas P, Clauser P, Woitek R, Wengert GJ, Lazar M, Pinker K, et al. Quantitative Multiparametric Breast Ultrasound: Application of Contrast-Enhanced Ultrasound and Elastography Leads to an Improved Differentiation of Benign and Malignant Lesions. Invest Radiol. 2019; 54(5):257-64.
13. Gao J, Perlman A, Kalache S, Berman N, Seshan S, Salvatore S, et al. Multiparametric Quantitative Ultrasound Imaging in Assessment of Chronic Kidney Disease. J Ultrasound Med. 2017; 36(11):2245-56.
14. Grgurevic I, Tjesic Drinkovic I, Pinzani M. Multiparametric ultrasound in liver diseases: an overview for the practising clinician. Postgraduate Medical Journal. 2019; 95(1126):425-32.
15. Moga TV, David C, Popescu A, Lupusoru R, Heredea D, Ghiuchici AM, et al. Multiparametric Ultrasound Approach Using a Tree-Based Decision Classifier for Inconclusive Focal Liver Lesions Evaluated by Contrast Enhanced Ultrasound. Journal of Personalized Medicine. 2021; 11(12):1388.

16. Yoo J, Lee JM. Diagnostic Value of High Frame Rate Contrast-enhanced Ultrasonography and Post-processing Contrast Vector Imaging for Evaluation of Focal Liver Lesions: A Feasibility Study. Ultrasound Med Biol. 2020; 46(9):2254-64.
17. Moga TV, David C, Popescu A, Lupusoru R, Heredea D, Ghiuchici AM, et al. Multiparametric Ultrasound Approach Using a Tree-Based Decision Classifier for Inconclusive Focal Liver Lesions Evaluated by Contrast Enhanced Ultrasound. J Pers Med. 2021; 11(12).
18. Ainora ME, Cerrito L, Liguori A, Mignini I, De Luca A, Galasso L, et al. Multiparametric Dynamic Ultrasound Approach for Differential Diagnosis of Primary Liver Tumors. International Journal of Molecular Sciences. 2023; 24(10):8548.

Chapter 6. The role of Elastography in pancreatic pathology

Bogdan Miutescu, Alexandru Popa, Adrian Săftoiu

Transabdominal Pancreatic Elastography

Over the past two decades, elastography has seen a continuous rise, proving to be an extremely useful technique that allows for the real-time assessment of the stiffness of various tissues. There is a considerable number of studies that have confirmed the utility of elastography in evaluating superficial organs (breast gland, thyroid) and the liver. Due to significant advancements in elastographic techniques in recent years, there has been increased interest in establishing the importance of elastography in the diagnosis and management of pancreatic pathology. However, due to the deep positioning of the pancreas, making precise and reproducible elastographic measurements remains a challenge. Moreover, verifying the concordance between elastographic measurements and the histological structure of the pancreas is difficult, considering the challenges in obtaining biopsies from this organ (1).

The elastic properties of the pancreas can be studied through both transabdominal and endoscopic approach. Impulse elastography-VCTE (FibroScan, EchoSense), used for assessing liver stiffness, cannot be applied to the pancreas since this organ is located deeply in the abdomen and it is difficult to explore without adequate visualization. Therefore, transabdominal elastographic evaluation of the pancreas requires that the elastography software module be integrated into the ultrasound device to use standard B-mode ultrasound as guidance. Thus, to evaluate the pancreas, two different types of elastography based on different principles can be used: strain elastography techniques and shear-wave elastography. Using strain elastography, tissue stiffness is estimated by measuring its distortion as a result of external (manual) or internal (heartbeats, pulsations of the aorta) compression. In shear-wave elastography, stiffness is estimated by measuring the propagation speed of shear-wave vibrations in tissues.

Strain Elastography

In clinical practice, the initial elastographic evaluation has been performed by using strain elastography. Strain elastography estimates the stiffness of the target tissue by measuring the degree of deformation caused by external pressure. There is a negative correlation between the degree of deformation and the stiffness of the target tissue: the greater the deformation, the softer the tissue stiffness. Since manual compression is inefficient for the pancreas, deformation must be generated by the pulsations of the aorta. Ideally, the targeted tissue should be located between the transducer and the aorta, thus facilitating the proper detection of deformation. An elastogram can be easily obtained in the

pancreatic body, except in patients with severe arteriosclerosis. Conversely, obtaining a proper elastogram in the head and tail of the pancreas is difficult.

The first clinical use of strain elastography was documented using Real-Time Elastography (RTE) technology, developed by Hitachi Aloka (2). Initially, RTE only allowed for qualitative assessments, through a color elastogram where harder tissues are indicated in shades of blue, while softer tissues are represented in red. Uchida reported that the diagnostic accuracy for pancreatic tumors using only standard ultrasound was approximately 70%-80%, while the accuracy of combining it with RTE significantly improved diagnostic accuracy (over 90%).

Initially, these qualitative evaluations were marked by subjectivity and largely depended on the operator. With the introduction of the strain-ratio concept, a more objective approach to evaluation was pursued. Thus, the strain-ratio was defined as the ratio between the deformation measured in the reference tissue (B) and the deformation recorded in the targeted tissue (A). However, there is still no consensus on establishing the reference area. In evaluating pancreatic cancer, some researchers have used non-tumoral pancreatic tissue as the reference area, while others have chosen a red area around the pancreas, assumed to be fat—this latter consideration is not supported by any evidence. On the other hand, shear-wave elastography (SWE) is a quantitative method, considered to be the more accurate method for assessing pancreatic stiffness.

Shear-Wave Elastography (SWE)

Given that the pancreas is an organ deeply situated within the abdomen, a qualitative elastogram cannot always be obtained using strain elastography. Therefore, elastographic techniques that use acoustic radiation force impulse (ARFI) to generate shear waves in the pancreatic tissue have been developed. One of the first techniques introduced was the Virtual Touch Quantification (VTQ) developed by Siemens. VTQ is a point-shear wave technique (p-SWE) that estimates the stiffness of the target tissue by measuring the speed of the shear waves generated through the initiation of an ultrasonic pulse (Fig. 6.1).

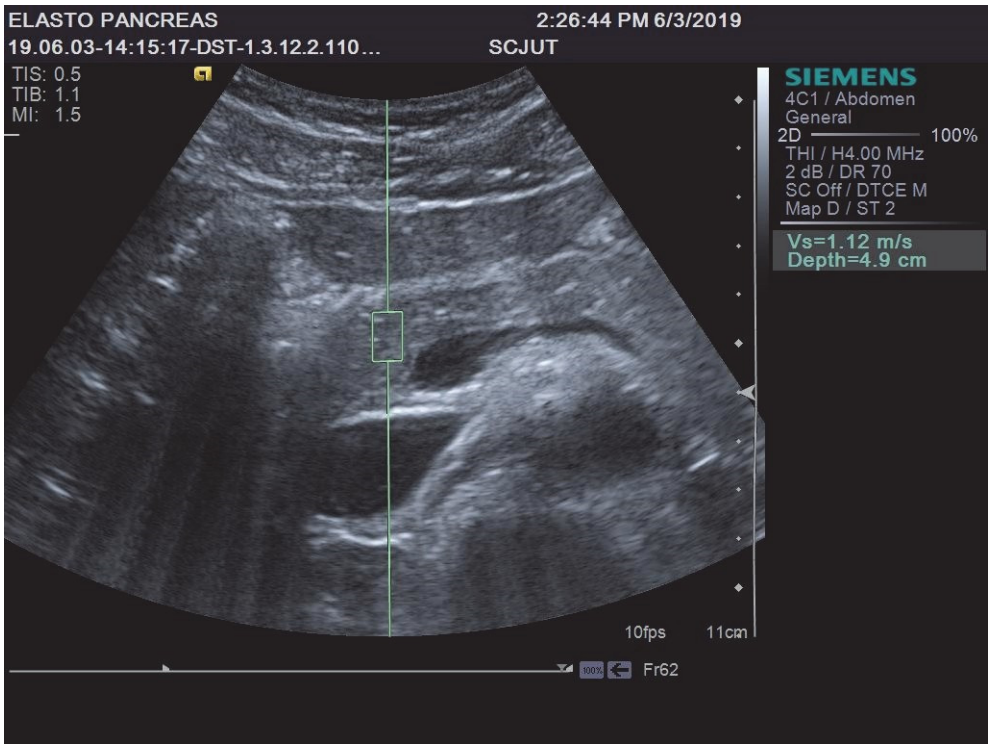

Fig. 6.1. p-SWE Elastography Developed by Siemens

Subsequently, several other p-SWE techniques have been developed and used, including ElastPQ developed by Philips, pSWE developed by Samsung, as well as 2D-SWE techniques (General Electric, Samsung, Canon, Supersonic) (Fig. 6.2).

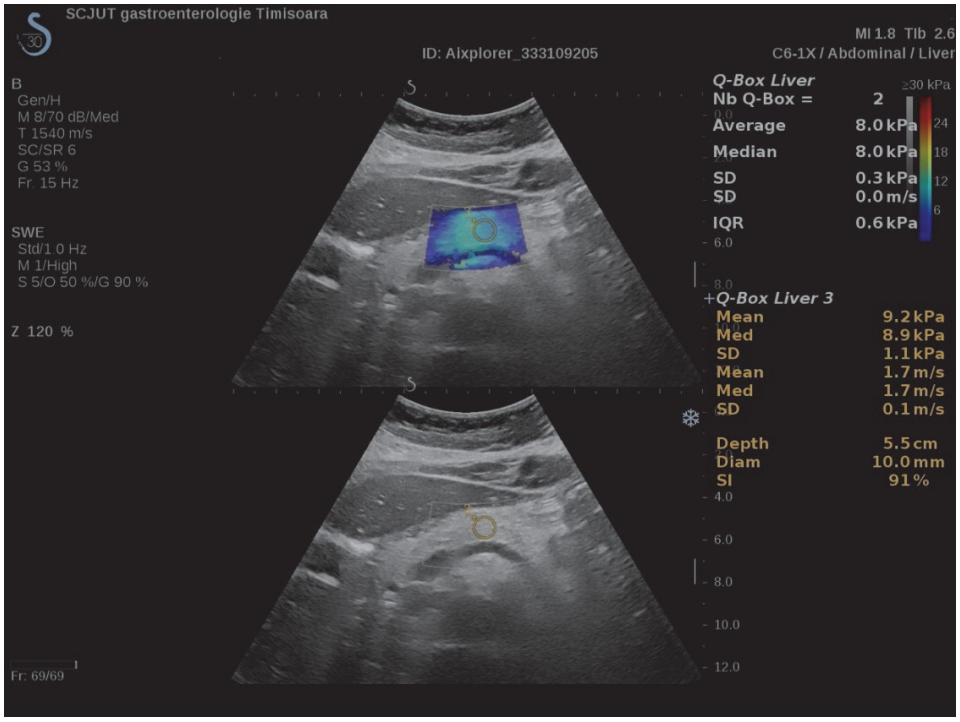

Fig. 6.2. 2D-SWE Elastography Developed by SuperSonic

Normal Values

Establishing normal values for the elastography of pancreatic parenchyma presents a challenge, given that, even using the same methodology, variations are observed among healthy control groups from different studies. One of the most comprehensive data sets, which included 210 healthy subjects, was analyzed by Xie and colleagues. According to them, the normal values for p-SWE elastography of the pancreatic head and body were 1.18 ± 0.23 m/s and 1.20 ± 0.20 m/s, respectively, unaffected by age, gender, body mass index (BMI), waist circumference, or organ dimensions (3).

On the other hand, the results of the study published by Stumpf and colleagues indicate significant differences based on sex, with lower average values recorded in men compared to women across all examined areas of the pancreas (head, body, and tail). Additionally, a significant correlation was observed between the age of participants and the measured values, suggesting that pancreatic tissue properties may change with age (4). Alcohol consumption and smoking did not have significant effects on the p-SWE values of the pancreas.

In a study that included 37 healthy subjects, Zaro investigated the pancreatic stiffness using the VTQ elastographic technique. The results indicate an average SWV (Shear-Wave Velocity) for the entire pancreatic parenchyma of 1.216 m/s ± 0.36, with similar values across the three segments of the pancreas: head (1.224 m/s), body (1.227 m/s), and tail (1.191 m/s). The study suggests that performing five SWV measurements per pancreatic segment is sufficient, with no statistically significant differences between the results obtained through 5 or 10 measurements (5).

Acute Pancreatitis

Several studies have explored the capability of elastographic techniques to differentiate acute pancreatitis from other pancreatic conditions. Mateen highlighted that p-SWE values were higher in patients with acute pancreatitis (n=68) compared to healthy subjects (n=52) and patients with chronic pancreatitis (n=46) (3.28 ± 0.85 vs. 1.28 ± 0.29 and 1.25 ± 0.24 m/s, $p < 0.001$). Using a cut-off value of 2.2 m/s, the negative predictive value of p-SWE to distinguish patients with acute pancreatitis from healthy individuals or those with chronic pancreatitis was 97.8% (6). However, Xie et al. found no significant differences between patients with acute pancreatitis (n=44) and healthy volunteers (3).

Given that the diagnosis of acute pancreatitis in typical cases is based on clinical presentation and biological changes that occur, elastography could improve the accuracy of diagnosis in unclear cases, even when imaging results are inconclusive. Using a cut-off value of 1.63 m/s, the p-SWE technique performed better than computed tomography (CT) in diagnosing acute pancreatitis, with a sensitivity of 100% and a specificity of 98% (7). Similarly, Durmaz showed that in patients diagnosed based on clinical symptoms and biological changes, who had a normal pancreatic appearance on standard ultrasound and CT, the 2D-SWE values

were significantly higher than in healthy volunteers (41.67 ± 9.65 vs. 23.77 ± 6.72 kPa, $p < 0.001$) (8).

Given that universal normal or pathological elastographic values have not been clearly established, in patients with acute pancreatitis, investigating the dynamics of elastographic values between the initial moment and subsequent re-evaluations is of real interest. In a prospective study where patients with acute pancreatitis were classified according to Atlanta criteria, the 2D-SWE values in patients with mild acute pancreatitis tended to be higher than those in patients with severe acute pancreatitis (9.05 ± 1.44 vs. 8.61 ± 1.72 kPa); however, the difference was not statistically significant. After clinical improvement, the 2D-SWE values decreased significantly compared to the initial value (10.97 vs. 8.8 kPa, $p = 0.000$), but remained elevated after one month. Furthermore, 2D-SWE was not correlated with hospital stay duration and biochemical parameters (9). Further studies on the dynamics of SWE values are needed.

Pancreatic elastography could also prove to be a valuable tool in monitoring the effectiveness of treatment. In patients diagnosed with type 1 autoimmune pancreatitis (n=23), it was observed that the 2D-SWE values were significantly higher compared to those of healthy volunteers (n=34) - 30.9 vs. 6.6 kPa, $p = 0.001$. Moreover, these values registered a significant decrease just two weeks after starting treatment with corticosteroids, thus highlighting the capability of elastography to accurately track the response to therapy (10).

Chronic Pancreatitis

A study conducted by Yashima investigated the efficacy of ARFI elastography in diagnosing chronic pancreatitis, comparing SWE values between healthy volunteers and patients with chronic pancreatitis. The study included 52 healthy volunteers and 46 patients with chronic pancreatitis, with elastographic measurements taken across all segments of the pancreas (head, body, and tail). The feasibility of the technique was good in the body, acceptable in the head, and low in the tail: 75%, 69%, and 42%, respectively. The study results show that pancreatic stiffness is significantly higher in patients with chronic pancreatitis. The optimal cut-off value for diagnosing chronic pancreatitis was 1.40 m/s with a sensitivity of 75%, specificity of 72%, positive predictive value of 69%, and negative predictive value of 78%. Additionally, alcoholic etiology ($r^2 = 0.142$) and lower BMI ($r^2 = 0.107$) were correlated with higher values of pancreatic stiffness (11).

In another study that included 52 patients with chronic pancreatitis and 42 healthy volunteers, pancreatic stiffness values were significantly higher in patients with chronic pancreatitis compared to healthy subjects ($p = 0.001$). Significantly higher values were also observed in patients with a longer duration of the disease (>10 years compared to ≤10 years) ($p = 0.01$), those using chronic analgesic medications ($p < 0.05$), and those with lower body weight ($p < 0.05$, $r = -0.38$) (12).

Kojima aimed to evaluate the role of SWE elastography in diagnosing chronic pancreatitis in a study that included 59 patients. The study demonstrated significant differences between the SWE values obtained in patients with chronic pancreatitis compared to those obtained in patients with a normal pancreas ($p = 0.001$) (13).

Another study conducted by Kawada, which included 85 patients with chronic alcohol use (AUD) and analyzed the p-SWE technique, concluded that pancreatic stiffness values were significantly higher in patients consuming >60 g ethanol/day ($p = 0.005$) (14).

In conclusion, the use of elastography consistently revealed that pancreatic stiffness is significantly higher in patients diagnosed with this condition compared to healthy individuals. This underscores the potential of such non-invasive techniques as promising tools for diagnosing chronic pancreatitis. However, further studies are needed to comprehensively evaluate their applicability in clinical practice.

Pancreatic Cancer

Although pancreatic elastography has proven useful in enhancing the diagnostic accuracy of standard ultrasound (B-mode) for the diagnosis of pancreatic cancer, the results regarding SWE values are mixed. Some authors have reported significantly higher values at the tumor site compared to healthy pancreatic parenchyma (15), yet, in other studies, no significant differences were identified using transabdominal elastography. Park and colleagues highlighted that the difference between the p-SWE values obtained in the lesion and in the surrounding healthy pancreatic parenchyma was significantly smaller for benign lesions compared to malignant lesions (0.4 ± 0.3 vs. 1.5 ± 0.8 m/s, $p = 0.011$) (16).

The results of the aforementioned studies indicate that transabdominal elastography holds significant potential in evaluating pancreatic pathologies, providing valuable details that can support the improvement of the accuracy of standard ultrasound diagnostics. However, variations between studies and the challenges in establishing reference normal or pathological values underscore the imperative need for further research to solidify the foundations of its use in clinical practice. Ecoendoscopic elastography seems to offer even more promising results, suggesting that it could be even more useful in detailed assessments of the pancreas, requiring additional studies for full validation of its effectiveness and applicability.

Endoscopic Ultrasound Elastography (EUS-E) of the Pancreas

The utility of EUS-E lies in its ability to access structures that are quite difficult to examine, such as the pancreas or adjacent lymph nodes. There are two elastography techniques available on endoscopy systems, similar to transabdominal ultrasound, which have been studied in pancreatic diseases: strain elastography and shear-wave elastography (17). One of the major differences between these techniques is that strain elastography provides relative values, as it is a semi-quantitative method, whereas shear-wave elastography

produces absolute values, which may be more relevant in the subsequent management of the patient. To perform this type of procedure, it is necessary for the endoscope to be connected to a compatible ultrasound machine, or for the endoscopy system to be equipped with a dedicated endoscopy processor (18).

Clinical Applications of Endoscopic Ultrasound Elastography in Pancreatic Pathology: Solid Pancreatic Tumors

Given the epidemiology of pancreatic adenocarcinoma, among focal pancreatic lesions, the most important consideration when faced with a pancreatic tumor is to exclude this diagnosis. The existence of elastographic cut-off values to define this tumor compared to other pancreatic tumors would be extremely useful, but these values are not yet available, even though there are studies that have tried to differentiate various types of tumors based on elastography (19).

There are multiple meta-analyses that have evaluated the diagnostic performance of strain-type endoscopic ultrasound elastography in characterizing malignant pancreatic lesions, with authors demonstrating high sensitivity but low specificity of elastography in clinical practice (20,21,22,23,24). (Table 6.I).

Table 6.I: Diagnostic Performance of Strain-Type Endoscopic Ultrasound Elastography in Characterizing Malignant Pancreatic Lesions

Author	**Number of Patients**	**Sensitivity (%)**	**Specificity (%)**
Pei et al. 2012	1042	98	69
Mei et al. 2013	1044	95	67
Ying et al 2013	893	98	69
Li et al. 2013	781	99	76
Hu et al. 2013	752	97	76
Xu et al. 2013	752	99	74
Lu et al. 2017	1537	97	67
Zhang et al. 2018	1687	98	63

In a study conducted by Ignee and colleagues that included 216 patients with small solid pancreatic tumors (up to 15 mm), elastographic measurements were performed using endoscopic ultrasound, and the results were subsequently compared with the histopathological diagnosis. The authors demonstrated that EUS-E had a sensitivity and specificity of 96% and 64%, respectively, for pancreatic adenocarcinoma (25).

Fine-needle aspiration or biopsy guided by endoscopic ultrasound plays an important role in diagnosing malignancy in pancreatic masses or certain lymph nodes. Elastography enhances this procedure by highlighting the hard areas within the masses being biopsied, thus selecting the most suitable region for biopsy while avoiding areas of necrosis and inflammation (Fig. 6.3 and Fig. 6.4). A study published by Facciorusso and colleagues on a cohort of 54 patients with solid pancreatic lesions with an average size of 35 mm showed that using elastography to guide the most appropriate area for fine-needle aspiration increased sensitivity from 86.4% to 93.4% and specificity from 75% to 100% (26).

EUS elastography can be considered a method for excluding a malignancy diagnosis rather than confirming it, but combined with other endoscopic ultrasound diagnostic methods, such as the administration of contrast agents during the examination, it can be very helpful in confirming the malignant nature of a solid pancreatic mass or lymph node (27).

In conclusion, qualitative and semi-quantitative elastography in pancreatic formations have a very high negative predictive value for excluding the diagnosis of pancreatic adenocarcinoma in a soft pancreatic lesion. Additionally, it can be used as a non-invasive technique that assists in guiding endoscopic ultrasound-guided fine-needle aspiration, the golden standard in the diagnosis of solid pancreatic tumors (27).

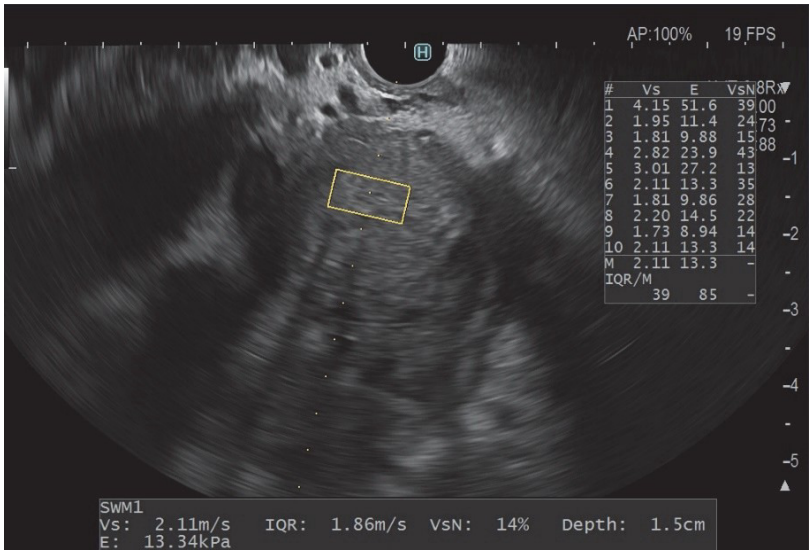

Fig. 6.3. Shear-Wave Type Endoscopic Ultrasound Elastography

Chronic Pancreatitis

The value of elastography for diagnosing chronic pancreatitis (CP) remains controversial. Although transabdominal elastography is the first-line choice due to its ease of use, EUS-guided elastography is the preferred method because of its better visualization of the pancreas compared to transabdominal ultrasound (28).

In general, fibrotic changes in chronic pancreatitis lead to increased pancreatic stiffness, while acute pancreatitis and necrotic areas appear softer on the elastogram (26). In

chronic pancreatitis, elastographic histogram analysis corresponds with histological changes and the likelihood of exocrine pancreatic insufficiency (29).

Using this method, a prospective study conducted in 2013 by Iglesias-Garcia and colleagues demonstrated a significant direct correlation ($r = 0.813$; $p < 0.0001$) between EUS criteria for CP (Rosemont criteria, Tables 6.II and 6.III) and strain elastography as an indicator of pancreatic fibrosis severity. The sensitivity of EUS elastography for diagnosing CP was 91.1% at a cut-off value of 2.25. Strain elastography values varied significantly according to the Rosemont classification (1.80 normal pancreas, 2.40 indeterminate group, 2.85 suggestive of CP, 3.62 consistent with CP, $p < 0.001$) (30).

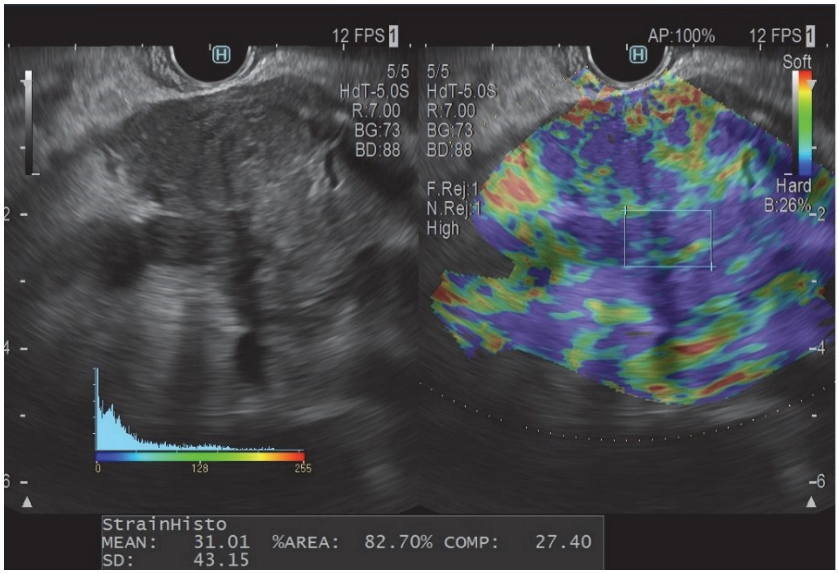

Fig. 6.4. Strain-Type Endoscopic Ultrasound Elastography

Table 6.II. Rosemont Criteria for Diagnosing Chronic Pancreatitis by EUS

Parenchyma	**Ducts**
Hyperechoic foci with posterior shadowing (major A); body/tail	Ductal calculi (major A criterion)
Honeycomb-type lobulation (major B); body/tail	Irregular main duct (minor criterion); body/tail
Lobulation without honeycomb (minor criterion); body/tail	Dilated secondary ducts (minor criterion); body/tail
Hyperechoic foci without posterior shadowing (minor criterion); body/tail	Dilated main duct (minor criterion); body/tail
Cysts (minor criterion)	Hyperechoic ductal margin (minor criterion); body/tail
Hyperechoic septa (minor criterion); body/tail	

Table 6.III. Interpretation of the Rosemont Criteria

Result	Criteria
Chronic Pancreatitis	1 major A + ≥ 3 minor 1 major A + 1 major B 2 major A
Suspected Chronic Pancreatitis	1 major A + < 3 minor 1 major B + ≥ 3 minor ≥ 5 minor
Possible Chronic Pancreatitis	3 or 4 minor, no major B +/- < 3 minor
Normal	< 3 minor, no major

An accurate diagnosis of pancreatic fibrosis is clinically important and has the potential to stage chronic pancreatitis. To this end, Itoh and colleagues demonstrated a very strong correlation between histology, the standardized fibrosis score, and elastographic assessment. The ROC curve for the diagnosis of mild fibrosis, marked fibrosis, and severe fibrosis were 0.90, 0.90, and 0.90, respectively (31,32).

In terms of applicability, shear wave elastography has also been described in chronic pancreatitis. A recent study published by Yamashit and colleagues, which included 52 patients, demonstrates a direct correlation between elastography results and the Rosemont classification (Tables 1,2), considered the golden standard for diagnosing chronic pancreatitis. At a cut-off value of 2.19 m/s, it showed a sensitivity of 100% and a specificity of 94% for chronic pancreatitis (33). These data showed good results in favor of EUS-SWM as a diagnostic modality for chronic pancreatitis compared to other studies on strain elastography. Iglesias-Garcia and colleagues reported a sensitivity and specificity of strain-type EUS elastography for diagnosing chronic pancreatitis of 91.2% and 91%, respectively. Given these results, EUS-SWM appears to be superior (34).

More recently, another study published in 2023 by Yamashit and colleagues showed that shear wave elastography values correlated better with the severity grades of the Rosemont classification, CT appearance, and the degree of exocrine pancreatic insufficiency compared to strain-type values (35).

In conclusion, EUS-guided elastography is considered an excellent tool today, capable of differentiating a normal pancreas from early chronic pancreatitis. Future research will continue to update and define the role of EUS elastography in clinical practice.

Autoimmune Pancreatitis

Autoimmune pancreatitis (AIP) is a distinct type of pancreatitis caused by a chronic inflammatory mechanism mediated by autoimmunity. AIP is morphologically characterized by diffuse or focal enlargement of the pancreas and irregular, diffuse narrowing of the main pancreatic duct, and serologically by elevated levels of serum gammaglobulins, including IgG, and especially IgG4 (36). AIP responds well to steroid therapy. However, the definitions of "remission" and "relapse" are ambiguous; therefore, a method to assess the degree or activity of AIP inflammation is necessary (37,38).

There is a wide spectrum of radiological features of AIP, ranging from a normal pancreas to diffuse parenchymal enlargement or the appearance of focal pancreatic lesions. The latter are characterized as focal AIP and can be easily confused with pancreatic adenocarcinoma. Correct diagnosis can be established by evaluating combined clinical, laboratory, and histopathological data along with EUS assessment. Elastography is an important tool that can help clinicians differentiate focal AIP from pancreatic carcinoma. Indeed, the former usually presents a homogeneous increase in stiffness throughout the entire organ, whereas the latter has increased stiffness limited only to the tumor area (39).

When using qualitative elastography in AIP, the inflamed area should present a predominantly green pattern with slight red or yellow lines, while a homogeneous green appearance should appear in the normal parenchyma. However, definitive cut-off values for diagnosing AIP and distinguishing between focal AIP and pancreatic carcinoma are not available. A prospective study was conducted using shear-wave measurements to evaluate the feasibility and ability to measure tissue elasticity in the pancreas and the correlation between disease activity and pancreatic tissue elasticity in patients with AIP (40).

To evaluate the utility of EUS-SWM, measurements and comparative analyses of pancreatic tissue elasticity were performed in patients with diffuse pancreatic lesions. Eight patients with AIP and 16 control patients were included in this analysis. The median Vs in the pancreatic body of the AIP group was 2.57 m/s (IQR 2.16–3.08), significantly higher than that of the normal control group (1.89 m/s (IQR 1.68–2.63)) (P=0.0185) (40). For patients who received corticosteroid therapy (n=6), EUS-SWM was performed before and 2 weeks after therapy (Prednisone 0.6 mg/kg/day). The mean Vs significantly decreased from 3.32 m/s (IQR 2.93–3.59) before to 2.46 m/s (1.84–2.96) after steroid therapy. The pancreatic body size on CT examination significantly decreased (21.3 mm vs. 15.9 mm). Serum IgG4 level (244 mg/dl vs. 209.5 mg/dl, P=0.3367) and pancreatic body size on EUS (24 mm vs. 16 mm, P=0.0863) showed a trend of decrease, but no statistically significant difference was observed 2 weeks after steroid therapy. There was no significant correlation between Vs level and IgG4 in patients with AIP (41).

In conclusion, even though elastography is not the main diagnostic tool for AIP, the use of EUS-SWM is feasible and represents a useful method for evaluating the effect of steroid therapy in patients with AIP. EUS-SWM is a promising method that can facilitate the implementation of EUS-E in the future.

Conclusions

The use of EUS elastography should be encouraged as it provides valuable complementary information. It is performed in real-time, it is easy to use and learn, it has no additional risks or costs, and only minimally increases the examination time. It has no known contraindications and does not require any specific preparation.

References

1. Kawada N, Tanaka S. Elastography for the pancreas: Current status and future perspective. World J Gastroenterol. 2016 Apr;22(14):3712–24.
2. Uchida H, Hirooka Y, Itoh A, Kawashima H, Hara K, Nonogaki K, et al. Feasibility of tissue elastography using transcutaneous ultrasonography for the diagnosis of pancreatic diseases. Pancreas. 2009 Jan;38(1):17–22.
3. Xie J, Zou L, Yao M, Xu G, Zhao L, Xu H, et al. A Preliminary Investigation of Normal Pancreas and Acute Pancreatitis Elasticity Using Virtual Touch Tissue Quantification (VTQ) Imaging. Med Sci Monit Int Med J Exp Clin Res. 2015 Jun;21:1693–9.
4. Stumpf S, Jaeger H, Graeter T, Oeztuerk S, Schmidberger J, Haenle MM, et al. Influence of age, sex, body mass index, alcohol, and smoking on shear wave velocity (p- SWE) of the pancreas. Abdom Radiol (New York). 2016 Jul;41(7):1310–6.
5. Zaro R, Lupsor-Platon M, Cheviet A, Badea R. The pursuit of normal reference values of pancreas stiffness by using Acoustic Radiation Force Impulse (ARFI) elastography. Med Ultrason, 2016 Dec 5;18(4):425-430
6. Mateen M, Muheet K, Mohan R, Rao P, Majaz H, Rao G, et al. Evaluation of Ultrasound Based Acoustic Radiation Force Impulse (ARFI) and eSie touch Sonoelastography for Diagnosis of Inflammatory Pancreatic Diseases. JOP J Pancreas 2012;13(1):36–44.
7. Göya C, Hamidi C, Hattapoğlu S, Çetinçakmak MG, Teke M, Degirmenci MS, et al. Use of Acoustic Radiation Force Impulse Elastography to Diagnose Acute Pancreatitis at Hospital Admission. J Ultrasound Med (Internet). 2014 Aug 1;33(8):1453–60.
8. Durmaz MS, Arslan S, Özbakır B, Güngör G, Tolu İ, Arslan FZ, et al. Effectiveness of Shear Wave Elastography in the diagnosis of acute pancreatitis on admission. 018 Aug 30;20(3):278-284
9. Kaya M, Değirmenci S, Göya C, Tuncel ET, Uçmak F, Kaplan MA. The importance of acoustic radiation force impulse (ARFI) elastography in the diagnosis and clinical course of acute pancreatitis. Turkish J Gastroenterol Off J Turkish Soc Gastroenterol. 2018 May;29(3):342–7.
10. Suzuki H, Ishikawa T, Ohno E, Iida T, Uetsuki K, Yashika J, et al. An initial trial of quantitative evaluation of autoimmune pancreatitis using shear wave elastography and shear wave dispersion in transabdominal ultrasound. Pancreatology. 2021;21(4):682–7.
11. Yashima Y, Sasahira N, Isayama H, Kogure H, Ikeda H, Hirano K, et al. Acoustic radiation force impulse elastography for noninvasive assessment of chronic pancreatitis. J Gastroenterol. 2012 Apr;47(4):427–32.
12. Pozzi R, Parzanese I, Baccarin A, Giunta M, Conti CB, Cantù P, et al. Point shear-wave elastography in chronic pancreatitis: A promising tool for staging disease severity. Pancreatology. 2017;17(6):905–10.

13. Kojima H, Sofuni A, Sugimoto K, Tsuchiya T, Ishii K, Tanaka R, et al. Efficacy of shear wave elastography for the diagnosis of chronic pancreatitis. J Hepatobiliary Pancreat Sci. 2023 Mar;30(3):351–9.
14. Kawada N, Tanaka S, Uehara H, Ohkawa K, Yamai T, Takada R, et al. Potential use of point shear wave elastography for the pancreas: a single center prospective study. Eur J Radiol. 2014 Apr;83(4):620–4.
15. Zaro R, Dina L, Pojoga C, Vesa S, Badea R. Evaluation of the pancreatic tumors by transabdominal Shear Wave Elastography: preliminary results of a pilot study. 2018 Aug 30;20(3):285-291
16. Park MK, Jo J, Kwon H, Cho JH, Oh JY, Noh MH, et al. Usefulness of acoustic radiation force impulse elastography in the differential diagnosis of benign and malignant solid pancreatic lesions. Ultrason (Seoul, Korea). 2014 Jan;33(1):26–33.
17. Iglesias-Garcia, J.; de la Iglesia-Garcia, D.; Lariño-Noia, J.; Dominguez-Muñoz, J.E. Endoscopic Ultrasound (EUS) Guided Elastography. *Diagnostics*, 2023 May 10;13(10):1686
18. Yasunobu Yamashita, Hirofumi Yamazaki, Toshio Shimokawa, Yuki Kawaji, Takashi Tamumra, Keiichi Hatamaru, Masahiro Itonaga, Reiko Ashida, Masayuki Kitano, Shear-wave versus strain elastography in endoscopic ultrasound for the diagnosis of chronic pancreatitis, Pancreatology. 2023 Jan;23(1):35-41
19. Ying L, Lin X, Xie ZL, et al. Clinical utility of endoscopic ultrasound elastography for identification of malignant pancreatic masses: A meta-analysis. J Gastroenterol Hepatol 2013;28:1434-43.
20. Iglesias-Garcia J, Larino-Noia J, Abdulkader I, Forteza J, Dominguez-Munoz JE. Quantitative endoscopic ultrasound elastography: an accurate method for the differentiation of solid pancreatic masses. Gastroenterology 2010;139:1172– 1180.
21. Mei M, Ni J, Liu D, et al. EUS elastography for diagnosis of solid pancreatic masses: A meta-analysis. Gastrointest Endosc 2013;77:578-89.
22. Hu DM, Gong TT, Zhu Q. Endoscopic ultrasound elastography for differential diagnosis of pancreatic masses: A meta-analysis. Dig Dis Sci 2013;58:1125-31.
23. Pei Q, Zou X, Zhang X, et al. Diagnostic value of EUS elastography in differentiation of benign and malignant solid pancreatic masses: A meta-analysis. Pancreatology 2012;12:402-8.
24. Li X, Xu W, Shi J, et al. Endoscopic ultrasound elastography for differentiating between pancreatic adenocarcinoma and inflammatory masses: A meta-analysis. World J Gastroenterol 2013;19:6284-91.
25. Ignee A, Jenssen C, Arcidiacono PG, et al. Endoscopic ultrasound elastography of small solid pancreatic lesions: A multicenter study. Endoscopy 2018;50:1071-9.
26. Facciorusso A, Martina M, Buccino RV, et al. Diagnostic accuracy of fine-needle aspiration of solid pancreatic lesions guided by endoscopic ultrasound elastography. Ann Gastroenterol 2018;31:513-8.
27. Dietrich CF, Burmeister S, Hollerbach S, Arcidiacono PG, Braden B, Fusaroli P, et al.. Do we need elastography for EUS? Endosc Ultrasound. 2020 Sep-Oct;9(5):284- 290.Janssen J, Papavassiliou I. Effect of aging and diffuse chronic pancreatitis on pancreas elasticity evaluated using semiquantitative EUS elastography. Ultraschall Med 2014;35:253–258.
28. Itoh Y, Itoh A, Kawashima H, *et al*. Quantitative analysis of diagnosing pancreatic fibrosis using EUS‐elastography (comparison with surgical specimens). *J Gastroenterol* 2014;49:1183‐92.

29. Iglesias-Garcia J, Domínguez-Muñoz J, Castiñeira-Alvariño M, Luaces-Regueira M, Lariño-Noia J. Quantitative elastography associated with endoscopic ultrasound for the diagnosis of chronic pancreatitis. Endoscopy 2013, 45, 781–788.
30. Yamamiya A, Irisawa A, Hoshi K, Yamabe A, Izawa N, Nagashima K, et al. Recent Advances in Endosonography-Elastography: Literature Review. J Clin Med. 2021;10(16),3739
31. Ungureanu SB, Saftoiu A. Endoscopic Ultrasound Elastography: New Advancement in Pancreatic Diseases. Elastography - Applications in Clinical Medicine. IntechOpen; 2022.
32. Yamashita Y, Tanioka K, Kawaji Y, Tamura T, Nuta J et al.; et al. Utility of Elastography with Endoscopic Ultrasonography Shear-Wave Measurement for Diagnosing Chronic Pancreatitis. *Gut Liver* 2020, *14*, 659–664.
33. Iglesias-Garcia J, Domínguez-Muñoz JE, Castiñeira-Alvariño M, Luaces-Regueira M, Lariño-Noia J. Quantitative elastography associated with endoscopic ultrasound for the diagnosis of chronic pancreatitis. Endoscopy. 2013;45:781–788.
34. Yamashita Y, Yamazaki H, Shimokawa T, Kawaji Y, Tamumra T et al. Shear-wave versus strain elastography in endoscopic ultrasound for the diagnosis of chronic pancreatitis. *Pancreatology* 2023, *23*, 35–41.
35. Shimosegawa T, International Association of Pancreatology. International consensus diagnostic criteria for autoimmune pancreatitis: guidelines of the International Association of Pancreatology. Pancreas. 2011;40:352–8.
36. Lee HW, Moon SH, Kim MH, et al. Relapse rate and predictors of relapse in a large single center cohort of type 1 autoimmune pancreatitis: long-term follow-up results after steroid therapy with short-duration maintenance treatment. J Gastroenterol. 2018;53:967–77.
37. Masamune A, Nishimori I, Kikuta K, Tsuji I, Mizuno N, Iiyama T, et al; Research Committee of Intractable Pancreas Diseases in Japan. Randomised controlled trial of long-term maintenance corticosteroid therapy in patients with autoimmune pancreatitis. Gut. 2017 Mar;66(3):487-494.
38. Conti CB, Cereatti F, Drago A, Grassia R. Focal Autoimmune Pancreatitis: A Simple Flow Chart for a Challenging Diagnosis. Ultrasound Int Open 2020; 6: E67-E75 .
39. Ohno E, Kawashima H, Ishikawa T, Iida T, Suzuki H, Uetsuki K, et al. Diagnostic performance of endoscopic ultrasonography-guided elastography for solid pancreatic lesions: Shear-wave measurements versus strain elastography with histogram analysis. Dig Endosc. 2021 May;33(4):629-638.
40. Ohno E, Hirooka Y, Kawashima H, *et al*. Feasibility and usefulness of endoscopic ultrasonography‐guided shear‐wave measurement for assessment of autoimmune pancreatitis activity: A prospective exploratorystudy. *J Med Ultrason* (2001) 2019;46:425‐33.
41. Poiraud M, Gkolfakis P, Arvanitakis M. Recent Developments in the Field of Endoscopic Ultrasound for Diagnosis, Staging, and Treatment of Pancreatic Lesions. Cancers (Basel). 2023 Apr 29;15(9):2547.

Chapter 7. Elastography in the Pathology of the Digestive Tract

Alina Popescu, Felix Bende

The wall of the gastrointestinal tract is a long and thin anatomical organ, surrounded by a serous layer and which includes a lumen, usually occupied by gas or fluid content, characterized by a natural peristalsis, a phenomenon that brings additional complexity to the elastographic evaluation. This anatomical structure can be examined by ultrasound, presenting it as a layered structure, characteristically consisting of five distinct layers (1, 2). In the context of ultrasonographic examination, it is recommended to use high ultrasonic frequencies, exceeding 7.5 MHz, to ensure optimal visualization of wall layers, of any thickening of the intestinal wall and possible focal lesions. This recommendation applies also to both the Strain Elastography (SE) and the shear wave (SWE) elastography techniques.

Pathological lesions that increase the thickness of the wall are most appropriate for elastographic evaluation, because the intestinal wall is a thin structure in ultrasound images, which shows natural peristalsis, and considerable movements are possible on both the serous and luminal sides. This adds artifacts to elastographic images and makes stiffness measurement more difficult and user-dependent. SE and SWE are the elastographic methods that can be used to measure the elasticity of the digestive tract wall, and the studies that have addressed the elastographic evaluation of intestinal wall lesions focus mainly on the use of the SE technique (Fig.7.1).

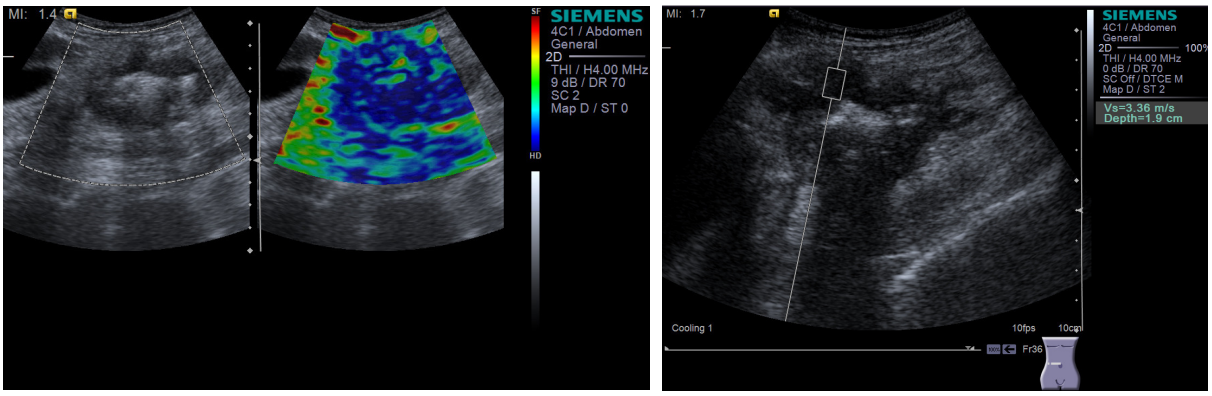

Fig. 7.1. Elastographic evaluation of a cecal tumor formation. The image on the left is taken using eSie Touch Elasticity Imaging (Siemens) elastography, where the blue color represents the harder areas and the green color the soft areas. The image on the right is taken using the pSWE technique where a small rectangular region of interest is positioned at the level of the modified wall of the cecum, obtaining a stiffness value of 3.36 m/s.

Pathological intestinal lesions usually induce a thickening of the intestinal wall and a reduction in peristalsis, thus improving the conditions of elastographic evaluation. The intestinal wall can become thickened in both neoplastic and inflammatory diseases,

predominantly in Crohn's disease (CD) (Fig.7.2). The elastographic study can provide important information in these pathologies, such as improving tissue characterization, differentiating between malignant and benign lesions or between inflammation and fibrosis.

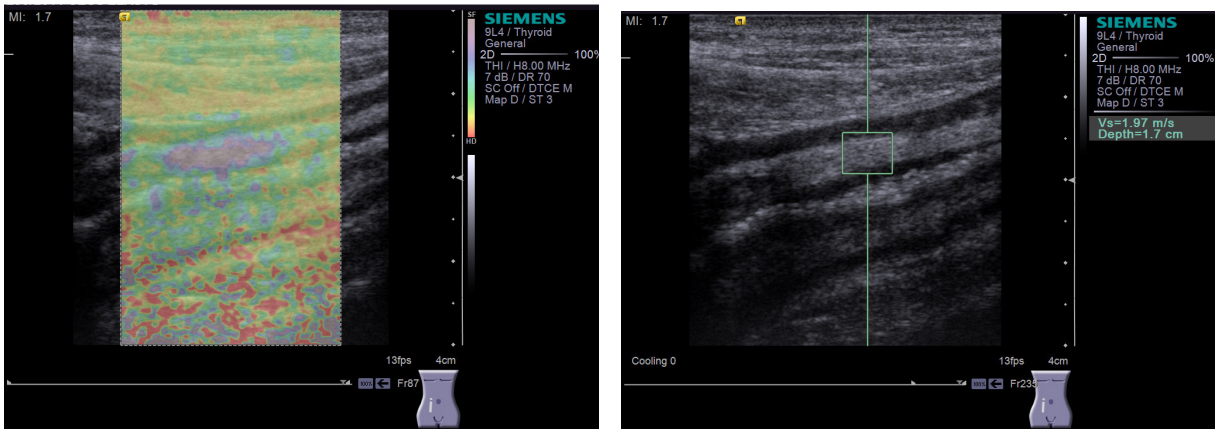

Fig. 7.2. Elastographic evaluation of the intestinal wall in Crohn's disease. The image on the left represents the elastographic evaluation using the strain elastographic (SE) technique. The image on the right represents elastographic evaluation using the pSWE technique where a small rectangular region of interest is positioned at the level of the intestinal wall, obtaining a stiffness value of 1.97 m/s.

Clinical Applications

Differentiation between fibrous and inflammatory strictures in Crohn's disease

Various studies on CD, which have involved both animal and human models, conclude that increased stiffness is associated with the presence of fibrotic structures. Some studies indicate that SE and SWE elastography can differentiate fibrosis from inflammatory lesions (3-5). One study evaluating SE performance in terminal ileum stenosis in CD, reported a higher tissue stiffness score in fibrosis using magnetic enterography as a reference (6). Another ex-vivo study of intestinal tissue samples from CD and neoplastic lesions also showed that stiffness is higher in both CD and adenocarcinoma lesions, but it is not possible to differentiate between the two pathologies (7). The same study showed that adenomas had significantly lower stiffness compared to adenocarcinomas, and that SE in intestinal pathology is a reproducible method.

A meta-analysis that included 154 CD lesions in 129 patients (8), suggested that the stiffness assessed using SE was significantly higher in fibrotic stenosis. In a study of ten patients, using SE at the level of the intestinal wall of the affected vs. unaffected segments before, during, and after surgery, found significant differences in stiffness values in the affected vs. unaffected segments, correlating well with the histological distribution of connective tissue and collagen content (9). Also, the SE measurements had an acceptable intraclass correlation coefficient (ICC) in the three examinations.

A study of 23 consecutive patients who underwent surgery for CD (10) achieved excellent differentiation between patients with severe ileal fibrosis, both histologically and by the use of the strain ratio (including excellent agreement between examiners). Conflicting results are reported in a prospective study using SE in 26 patients who underwent surgery for CD. Preoperatively, the strain ratio did not correlate with histological scores of fibrosis or inflammation (11).

A systematic review of the literature on elastography in patients with inflammatory bowel disease (IBD) that included 12 published studies and a number of 275 patients with IBD showed moderate to good accuracy of ultrasound-based elastography in the detection of histological fibrosis. SWE outperformed SE (12).

Strain elastography of intestinal lesions in CD can also predict the response to anti-inflammatory treatment. In a prospective study of 30 patients with CD, five patients who required surgery had significantly higher values of the strain ratio at baseline, with a significantly negative correlation between baseline strain ratio and intestinal wall thickness after 52 weeks of anti-tumor necrosis factor (TNF) therapy (13).

In ulcerative colitis, a published study evaluating SE demonstrated a correspondence between elastographically increased stiffness and the severity of inflammation by endoscopic scores (14). Another published study evaluated 37 patients with ulcerative colitis in whom descending colon changes were evaluated by SE, using endoscopic scores as a reference, classifying elastographic changes into 4 types: normal, homogeneous, random, and hard. In the active phase of colitis, the colonic wall was classified as hard (elastographically blue) (15).

Diagnosis of acute appendicitis

The performance of 2D-SWE in the diagnosis of acute appendicitis was evaluated in a study that included a group of 30 patients with acute appendicitis and a control group of 11 patients. This study showed that 2D-SWE can differentiate between an inflamed appendix and a normal one using a cut-off value of 12.5 kPa (Sensitivity 93%, Specificity 100%), but is not superior to computed tomography (16).

The role and efficacy of SE in the diagnosis of acute appendicitis was evaluated in a study that included 225 pediatric patients with clinical and biological suspicion of acute appendicitis. Appendectomy was performed in all cases and the histopathological result was compared with imaging methods (SE examination together with ultrasound examination in B mode). Using B-mode ultrasonography together with SE, the following values of sensitivity, specificity, positive predictive value, negative predictive value, and accuracy for the diagnosis of acute appendicitis were obtained: 96%, 96%, 95%, 96.8% and 96%. This study concluded that SE in acute appendicitis can be used as a complementary method, with the results having a good correlation with the histopathological stage of appendicular inflammation (17).

Differentiation of intramural gastrointestinal tumors

Echoendoscopic elastography (EUS) may be useful in the evaluation of intramural tumors in the upper gastrointestinal tract. Measuring the stiffness of intramural tumours can be useful in differentiating leiomyomas, lipomas or ectopic pancreatic tumours, as well as in assessing the degree of aggressiveness of gastrointestinal stromal tumours (GIST) (18).

A published study evaluated the usefulness of EUS elastography in the differential diagnosis of GIST from gastrointestinal leiomyomas (GIL), differentiation that is not possible by conventional EUS. The authors used the elastographic images obtained by EUS for post-processing analysis by tinted histogram in Photoshop software, obtaining the hue values of the R (red), G (green), B (blue) channels of each group. The statistical t-test showed significant differences between the mean shade values between GIST and GIL in channels B and G, but not in the RGB and R channels, obtaining an area value below the ROC curve of shades B and G for differentiating the diagnosis of GIST or GIL using EUS elastography of 0.723 (19). Another published study demonstrated that EUS elastography has a good value in the differential diagnosis between GIST and GIL, with sensitivity of 100% and specificity of 94% (20). However, there are studies such as the one published by Ignee et al., which have shown that EUS elastography is not useful in the differential diagnosis between GIST and GIL (21).

Characterization and staging of rectal tumors

In rectal tumors, differentiating between adenomas and adenocarcinomas is important for planning the optimal treatment option. Endorectal ultrasonography (ERUS) is a good imaging method for the T staging of rectal tumors. Elastography has demonstrated its ability to characterize harder neoplastic tissue compared to benign tissue. However, differentiating between rectal adenomas and early rectal cancer remains a challenge (T1 vs. T2) (22).

Differentiation and staging of rectal tumors can be achieved using SE as a complementary ERUS method. Thus, SE can improve the staging of rectal cancer and differentiate adenoma from adenocarcinoma, compared to ERUS alone and magnetic resonance imaging, with high interobserver agreement (23–25). Another published study demonstrated a good correlation between diffusely weighted magnetic resonance imaging associated with fibrosis, and SWE of rectal malignancies (26). Another study evaluated the performance of ERUS for rectal tumours using SWE with an 8 MHz endorectal transducer, finding that tumour stiffness measurements accurately corresponded to pathological T stage and the accuracy of tumour staging diagnosis increased from 76.7 % to 93.3 % (27).

A systematic review of the diagnostic performance of ERUS elastography in differentiating rectal adenomas from adenocarcinomas identified 6 published studies that reported increased diagnostic accuracy of ERUS elastography compared to ERUS. The sensitivity, specificity and accuracy ranged from 0.93-1.00, 0.83-1.00, 0.91-1.00 for the

differentiation of rectal adenoma from rectal adenocarcinoma, and for the differentiation of adenoma from incipient rectal cancer ranged from 0.82-1.00, 0.86-1.00 and 0.84-1.00, concluding that elastography increases the diagnostic accuracy of ERUS and provides valuable information on the malignant transformation of rectal lesions (28).

Despite the advances in the field of elastographic techniques and the interest of researchers in their use in the pathology of the digestive tract, it still remains an open field for research, in which further studies are needed to establish the role and indications where elastography can be useful.

References

1. Nylund K, Ødegaard S, Hausken T et al. Sonography of the small intestine. World J Gastroenterol 2009; 15: 1319–1330
2. Nylund K, Maconi G, Hollerweger A et al. EFSUMB Recommendations and Guidelines for Gastrointestinal Ultrasound Part 1: Examination Techniques and Normal Findings (Long version). Ultraschall in Der Medizin 2017; 38: E1–E15
3. Kim K, Johnson LA, Jia C et al. Noninvasive ultrasound elasticity imaging (UEI) of Crohn's disease: animal model. Ultrasound Med Biol 2008; 34: 902–912.
4. Stidham RW, Higgins PD. Imaging of intestinal fibrosis: current challenges and future methods. United European Gastroenterol J 2016; 4: 515–522.
5. Dillman JR, Stidham RW, Higgins PD et al. US elastography-derived shear wave velocity helps distinguish acutely inflamed from fibrotic bowel in a Crohn disease animal model. Radiology 2013; 267: 757– 766.
6. Sconfienza LM, Cavallaro F, Colombi V et al. In-vivo Axial-strain Sonoelastography Helps Distinguish Acutely-inflamed from Fibrotic Terminal Ileum Strictures in Patients with Crohn's Disease: Preliminary Results. Ultrasound Med Biol 2016; 42: 855–863.
7. Havre RF, Leh S, Gilja OH et al. Strain assessment in surgically resected inflammatory and neoplastic bowel lesions. Ultraschall in Med 2014; 35: 149–158.
8. Pescatori LC, Mauri G, Savarino E et al. Bowel Sonoelastography in Patients with Crohn's Disease: A Systematic Review. Ultrasound Med Biol 2018; 44: 297–302.
9. Baumgart DC, Müller HP, Grittner U et al. US-based Real-time Elastography for the Detection of Fibrotic Gut Tissue in Patients with Stricturing Crohn Disease. Radiology 2015; 275: 889–899.
10. Fraquelli M, Branchi F, Cribiù FM et al. The Role of Ultrasound Elasticity Imaging in Predicting Ileal Fibrosis in Crohn's Disease Patients. Inflamm Bowel Dis 2015; 21: 2605–2612.
11. Serra C, Rizzello F, Pratico' C et al. Real-time elastography for the detection of fibrotic and inflammatory tissue in patients with stricturingCrohn's disease. J Ultrasound 2017; 20: 273–284.
12. Dal Buono A, Faita F, Peyrin-Biroulet L, Danese S, Allocca M. Ultrasound Elastography in Inflammatory Bowel Diseases: A Systematic Review of Accuracy Compared with Histopathological Assessment. J Crohn's Colitis. 2022 Nov 1; 16(10):1637-1646.
13. Orlando S, Fraquelli M, Coletta M et al. Ultrasound Elasticity Imaging predicts therapeutic outcomes of patients with Crohn's disease treated with anti-tumour necrosis factor antibodies. J Crohns Colitis 2018; 12: 63–70.

14. Rustemovic N, Cukovic-Cavka S, Brinar M, et al. A pilot study of transrectal endoscopic ultrasound elastography in inflammatory bowel disease. BMC Gastroenterol 2011; 11(October (1)):113.
15. Ishikawa D et al: Images of colonic real-time tissue sonoelastography correlate with those of colonoscopy and may predict response to therapy in patients with ulcerative colitis. BMC Gastroenterology 2011;11:29-34.
16. Cha SW, Kim IY, Kim YW. Quantitative measurement of elasticity of the appendix using shear wave elastography in patients with suspected acute appendicitis. PLoS One 2014; 9: E101292.
17. Arslan H, Akdemir Z, Yavuz A, Gökçal F, Parlakgümüş C, İslamoglu N, Akdeniz H. Efficacy of Strain Elastography in Diagnosis and Staging of Acute Appendicitis in Pediatric Patients. Med Sci Monit. 2018 Feb 11;24:855-862.
18. Havre R, Gilja OH. Elastography and strain rate imaging of the gastrointestinal tract. Eur J Radiol. 2014 Mar; 83(3):438-41.
19. Guo J, Bai T, Ding Z, Du F, Liu S. Efficacy of Endoscopic Ultrasound Elastography in Differential Diagnosis of Gastrointestinal Stromal Tumor Versus Gastrointestinal Leiomyoma. Med Sci Monit. 2021 Feb 4; 27:E927619.
20. Kim SH, Yoo IK, Kwon CI, et al. Utility of eus elastography in the diagnosis of gastric subepithelial tumors: A pilot study (with video). Gastrointest Endosc, 2020; 91(1):172-77.
21. Ignee A, Jenssen C, Hocke M, et al. Contrast-enhanced (endoscopic) ultrasound and endoscopic ultrasound elastography in gastrointestinal stromal tumors. Endosc Ultrasound, 2017; 6(1):55.
22. Waage JE, Havre RF, Odegaard S, Leh S, Eide GE, Baatrup G. Endorectal elastography in the evaluation of rectal tumours. Colorectal Disease 2011; 13(10):1130–7.
23. Waage JE, Bach SP, Pfeffer F et al. Combined endorectal ultrasonography and strain elastography for the staging of early rectal cancer. Colorectal Dis 2015; 17: 50–56.
24. Waage JE, Leh S, Røsler C et al. Endorectal ultrasonography, strain elastography and MRI differentiation of rectal adenomas and adenocarcinomas. Colorectal Dis 2015; 17: 124–131.
25. Waage JE, Rafaelsen SR, Borley NR et al. Strain Elastography Evaluation of Rectal Tumours: Inter- and Intraobserver Reproducibility. Ultraschall in Med 2015; 36: 611–617.
26. Rafaelsen SR, Vagn-Hansen C, Sørensen T et al. Elastography and diffusion- weighted MRI in patients with rectal cancer. Br J Radiol 2015; 88: 20150294.
27. Chen LD, Wang W, Xu JB et al. Assessment of Rectal Tumours with Shear-Wave Elastography before Surgery: Comparison with Endorectal US. Radiology 2017; 285: 279–292.
28. Loft MK, Pedersen MRV, Rahr HB, Rafaelsen SR. Can Ultrasound Elastography Discriminate between Rectal Adenoma and Cancer? A Systematic Review. Cancers (Basel). 2021 Aug 18; 13(16):4158.

Chapter 8. Artificial Intelligence in Elastography

Angela Peltec, Ioan Sporea

Introduction

Artificial intelligence (AI) is a vast and rapidly growing field that uses software that mimics human cognitive abilities to perform complex tasks. The contribution of artificial intelligence to the global economy by 2030 is estimated to be $15.7 trillion (1). AI has been recognized as the fourth industrial revolution, as it is reshaping many areas of human activity. Let's explore the most promising AI trends in the healthcare industry that are expected to see the most growth in the coming years. We'll see how AI will move from experiments and testing to real-world use cases, especially in areas that reduce administrative burdens, help clinicians easily find information, assist agents in medical call centers, and ultimately help organizations run more efficiently. Of course, we will continue to see the development of medical imaging in relation to AI application. Ultimately, this technology will drive a new understanding of health and healthcare. This will influence the big changes we will see over the next decade. In other words, radical change doesn't arrive like a bolt from the blue, it builds gradually.

Imaging diagnostics is increasingly becoming a top priority for AI utilization. AI-powered medical imaging solutions have initiated a transformative period in healthcare. With the amalgamation of artificial intelligence and medical imaging, the accuracy and efficiency of diagnosis has reached new heights. These advanced imaging technologies facilitate faster analysis, early disease detection and personalized treatment planning, bringing great benefits to both patients and healthcare professionals. According to BIS Research, the global market for AI-powered medical imaging solutions is anticipated to reach $18.35 billion by 2032, up from $1.85 billion in 2022 (1).

Tissue stiffness is a biological marker of changes in tissue strength, which is often associated with the progression of pathologic changes in tissue. It is also well known that cancerous tissue tends to be stiffer than normal. Ultrasound-based elastography is an imaging technology that enables the assessment of tissue elasticity. The application of tissue elasticity measurement during conventional ultrasonography enhances the diagnostic performance of the exploration. US elastography has gradually been used to evaluate the pathology of superficial organs, in which tissue elasticity is found in close relationships with specific pathological processes and can characterize tumour formations of mammary glands (2), thyroid nodules (3) and prostate lesions (4).

However, the analysis of medical images is challenging due to significant intra- and inter-observer variability, to unstable diagnostic performance, to particularly low image acquisition accuracy due to low operator experience, especially for images where the boundary of a lesion is usually less well specified (7). The difficulty in identifying the optimal

cutoff for stiffness values, the variability in the selection of the region of interest (ROI), and the lack of image quality verification (8) are the basic limitations of the method.

AI can be applied in the medical field for image interpretation. As the rapid development of machine learning (ML), particularly advanced deep learning (DL) architectures, offers significant potential for automating the analysis of medical images, including segmentation, detection, and classification. (9).

The need for artificial intelligence to optimize the interpretation processes of organ-specific elastography results is crucial in the current medical context, and this can be supported by a series of solid arguments. Machine learning algorithms can detect subtle changes and provide early clues about potential conditions, contributing to early diagnosis and treatment. The increased volume of data generated by modern medical imaging can surpass a human operator's ability to process information efficiently. Artificial intelligence can quickly manage and analyze large amounts of data, providing a correct approach for interpreting elastographic results. By adapting to the particularities of each organ, artificial intelligence can contribute to personalized diagnosis, considering patient-specific variables and thus providing a more accurate framework for medical decision-making.

Therefore, in this chapter, we explore how the integration of artificial intelligence in elastography can redefine diagnostic processes and how this may influence the evolution of medicine in the next decade. In this context, it is essential to explore the potential of AI (including ML, DL and radiomics) in elastography and to identify the scientific, cultural, educational and ethical issues. We present existing challenges and future trends regarding the application of AI based on ultrasound-based elastography.

1. Principles of Elastography Techniques

In general, ultrasound elastography technique can be categorized into **Strain Elastography** (SE), which applies a constant tension method of tissue excitation, and **Shear Wave Elastography** (SWE), which uses a time-varying force. Figure 1 shows the categories of elastography techniques according to the excitation methods, including external compression or internal physiological motions, Acoustic Radiation Force Impulse (ARFI) and mechanical vibration. All approaches are based on the three-phase methodology: (a) tissue is compressed by static stress or shear wave propagation; (b) tissue displacement is tracked using ultrasound; and (c) tissue elasticity is estimated quantitatively or qualitatively by displacement measurement. In addition, a physical property called Young's modulus (E) is calculated to estimate tissue stiffness. Harder lesions have smaller deformations and higher E values (10). Details of ultrasound elastography techniques can be found in the chapter of the same name.

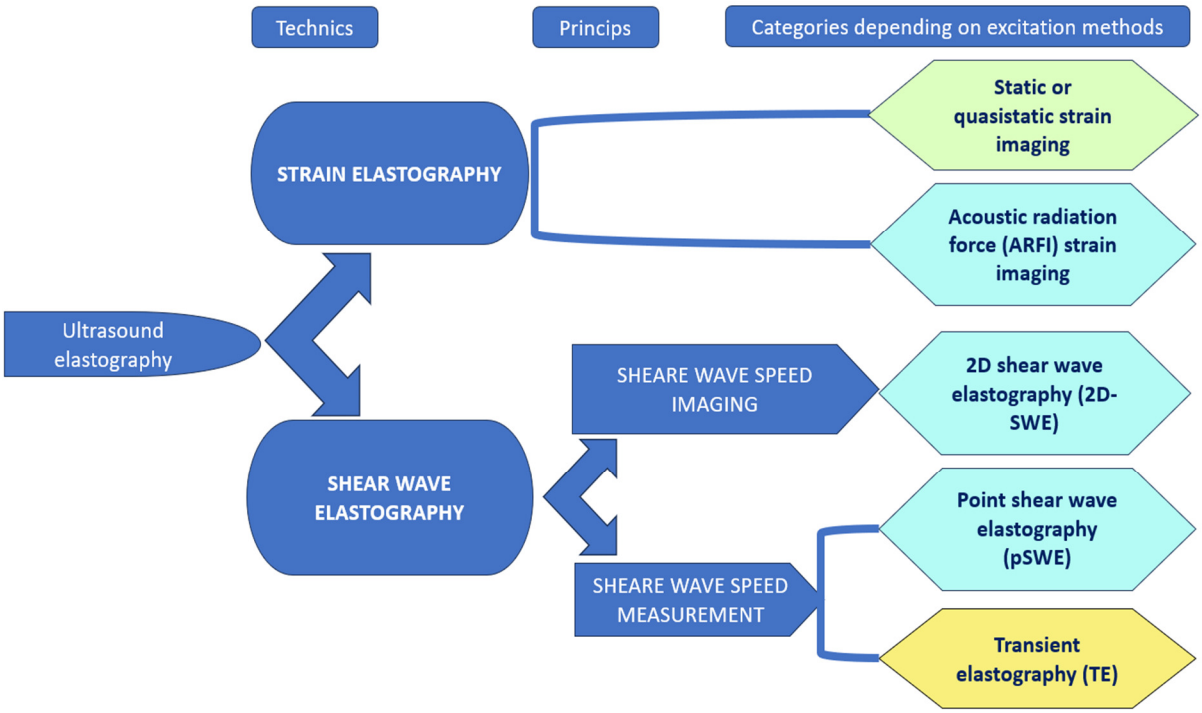

Figure 1. Categories of ultrasound-based elastography techniques depending on excitation methods, including external compression or internal physiological motions (green), acoustic radiation force impulse (ARFI) (blue) and mechanical vibration (yellow).

2. Artificial Intelligence - an Overview

Over the past decade, AI has become a popular topic both inside and outside the scientific community; an abundance of studies from the technology and non-technology fields have covered the topics of ML, DL and AI. However, there is still confusion around AI, ML and DL. The terms are highly associated, but not interchangeable. In this review, we attempt to drop the technical language to better explain these concepts to a clinical audience.

In 1956, a group of computer science researchers proposed that computers could be programmed to simulate intelligence, suggesting that "every aspect of learning or any other feature of intelligence could, in principle, be described so precisely that a machine could replicate these processes." (13). In simple terms, AI is a field focused on automating intellectual tasks typically performed by humans, and ML and DL are specific methods of achieving this goal. In other words, they fall under the umbrella of AI (Figure 2).

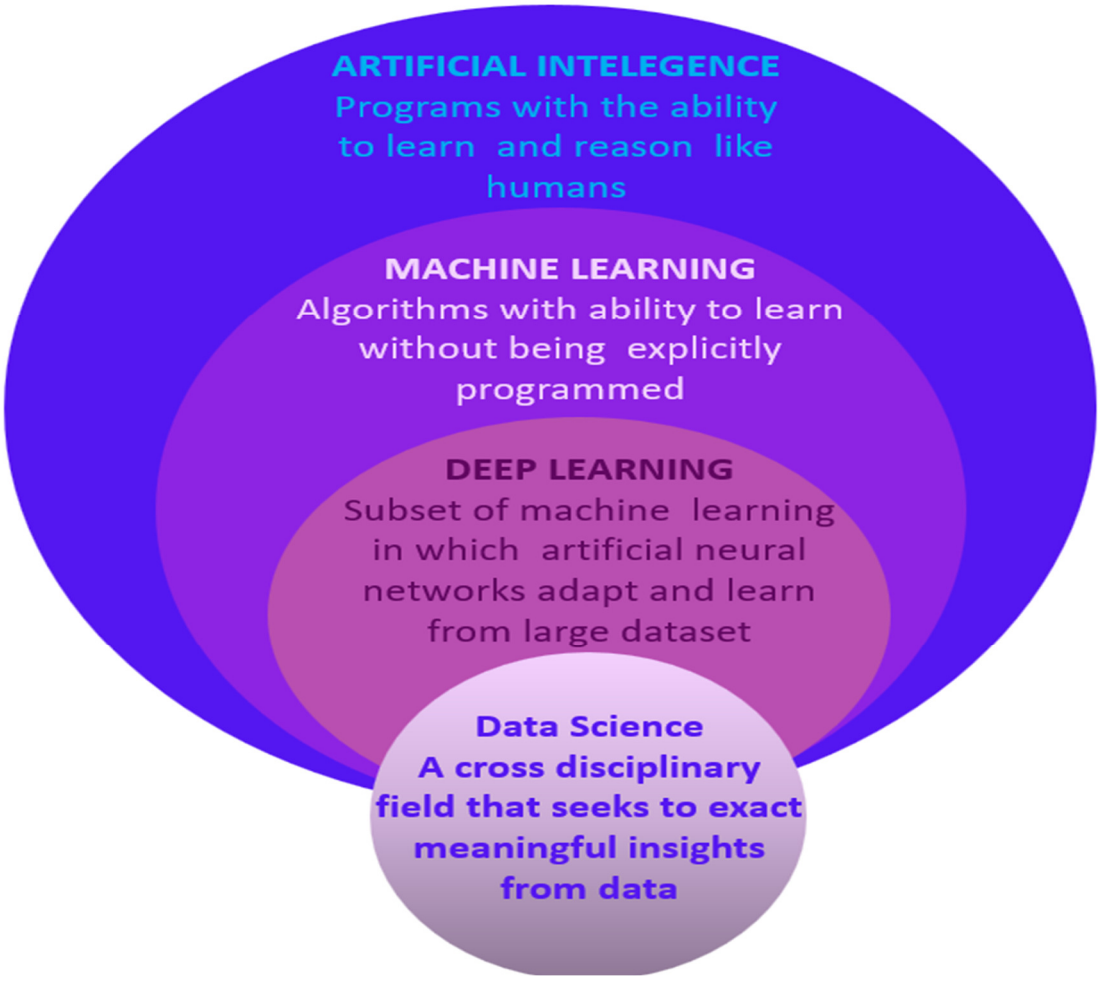

Figure 2. The difference between artificial intelligence, machine learning, deep learning and data science

However, AI includes approaches that do not involve any form of "learning". The sub-domain known as symbolic AI, for example, focuses on hardcoding (i.e. explicitly writing) rules for every possible scenario within a specific area of interest. These rules, written by humans, come from the "a priori" knowledge of the subject and in this way, specific tasks will be accomplished. For example, if someone were to program an algorithm for modulating the air temperature in an office, he or she would likely already know what temperatures are comfortable for humans and would program it to cool the room if temperatures rise above a certain threshold and to heat it if they fall below a lower threshold. Although symbolic artificial intelligence can solve clearly defined logical problems, it often fails at tasks that require higher-level pattern recognition, such as speech recognition or image classification. These more complicated processes are the tasks in which ML and DL methods perform well. We will try to summarize ML and DL for the audience without extensive technical knowledge of computer programming.

2.1. Machine Learning

Machine Learning is a field that focuses on the learning aspect of AI by developing algorithms that best represent a dataset. Unlike classical programming **(Figure 3A)**, in which an algorithm can be explicitly encoded using known features, ML uses subsets of data to generate an algorithm that can use novel combinations or different features and weights than those that can be derived from the first principles **(Figure 3B)** (14).

AI encompasses a broad array of techniques, with machine learning being one of the most significant methods used in the medical field. As a branch of AI, Machine Learning (ML) allows the creation of a system of algorithms and computational models. This system can learn from data and experience without being explicitly programmed for a particular task and can make predictions, thus allowing computers to learn like humans (11). A machine learning system is trained to interpret data and enhance its performance in a specific task or area by learning from experience. ML has numerous applications in various domains such as speech recognition, facial recognition, image classification, personalized recommendations, data analytics, and many others. It is an interdisciplinary field involving computer science and statistics.

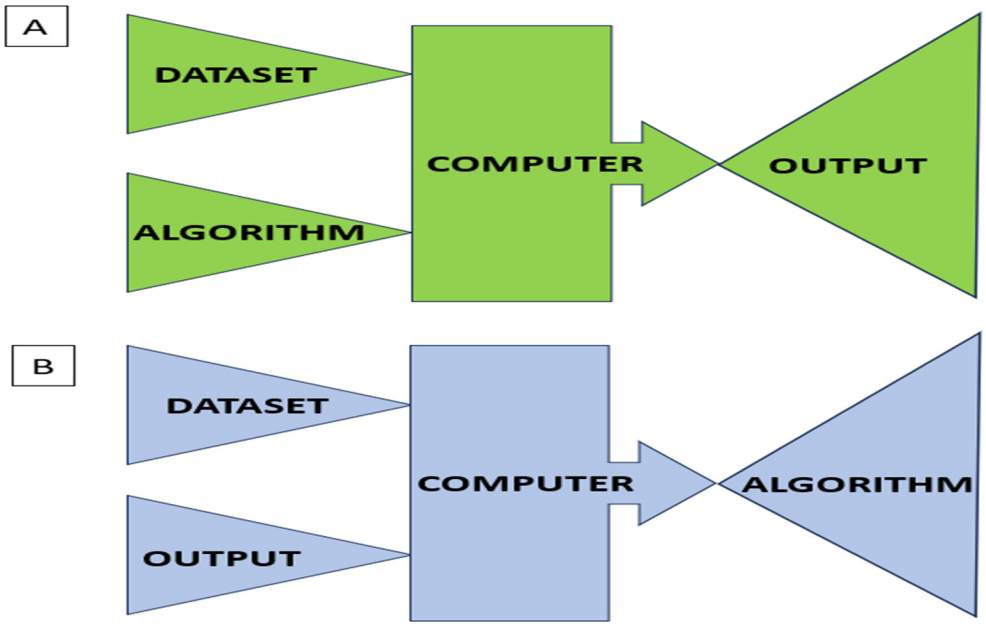

Figure 3. Classical programming versus machine learning paradigm. A. In the classical paradigm the computer is supplied with datasets and algorithms. The algorithm provides information to the computer how the data set needs to be operated to obtain the desired result. B. In machine learning, the computer is provided with datasets and corresponding results. It then learns from this information and creates an algorithm that describes the relationship between them. This algorithm can be used to predict future datasets.

2.1.1 Types of Learning Methods in ML

Generally, ML techniques can be categorized based on the types of datasets used for training. There are four commonly used learning methods in ML, each suited for different tasks: supervised, unsupervised, semi-supervised, and reinforcement learning (Figure 4).

Supervised learning involves training models with labelled data. Each dataset includes features associated with correct diagnoses. This guides the model in recognizing features and making predictions. For example, to make liver steatosis prediction, a model is fed with data from patients in whom the diagnosis of liver steatosis was made by liver biopsy. The model learns to predict in patients with the same characteristics (e.g. body mass index, visceral obesity, blood glucose, triglyceride levels) the presence of hepatic steatosis. This method is crucial to predict different real-life scenarios. The process is simple, first the model is trained with labelled examples and then applies what it has learned to new, unseen data. Gradually, the accuracy and reliability of the method improves.

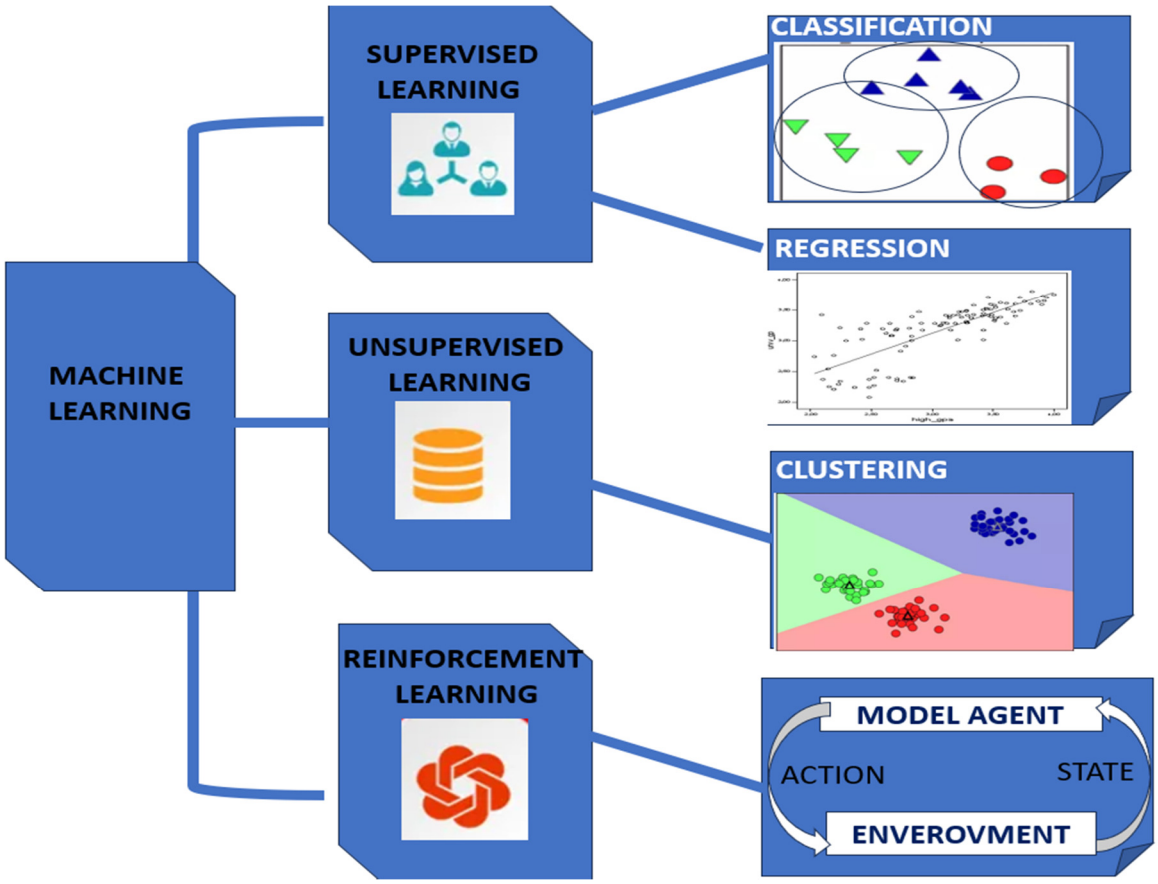

Figure 4 Types of machine learning models. Supervised learning models use labelled data; Unsupervised learning models use unlabelled data; Reinforcement learning models take actions in the environment, then receive state updates and feedback

There are two main types of supervised models:

Regression models find connections between variables. One can visualize such connections in a graph with X and Y axes, as in the picture above. If body weight increases, one can predict the increase in body mass index. This is called linear regression.

Classification models sort items into categories. Imagine a full bowl of fruit. If one is asked to pick out all the bananas, one will instinctively look at shape, color and so on. For humans, categorization is simple and automatic. We don't need to have seen a billion bananas to tell them apart. Computers must do it, though, and that was a challenge (although robots have gotten better and better at it).

Supervised models are ideal when we have a large amount of labelled data. They are perfect for content recommender systems, automatic categorization and language learning tools.

Datasets are generally divided into three categories: training, validation, and testing (models will always perform optimally on the dataset on which they are trained). Supervised learning uses the models in the training dataset to draw features for the target so that an algorithm can make predictions about presence, for example steatosis, based on future datasets. This approach is supervised, as the model infers an algorithm from the feature-target pairs and is informed, via the target, whether the prediction was correct. In other words, the features x are mapped to the target Y by learning the function f, allowing the algorithm to approximate the probability of steatosis as $Y = f(x)$. That is, the features x is mapped to the target Y by learning the mapping function, f, so that the probability of the presence of steatosis can be approximated by the algorithm $Y = f(x)$. The performance of the algorithm is evaluated against testing on another dataset, which the algorithm has never seen.

Unsupervised learning operates without human guidance, utilizing algorithms to discover patterns in unlabelled data without predefined outcomes. It is essential for analysing large amounts of unstructured and unlabelled data. *Clustering* is a common type of unsupervised learning that groups similar data to uncover insights. It is like classification, but the data isn't labelled. For example, if one is asked to sort gemstones by type without providing specific labels, one would use clustering techniques to group them based on their similarities. Even if one has never encountered a gemstone before, one could likely distinguish between rubies and emeralds simply because they have distinct colors: one is red and the other is green. Similarly, unsupervised learning is used to identify trends or organize content without direct guidance, mimicking human pattern recognition.

Semi-supervised learning can be considered the "happy medium" between supervised and unsupervised learning and is particularly useful for datasets that contain both labelled and unlabelled data (for example, where all feature data is available, but not all features have associated targets). This situation typically arises when image labelling is time-consuming or difficult due to cost. In such cases, semi-supervised learning is frequently applied in medical imaging, where a clinician labels a small sample of images to train a model. This model is then

used to classify the remaining unlabelled images in the dataset. The newly labelled dataset can then be used to train a more effective model, which is expected to perform better than unsupervised models.

Reinforcement Learning (RL) is a machine learning method where a software agent learns to make decisions by trial and error, aiming to maximize rewards. Unlike other learning models, RL does not rely on pre-existing training data. Instead, the agent improves its performance through experience gained from its actions over time. This approach is particularly valuable in robotics and gaming, where actions have direct consequences, such as scoring in video games. In RL, the computer determines which actions lead to the highest rewards through repeated trials. For example, teaching a dog a trick involves rewarding or correcting its behaviour rather than giving instructions. Similarly, RL begins with imprecise actions but gradually becomes more proficient. In a practical RL scenario, if a system misidentifies an apple as an orange, feedback helps it learn the correct identification for future instances.

2.1.2. Machine Learning Algorithms

Examining various ML algorithms reveals that each offers a unique approach to data analysis and interpretation.

Decision tree

In ML models, decision trees use tree-like graphs to make decisions. Each branch represents attributes of the observed data, and the leaves signify conclusions. These branches simplify the complex decision process by breaking down conditions into hierarchical paths, much like how we make everyday decisions, such as choosing activities based on the weather.

Random forest

Developed by Leo Breiman and Adele Cutler, the random forest (RF) algorithm combines multiple decision trees to generate unified results. Renowned for its simplicity and versatility, RF is effective for both classification and regression tasks.

Logistic regression

Logistic regression is a technique that mathematically establishes the relationship between two data variables. It predicts the outcome of a variable, providing binary results such as "yes" or "no."

Linear regression

Linear regression predicts a dependent variable based on an independent one by finding the smallest error in their linear relationship. It is like drawing a line through the data points to estimate the results. It reduces the difference between observed and predicted values.

K-means clustering

K-means clustering is an unsupervised learning algorithm that organizes unlabelled data into a predefined number of clusters, "K". It iteratively assigns data points to clusters based on their similarity, optimizing the distance between the points and the centroids (the mean value of a cluster's elements, representing its center of gravity, though not necessarily part of the dataset). This approach allows for the discovery of clusters in the data without prior training, enabling insightful classification.

2.1.3. The Most Widely Used Application Directions of ML

Here is a list of some of the most common uses of machine learning:

Pattern recognition

Pattern recognition uses ML to identify patterns automatically. It observes different types of data, including text, image and sound data. These systems quickly and accurately detect familiar patterns, simplifying data analysis. Common applications of pattern recognition are image recognition, fingerprint scanning and seismic activity analysis.

Regression analysis

Regression models predict a continuous outcome variable (y) based on one or more predictor variables (x). Regression analysis is a fundamental technique in ML.

Automation

ML recognizes patterns in the tested system and autonomously generates test cases. This decreases dependency on manual creation, improving productivity and accelerating processes.

Data Extraction

Data extraction involves the following key steps: detecting patterns, predicting results, and obtaining meaningful insights from extensive datasets.

The process of model building in machine learning generally involves the following steps:

Step 0. *Understand the problem and objectives.*

Step 1. *Data collection*: gathering data relevant to the specific problem or task that the system is required to learn.

Sources of datasets:

- Open-source datasets. Large technology companies and even governments provide free data for modelling.

- Web scraping. Collecting data from websites is often done manually. Popular "scrapers" are Scrapy and ProWebScraper.

- Internal data. With customized data, one can build highly specific models. Sometimes, it is the only way to achieve optimal results, as public data often has its limitations.

Step 2. *Data preparation and preprocessing:* cleaning and preparing the data for use in the training process. This may include normalizing the data, removing missing values or handling other anomalies.

The steps in data preprocessing are (Figure 5):

I. *Data cleaning.* Machine learning engineers correct errors and handle missing data through various data cleaning techniques, such as imputation, elimination, and transformation. Data cleaning addresses two main issues: missing data and noisy data. For missing data, values are often filled in through imputation. For noisy data, the problematic entries are typically removed. Noisy data can be managed using techniques like binning, regression, and clustering.

II. *Data transformation* is the conversion of raw data into a structured and usable format. These methods help in preparing data for analysis and improving the performance of machine learning models. These are the main ways of transforming data:

- Data normalization. Adjusts data to fit within a specific range, making sure all values are on the same scale. Think of normalization as adjusting the volume on a music player. It is a method to ensure that all data values are on the same scale by placing them within a specific range, like setting the volume knob between 0 and 100.

- Attribute selection. It chooses the most relevant features from the data to simplify and improve the model. Imagine having a lot of tools, and one wants to choose only the most useful ones for a particular task. Attribute selection is like picking the best tools from the toolbox and creating new, more focused tools to make work easier.

- Discretization. Rounds or bins continuous data into more manageable categories. If one has a bunch of numbers and wants to simplify things, discretization is like rounding those numbers to make them more manageable.

- Concept Hierarchy Generation. It might sound intimidating, but it simply means converting detailed information into broader, more general categories.

III. *Data reduction* means reducing the data set while retaining important information.

- Feature selection. This involves choosing a subset of relevant features from the dataset, eliminating unnecessary or duplicate ones. Techniques such as correlation analysis, mutual information and principal component analysis (PCA) are commonly used.

- Feature extraction. Transforming data into a smaller dimensional space while retaining the important information. This is beneficial for large and complex datasets. Techniques include PCA, linear discriminant analysis (LDA) and non-negative matrix factorization (NMF).

- Sampling. Selecting a subset of data points to reducing the size of the data set while retaining essential information. Techniques such as random sampling, stratified sampling and systematic sampling are used.

- Clustering. Grouping similar data points into clusters, replacing them with a representative centroid. Methods include k-means, hierarchical clustering and density-based clustering.

- Compression. Reducing the size of the data set for storage and transmission without losing vital information. Techniques such as wavelet compression, JPEG compression and gzip compression are commonly used.

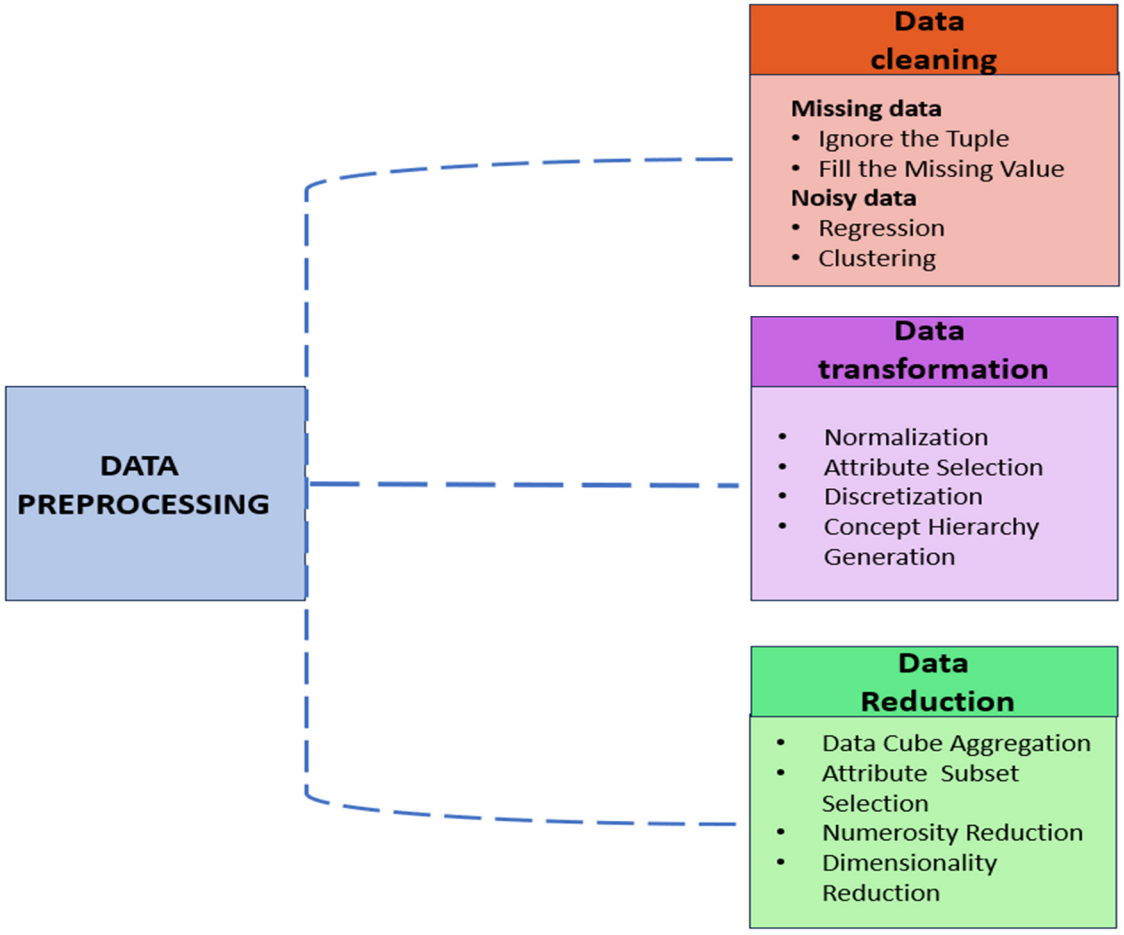

Figure 5. Data processing steps

Step 3. *Model selection:* choosing a suitable ML algorithm or model for the given task. There are a variety of models such as decision trees, support vector machines, neural networks, etc.

Step 4. *Train the model:* Feed the model with training data and adjust its parameters to improve performance. The goal is to make the model able to make correct predictions or decision making on new data.

Step 5. *Performance Evaluation:* Test the model on data that was not used in the training process and evaluate the accuracy, recall, or other relevant metrics to measure model performance.

Step 6. *Production Deployment:* If the model meets the desired performance, it can be deployed into a production system to make decisions or perform specific tasks. (Figure 6)

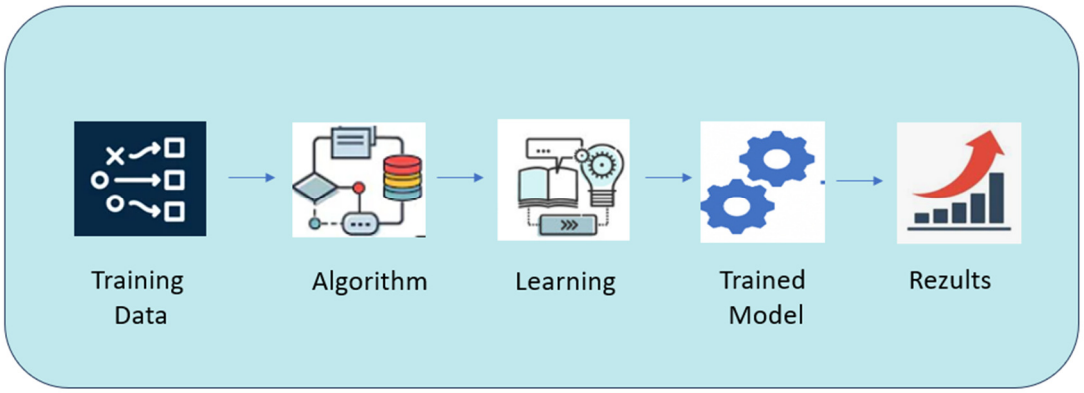

Figure 6. Machine learning process

2.2 Deep Learning

The availability of labelled datasets, faster algorithms, and more powerful hardware have enabled the rapid application of Deep Learning (DL) (13). DL has facilitated the use of multiple features and the application of data with various levels of hierarchy and abstraction, leading to enhanced universal approximation capabilities. Convolutional neural networks (CNNs) have been considered as the state-of-the-art algorithms of DL methods in the field of radiology, for computerized image recognition tasks such as segmentation (a technique that divides a digital image into groups of pixels - image segments - to inform object detection and other related tasks; by dividing an image's complex visual data into shape-specific segments, image segmentation enables faster and more advanced image processing) (15), detection (16,17), and image classification ("few-shot image classification" a computerized image recognition task that involves training machine learning models to classify images into predefined categories using only a few labelled examples from each category (typically < 6 examples) (18). There are four key ideas underlying CNNs: local connections, shared weights, pooling, and the use of multiple layers, which results in improving the accuracy and efficiency of the whole system (14). The relationship between IA, ML, DL, and CNNs is shown in **Figure 7**. CNNs consist of a stack containing an input layer, an output layer, and several hidden layers, which consist of convolutional layers, clustering layers, and fully connected layers (19) (Figure 8). Fully connected convolutional and pooling layers, which are applied repeatedly, are used to make

classifications or predictions (20). The combinations of layers are diverse, and some deep neural network architectures have been successfully used in the field of image analysis, such as GoogleNet (21), AlexNet (22), VGGNet (23), ResNet (24).

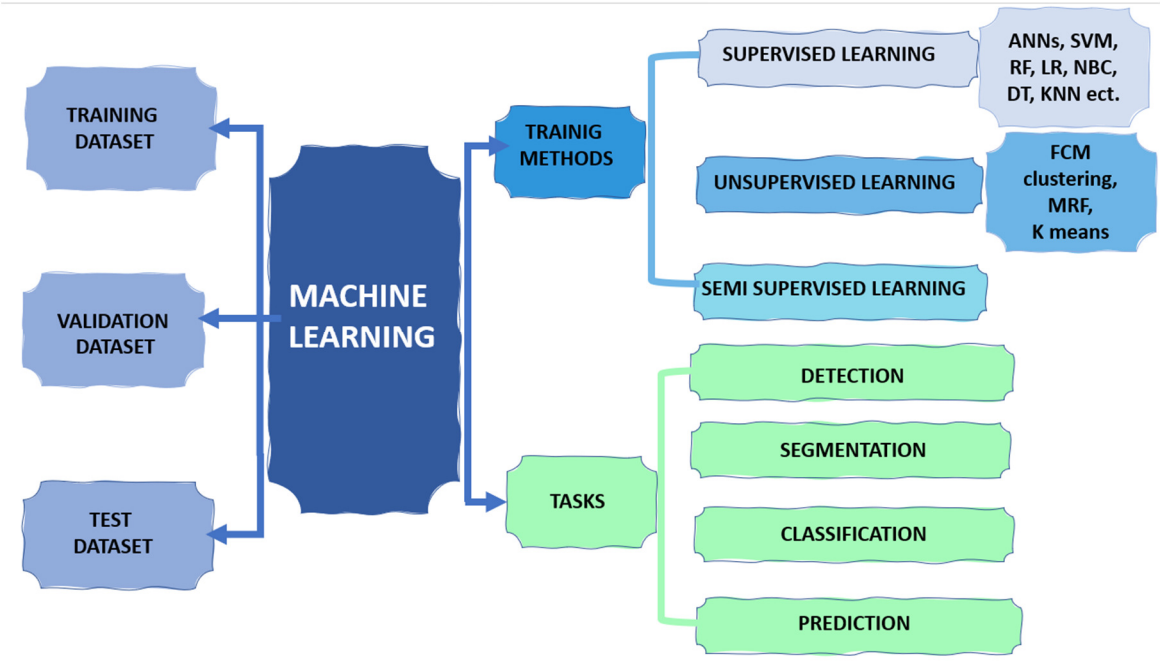

Figure 7. Classification and tasks of machine learning computer vision systems. ANN, artificial neural networks; DT, decision tree; FCM clustering, fuzzy C mean clustering; KNN, K nearest neighbour; RL, logistic regression; MRF, Markov random fields; RF, random forest; SVM, support vector machine

2.3. Transfer Learning

Transfer Learning (TL) strategies have recently been used in the medical world to avoid "overfitting" problems caused by lack of data. In the TL method, knowledge can be shared and transferred between different tasks (25). The work process involves two steps: pretraining on a large dataset (ImageNet, for example) and fine-tuning on the target dataset (a limited volume of ultrasonographic images). In other words, by fine-tuning the DL constructs, the knowledge obtained from one dataset can be transferred to another dataset obtained from another center.

2.4. Radiomics

Radiomics involves quantitatively mapping and analysing large, complex medical image data to extract information linked to predictive targets. (26). Radiomic features such as intensity, shape or texture reflect the underlying pathophysiology and provide information on tumour phenotype and microenvironment (27). For strong evidence-based decision support in prediction, diagnosis, prognosis, or monitoring, these features can be utilized either on their own or combined with other relevant data, such as clinical data, laboratory tests, or genomic information. (26). Radiomic features can be evaluated semantically by experienced

radiologists, computed mathematically by computer algorithms to describe the size, shape, and textures of regions of interest (ROIs), or generated by DL algorithms. (27). The computed features are further analyzed, typically with traditional machine learning methods, to develop predictive models (28). Research has shown that radiomic analysis can enhance diagnostic, prognostic, and predictive capabilities (29).

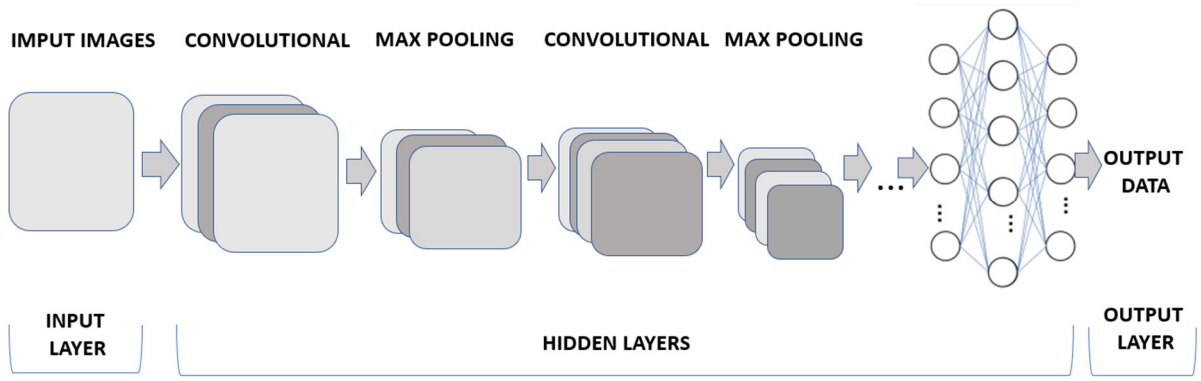

Figure 8. The architecture of convolutional neural networks (CNNs) that consist of an input layer, multiple hidden states and an output layer. The convolutional and unification layers can be laid alternately until the network is deep enough to recognize the optimal features of the images which are enough to perform classification

3. Artificial intelligence in imaging

The field of medical imaging has been pivotal in advancing medicine into the digital era and now stands poised to lead in exploring AI applications in healthcare. The vast number of radiology reports and billions of digital images exemplify "big data" and provide a rich foundation for AI research. Three converging technical advances have facilitated medical applications of machine learning:

- the global rise of ''big data'', i.e. the building and analysis of very large databases
- the dramatic increase in computing power of processors
- the design of new deep learning algorithms.

Healthcare is currently facing a massive increase in the volume, complexity and heterogeneity of raw data. The efficient and medically oriented analysis of big data is a major issue in public health.

AI offers three promising insights in this area:

- risk prediction through correlation analysis
- genomic analysis and phenotype-genotype association studies
- automation of medical image analysis.

In this chapter, we focused on the third topic and investigated the following question: ''Can deep learning algorithms for image recognition improve medical visual diagnosis?"

3.1 Artificial Intelligence in Ultrasound-based Elastography

The fundamental question is whether AI applications in imaging can add diagnostic value. The main tasks for automated analysis of ultrasound-based elastography patterns using AI involve - (a) *classification*: predicting the character of changes in the ultrasonographic image (e.g., classifying breast tumours into benign or malignant) (30); (b) *detection*: to predict the location of focal lesions, which is a preliminary step for the operator to characterize the lesions; (c) *segmentation*: to distinguish suspicious lesions from surrounding normal tissues, i.e. to acquire ROIs; and (d): *prediction*: to predict the stage of diseases or events that may occur.

Unlike conventional ML methods, the distinctive feature of DL is that the feature layers are not manually designed by experts but are instead automatically learned from the data through a general-purpose learning approach (14). This enables image classification using the image-to-classification method (30). In traditional ML methods, success relies heavily on accurate segmentation and the choice of features proposed by experts. These limitations can be addressed by DL approaches, as such algorithms can autonomously identify the regions in the image most closely associated with the outcome through self-learning (27). A comparison between traditional ML methods and DL models is illustrated in Figure 9.

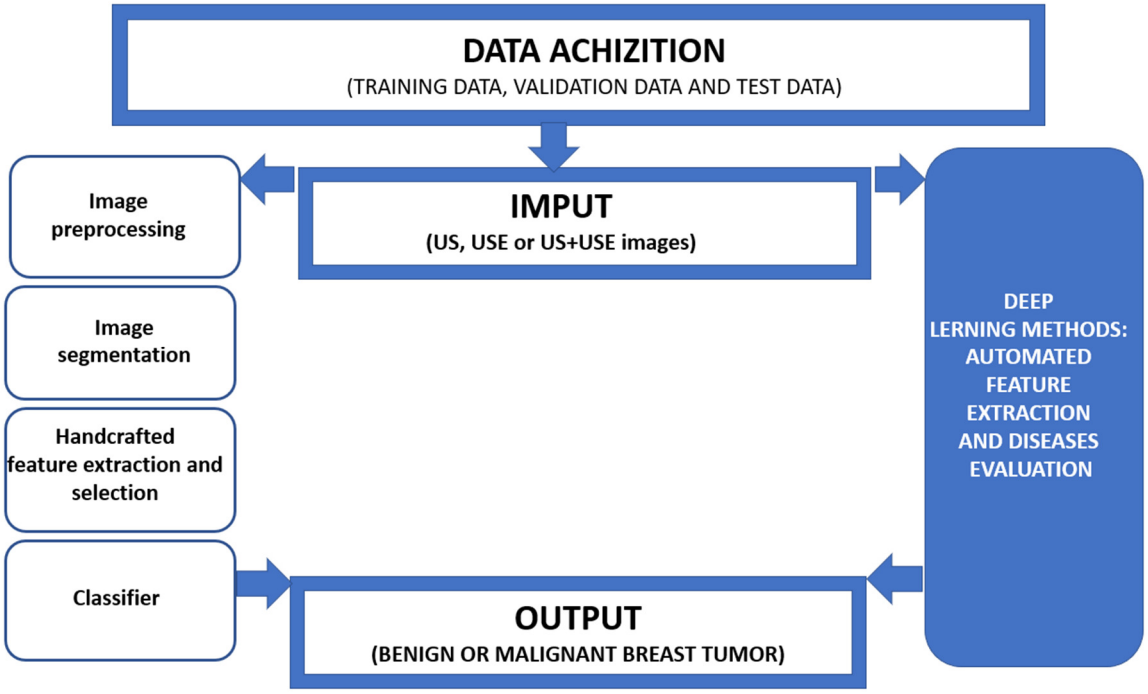

Figure 9. Conventional machine learning models of ultrasound-based elastography versus deep learning models of ultrasound-based elastography. Conventional machine learning models for ultrasound-based elastography depend on carefully human-selected features, whereas deep learning models allow learning by automatic feature extraction and assessment of pathological conditions

3.1.1. Assessment of Liver Pathology

Many etiologies of chronic liver diseases follow a common pathway to liver fibrosis, cirrhosis and hepatocellular carcinoma (HCC). Hepatocellular carcinoma, the 6th most common form of cancer worldwide and the third leading cause of death (31). Liver biopsy has traditionally served as the golden standard for staging hepatic fibrosis in chronic liver disease and for diagnosing HCC. However, it is invasive and has some limitations such as sampling error and post-procedural complications. Compared with standard ultrasonography, elastography has become a popular non-invasive technique that provides additional information on liver tissue stiffness. Artificial intelligence-based elastography models may help improve diagnostic accuracy while reducing the need for unnecessary biopsies for either staging liver fibrosis in these patients or differentiating focal liver lesions (FLL) from benign to malignant.

3.1.1.1. Staging of Liver Fibrosis

Liver fibrosis is a critical factor in the progression of chronic liver disease. Accurate evaluation of its extent and progression is crucial for managing and predicting patient outcomes. Elastography, which measures liver stiffness, is widely regarded as the primary non-invasive method for this assessment. AI-based elastography models are being developed to minimize variability in liver stiffness measurements and enhance the diagnostic accuracy of liver fibrosis evaluations.

Currently, it is anticipated that AI using DL methods will enable direct handling of input images and reveal information that human experts may not recognize. The superior diagnostic performance of deep neural networks (DNNs) compared to conventional machine learning classifiers for liver fibrosis staging was demonstrated in Brattain's study (32). To achieve more standardized measurements of shear wave elastography (SWE) and detect significant fibrosis in patients with non-alcoholic fatty liver disease, an automated framework called "SWE-Assist" was developed. This model can automatically verify the quality of SWE images, select a region of interest (ROI), and classify the ROI using classifiers such as random forests (RF), support vector machines (SVM), and CNNs. CNNs have provided the most significant improvement in classification, with an AUROC of 0.89 in a large dataset of 3,392 SWE images. A new method called “DL radiomics of elastography” (DLRE) was proposed by Wang (33) with the expectation of extracting additional radiomic features. In a study involving 398 patients with 1,990 images from 12 hospitals, DLRE achieved AUROC scores of 0.97 for F4, 0.98 for ≥ F3, and 0.85 for ≥ F2, which were significantly better than those obtained with LSM and biomarkers (33). The model also demonstrated improved performance with an increasing volume of acquired images. Since Wang's DLRE model showed limited accuracy in evaluating ≥ F2 fibrosis, Lu (34) developed a new model called DLRE 2.0, based on the previous model and utilizing TL for more precise assessment of liver fibrosis levels ≥ F2 (34).

3.1.1.2. Classification and Assessment of Focal Liver Lesions

Early detection and precise diagnosis of HCC are essential for choosing the right treatment and assessing patient prognosis, making the differentiation of focal liver lesions (FLL) a critical task. Because structural changes can be reflected by changes in tissue stiffness, ultrasound-based elastography, especially SWE, has been widely used to differentiate benign from malignant FLL (35).

Radiomic approaches have been suggested for various diagnostic applications, focusing on extracting features from ultrasonographic images and combining them with expert-designed SWE parameters or serologic data (36).

Specifically, to classify FLL, Wang (37) established two radiomic models: the ultrasonic score (based on radiomic features alone) and the combined score (based on radiomic features and quantitative features of SWE measurements). With 1,044 features extracted from the ultrasonic, they found that the combined score had the best performance, yielding an AUROC of 0.92.

3.1.2. Evaluarea tumorilor mamare

Breast cancer is the most frequently diagnosed cancer among women (38). Precise evaluation of breast tumours—including tasks like segmentation, detection, distinguishing between benign and malignant masses, predicting axillary lymph node (ALL) status, and assessing treatment response—is essential for personalized treatment and better prognosis. AI techniques applied to ultrasound-based elastography are anticipated to offer more objective and consistent assessments of breast masses. Accurate delineation of these masses in ultrasound images is crucial for proper image interpretation. However, manual segmentation is labour-intensive and time-consuming (39). Additionally, artifacts, uneven intensity, and blurred boundaries in elastography images make automated segmentation challenging.

Early detection and treatment of breast cancer can significantly decrease mortality. Therefore, distinguishing between benign and malignant breast masses holds significant value. Although the American College of Radiology Breast Imaging Data System (ACR BI-RADS) can provide a standardized and systematic interpretation of breast ultrasound, the problems of inter- and intra-observer variability can be effectively addressed by AI solutions (41). The most used machine learning algorithms are artificial neural networks and support vector machines. Fusion of B-mode ultrasound and elastography ultrasound features generates better results than unimodal imaging (42,43). Additionally, research has shown that utilizing elasticity features along the edges surrounding the lesion is valuable for breast mass classification. (44).

However, extracting human-created features from elastography images is challenging because they often contain irrelevant data (45). Moreover, the performance of classification is greatly affected by the choice of specific features. Recently, DL algorithms, especially CNNs, have made significant strides in developing AI-based elastography models for classifying

breast tumour formations. *Zhang et al.* (46) utilized CNNs to extract 768 radiomic features from segmented B-mode and SWE ultrasonographic images. These features were used to develop radiomic scores, which were found to be superior to expert assessments using BI-RADS and quantitative SWE features in distinguishing benign from malignant breast masses.

Accurate preoperative assessment of axillary lymph node (ALN) status in breast tumour patients is crucial for surgical decisions and prognosis (47). Various AI models have been proposed to analyse ALN status using ultrasound images of ALN or the mammary gland (48). *Zheng et al.* (49), developed a deep learning-based radiomics model that can differentiate metastatic axillary lymph nodes with an AUROC of 0.905. Understanding how a tumour responds to treatment can be valuable for selecting subsequent therapies. Additionally, evaluating pathological complete response in breast cancer is crucial, as it is associated with long-term survival rates. Fernandes found that the strain ratio—a semi-quantitative measure calculated by comparing the strain in a normal reference region to the strain in the region of interest—could predict the response to neoadjuvant chemotherapy in locally advanced breast cancer. Notably, significant changes in tumor stiffness were observed as early as 2 weeks into the treatment.

3.1.3. Evaluation of Thyroid Nodules

Thyroid nodules are very common findings during ultrasonographic examination, and the incidence of thyroid cancer is increasing worldwide year by year (51). However, only 5%-15% of thyroid nodules are malignant, and most of those selected for fine-needle aspiration biopsy are benign (52). Differentiating clinically significant malignant nodules from the many benign ones remains a major clinical challenge. Effective differentiation would help identify patients who need surgical treatment, reduce medical costs, and lessen patient suffering. Additionally, lymph node metastases (LNM) are linked to local recurrence, the occurrence of distant metastases, and affect the staging of thyroid cancer, which in turn influences surgical strategies. Therefore, a reliable and non-invasive diagnostic method is needed to evaluate thyroid nodules and predict lymph node metastases.

3.1.3.1. Segmentation and Delineation of Thyroid Nodules

Segmentation is crucial in AI-based elastography models, as accurately delineated features are key to diagnosing malignant thyroid nodules. However, ultrasound images often suffer from low quality due to noise, making automatic nodule segmentation a challenging task. *Huang et al.* introduced a novel method for segmenting thyroid nodules that uses an adaptive fast generalized clustering algorithm, incorporating both grey level and spatial position information from the original image (53). The proposed method achieved an accuracy of 0.9981 with Gaussian noise at 0.03 and 0.9986 with Gaussian noise at 0.05. This demonstrates its strong ability to suppress noise and its effectiveness in producing more accurate results when clustering images with high noise.

3.1.3.2. Classification of Thyroid Nodules

Although elasticity scoring has been introduced in elastography, strain elastography (SE) remains a quantitative yet somewhat subjective imaging method. *Ding et al.* (54) proposed a quantitative "hard area ratio" index by converting the original colour elastograms of the thyroid from the red-green-blue colour space to the colour-saturation-value hue space. The SVM classifier achieved an accuracy of 93.6% when both the hard-area ratio and textural features were utilized. Additionally, two studies employed logistic regression analysis to examine which sonographic features were linked to thyroid nodule malignancy, and they developed formulas to predict whether thyroid nodules were malignant or benign (55,56).

It remains uncertain whether ML-based diagnostic models can offer a more efficient and accurate diagnosis compared to experts in thyroid nodule classification. In a large study involving 2,064 thyroid nodules, *Zhang et al.* (57) compared the diagnostic performance of nine ML classifiers, trained on 11 ultrasonographic B-mode (USBM) features and one SE feature, with that of radiology experts. The RF classifier achieved the highest AUROC of 0.938, surpassing expert diagnosis based on USBM alone (AUROC = 0.924 vs. 0.834) and on both USBM and SE (AUROC = 0.938 vs. 0.843).

Both ML-based visual and radiomic methods are commonly used for diagnosing thyroid nodules. Recently, *Zhao et al.* (58) found that the ML-assisted visual ultrasound (US) approach outperformed the radiomic approach and the American College of Radiology Thyroid Imaging Reporting and Data System (ACR TIRADS) in diagnostic ability (AUROC: 0.900 vs. 0.789 vs. 0.689 for the validation dataset; 0.917 vs. 0.770 vs. 0.681 for the test dataset). Moreover, using the ML-assisted visual US combined with SE reduced the rate of unnecessary fine-needle aspiration biopsies from 30.0% to 4.5% in the validation dataset and from 37.7% to 4.7% in the test dataset. Because DL is data-intensive and the absence of standardized images can lead to overfitting, TL strategies have been applied in some studies for thyroid nodule classification (59,60). *Qin et al.* (59) proposed transferring feature parameters learned from VGG16, pretrained on ImageNet, to ultrasonographic images. By using a combination of USBM and SE features, a CNNs model was built. This AI-based method achieved an accuracy of 0.947, outperforming other methods that relied on a single data source. *Pereira et al.* (60) compared the performance of conventional ML approaches based on feature extraction, fully trained CNNs, and TL-based pretrained CNNs for detecting malignant thyroid nodules. The results showed that the pretrained network achieved the best classification performance, with an accuracy of 0.83, which was superior to that of the fully trained CNNs. This may be due to the relatively limited sample size used to train the fully trained network.

3.1.4. Evaluation of Cervical Lymph Nodes

Although papillary thyroid cancer (PTC) is an indolent cancer, 20 to 90% of patients with PTC are diagnosed with cervical lymph node metastases (CLNM) (61), which are correlated with recurrence and decreased survival. Accurate estimation of CLNM in PTC

patients is clinically important. *Liu et al.* (62) constructed a radiomics-based model that extracted 684 radiomic features from both USBM and SE images to estimate CLNM in patients with PTC, obtaining an AUROC of 0.90, which was better than using features extracted from USBM or SE images separately. However, it used only radiomic features without considering other clinical information. *Jiang's* team (63) developed a radiomic nomogram by incorporating the radiomic features of SE as well as clinico-pathologic risk factors to predict CLNM in patients with PTC, which showed good diagnostic performance in the training set (AUROC of 0.851) and the validation set (AUROC of 0.832).

3.2 Multiparametric Ultrasonography (MPUS)

The diagnostic abilities will be greatly improved with the help of AI methods applied on elastography images, especially multiparametric ones, which contain several ultrasound imaging methods (standard ultrasound, elastography and contrast-enhanced ultrasonography-CEUS) and other medical imaging techniques (MRI and Computed Tomography). Although all available studies showed that models based on multiparametric imaging outperformed those based on a single modality, the efficiency in model development depends on the availability of datasets. On the one hand, an additional imaging modality may help provide more efficient and comprehensive information.

If multimodality imaging data are available and acquired in a standardized fashion, it is expected that elastography imaging in combination with standard ultrasound or other modalities will help improve diagnostic accuracy. On the other hand, the model based on unimodal images gave acceptable performance and can be more easily obtained. AI models based on these are also easier to use and generalize in the clinic, especially in primary care hospitals. Thus, higher accuracy should not be the only factor considered when selecting a unimodal or multimodal prediction model; the applicability of the model in different institutions should also be considered.

Overall, available studies suggest that AI is a powerful tool for assisting with various clinical tasks across different pathologies with consistent results. While diagnostic performance can vary depending on the disease, AI methods applied in elastography have shown exceptional capability in differentiating between malignant and benign breast masses, identifying focal liver lesions and thyroid nodules, staging liver fibrosis, and predicting lymph node metastases. The performance of many AI applications has been shown to be comparable to or even exceed that of experts, partly due to the growing availability of high-quality datasets and optimized AI methods. However, further validation with larger datasets is necessary to confirm these results. Additionally, non-uniform acquisition methods and variability in ultrasound data present significant challenges that affect the comparison and generalizability of different methods across various tasks. Developing standard databases for different ultrasound applications is a key future direction for advancing these studies.

3.3. Advantages and Limitations of Artificial Intelligence Technologies in Elastography

Early ML-based elastography models primarily focused on extracting discriminative features from elastography images or from a combination of standard ultrasound and elastography images, often using texture features and elasticity indices. These features were then input into classical ML classifiers, such as SVM, RF, or artificial neural networks, to improve diagnostic accuracy and efficiency. However, with DL models, such as CNNs and those based on various training strategies like GoogleNet, AlexNet, VGG, ResNet, and DenseNet, there is no need for manual feature computation and image segmentation. These DL models can automatically learn hierarchical features, addressing some of the limitations of traditional ML processes. Additionally, numerous significant radiomics studies have been conducted. Radiomics enables the quantitative extraction of high-throughput features from medical images that are not immediately apparent. These features can then be used to build classification or prediction models using ML methods, either based solely on radiomic features or in combination with clinical disease-related information.

However, there are still challenges in generalizing AI methods applied to ultrasound-based elastography in clinical practice. One of the main challenges is the lack of large, high-quality datasets. Since deep learning algorithms are "data hungry," large-scale multicenter studies with well-annotated datasets are necessary to better assess the diagnostic value of AI in elastography imaging. A common approach to addressing this issue is to increase the available data through artificial augmentation, which includes random transformations such as flipping, rotating, translating, and zooming (9). Another common strategy is TL, which can transfer learned parameters from one dataset to another target dataset. Recent advances in novel DL architectures, including unsupervised learning, Generative Adversarial Networks (GANs) (64), for example, and Federated Learning (65), have shown great promise to circumvent the data sparsity obstacle. GANs, which consist of a generator and a classifier, can help generate synthetic medical images to train deeper architectures. GANs have been shown to be very effective at synthesizing medical images between MRI and CT images (66, 67).

Federated Learning allows multiple centers to collaboratively build an ML model based on datasets that are distributed across multiple devices, while preserving the confidentiality of private data. This can be useful to help address privacy and ethical concerns when patient data is shared between different centers. Also worth mentioning are Graph Neural Networks (GNNs), which focus on learning data represented as graphs (68). GNNs have been applied to several computational tasks, including image classification (69) and image segmentation (70).

Another challenge is the lack of transparency in interpreting deep learning (DL) approaches, often referred to as the "black box" problem. This means it is difficult for experts to explain the results produced by DL models. Without a clear understanding of how input data relates to output, identifying the features used for interpretation can be nearly impossible, which may lead to reluctance among experts to accept conclusions drawn from such AI models. The development of "heatmaps" (AI-generated "attention heatmaps" that

highlight the elements of the model design most likely to be noticed) can help address this issue.

In addition to the previously mentioned impediments, ultrasound-based elastography presents unique difficulties. Firstly, irrelevant patterns such as noise, artifacts, and regions lacking elastography information can complicate both manual and automated feature extraction. Consequently, there is a need for further improvement in elastography image quality. Secondly, because ultrasound is frequently used as a first-line imaging modality, there is often an imbalance with an overabundance of normal images, which can diminish the diagnostic accuracy of AI models. Additionally, the generalizability of developed AI models presents another challenge. Most datasets are generated by a single type of device and from a single collection center, and current AI research often focuses on specific tasks within a broader system, such as segmentation or classification. All these factors contribute to limitations in the generalizability of AI models.

It is unlikely that artificial intelligence will replace experts in the near or distant future due to the complexity involved in creating and training an AI model. What is imperative is for experts to understand the fundamental principles of AI and apply them effectively to the interpretation and analysis of medical images (which is, in fact, the basis of this chapter). While AI can provide a second opinion based on elastography models using ML or DL techniques, the final diagnostic decision should always be made by the expert.

In 2016, Geoffrey Hinton, often considered a pioneer in artificial intelligence, stated: “We should stop training radiologists now. In 5 years, deep learning will probably be better than radiologists.” However, a more plausible scenario might be: “AI will not replace doctors, but doctors who use AI will replace those who do not.” AI has the potential to reduce the workload for doctors and decrease the risk of burnout. The future will reveal the exact role of AI in medical practice (and in elastography), in a field where time seems to be accelerating.

References

1. AI-Enabled Medical Imaging Solutions Market - A Global and Regional Analysis: Focus on Modality, Product, Deployment Model, Workflow, Therapeutic Application, and Country - Analysis and Forecast, 2022-2032**.** BIS research. Report. https://bisresearch.com/requestsample**.**
2. Fujioka T, Mori M, Kubota K, Kikuchi Y, Katsuta L, Kasahara M, et al. Simultaneous comparison between strain and shear wave elastography of breast masses for the differentiation of benign and malignant lesions by qualitative and quantitative assessments. Breast Cancer. 2019; 26:792–8. doi: 10.1007/s12282-019- 00985-0
3. Cosgrove D, Barr R, Bojunga J, Cantisani V, Chammas MC, Dighe M, et al. WFUMB guidelines and recommendations on the clinical use of ultrasound elastography: part 4. Thyroid Ultrasound Med Biol. 2017; 43:4–26. doi: 10.1016/ j.ultrasmedbio.2016.06.022

4. Barr RG, Cosgrove D, Brock M, Cantisani V, Correas JM, Postema AW, et al. WFUMB guidelines and recommendations on the clinical use of ultrasound elastography: part 5. Prostate. Ultrasound Med Biol (2017) 43:27–48. doi: 10.1016/ j.ultrasmedbio.2016.06.020
5. Gao J, Jiang Q, Zhou B, Chen D. Convolutional neural networks for computeraided detection or diagnosis in medical image analysis: an overview. Math Biosci Eng. 2019; 16:6536–61. doi: 10.3934/mbe.201932
6. Milas M, Mandel SJ, Langer JE. Elastography: applications and limitations of a new technology. Adv Thyroid Parathyr Ultrasound. 2017: 67–73. doi: 10.1007/978-3- 319-44100-9_8
7. Chartrand G, Cheng PM, Vorontsov E, Drozdzal M, Turcotte S, Pal CJ, et al. Deep learning: a primer for radiologists. Radiographics. 2017; 37:2113–31. doi: 10.1148/rg.2017170077
8. Ozturk A, Grajo JR, Dhyani M, Anthony BW. Principles of ultrasound and elastography. Physiol Behav. 2016; 176:139–48. doi: 10.1007/s00261-018-1475-6
9. Choy G, Khalilzadeh O, Michalski M, Do S, Samir AE, Pianykh OS, et al. Current applications and future impact of machine learning in radiology. Radiology. 2018; 288:318–28. doi: 10.1148/radiol.2018171820.
10. Wang S, Summers RM. Machine learning and radiology. Med Image Anal. 2012; 16:933–51. doi: 10.1016/j.media.2012.02.005
11. Brattain LJ, Telfer BA, Dhyani M, Grajo JR, Samir AE. Machine learning for medical ultrasound: status, methods, and future opportunities. Abdom Radiol. 2018; 43:786–99. doi: 10.1007/s00261-018-1517-0
12. Lecun Y, Bengio Y, Hinton G. Deep learning. Nature. 2015; 521:436–44. doi: 10.1038/nature14539
13. Abdelhafiz D, Bi J, Ammar R, Yang C, Nabavi S. Convolutional neural network for automated mass segmentation in mammography. BMC Bioinf. 2020; 21:1–19. doi: 10.1186/s12859-020-3521-y
14. Kooi T, Litjens G, van Ginneken B, Gubern-Mérida A, Sánchez CI, Mann R, et al. Large Scale deep learning for computer aided detection of mammographic lesions. Med Image Anal. 2017; 35:303–12. doi: 10.1016/j.media.2016.07.007
15. Khan AI, Shah JL, Bhat M. CoroNet: a deep neural network for detection and diagnosis of covid-19 from chest X-ray images. Comput Methods Programs BioMed. 2020; 196:105581. doi: 10.1016/j.cmpb.2020.105581
16. Choi B-K, Madusanka N, Choi H-K, So J-H, Kim C-H, Park H-G, et al. Convolutional neural network-based MR image analysis for alzheimer's disease classification. Curr Med Imaging Rev (2019) 16:27–35. doi: 10.2174/ 1573405615666191021123854
17. Yasaka K, Akai H, Kunimatsu A, Kiryu S, Abe O. Deep learning with convolutional neural network in radiology. Jpn J Radiol (2018) 36:257–72. doi: 10.1007/s11604-018-0726-3
18. Erickson BJ, Korfiatis P, Kline TL, Akkus Z, Philbrick K, Weston AD. Deep learning in radiology: does one size fit all? J Am Coll Radiol (2018) 15:521–6. doi: 10.1016/j.jacr.2017.12.027
19. Szegedy C, Liu W, Jia Y, Sermanet P, Reed S, Anguelov D, et al. Going deeper with convolutions, in: 2015 IEEE Conference on Computer Vision and Pattern Recognition (CVPR). 2015. Boston, MA, USA: IEEE p. 1–9. doi: 10.1109/ CVPR.2015.7298594
20. Krizhevsky BA, Sutskever I, Hinton GE. ImageNet classification with deep convolutional neural networks. Commun ACM (2017) 60:84–90. doi: 10.1145/3065386

21. Simonyan K, Zisserman A. Very deep convolutional networks for large-scale image recognition. Computer Science (2014). doi: 10.48550/arXiv.1409.1556
22. He K, Zhang X, Ren S, Sun J. Deep residual learning for image recognition. 2016 IEEE Conference on Computer Vision and Pattern Recognition (CVPR). 2016; Las Vegas, NV, USA: IEEE. p. 770–8. doi: 10.1109/CVPR.2016.90
23. Bengio Y, Courville A, Vincent P. Representation learning: a review and new perspectives. IEEE Trans Pattern Anal Mach Intell. 2013; 35:1798–828. doi: 10.1109/TPAMI.2013.50
24. Lambin P, Leijenaar RTH, Deist TM, Peerlings J, De Jong EEC, Van Timmeren J, et al. Radiomics: the bridge between medical imaging and personalized medicine. Nat Rev Clin Oncol. 2017; 14:749–62. doi: 10.1038/nrclinonc.2017.141
25. Gillies RJ, Schabath MB. Radiomics improves cancer screening and early detection. Cancer Epidemiol Biomarkers Prev (2020) 29:2556–67. doi: 10.1158/1055- 9965.EPI-20-0075
26. Bi Q, Goodman KE, Kaminsky J, Lessler J. What is machine learning? a primer for the epidemiologist. Am J Epidemiol (2019) 188:2222–39. doi: 10.1093/aje/kwz189
27. Gillies RJ, Kinahan PE, Hricak H. Radiomics: images are more than pictures, they are data. Radiology (2016) 278:563–77. doi: 10.1148/radiol.2015151169
28. Chartrand G, Cheng PM, Vorontsov E, Drozdzal M, Turcotte S, Pal CJ, et al. Deep learning: a primer for radiologists. Radiographics (2017) 37:2113–31. doi: 10.1148/rg.2017170077
29. Ferlay J, Colombet M, Soerjomataram I, Parkin DM, Pineros M, Znaor A, et al. Cancer statistics for the year 2020: An overview. Int J Cancer. 2021 Apr 5. doi: 10.1002/ijc.33588. Epub ahead of print.
30. Brattain LJ, Telfer BA, Dhyani M, Grajo JR, Samir AE. Objective liver fibrosis estimation from shear wave elastography. Annu Int Conf IEEE Eng Med Biol Soc. 2018:1–5. doi: 10.1109/EMBC.2018.8513011
31. Wang K, Lu X, Zhou H, Gao Y, Zheng J, Tong M, et al. Deep learning radiomics of shear wave elastography significantly improved diagnostic performance for assessing liver fibrosis in chronic hepatitis b: a prospective multicentre study. Gut (2019) 68:729– 41. doi: 10.1136/gutjnl-2018-316204
32. Lu X, Zhou H, Wang K, Jin J, Meng F, Mu X, et al. Comparing radiomics models with different inputs for accurate diagnosis of significant fibrosis in chronic liver disease. Eur Radiol. 2021; 31:8743–54. doi: 10.1007/s00330-021-07934-6
33. Tian WS, Lin MX, Zhou LY, Pan FS, Huang GL, Wang W, et al. Maximum value measured by 2-d shear wave elastography helps in differentiating malignancy from benign focal liver lesions. Ultrasound Med Biol. 2016; 42:2156–66. doi: 10.1016/j.ultrasmedbio.2016.05.002
34. Jin J, Yao Z, Zhang T, Zeng J, Wu L, Wu M, et al. Deep learning radiomics model accurately predicts hepatocellular carcinoma occurrence in chronic hepatitis b patients: a five-year follow-up. Am J Cancer Res. 2021; 11:576–89.
35. Wang W, Zhang JC, Tian WS, Chen LD, Zheng Q, Hu HT, et al. Shear wave elastography-based ultrasomics: differentiating malignant from benign focal liver lesions. Abdom Radiol. 2021; 46:237–48. doi: 10.1007/s00261-020-02614-3
36. Siegel RL, Miller KD, Fuchs HE, Jemal A. Cancer statistics, 2021. CA Cancer J Clin. 2021; 71:7–33. doi: 10.3322/caac.21654

37. Xu Y, Wang Y, Yuan J, Cheng Q, Wang X, Carson PL. Medical breast ultrasound image segmentation by machine learning. Ultrasonics. 2019; 91:1–9. doi: 10.1016/j.ultras.2018.07.006
38. Guo Y, Duan X, Wang C, Guo H. Segmentation and recognition of breast ultrasound images based on an expanded U-net. PloS One. 2021; 16:e0253202. doi: 10.1371/journal.pone.0253202
39. Nedevschi S, Pantilie C, Mariţa T, Dudea S. Statistical methods for automatic segmentation of elastographic images. 2008 4th International Conference on Intelligent Computer Communication and Processing. 2008; Cluj-Napoca: IEEE. p. 287–90. doi: 10.1109/ICCP.2008.4648388
40. Kim J, Kim HJ, Kim C, Kim WH. Artificial intelligence in breast ultrasonography. Ultrasonography. 2021; 40:183–90. doi: 10.14366/usg.20117.
41. Destrempes F, Trop I, Allard L, Chayer B, Garcia-Duitama J, El Khoury M, et al. Added value of quantitative ultrasound and machine learning in BI-RADS 4–5 assessment of solid breast lesions. Ultrasound Med Biol. 2020; 46:436–44. doi: 10.1016/j.ultrasmedbio.2019.10.02
42. Zhang Q, Xiao Y, Dai W, Suo J, Wang C, Shi J, et al. Deep learning-based classification of breast tumors with shear-wave elastography. Ultrasonics (2016) 72:150–7. doi: 10.1016/j.ultras.2016.08.004
43. Brattain LJ, Telfer BA, Dhyani M, Grajo JR, Samir AE. Machine learning for medical ultrasound: status, methods, and future opportunities. Abdom Radiol. 2018; 43:786–99. doi: 10.1007/s00261-018-1517-0
44. Zhang X, Liang M, Yang Z, Zheng C, Wu J, Ou B, et al. Deep learning-based radiomics of B-mode ultrasonography and shear-wave elastography: improved performance in breast mass classification. Front Oncol. 2020; 10:1621. doi: 10.3389/fonc.2020.01621
45. Ahmed M, Purushotham AD, Douek M. Novel techniques for sentinel lymph node biopsy in breast cancer: a systematic review. Lancet Oncol. 2014; 15:e351–62. doi: 10.1016/S1470-2045(13)70590-4
46. Zhang Q, Suo J, Chang W, Shi J, Chen M. Dual-modal computer-assisted evaluation of axillary lymph node metastasis in breast cancer patients on both real-time elastography and b-mode ultrasound. Eur J Radiol. 2017; 95:66–74. doi: 10.1016/j.ejrad.2017.07.027
47. Zheng X, Yao Z, Huang Y, Yu Y, Wang Y, Liu Y, et al. Deep learning radiomics can predict axillary lymph node status in early-stage breast cancer. Nat Commun. 2020 11:1–9. doi: 10.1038/s41467-020-15027-z
48. Fernandes J, Sannachi L, Tran WT, Koven A, Watkins E, Hadizad F, et al. Monitoring breast cancer response to neoadjuvant chemotherapy using ultrasound strain elastography. Transl Oncol. 2019; 12:1177–84. doi: 10.1016/j.tranon.2019.05.004
49. Cooper DS, Doherty GM, Haugen BR, Kloos RT, Lee SL, Mandel SJ, et al. Revised American thyroid association management guidelines for patients with thyroid nodules and differentiated thyroid cancer. Thyroid. 2009; 19:1167–214. doi: 10.1089/thy.2009.0110
50. Guille JT, Opoku-Boateng A, Thibeault SL, Chen H. Evaluation and management of the pediatric thyroid nodule. Oncologist. 2015; 20:19–27. doi:10.1634/theoncologist.2014-0115
51. Huang W. Segmentation and diagnosis of papillary thyroid carcinomas based on generalized clustering algorithm in ultrasound elastography. J Med Syst (2020) 44:13. doi: 10.1007/s10916-019-1462-7

52. Ding J, Cheng H, Ning C, Huang J, Zhang Y. Quantitative measurement for thyroid cancer characterization based on elastography. J Ultrasound Med (2011) 30:1259–66. doi: 10.7863/jum.2011.30.9.1259
53. Bhatia KSS, Lam ACL, Pang SWA, Wang D, Ahuja AT. Feasibility study of texture analysis using ultrasound shear wave elastography to predict malignancy in thyroid nodules. Ultrasound Med Biol. 2016; 42:1671–80. doi: 10.1016/j.ultrasmedbio.2016.01.013
54. Pang T, Huang L, Deng Y, Wang T, Chen S, Gong X, et al. Logistic regression analysis of conventional ultrasonography, strain elastosonography, and contrastenhanced ultrasound characteristics for the differentiation of benign and malignant thyroid nodules. PloS One. 2017; 12:1–11. doi: 10.1371/journal.pone.0188987
55. Zhang B, Tian J, Pei S, Chen Y, He X, Dong Y, et al. Machine learning-assisted system for thyroid nodule diagnosis. Thyroid. 2019; 29:858–67. doi: 10.1089/thy.2018.0380
56. Zhao C-K, Ren T-T, Yin Y-F, Shi H, Wang H-X, Zhou B-Y, et al. A comparative analysis of two machine learning-based diagnostic patterns with thyroid imaging reporting and data system for thyroid nodules: diagnostic performance and unnecessary biopsy rate. Thyroid. 2021; 31:470–81. doi: 10.1089/thy.2020.0305
57. Qin P, Wu K, Hu Y, Zeng J, Chai X. Diagnosis of benign and malignant thyroid nodules using combined conventional ultrasound and ultrasound elasticity imaging. IEEE J BioMed Heal Inf. 2020; 24:1028–36. doi: 10.1109/JBHI.2019.2950994
58. Pereira C, Dighe MK, Alessio AM. Comparison of machine learned approaches for thyroid nodule characterization from shear wave elastography images. In: Mori K, Petrick N, editors. Medical Imaging 2018: Computer-Aided Diagnosis. 2018. Houston, United States: SPIE. p. 68. doi: 10.1117/12.2294572
59. Kim SK, Chai YJ, Park I, Woo JW, Lee JH, Lee KE, et al. Nomogram for predicting central node metastasis in papillary thyroid carcinoma. J Surg Oncol. 2017; 115:266–72. doi: 10.1002/jso.24512
60. Liu T, Ge X, Yu J, Guo Y, Wang Y, Wang W, et al. Comparison of the application of b-mode and strain elastography ultrasound in the estimation of lymph node metastasis of papillary thyroid carcinoma based on a radiomics approach. Int J Comput Assist Radiol Surg. 2018; 13:1617–27. doi: 10.1007/s11548-018-1796-5
61. Jiang M, Li C, Tang S, Lv W, Yi A, Wang B, et al. Nomogram based on shearwave elastography radiomics can improve preoperative cervical lymph node staging for papillary thyroid carcinoma. Thyroid (2020) 30:885–97. doi: 10.1089/thy.2019.0780
62. Goodfellow BI, Pouget-abadie J, Mirza M, Xu B, Warde-farley D, Ozair S, et al. Generative adversarial networks. Commun ACM. 2020; 63:139–44. doi: 10.1145/3422622
63. Yang Q, Liu Y, Chen T, Tong Y. Federated machine Learning: concept and applications. ACM Trans Intell Syst Technol. 2019; 10:1–19. doi: 10.1145/3298981
64. Li Y, Li W, Xiong J, Xia J, Xie Y. Comparison of supervised and unsupervised deep learning methods for medical image synthesis between computed tomography and magnetic resonance images. BioMed Res Int (2020) 2020:5193707. doi: 10.1155/2020/5193707
65. Nie D, Trullo R, Lian J, Petitjean C, Ruan S, Wang Q, et al. “Medical Image Synthesis with Context-Aware Generative Adversarial Networks.,” In: Descoteaux M, Maier-Hein L, Franz A, Jannin P, Collins DL, Duchesne S, editors. Medical Image Computing and Computer Assisted Intervention − MICCAI 2017. Lecture Notes in Computer Science. 2017. Cham: Springer International Publishing. p. 417–25. doi: 10.1007/978-3-319-66179-7_48

66. Wu Z, Pan S, Chen F, Long G, Zhang C, Member S, et al. A comprehensive survey on graph neural networks. IEEE Trans Neural Networks Learn Syst. 2021; 32:4–24. doi: 10.1109/TNNLS.2020.2978386
67. Garcia V, Bruna J. Few-Shot Learning with Graph Neural Networks. 2018, 1–13. doi: 10.48550/arXiv.1711.04043
68. Yi L, Su H, Guo X, Guibas L. SyncSpecCNN: Synchronized Spectral CNN for 3D Shape Segmentation. 2017 IEEE Conference on Computer Vision and Pattern Recognition (CVPR) (2017). Honolulu, HI: IEEE. p. 6584–92. doi: 10.1109/CVPR.2017.697
69. Byrne DW, Domenico HJ, Moore RP. Artificial Intelligence for Improved Patient Outcomes—The Pragmatic Randomized Controlled Trial Is the Secret Sauce. Korean J Radiol 2024;25(2):123-125

Chapter 9. Breast Elastography

Dana Stoian

We may think of elastography as a continuation of the palpation, as a quantitative palpation, more objective than the qualitative clinical examination by convectional palpation. The evaluation of structures dislocation, when exposed to external pressure, estimates the tissue stiffness. This principle is used not only in ultrasound diagnostic techniques, but also in optical and magnetic resonance evaluations.

From the exiting elastographic techniques, breast elastography uses free hand compression elastography, the strain technique (SE), where the different deformation of the tissue exposed to externally applied pressure is assessed and compared, respectively the shear wave technique (SWE), evaluating the propagation of the shear wave, generated by the ultrasound probe, within the scrutinized tissues.

Regardless of the technique, the results of elastography pertain to the BIRADS classification system (1), being considered as associated features, along with architectural distortions, ductal and skin aspects, oedema, and vascularization, as part of the comprehensive multiparametric evaluation of breast lesions, besides gray scale conventional diagnostic criteria. The need to improve breast ultrasound diagnosis derives from the limited positive predictive value of combined gray scale and Doppler techniques, described as up to 40-60% (2–6).

The premises of the use of elastography in the ultrasound diagnosis of breast lesions are supported by demonstrated data (7,8) regarding the significant differences in the elastic module of preglandular fatty tissue, healthy breast tissue, respectively breast cancers, which showed increased stiffness, when exposed to moderate pressure, whether it was the ductal *in situ*, the infiltrative variant, or the isolated lobar carcinoma. When applied to breast, elastography is offered just in the presence of circumscribed/localised lesions, the stiffness of which is to be compared to the one of the healthy surrounding tissues.

9.1. Technique of examination

The elastographic examination, either by strain (SE), or shear-wave (SWE) technique, is made by using multifrequency linear transducers. The choice of the right frequency depends on the depth of the lesion: superficially located nodules require high frequency probes, while more deeply located nodules require lower frequencies, but the vast majority of lesions can be evaluated by the standard frequency range offered by the vendors, comprised between 5 and18 MHz. There are some general rules to be applied in any elastographic evaluation, in order for the results to be correct and valid (3).

The transducer will be placed in a perpendicular position to the breast examination plane (Fig. 9.1.1), and not obliquely (Fig. 9.1.2), (3), with the arm of the examiner in a fixed position, avoiding exerting excessive external pressure.

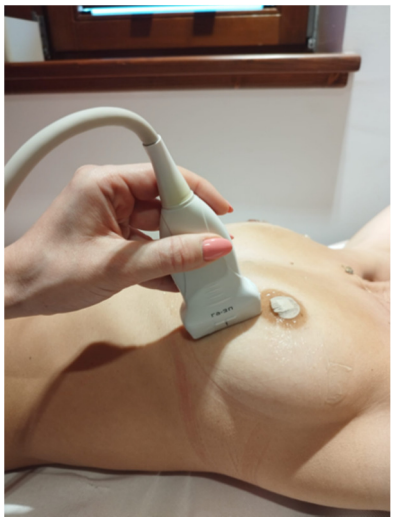

Fig. 9.1.1: Perpendicular position of the transducer on the examination plane

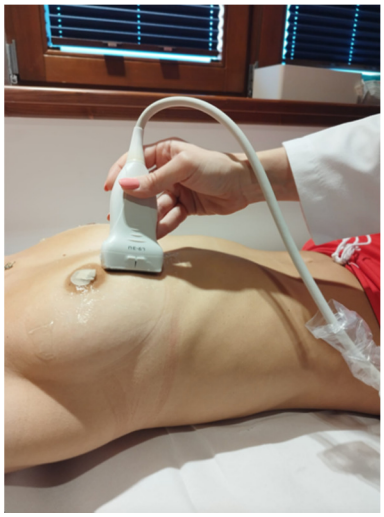

Fig. 9.1.2: Oblique position of the transducer on the examination plane

Using the perpendicular position to the examination plane, the examination failures due to unneeded transducer movements or excessive external pressure are avoided. For big breasts, lower frequencies of up to 10 MHz are preferred (9), (Fig. 9.1.4), because of their deeper penetration power compared to the standard frequencies, 15 MHz, as seen in Fig. 9.1.3, regardless of the vendor. We can observe the differences between the two images, where a deeper penetration enables a better evaluation of the examined ectatic duct.

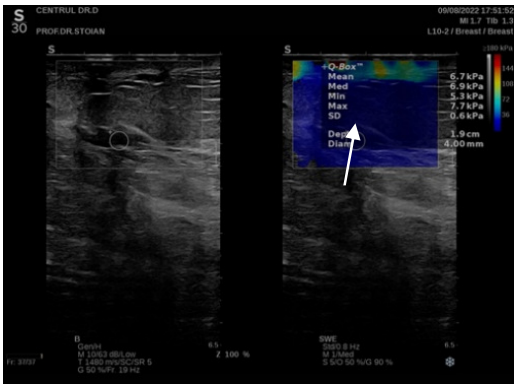

Fig. 9.1.3: 15 MHz linear transducer

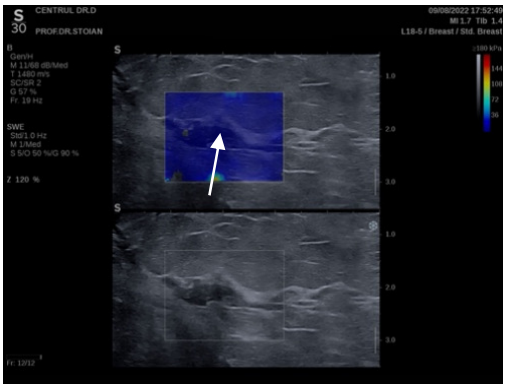

Fig. 9.1.4: 10 MHz linear transducer

The avoidance of excessive external pressure during examination (10) is one of the most important prerequisites for a correct breast elastography examination. The recommendation is to perform elastography, after the gray scale ultrasound evaluation, with a fine withdrawal of the transducer, until it offers a minimum contact with the skin (9). External pressure quality control system is offered by each vendor, quality images being those where the pressure level is maintained constant in the recommended range, displayed on the screen. - Fig. 9.1.5-6.

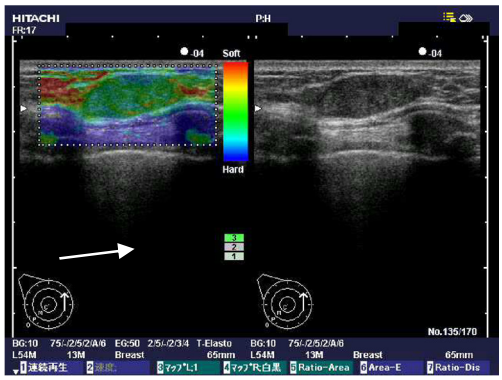

Fig. 9.1.5: Correct pressure: level 3-4
Hitachi/Fujifilm US machine

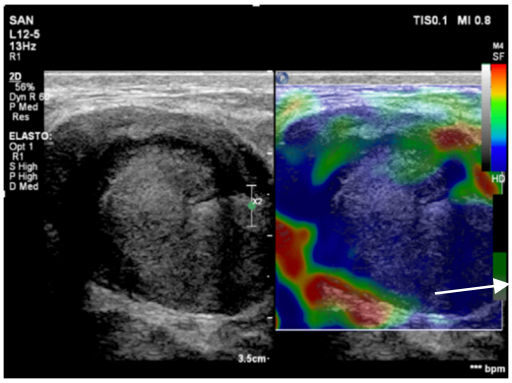

Fig. 9.1.6: Correct pressure: stable green bar
Philips US machine

Using external pressure outside the recommended range will generate distorsioned images; insufficient external pressure will yield a false reduction of the stiffness, as seen in Fig. 9.1.8, compared to the actual stiffness - Fig. 9.1.7, respectively applying an increased external pressure will induce an exaggerated tissue displacement, generating false increased stiffness, as seen in Fig. 9.1.9 (9). This phenomenon is described both in strain and in shear wave elastography (3).

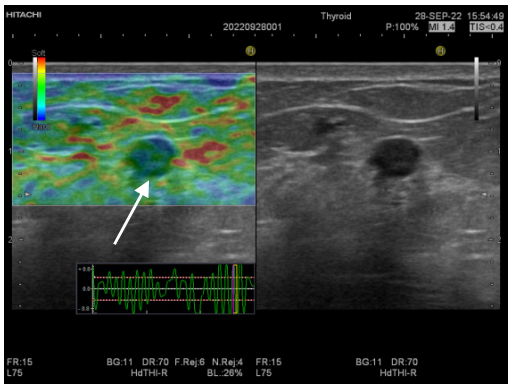

Fig. 9.1.7: Correct external pressure - actual stiffens (Rago 2)

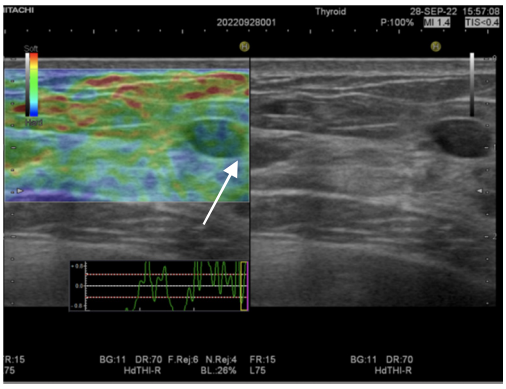

Fig. 9.1.8: Insufficient pressure - low stiffness (Rago1)

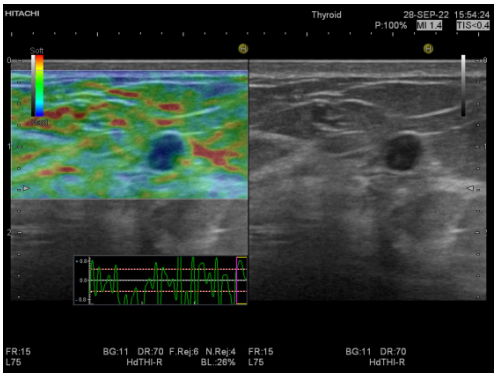

Fig. 9.1.9: Excessive external pressure - Increased stiffness (Rago 4)

Not only in SE but also in SWE (Fig. 9.1.10), there are signs suggesting excessive external pressure: appearance of vertical, parallel lines, coloured in blue, yellow, or red are highly suggestive images for high external pressure (Fig. 9.1.11 and 9.1.12), generating falsely increased stiffness in the subjacent region. Insufficient pressure with incomplete contact of the transducer to the skin will generate incomplete images.

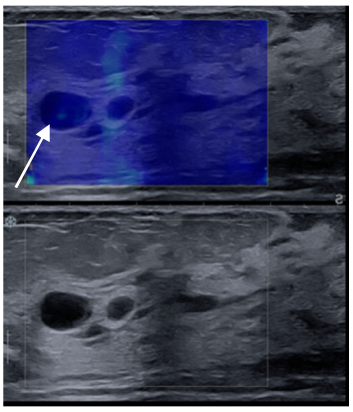

Fig. 9.1.10: Sufficient pressure Homogenous image Soft nodule (cyst)

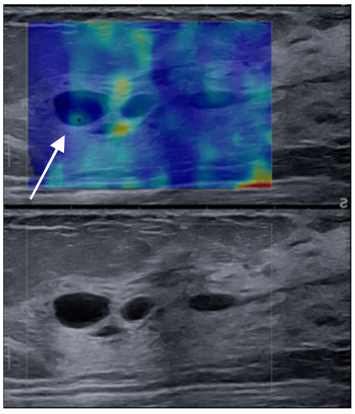

Fig. 9.1.11: Excessive pressure Vertical yellow lines Mimicking solid nodule

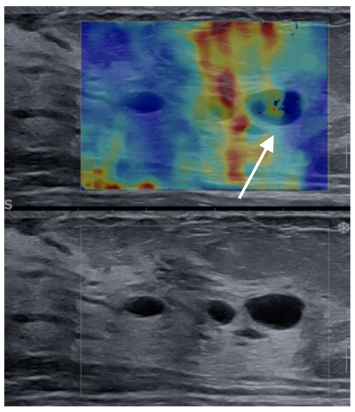

Fig.9.1.12: Intense pressure Vertical red lines Falsely increased stiffness

The necessary movements of the transducer are different for different providers and elastographic techniques. The strain technique usually needs the so-called ”Parkinson vibrating technique” with minimum movements, high frequency and low amplitude around 1 mm (3) – an excellent technique for the evaluation of superficial lesions, like nodular breast disease (9). In the case of SWE technique, it is mandatory not to use any movement of the transducer, in order to not induce any deformation/flattening of the breast tissue to be evaluated (9). The scanning must be performed slowly, with stable images of at least 0.5 seconds (2,3).

There are some US machines offering evaluation systems for both quality (M STB scale) and stability of the image, (RLB index), displayed as a scale, rated from 1 to 5, with 1 to 3 stars suggestive for unstable image due to unstable transducer, - Fig. 9.1.13, respectively 4 to 5 star images, optimal images for use, because of pressure and position stability, ideally for the clinical use. Images with reliability indexes higher than 80% should be used.

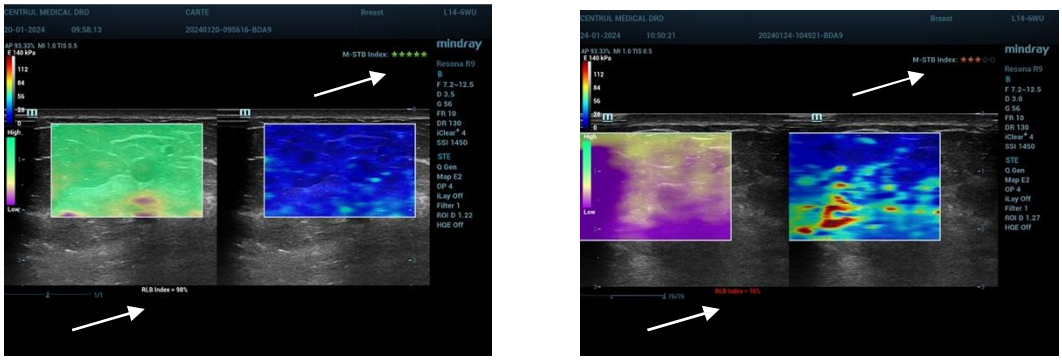

a **b**

Fig. 9.1.13: 2D-SWE evaluation Mindray Reasona 9 US machine
a. RLB index of 95%, 5 star stability map - ideal image
b. RLB index of 16%, 3 star stability map – not to be used image

The Field of View (FOV) needs to be correctly identified. Since SE evaluates the differences in the stiffness of different tissues, any measurement needs to comprise sufficient healthy tissue, shrouding the observed lesion. The evaluated lesion needs to be positioned in the centre of the FOV occupying up to a maximum of 25-50% from the total area of the FOV (9) (Fig. 9.1.14). The same principle of the centrality of the lesion needs to be applied both in sagittal as in the orthogonal plane. The FOV must comprise all the anatomical layers, starting with the skin, the subcutaneous tissue to the muscular pectoralis plane, respectively the bone plane (9) (Fig.9.1.15). In case of large nodules, exceeding the length of the transducer, respectively larger than the maximum obtainable FOV, there are recommendations to place the lesion eccentrically, with a minimum layer of healthy tissue surrounding the lesion, in order to perform an acceptable measurement (3), as described in Fig.9.1.16 and 9.1.17.

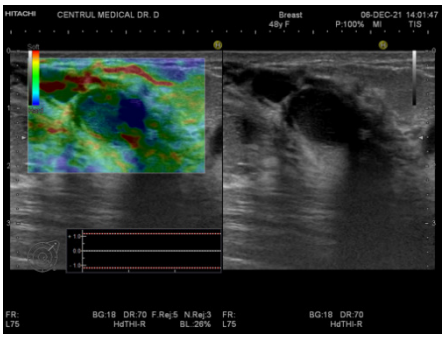

Fig. 9.1.14: Nodular lesion placed in the centre of the FOV (transversal section)

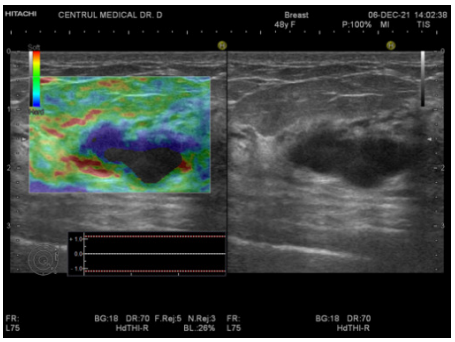

Fig. 9.1.15: Nodular lesion placed in the centre of the FOV (anteroposterior section)

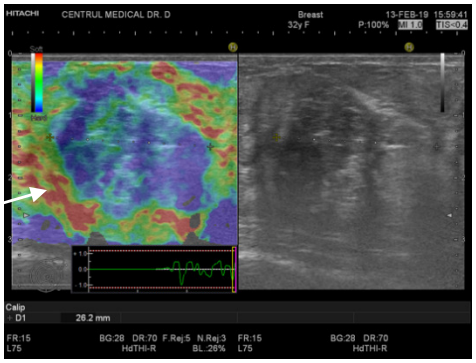

Fig. 9.1.16: Large nodule occupying more than 50% of the FOV

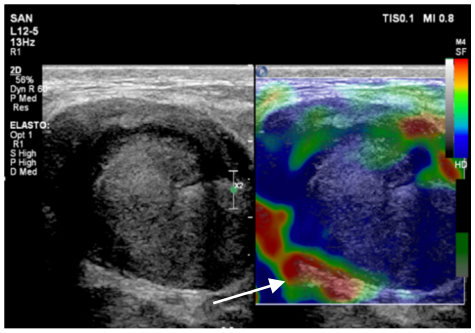

Fig. 9.1.17: Large nodule occupying more than 50% of the FOV

The same principle is valid for the SWE technique, where the FOV needs to comprise both the breast lesion which needs to be evaluated, and the healthy perilesional breast tissue, of at least 5 mm in size, respectively all the anatomical layers, for the skin to the pectoral muscles structure (11).

For the SE examination, the patient must be positioned so as to minimise the impact of respiratory movements (12), with the rotation of the patient in the plane of the movement (13). The examination of external quadrants requires an internal oblique position, respectively the evaluation of inner quadrants requires an external oblique position of the patient (3). In SWE examination, the lesion must be positioned more than 5 mm and less than 4 cm to the skin, (12) and positions that reduce the depth of the preglandular fat layer are to be preferred.

The optimum SWE image requires, besides the general conditions previously mentioned, regarding pressure, size and position of FOV, the adjustment of gain, in order to limit the noise artefacts, as seen inn Fig 9.1.18, observed in cases of excessive intensity, as seen in Fig 9.1.19.

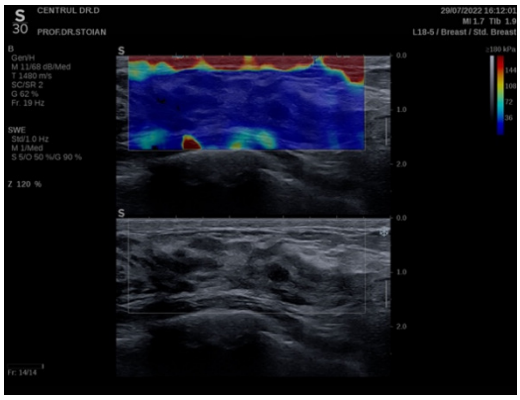

Fig. 9.1.18: Optimal gain, complete image, no artefacts/noise gain of 90%

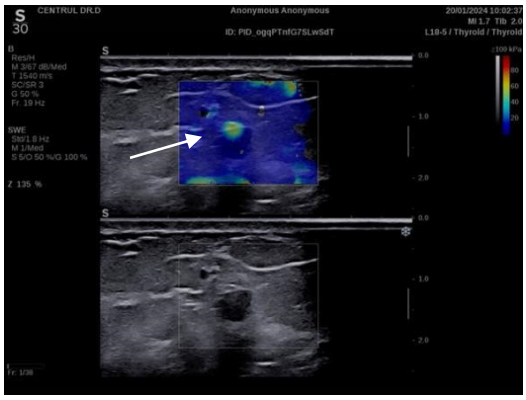

Fig. 9.1.19: Increased gain, complete image with additional visible pixels gain of 100%

The optimisation of the ratio of resolution versus penetration imposes the adjustment of resolution, in the case of small lesions, respectively of the penetration, in the case of profound lesions. The image scale can be adjusted: usually the upper normal value is 180 kPa, but it can be increased up to 300 kPa. This adjustment is needed for very dense lesions, for a better colour code map classification, as seen in Fig. 9.1.20 (a-c).

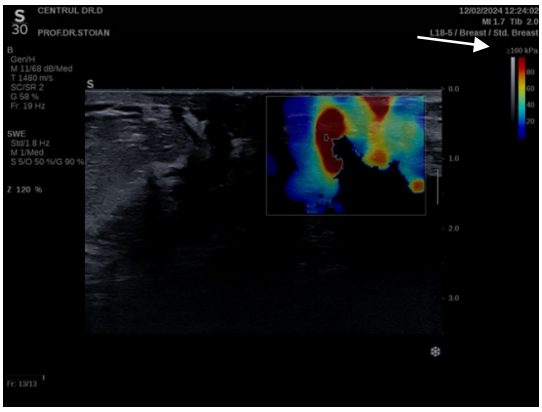

Fig.9.1.20.a: B-5 ES=5 Scale maximum 100 kPa

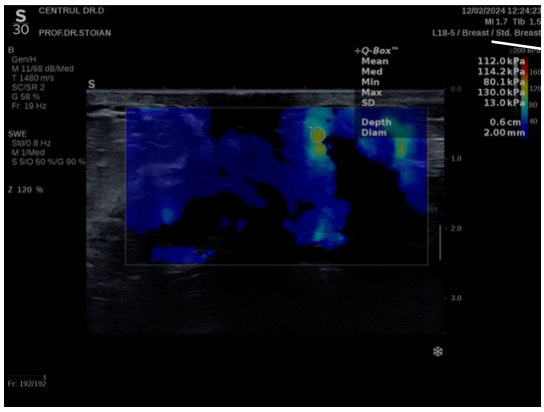

Fig.9.1.20.b: B-5 ES=4 Scale maximum 200 kPa

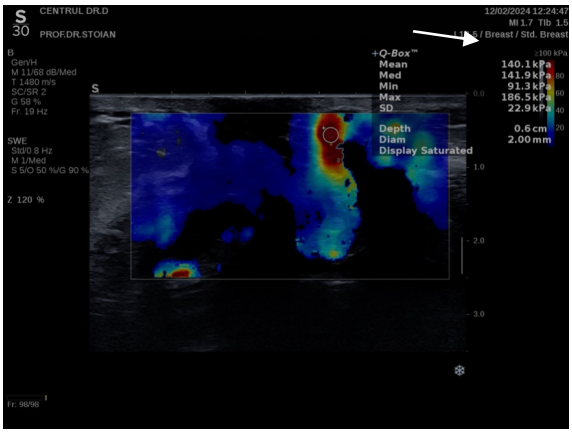

Fig.9.1.20.c: B-5 ES-5 Scale maximum 300 kPa

9.2. Strain elastography (SE)

The main premise in the elastographic diagnosis of nodular diseases is that most cancers are stiff, respectively most benign lesions are soft. The stiffness of cancer lesions is induced by desmoplastic peritumoral reaction, the infiltration of the interstitial tissue or of the ductal compartment by the neoformation tumoral tissue (14).

SE does not directly measure the tissue elasticity, but it evaluates the differences in stiffnes in the exposed tissues to the external pressure and displays such differences as a colour code map. The colour code and legend can be different for different manufacturers. The colour convention from soft to stiff is displayed on the screen of the ultrasound machine, as seen in Fig. 9.2.1 and 9.2.2. Regardless of the producer, in SE, the elastography image is displayed in real time, concurrently with the grey scale image, thus allowing a complete and integrative image evaluation.

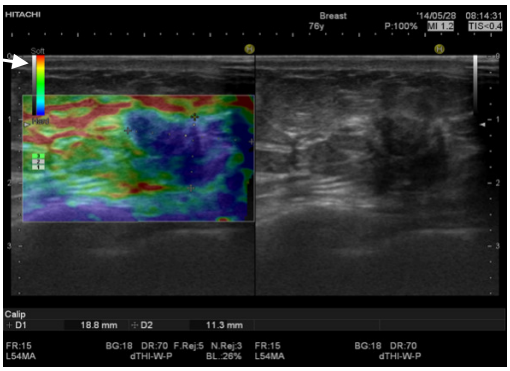

Fig. 9.2.1: Scale red/stiff – blue/soft Hitachi Machine

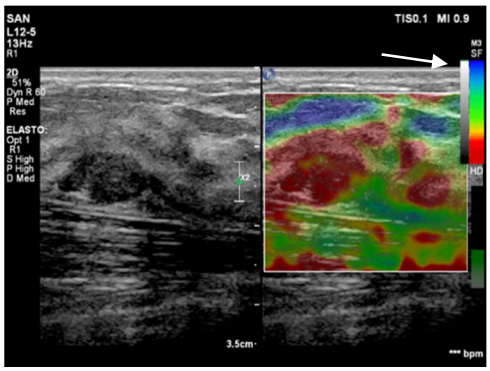

Fig. 9.2.2: Scale red/stiff – blue/soft E 7500 Philips EPIQ

The double checking of the quality of the elastography image requires the retrospective evaluation of the screen loop, by choosing the most stable colour distribution of the pre-recorded frames (3).

The SE is a relative technique which evaluates the differences in the tissue dislocation when exposed to the same external pressure (13). Results can be displayed by three methods: *a. qualitative technique*, colorimetric evaluation of the predominant colour in the nodule; b. *semiquantitative technique,* with the computed ratio between the stiffness of the nodule and the pre-glandular fatty tissue and c. the ratio between the maximum size of the lesions in elastography compared to the same axis size, in grey scale evaluation, the *E/B ratio.*

a. *Qualitative evaluation* quantifies the stiffness of the lesion. In breast elastography, the Tsukuba score is generally used. It comprises five categories: score 1 with the whole nodule soft (Fig. 9.2.3), score 2 with predominance of stiffness in the nodule, with some point of increased stiffness, (Fig. 9.2.4), score 3 with the centre of the lesion hard and the periphery soft, respectively predominant stiffness (Fig. 9.2.5), score 4 with the entire lesion stiff (Fig. 9.2.6), and score 5 when the stiffness exceeds the size in grey scale (Fig. 9.2.7-8).

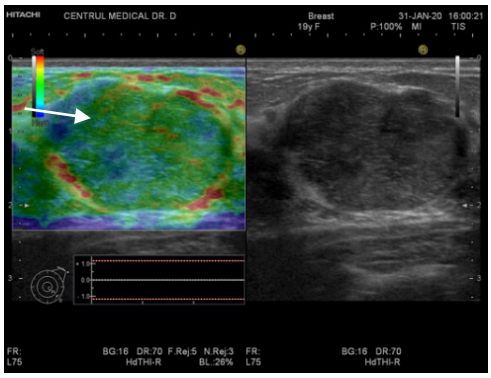

Fig. 9.2.3: Score 1: complete elasticity

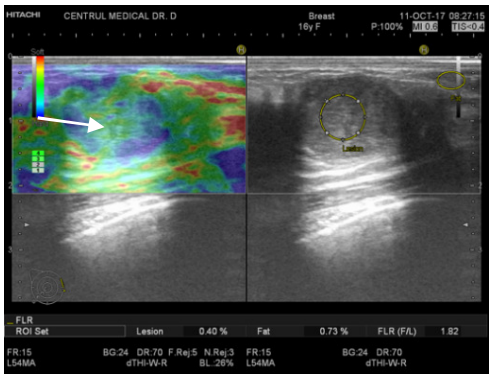

Fig. 9.2.4: Score 2: stiffness points

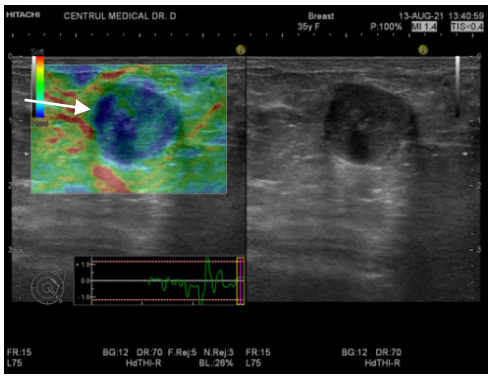

Fig. 9.2.5: Score 3: central stiffness

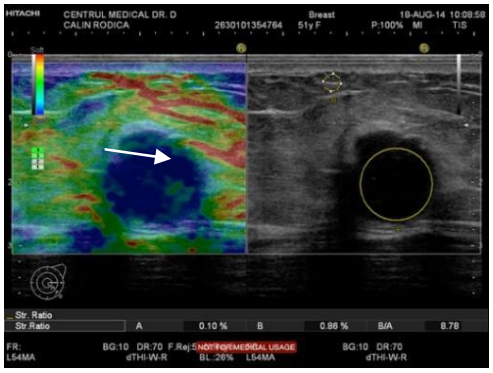

Fig. 9.2.6: Score 4: complete stiffness

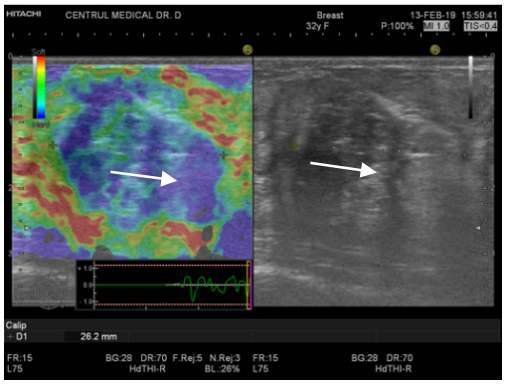

Fig. 9.2.7: Score 5 with the stiffness exceeding the contour of the nodule

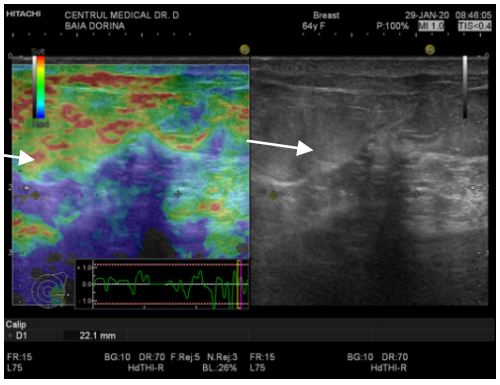

Fig. 9.2.8: Score 5 with the stiffness exceeding the contour of the distortion

Additionally, there is a subcategory to be considered, 1* (3,12) presented in Fig. 9.2.9, the so-called Blue-Red-Green sign– BRG, an artefact described in cystic lesions, regardless of simple or complex cyst (14). This aspect is characteristic to mobile fluid collections, the presence of a solid part inducing a defect in the area of the artefact (Fig. 9.2.10), with a diagnostic sensitivity and specificity of 100% (14). Mucinous or medullar lesions, even if soft, do not show this artefact (14), despite their increased elasticity.

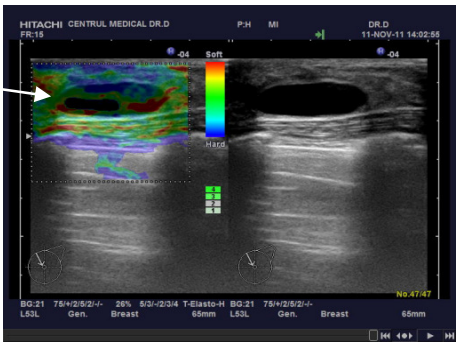

Fig. 9.2.9: complete BRG sign
Fluid only content

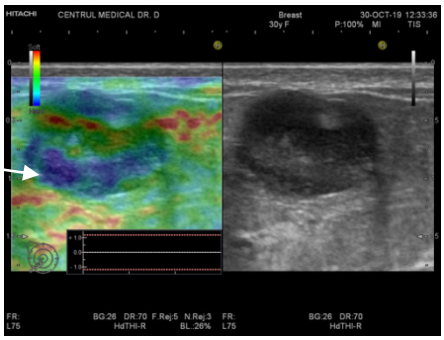

Fig. 9.2.10: stiff area in the BRG area induced by the solid intralesional vegetation

In the case of a voluminous fluid lesion, the transmission of the dislocation waves is interrupted, resulting in the partial or total absence of an elastogram (Fig. 9.2.11 and 9.2.12).

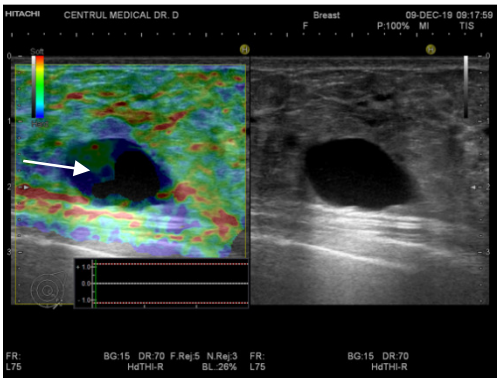

Fig. 9.2.11: Large simple cyst
Incomplete BRG artefact

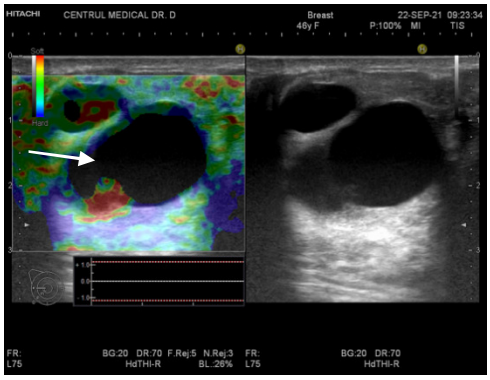

Fig.9. 2.12: Multiple simple cysts
small lesion – complete BRG sign
large lesion – absent BRG sign

Adherence to this classification is justified also by a very small intra- and interobserver variability, comparable to the classic BIRADS criteria (14). From the colour code perspective, categories 1, 1* and 2 are typical benign, respectively scores 4 and 5 are typical malignant (2,9,14,15), some authors describing category 3 and 4 (14) as suggestive for malignancy. Other authors consider score 3 lesions as equivocal (16) between benign and malignant. The qualitative technique shows a sensitivity between 87 to 93% and a specificity of 83 to 90% (9,13,17,18).

b. The *semiquantitative technique* is used for the quantification of the stiffness of any circumscribed lesion, relative to the one of the surrounding tissues. Since pre-glandular fatty tissue proved to have constant elastic modulus, in different compression models (7), with minimum inter-patient variations patients (9), this tissue is always used as a reference for the stiffness ratio calculation, the so-called Fat Lesion Ratio, (FLR). The ratio is automatically computed by the ultrasound machine, as a division between the mean dislocation in the pre-

glandular fatty tissue and the mean dislocation of the evaluated lesion, when exposed to the same external perpendicular pressure. After freezing the image and choosing the best image for the pre-recorded loop, a region of interest (ROI) is defined, to comprise the entire lesion under measurement, and the second ROI, automatically generated, is placed in the pre-glandular suprajacent tissue (2,9,12) (Fig. 9.2.13.a-d and Fig. 9.2.14). The visualisation of ROI is different according to the graphic interface of each vendor.

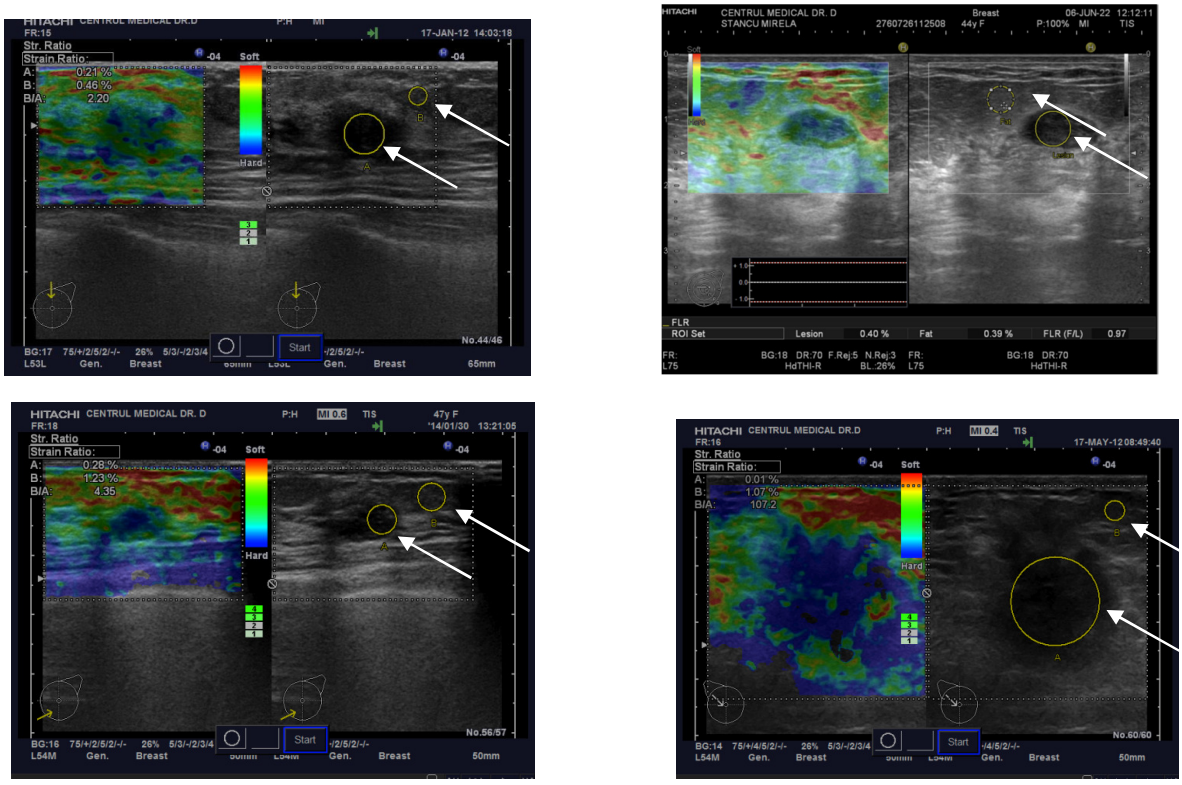

Fig. 9.2.13: Semiquantitative SE with FLR evaluation. Hitachi Preirus US machine.
a. Score 1, FLR = 2.20 b. Score 2, FLR = 0.97 c. Score 3, FLR = 4.35 d. Score 4 FLR = 107.2

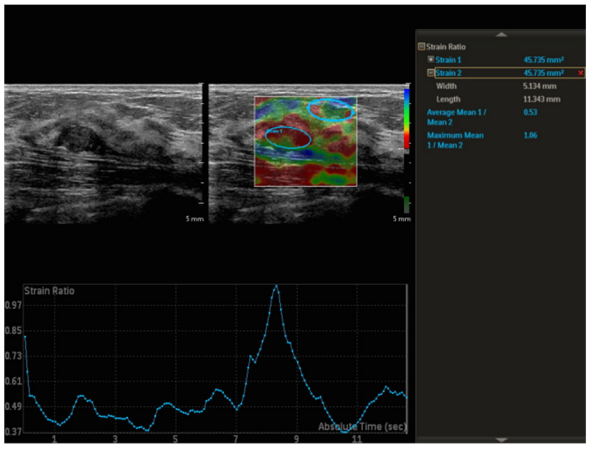

Fig. 9.2.14: Automatic in real time FLR calculation. Philips Equip US machine

The elasticity curves are obtained for each tissue with automatic comparison. Since the algorithms behind the calculation of FLR are different for each major vendor, no unique threshold value of FLR is defined and validated (9) in terms of defining benign versus malignant lesions. Values between 0.5 to 4.5 are described in the literature as being suggestive for malignancy, with a mean sensibility of 88% (84-91%) and a mean specificity of 83% (78-88%) (18). Other publications suggest a higher sensitivity of 83-91% compared to the global specificity of 68-91%, for FLR threshold values from 2.3 to 4.8. Despite this robust data, a new metanalysis (19) reemphasise the unsolved problem of the agreement for the suggestive FLR ratio.

c. *The E/B ratio* evaluation assesses the ratio between the maximum diameter in gray scale (B) (Fig. 9.2.15.a) and the same axis diameter of the lesion observed on elastography (E) (Fig. 9.2.15.b). The rationale behind this procedure is the fact that most malignant lesions seem larger in elastography compared to conventional ultrasound evaluation (13). The ratio can be calculated in any incidence, but same plane diameters must be compared (9). Three consecutive measurements are recommended, and the higher ratio will be taken into account in the the final evaluation. A value higher than 1 is suggestive for malignancy, values less than 1 are characteristic for benign lesions, with an excellent sensitivity of 98% (93-99%) and a good specificity of 72% (31-96%) (20). This technique is available for any US machine able to perform elastography.

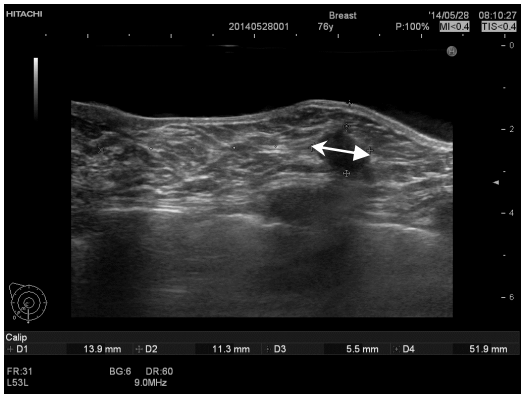

Fig. 9.2.15.a: Gray scale: BI- 4 lesion size = 13.9/11.3 mm E/B ration = 18.8/13.9 = 1.4

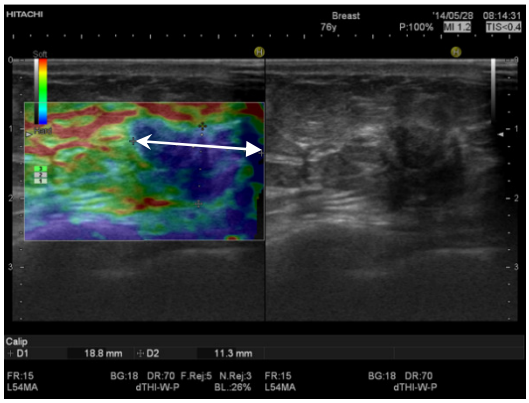

Fig. 9.2.15.b: Elastography image BI-4 lesion size = 18.8/11.3 mm Hitachi Preirus US machine, Path: CDI

False negative results of the E/B ratio are observed in soft cancers, such as metastatic foci or intramammary lymphoma (21) (Fig. 9.2.16).

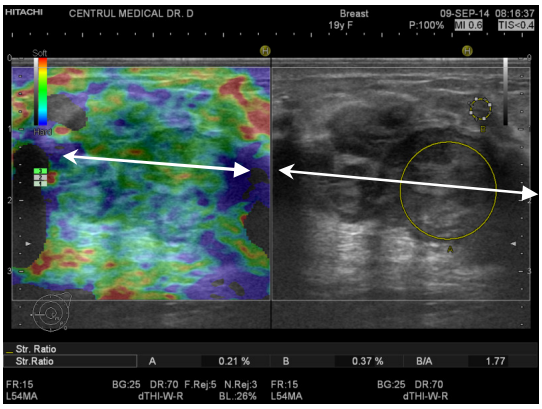

Fig. 9.2.16: Polilobulated Bi-4 lesion
Gray scale diameter = 35 mm
Elastography image diameter = 28 mm
E/B ration = 28mm/35mm = 0.8
Hitachi EUB 7500 US device
Path: Multiple myeloma

False positive results of the E/B ratio can be observed in mastitis cases (22) (Fig. 9.2.17), probably due to the perilesional oedema.

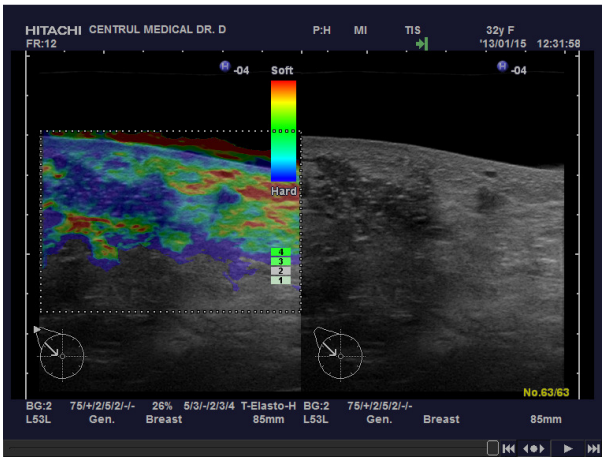

Fig. 9.2.17: Architectural distortion Bi-4: gray scale size= 22 mm, elastography size = 28mm E/B ratio= 28/22= 1.27 Hitachi EUB 7500. Path: acute mastitis

Despite these limitations, E/BB ratio offers the best accuracy among all semiqualitative techniques that can be applied with strain elastography, differentiating between malignant and benign lesions with a sensitivity of 96%, respectively a specificity of 88% (23).

Subchapter 9.7 summarise the clinical use of elastography in the diagnosis of breast lesions.

9.3. Limits of strain elastography

The most important limits in the strain technique evaluation, besides the rules to comply with, like external pressure intensity, the position or size of ROI, and the majority of the pitfalls described in the strain elastography technique are presented below.

The absence of pre-glandular fatty tissue does not allow for the calculation of the stiffness ratio. The comparison with other adjacent structure, besides pre-glandular fatty tissue, is not recommended (Fig. 9.3.1).

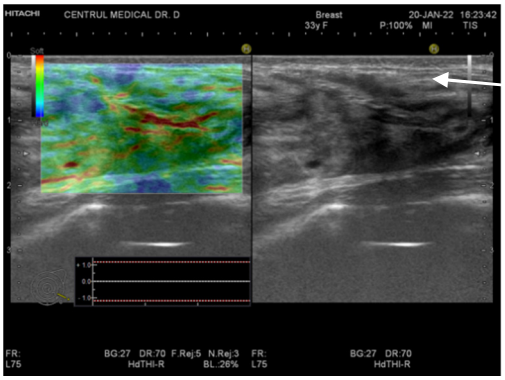

Fig. 9.3.1: Absence of pre-glandular fatty tissue

The size of the lesion limits the quality of the image, if the size exceeds the size of the ROI and also due to the deformation of the tissues and the alteration of the contact transducer – teguments, altering the final elastography image (Fig 9.3.2 and 9.3.3) (20,24).

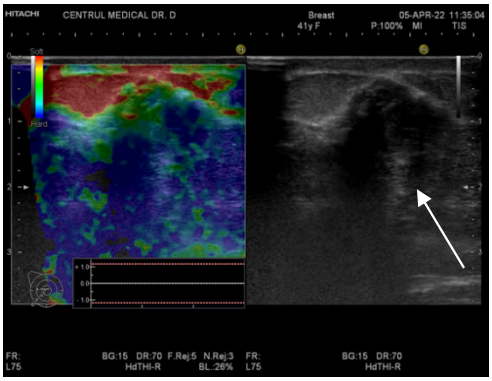

Fig. 9.3.2: Lobar cancer
Large size lesion exceeding the ROI
Inability for a correct measurement

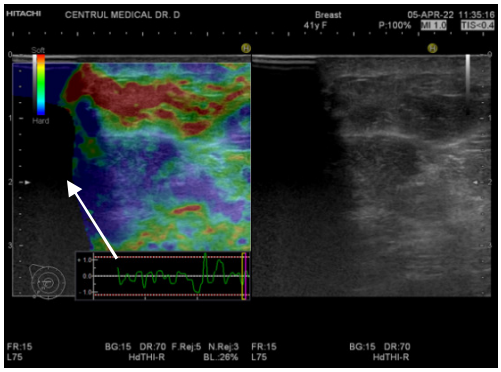

Fig. 9.3.3: Lobar cancer
deformation of the teguments
incomplete elastogram

The depth of the lesion is one of the most important causes of altered elastographic images (20,24,25), due to the alteration of the waves induced by the external pressure imposed by the examiner. There is not a threshold for the perfect penetration of the dislocation waves, and depths comprised between 2.5 cm (26,27) and 4 cm (28), for the most inferior point of the lesion compared to the skin surface, are mentioned in the literature.

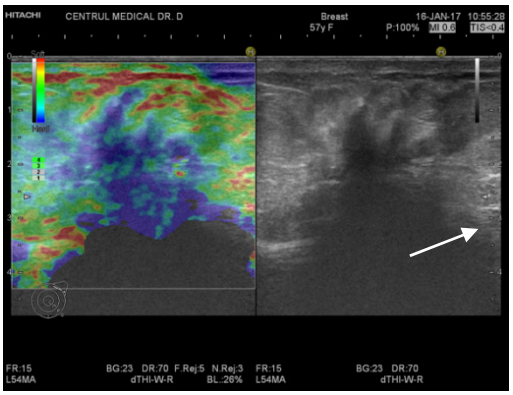

Fig.9.3.4: Partial visualisation of the Inferior portion of the tumour (3.2 cm) BI-5, Path: CDNS

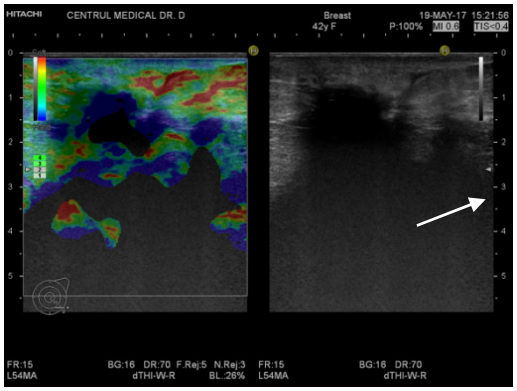

Fig. 9.3.5: Partial visualisation of the Inferior portion of the tumour (3.5 cm) BI-5, Path: LC

The presence of a **breast implant** changes the dislocation of suprajacent tissues (29). The submuscular implant can alter the elastography, due to the compression effect that is induced on the surrounding tissues located in a superior position. This effect is more prone on profound, pre-pectoral located breast solid nodules (30) (Fig. 9.3.6), which effect is not observed in superficial located nodules (Fig. 9.3.7).

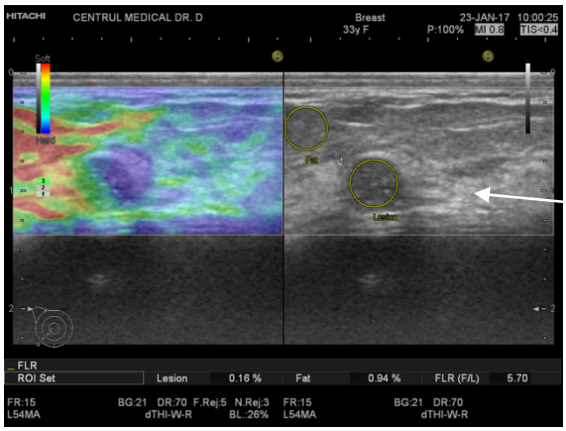

Fig. 9.3.6: Bi-4. TSUKUBA 3 Prepectoral located solid lesion Path: Fibroadenoma

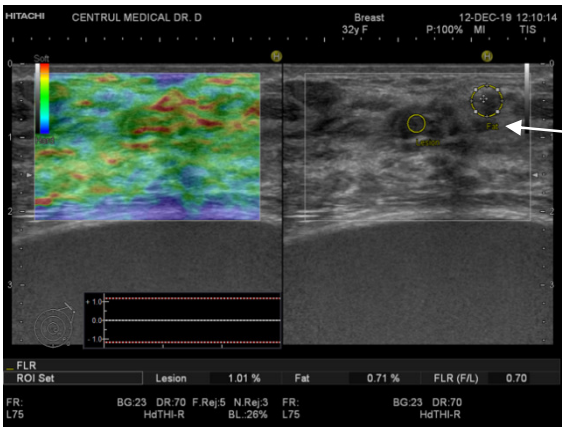

Fig. 9.3.7: Bi-3. TSUKUBA 1 Intraglandular located solid lesion Path: Fibroadenoma

False negative results are rare and characteristic for soft cancers, such as medullary, papillary or mucinous variants (31). The fact that accelerated growing aggressive tumours, due to high growing speed and increased cellularity, develop intra-tumoral necrosis with less fibrosis, is general accepted (32), and can explain low stiffness in some very aggressive cancers, as an exception to the rule. Besides these situations, mucinous cancers, very rare, representing 1-2% of false diagnoses of breast malignancy, due to the predominant mucinous content (33), with an associated low rate of cell proliferation (9), are the typical examples of soft breast cancers (20, 25), as depicted in Fig 9.3.8. Despite such general considerations, there are series of cases of mucinous cancers, presented in the literature, that tended to be stiff (32-34), with a heterogenous aspect, in an inversed relationship between the mucinous content and the degree of stiffness (Fig 9.3.9) (35).

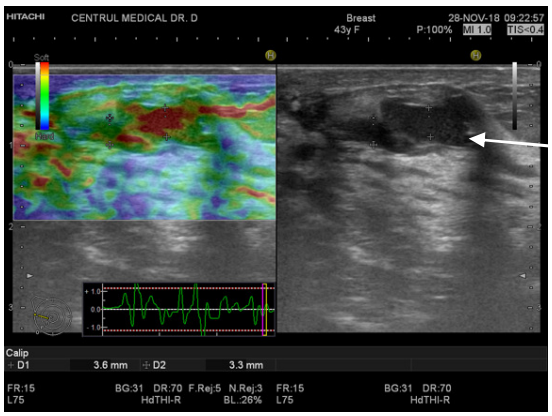

Fig. 9.3.8: Soft mucinous carcinoma TSUKUBA 1 colour code score

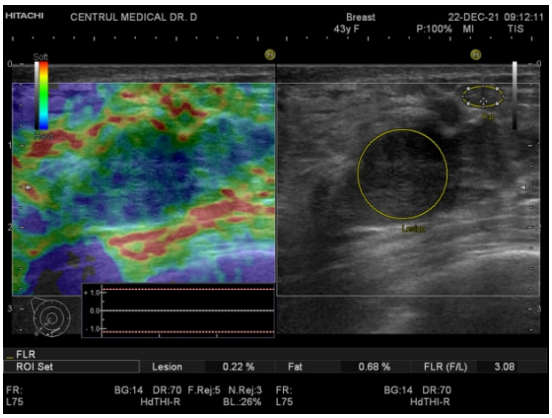

Fig. 9.3.9: Stiff mucinous carcinoma TSUKUBA 3 colour code score

In nonglandular tumours, with intramammary location, such as multiple myeloma, lymphoma, metastases, the general rule of stiffness suggestive for malignancy does not apply, these tumours being usually soft (Fig.9.3.10) (12,13,21).

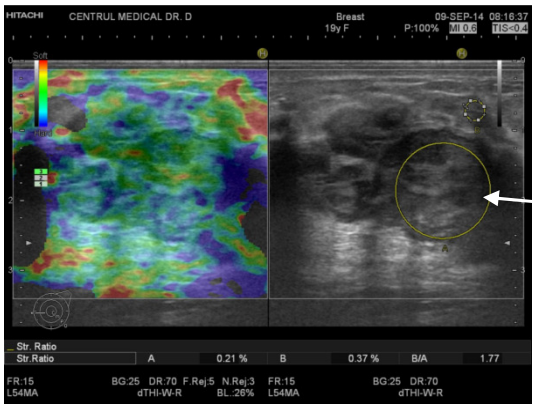

Fig. 9.3.10: Intramammary metastasis of multiple myeloma. TSUKUBA score 2. FLR =1,77

The tumoral necrosis parts of breast cancers, often induced by the imbalance between the increased cell population and the neovascularisation (32), is soft, but the conventional image remains highly suggestive of malignancy, which does not alter the BIRADS category of the nodule (Fig. 9.3.11).

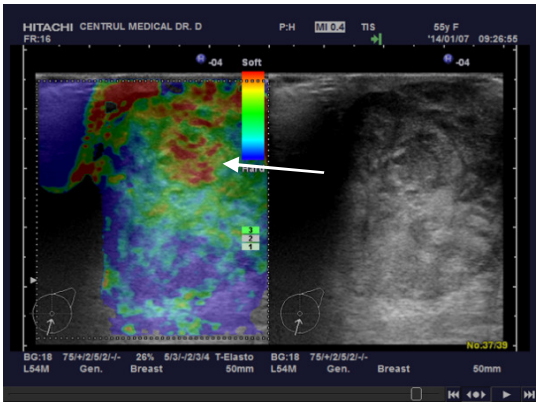

Fig.9.3.11: Invasive lobar carcinoma B-5 on gray scale ultrasound. TSUKUBA score 2

False positive results are to be expected in the case of benign lesions difficult to compress due to fibrotic tissue, as in fibrotic scars or postmenopausal fibrosis, these being the most frequent causes of false negatives (38–40) (Fig. 9.3.12) or if the lesion has high cellularity such as in sclerosant adenosis (28), intraductal or old fibroadenomas (36,37). Additionally, the presence of breast implants may falsely increase the stiffness in profoundly located solid lesions.

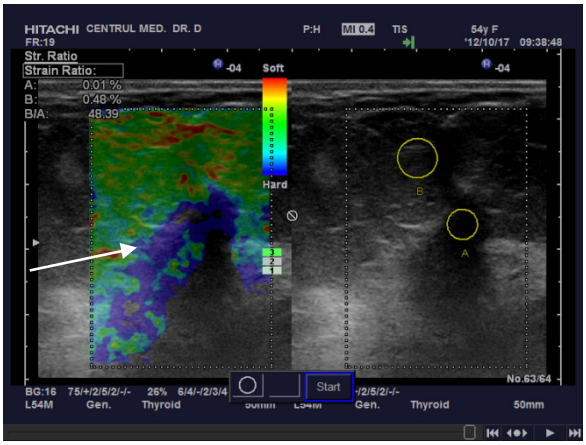

Fig. 9.3.12: B-5 lesion. TSUKUBA score 4
Path: nontumoral postmenopausal fibrosis

Calcifications are also associated with the alteration of the elastogram, inducing high stiffness in the evaluated region (2,20,25), but the phenomenon is not universal (Fig.9.3.13). The presence of an eggshell calcification does alter the elastogram, because of the lack of penetration of the dislocation waves in the central part of the nodule, not calcified (Fig. 9.3.14) (41).

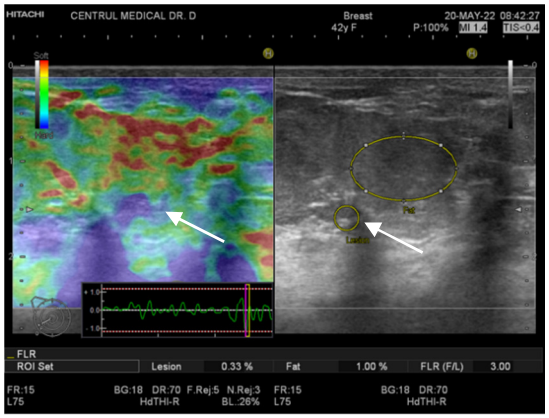

Fig. 9.3.13: B-3 Punctiform calcification
B -3 TSUKUBA 3 Path: adenosis sclerosant

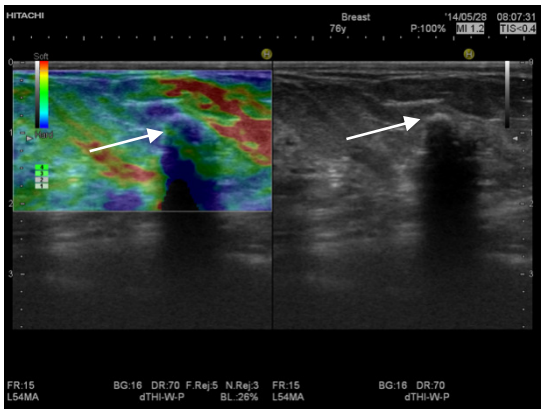

Fig. 9.3.14: Eggshell calcification,
B-5 Tsukuba 4 Path: calcified fibroadenoma

Sclerosant adenosis, a variant of mastopathy, can mimic the breast cancer observed in both clinic and conventional ultrasound examinations (42,43), and with elastography (44) (Fig. 9.3.15 and 9.3.16). Caution is needed, because this proliferative variant of adenosis can coexist

with in situ mammary carcinoma (Fig. 9.3.17 and 9.3.18), and elastography is not always suggestive.

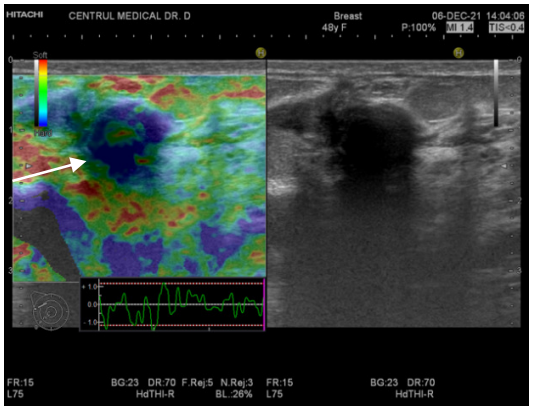

Fig. 9.3.15: B-4. TSUKUBA score 3
Path: adenosis sclerosant

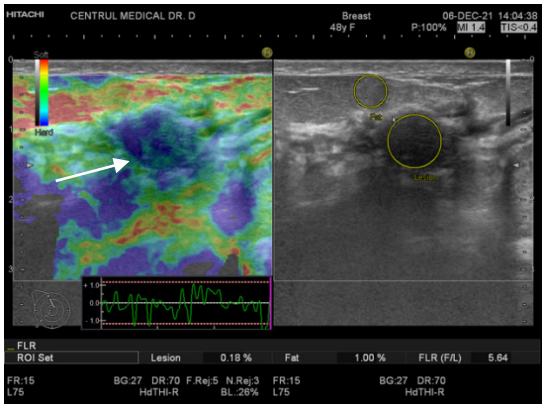

Fig. 9.3.16: B-4. TSUKUBA score 4
Path: adenosis sclerosant

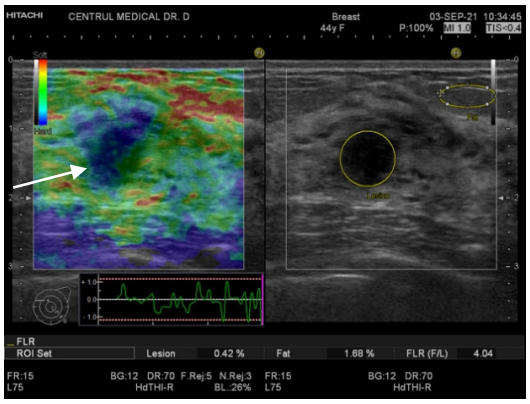

Fig. 9.3.17: B-3. TSUKUBA score 2
HP: adenosis sclerosant + CDI NOS

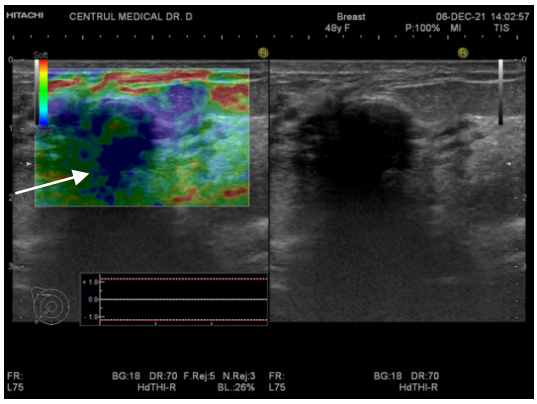

Fig. 9.3.18: B-5 . TSUKUBA score 3
HP: adenosis sclerosant + CDIS

In the same category of lesions which are difficult to assess, *cystic carcinomas* have to be considered (12,13,45). In their case, perilesional fibrosis, revealed by elastography, is a valuable, highly suggestive sign, for a peritumoral desmoplastic reaction (Fig 9.3.19 and 9.3.20) (46,47).

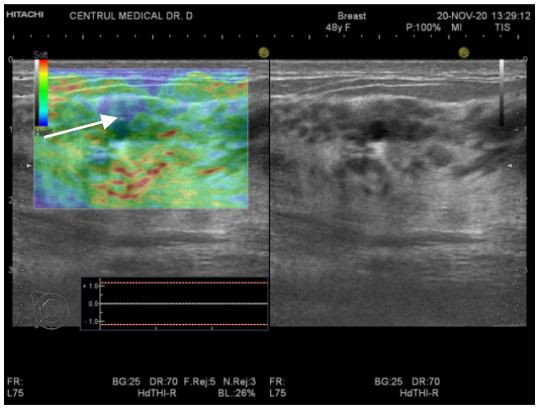

Fig. 9.3.19: B-4. TSUKUBA score 3
Path: adenoid cystic carcinoma

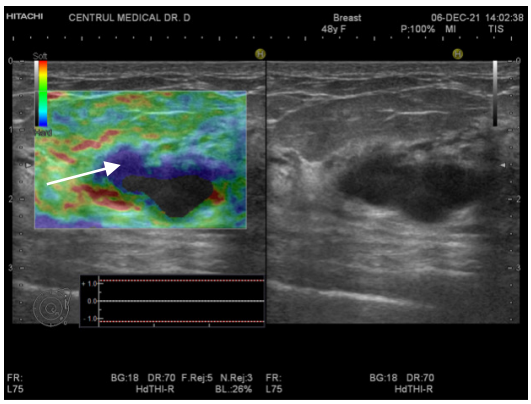

Fig. 9.3.20: B-2. TSUKUBA score 1
Path: sclerosant adenosis (48,49) + CDIS

Breast abscess can also result in false negative results in elastography. Classic ultrasound criteria are usually highly suggestive for the final diagnosis (Fig.9.3.21), but, in the absence of typical signs and a relevant clinical history, such lesions can be erroneously referred to CORE biopsy, due to their increased stiffness (Fig. 9.3.22).

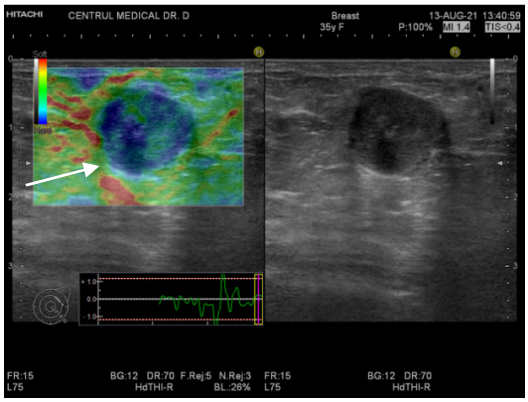

Fig. 9.3.21: B-4. TSUKUBA score 4
Path: Abscess

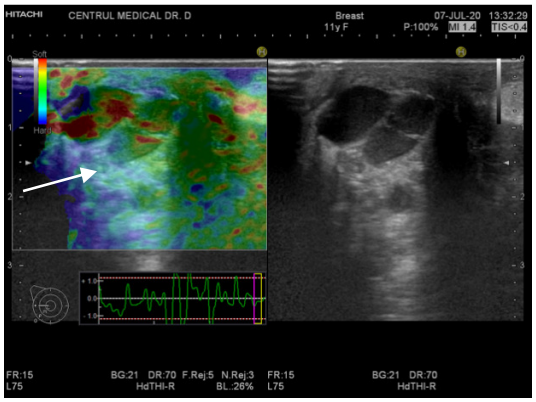

Fig. 9.3.22: B-3. TSUKUBA score 3
Path: Abscess

Previous published papers mention that intraductal papilloma can associate secondary increased stiffness (37), representing the higher rate of false positive results, due to the overlapping of elastographic characteristics, so any intraductal proliferation imposes diagnostic caution (50) (Fig. 9.3.23 and 9.3.24).

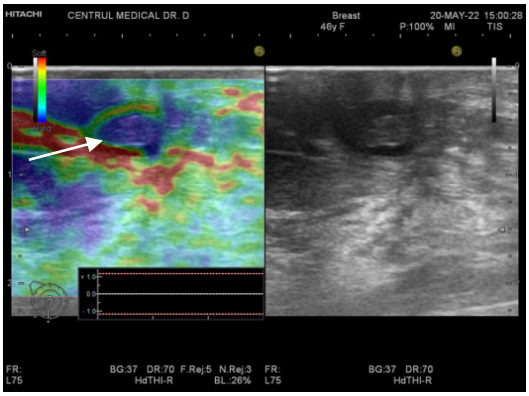

Fig. 9.3.23: B - 3. TSUKUBA score 4
Path: intraductal papilloma

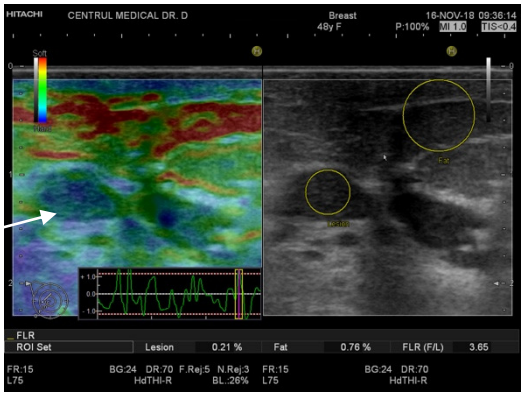

Fig. 9.3.24: B-3. Scor TSUKUBA score 2
Path: intraductal papilloma

Breastfeeding adenoma is another example for difficult-to-diagnose lesions. This is characterised as a solid lesion, partial circumscribed, usually with a pseudo-capsule, with central inhomogeneity, intralesional fibrotic septae (51–53). Increased stiffness can be expected in such cases, usually heterogenous, mainly stiff (54) - Fig. 9.3.25.

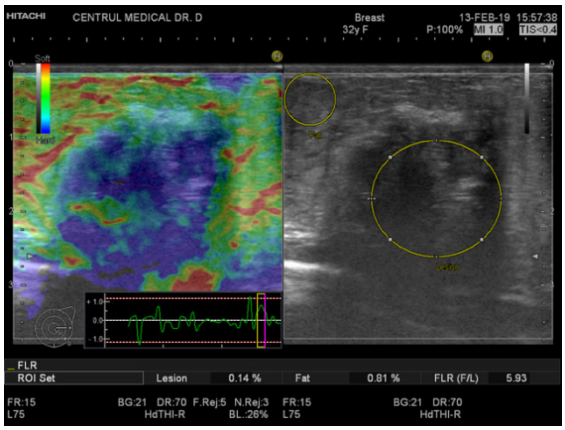

Fig. 9.3.25: B-5. TSUKUBA 4 score, Path: breastfeeding adenoma

9.4. Shear Wave Elastography (SWE)

Shear wave elastography, SWE, has a different basic principle: the propagation of shear waves with different speeds according to the stiffness of different tissues (3). Significant differences are described between the speed of waves when traveling through preglandular fatty tissue, breast glandular tissue, cystic lesions, or solid masses (55). The technique is based on the measurement of speed in the region of interest, in real time. The shear waves are automatically generated by the transducer (56), the phenomenon being known as radiation force of the ultrasounds beam. Technically, there are systems that generate a unique wave for each impulse, with postexposure image reconstruction, namely point SWE, respectively systems that are able to generate multiplane beams, with a real time image, the 2D-SWE variant.

Point SWE is mentioned among the elastographic techniques used in breast diagnosis, as a possible option to assess tissue stiffness, measuring the speed of the acoustic force generated by a focused ultrasonic impulse (57). The technique is considered to be able to generate valuable information related to solid breast masses (58,59). The evaluation is usually made quantitatively, VTQ, measuring the shear wave, perpendicular to the direction of the acoustic pulse, calculating the speed, in m/s, which speed is called velocity of the shear wave and is proportional with the consistency of the penetrated tissues, (VS) (Fig. 9.4.1).

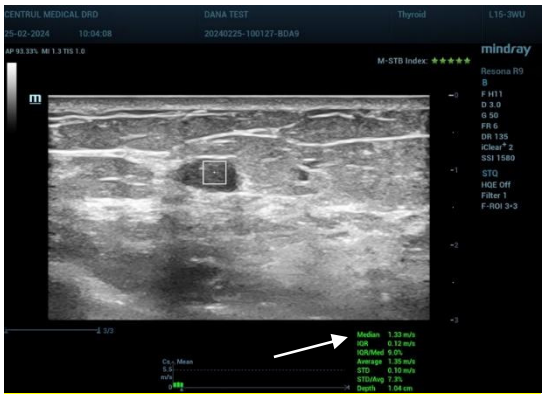

Fig. 9.4.1: point SWE evaluation, with the value of SWV (m/sec)

Additionally, qualitative variants are also offered, VTI technique using a short acoustic impulse that compresses the structures/tissues within the ROI, generating an acoustic map in grey scale, with the grey intensity proportional to the stiffness of the structure (31,60). The map does not appear in real time but offers static images of the structures present in the ROI. (31). Because breast cancers are usually very heterogenous, this technique cannot offer a comprehensive image of an entire breast nodule, so there are voices advising against the use of this technique in the diagnosis of the breast (9,25).

Fig. 9.4.2 6.2. Grey scale color code map pSWE

The studies related to the use of pSWE in the diagnosis of breast nodular pathology are limited, suggesting significant differences between benign and malignant lesions (61–63), with a threshold value of 3.6 m/s for the shear wave velocity, as suggestive for malignancy, with a sensitivity of 90% and a specificity of 80.6% (64).

If the most important limit of pSWE is intended to be overcome, namely the techniques's blind/randomly way of placing the ROI in an observed nodule, in the presence of increased speed, the specificity of the method reaches 100% but with a significant decrease in sensitivity (31).

The Aixplorer system (Supersonic Imagine - Hologic) is able to evaluate 20,000 images/second, due to the high number of acoustic beams generated by the transducer,

creating a moving picture of the wave propagation in the ROI, as well as a secondary map of the elasticity/stiffness. These events are in real time, with a short delay of just milliseconds. There is no need for additional movements from the operator. The final real time image always displays the elastographic image parallel to the grey scale image, allowing for a correct and integrated evaluation of the obtained images. This technique is called multiplane SWE or 2D-SWE.

A stable image is chosen, without any pressure artefacts, usually displayed as vertical greenish lines, as depicted in Fig. 9.1.10, and without any movements, as seen in Fig. 9.1.17, with correct gain and amplification avoiding noise artefacts as depicted in Fig. 9.1.18, using the elasticity standard scale, Fig. 9.1.19. The circumscribed lesion needs to be placed in the middle of the FOV (Fig. 9.4.3), on both transversal and anteroposterior directions, with all the anatomical layers visible in the FOV, from the skin to the entire muscle plane (Fig. 9.4.4) (3).

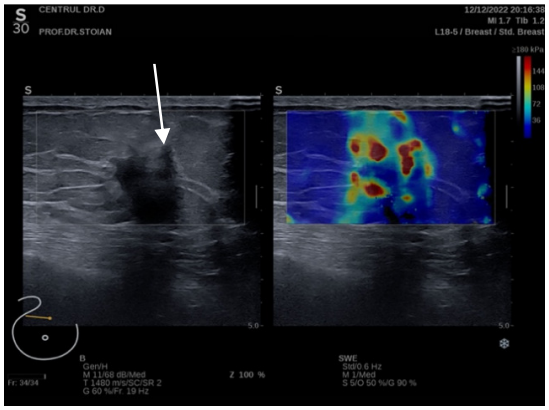

Fig. 9.4.3: Nodular lesion placed in the center of FOV (transversal)

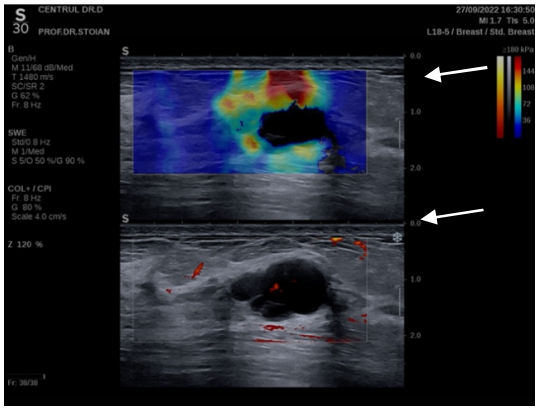

Fig. 9.4.4: Nodular lesion place in the center of FOV (frontal)

Three consecutive measurements are recommended (9). Unlike SE, where the recommendation is to define a large elastographic window, that needs to comprise the entire nodule, in 2D SWE small ROIs are recommended, up to 3-4 mm in diameter (9,20,25). There are some studies suggesting that even very small ROIs of around 1 mm in diameter can be used, without altering the diagnostic capacity of the method (65). Usually, a standard ROI of 2 mm is recommended, placed in the stiffest part of the nodule or in the shallowest 3 mm of the peritumoral tissue (Fig 9.4.5 and 9.4.6) (11).

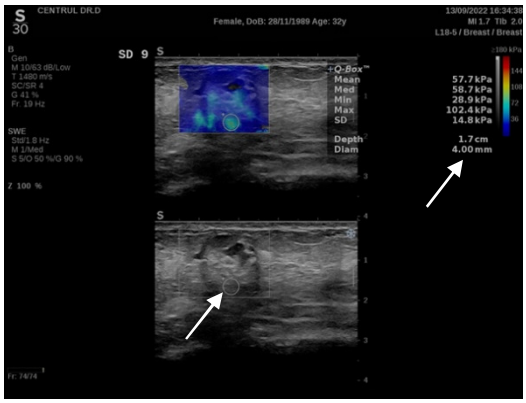

Fig. 9.4.5: 4 mm large diagnostic ROI
Path: CDIS

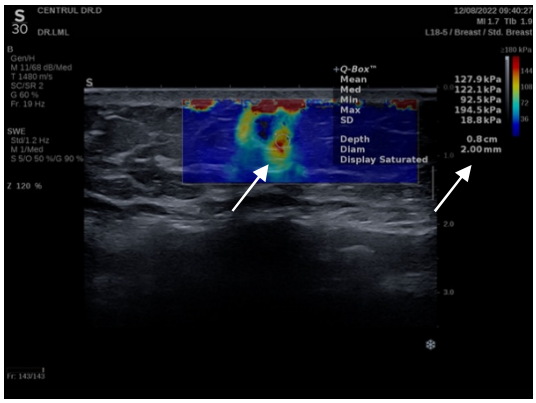

Fig. 9.4.6: 2 mm large diagnostic ROI
Path: CD NOS

In the case of heterogenous lesions, the stiffest region of the nodule is chosen for the elastographic evaluation, as well as the first 2-3 peri nodular mm, which comprise the possible desmoplastic peritumoral reaction, essential for the diagnosis of breast cancers, regardless of the intranodular cancer composition and homogeneity/heterogeneity of the stiffness (Fig. 9.4.7) and (Fig. 9.4.8).

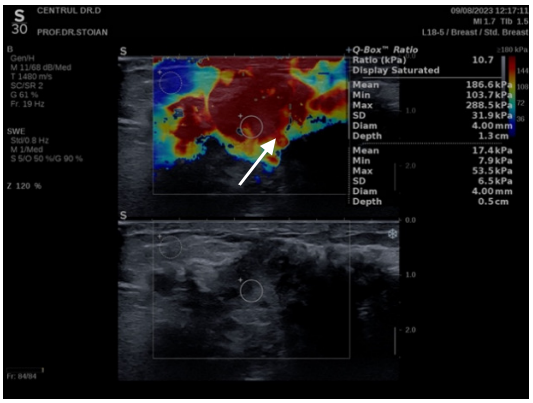

Fig. 9.4.7.a: Intra and perinodular stiffness
Path: lobular cancer

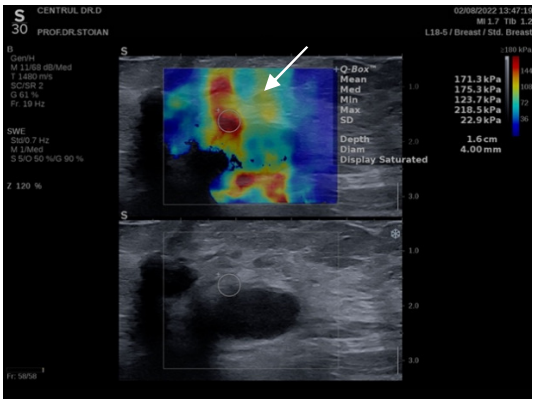

Fig. 9.4.7.b: Perinodular stiffness
Path: CDI cystic variant

The image stability is very important in the SWE technique. Aixplorer systems recommend a simple touch of the skin, without any compression, for some seconds, so as to obtain a stable image (2). There are systems that quantify the image stability as well as the quality of the elastographic image, the so-called Reability Map (RLM) offered by General Electric or Mindray machines, with a quality level of at least 80% (9) (Fig.9.4.8) confirming the homogeneity of the elastogram.

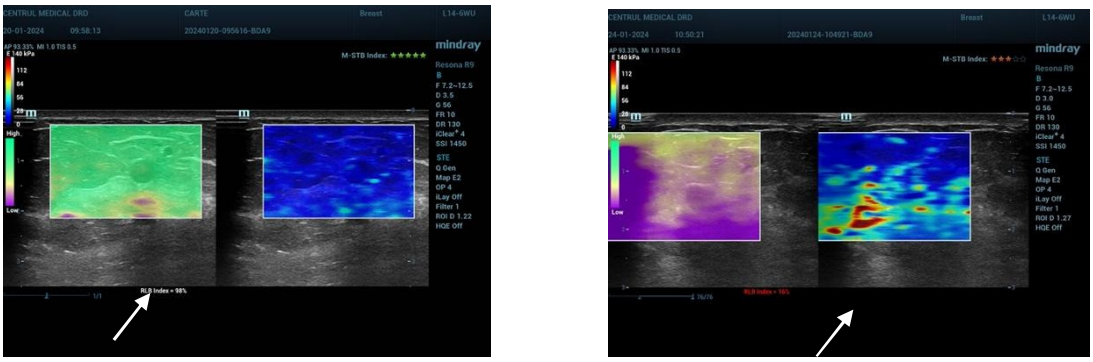

Fig. 9.4.8: 2D-SWE elastography with Reasona 9 Mindray US Machine
a. excellent image quality RLM = 95%
b. unreliable image quality RLM= 16%

The 2D-SWE elastographic results are qualitative, as a color code map, but also quantitative, measuring stiffness. The qualitative measurements use the same principle as the strain elastography, displaying different colors according to the pre-set color code map, in relation to the relative stiffness (66): Type 1: homogenous blue (Fig. 9.4.9); Type 2: minimal vertical green lines against the predominant blue background (Fig. 9.4.10); Type 3: heterogenous colours in nodule periphery (Fig. 9.4.11); respectively Type 4: multiple heterogenous zones in the core of the nodule (Fig. 9.4.12). Color code 1 and 2 are suggestive for benignity, 3 and 4 are suggestive for malignancy, with a sensitivity of 91.3% and a specificity of about 80%.

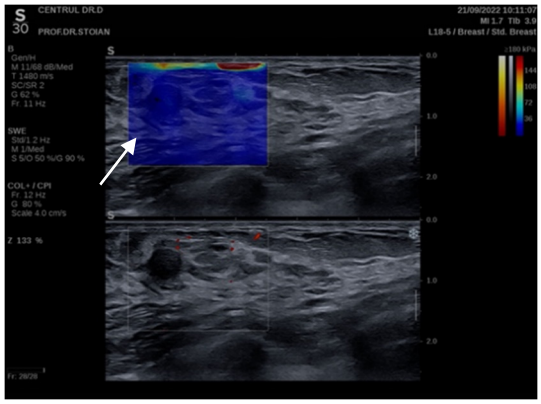

Fig. 9.4.10: Color code 1 (blue)

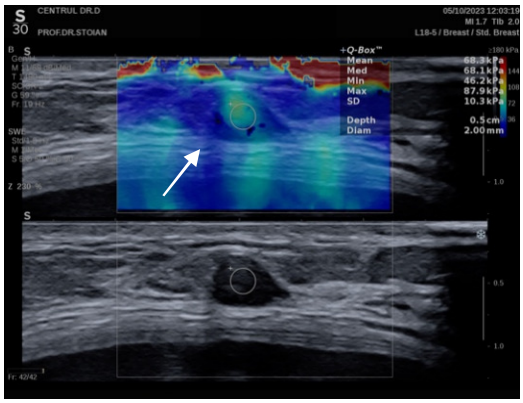

Fig. 9.4.11: Color code 2 (green vertical)

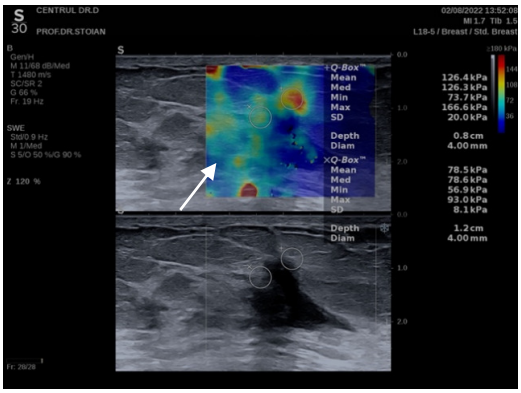

Fig. 9.4.12: Color code 3 (heterogenous)

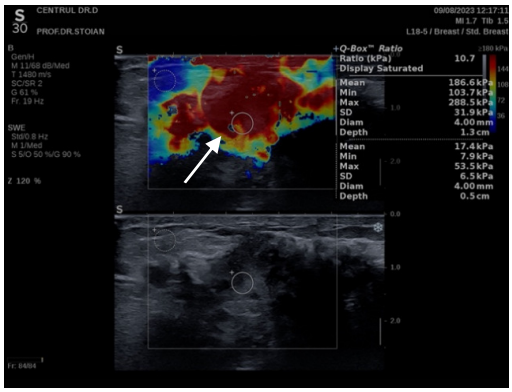

Fig. 9.4.13: Color code 4 (completely stiff)

An interesting algorithm is proposed in some previous published studies, (67), combining color code information with the maximum stiffness in the lesion, as threshold values: low risk, with a positive predictive value of 0.04% for completely blue color (color code type 1) respectively a maximum stiffness less than 72 kPa; intermediate risk for lesions with increased risk of the presence of green, yellow, orange colours, corresponding to stiffness values between 72 to 144 kPa; respectively high risk category for red colour associated with values higher than 144 kPa.

Another classification system proposed a side by side qualitative/quantitative assessment integrating both color code map and stiffness values, in six categories (Fig. 9.4.14) (67).

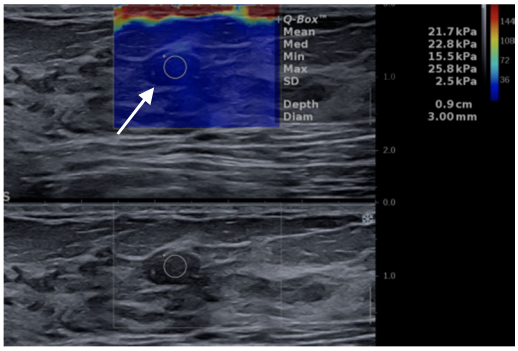

a: Score 1 Dark blue 0-36 kPa/0-3,5 m/s

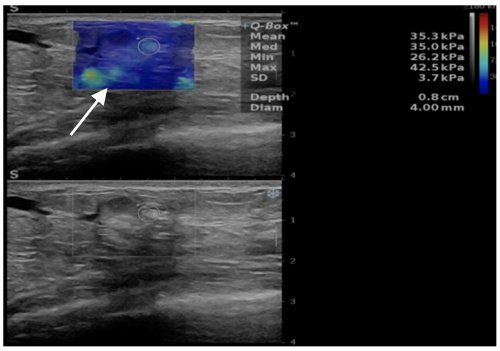

b: Score 2 Light blue 36-72 kPa

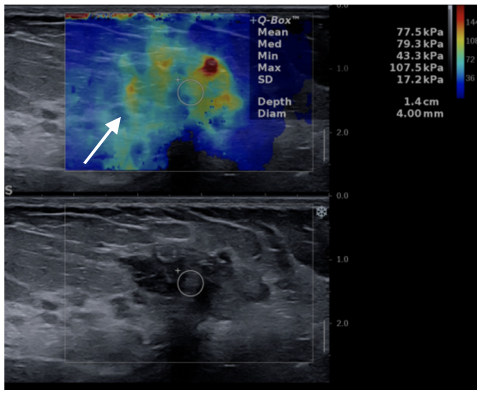

c: Score 3 Green 72-108 kPa/4,9-6,0 m/s

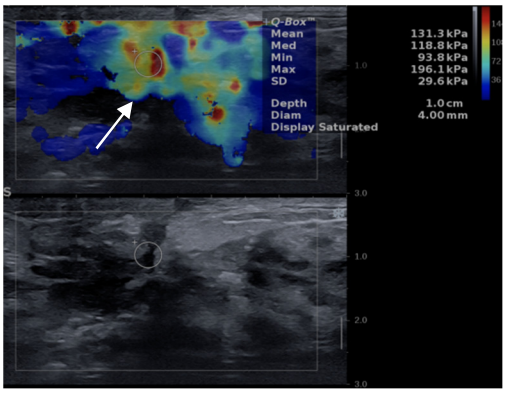

d: Score 4 Orange 108.8-144 kPa/6,0-6,9 m/s

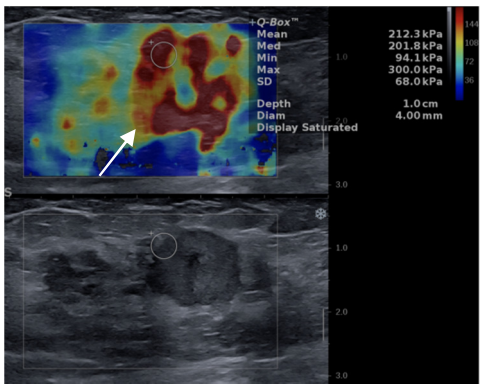

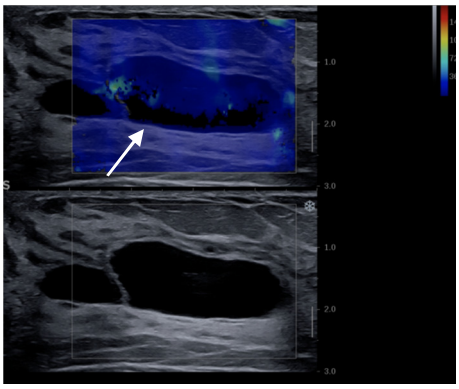

e: Score 5 Red 144-180 kPa/6,9 - 7,7 m/s **f: Score 6 Black <36 kPa/ <3,5 m/s**

Fig. 9.4.14: Combined quantitative evaluation (kPa, or m/sec) with color code map 6 (a-f)

In the presence of black/dark blue colour, the malignancy risk is 0 (68) and a complete blue lesion allows the downgrade of B-4a cases to B-3.

When evaluating the qualitative report of 2-D-SWE, the measured parameters are: mean = E_{Mean}, maximum = E_{Max}, minimum= E_{Min}, and standard deviation E_{SD}. The values are measured for each pixel comprised in the ROI and are displayed in kPa or m/sec according to the selection made (Fig. 9.4.15) (69). Furthermore, a stiffness ratio, QR, between the stiffest part of the nodule and the preglandular fatty tissue can also be measured and is calculated automatically (Fig 9.4.15).

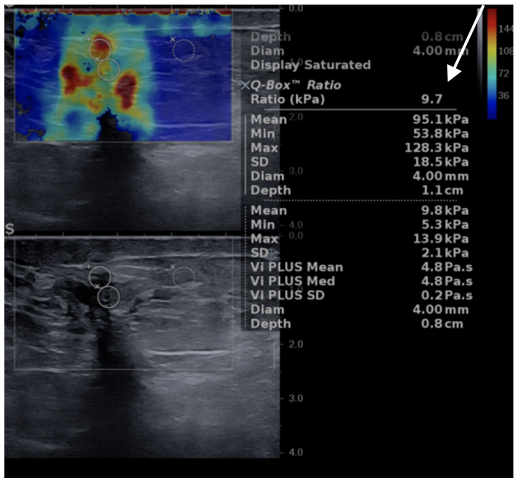

Fig. 9.4.15: Measurement of stiffness ratio nodule/preglandular fatty tissue

Since even very small, 2mm in diameter large ROIs can be used, with different positions in the nodule, E max can be very different in heterogenous nodules, but E_{Mean} is considered stable (70). The threshold values in defining malignancy, for E_{Mean}, are comprised between 33 and 80 kPa, respectively for E_{Max} 43.6-93.8 kPa, 6.3-13.9 kPa for E_{SD} respectively 3.18-5.14 kPa for E_{ratio} (61). There is no unanimous consensus for these threshold values (25), different values being described: 145.7 kPa for E_{Max} and 89.1 for E_{Mean} (71) or 46.7 kPa for E_{Max} and 42.5

kPa for E_{Mean} (72), respectively 50.85 kPa for E_{Max} and of 42.08 kPa for E_{Mean} (73). Differences can be explained by the different types of ultrasound machines used, the number of consecutive measurements, the size of ROI or the rule of choice about where to place the ROI within the intranodular portion (73), since not all users recommend placing the ROI in the stiffest part of the nodule (9,65).

SWE offers more qualitative parameters, as shown before, the question rises which is the most accurate, which should be used in daily practice. Some studies recommend E_{Mean} as the parameter to be considered (11,69), with a described value of 80.17 kPa, differentiating between benign and malignant with a sensitivity of 88.8% and specificity of 84.9% . Other studies consider E_{Max} (68) as the ideal diagnostic parameter, it being able to even predict the low differentiated grade lesions, the negative progesterone receptor levels, respectively the expression of Ki-67 (73), values less than 20 kPa being predictive for benignity with an error of up to 0.3%. From the clinical perspective, there are algorithms proposing BIRAS regrading, after integrating the elastographyc data (11,25,68,74). Subchapter 9.7 summarises the clinical implication of the use of elastography in the multiparametric diagnosis of breast lesions.

Special aspects of 2D SWE

No elastographic color on SWE appears when the examined tissue cannot measure the shear waves, because of the lack of transmission, either in the presence of large fluid collections, (Fig. 9.4.16 and 9.4.17), or in intensely stiff solid lesions, (Fig. 9.4.18 and 9.4.19).

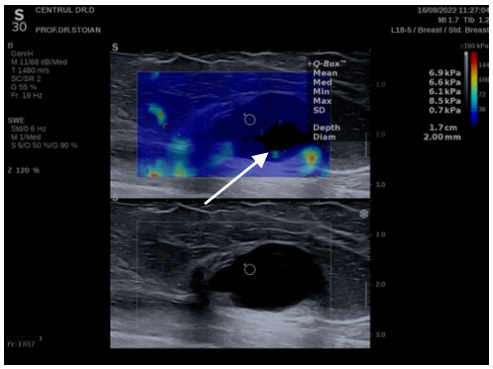

Fig. 9.4.16: Incomplete elastogram
Path: colloid cystic lesion B - 2

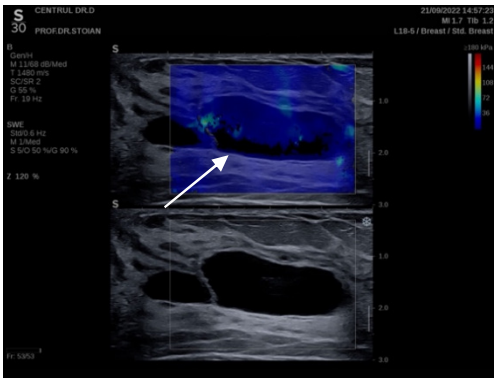

Fig. 9.4.17: Incomplete elastogram
Path: simple cyst B - 2

The explanation of the phenomenon is the lack of shear wave propagation through low viscosity fluids (25).

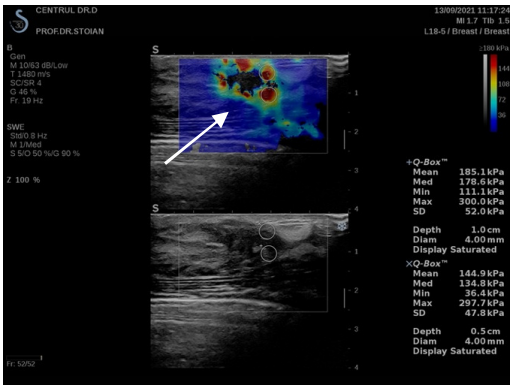

Fig. 9.4.18: Strictly peritumoral elastogram
Path: DCI

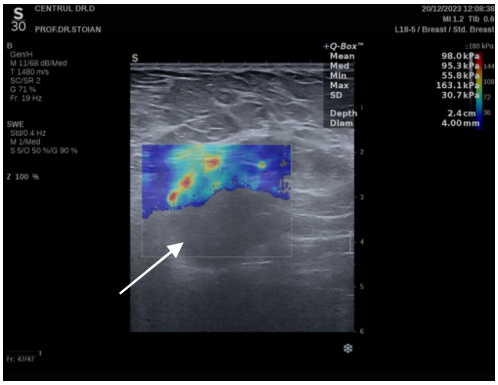

Fig. 9.4.19: Strictly pretumoral elastogram
Path: DCI

Even in these situations, the information offered by elastography can be useful, since peritumoral tissue offers sufficient areas to position the ROI in the immediate peritumoral zone(2).

9.5. Limits of Shear Wave Elastography (SWE)

The most important limits of SWE, beyond the technical requirements such as pressure intensity and stability, the size and position of ROI, the penetration adjustment, are the absence of preglandular fatty tissue, the size and depth of the lesion, the proximity to a hard plane, respectively the lesions generating falsely increased stiffness.

The absence of preglandular fatty tissue makes the calculation of the stiffness ratio impossible, but, unlike strain elastography, all the other qualitative parameters can be measured without restraint (Fig 9.5.1).

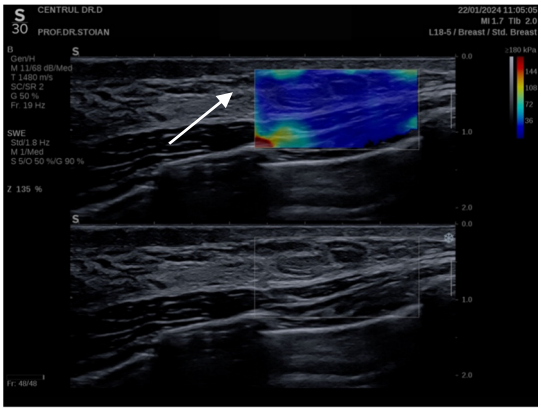

Fig. 9.5.1: Absent preglandular tissue. No stiffness ratio measurement

Large tumours generate uneven pressure application on the surface of the tumour, altering the quality of the image collection (75) and generating false results (Fig.9.5.2).

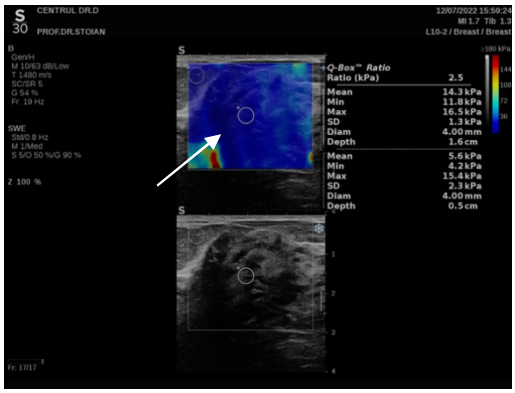

Fig. 9.5.2: Primary lesion 2.5 cm
Path: adenosis

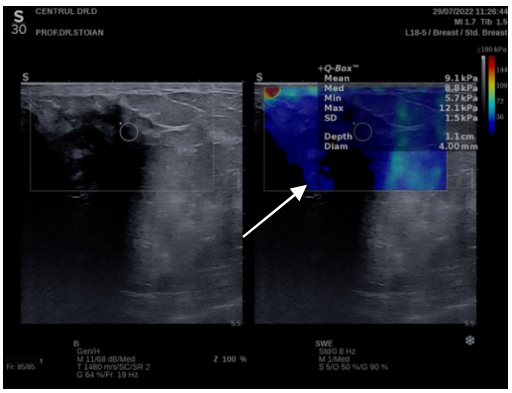

Fig. 9.5.3: Primary lesion 4.5 cm
Path: Lobar carcinoma

No echogenic areas in the tumors, in grey scale mode, will induce null elastogram, as seen in Fig. 9.5.3 (76).

A significant variation of results is seen in differently sized breast cancers, due to an intrinsic factor of the tumor biology, that induces different intra and peritumoral stiffness (77). Different discriminative threshold values are described for differently sized tumours: 109 kPa (for tumors smaller than 15 mm) versus 167 kPa (for tumors larger than 15 mm) (78) respectively values of 64 kPa for tumor diameters smaller than 1 cm, of 110 kPa for lesions comprised between 1 and 2 cm (77), and of more than 86 kPa for cancers smaller than 5 mm in diameter (11).

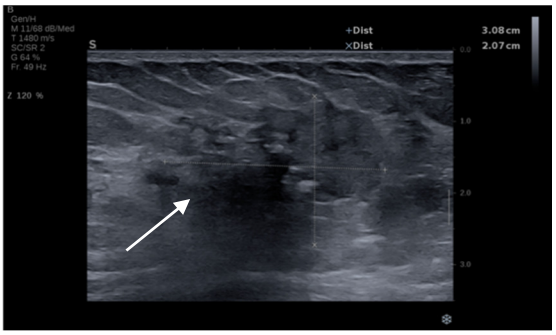

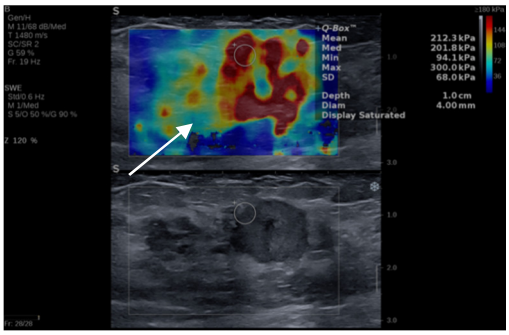

Fig. 9.5.4: solid lesion B-5, diameter of 3 cm, ES=4, E Max=300 kPa, Path: CDI

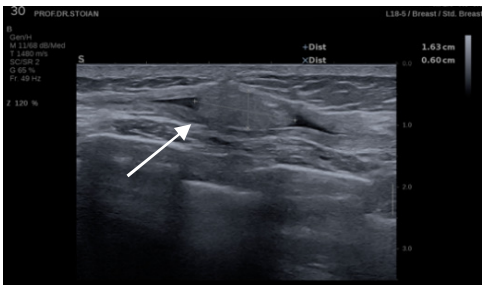

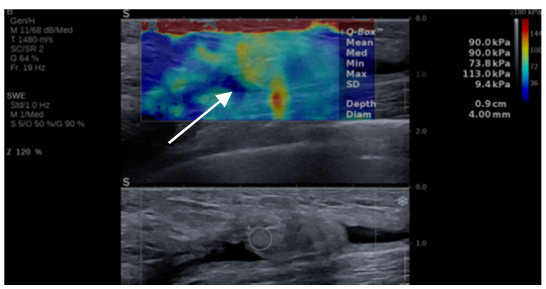

Fig. 9.5.5: Solid lesion of 1.6 cm, pre-pectoral layer B-3, ES=3, E Max=113 kPa
Path: CDI tumoral relapse after total mastectomy

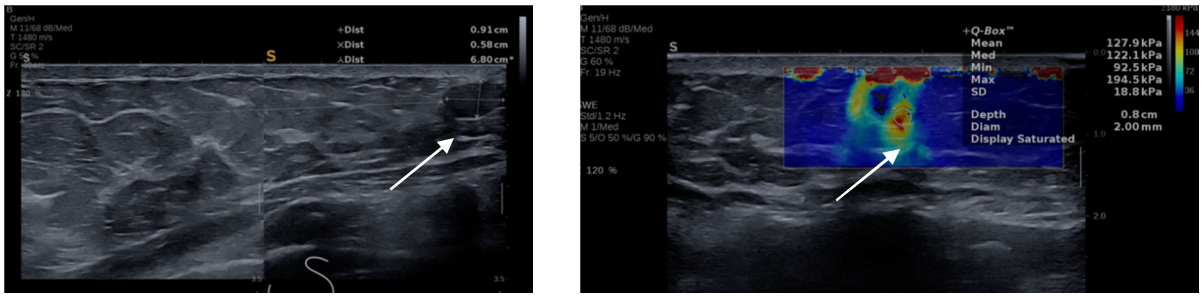

Fig. 9.5.6: Solid lesion B-4a diameter of 9.1 mm, ES=3, E Max=194.5 kPa, Path: CDI

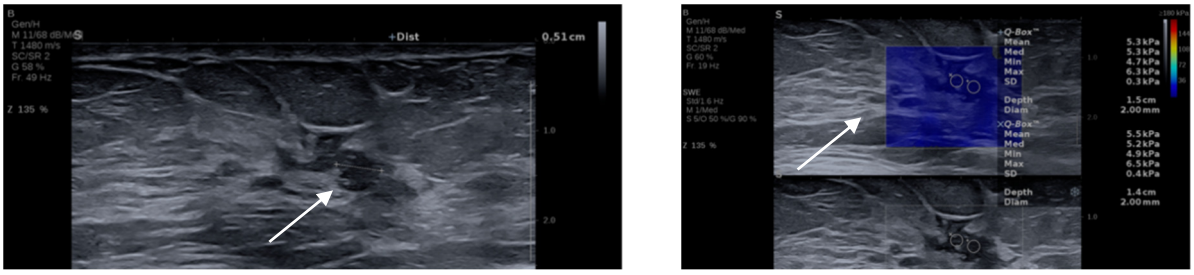

Fig. 9.5.7: Intraductal solid lesion, 5 mm diameter, B-4a, ES=1, E MAX = 6.5 kPa, Path: intraductal papyloma

It is recommended to define threshold values for differently sized tumors (<1, 1-4, >4 cm) (79).

The use of very small ROIs, intratumorally or in immediate peritumoral position, aiming to the stiffest part of the lesion, (according to the colour code) reduces the impact of the tumor size on the result of the elastography (65). When the tumour size is larger than the size of the FOV, the elastography cannot be performed or used (Fig 9.5.8) (25).

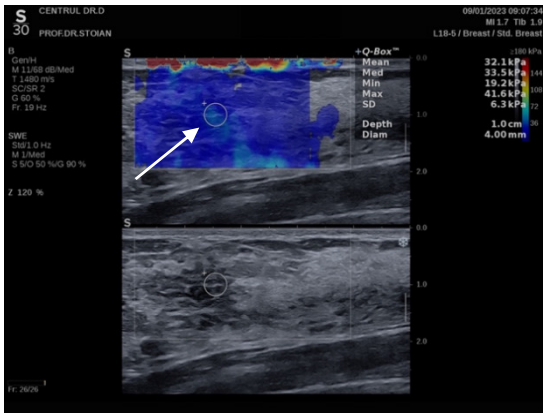

Fig. 9.5.8: Solid lesion, 5 cm in diameter, B-4a, covering the entire FOV Path: Hamartoma

The depth of the lesions is important, since the conventional ultrasound probes, with frequencies between 5 and 15 MHz, allow for a penetration of the shear wave up to 4 cm in depth (Fig. 9.5.9) (9). The evaluation of deeply positioned tumors (more than 4 cm deep) is therefore limited.

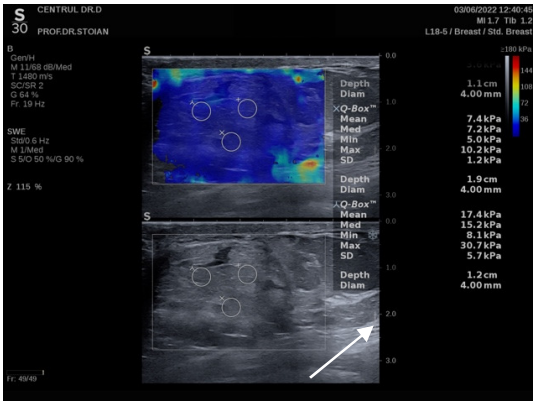

Fig. 9.5.9: Correct penetration to 3.5 cm, Path: Hamartoma

Similarly, very superficial lesions, situated in the first 3 mm, cannot be correctly evaluated by means of elastography (Fig 9.5.10 and 9.5.11) (25).

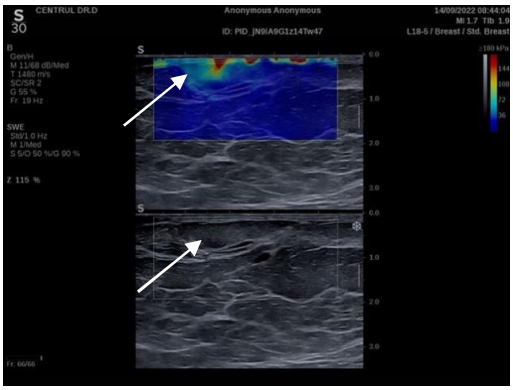

Fig. 9.5.10: Superficial solid lesion B2, ES=3
Path: lipoma

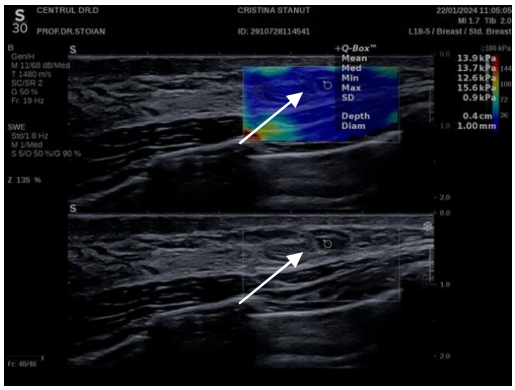

Fig. 9.5.11: Solid lesion B-3. ES=3
Path: Fibroadenoma

The proximity of a stiff plane can alter the elastographic evaluation due to an apparent increase of the stiffness surrounding the bone plane generating falsely increased stiffness of the lesion situated in the proximity of thoraco-costal plane. Fig. 9.5.12 presents a prepectoral glandular lesion generating increased stiffness.

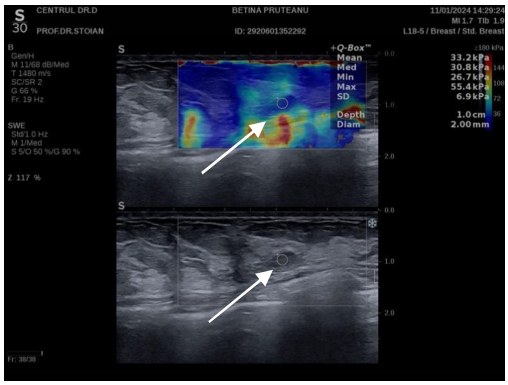

Fig. 9.5.12: Solid circumscribed B-3 lesion, prepectoral position, ES =3, E Max = 55.4 kPa Path: fibroadenoma

A high grade histological type, the degree of invasion, vascular invasion, the lymph node involvement, and the type of tumour associate with increased stiffness (77). Fibrosis areas, collagenous matrix proliferation, and necrotic areas inversely correlate with attenuation (80).

SWE can also generate false **negative results.** As mentioned before, there are some cancers not visible in elastography because of the lack of transmission of the shear wave echoes, due to increased stiffness (9,76). The so-called blue cancers (Fig 9.5.13 and 9.5.14) generate false black or blue color code on 2D SWE.

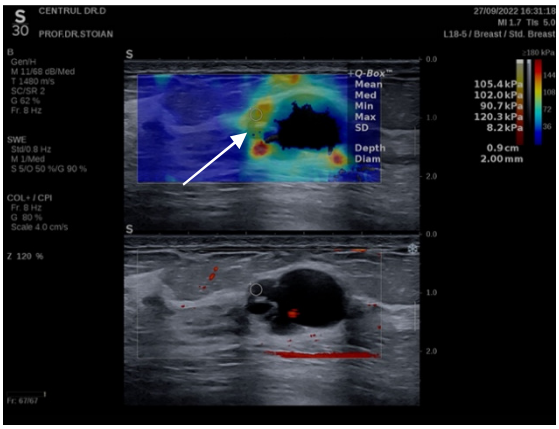

Fig. 9.5.13: Intense hypoechoic lesion. ES=0 Desmoplastic peritumoral reaction ES =4, E Max = 120 kPa, Path CDI

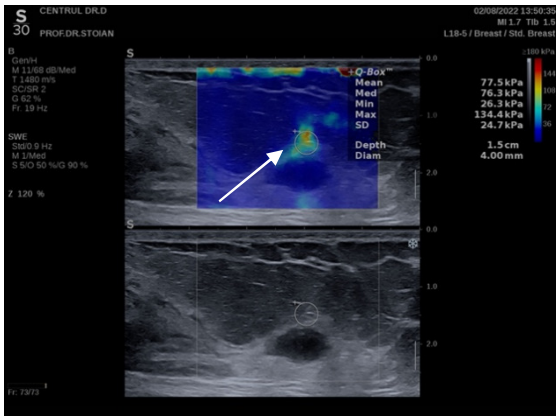

Fig. 9.5.14: Markedly hypoechoic solid lesion ES=1 Desmoplastic peritumoral reaction ES=3 E Max = 134 kPa, Path: CDI

There also really soft cancers, usually small, low grade invasion cancers, mucinous, papillary metaplastic or tubular cancers, with high elasticity compared to the invasive ones, either ductal or lobar variants (73,80,81) (Fig. 9.5.15 and 9.5.16).

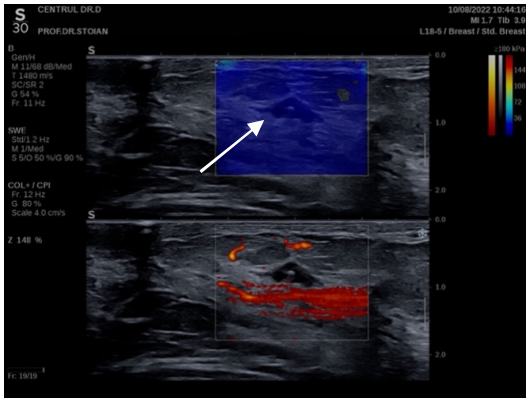

Fig. 9.5.15: Solid lesion B3, ES=1, Path: CDIS

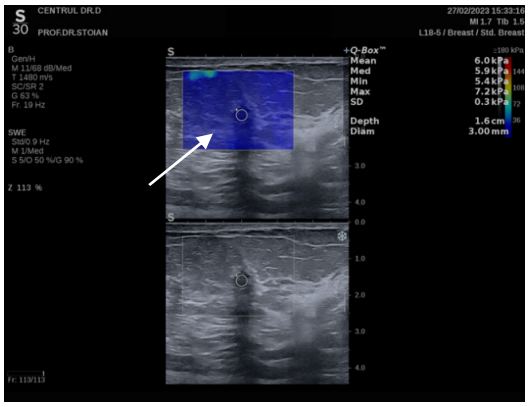

Fig. 9.5.16: Solid lesion B5 ES=1, Path: Mucinous cancer

False positive results are more frequent, such as fibrosis, tumoral necrosis or cheloid scars (82), which are some of the intraglandular entities that can falsely induce increased stiffness. Sclerosant adenosis (83) is stiffer than healthy glandular tissue, but softer than most breast cancers (73,84). There are no significant differences among benign disease entities, such as fibrocystic mastosis, adenosis, fibroadenoma, intraglandular papilloma or inflammation (84). Mastitis and fat necrosis also generate false positive results (9). The same is observed in radial sclerosant scars that can associate increase rigidity (9,85).

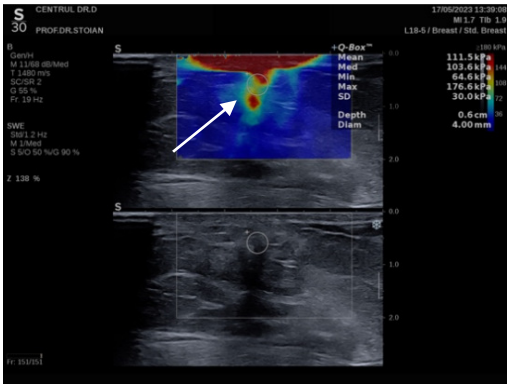

Fig. 9.5.17: B-4c, ES=4, E Max = 176 kPa Path: Steatonecrosis

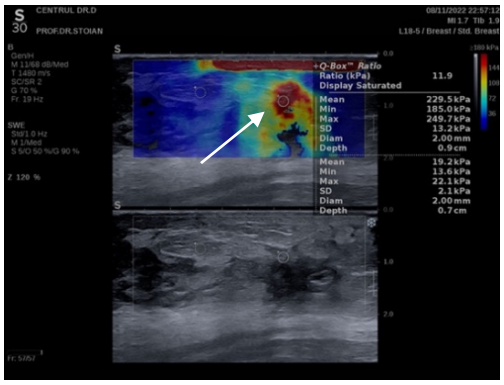

Fig 9.5.18: B-4a, ES=5, E Max = 249.7 kPa Path: Sclerosant scar tissue

Foreign body granuloma, respectively intraglandular cheloid scars can also mimic malignancy, due to increased stiffness (Fig. 9.5.19)

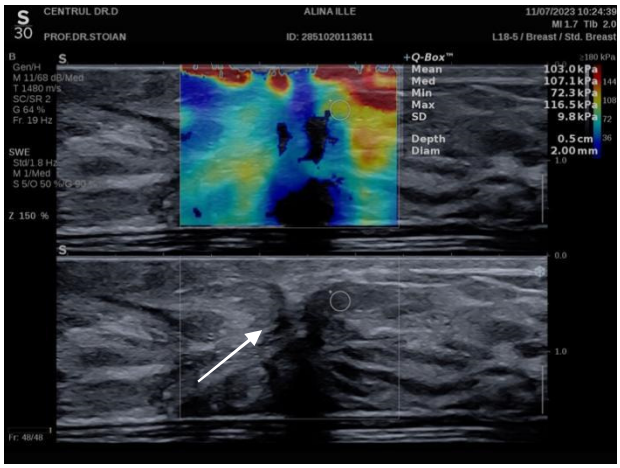

Fig. 9.5.19 Architectural distortion, retractile effect B-4, ES=4, E_{Max} = 116/5 kPa. Path: foreign body granuloma

Calcification, that can frequently induce distortion both in gray scale and strain elastography (42–44), alter the 2D – SWE measurements less (70) (86). Calcification can be seen both in benign and malignant lesions, but shear wave elastography can differentiate between these, with benign calcification defined by values of elasticity E_{Max} 62.8 ± 64.7 kPa, respectively malignant calcification identified by elasticity values of 114.6 ± 70.0 kPa, for in situ carcinoma respectively of E_{Max} 171.9 ± 59.0 kPa (Fig 9.5.2- - 9.5.23) for invasive variants (70).

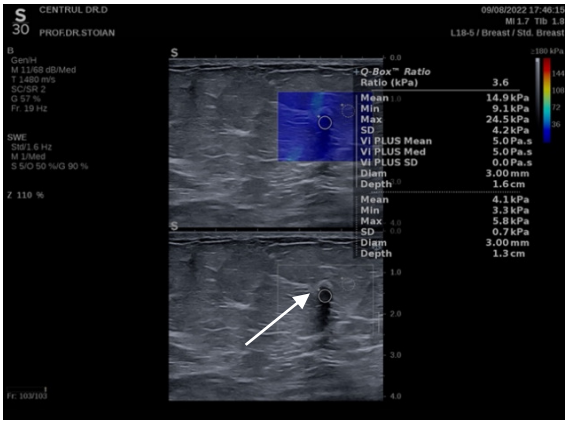

Fig. 9.5.20: Eggshell calcification ES=1
E_{Max} = 24.5 kPa, Path: calcified fibroadenoma

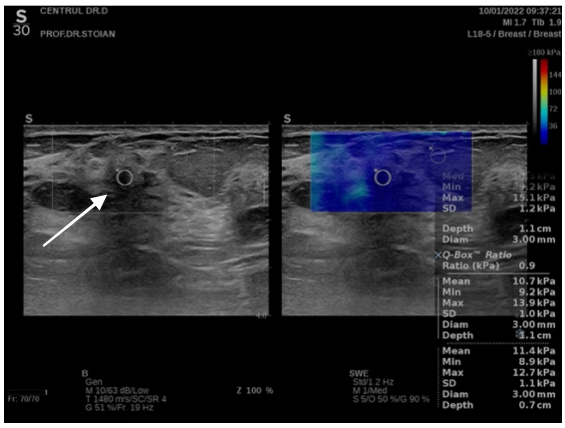

Fig. 9.5.21: Non mass microcalcification ES=1
E_{Max} = 13.9 kPa Path: sclerosant adenosis

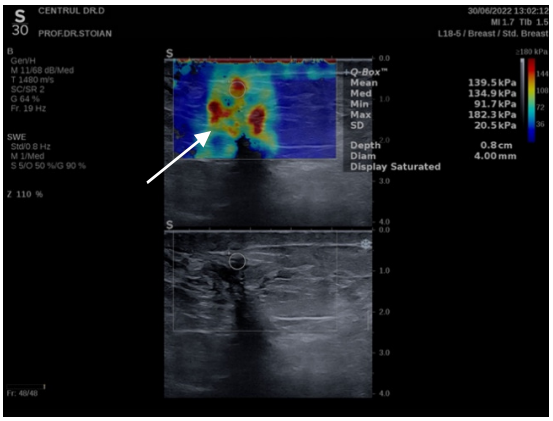

Fig. 9.5.22. Intranodular calcifications ES=4
E_{Max} = 182.3 kPa Path: CDI

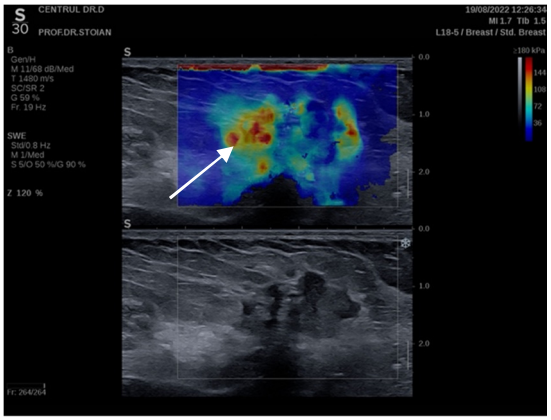

Fig. 9.5.23. Non-mass macrocalcification ES= 4
E_{Max} = 107.5 kPa, Path: CLI

We should mention that there is an overlap between the stiffness of clustered benign calcifications and the punctiform microcalcifications characteristic for in situ carcinoma, so caution is recommended in the integration of 2D SWE elastographic evaluations.

9.6. Integration of Elastography in the Multiparametric Diagnosis of Breast Pathology

It is generally accepted that elastographic information adds value to the gray scale ultrasound evaluation in the diagnosis of breast masses (2,3,9,12,13), by means of complementary data (25). Strain elastography offers greater sensitivity, whereas 2D-SWE offers greater in the differential diagnosis of benign versus malignant pathology (67,87). In an ideal situation, both elastography methods can be offered, since the two techniques are complementary (9). There are already vendors that offer this concomitant elastography technique.

From the perspective of integrating elastographic information in the BIRADS system, the WFUMB proposes the following arguments, valid for each elastographic technique (25):

- BIRADS 2: Tsukuba 1, E/B < 1, SR < 2.8, E_{Max} < 20 kPa or SWV < 2.6 m/s
- BIRADS 3: Tsukuba 2, E/B =1, SR = 2.9 – 4.5, E_{Max} 20-60 kPa or SWV = 2.6 – 4.5m/s
- BIRADS 4: Tsukuba 3, E/B > 1, SR > 4.5, E_{Max} > 60 kPa or SWV > 4.5 – 5.2 m/s
- BIRADS 5: Tsukuba 4 or 5, E/B > 1, SR > 4.5, E_{Max} > 80 kPa or SWV > 5.2 m/s

The ideal proposed scenario, with **concomitant stepwise elastography** evaluation, with referral to core biopsy if there is concordance of stiffness in both strain and shear wave elastography, regardless of the BIRADS category. False results are expected in mastitis, fat necrosis and some old calcified fibroadenoma.

When both elastography images are concordant to benignity, risk downgrade from B 4a category is recommended, to B 3, and ultrasound follow-up instead of core biopsy. False negative results are expected in lymphoma, which are always soft. B-4b, B-4c and B-5 categories are never to be downgraded, regardless of elastographic characteristics.

In case of discordance in elastography, strain versus shear wave, shear wave elastography upgrades strain elastography (9).

Currently, most diagnostic centres only offer one elastographic technique, SE or SWE. Most international guidelines recommend elastography as additional evaluation besides conventional gray scale ultrasound evaluation, to increase confidence in the diagnosis, and risk reassignment according to the lesion elasticity (1,20,25).

Risk downgrade, with routine follow-up, is recommended in soft B-3 lesions (Fig 9.6.1 a, b) (20,25) defined by TSUKUBA 1 color code (SE) dark blue color code (2D-SWE), respectively a value of E_{Max} lower than 20 kPa (11).

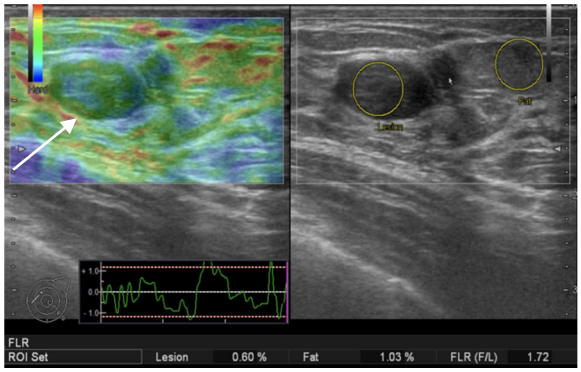

Fig. 9.6.1.a: B-3. TSUKUBA 1
Path: Fibroadenoma

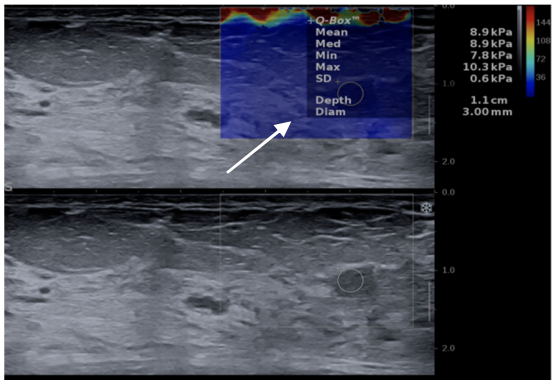

Fig. 9.6.1.b. B-3. ES=1, E_{Max} = 10,3 kPa
Path: Simple hyperplasia

Risk downgrade of B4a to B3 category, with active follow-up after three months instead of core biopsy, is recommended for entirely soft lesions (Fig. 9.6.2.a-b) (20,25). Soft is defined as Tsukuba category 1 and 2, for SE, respectively dark or light blue for 2D-SWE, respectively a value of E_{Max} lower than 80 kPa (11). The previously described threshold for E_{Max} lower than 20 kPa generates a 0% rate of false negative results.

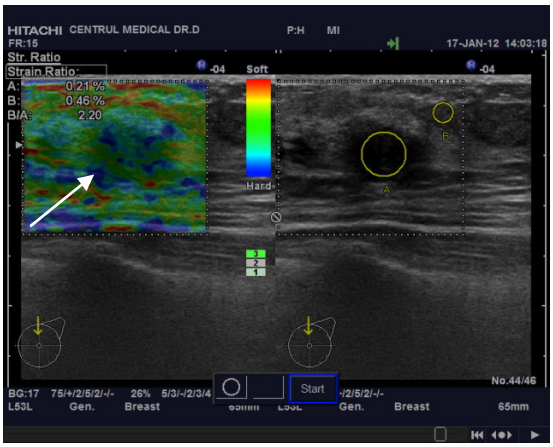

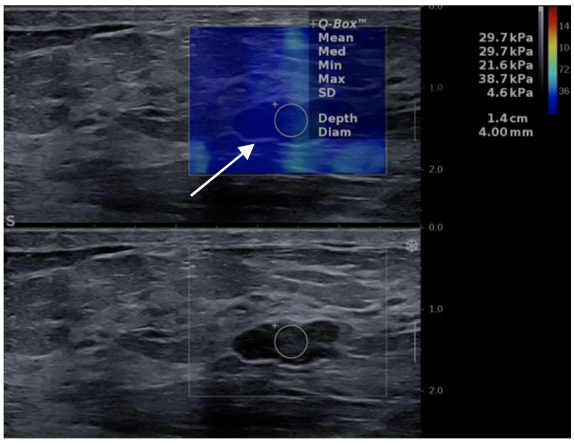

Fig 9.7.2.a: Downgrade B-4a to B-3, TSUKUBA 2 **b: Downgrade B-4a B-3 ES=2, E_{Max} =38,7 kPa**

The identification of stiffness imposes the risk upgrade for B-3 to B-4a, with immediate referral to core biopsy (20,25). Stiffness is considered for Tsukuba 3 or 4 (SE) category, yellow/red colour code for 2D-SWE or for a E_{MAX} value higher than 160 kPa (2D-SWE) (Fig. 9.7.3.a-b).

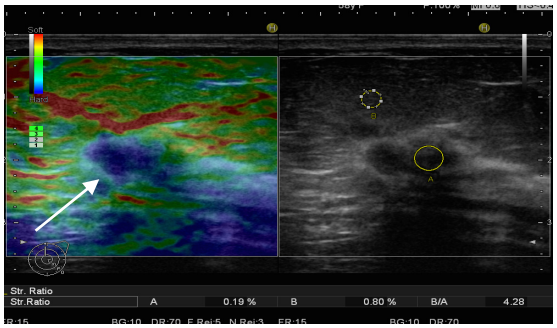

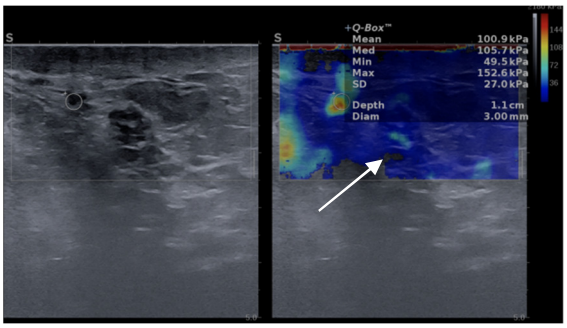

Fig. 9.7.3.a: Upgrade B-3 to B-4a, TSUKUBA 4 **b: Upgrade B-3 to B-4a,ES=2, E_{Max}=152.6 kPa**

BIRADS 4b and 5 categories are never to be downgraded (Fig. 9.7.4.a-b), but additional stiffness re-emphasizes the urgent need for core biopsy (11,20,25) (Fig. 9.7.5 a-b).

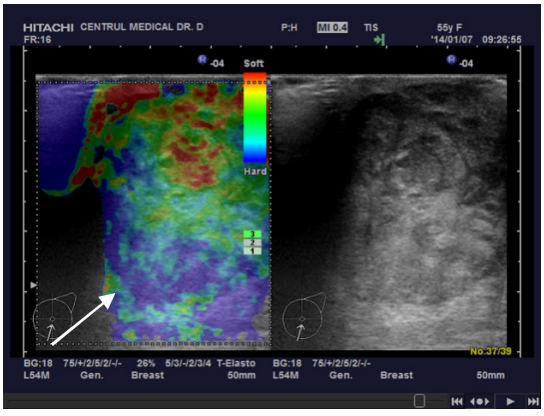

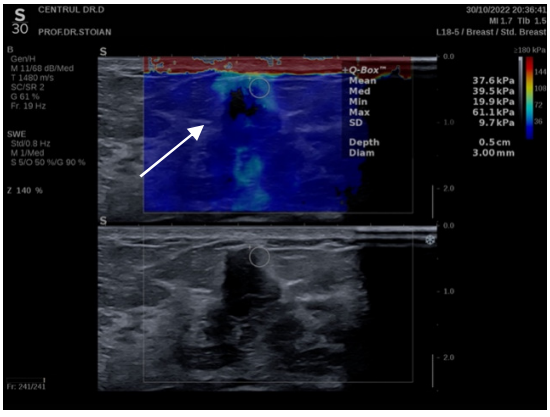

Fig. 9.7.4.a. B- 5 regardless TSUKUBA 2 **b. B-5 regardless ES=2, E_{Max} = 61.1 kPa**

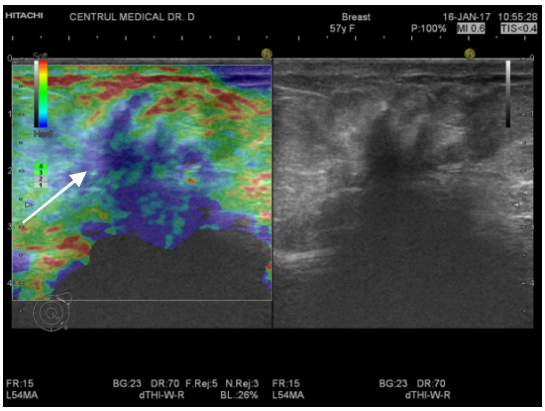

Fig. 9.7.4.a: B - 5, TSUKUBA 4

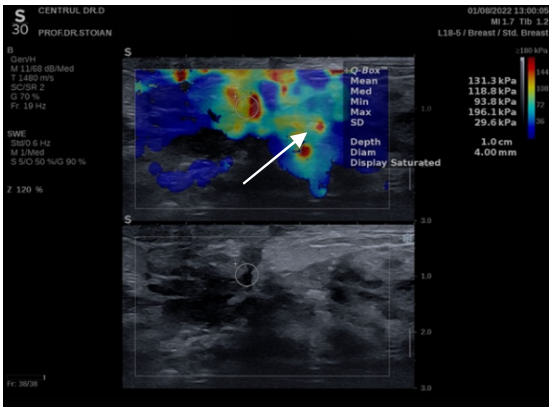

b: BIRADS 4b, B – 5, ES-4, E_{Max}=196 kPa

Additionally, current guidelines suggest, as possible clinical applications of elastography, the reconfirmation of benignity in soft B-3 cases (20), the reconfirmation of fluid content in mixed lesions, as well as the study of the ductal impact of any solid mass (25). Benefits are greater for equivocal nodules, where elastography adds clarifying information. In clear cases, very low risk cystic B-2 cases, or high and very high-risk B-4b, 4c, 5 cases, elastography adds no additional diagnostic value, even if it re-emphasizes the risk category.

Finally, there are data in the literature suggesting the role of 2D SWE in the prediction of the tumoral response to neoadjuvant chemotherapy (74). The reason behind this phenomenon is defined by the predictive role of gene expression in the breast stromal structures in the response to treatment, the tumor stiffness being dependent of the characteristics/content of the stroma compartment (88). In breast cancers, the elasticity of naïve tumor cells is predictive for the cell involution under neoadjuvant treatment (81). The decrease of tumoral stiffness under treatment is a good predictor of the response to treatment, (88–90), and there are descriptions of discriminative threshold values of such variation (89), of at least 36%, differentiating responders from non-responders.

The place of elastography as part of the morphological diagnostic of breast pathology is well defined. There is consensus in respect to the use of elastography, regardless of the technique, in the following aspects:

1. Elastography can be used only in the presence of a mass able to be visualised in grey scale mode.
2. B-3 and 4a lesions can be downgraded in the presence of complete elasticity of the nodule.
3. It confirms the fluid content in transonic or apparent intense hypoechoic lesions.
4. It identifies B-3 lesions that are suspect in the presence of stiffness, with risk upgrade.
5. It indicates risk re-assignment anytime stiffness appears.
6. Additionally, the shear-wave technique allows for active follow-up of breast cancer lesions, with a predictive role in the response to neoadjuvant treatment.
7. The degree of tumoral stiffness is an evolution predictor.

References

1. Breast Imaging Reporting & Data System | American College of Radiology [Internet]. [cited 2024 Jan 6]. Available from: https://www.acr.org/Clinical-Resources/Reporting-and-Data-Systems/Bi-Rads
2. Amy D, Amy D. Breast Elastography. Elastography - Applications in Clinical Medicine. 2022 Apr 9; Available from: https://www.intechopen.com/chapters/81178
3. Amy D, Bercoff J, Bibby E. Breast elastography. Lobar Approach to Breast Ultrasound 2018 Jun 6; 85–106. Available from: https://link.springer.com/chapter/10.1007/978-3-319-61681-0_7
4. Zanello PA, Robim AFC, de Oliveira TMG, Elias J, de Andrade JM, Monteiro CR, et al. Breast ultrasound diagnostic performance and outcomes for mass lesions using Breast Imaging Reporting and Data System category 0 mammogram. Clinics. 2011 Jan 1;66(3):443–8.
5. Duijm L, Guit GL, Zaat JOM, Koomen AR, Willebrand D. Sensitivity, specificity and predictive values of breast imaging in the detection of cancer. British Journal of Cancer 1997;76(3):377–81.
6. Hong AS, Rosen EL, Soo MS, Baker JA, Hong AS, Rosen EL, et al. BI-RADS for Sonography: Positive and Negative Predictive Values of Sonographic Features. AJR 2012 Nov 23;184(4):1260–5.
7. Krouskop TA, Wheeler TM, Kallel F, Garra BS, Hall T. Elastic Moduli of Breast and Prostate Tissues under Compression. Ultrason Imaging 1998 Oct 1;20(4):260–74.
8. Garra BS, Cespedes EI, Ophir J, Spratt SR, Zuurbier RA, Magnant CM, et al. Elastography of breast lesions: initial clinical results. Radiology. 1997 ;202(1):79–86.
9. Barr RG. Breast Elastography: How to Perform and Integrate Into a “Best-Practice” Patient Treatment Algorithm. J Ultrasound Med [Internet]. 2020 Jan 1 ;39(1):7–17.
10. Barr RG, Zhang Z. Effects of precompression on elasticity imaging of the breast: development of a clinically useful semiquantitative method of precompression assessment. J Ultrasound Med. 2012 Jun 1 [cited 2024 Jan 9];31(6):895–902.
11. Chang JM, Moon WK, Cho N, Yi A, Koo HR, Han W, et al. Clinical application of shear wave elastography (SWE) in the diagnosis of benign and malignant breast diseases. Breast Cancer Res Treat. 2011 Aug [cited 2024 Jan 16];129(1):89–97.
12. Barr RG. Future of breast elastography. Ultrasonography. 2019;38(2):93–105.
13. Barr RG. Sonographic breast elastography: a primer. J Ultrasound Med [Internet]. 2012 May 1;31(5):773–83.
14. Itoh A, Ueno E, Tohno E, Kamma H, Takahashi H, Shiina T, et al. Breast disease: clinical application of US elastography for diagnosis. Radiology. 2006 May;239(2):341–50.
15. Barr RG, Lackey AE. The utility of the “bull’s-eye” artifact on breast elasticity imaging in reducing breast lesion biopsy rate. Ultrasound Q. 2011 Sep 1;27(3):151–5.
16. Breast elastography: A new paradigm in diagnostic breast imaging • APPLIED RADIOLOGY.
17. Dong M, Xing B, Zhang B, Xu X, Zhou Q. META-ANALYSIS OPEN ACCESS Diagnostic Performance and Accuracy of Strain Elastography for BI-RADS Category 4 Lesions among Asian Females. Journal of the College of Physicians and Surgeons Pakistan.;2023(10):1181–7.
18. Sadigh G, Carlos RC, Neal CH, Dwamena BA. Accuracy of quantitative ultrasound elastography for differentiation of malignant and benign breast abnormalities: a meta-analysis. Breast Cancer Res Treat. 2012 Aug;134(3):923–31.

19. Mutala TM, Mwango GN, Aywak A, Cioni D, Neri E. Determining the elastography strain ratio cut off value for differentiating benign from malignant breast lesions: systematic review and meta-analysis. Cancer Imaging. 2022 Dec 1;22(1):1–13.
20. Cosgrove D, Piscaglia F, Bamber J, Bojunga J, Correas JM, Gilja OH, et al. EFSUMB Guidelines and Recommendations on the Clinical Use of Ultrasound Elastography. Part 2: Clinical Applications Ultraschall in Med 2013; 34: 238-253 © Georg Thieme Verlag KG Stuttgart · New York ·. 2013
21. Sousaris N, Barr RG. Sonoelastography of Breast Lymphoma. Ultrasound Q [Internet]. 2016 Sep 1;32(3):208–11.
22. Sousaris N, Barr RG. Sonographic Elastography of Mastitis. J Ultrasound Med [Internet]. 2016 Aug 1 [cited 2024 Jan 7];35(8):1791–7.
23. Barr RG, De Silvestri A, Scotti V, Manzoni F, Rebuffi C, Capittini C, et al. Diagnostic Performance and Accuracy of the 3 Interpreting Methods of Breast Strain Elastography: A Systematic Review and Meta-analysis. J Ultrasound Med. 2019 Jun 1;38(6):1397–404.
24. Chang JM, Moon WK, Cho N, Kim SJ. Breast mass evaluation: factors influencing the quality of US elastography. Radiology. 2011 Apr;259(1):59–64.
25. Barr RG, Nakashima K, Amy D, Cosgrove D, Farrokh A, Schafer F, et al. WFUMB guidelines and recommendations for clinical use of ultrasound elastography: Part 2: Breast. Ultrasound Med Biol. 2015 May 1;41(5):1148–60.
26. Song G, Jing L, Yan M, Cong S, Xuejiao W. Influence of various breast factors on the quality of strain elastograms. J Ultrasound Med [Internet]. 2015 Mar 1;34(3):395–400.
27. Zou H, Xue Y, Ou Y, Li S, Zhao Y, Shao L, et al. Factors Affecting the Quality of Breast Quasistatic Ultrasound Elastograms. J Ultrasound Med. 2018 Jul 1;37(7):1701–12.
28. Faruk T, Islam MK, Arefin S, Haq MZ. The Journey of Elastography: Background, Current Status, and Future Possibilities in Breast Cancer Diagnosis. Clin Breast Cancer . 2015 Oct 1;15(5):313–24.
29. Balleyguier C, Ciolovan L, Ammari S, Canale S, Sethom S, Al Rouhbane R, et al. Breast elastography: The technical process and its applications. Diagn Interv Imaging. 2013 May 1;94(5):503–13.
30. Rad Tech CE, ASRT, ARRT® CE, Category A Credits | Radiology Continuing Education.
31. Goddi A, Bonardi M, Alessi S. Breast elastography: A literature review. J Ultrasound. 2012 Sep;15(3):192.
32. Wang Y, Ikeda DM, Narasimhan B, Longacre TA, Bleicher RJ, Pal S, et al. Estrogen receptor-negative invasive breast cancer: imaging features of tumors with and without human epidermal growth factor receptor type 2 overexpression. Radiology. 2008 Feb;246(2):367–75.
33. Rare types of breast cancer | Cancer Research UK https://www.cancerresearchuk.org/about-cancer/breast-cancer/types/rare-types-breast-cancer
34. Mori M, Tsunoda H, Kawauchi N, Kikuchi M, Honda S, Suzuki K, et al. Elastographic evaluation of mucinous carcinoma of the breast. Breast Cancer. 2012 ;19(1):60–3.
35. Wang PL, Zheng FY, Lu Q, Xia HS, Huang BJ, Liu LM, et al. Imaging features of pure mucinous breast carcinoma: correlation with extracellular mucus content. Clin Radiol. 2019 Jul 1;74(7):569.e9-569.e17.
36. Balleyguier C, Ciolovan L, Ammari S, Canale S, Sethom S, Al Rouhbane R, et al. Breast elastography: The technical process and its applications. Diagn Interv Imaging. 2013 May 1;94(5):503–13.

37. Farrokh A, Wojcinski S, Degenhardt F. Evaluation of Real-Time Tissue Sono-elastography in the Assessment of 214 Breast Lesions: Limitations of This Method Resulting from Different Histologic Subtypes, Tumor Size and Tumor Localization. Ultrasound Med Biol. 2013 Dec 1;39(12):2264–71.
38. Lee NR, Oh HK, Jeong YJ. Clinical Significance of Ultrasound Elastography and Fibrotic Focus and Their Association in Breast Cancer. J Clin Med. 2022 Dec 1;11(24):7435.
39. Liu T, Babaniyi OA, Hall TJ, Barbone PE, Oberai AA. Noninvasive In-Vivo Quantification of Mechanical Heterogeneity of Invasive Breast Carcinomas. PLoS One. 2015 Jul 8 ;10(7):e0130258.
40. Hayashi M, Yamamoto Y, Sueta A, Tomiguchi M, Yamamoto-Ibusuki M, Kawasoe T, et al. Associations Between Elastography Findings and Clinicopathological Factors in Breast Cancer. Medicine. 2015;94(50).
41. Rago T, Santini F, Scutari M, Pinchera A, Vitti P. Elastography: New Developments in Ultrasound for Predicting Malignancy in Thyroid Nodules. J Clin Endocrinol Metab. 2007 Aug 1;92(8):2917–22.
42. Li Y, Wei XL, Pang KK, Ni PJ, Wu M, Xiao J, et al. A comparative study on the features of breast sclerosing adenosis and invasive ductal carcinoma via ultrasound and establishment of a predictive nomogram. Front Oncol. 2023;13.
43. Huang Q, Nong W, Tang X, Gao Y. An ultrasound-based radiomics model to distinguish between sclerosing adenosis and invasive ductal carcinoma. Front Oncol. 2023;13.
44. Liu W, Li W, Li Z, Shi L, Zhao P, Guo Z, et al. Ultrasound characteristics of sclerosing adenosis mimicking breast carcinoma. Breast Cancer Res Treat . 2020 May 1;181(1):127–34.
45. De Faria E, Fleury C, Rinaldi JF, Piato S, Fleury JC, Roveda D. Radiol Bras. Mai. 2008;41(3):167–72.
46. Liu L, Lin X, Xiang H, Tang G, Li C. Adenoid cystic carcinoma of the breast: a study of five cases. J Radiol Case Rep [Internet]. 2020;14(11)47. Guldogan N, Esen G, Kayadibi Y, Taskin F, Alfatli AO, Boy FNS, et al. Adenoid Cystic Carcinoma of the Breast: Multimodality Imaging Findings and Review of the Literature. Acad Radiol. 2023 Jun 1;30(6):1107–17.
48. Kanagaraju V, Dhivya B, Devanand B, Maheswaran V. Utility of Ultrasound Strain Elastography to Differentiate Benign from Malignant Lesions of the Breast. J Med Ultrasound. 2021 Apr 1;29(2):89.
49. Shehata RMA, El-Sharkawy MAM, Mahmoud OM, Kamel HM. Qualitative and quantitative strain and shear wave elastography paradigm in differentiation of breast lesions. Egyptian Journal of Radiology and Nuclear Medicine. 2022 Dec 1;53(1):1–8.
50. AKO I. Ultrasonic diagnosis of breast lesions combined with “Real-time Tissue Elastography.” 超音波医学 [Internet]. 2013;40(3):257–66.
51. Chico MJ, Causa Andrieu PI, Wernicke A, Pesce K. Breast lactating adenoma, an example of the utility of the radiological-pathological correlation. Clin Imaging. 2021 Mar 1;71:136.
52. Vashi R, Hooley R, Butler R, Geisel J, Philpotts L. Breast imaging of the pregnant and lactating patient: physiologic changes and common benign entities. AJR Am J Roentgenol. 2013;200(2):329–36.
53. Szabo J, Garcia D, Ciomek N, Margolies L. Spuriously aggressive features of a lactating adenoma prompting repeated biopsies. Radiol Case Rep. 2017 Jun 1;12(2):215.

54. Samad S, Phatak S. Role of ultrasonography and elastography of palpable breast masses in pregnancy and lactation with clinical correlation. Journal of Datta Meghe Institute of Medical Sciences University. 2020 Oct 1;15(4):539–46.
55. Tanter M, Bercoff J, Athanasiou A, Deffieux T, Gennisson JL, Montaldo G, et al. Quantitative assessment of breast lesion viscoelasticity: initial clinical results using supersonic shear imaging. Ultrasound Med Biol. 2008 Sep ;34(9):1373–86.
56. Bercoff J, Tanter M, Fink M. Supersonic shear imaging: a new technique for soft tissue elasticity mapping. IEEE Trans Ultrason Ferroelectr Freq Control. 2004 Apr;51(4):396–409.
57. Nightingale K, Bentley R, Trahey G. Observations of Tissue Response to Acoustic Radiation Force: Opportunities for Imaging. http://dx.doi.org/101177/016173460202400301. 2002 Jul 1;24(3):129–38.
58. Bai M, Du L, Gu J, Li F, Jia X. Virtual touch tissue quantification using acoustic radiation force impulse technology: initial clinical experience with solid breast masses. J Ultrasound Med. 2012 Feb 1;31(2):289–94.
59. Balleyguier C, Ciolovan L, Ammari S, Canale S, Sethom S, Al Rouhbane R, et al. Breast elastography: the technical process and its applications. Diagn Interv Imaging. 2013];94(5):503–13.
60. Nightingale K, Soo MS, Nightingale R, Bentley R, Trahey G. In vivo demonstration of acoustic radiation force impulse (ARFI) imaging in the thyroid, abdomen, and breast. Proceedings of the IEEE Ultrasonics Symposium. 2001;2:1633–8.
61. Meng W, Zhang G, Wu C, Wu G, Song Y, Lu Z. Preliminary results of acoustic radiation force impulse (ARFI) ultrasound imaging of breast lesions. Ultrasound Med Biol. 2011 Sep ;37(9):1436–43.
62. Magalhães M, Belo-Oliveira P, Casalta-Lopes J, Costa Y, Gonçalo M, Gomes P, et al. Diagnostic Value of ARFI (Acoustic Radiation Force Impulse) in Differentiating Benign From Malignant Breast Lesions. Acad Radiol. 2017 Jan 1;24(1):45–52.
63. Bai M, Du L, Gu J, Li F, Jia X. Virtual touch tissue quantification using acoustic radiation force impulse technology: initial clinical experience with solid breast masses. J Ultrasound Med. 2012 Feb 1;31(2):289–94.
64. Tozaki M, Isobe S, Yamaguchi M, Ogawa Y, Homma K, Saito M, et al. Ultrasonographic elastography of the breast using acoustic radiation force impulse technology: preliminary study. Jpn J Radiol. 2011 Jul;29(6):452–6.
65. Bulum A, Ivanac G, Divjak E, Biondić Špoljar I, Džoić Dominković M, Bojanić K, et al. Elastic Modulus and Elasticity Ratio of Malignant Breast Lesions with Shear Wave Ultrasound Elastography: Variations with Different Region of Interest and Lesion Size. Diagnostics 2021, Vol 11, Page 1015. 2021 Jun 1 [cited 2024 Jan 14];11(6):1015.
66. Tozaki M, Fukuma E. Pattern classification of ShearWave™ Elastography images for differential diagnosis between benign and malignant solid breast masses. Acta Radiol. 2011 Dec;52(10):1069–75.
67. Berg WA, Cosgrove DO, Doré CJ, Schäfer FKW, Svensson WE, Hooley RJ, et al. Shear-wave elastography improves the specificity of breast US: The BE1 multinational study of 939 masses. Radiology. 2012 Feb 1;262(2):435–49.
68. Schäfer FKW, Hooley RJ, Ohlinger R, Hahne U, Madjar H, Svensson WE, et al. ShearWave™ Elastography BE1 multinational breast study: additional SWE™ features support potential to downgrade BI-RADS®-3 lesions. Ultraschall Med. 2013;34(3):254–9.

69. Youk JH, Gweon HM, Son EJ. Shear-wave elastography in breast ultrasonography: the state of the art. Ultrasonography. 2017 Oct 1;36(4):300.
70. Seung P, Choi H, Ko EY, Han BK, Ko ES, Choi JS, et al. Original Contribution EFFECT OF CALCIFICATIONS ON SHEAR-WAVE ELASTOGRAPHY IN EVALUATING BREAST LESIONS. 2021;
71. Park J, Woo OH, Shin HS, Cho KR, Seo BK, Kang EY. Diagnostic performance and color overlay pattern in shear wave elastography (SWE) for palpable breast mass. Eur J Radiol. 2015 Oct 1;84(10):1943–8.
72. Au FWF, Ghai S, Moshonov H, Kahn H, Brennan C, Dua H, et al. Diagnostic performance of quantitative shear wave elastography in the evaluation of solid breast masses: determination of the most discriminatory parameter. AJR Am J Roentgenol. 2014 Sep 1;203(3):E328–36.
73. Kim H, Lee J, Kang BJ, Kim SH. What shear wave elastography parameter best differentiates breast cancer and predicts its histologic aggressiveness? Ultrasonography. 2021;40(2):265.
74. Youk JH, Gweon HM, Son EJ. Shear-wave elastography in breast ultrasonography: the state of the art. Ultrasonography. 2017 Oct 1;36(4):300.
75. Yoon JH, Ko KH, Jung HK, Lee JT. Qualitative pattern classification of shear wave elastography for breast masses: how it correlates to quantitative measurements. Eur J Radiol. 2013;82(12):2199–204.
76. Barr RG. Still on the Learning Curve Shear Wave Imaging of the Breast.;
77. Evans A, Whelehan P, Thomson K, McLean D, Brauer K, Purdie C, et al. Invasive breast cancer: relationship between shear-wave elastographic findings and histologic prognostic factors. Radiology. 2012;263(3):673–7.
78. Evans A, Whelehan P, Thomson K, McLean D, Brauer K, Purdie C, et al. Quantitative shear wave ultrasound elastography: initial experience in solid breast masses. Breast Cancer Res. 2010 Dec 1;12(6).
79. Qu W, He N, Yang X, Yuan C, Zhang G, Wei J, et al. Influence of lesion size on differential diagnosis of benign and malignant breast lesions by real-time two-dimensional shear wave elastography. 2022;
80. Chamming'S F, Latorre-Ossa H, Le Frère-Belda MA, Fitoussi V, Quibel T, Assayag F, et al. Shear wave elastography of tumour growth in a human breast cancer model with pathological correlation. Eur Radiol. 2013 Aug;23(8):2079–86.
81. Evans A, Sim YT, Thomson K, Jordan L, Purdie C, Vinnicombe SJ. Shear wave elastography of breast cancer: Sensitivity according to histological type in a large cohort. Breast. 2016 Apr 1;26:115–8.
82. Aya R, Yamawaki S, Muneuchi G, Naitoh M, Suzuki S. Ultrasound Elastography to Evaluate Keloids. Plast Reconstr Surg Glob Open. 2014 Feb 11;2(2).
83. Hari S, Paul SB, Vidyasagar R, Dhamija E, Adarsh AD, Thulkar S, et al. Breast mass characterization using shear wave elastography and ultrasound. Diagn Interv Imaging. 2018 Nov 1;99(11):699–707.
84. Xu J, Zhang L, Wen W, He Y, Wei T, Zheng Y, et al. Evaluation of standard breast ultrasonography by adding two-dimensional and three-dimensional shear wave elastography: a prospective, multicenter trial. Eur Radiol. 2023 Aug 30;1:1–12.
85. Barr RG. Elastography in clinical practice. Radiol Clin North Am. 2014 Nov 1 ;52(6):1145–62.

86. Gregory A, Mehrmohammadi M, Denis M, Bayat M, Stan DL, Fatemi M, et al. Effect of Calcifications on Breast Ultrasound Shear Wave Elastography: An Investigational Study. PLoS One. 2015 Sep 14;10(9):e0137898.
87. Barr RG, Zhang Z. Shear-wave elastography of the breast: value of a quality measure and comparison with strain elastography. Radiology. 2015 Apr 1;275(1):45–53.
88. Ma Y, Zhang S, Zang L, Li J, Li J, Kang Y, et al. Combination of shear wave elastography and Ki-67 index as a novel predictive modality for the pathological response to neoadjuvant chemotherapy in patients with invasive breast cancer. Eur J Cancer. 2016 Dec 1. 69:86–101.
89. Jing H, Cheng W, Li ZY, Ying L, Wang QC, Wu T, et al. Early evaluation of relative changes in tumor stiffness by shear wave elastography predicts the response to neoadjuvant chemotherapy in patients with breast cancer. Journal of Ultrasound in Medicine. 2016 Aug 1;35(8):1619–27.
90. Ma Y, Zhang S, Li J, Li J, Kang Y, Ren W. Comparison of strain and shear-wave ultrasonic elastography in predicting the pathological response to neoadjuvant chemotherapy in breast cancers. Eur Radiol 2017 Jun 1;27(6):2282–91.

Chapter 10. Elastography of the Thyroid and Parathyroids

Dana Stoian, Andreea Bena, Laura Tăban

Elastography can be considered an extension of clinical examination, specifically palpation. It is viewed as a virtual palpation, with the ability to assess circumscribed nodular lesions beyond the strict evaluation of palpable ones.

Elastography techniques applied in breast nodular pathology (Chapter 9.1) are also used in the evaluation of thyroid pathology: strain elastography (SE) and shear-wave elastography (SWE), as real-time shear-wave elastography, two-dimensional shear-wave elastography (2D-SWE), as well as point shear-wave elastography (pSWE).

The need to implement elastography in the routine ultrasound evaluation of the thyroid arises from several reasons. In the case of diffuse thyroid pathology, by extrapolating findings from hepatology, where elastography is a method for assessing liver fibrosis, with a diagnostic and predictive role for the progression of chronic liver disease (1), efforts are being made to incorporate elastography into the active diagnosis of autoimmune thyroid disease. In the case of nodular thyroid pathology, its significant prevalence in the general population (2), coupled with a relatively low incidence of thyroid cancer in the subgroup of nodular goiter, about 7-15% (3), with extremes ranging from 1 to 35% (4,5), to 38% in thyroidectomy series, requires the most accurate post-ultrasound cases evaluation.

The premises for the use of elastography in the diagnosis of circumscribed thyroid lesions are justified by previous findings (6,7) regarding significant differences between the elastic modulus of healthy thyroid tissue and the tissue affected by autoimmune thyroid disease (8), thyroid adenomas, and malignant pathology (9), with distinctions between follicular and papillary tumors. As mentioned in the chapter dedicated to breast pathology, in the case of nodules, elastography is not a screening technique; it requires the pre-existence of a circumscribed lesion, detected and evaluated through grayscale ultrasound, whose stiffness is directly assessed and compared with that of an adjacent healthy region, either thyroid or muscular structure. The thyroid application of elastography has been available since 2005 for the strain technique (9) and since 2010 for the SWE technique (10).

The guidelines of thyroid societies, such as the American Thyroid Association (ATA) (11) and the American Association of Clinical Endocrinologists (AACE) (12), include elastography in the evaluation algorithm for thyroid nodules, considering it among additional ultrasound criteria. They consider the stiffness of a nodule as a high-risk factor, comparable to the presence of suspicious lateral cervical adenopathies, with valuable roles including the subgroup of nodules with indeterminate cytology on fine-needle aspiration, classified as BETHESDA III and IV (13–19). Additionally, the guidelines of the European Federation of Societies for Ultrasound in Medicine and Biology, (EFSUMB) (20) and the World Federation for Ultrasound in Medicine and Biology (WFUMB) (21) recommend the use of elastography as an additional criterion for monitoring the dynamic evolution of thyroid nodules.

10.1. The Technique of Thyroid Elastography Examination

Elastographic evaluation, either by SE or SWE, is performed using linear, multi-frequency transducers. Correct evaluation requires the adherence to the general rules of the elastographic technique. The depth of the lesion dictates the choice of the transducer frequency. Superficial lesions require the selection of high frequencies, ranging from 12-16 MHz, while deeper lesions necessitate the use of lower frequencies, around 10 MHz. However, the range offered by most vendors, from 5 to18 MHz, is sufficient for a satisfactory elastographic examination (Fig. 10.1.1). The presence of deep lesions, either by profound location of the lesion per se or secondary to a well-represented subcutaneous adipose layer, requires the choice of a lower frequency transducer to ensure deeper penetration (Fig. 10.1.2).

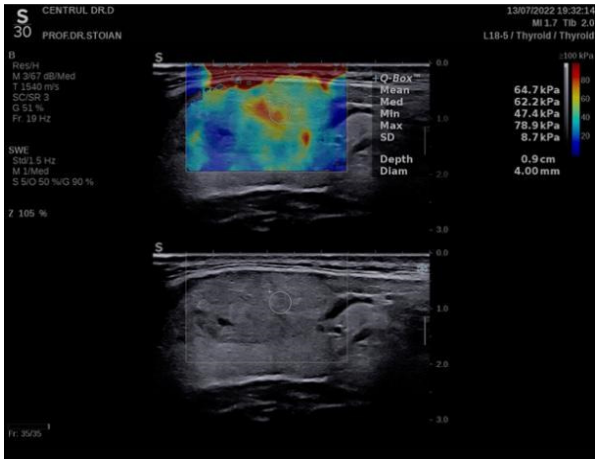

Fig. 10.1.1. Superficial thyroid nodule (1-2 cm); Linear multi-frequency probe 10-15 MHz

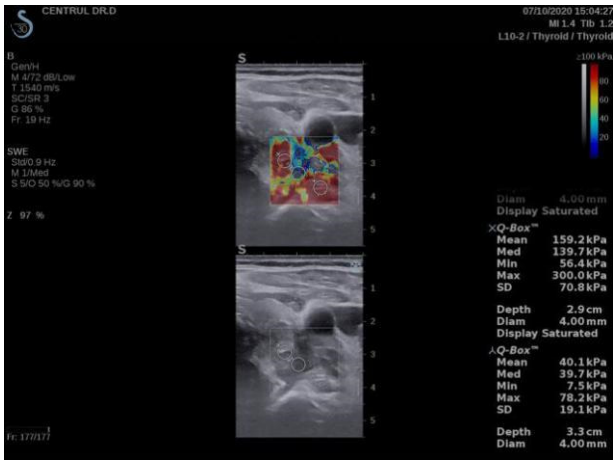

Fig. 10.1.2. Deep thyroid nodule (2.5-4 cm); Linear multi-frequency probe 3-10 MHz

The position of the transducer should be perpendicular to the region being examined, as illustrated in Fig. 10.1.3 (21). Choosing an oblique plane of the transducer relative to the underlying layers is incorrect (Fig. 10.1.4).

Fig.10.1.3. Correct transducer position perpendicular to the examined region

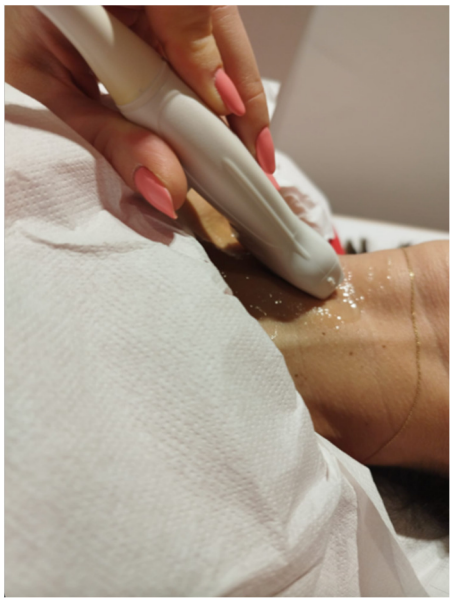

Fig.10.1.4. Incorrect transducer position oblique to the underlying layers

The pressure applied varies across different types of elastography. Each ultrasound device presents a pressure scale, with an optimal range recommended for each vendor. Real-time verification of the pressure quality is achieved by staying within the permissible variation range (Fig 10.1.5) or by maintaining a stable pressure indicator, shown as the green bar in Fig. 10.1.6.

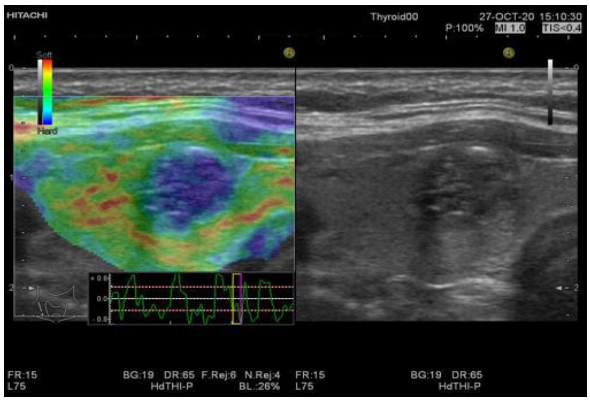

Fig. 10.1.5. Correct Pressure - Hitachi Preirus device

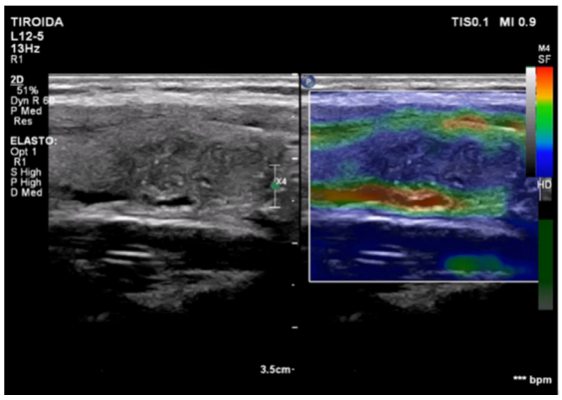

Fig. 10.1.6. Correct Pressure - Philips Epique 10 device

Applying pressures that are too low generates a false-negative image, while high pressures generate false-positive images of increased stiffness (9), as shown in Fig. 10.1.7 and Fig. 10.1.8.

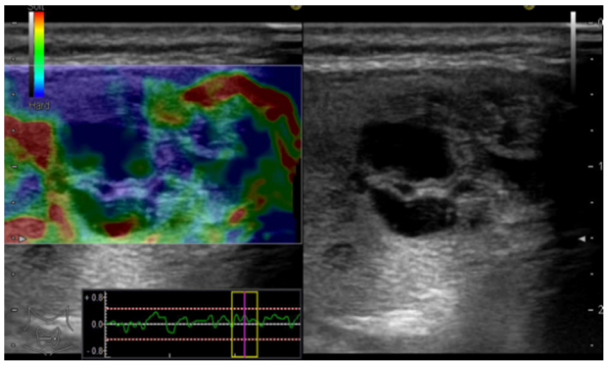

Fig. 10.1.7. Normal Pressure - Correct elastographic score 1

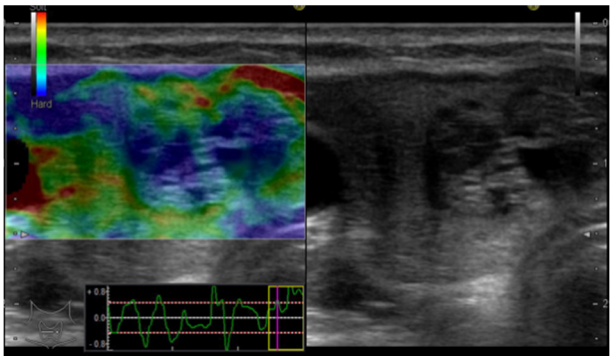

Fig. 10.1.8: Intense External Pressure - False positive score 3

For SWE techniques, applying external pressure is not recommended; rather, the touch should be gentle, without compression. Applying external compression will alter the image, causing vertical artifacts, which will affect the quality of the elastogram (Fig. 10.1.9 a–c).

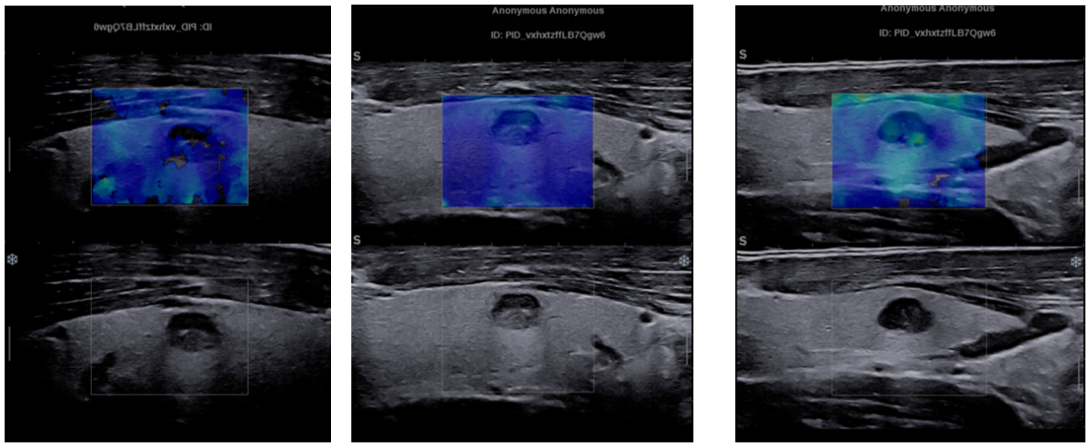

a **b** **c**

Fig. 10.1.9: 2D SWE Elastography:

a) Insufficient pressure – incomplete elastogram
b) Sufficient pressure – complete elastogram
c) Excessive pressure – elastogram with artifacts

Alongside the elastographic image, some systems measure, the technical quality of the procedure in terms of external pressure stability, facilitating the correct selection of image sequences for an elastogram evaluation, as do systems offered by Mindray. Thus, a score of 1-3 stars indicates unstable pressure, resulting in an unusable elastogram, as shown in Fig. 10.1.10, while a score of 4-5 stars confirms the stability of the applied pressure, resulting in a reliable elastographic outcome, as shown in Fig. 10.1.11.

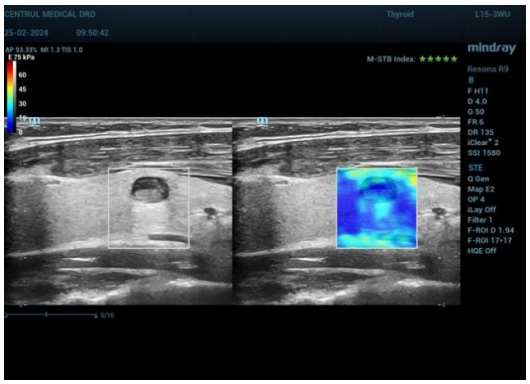

Fig. 10.1.10. Stable Pressure (5 stars)

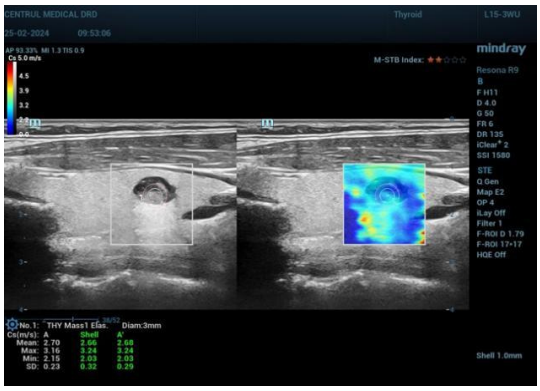

Fig. 10.1.11. Unstable Pressure (2 stars)

Some ultrasound systems ensure the quality of the elastogram by real-time image quality checks, known as the reliability quality map (RLM), where a minimum index of 90% is desired to confirm the quality and accuracy of the elastogram (22).

The **movement of the transducer** varies with the type of elastography, adhering to vendor recommendations. In SWE, no precompression is recommended (1). In strain elastography, external pressure is applied axially with fine, Parkinsonian-type movements (23), used for Hitachi devices. Some vendors recommend avoiding external pressure, utilizing regional pulsations generated physiologically by the carotid artery (18, 24), reducing the variability caused by different levels of external pressure (24, 25). The goal is to maintain a constant displacement rate (26).

Choosing **the field of view (FOV)** involves positioning the nodule in the center of the image, with sufficient adjacent non-nodular thyroid tissue visible for stiffness ratio calculation. Rectangular areas are commonly used, rarely elliptical (27) (Fig. 10.1.12). The neck should be in hyperextension to obtain thinner overlying layers, aiming for superficial sections, as close to the dermis as possible (21).

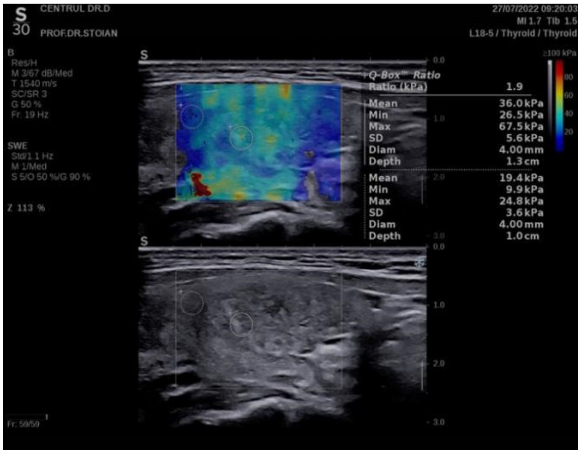

Fig. 10.1.12. Rectangular FOV. Thyroid nodule positioned in the centre of the FOV

As with breast elastography, the SWE technique in thyroid evaluation requires additional **image optimization**. The SWE intensity should be adjusted to the maximum value that does not introduce additional noise artifacts, visible as random hard points in the FOV (Fig. 10.1.13 and 10.1.14).

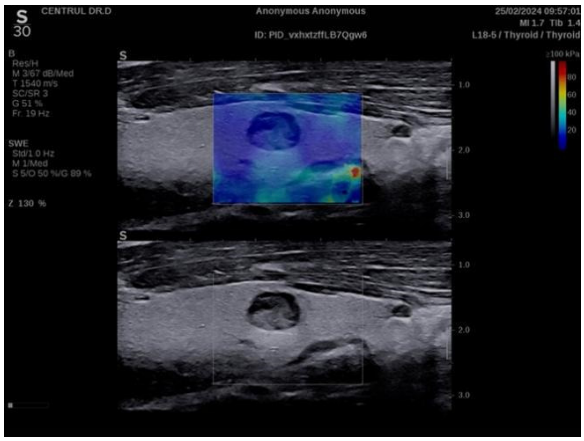

Fig. 10.1.13. Good intensity, complete image without artifacts/noise
Amplification 80%

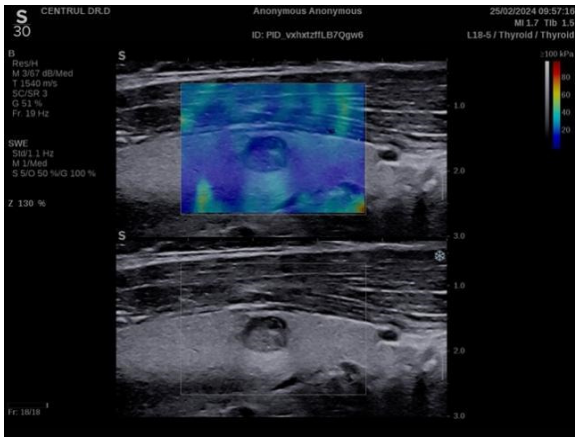

Fig. 10.1.14. Increased intensity, complete image but with visible additional pixels
Amplification 100%

Adjusting the resolution/penetration ratio compared to the standard device settings is necessary when enhancing the resolution for small lesions or adapting the penetration for deep lesions. Additionally, the stiffness scale can be adjusted. Typically, the stiffness scale is automatically calibrated to a maximum of 100 kPa (Fig. 10.1.15.a), but the upper limit can be adjusted up to a maximum of 300 kPa. Adjusting the scale is necessary for a superior visualization of usually hard images (Fig. 10.1.15 c).

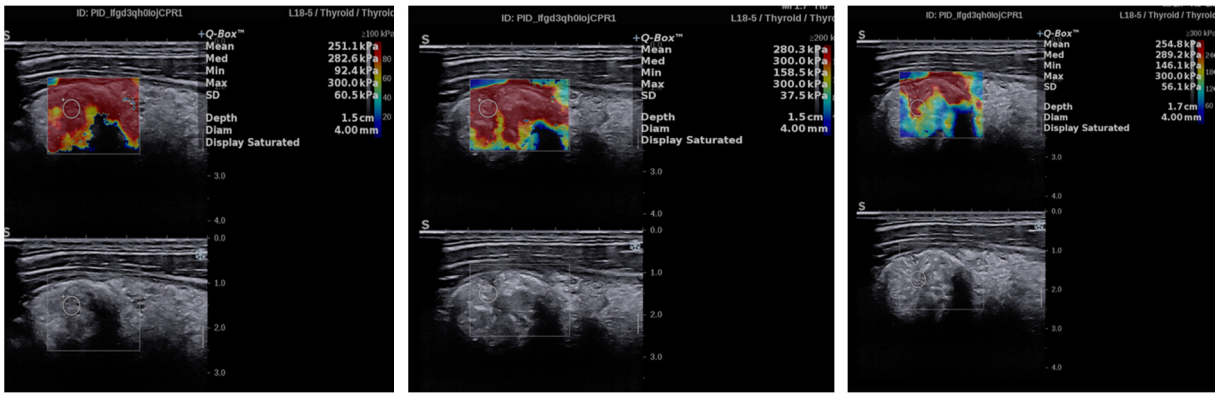

a) Score 5, E_{mean} = 251.1 kPa; b) Score 4, E_{mean} = 280.3 kPa; c) Score 3, E_{mean} = 254.8 kPa

Fig. 10.1.15: Thyroid nodule TIRADS 5. High stiffness

a) Maximum pressure scale 100 kPa
b) Maximum pressure scale 200 kPa
c) Maximum pressure scale 300 kPa

The **patient's position** is a standard one, supine with the neck in hyperextension, holding their breath during the examination (28) and without swallowing during the examination.

10.2. Strain Elastography

Strain elastography, also known as real-time elastography or free hand elastography, evaluates the deformation of structures exposed to a perpendicular displacement force, comparing the deformation of various tissues (21), without directly measuring the stiffness (21). These differences are depicted in the elastographic image alongside real-time B-mode images, allowing for a qualitative or semi-quantitative evaluation (29).

Qualitative reporting presents a map of different tissue deformability (30), resulting in an elastogram in various colours. Typically, red indicates very soft structures with maximum displacement (27), and blue indicates very hard structures with minimal or no deformation. With the increasing number of vendors offering strain elastography equipment, the color codes have become varied.

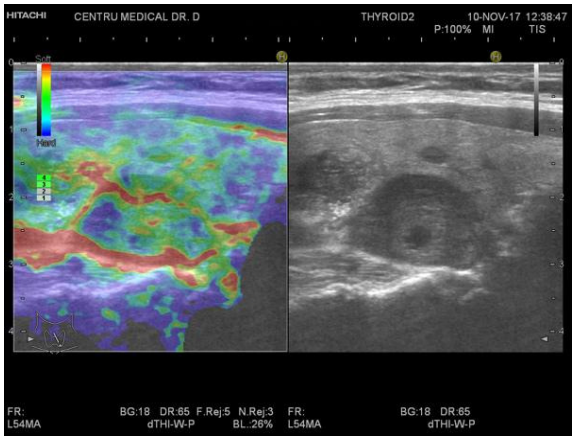

Fig. 10.2.1. Hitachi device color code blue (elastic) – red (hard)

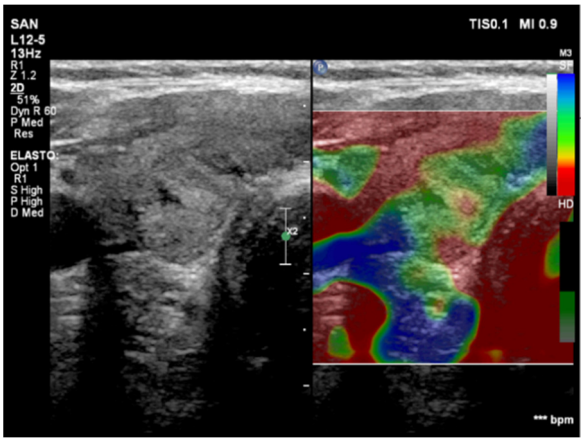

Fig. 10.2.2. Philips device color code red (elastic) – blue (hard)

In qualitative thyroid SE quantification, two classification scales are generally accepted: the Asteria system (31), similar to the breast classification system proposed by Itoh (32), which categorizes nodules into: score 1 – completely soft (Fig. 10.2.3), score 2, predominantly soft nodule (Fig. 10.2.4), score 3 predominantly rigid (Fig. 10.2.5), and score 4 when the nodule is entirely rigid, as in Fig. 10.2.6. Rubaltelli (33) modifies this score, defining subcategories 3a with hard periphery and 3b with a hard centre (Fig. 10.2.7 and 10.2.8).

Scores 1 and 2 are considered suggestive of benignity, while scores 3 and 4 are suggestive of malignancy (31). Considering category 3 as suggestive of benignity increases the method's specificity at the expense of diagnostic sensitivity (27).

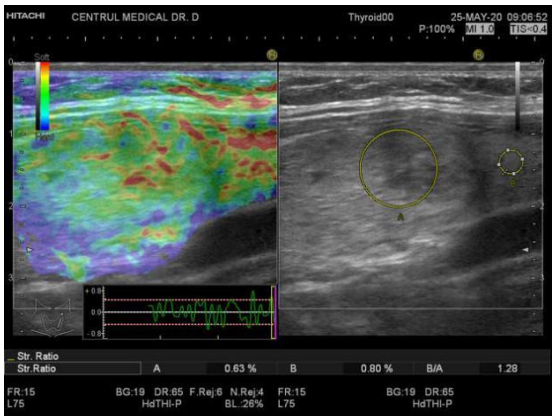

Fig. 10.2.3. ASTERIA 1 - completely soft, HP: Follicular adenoma

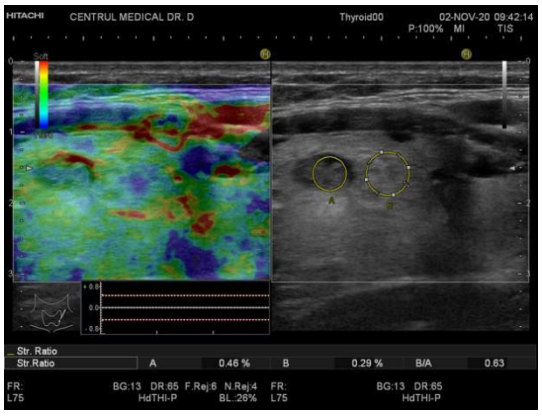

Fig. 10.2.4. ASTERIA 2 - heterogeneous soft, HP: Colloid nodule

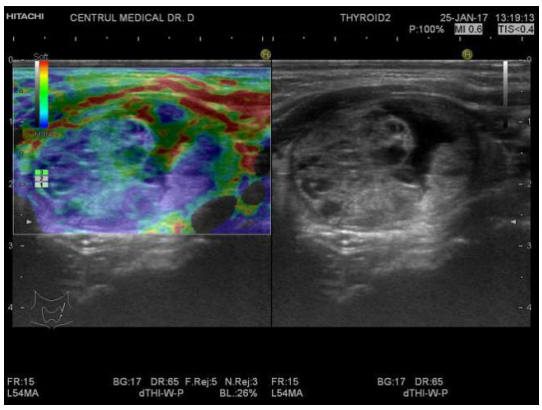

Fig. 10.2.5. ASTERIA 3 central soft, HP: Hurthle Cell Adenoma

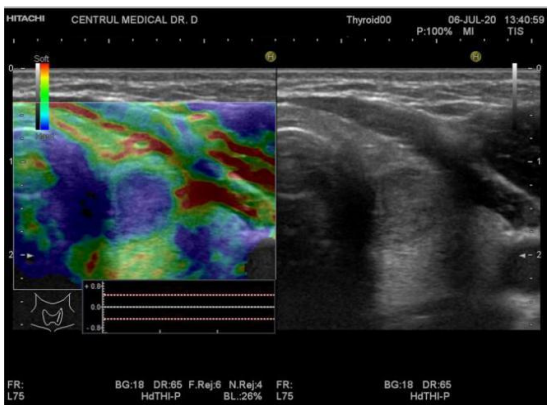

Fig. 10.2.6. ASTERIA 4 completely hard, HP: Papillary thyroid carcinoma (PTC)

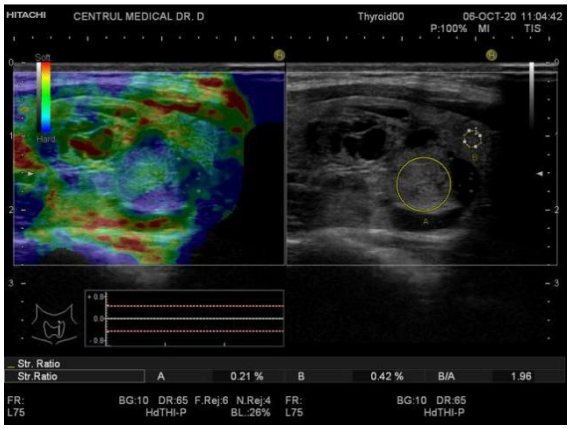

Fig. 10.2.7. ASTERIA 3a central hardness, HP: Nodular autoimmune thyroiditis

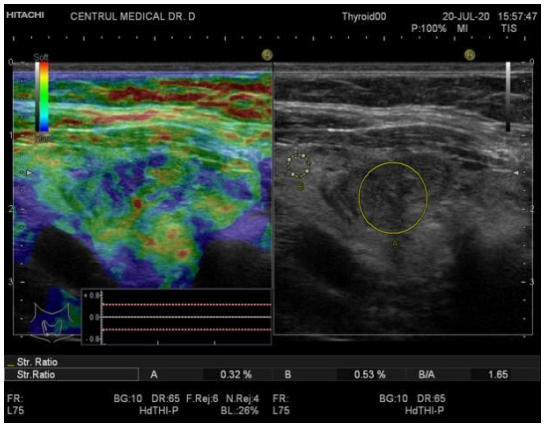

Fig. 10.2.8. ASTERIA 3b, HP: Follicular neoplasia of uncertain potential

The second classification system, known as the Rago score (34), is an extension of the UENO model used in breast elastography. It classifies nodules into five categories: score 1 for completely soft nodules (Fig. 10.2.9), score 2 when elasticity is present in most of the nodule (Fig. 10.2.10), score 3 for elasticity restricted to the nodule periphery (Fig. 10.2.11), score 4 for entirely rigid nodules (Fig. 10.2.12), and score 5 when rigidity extends beyond the nodule as seen in 2B mode (Fig. 10.2.13). Scores 1, 2, and 3 typically indicate benignity, while scores 4 and 5 suggest malignancy (19, 34).

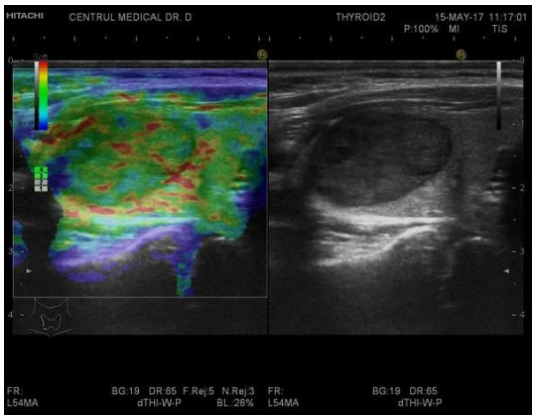

Fig. 10.2.9. RAGO 1 completely soft,
HP: Follicular adenoma

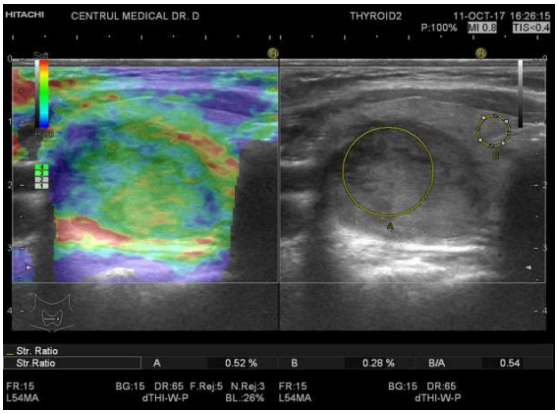

Fig. 10.2.10. RAGO 2 predominantly soft,
HP: Follicular adenoma

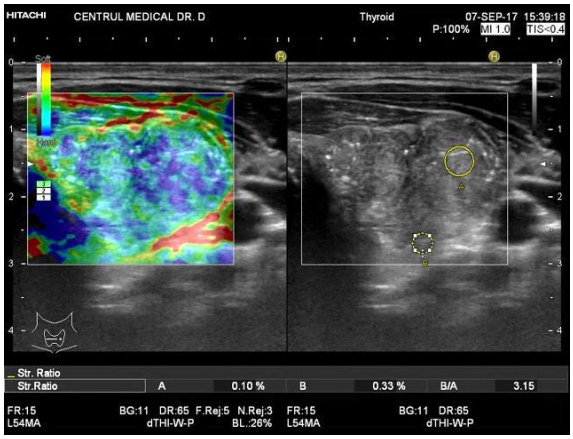

Fig. 10.2.11. RAGO 3 central hard,
HP: PTC

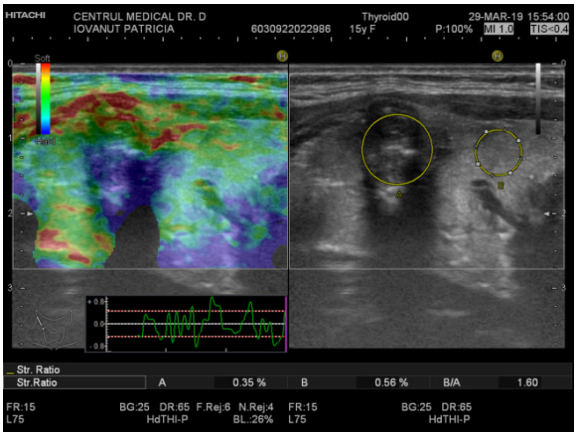

Fig. 10.2.12. RAGO 4 completely hard,
HP: PTC

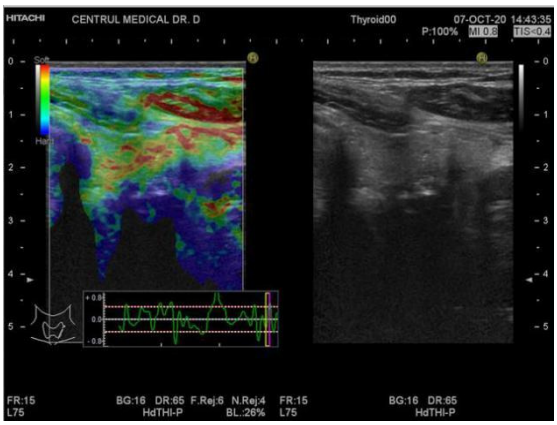

Fig. 10.2.13. RAGO 5,
HP: PTC

In mixed lesions, the elastographic evaluation focuses strictly on the solid component (Fig. 10.2.14 and 10.2.15) (35).

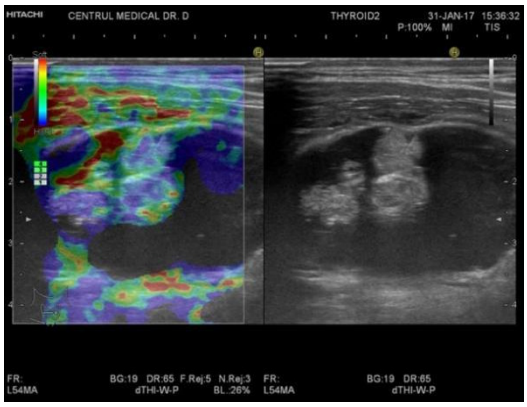

Fig. 10.2.14. Measurement of nodular elasticity in the solid part of the mixed nodule - Score 3, HP: Cystic variant of PTC

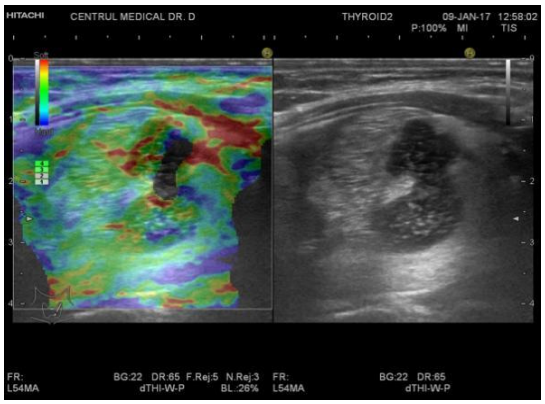

Fig. 10.2.15. Measurement of nodular elasticity in the solid part of the mixed nodule - Score 1, HP: Colloid cystic goiter

There are no differences between elastographic classification systems regarding diagnostic quality (28,36,37). Literature data validate elastography as an additional technique to classical ultrasound. Recent meta-analyses (35,36,38) consider that the stiffness score surpasses standard ultrasound parameters in terms of sensitivity and specificity, with a sensitivity of about 78% and specificity of 78-80%, superior to hypoechogenicity (78% and 55%), irregular margins (66 and 81%), tall shape (46 and 77%), and even the presence of intranodular microcalcifications (50 and 80%). The positive predictive value of higher stiffness scores, 3 and 4, is 13.6%, comparable to the presence of microcalcifications, 16.9%, while the negative predictive value, 97.2%, is superior to any classical ultrasound criterion (35).

There is consensus regarding the diagnostic value of elastography in differentiating benign/malignant nodular pathology (26,29), it being performed as a unique ultrasound evaluation in a cohort of over 13,000 patients (39), with the strain technique showing a cumulative sensitivity of 84%, a cumulative specificity of 81%, and an accuracy of 87.1%.

The rainbow or blue-green-red (BGR) artifact, specific to fluids, is also observed in thyroid fluid lesions (40–42), whether simple cystic lesions (Fig. 10.2.16) or colloidal ones (Fig. 10.2.17).

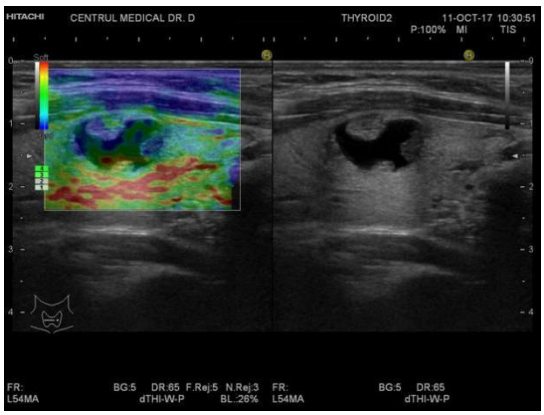

Fig. 10.2.16. BGR artifact, HP: Cystic lesion

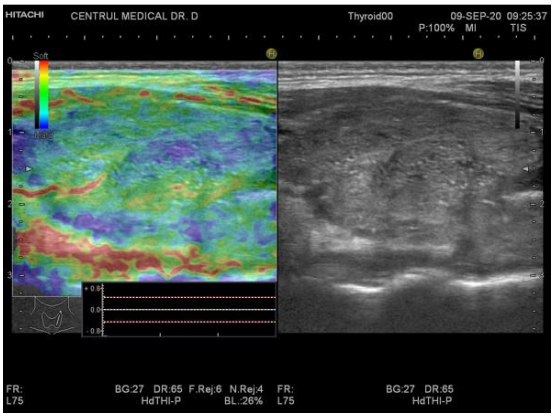

Fig. 10.2.17. BGR artifact, HP: Colloid lesion (granular colloid)

It should be noted that a null elastographic result, observed in large or deep cystic lesions due to the absence of displacement wave transmission (Fig. 10.2.18), is a useful result.

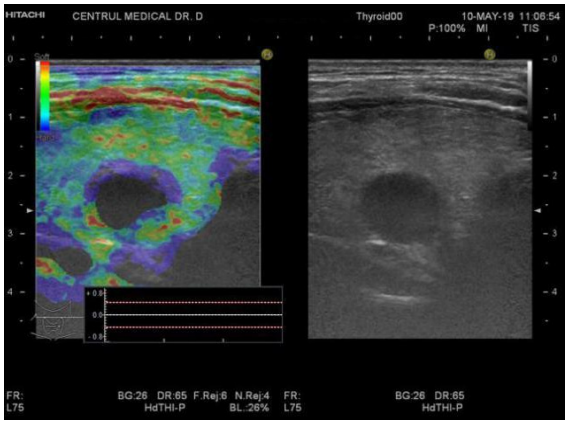

Fig. 10.2.18. Absence of intralesional elastographic image, HP: Simple cystic lesion

Semi-quantitative evaluation compares the stiffness of the nodule to that of the chosen standard, in the case of the thyroid, the adjacent thyroid parenchyma, preferably located at similar depths to the nodule, with a maximum depth difference of 10 mm, as displacement decreases with depth/distance from the plane of the applied external force (28). It is worth mentioning that SE does not directly measure Young's modulus but only evaluates deformability differences between the compared structures (43). Some authors recommend performing three measurements and using their average in the final report (Fig. 10.2.19) (44,45).

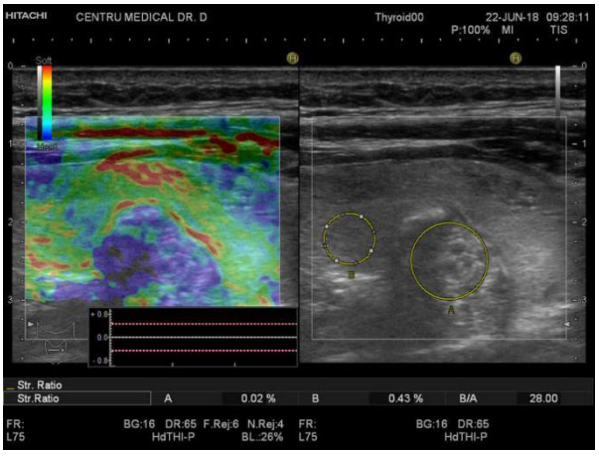

Fig. 10.2.19. Comparable ROI sizes/depths nodule vs. adjacent thyroid parenchyma, HP: PTC

There are controversies in the literature regarding the size and position of the ROI, as to which are the correct size and position. Some authors recommend that the ROI includes the entire nodule and up to 5 mm of perinodular tissue (43,46), but avoiding bone, vascular, or non-thyroid inclusions (21,43). There is no defined single threshold value to discriminate between benign and malignant, with most values falling between 2 and 4 (47), with a wide range between 1 and 5 (21). The stiffness ratio value correlates with the probability of thyroid

cancer, all studies describing significant differences between the mean values of benign tumors and thyroid cancers. If there is no healthy perinodular thyroid parenchyma, an alternative is to use the ipsilateral prethyroid muscle ratio (47).

Although the semi-quantitative technique is more accurate than the qualitative technique (38), its universal use is hindered by the absence of a single threshold value (20). As with breast elastography, there is no single threshold value described (20,21) for differentiating between benign and malignant. Literature articles use threshold values ranging from 2.32 (48) to 2.69 (22), to 4.0 (49) and to 5.03 (50), generally the most widely described range being 1.5 to 5 (21), with different results regarding the method's accuracy for each study. The diagnostic performance of the semi-quantitative technique ranges from 83-96% for sensitivity, 71-85% for specificity (38), with overall diagnostic quality assessed by AUROC at 93%.

Performance data for the semi-quantitative technique vary, some of them demonstrating superiority over qualitative techniques (38,39) with AUROC = 92.9% vs. 89%. However, these data are challenged by other meta-analyses, which either describe similar performance (51) or even inferior performance of the displacement ratio compared to the qualitative elastographic risk score (47). Regardless of the threshold value used, for each vendor and research group, the concept of risk upgrade is also described for the displacement ratio value, SR, considering that each unit added to its value doubles the risk of malignancy (48).

There are a few studies evaluating an alternative technique of strain ultrasound, also called quasistatic, where carotid pulsations are used as the only displacement source. These studies describe encouraging results, with differences between the mean hardness of benign versus malignant lesions (52), including nodules under 1 cm in diameter (52). However, most studies describe carotid-generated displacement as a factor that alters elastogram quality (21). Numerical indices, such as the Thyroid Stiffness index or the systolic thyroid strain index (TSI), and the elasticity contrast index (ECI) are described. For TSI, the carotid and the nodular lesion are placed in the same examination window, implicitly using the transverse section, with the calculation of the ratio between carotid elasticity and maximum intranodular elasticity (43,53). ECI is a parameter measured by Samsung devices, using quasistatic elastography (28), and it compares, similarly to the SR semi-quantitative method, the elasticity ratio between the nodule and the adjacent thyroid parenchyma (54). The dependency of carotid pulsations on age, cardiac pump function, and changes described in cases of pulmonary hypertension, tachyarrhythmias, arteriosclerosis, and pregnancy have limited the widespread use of this alternative technique (21,28).

10.3. Limitations of Strain Elastography

Practicing strain elastography requires an understanding of the technique's limitations. These limitations originate from the specific characteristics of nodular lesions, such as size, position, and the amount of liquid componence, as well as from technical issues like motion artifacts and the proximity of solid planes. Additionally, certain conditions can lead to false-positive and false-negative results.

It is widely accepted that strain elastography is **operator**-dependent (21,27,39). This dependence necessitates an experienced operator skilled in the technique of fine compressive vibrations, which can vary between vendors. Variations in pre-compression contribute to intra- and inter-observer variability (19,55,56). Repeating compression cycles and selecting similar images is recommended to reduce this limitation. The definition of an expert technician is also debatable, with one study suggesting that a minimum of 7 patients is required for expertise, compared to a minimum of 50 patients for expertise in hepatic elastography (57).

Carotid pulsation affects elastographic image stability, especially in tachycardic patients. Transverse section elastograms are more susceptible to this influence than longitudinal sections (21). Moreover, the presence of arrhythmias, atherosclerotic changes, or hypertension can affect the displacement of adjacent tissues (56,58).

The morphological characteristics of the nodular lesion can influence elastography results. The depth of the nodule affects the elastogram quality due to both the penetration limits of the displacement wave and the decrease in displacement wave amplitude with depth (59). Depths greater than 2.5 cm are considered potentially problematic (59,60) (Fig. 10.3.1).

Large nodules that exceed the field of view (FOV) cannot be evaluated elastographically, as seen in Fig. 10.3.2. This is also true for nodules larger than 3 cm or those occupying an entire thyroid lobe (27), preventing the comparison with the adjacent thyroid tissue (21). Some studies consider 3.5 cm as the size limit (61,62).

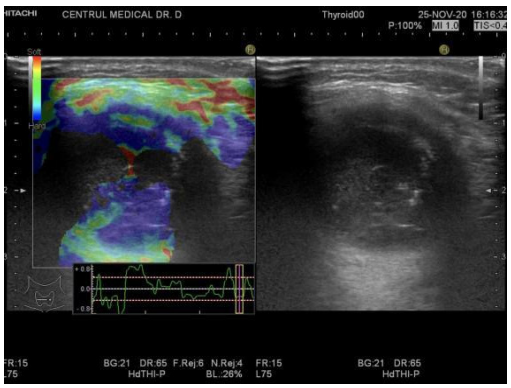

Fig. 10.3.1. Solid nodule, apparently spongiform. Inferior pole at about 3.5 cm in depth. Incomplete elastogram

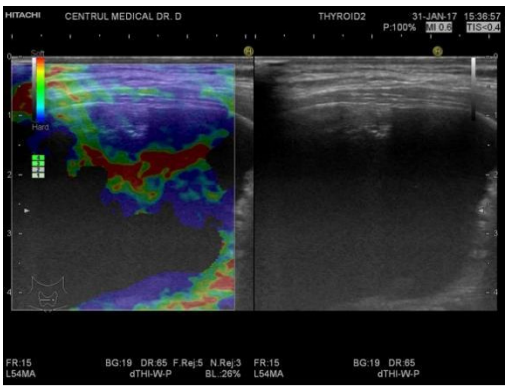

Fig. 10.3.2. Predominantly cystic nodule. Dmax > 4 cm. Intranodular vegetation. Incomplete elastogram

Regarding the optimal minimum nodular size, some studies suggest that elastographic examination is suitable for nodules larger than 1 cm (63,64), while others show diagnostic accuracy for elastography in nodules between 3 and 10 mm (65).

Nodules with a significant *cystic component* will also generate incomplete and unsatisfactory images (Fig. 10.3.3 and 10.3.4) (21).

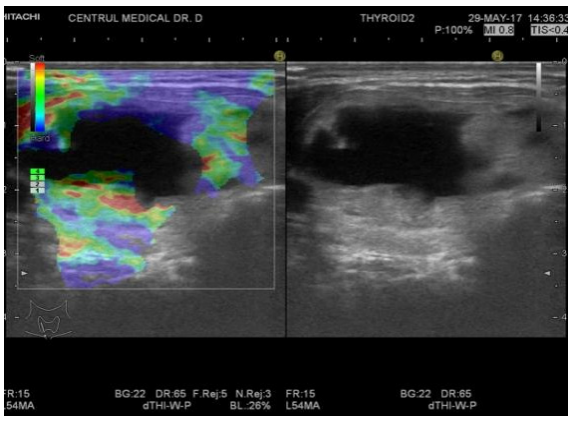

Fig. 10.3.3. Predominantly cystic lesion. Solid vegetation Score 1. Hyperplasia

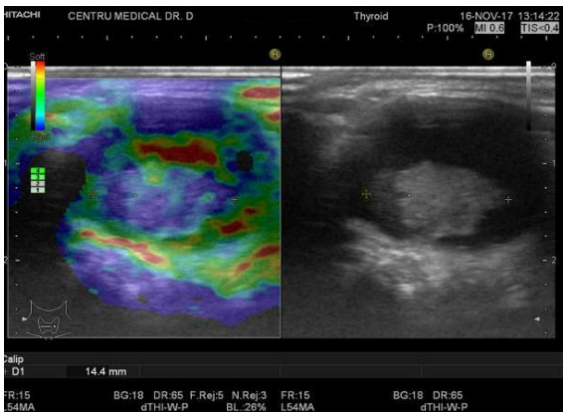

Fig. 10.3.4. Mixed lesion, BGR effect in the fluid portion. Solid vegetation Score 3. Cystic PTC

Another limitation in the elastography interpretation is observed in *coalescent nodules* (66), where such evaluation is not recommended (Fig. 10.3.5).

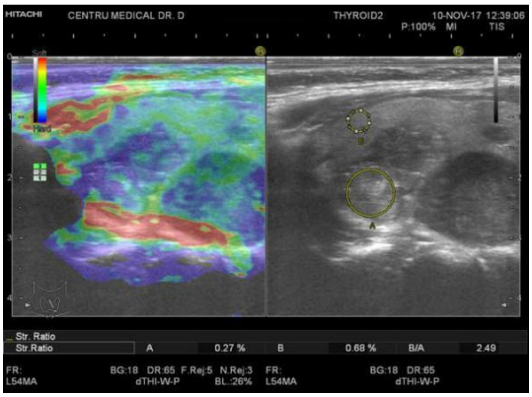

Fig. 10.3.5. Longitudinal section of LTD with 3 adjacent nodular lesions, apparent ES = 4 Multifocal PTC (lateral nodules) + FTC (inferomedial nodule)

Calcifications are part of the classical ultrasound risk criteria (12,67), but not all calcifications are highly suspicious. Marginal, complete shell, or intraparenchymal calcifications are not considered specific for malignancy. Unfortunately, strain elastography does not discriminate between different types of calcifications, all of which generate stiffness. Thus, high-risk calcifications (68), such as intraparenchymal "salt and pepper" type (47) (Fig. 10.3.6) or disseminated microcalcifications (Fig. 10.3.7), interrupted shell calcifications (Fig. 10.3.8), and rough intranodular calcifications (Fig. 10.3.9), all show increased stiffness similar to isolated intraparenchymal calcifications (Fig. 10.3.10) or complete shell calcifications (Fig. 10.3.11), both typically benign (69).

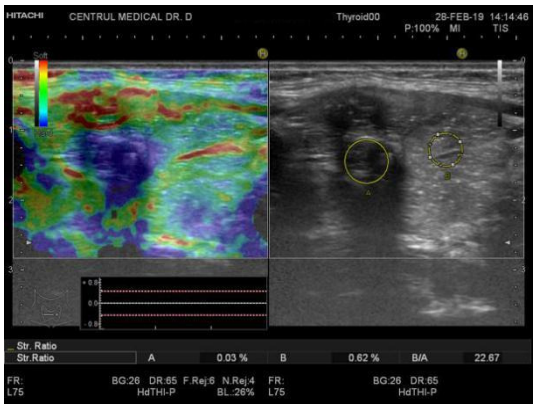

Fig. 10.3.6. "Salt and pepper" microcalcifications. Rago 4. HP: Sclerosing PTC

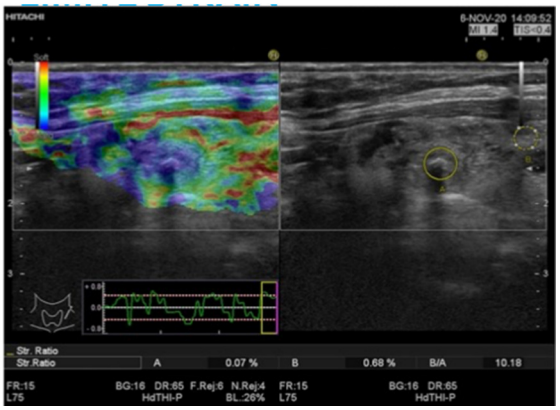

Fig. 10.3.7. Intraparenchymal calcifications RAGO 3 HP: Classic PTC

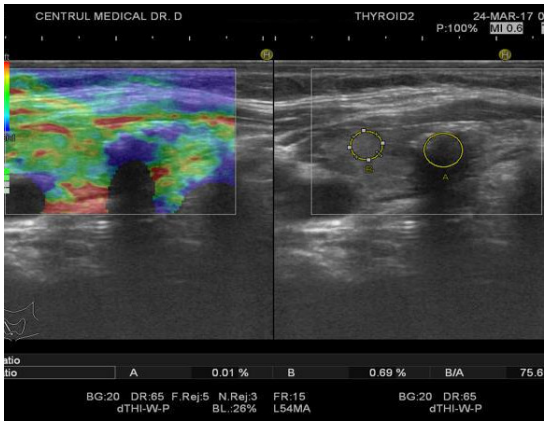

Fig. 10.3.8. Partial shell calcification. Rago 4 HP: Follicular variant of PTC

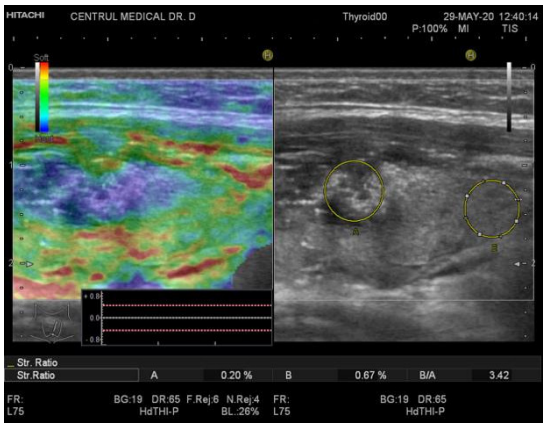

Fig. 10.3.9. Rough calcifications. Rago 4 HP: Classic PTC

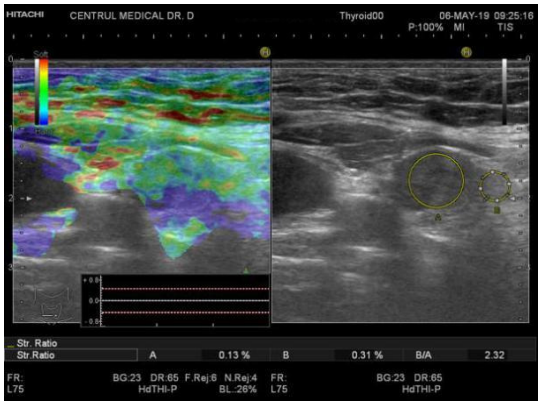

Fig. 10.3.10. Marginal calcification, Rago 3 HP: Granulomatous thyroiditis

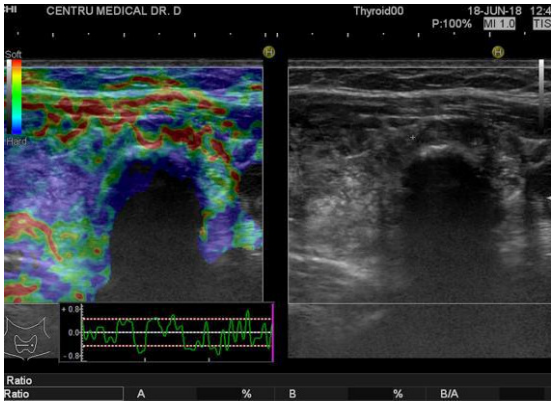

Fig. 10.3.11. Complete shell calcification. HP: Follicular adenoma

Fibrosis is another potential phenomenon in the thyroid that alters thyroid elasticity (27). The most common situation where fibrosis is observed is in chronic autoimmune thyroiditis (70) (Fig. 10.3.12 and 10.3.13), but fibrosis can accompany both benign and malignant nodular lesions (58). The impact of diffuse fibrosis is noteworthy in cases with nodules on a background of autoimmune thyroiditis, where the displacement ratio is falsely lower (71) due to a modified elasticity of the non-nodular parenchyma.

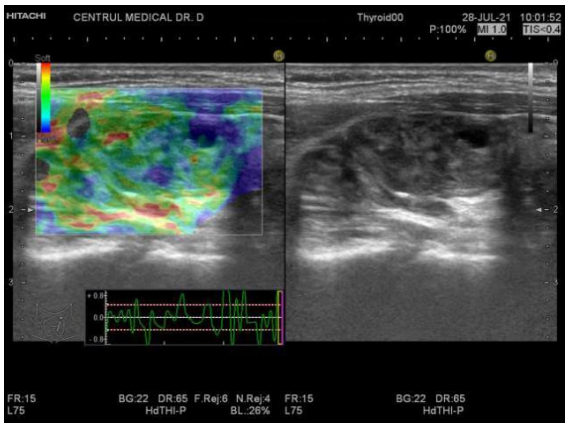

Fig. 10.3.12. TIRADS 4 nodule. RAGO 4
HP: Autoimmune thyroiditis

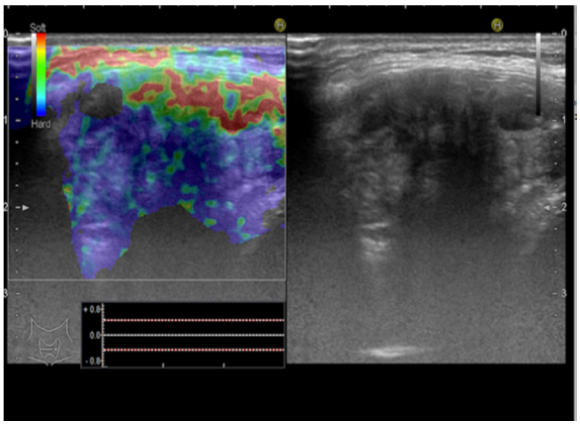

Fig. 10.3.13. Architectural distortion TIRADS 5.
HP: Autoimmune thyroiditis

Certain entities are controversial regarding their elastographic appearance. **False positives** are described in granulomatous thyroiditis (Fig. 10.3.14), Riedel's thyroiditis (Fig. 10.3.15), or subacute thyroiditis (Fig. 10.3.16) in the initial phase of silencing (43). Additionally, many nodular forms of autoimmune thyroiditis can mimic thyroid cancer in both classical ultrasound and elastography (72) (Fig. 10.3.17).

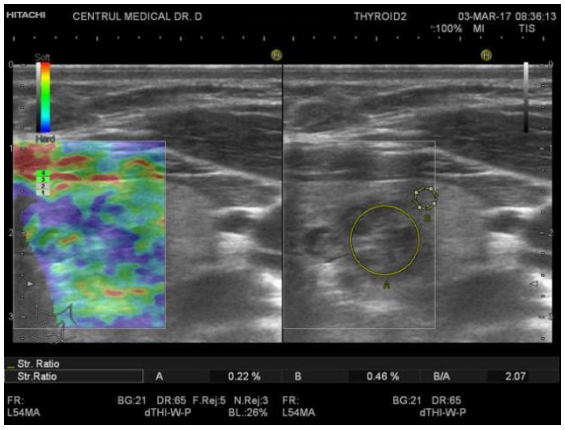

Fig. 10.3.14. TIRADS 4. Rago 3.
HP: Granulomatous thyroiditis

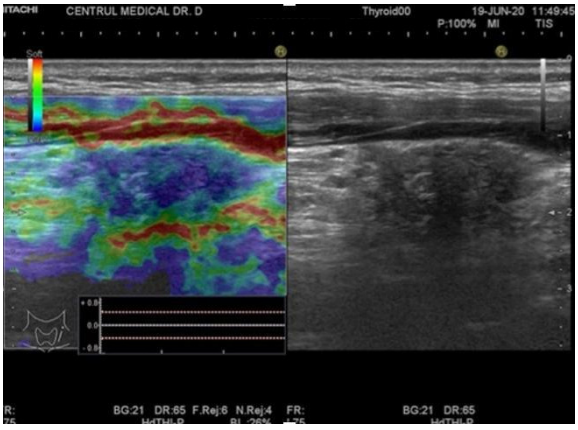

Fig. 10.3.15. TIRADS 5. RAGO 4
HP: Riedel's thyroiditis

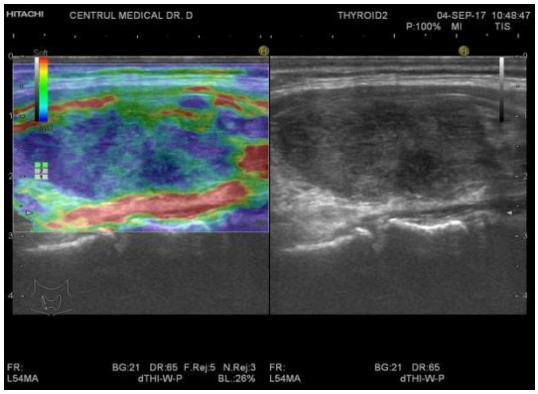

Fig. 10.3.16. TIRADS 4. Rago 3.
HP: Subacute thyroiditis

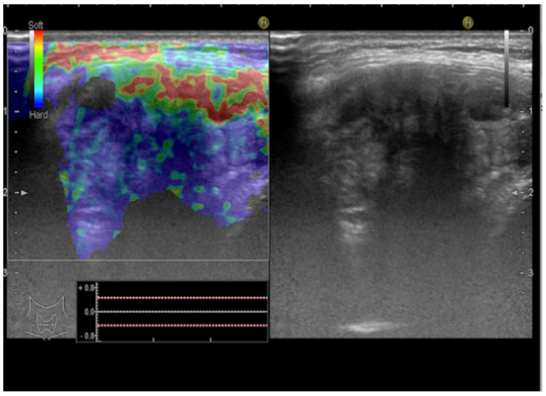

Fig. 10.3.17. TIRADS 5. RAGO 4
HP: Chronic autoimmune Hashimoto thyroiditis

The presence of autoimmune thyroiditis can also alter the strain ratio (73) (Fig. 10.3.18), similar to the phenomenon described in liver pathology, although there is no consensus in the literature (74). An alternative, though less standardized, is using the stiffness ratio between the thyroid nodule and the prethyroid muscle (SR2), preferably in longitudinal section, specifically the ipsilateral sternocleidomastoid muscle (SCLM) (73) (Fig. 10.3.19).

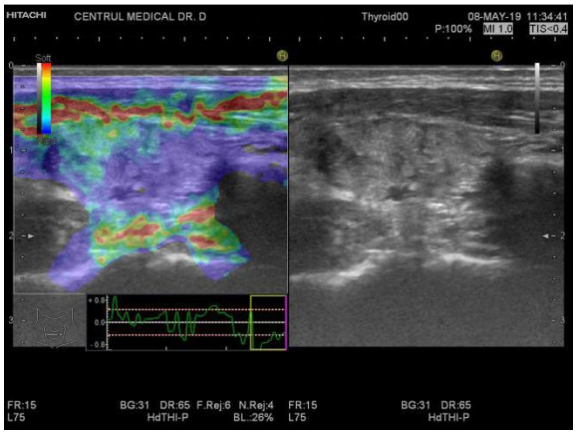

Fig. 10.3.18. TIRADS 4 nodule on an AITD background. Perinodular stiffness exceeds nodular stiffness. HP: AITD

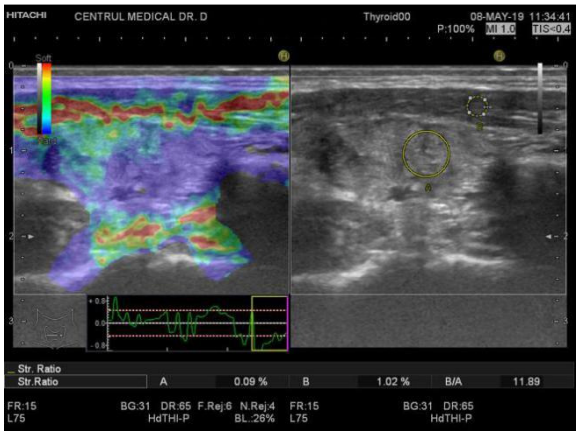

Fig. 10.3.19. TIRADS 4 nodule on an AITD background. SR2 calculation (nodule/SCLM)

Among circumscribed benign nodular lesions, follicular adenomas often exhibit stiffness (75,76), contributing to false positives. Follicular lesions are generally a diagnostic pitfall (13) and the most common category of **false negatives** described in the literature (77).

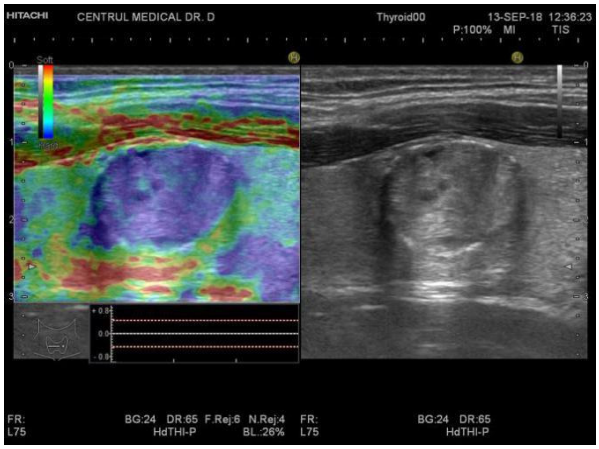

Fig. 10.3.20. TIRADS 4. Rago 4.
HP: Follicular adenoma

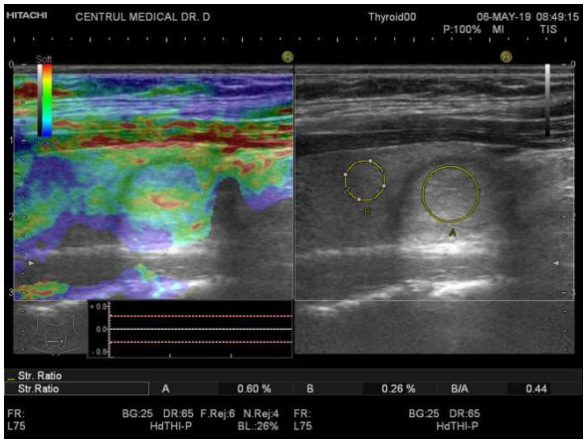

Fig. 10.3.21. TIRADS 3. Rago 1
HP: Follicular adenoma

Hurthle cell neoplasms, another variant of follicular neoplasms, fall into the same category (Fig. 10.3.22 and 10.3.23).

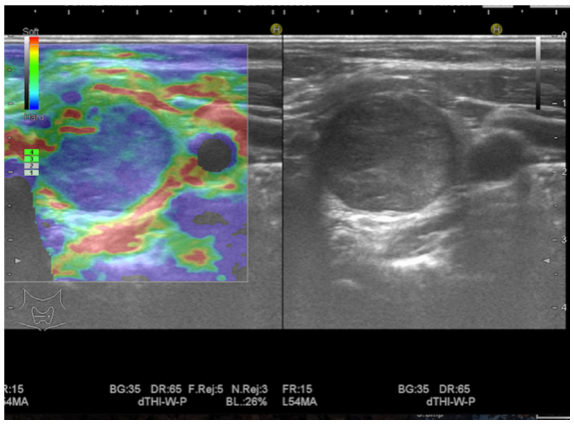

Fig. 10.3.22. TIRADS 4. Rago 4.
HP: Hurthle cell adenoma

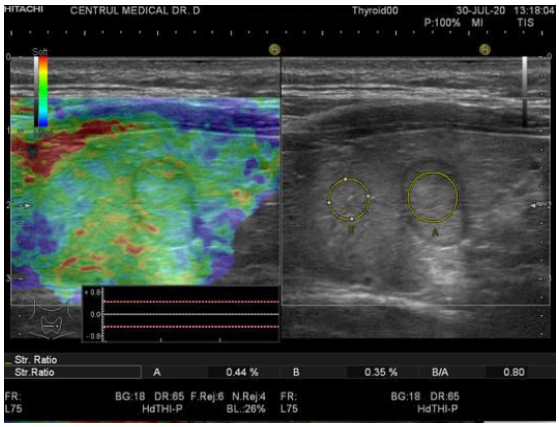

Fig. 10.3.23. TIRADS 4. RAGO 1
HP: Follicular neoplasm of uncertain potential

The uncertainty of elastographic images in follicular neoplasms extends to the subgroup of follicular cancers. While papillary thyroid carcinoma, representing over 80% of thyroid cancers worldwide (67) and regionally (78), is associated with increased stiffness, the data on follicular or medullary cancers are controversial (21,29). Follicular carcinomas are described as potentially elastic and soft (27,28,47), generating the most frequent errors in strain elastography (56), and thus being the most commonly undiagnosed cancers (77) (Fig. 10.3.24).

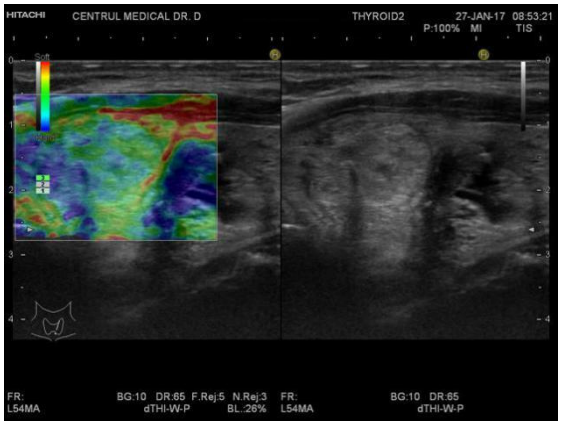

Fig. 10.3.24. Lateral nodule TIRADS 4, Rago 1. Central nodule TIRADS 5, RAGO 4.
HP: Multifocal FTC

Microcarcinomas are entities with diameters up to 1 cm, present either as isolated nodules or part of a macronodule. Some studies suggest that strain elastography can be beneficial in diagnosing malignancy even in subcentimeter nodules (79,80) (Fig. 10.3.25). However, the limitations of this method become evident when there are disseminated microPTC foci within macronodules (21) (Fig. 10.3.26).

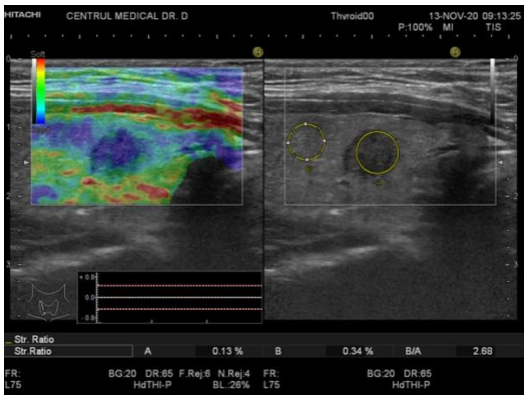

Fig. 10.3.25. Isolated subcentimeter nodule
TIRADS 3, Rago 4
HP: Classic variant of microPTC

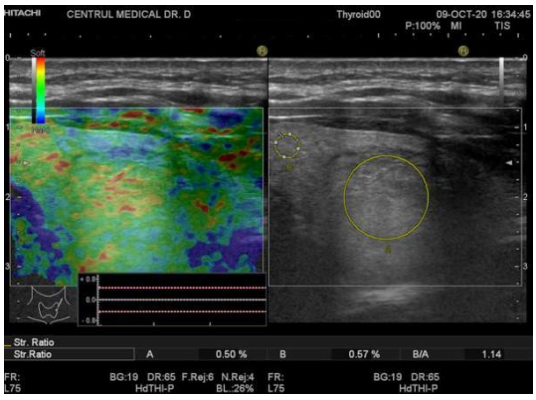

Fig. 10.3.26. Isolated 2cm nodule
TIRADS 3, Rago 1
HP: MicroPTC in an adenomatous nodule

For medullary or anaplastic cancers, their elastographic appearances can also vary (21,29). However, literature data are limited due to the small number of such carcinomas. Studies dedicated exclusively to cases of medullary thyroid carcinoma (MTC) (81) describe the predominant elastographic appearance as Rago 2, with 60% of MTCs mimicking benignity.

Intra- and inter-observer variability is low, with a minimum of four to seven patient evaluations considered sufficient for learning (21). Qualitative interpretation is more challenging than quantitative interpretation (47,82).

10.4. Shear Wave Elastography

The principle of **shear wave elastography** is identical to the one used in breast evaluation (subchapter 9.4). As with other applications, vendors offer either the single-plane variant pSWE, or the multiplane two-dimensional variant 2D-SWE (8). Measuring the transverse attenuation component (83) allows for the evaluation of shear wave velocity, which is closely linked to Young's modulus; thus, the numerical data provided by SWE are direct indicators of the elasticity of the underlying tissues (26). The point technique offers strictly a quantitative evaluation without a color code. The measured value is the shear wave velocity (SWV), expressed in m/sec (84) (Fig. 10.4.1).

Fig. 10.4.1. pSWE technique – Isolated nodule, TIRADS 3, HP: Follicular adenoma

Normal thyroid texture, with a follicular structure, has a low cellular density, resulting in low SWV values, with an average value of up to 1.55 m/s. Autoimmune thyroid disease, associated with fibrosis, generates higher velocities, over 2.55 m/s. Thyroid adenomas, with rich cellularity, have higher velocities than healthy parenchyma but lower than those in autoimmune thyroiditis, around 1.72 m/s. Papillary cancers, which associate solid cells, fibrosis, and adipose tissue, generate velocities higher than approximately 2.66 m/s (85). The point technique is recommended as an additional method to conventional ultrasound (21), including in cases with nodules smaller than 1 cm in diameter (86).

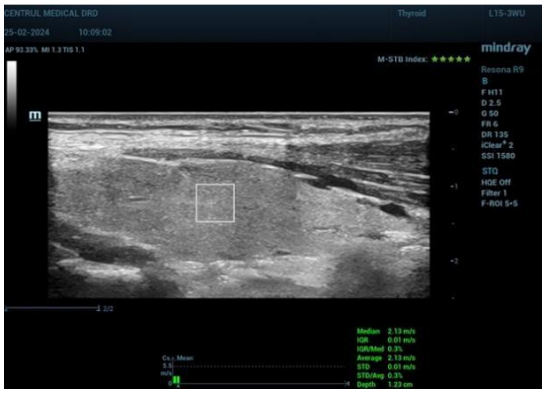

Fig. 10.4.2. Normal thyroid parenchyma

Fig. 10.4.3. Autoimmune thyroid disease

The multiplane technique offers either real-time examination or the one-shot variant. This technique allows for the propagation velocities to be measured at several points around the lesion, with an acquisition window of up to 700 milliseconds (8). This technique, offered by Toshiba, generates both qualitative and quantitative reports.

The real-time technique involves exposing tissues to multiple ultrarapid multiplane ultrasound waves, 2D-SWE. It generates both qualitative and quantitative reports. Recently, a three-dimensional elastography variant has been offered, using a volumetric probe with the addition of a frontal image acquisition plane.

The 2D-SWE ratio provides both qualitative and quantitative information. The qualitative evaluation offers a real-time color elastogram, which reveals differences in the shear wave propagation velocity through tissues located beneath the transducer in the transverse plane (8). The color scale typically ranges from dark blue (very soft lesions), through green and yellow (intermediate lesions), to red (very hard lesions) (87) (Fig. 10.4.4).

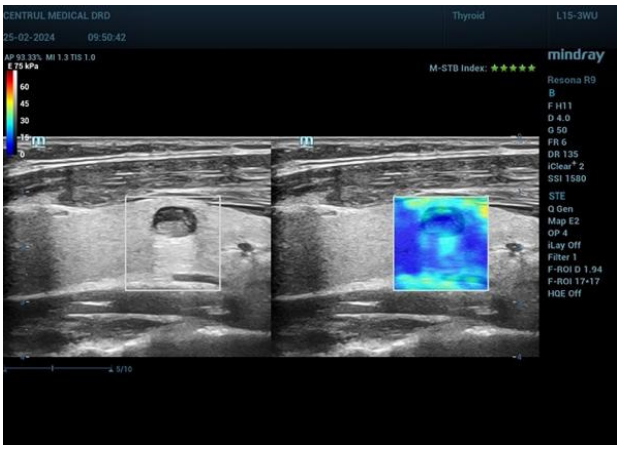

Fig. 10.4.4. SWE color scale from blue (soft tissue) to red (stiff tissue)

Color classification is not as well-standardized as in strain elastography, with some authors proposing a variant extrapolated from breast evaluation (88). The color estimation is proposed on a standard thyroid evaluation scale, with a maximum of 100 kPa. From a qualitative perspective, several parameters can be defined for evaluation (89), beyond the classical evaluation used in breast elastography: the *predominant color in the nodule* (Fig. 10.4.5 a – d), the *maximum intranodular stiffness* (Fig. 10.4.6 a – d), the *appearance of the nodular margin* (the stiffest part, the perinodular transition zone) (Fig. 10.4.7 a-b), the *intranodular homogeneity* (defining homogeneity as the presence of a single color and heterogeneity when displaying at least two colours), and lastly*, the perinodular parenchymal homogeneity* (Fig. 10.4.8).

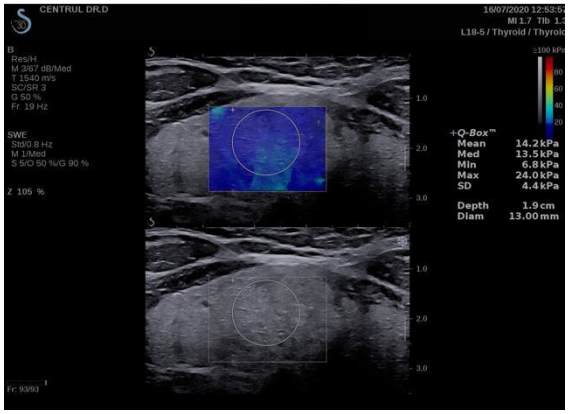

Fig. 10.4.5.a: Homogeneous Blue
HP: Follicular adenoma

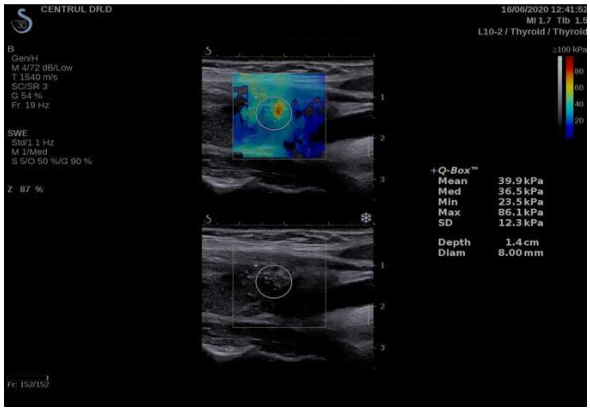

Fig. 10.4.5.b: Homogeneous Green
HP: Granulomatous thyroiditis

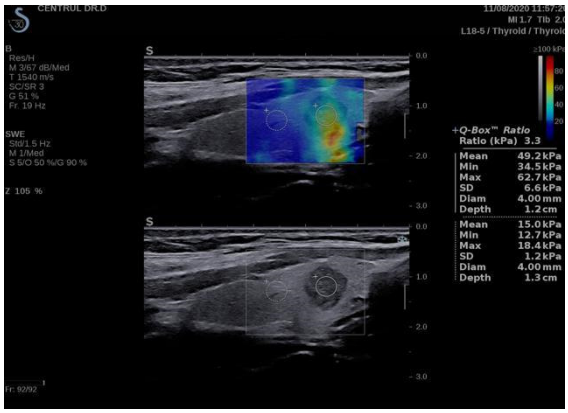

Fig. 10.4.5.c: Homogeneous Orange
HP: Micro papillary carcinoma (MicroPTC)

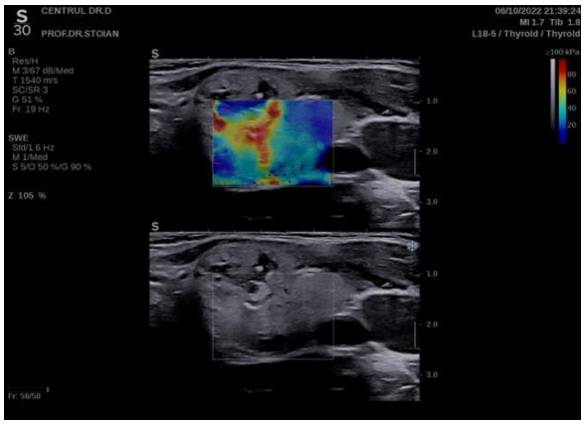

Fig. 10.4.5.d: Homogeneous Red
HP: PTC pT2

Figures 10.4.6 a–d display the qualitative quantification of maximum nodular stiffness.

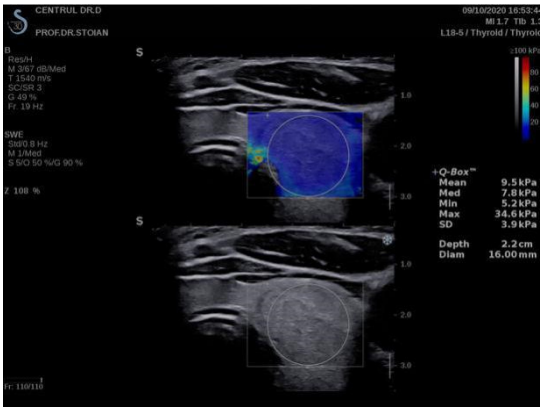

Fig. 10.4.6.a: Maximum intranodular blue
HP: Follicular adenoma

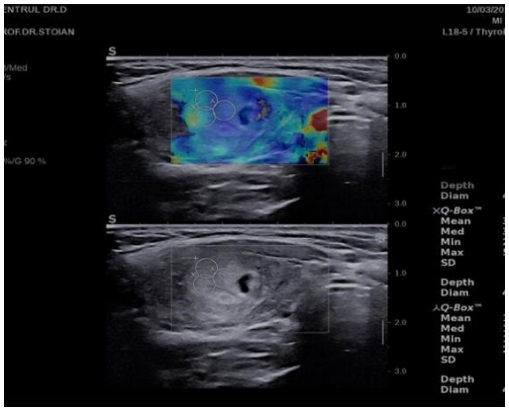

Fig. 10.4.6.b: Maximum intranodular green
HP: Autoimmune thyroiditis

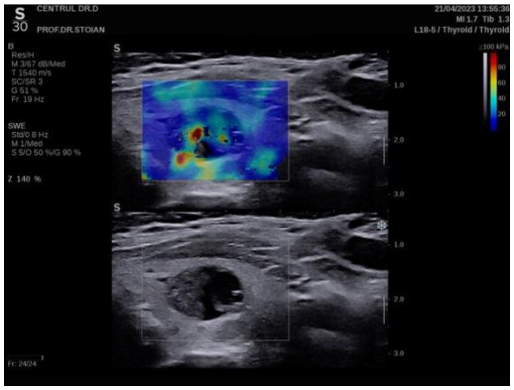

Fig. 10.4.6.c: Maximum intranodular orange
HP: Cystic PTC

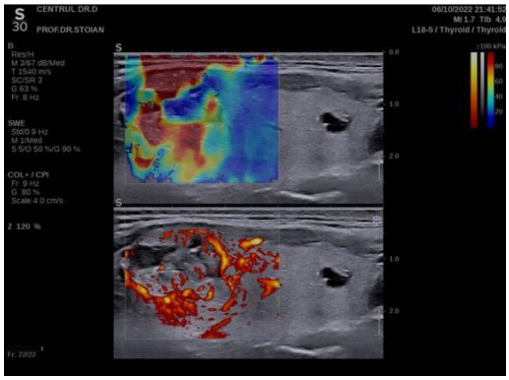

Fig. 10.4.6.d: Maximum intranodular red
HP: Follicular thyroid carcinoma (FTC)

Figures 10.4.7 a and b show homogeneous and heterogeneous intranodular aspects, respectively.

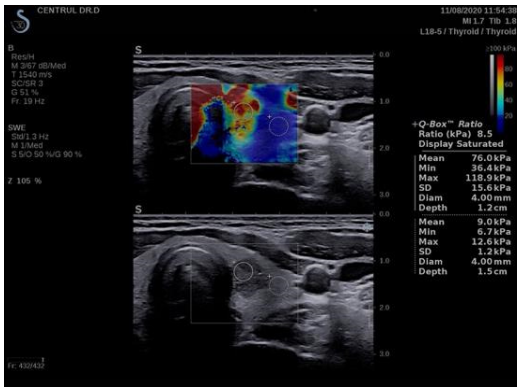

Fig. 10.4.7.a: Intranodular homogeneity
HP: Classical variant of PTC

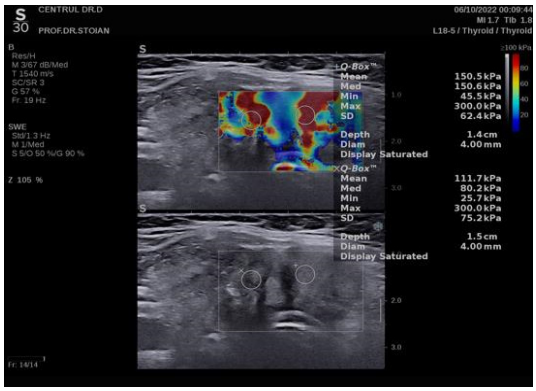

Fig. 10.4.7.b: Intranodular heterogeneity
HP: Sclerosing variant of PTC

Figures 10.4.8 a and b show homogeneous and heterogeneous perinodular aspects, respectively.

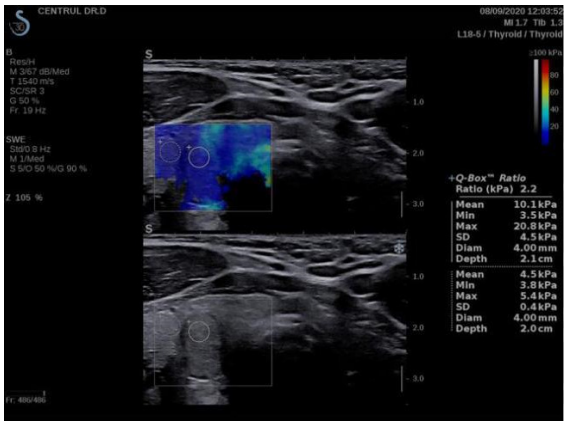

Fig. 10.4.8.a: Perinodular homogeneity
HP: Granulomatous thyroiditis focus

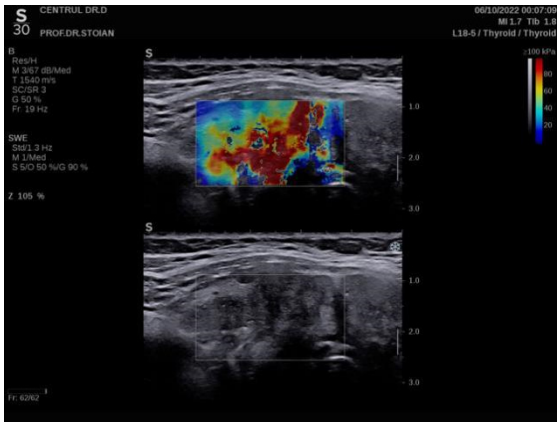

Fig. 10.4.8.b: Perinodular heterogeneity
HP: FTC on AITD background

Intranodular and perinodular heterogeneity, and the predominance of green intranodular color, with the hardest area at least orange coloured, characterize malignancy (Fig. 10.4.9). On the other hand, homogeneity, the absence of perinodular stiffness, and the predominance of blue intranodular color, with the hardest area also blue, characterize benign lesions (Fig. 10.4.10) (89).

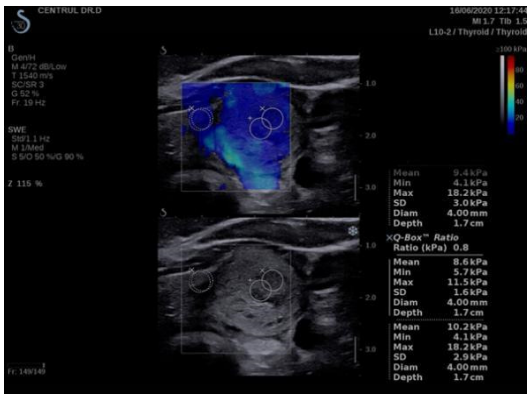

Fig. 10.4.9. Soft nodule (predominantly soft);
Maximum stiffness area = soft, homogeneous intra and perinodular

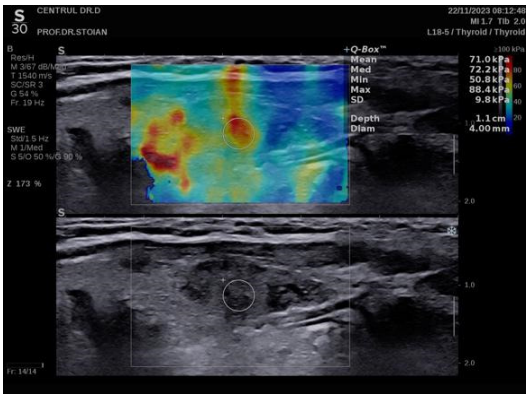

Fig. 10.4.10. Hard nodule (predominantly orange);
Maximum stiffness area = hard, heterogeneous intra and perinodular

Some authors only use the perinodular margin aspect as a single qualitative criterion (Fig. 10.4.11) (90), describing perinodular anelasticity as highly predictive for malignancy, even in subcentimeter nodules (Fig. 10.4.12).

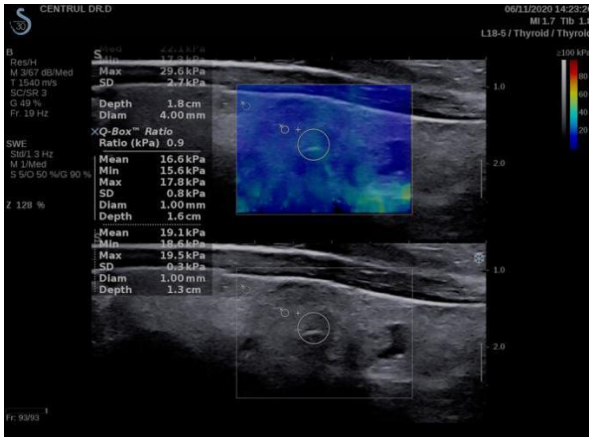

Fig. 10.4.11. Solid nodule TIRADS 3
Intranodular stiffness 1
Elastic nodular margin
HP: Follicular adenoma

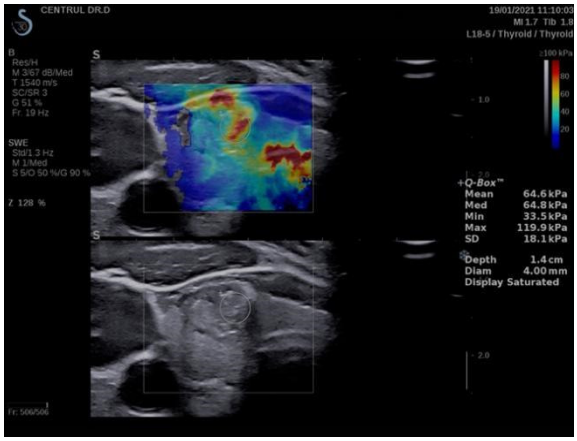

Fig. 10.4.12. Solid nodule TIRADS 4
Intranodular stiffness 2
Stiff nodular margin
HP: Hobnail variant of PTC

Other authors propose a simpler scale (91), with four color categories, similar to the Tozaki scale (92): Type 1 homogeneous, elastic (completely blue), Type 2 blue with vertical lines of green stiffness, Type 3 eccentric stiffness, and Type 4 central stiffness and heterogeneity (Fig. 10.4.13 a-d).

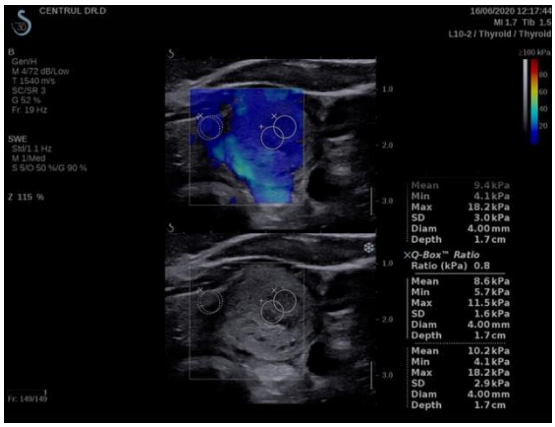

Fig. 10.4.13.a: Score 1: completely blue

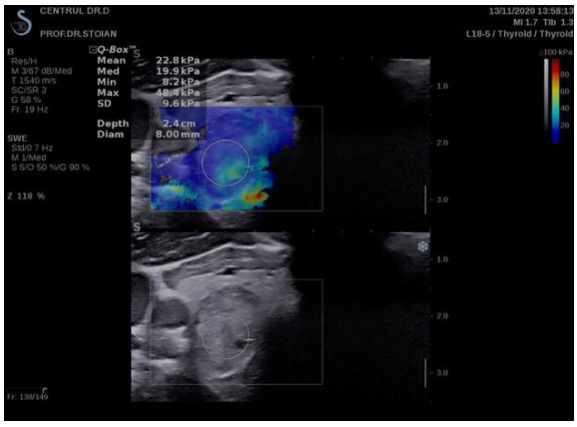

Fig. 10.4.13.b: Score 2: stiffness lines (green)

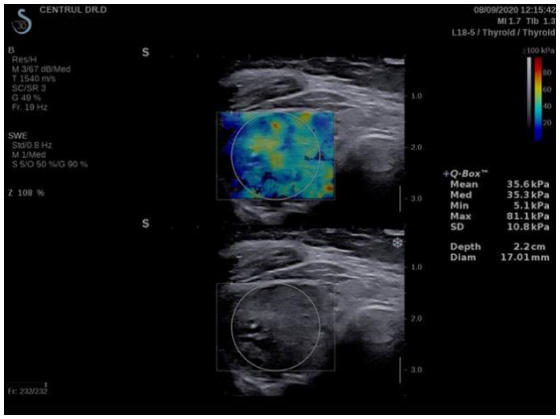

Fig. 10.4.13.c: Score 3: eccentric stiffness

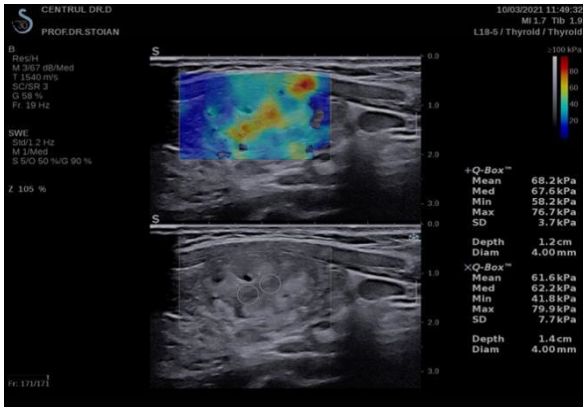

Fig. 10.4.13.d: Score 4: stiffness + heterogeneity

Despite this, the advantage of 2D-SWE lies in the multitude of quantitative parameters measured. Thus, 2D-SWE directly measures ultrasound propagation speed, directly estimating stiffness through minimum elasticity (E_{Min}), mean elasticity (E_{Mean}), maximum elasticity (E_{Max}), and standard deviation, expressed either in m/s or kPa (Fig. 10.4.14 and 10.4.15). It is recommended to perform three consecutive measurements (93).

Fig. 10.4.14: Elastographic parameters (kPa)

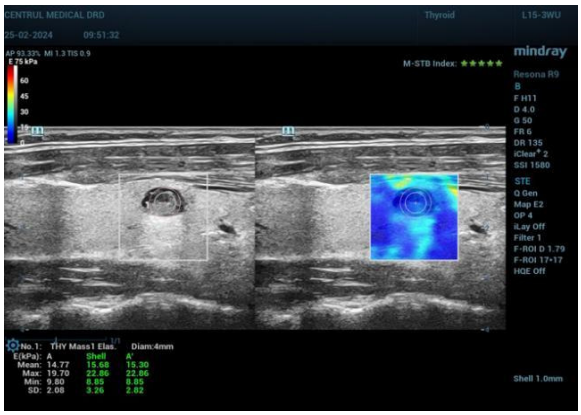

Fig. 10.4.15: Elastographic parameters (m/s)

There is no consensus on the optimal parameter to use; some studies use E_{Max} as the optimal diagnostic parameter, with threshold values ranging between 36-49-65-95 kPa (8,94–96), while others use the mean value, ranging between 38-62-85 kPa (87,97). Some authors recommend E_{Max} as the most effective parameter (90,93,98), while others support the superiority of E_{Mean} (99).

The performance of E_{Max} is also considered dependent on nodule size (96), with the discriminative threshold increasing with nodule size (93,96,100): 33.7 kPa (for sizes smaller than 1 cm), 37.7 kPa (for nodules between 1 and 2 cm), and 55.1 kPa (for nodules larger than 2 cm) (96). It is considered that 2D-SWE has low sensitivity for nodules smaller than 1 cm and low specificity for nodules larger than 2 cm (101). Other authors have not noticed an impact of nodule size on the diagnostic performance of 2D-SWE (102,103).

Studies evaluating the impact of size on SWE performance used a ROI encompassing the entire nodule (Fig. 10.4.17). Discrepancies in the discriminative threshold values of elasticity indices can be explained by different sample sizes, nodule sizes, chosen ROI size/technique, and cancer prevalence in the study group (21).

In general, the literature describes good diagnostic performance of elastography, whether evaluated alone (85,88,94,104,105) or incorporated into various TIRADS models (96,106,107). The advantages of 2D-SWE are evident in improving the diagnostic quality of TIRADS models, considering stiffness as an additional risk factor, increasing accuracy from 85.5% to 92.6% (106) for TIRADS 4a category, and from 78.4% to 84% for TIRADS 4b category (108). There are meta-analyses that also verify the diagnostic performance of different vendors, expressed through the area under the receiver operating characteristic curve (AUROC) (109), with the following results: 0.84 for Toshiba, 0.85 for Siemens VFI, and 0.61 and 0.88 for Aixplorer, indicating diagnostic value independently of the type of device used. However, there are also negative studies, such as a recent meta-analysis (110) comprising over 2,500 nodules and describing a sensitivity of only 66% and a specificity of 85%, considering the diagnostic performance as mediocre.

In quantitative evaluation, a qualitative elasticity ratio (ER) can also be calculated, automatically performed by the ultrasound machine, with direct comparison between the ROI in the nodule and a similarly sized ROI in the adjacent non-nodular thyroid parenchyma, preferably at the same depth (43) (Fig. 10.4.16). The lack of ROI standardization (111) impacts the diagnostic accuracy of ER. Generally, ER is considered to have superior diagnostic sensitivity compared to other quantitative parameters but with lower specificity (112), with diagnostic performance inferior to the preferred parameter, E_{Max}, with values ranging between 77.03 - 86.71%, averaging 81.85%, compared to 84.27 - 92.09%, averaging 78.19%. The threshold value of ER is not standardized, with values ranging between 1.35 (112) - 3.7 (113) - 3.9 (99).

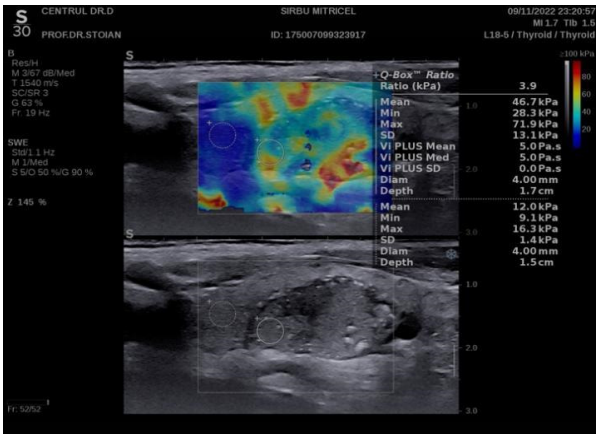

Fig. 10.4.16. Quantitative Evaluation of Elastographic Indices

10.5. Limitations of Shear Wave Elastography

The **size of the ROI** is not standardized in thyroid evaluation guidelines, with recommendations varying from minimal regions of 1-3 mm (8, 51, 114) to the use of a window covering the entire nodular lesion (107, 115). The placement of the ROI should correspond to the hardest intranodular area (105) (Fig. 10.5.1), avoiding heterogeneous zones (56, 74). Several studies directly compare the diagnostic performance of different ROI sizes, showing the superiority of small ROIs (Figs. 10.5.2 and 10.5.3) for the parameters E_{Max} and E_{Min} (116), with no performance differences in E_{Mean} (111). Other authors recommend choosing an ROI that encompasses the entire nodule (21).

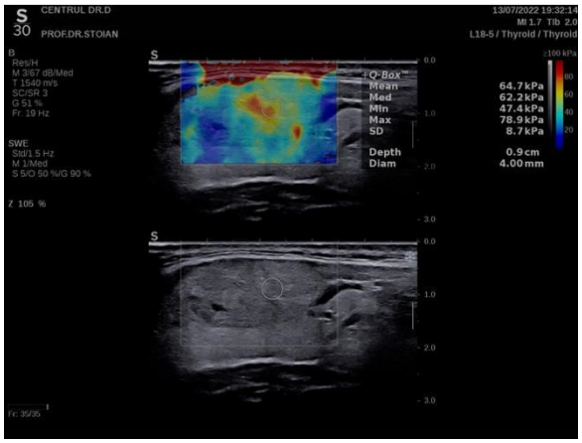

Fig. 10.5.1. TIRADS 4 Nodular Lesion, ROI 4 mm

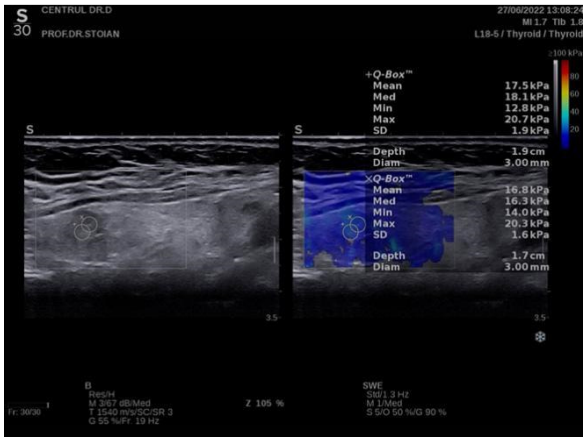

Fig. 10.5.2. TIRADS 4 Nodular Lesion, ROI 3 mm

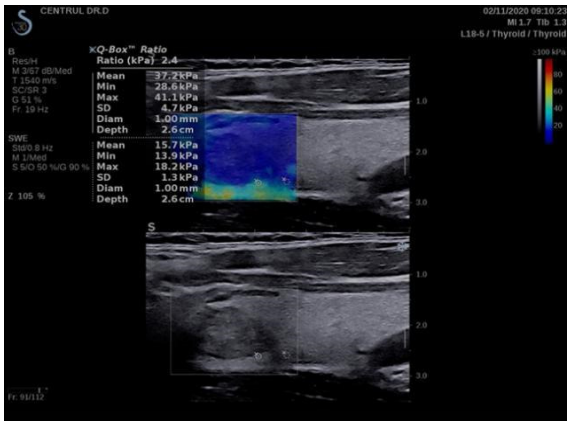

Fig. 10.5.3. TIRADS 1 Nodular Lesion, ROI 1 mm, HP: Follicular Adenoma

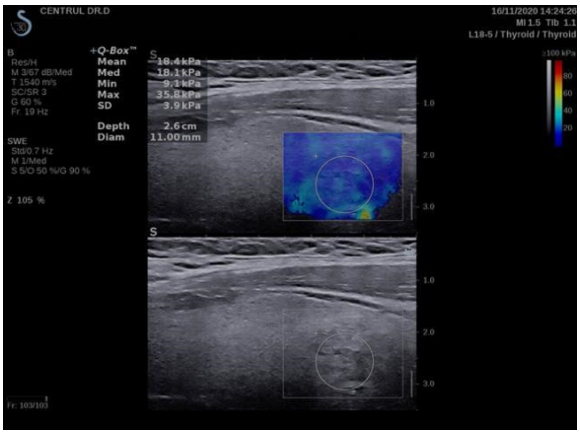

Fig. 10.5.4. TIRADS 4 Nodular Lesion, ROI 11 mm, HP: Hurthle Cell Adenoma

Nodule Depth. Generally, nodular lesions deeper than 3 cm do not allow for a complete elastogram, with images often being incomplete (116) because the penetration limit of shear waves is around 3 cm (117) (Fig. 10.5.5). For very deep nodules, a lower frequency probe, up to 10 MHz, can be used in elastographic mode, but even under these conditions, the elastogram is often incomplete, as shown in Fig. 10.5.6.

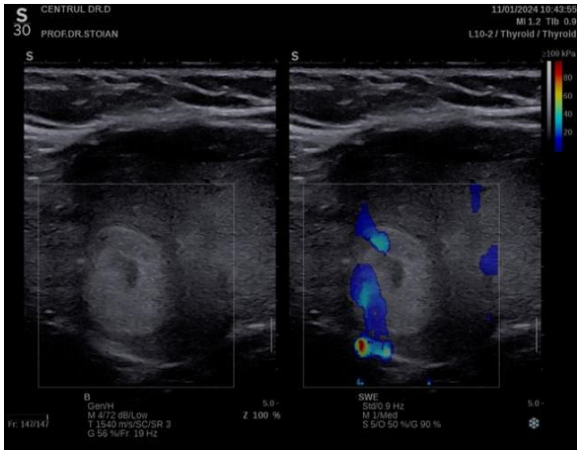

Fig. 10.5.5. Solid TIRADS 4a Lesion, Depth 4 cm, Incomplete Elastogram

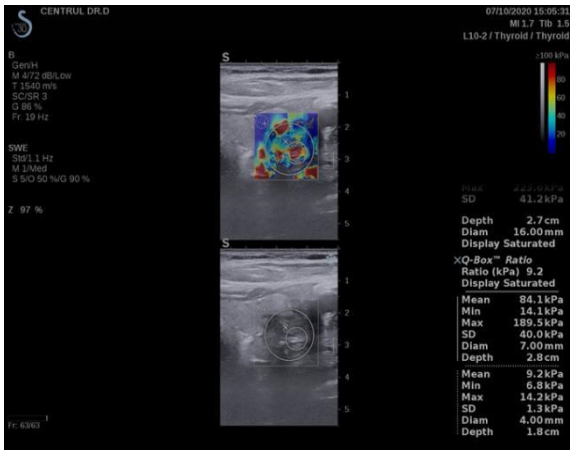

Fig. 10.5.6. Solid TIRADS 5 Lesion, Depth 3.5 cm, Incomplete Elastogram

In overweight patients, ultrasound attenuation due to adipose tissue can further alter the elastogram quality (Figs. 10.5.7 and 10.5.8).

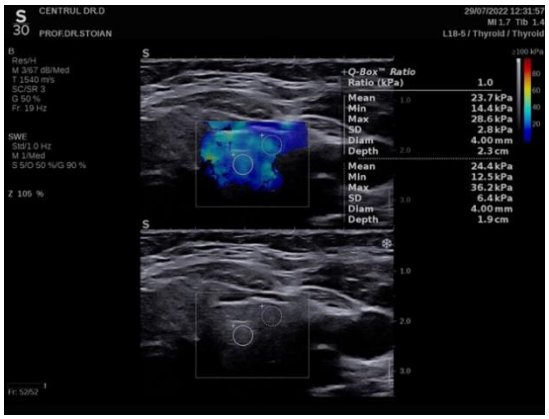

Fig. 10.5.7. Nodular Lesion at 1.9 cm Depth, Complete Elastogram

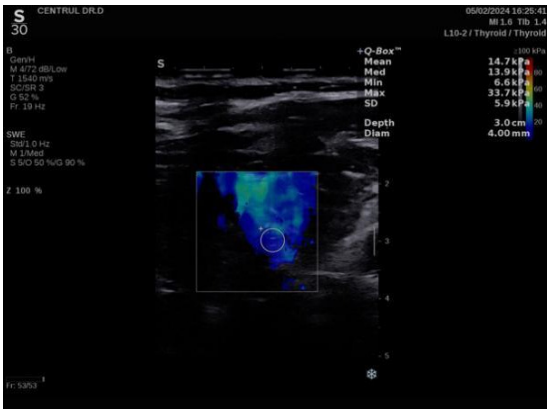

Fig. 10.5.8. Nodular Lesion at 3.0 cm Depth, Incomplete Elastogram

Nodule size has an impact on the quality and reliability of the elastography evaluation, as it was already described. Large nodular lesions affect the elastography performance, with different diagnostic outcomes for various nodule sizes (Fig. 10.5.9). However, the impact of the nodule size on elastography eligibility is unclear (21).

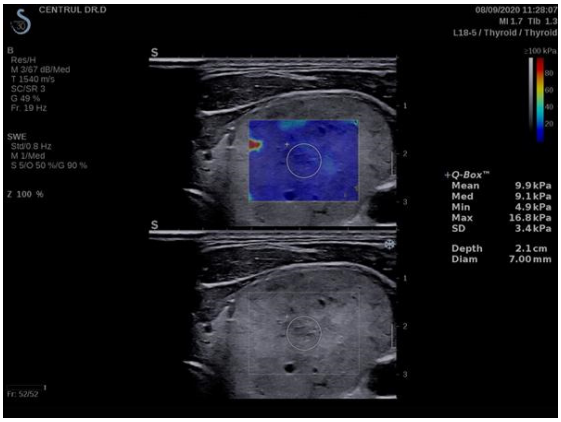

Fig. 10.5.9. Solid TIRADS 3 Lesion, Maximum Diameter 4.2 cm, Exceeding Elastographic FOV Size

Pretracheal nodule position limits the use of shear wave elastography due to the proximity of the tracheal cartilage, which can cause falsely increased stiffness (Figs. 10.5.10 and 10.5.11).

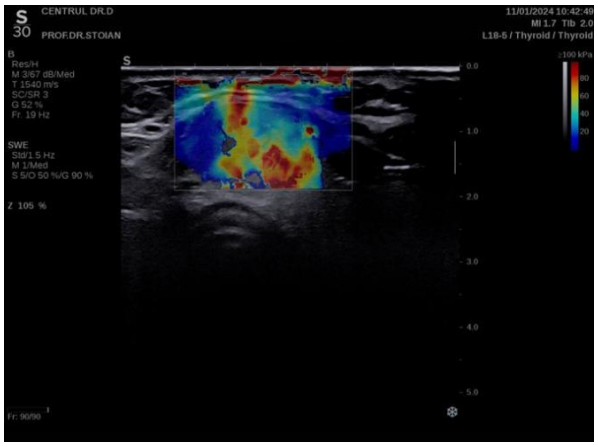

Fig. 10.5.10. Isthmic Nodular Lesion, False Increased Intranodular Stiffness,
HP: Follicular Adenoma

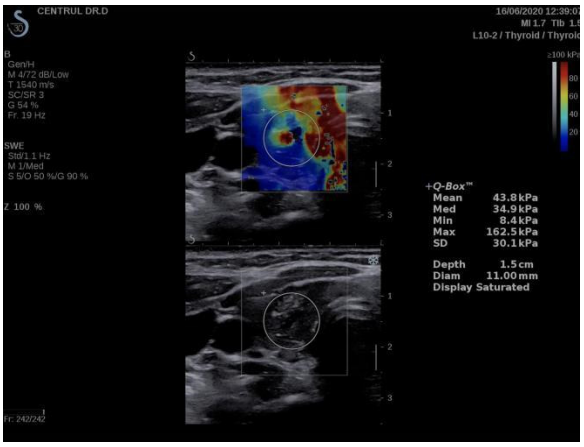

Fig. 10.5.11. Isthmic Nodular Lesion, Apparent False Increased Intranodular Stiffness,
HP: Sclerosing Variant of PTC

Nodule composition influences elastographic results due to inhomogeneity from cystic inclusions, calcifications, or heterogeneity. Calcifications increase shear wave speed (118), with a threshold value of 66 kPA for the elastic index in distinguishing benign from malignant calcifications (119). Microcalcifications and macrocalcifications within nodules show different velocities (118). Some authors report decreased diagnostic capability due to calcifications (21, 118-120), but there is no literature consensus(121). Macrocalcifications, both intranodular (Fig. 10.5.12) and egg-shell (Fig. 10.5.13), can cause increased stiffness and false-positive results (122), though this effect is not universally observed (121).

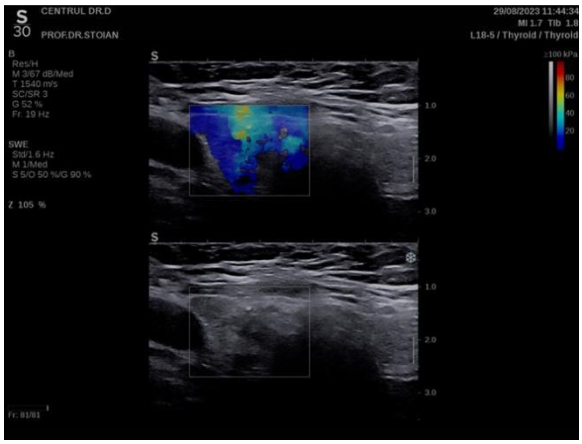

Fig. 10.5.12. Intraparenchymal Macrocalcification, Score 3
HP: PTC

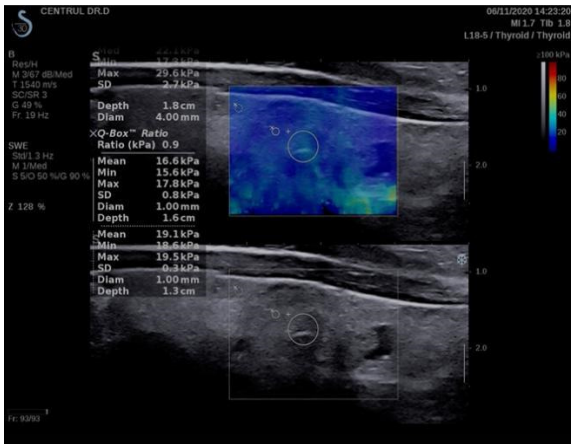

Fig. 10.5.13. Intraparenchymal Macrocalcification, Score 1
HP: Colloid Goiter

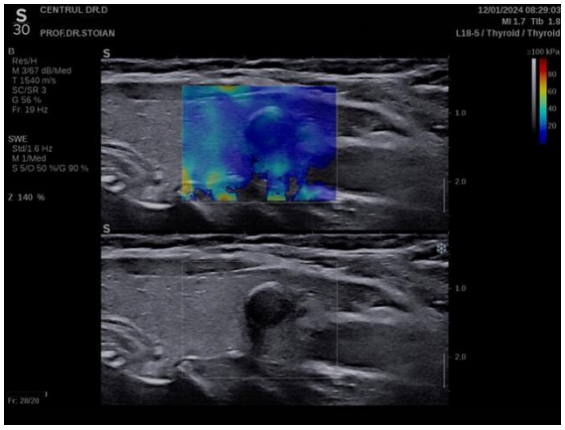

Fig. 10.5.14. Egg-shell Macrocalcification, Incomplete. ES = 2. HP: MicroPTC

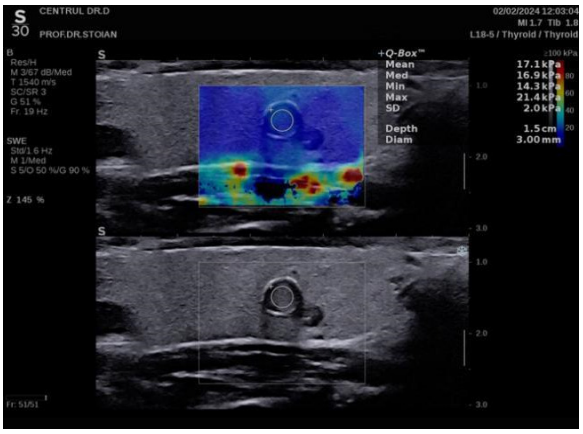

Fig. 10.5.15. Egg-shell Macrocalcification, Complete. ES = 1. HP: Follicular Adenoma

Only rough or diffuse salt-and-pepper calcifications affect elasticity (93) (Figs. 10.5.16 and 10.5.17).

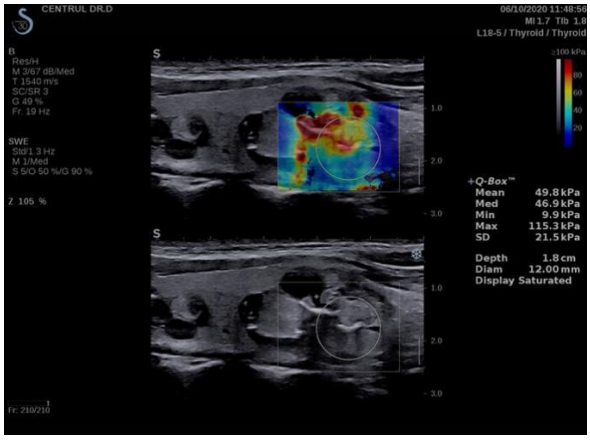

Fig. 10.5.16. Rough Calcifications, Score 4, HP: PTC

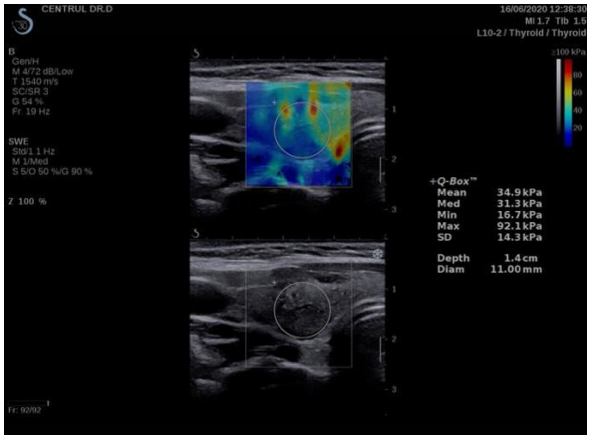

Fig. 10.5.17. Punctate Calcifications, Score 3, HP: PTC

Nodule heterogeneity complicates elastographic evaluation (21), with cystic components being particularly disruptive (Figs. 10.5.18 and 10.5.19). Using a small ROI decreases the negative impact of intranodular heterogeneity (111).

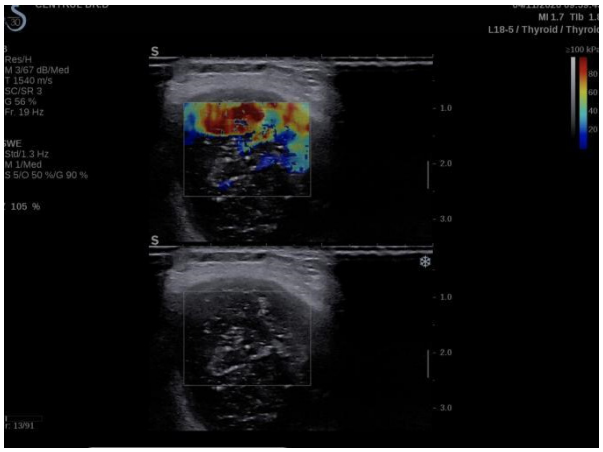

Fig. 10.5.18. Mixed nodule, dispersion phenomenon, falsely hard and incomplete elastogram

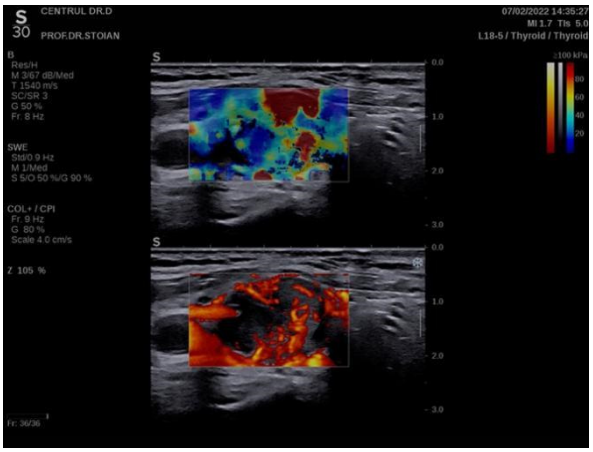

Fig. 10.5.19. Mixed nodule, heterogeneous and incomplete elastogram

The impact of **diffuse heterogeneity** on benign/malignant diagnostic capacity is also discussed (112, 123), with chronic autoimmune thyroiditis increasing diffuse elasticity indices (72), altering the absolute elasticity ratio but not affecting the diagnostic capability of 2D-SWE (123).

Apart from technique-related limitations (transducer position, FOV size, ROI size, pressure intensity), and nodule characteristics (position, depth, size, structure), shear wave elastography also associates a range of false-positive and false-negative results due to overlapping elasticity values of **various pathologies**. Results are explicable by differences in intranodular fibrosis quantification: papillary cancer elasticity correlates with fibrosis degree (19), and follicular neoplasia is more elastic than nodular hyperplasia (124).

Follicular neoplasia includes benign lesions, precancerous entities like NIFTP, and cancers. Conventional ultrasound and strain elastography do not offer accurate morphological diagnoses. SWE data indicate that follicular neoplasia, both benign and malignant, shows lower elasticity indices than those measured in chronic autoimmune thyroiditis or papillary cancers (125) (Figs. 10.5.20 and 10.5.21). Thus, the predictive value for follicular cancer is low (Fig. 10.5.22), even though malignant follicular neoplasia has a mean value above 22.3 kPa (Figs. 10.5.23 and 10.5.24). Follicular neoplasia is one of the most frequent causes of both false-positive and false-negative results.

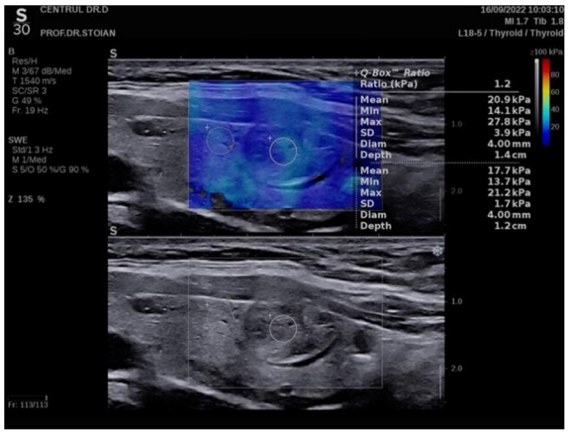

Fig. 10.5.20. TIRADS 4a, Elastographic Score 2, HP: Follicular Adenoma

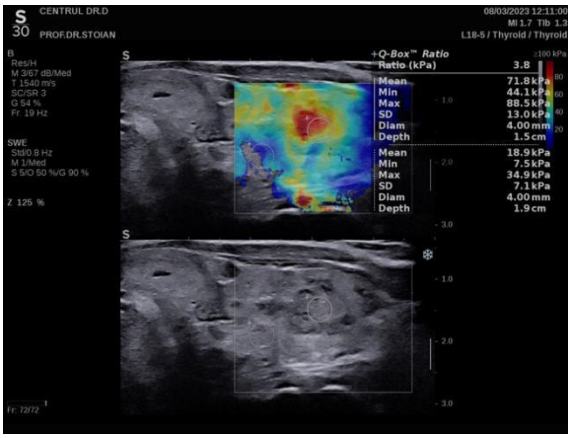

Fig. 10.5.21. TIRADS 3, Elastographic Score 4, HP: NIFTP

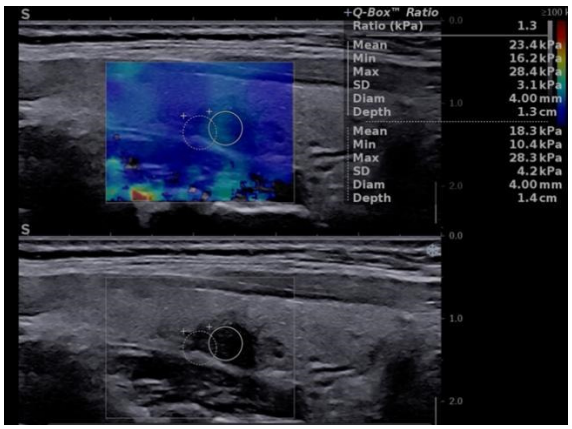

Fig. 10.5.22. TIRADS 4, Score 1, HP: Classic FTC

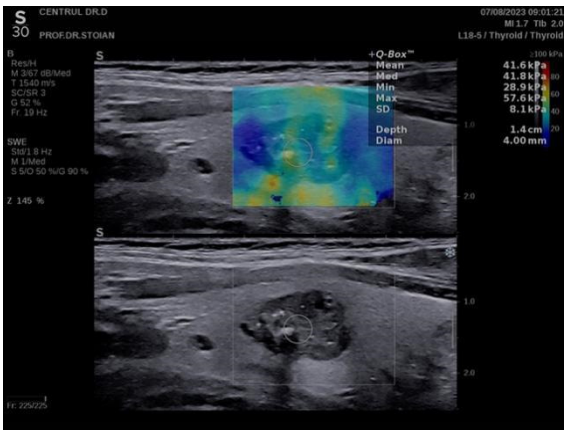

Fig. 10.5.23. TIRADS 4, Score 3, HP: Cystic Variant FTC

Regarding fibrosis distribution, follicular neoplasia shows stiffness at the nodule margin, while simple nodular hyperplasia has uniform stiffness distribution (124, 126).

Despite classical theories that most **medullary thyroid cancers** (MTC) are soft due to their high amyloid content and to the absence of fibrosis, SE results do not fully extrapolate to SWE. MTCs present higher elasticity indices than healthy thyroid parenchyma, with a mean of 85.9 kPa (127), but significantly lower compared to papillary cancers, which average over 100 kPa (125). Figs. 10.5.24 and 10.5.25 show cases diagnosed with MTC, with increased and reduced elasticity, respectively.

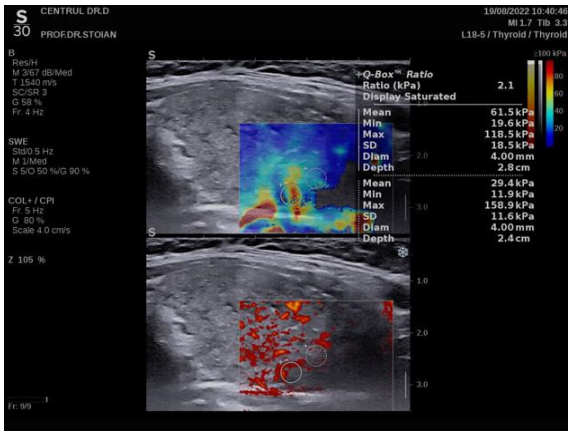

Fig. 10.5.24. TIRADS 5, ES 4, HP: Isolated MTC MTC

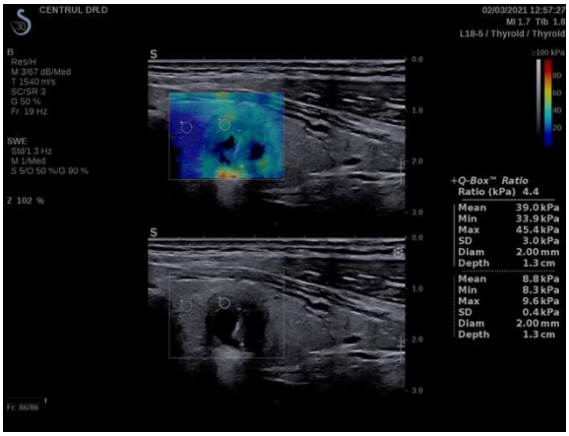

Fig. 10.5.25. TIRADS 3, Elastographic Score 2, HP: Isolated HP: Isolated MTC

Papillary microcarcinomas can exist isolated in the thyroid parenchyma or within macronodules. Several studies on papillary microcarcinomas describe small benign/malignant differentiation threshold values under 36 kPa (128, 129) for E_{Mean}, the most diagnostically accurate qualitative parameter.

Excessive fibrosis presence, as in nodular autoimmune thyroid disease (123) (Fig. 10.5.26), granulomatous thyroiditis (Fig. 10.5.27), or non-autoimmune contexts like post-regional radiotherapy (21, 125), generates frequent **false-positive situations**. Riedel's thyroiditis (Fig. 10.5.29), part of the thyroiditis group, fibroblastic infiltration, as seen in subacute thyroiditis during the sideration phase, mimic thyroid cancer by generating the highest stiffness values encountered in thyroid elastography (72, 125). Healing allows for a return to normal. Fig. 10.5.30 shows the initial aspect of subacute thyroiditis during the sideration phase, and Fig. 10.5.31 shows the ultrasound evolution in the same patient as the fibroblastic infiltrate disappears during the healing process.

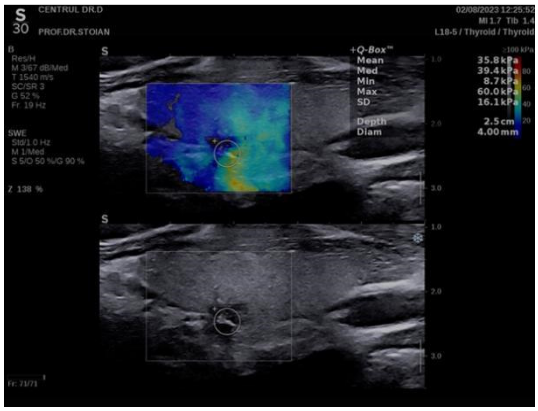

Fig. 10.5.26. TIRADS 4, Elastographic Score 2, HP: BTA, Pseudonodular Form

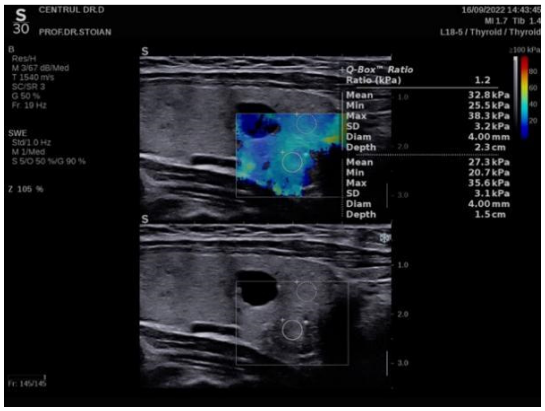

Fig. 10.5.27. Elastographic Score 2, HP: Granulomatous Thyroiditis

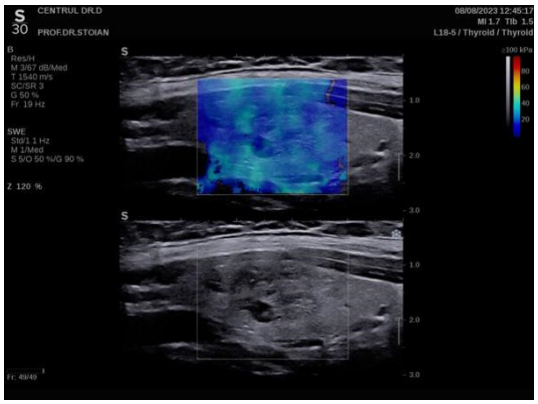

Fig. 10.5.28. TIRADS 4a Nodule, Score 2, HP: Post-Radiation Thyroiditis

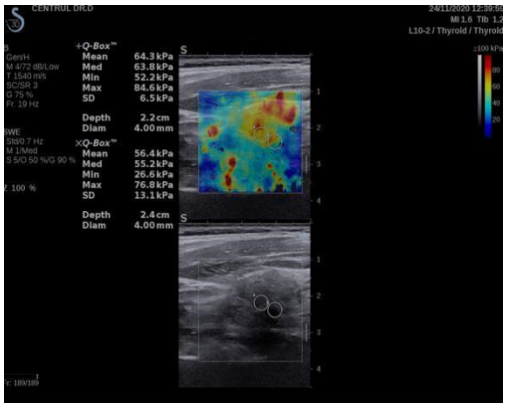

Fig. 10.5.29. TIRADS 4c Nodule, Score 4, HP: Riedel's Thyroiditis

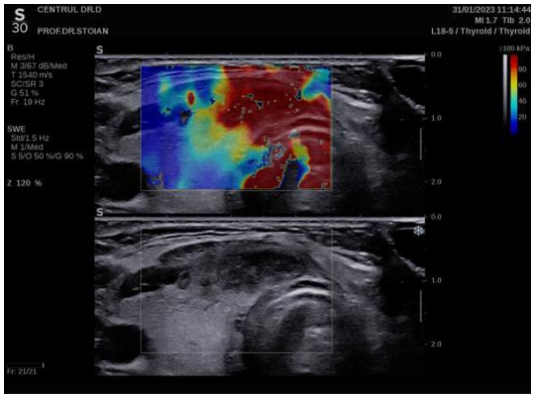

Fig. 10.5.30. TIRADS 5 Nodule, Score 4, HP: Subacute Thyroiditis (attack 01.2023)

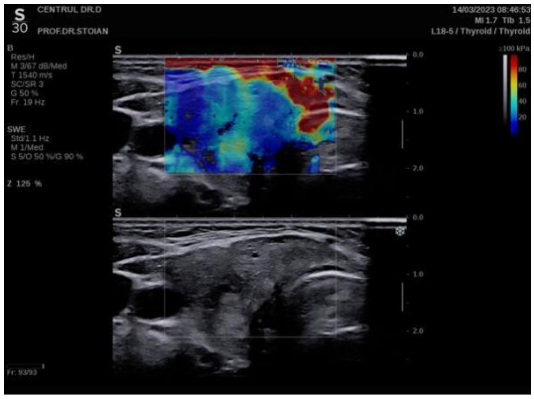

Fig. 10.5.31. TIRADS 4c Nodule, Score 4, HP: Subacute Thyroiditis (recovery 03.2023)

Unlike strain elastography, the learning curve for 2D-SWE is steeper (43, 131), with a small intra- and inter-observer variability (21, 22) and a concordance of 0.97 (119).

10.6. The Use of Elastography in Nodular Pathology

Many current guidelines (12, 20, 21, 67) recommend integrating elastographic information into the multiparametric thyroid evaluation. Integrating nodular elasticity as an additional evaluation factor enhances diagnostic performance (77, 133–135), including in improving TIRADS prediction models (39), where Asteria color score 3 and 4, and Rago 4 and 5, are considered additional risk factors by increasing specificity and negative predictive value (49, 136, 137) (Figs. 10.6.1 – 10.6.4).

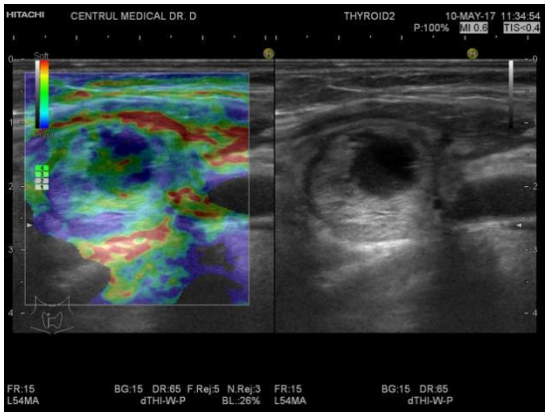

Fig. 10.6.1. TIRADS 2 Nodule, RAGO 3, Reclassified as TIRADS 4, HP: Cystic PTC

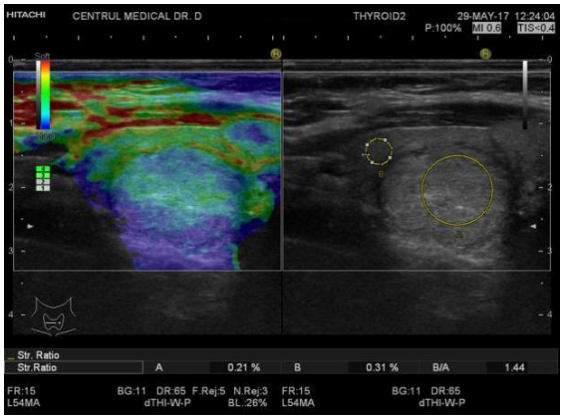

Fig. 10.6.2. TIRADS 3 Nodule, RAGO 3, Reclassified as TIRADS 4, HP: NIFTP

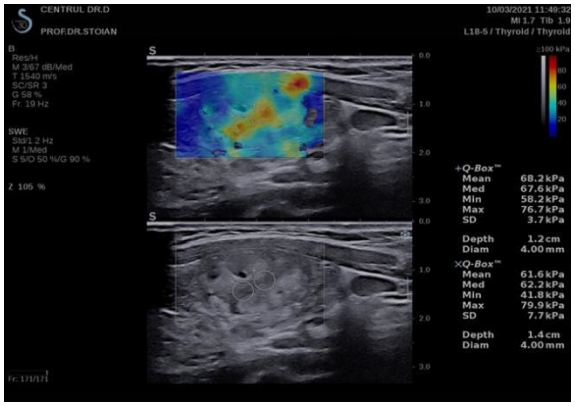

Fig. 10.6.3. TIRADS 3, RAGO 3, Reclassified as TIRADS 4, HP: Granulomatous Thyroiditis

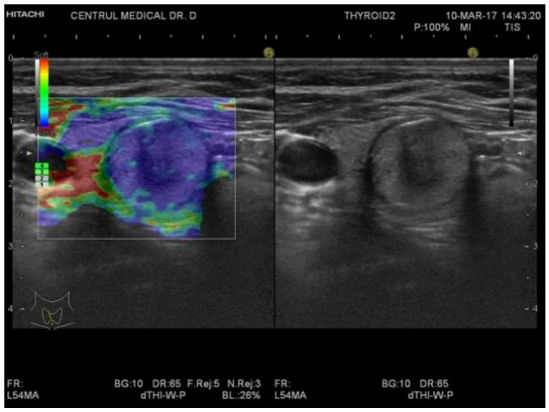

Fig. 10.6.4. TIRADS 4 Nodule, RAGO 4, Reclassified as TIRADS 5, HP: FTC

The same principle applies to 2D-SWE, where stiffness requires a risk reclassification (8, 11, 28, 88, 112, 125, 138) (Figs. 10.6.5 and 10.6.6).

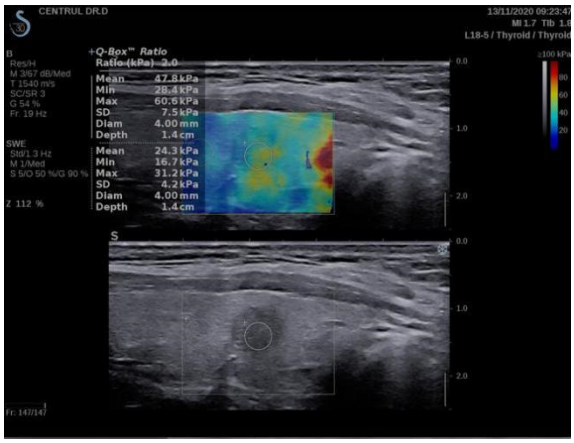

Fig. 10.6.5. TIRADS 3, Elastographic Score 3, Reclassified as TIRADS 4, HP: PTC

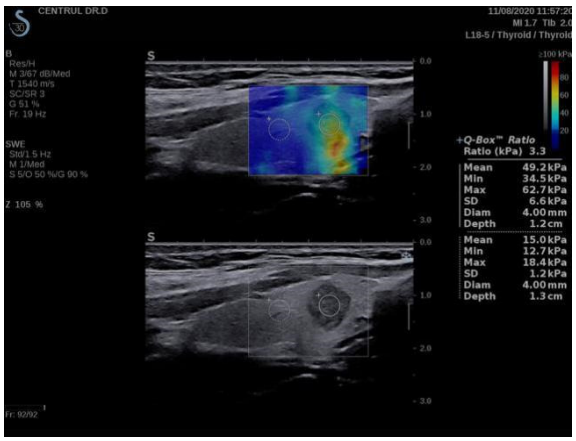

Fig. 10.6.6. TIRADS 4a Nodule, Elastographic Score 4, Reclassified as TIRADS 5, HP: PTC

In the case of multinodular goiters, reclassifying to a higher risk class facilitates choosing the nodule for biopsy. Figs. 10.6.7 and 10.6.8 show the same patient with multinodular involvement, where the stiffness of the caudal nodule was decisive in its selection for biopsy (76).

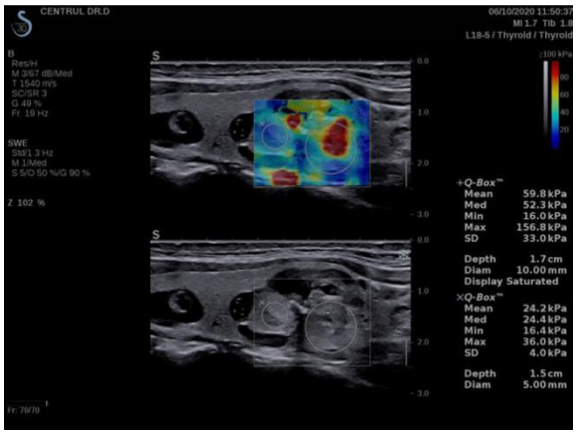

Fig. 10.6.7. Multinodular Goiter, Choosing the Caudal Nodule (Rago 3) for Biopsy

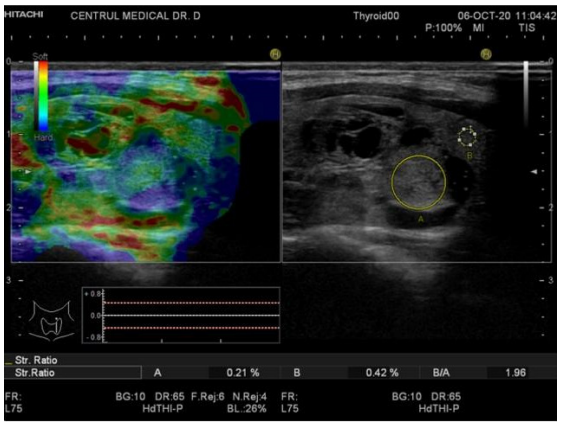

Fig. 10.6.8. Multinodular Goiter, Choosing the Caudal Nodule (Score 3) for Biopsy

Studies indicate a role for elastography even in heterogeneous nodules, where biopsy orientation is facilitated by elastography towards hard areas (139), as demonstrated by the ventro-apical position of the nodule in the left thyroid lobe, with consistent stiffness in SE (Fig. 10.6.9) and SWE (Fig. 10.6.10).

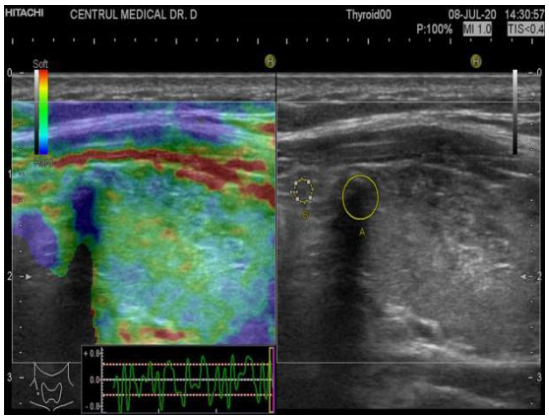

Fig. 10.6.9. SE Evaluation

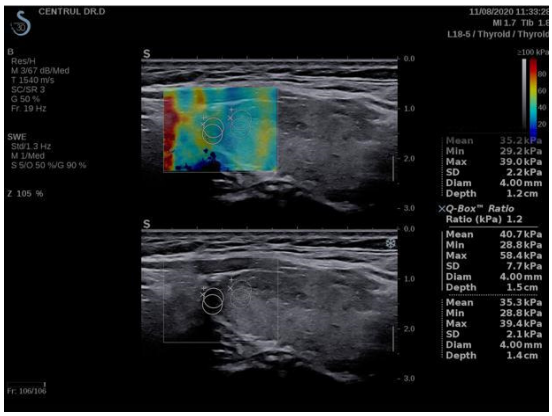

Fig. 10.6.10. SWE Evaluation

Risk downgrading is not recommended (29, 47). However, we can hypothesize that a soft TIRADS 3 nodule should not be referred for biopsy, with elastography reaffirming the nodule's benignity (137), having a diagnostic failure rate of 0.03%. Elastography's malignancy exclusion probability is higher than that of B-mode ultrasound (38). Figures 10.6.11 and 10.6.12 show the same solid nodule, evaluated by strain and 2D-SWE techniques, where elasticity reiterates the minimal malignancy probability. Thus, increased diagnostic accuracy through elastography, regardless of type, allows for reducing invasive explorations by up to 33% (137).

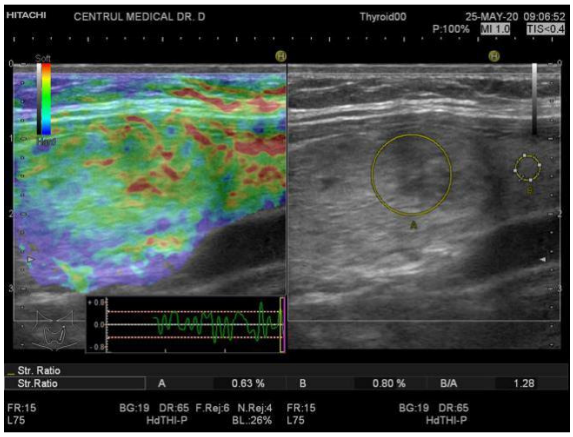

Fig. 10.6.11. TIRADS 3, RAGO 1,
HP: Autonomous Follicular Adenoma

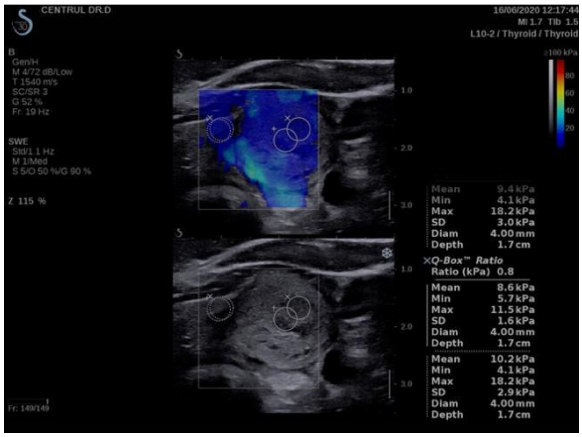

Fig. 10.6.12. TIRADS 3, Score 1,
HP: Autonomous Follicular Adenoma

Regardless of classical ultrasound criteria, the presence of stiffness in solid nodular lesions requires a risk upgrade with fine-needle aspiration (FNA) indication (141). The following figures display the same solid nodule evaluated by strain (Fig. 10.6.13) and 2D-SWE (Fig. 10.6.14) techniques, stiff and referred for FNA at about 8 mm size, confirming the diagnosis of papillary microcarcinoma with secondary lymph node metastases.

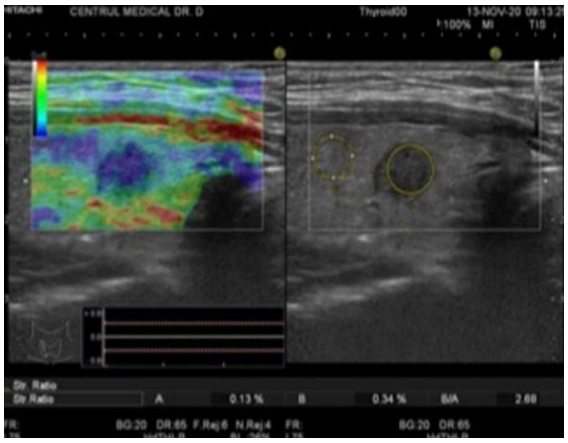

Fig. 10.6.13. TIRADS 3, RAGO 4, Reclassified as TIRADS 4, Micro PTC

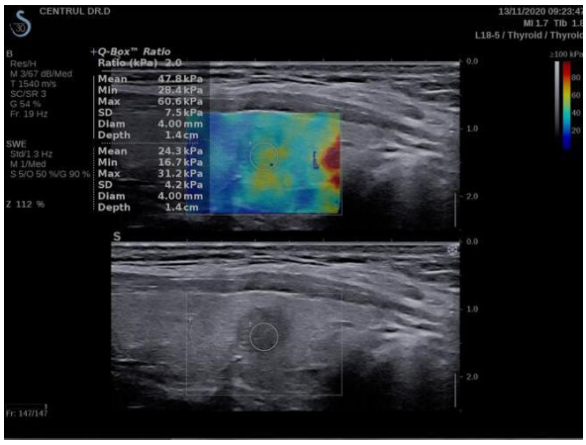

Fig. 10.6.14. TIRADS 3, Elastographic Score 4, Reclassified as TIRADS 4, Micro PTC

A special category of nodules includes those with indeterminate results on FNA, which represent up to 25% of biopsied nodules (12). There are no universal recommendations for this situation, with individual risk, whether clinical, anamnestic, or molecular, usually necessitating total thyroidectomy (12, 67). Positive studies indicate that rigidity, either qualitatively defined (142) or semi-quantitatively assessed (14), increases thyroid cancer diagnostic prediction with a sensitivity of about 96-98% and a specificity of over 90%, though not universally demonstrated (15). Our working group considers nodule rigidity as an individual risk addition (75), especially as recent meta-analyses confirm this (39, 77). Similar results are described for the 2D-SWE technique (16, 17, 143), though there is no consensus on the discriminative parameters to use (E_{Mean} or E_{Max}), noting a sensitivity of 79.2% and specificity of 84.5%. Figures 10.6.15 and 10.6.16 present the same case with indeterminate cytology on FNA, upgraded in risk category and referred for surgical cure due to increased stiffness evaluated by strain and 2D-SWE techniques.

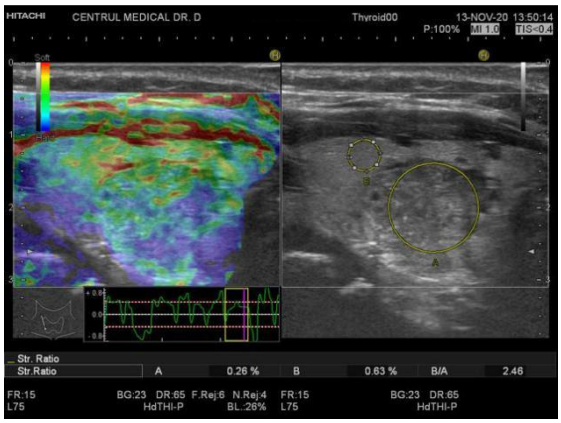

Fig. 10.6.15. BETHESDA III, RAGO 3, HP: PTC

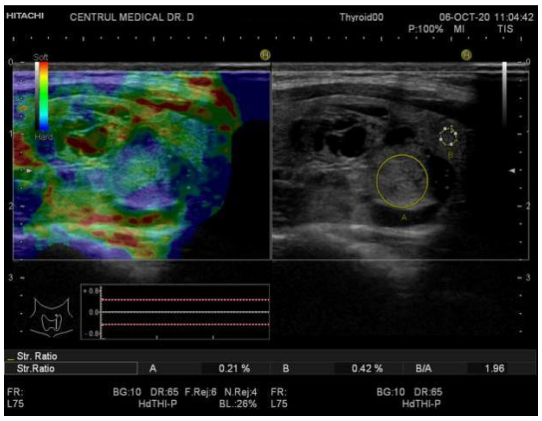

Fig. 10.6.16. BETHESDA III, Elastographic Score 3, HP: NIFTP

Most literature data provide a comparison between SE and SWE in different study populations. A meta-analysis including 80 studies with a total of 16,624 subjects shows

superior diagnostic quality overall for SE compared to SWE in differentiating malignant and benign thyroid nodules (144). Significant is the proportion of SE studies included compared to SWE and the lack of uniformity and standardization in ultrasound evaluation, elastographic techniques, and cancer thresholds. Some smaller studies comparing both methods in the same populations using different ultrasound machines for measurements generally favoured SE, though SWE had comparable value (specificity of 68.4% vs. 79.0%, sensitivity of 86.7% vs. 84.4%, and accuracy of 81.3% vs. 78.1%) (145). There are also studies showing superior values for SWE, with no significant statistical differences in terms of AUROC: 0.912 for mean EI and 0.905 for SR (p=0.0952) (146). Nodule-to-parenchyma or nodule-to-muscle SR was shown to be a better predictor than qualitative SE assessment, providing a numerical, quantitative evaluation for SE (147). A considerable advantage of SWE refers to evaluating nodules coexisting with autoimmune thyroid disease, while SE is described as less feasible in this context (144, 148).

Operator experience is crucial, especially in the case of strain elastography (149). SWE generally shows better reproducibility. However, certain factors, such as external compression on the transducer, can interfere with measurements. The most common type of error in SWE evaluation relates to operator-dependent artifacts. Therefore, although SWE is perceived as an easier technique to learn, both elastographic techniques should invariably be performed by trained, experienced examiners. Interobserver variability has been assessed in several recent studies, indicating excellent agreement among observers (149).

Our team has described that nodules near the trachea, particularly those located on the isthmus, can be associated with more artifacts in SWE evaluation. For this location, SE seems to have more reliable results (146). Fig. 10.6.17 and 10.6.18 present a case with an isthmic nodule, where SE shows elasticity, while SWE shows false stiffness.

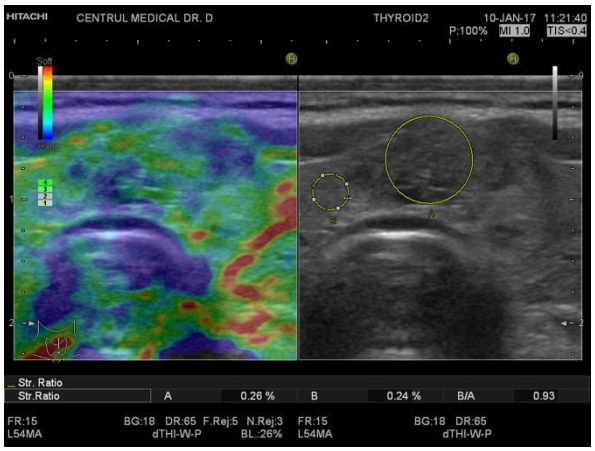

Fig. 10.6.17. Isthmic nodule evaluated with SE, TIRADS 3. RAGO 2

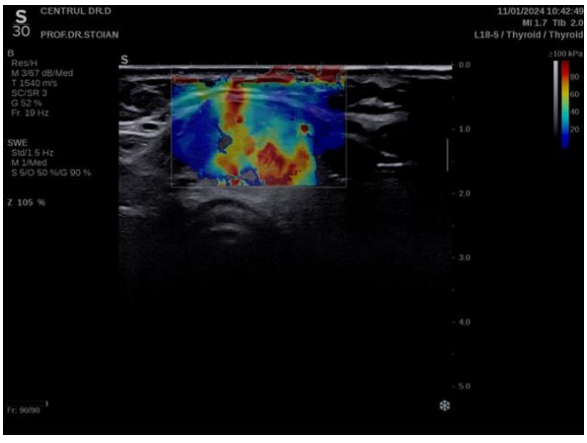

Fig. 10.6.18. Isthmic nodule evaluated with SWE, TIRADS 3. Stiffness score 4

Follicular carcinomas can appear elastic in SE, with a false-negative rate of 44%, but most are stiff when evaluated using 2D-SWE. Follicular adenomas also appear stiff in SE, but, in most cases, they do not exhibit stiffness in SWE. Medullary and metastatic carcinomas can also present false-negative results in SE (150, 151).

Some studies have reported lower diagnostic performance for nodules *exceeding 3 cm* or very small lesions. Additionally, the idea of validating different elastographic thresholds in SWE evaluation has been proposed, depending on the size of the nodule being analyzed, with thresholds increasing as the size of the nodules grows (152).

In *obese* patients, as well as in deeply situated lesions, which can generate false images or be unevaluable by elastography regardless of the method used, elastographic evaluation is limited, especially for SWE (153, 154). Other limitations of elastography, regardless of the technique, include peripheral calcifications, which increase rigidity and can generate a posterior shadow. Intranodular macrocalcifications always produce stiff images in SWE without significantly influencing the elastographic map in SE (155).

Large cystic components do not allow for the passage of shear waves in SWE, leading to artifacts that can confirm the presence of a cystic component. Since shear waves do not travel well through fluid-filled areas, these regions will appear without a shear wave signal on elastographic images; the characteristic RGB aspect confirms the cystic nature in strain elastography (156). In mixed lesions with a cystic component, strain elastography can be useful in detecting thyroid cancer by identifying a high SR value in the solid component (157).

Necrosis areas are often present in the centre of differentiated thyroid carcinomas and can induce soft elastographic images, especially in SWE (158).

Strain elastography has limitations in nodules *smaller than 5 mm*, although no lower size limit for its use has been established. For subcentimeter nodules, SWE provides more accurate diagnostic elastographic information compared to SE (150).

10.7. The Role of Elastography in Diffuse Thyroid Pathology

The introduction of elastography in evaluating diffuse thyroid pathology originates from its diagnostic and prognostic role in hepatic pathology regarding chronic disease progression.

There are several studies defining normal values in thyroid elastography. Since strain elastography does not provide direct quantitative measurement, normal thyroid elasticity is defined by shear wave elastography, particularly 2D-SWE, with values of 9.0 ± 11.3 kPa (159), 13.5 ± 3.3 kPa (160), 13.34 ± 3.2 kPa (161), and 10.97 ± 3.1 kPa (162). Normative values are also described for the point technique, with corresponding SWV values of 1.60 ± 0.18 m/s (163) and an average of 1.98 m/s (163) (74). The measurement is considered accurate, with minimal inter-observer variability of 0.97-0.98 (164) and intra-observer reproducibility of 0.78-0.85 (165). It is recommended to perform three determinations per lobe, using the median values (166).

Elastography is useful in diagnosing autoimmune thyroid disease in both adult (159, 160, 163, 165, 167-172) and pediatric populations (170, 172-176). In the pediatric population, no correlation is observed between the degree of fibrosis and age, weight, or pubertal stage (70, 164). Other authors describe a positive correlation between elasticity indices and age in the adolescent population (176).

Both strain elastography (170, 175), monoplane ARFI, and 2D-SWE techniques have been studied by various groups, all revealing that, regardless of the disease stage, autoimmune thyroid disease associates with increased elasticity indices (72, 74, 159-165, 172, 176) compared to the non-thyroid population. The diagnostic value is certain, predicting autoimmune thyroid disease with a sensitivity of up to 96.9% and specificity of 100% (174).

There are also various threshold values indicative of autoimmune thyroid disease presence, but no consensus exists on the discriminative values of elasticity indices (21). Data related to the predictive value of elastography regarding disease progression, especially towards hypothyroidism, are controversial. Some studies reveal higher elasticity indices due to fibrosis progression in cases requiring thyroid hormone replacement therapy (123, 170), but this finding is not universally demonstrated (169, 175).

The subtypes of autoimmune thyroid disease, including asymptomatic, hypothyroid, or hyperthyroid phases, are difficult to differentiate strictly based on elastography, essentially showing differences between autoimmune and non-autoimmune types, with minimal, non-significant differences between Hashimoto's and Graves' disease variants (168). Additionally, there are controversies regarding the correlation between elastographic parameters and antithyroid antibody titers, which are pathognomonic for the positive diagnosis of thyroid autoimmunity (173).

Elastographic evaluation of diffuse pathology should be integrated into the multiparametric thyroid model in stages: 2B ultrasound identifies cases with diffuse thyroid pathology, power Doppler evaluation identifies hyperfunctional cases, elastography differentiates autoimmune from non-autoimmune substrates, and subacute thyroid destruction from non-subacute to correctly identify treatment categories: replacement therapy, anti-inflammatory, or antithyroid treatment (167).

In conclusion, elastography finds a well-deserved place in the multiparametric ultrasound evaluation of thyroid pathology. It contributes to discriminating most solid thyroid nodular lesions, as rigid thyroid cancers, predominantly papillary ones, are identified. Detecting a rigid intranodular area implies referral for FNA, facilitates biopsy guidance, or nodule selection for the procedure. Rigidity can be considered an additional risk factor in nodules with indeterminate cytology, alongside anamnestic, clinical, or molecular factors. Lastly, elastographic evaluation of diffuse thyroid pathology helps classify patients into subcategories: healthy, autoimmune thyroiditis with hypothyroidism, hyperthyroidism due to aggression, or hyperproduction.

10.8. Role of Elastography in Parathyroid Gland Evaluation

Medical advances have improved diagnostic methods, therefore increasing the incidence of various endocrine disorders (177, 178). Hyperparathyroidism is a common endocrine disorder, often referred to as primary hyperparathyroidism. In terms of incidence, it is the third most common endocrinopathy after type 2 diabetes and thyroid diseases (179). The most common cause of primary hyperparathyroidism is a parathyroid adenoma, followed by parathyroid hyperplasia and parathyroid carcinoma (180-182). Secondary hyperparathyroidism is a frequent complication of chronic kidney disease, with a high prevalence in patients undergoing renal replacement therapy, dialysis (183, 184). Currently, primary hyperparathyroidism is diagnosed in asymptomatic forms, especially in premenopausal women, through active screening with high serum parathyroid hormone (PTH) levels and consequently high serum calcium levels (177, 185-187). Secondary hyperparathyroidism is common in the chronic kidney disease population and is caused by calcium-phosphorus metabolism disorders. The reported prevalence in the literature is high among dialysis patients, about 54% in the United States and Europe, up to 43.8% in France, 46.8% in Russia, and 42.9% in the United Kingdom (183).

The pathophysiological mechanism of primary hyperparathyroidism (PHPT) shows a loss of homeostatic control in the synthesis and secretion pathway of parathyroid hormone, resulting in increased PTH secretion and/or marked proliferation of cells with normal PTH levels. Single adenomas are of monoclonal origin, suggesting tumors that originate from a single abnormal cell (188), while hyperplastic parathyroid tumors are usually genetically polyclonal (177). On the other hand, secondary hyperparathyroidism (sHPT) has a multifactorial and complex mechanism caused by hypocalcemia, vitamin D deficiency, hyperphosphatemia, and high levels of fibroblast growth factor (FGF23). In this case, sHPT could be modified by treating the underlying disease, chronic renal failure, or vitamin D deficiency. However, chronic stimulation of the parathyroid glands can become autonomous, resulting in persistent tertiary hyperparathyroidism (180, 189-191).

Regardless of hyperparathyroidism etiology, surgery is a legitimate, validated, and corrective treatment for both primary and secondary hyperparathyroidism. Minimally invasive parathyroidectomy (MIP) is considered the preferred approach and is currently recommended; therefore, correctly identifying the number and location of affected parathyroid glands in preoperative evaluation is necessary, with ultrasound being the most cost-effective method (192). Given the positive characteristics of ultrasound, such as its non-invasive nature, real-time high resolution, reproducibility, ease of manipulation, safety for children and pregnant women, and the absence of X-ray exposure or contrast agent administration, it is the most accessible, reliable, and cost-effective imaging technique for identifying pathological parathyroid glands (193, 194).

Ultrasound visualization of the parathyroid glands includes both normal parathyroids (Fig. 10.8.1) and hypertrophied parathyroids, such as parathyroid adenomas (Fig. 10.8.2). The localization of hypertrophied or hyperplastic parathyroids is necessary only in cases of hyperparathyroidism (primary, secondary, or tertiary) that require surgical intervention.

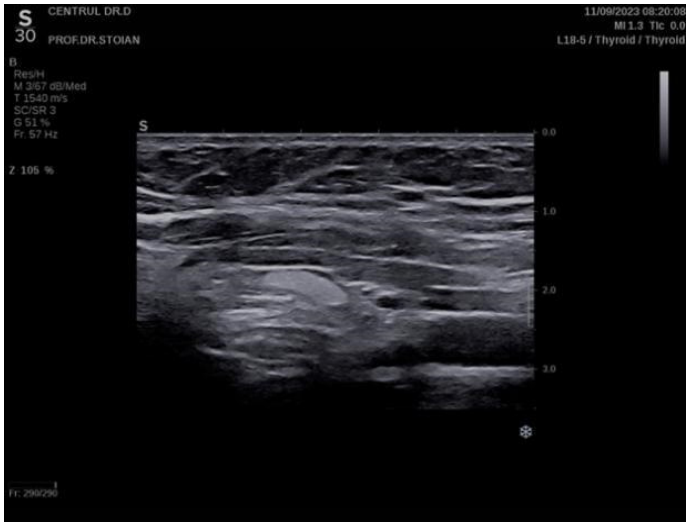

Fig. 10.8.1. Physiologic Parathyroid

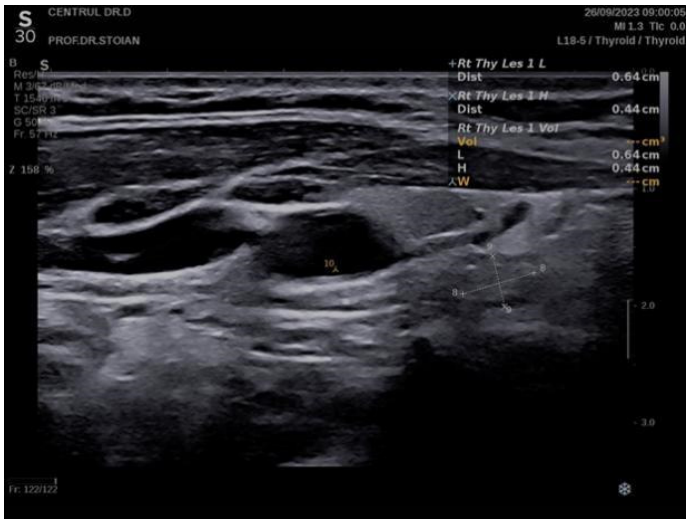

Fig. 10.8.2. Parathyroid Adenoma

Elastography is a validated and complementary method, referred to as "palpation imaging," which provides qualitative and quantitative information about the examined tissue, such as anatomical architecture and changes in tissue elasticity (193, 195-197). It is recognized as a marker of pathological conditions in many clinical fields, contributing to positive identification, differential diagnosis, and therapeutic management. Its role is established in endocrinology for the evaluation of the thyroid and parathyroids (187, 189, 198), hepatogastroenterology (199-201), senology (202, 203), urology (204), and otorhinolaryngology (205).

Elastography has been used in the evaluation of primary and secondary hyperparathyroidism, demonstrating its clinical importance (187, 189, 206, 207). It can accurately differentiate parathyroid tissue from thyroid or muscle tissue. However, the technique is not useful for evaluating physiologic parathyroids.

US is a highly accessible imaging technique in endocrinology, the golden standard for evaluating the thyroid and parathyroids (208-210). Ultrasound evaluation requires precise observation and identification of anatomical structures in both longitudinal and transverse views (211, 212). Additional techniques, such as head rotation or swallowing, can improve the identification of anatomical structures and ectopic parathyroid glands (211). The sensitivity of ultrasound identification of parathyroid tumors varies from 70-80% (213), with a higher positive identification rate for parathyroid hyperplasia ranging from 30-90% (214). However, the accuracy depends on the tumour's location and size (215), the patient's body habitus and gland morphology, as well as the operator's experience (212). The common false-positive ultrasound results are due to structures that mimic parathyroid adenomas, such as thyroid nodules, lymph nodes, thymus, muscles, vessels, and the oesophagus (216).

Parathyroid adenomas typically have a peripheral vascular margin and an abnormally increased blood flow compared to that of the thyroid (217). Therefore, adding the color Doppler mode to the ultrasound evaluation can increase the accuracy and sensitivity of ultrasound by 54% (218) (Fig. 10.8.3).

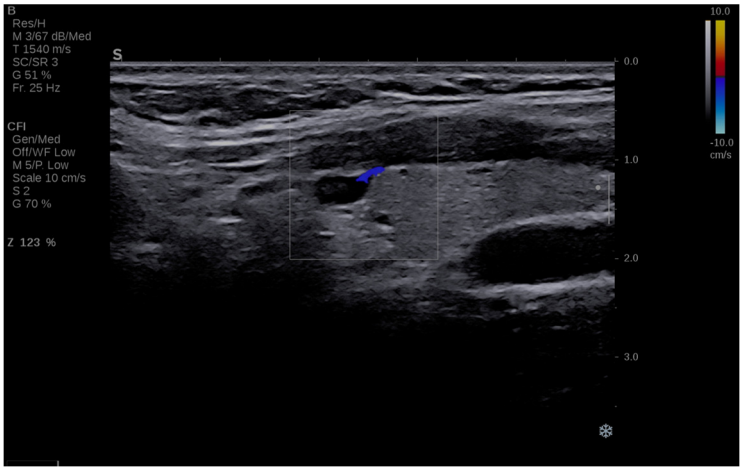

Fig. 10.8.3. Identification of peripheral flow using Color Doppler mode, complementary to 2B mode ultrasound.

Elastography can provide additional information on tissue stiffness, useful in evaluating parathyroid disease. Neoplastic, fibrous, or atherosclerotic tissue changes are reflected in tissue stiffness in elastographic evaluation. The development of neoplastic tissue can be identified at an early stage because, physiopathologically, there may be an increased production of connective tissue, changes in cellular density, and increased blood flow, all of which lead to changes in the tissue matrix and, consequently, tissue elasticity. Elastography can identify differences between benign and malignant tissues at the beginning of the disease

development, offering high sensitivity and resolution for deep structures (197, 220, 221). Elastography is performed after a 2B ultrasound of the parathyroid glands. It can be performed on all patients, is cost-effective, and adds valuable information. The elastography module is available on several ultrasound machines, such as the Aixplorer Mach 30 (SuperSonic Imagine, France), Philips, Fujifilm, and Hitachi Preirus (Hitachi Medical Corporation, Tokyo, Japan) (219).

Parathyroid elastography is performed with a high-resolution linear transducer of 15-4 or 18-5 MHz, chosen based on image clarity; deep parathyroid glands are evaluated with the 15-4 probe, which provides better images. The patient is examined in a supine position with neck extension, maintaining regular shallow breathing. The following parathyroid parameters are evaluated: location, shape, dimensions, and total gland volume.

As in thyroid pathology, SE requires the application of external pressure to induce tissue deformation, which is subsequently quantified by the device's software. An elastographic map is superimposed on the grayscale 2B image, displayed as a color map (red for fluid, green for soft tissue, blue for hard tissue), allowing the examiner to obtain qualitative information about tissue stiffness for the examined area (219). Semi-quantitative values are obtained by comparing tissue stiffness in the ROI of the target tissue with adjacent tissue, calculating a stiffness ratio, or strain ratio, as shown in Fig. 10.8.

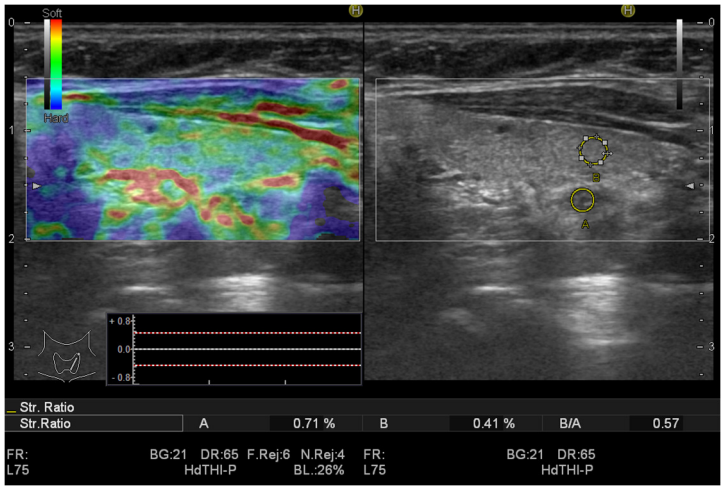

Fig. 10.8.4. SE Elastogram. Left inferior parathyroid adenoma, soft, strain ratio = 0.57

In the case of SWE, the examiner must maintain precise adherence of the probe to the examined area for at least 6 seconds, avoiding compression, allowing the transducer to induce acoustic vibrations in the parathyroid tissue. After the image stabilizes, a real-time elastogram with a color map is superimposed on the B-mode image. Once the image is stabilized, quantitative measurements can be performed on a static image.

Quantitative information, described as the elasticity index, is obtained from the static elastogram image using a quantification area Q-box placed in the ROI. After calculation by the software, elasticity parameters are displayed E_{Mean}, E_{Min}, E_{Max}, and standard deviation (SD). All

measurements are numerically expressed in kPa. Since there is no recommended scale setting for parathyroid examination, we recommend using a thyroid scale (0-100 kPa) (Fig. 10.8.5).

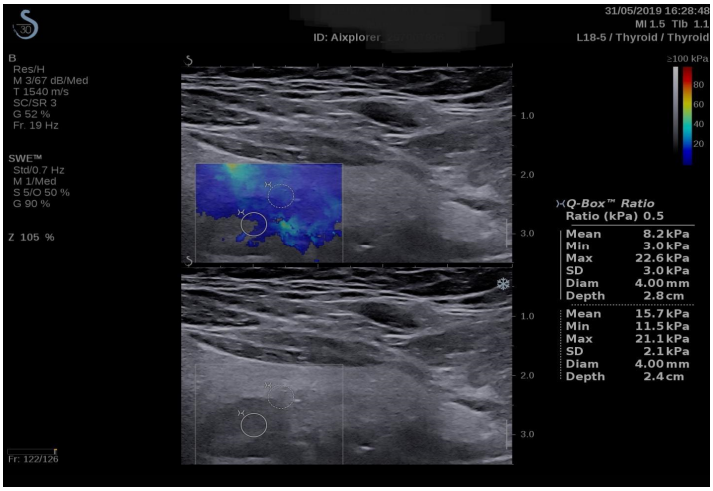

Fig. 10.8.5. Elastogram in shear wave elastography displaying incomplete colormap in a profound parathyroid lesion.

Experience with strain elastography in parathyroid disease has mainly focused on parathyroid adenomas, as parathyroid hyperplasia is more challenging to evaluate with this form of elastography (189). The classification scale used for evaluating parathyroid lesions is represented by the Rago criteria, often used for thyroid pathology. The Rago criteria (222), described for thyroid pathology, especially for nodular goiter, have been used for the qualitative assessment of strain elastography as follows: a score of 1 means that the elasticity in the entire lesion is soft tissue, a score of 2 means that the tissue is mostly soft, a score of 3 is defined by soft tissue in the peripheral part of the lesion, a score of 4 means that the examined lesion is completely rigid, and a score of 5 means that the rigidity extends beyond the lesion margins and infiltrates the surrounding tissues. The main disadvantage of this qualitative technique is the depth of the evaluated tissue or lesion, which leads to an incomplete, unusable, and uninterpretable color map at greater depths. Most parathyroid adenomas evaluated by our group in previously published work had a score of 1 according to the Rago criteria (Fig. 10.8.6) (223).

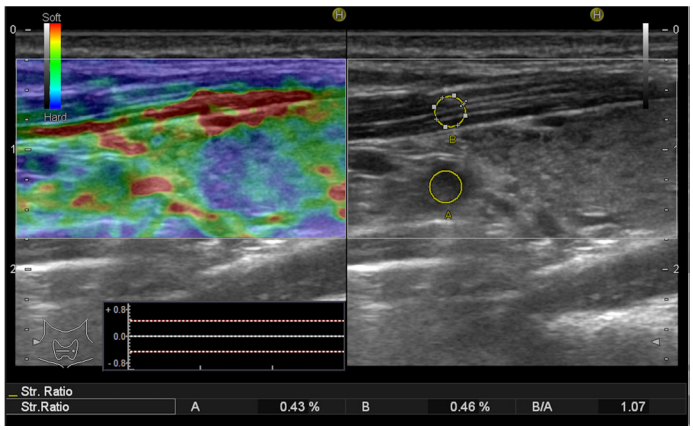

Fig. 10.8.6. Parathyroid adenoma evaluated according to the Rago criteria, score 1.

In the first study conducted by our group on the utility of strain elastography in primary hyperparathyroidism, we evaluated the qualitative and semi-quantitative elastographic values of identified parathyroid adenomas in 20 consecutive patients diagnosed with primary hyperparathyroidism. Of the 20 cases, two parathyroid adenomas could not be evaluated, and the rest had a score of 1 according to the Rago criteria (223). The size and location of the parathyroid adenomas were also quantified, with the average size of the parathyroid adenoma on ultrasound being 0.776 ± 0.50 cm, with a maximum size of 2.46 cm and a minimum size of 0.34 cm. Most parathyroid adenomas were found near the right superior lobe (nine adenomas), three near the right inferior lobe, three near the left superior lobe, and five near the left inferior lobe. In terms of ultrasound appearance, 13 parathyroid adenomas had a cystic appearance (65%), five had a solid homogeneous and hypoechoic appearance (25%), and two adenomas had a mixed appearance (10%) - mostly cystic, with one having an elongated shape. Semi-quantitative information was obtained by comparing the tissue strain of the parathyroid adenoma parenchyma with thyroid or muscle tissue. No significant differences were found between the strain ratio determined by calculating the mean elasticity ratio (ER) between the parathyroid adenoma and thyroid tissue (nine cases out of twenty) with a mean ER of 1.465 ± 1.458, and the stiffness ratio of the parathyroid adenoma compared to the stiffness ratio of thyroid tissue with autoimmune disease (11 cases out of 20) with a mean ER = 1.656 ± 1.746, p = 0.481 (223).

Our working group also studied 2D-SWE elastography in parathyroid pathology. We conducted several prospective studies on primary and secondary hyperparathyroidism, comparing elastographic results from parathyroid tissue to evaluate differences between the two clinical entities, as the pathophysiological mechanism is quite different. The first study (223) evaluated shear wave elastography values in primary hyperparathyroidism. Twenty patients with primary hyperparathyroidism and a solitary adenoma were included. Parathyroid tissue was compared with thyroid and muscle tissue, as normal parathyroid adenomas cannot be evaluated by ultrasound. The best parameter identified for evaluating parathyroid adenomas was the E_{Mean} elastographic index, with the highest specificity, sensitivity, and accuracy. The results are presented in Table 10 (223).

Table 10.1. Sensitivity, specificity, ROC curve for mean elastographic index measured ER for primary and secondary hyperparathyroidism (223).

	ER Mean Parathyroid Adenoma/Thyroid Tissue	ER Mean Parathyroid Adenoma/Muscle Tissue	ER Mean Parathyroid Hyperplasia/Thyroid Tissue	ER Mean Parathyroid Hyperplasia/Muscle Tissue
AUC value	0.950	0.997	0.940	0.949
Specificity	90.0%	95.0%	90.7%	90.7%
Sensitivity	95.0%	100.0%	94.8%	93.8%
PPV	90.5%	95.2%	91.1%	91.0%
NPV	94.7%	100.0%	94.6%	93.6%
Accuracy	92.5%	97.5%	92.26%	91.75%
p-value	<0.001	<0.001	<0.001	<0.001
Cut-off value	***<7.28 kPa***	***<10.47 kPa***	***<9.74 kPa***	***<9.98 kPa***

PPV: Positive Predictive Value, NPV: Negative Predictive Value

Statistical analysis showed a significant difference between parathyroid elasticity (kPa) and thyroid and muscle elasticity ($p < 0.001$). A second study (224), previously published, was conducted on patients undergoing renal replacement therapy with secondary hyperparathyroidism. A cohort of 120 patients was evaluated, of which 59 were found to have secondary parathyroid hyperplasia. Ninety-seven hyperplastic parathyroid glands were evaluated, comparing normal thyroid and muscle tissue with hyperplastic parathyroid tissue. Statistical differences were found in this cohort, and the best parameter for evaluating parathyroid tissue elasticity and cut-off values were identified (Table 1) (224). After analysing the two cohorts, a natural question arose - are there differences between primary and secondary hyperparathyroidism in elastographic evaluation? In a third study our group addressed this question by evaluating 68 patients: 27 with primary hyperparathyroidism (Fig. 10.8.7.b) and 41 with secondary hyperparathyroidism (Fig. 10.8.7.a). The results are presented in Table 10.II (225). Statistically significant differences in sex distribution were found between the groups ($p < 0.001$, Fisher's exact test). Given the different pathophysiological pathways, diagnostic tests were performed to evaluate elastographic differences between primary and secondary hyperparathyroidism (225).

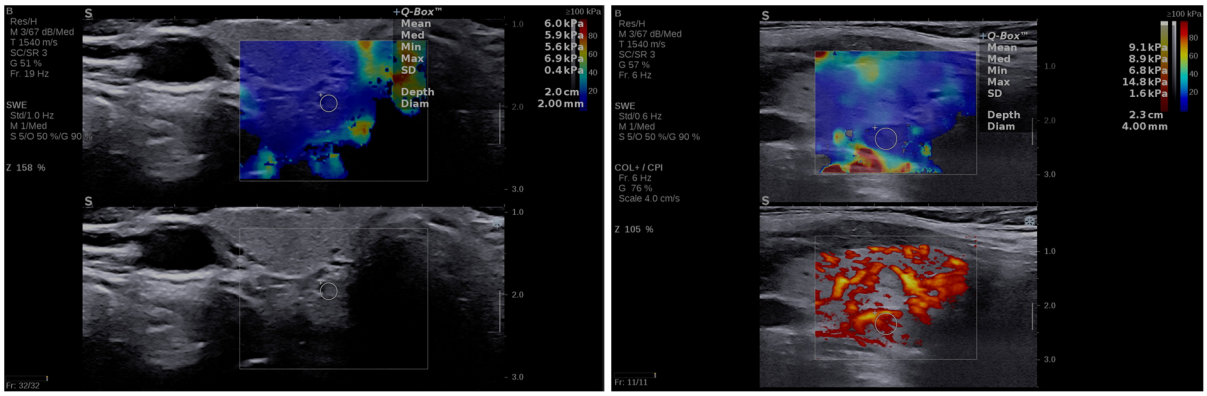

Fig. 10.8.7.a: Primary hyperparathyroidism; b: Secondary hyperparathyroidism

Table 10.2. SWE results of the study comparing primary and secondary hyperparathyroidism (225).

	pHPT	sHPT	p-value
E_{Mean} parathyroid	4.86 [3.42 – 5.84]	6.96 [6.09 – 8.44]	<0.001
ER parathyroid/thyroid tissue	0.4040 [0.324 – 0.486]	0.520 [0.420 – 0.660]	<0.001
ER parathyroid/thyroid	0.2960 [0.226 – 0.372]	0.452 [0.348 – 0.667]	<0.001

pHPT – primary hyperparathyroidism; sHPT – secondary hyperparathyroidism

Note: Specific values for these parameters were not provided in the text; they would be filled in based on the study results. PPV: Positive Predictive Value, NPV: Negative Predictive Value.

There is no "when and how" in the current literature, i.e., applied studies for conventional parathyroid ultrasound examination and ultrasound elastography in cases of secondary renal hyperparathyroidism. The prevalence of this endocrine disease and the necessity of discriminatory diagnosis, identification, and localization before definitive treatment is mandatory (225). This study confirms significant differences in elasticity between parathyroid, thyroid, and muscle tissues, both in parathyroid adenomas and hyperplasia, with parathyroid tissue exhibiting significantly lower elasticity than the other two tissues studied.

Comparing the two groups of patients with primary and secondary renal hyperparathyroidism, we can confirm that, regardless of etiology, using elastography as a complementary technique to ultrasound, we can differentiate parathyroid tissue, as it will present a lower elasticity index than thyroid or muscle tissue (225).

Parathyroid adenoma has a lower elasticity index than parathyroid hyperplasia in secondary renal hyperparathyroidism, likely due to the high cell occupancy rate resulting from renal disease. However, the EI will be lower than the thyroid EI and significantly lower than the muscle tissue elasticity index in both cases.

There are clinical implications for using elastography in the localization and treatment decisions in patients with primary and secondary hyperparathyroidism. It is a simple, operator-independent, repeatable, and reproducible method that can be used in addition to conventional ultrasound to accurately differentiate between thyroid and muscle tissue. Elastography could provide important information about parathyroid elasticity and be valuable in the localization and study of hyperparathyroidism.

When comparing the two types of hyperparathyroidism using the ROC curve, the best cut-off value for parathyroid adenoma is a mean SWE value of less than 5.96 kPa, highlighting the differences between primary and secondary hyperparathyroidism in cases of doubt. Given these significant differences, even when adjusting PTH values by age, the difference between serum PTH levels remains substantial, indicating that age has no effect on parathyroid hormone levels.

Elastography can be a useful qualitative and quantitative tool and can provide better differentiation of tissue elasticity in diagnosing parathyroid disease. Using 2D shear wave elastography, an elastographic value of less than 7 kPa is highly suggestive of parathyroid adenoma, and a value of less than 9.98 kPa is highly suggestive of parathyroid tissue in patients with secondary renal hyperparathyroidism.

In the field of primary hyperparathyroidism, different authors have reported various thresholds for parathyroid adenoma depending on the elastographic technique used. Using shear wave elastography, higher values were found for parathyroid adenoma (2.16 ± 0.33 m/s) compared to parathyroid hyperplasia (1.75 ± 0.28 m/s), identifying a threshold value for parathyroid adenoma greater than 1.92 m/s (210). Another study that compared elastographic results between thyroid and parathyroid tissue, using the same elastographic method as the previous one, concluded that the elastographic index of parathyroid adenomas is lower than that of thyroid tissue, with a shear wave velocity of 2.01 m/s and 2.77 m/s, respectively (226). Another representative study conducted an analysis using the 2D-SWE technique, comparing parathyroid adenomas with benign and malignant thyroid pathology. They found that parathyroid adenomas had a higher elasticity index than benign thyroid pathology (3.09 ± 0.75 m/s compared to 2.20 ± 0.39 m/s) and even higher elasticity than malignant thyroid lesions, with a mean SWV of 3.59 ± 0.43 m/s (227).

In 2D-SWE elastography, a study of parathyroid adenomas and benign thyroid nodules found that parathyroid adenomas had a significantly lower elasticity index than benign thyroid nodules (mean SWE 5.2 ± 7.2 kPa and 24.3 ± 33.8 kPa, respectively) (209). The results are similar to our conclusion when using the same elastographic method.

Some elastographic studies on parathyroid hyperplasia have been published, but they have not focused on patients with chronic kidney disease and haemodialysis. Currently, there are no other cut-off values for secondary hyperparathyroidism than those presented (207, 224).

Limitations and False-Positives

There are certain limitations of elastography in evaluating parathyroid glands, the most important being the difficulty in assessing ectopic and supernumerary parathyroid glands, especially when located in the thymus or posterior mediastinum. When using elastography, a low value close to zero might indicate the presence of a fluid lesion or a deep lesion inaccessible to the linear probe. It is very important to check the signal intensity to distinguish between fluid and deep lesions and to choose a linear probe with lower frequencies if available. Another limitation to consider is that tracheal or carotid artery movements can cause artifacts, in which case elastographic noise can be reduced by increasing the gain. One of the most important aspects of elastography is the external pressure applied to the probe, which can cause false-positive results. This is a limitation because it is operator-dependent and is less present in shear wave elastography than in strain elastography. Another aspect to consider is the choice of the elastography scale; since there is no recommendation for evaluating parathyroids, in our studies, we used a scale between 0 and 100 kPa.

The clinical importance of elastography in evaluating primary or secondary hyperparathyroidism is undeniable. As an adjunct to conventional ultrasound, elastography is a simple, non-invasive, repeatable, and reproducible method that can improve the diagnosis and preoperative evaluation of patients with primary or secondary hyperparathyroidism. Although there are certain limitations of the technique, such as operator experience, and some techniques are more operator-dependent than others, we must keep in mind that it is a complementary technique that is non-invasive, highly reproducible, easy to handle, offers high real-time resolution, is safe for children and pregnant women, and does not require exposure to X-rays or contrast agents, making it a very accessible and cost-effective imaging technique for the complementary evaluation of the parathyroid disease.

We found significant differences between primary and secondary hyperparathyroidism and identified a cut-off elastographic value for parathyroid adenomas below 5.96 kPa (223). One of the main questions of the studies was answered, and the next question was to determine a general cut-off value for parathyroid tissue. Therefore, we included both parathyroid adenoma and hyperplasia values in the analysis, allowing us to establish an average SWE cut-off value for parathyroid tissue below 9.58 kPa (207). Further studies may help determine elastographic differences between pathological parathyroid tissue and thyroid nodules. Recent studies in the literature have shown that there is a significant difference between malignant and benign thyroid nodules, with the former being stiffer than the latter. Additionally, benign thyroid nodules have a higher elasticity index than normal thyroid tissue. We can imagine that if parathyroid tissue were compared with benign or malignant thyroid tissue, a significant difference in elasticity would be found.

Elastography is a proven and validated method in many clinical fields and is recognized by current guidelines, including for thyroid diseases (228, 229). It undoubtedly plays an important role in locating parathyroid disease, being a useful tool for the qualitative and particularly for the quantitative assessment of the parathyroid tissue. Significant elastographic

differences were found between parathyroid adenoma and hyperplasia, but, in both cases, parathyroid tissue is significantly less elastic than healthy thyroid and surrounding muscle tissue.

Conflict of Interest

The authors declare no conflicts of interest.

References

1. Ferraioli G, Wong VWS, Castera L, Berzigotti A, Sporea I, Dietrich CF, et al. Liver Ultrasound Elastography: An Update to the World Federation for Ultrasound in Medicine and Biology Guidelines and Recommendations. Ultrasound Med Biol. 2018 Dec 1;44(12):2419–40.
2. Moon JH, Hyun MK, Lee JY, Shim JI, Kim TH, Choi HS, et al. Prevalence of thyroid nodules and their associated clinical parameters: a large-scale, multicenter-based health checkup study. Korean J Intern Med. 2018 Jul 1.
3. Paschou S, Vryonidou A, Goulis DG. Thyroid nodules: A guide to assessment, treatment and follow-up. Maturitas [Internet]. 2017 Feb 1 96:1–9.
4. Grussendorf M, Ruschenburg I, Brabant G. Malignancy rates in thyroid nodules: a long-term cohort study of 17,592 patients. Eur Thyroid J. 2022 Aug 8;11(4).
5. Marqusee E, Benson CB, Frates MC, Doubilet PM, Larsen PR, Cibas ES, et al. Usefulness of ultrasonography in the management of nodular thyroid disease. Ann Intern Med. 2000 Nov 7;133(9):696–700.
6. Krouskop TA, Wheeler TM, Kallel F, Garra BS, Hall T. Elastic Moduli of Breast and Prostate Tissues under Compression. http://dx.doi.org/101177/016173469802000403. 1998 Oct 1:260–74.
7. Garra BS, Cespedes EI, Ophir J, Spratt SR, Zuurbier RA, Magnant CM, et al. Elastography of breast lesions: initial clinical results. Radiology . 1997;202(1):79–86.
8. Zhao CK, Xu HX. Ultrasound elastography of the thyroid: principles and current status. Ultrasonography . 2019 Apr 1 38(2):106.
9. Lyshchik A, Higashi T, Asato R, Tanaka S, Ito J, Hiraoka M, et al. Elastic Moduli of Thyroid Tissues under Compression. http://dx.doi.org/101177/016173460502700204. 2005 Apr;27(2):101–10.
10. Sebag F, Vaillant-Lombard J, Berbis J, Griset V, Henry JF, Petit P, et al. Shear wave elastography: a new ultrasound imaging mode for the differential diagnosis of benign and malignant thyroid nodules. J Clin Endocrinol Metab. 2010;95(12):5281–8.
11. Haugen BR, Alexander EK, Bible KC, Doherty GM, Mandel SJ, Nikiforov YE, et al. 2015 American Thyroid Association Management Guidelines for Adult Patients with Thyroid Nodules and Differentiated Thyroid Cancer: The American Thyroid Association Guidelines Task Force on Thyroid Nodules and Differentiated Thyroid Cancer. Thyroid. 2016 Jan 1;26(1):1.

12. Gharib H, Papini E, Garber JR, Duick DS, Harrell RM, Hegedüs L, et al. AMERICAN ASSOCIATION OF CLINICAL ENDOCRINOLOGISTS, AMERICAN COLLEGE OF ENDOCRINOLOGY, AND ASSOCIAZIONE MEDICI ENDOCRINOLOGI MEDICAL GUIDELINES FOR CLINICAL PRACTICE FOR THE DIAGNOSIS AND MANAGEMENT OF THYROID NODULES--2016 UPDATE. Endocr Pract. 2016 May 1;22(5).
13. Ríos A, Rodríguez JM, Cepero A, Hernandez AM. Utility of elastography in thyroid nodules with indeterminate cytology. Endocrinología, Diabetes y Nutrición (English ed). 2017 Mar 1 [cited 2024 Feb 18];64(3):180–2.
14. Cantisani V, Ulisse S, Guaitoli E, de Vito C, Caruso R, Mocini R, et al. Q-Elastography in the Presurgical Diagnosis of Thyroid Nodules with Indeterminate Cytology. PLoS One. 2012 Nov 29 [cited 2024 Feb 17];7(11):e50725.
15. Lippolis P V., Tognini S, Materazzi G, Polini A, Mancini R, Ambrosini CE, et al. Is Elastography Actually Useful in the Presurgical Selection of Thyroid Nodules with Indeterminate Cytology? J Clin Endocrinol Metab. 2011 Nov 1;96(11):E1826–30.
16. Bardet S, Ciappuccini R, Pellot-Barakat C, Monpeyssen H, Michels JJ, Tissier F, et al. Shear Wave Elastography in Thyroid Nodules with Indeterminate Cytology: Results of a Prospective Bicentric Study. https://home.liebertpub.com/thy [Internet]. 2017 Nov 1;27(11):1441–9.
17. Qiu Y, Xing Z, Yang Q, Luo Y, Ma B. Diagnostic performance of shear wave elastography in thyroid nodules with indeterminate cytology: A systematic review and meta-analysis. Heliyon. 2023 Oct 1 [cited 2024 Feb 29];9(10):2405–8440.
18. Choi WJ, Park JS, Koo HR, Kim SY, Chung MS, Tae K. Ultrasound elastography using carotid artery pulsation in the differential diagnosis of sonographically indeterminate thyroid nodules. American Journal of Roentgenology . 2015 Feb 1;204(2):396–401.
19. Rago T, Scutari M, Santini F, Loiacono V, Piaggi P, Di Coscio G, et al. Real-time elastosonography: useful tool for refining the presurgical diagnosis in thyroid nodules with indeterminate or nondiagnostic cytology. J Clin Endocrinol Meta. 2010 ;95(12):5274–80.
20. Cosgrove D, Piscaglia F, Bamber J, Bojunga J, Correas JM, Gilja OH, et al. EFSUMB Guidelines and Recommendations on the Clinical Use of Ultrasound Elastography. Part 2: Clinical Applications Ultraschall in Med 2013; 34: 238-253 © Georg Thieme Verlag KG Stuttgart · New York ·. 2013 [cited 2024 Jan 7];
21. Cosgrove D, Barr R, Bojunga J, Cantisani V, Chammas MC, Dighe M, et al. WFUMB Guidelines and Recommendations on the Clinical Use of Ultrasound Elastography: Part 4. Thyroid. Ultrasound Med Biol [Internet]. 2017 Jan 1;43(1):4–26.
22. Mena G, Montalvo A, Ubidia M, Olmedo J, Guerrero A, Leon-Rojas JE. Elastography of the thyroid nodule, cut-off points between benign and malignant lesions for strain, 2D shear wave real time and point shear wave: a correlation with pathology, ACR TIRADS and Alpha Score. Front Endocrinol (Lausanne). 2023 Jun 16;14:1182557.
23. Amy D, Bercoff J, Bibby E. Breast elastography. Lobar Approach to Breast Ultrasound. 2018 Jun 6 ;85–106. Available from: https://link.springer.com/chapter/10.1007/978-3-319-61681-0_7
24. Bae U, Dighe M, Dubinsky T, Minoshima S, Shamdasani V, Kim Y. Ultrasound thyroid elastography using carotid artery pulsation: preliminary study. J Ultrasound Med. 2007;26(6):797–805. Available from: https://pubmed.ncbi.nlm.nih.gov/17526611/

25. Dighe M, Bae U, Richardson ML, Dubinsky TJ, Minoshima S, Kim Y. Differential diagnosis of thyroid nodules with US elastography using carotid artery pulsation. Radiology. 2008 Aug;248(2):662–9.
26. Bamber J, Cosgrove D, Dietrich CF, Fromageau J, Bojunga J, Calliada F, et al. EFSUMB guidelines and recommendations on the clinical use of ultrasound elastographypart 1: Basic principles and technology. Ultraschall in der Medizin [Internet]. 2013;34(2):169–84.
27. Cantisani V, Grazhdani H, Drakonaki E, D'Andrea V, Di Segni M, Kaleshi E, et al. Strain US Elastography for the Characterization of Thyroid Nodules: Advantages and Limitation. Int J Endocrinol. 2015;2015. Available from: /pmc/articles/PMC4411438/
28. Elastography of the Thyroid Gland | Radiology Key.
29. Cosgrove [1]D, Piscaglia F, Bamber J, Bojunga J, Correas JM, Gilja OH, et al. EFSUMB guidelines and recommendations on the clinical use of ultrasound elastography. Part 2: Clinical applications. Ultraschall Med. 2013;34(3):238–53.
30. Ophir J, Céspedes I, Ponnekanti H, Yazdi Y, li X. Elastography: a quantitative method for imaging the elasticity of biological tissues. Ultrason Imaging. 1991;13(2):111–34.
31. Asteria C, Giovanardi A, Pizzocaro A, Cozzaglio L, Morabito A, Somalvico F, et al. US-elastography in the differential diagnosis of benign and malignant thyroid nodules. Thyroid. 2008 May 1;18(5):523–31.
32. Itoh A, Ueno E, Tohno E, Kamma H, Takahashi H, Shiina T, et al. Breast disease: clinical application of US elastography for diagnosis. Radiology. 2006 May;239(2):341–50.
33. Rubaltelli L, Stramare R, Tregnaghi A, Scagliori E, Cecchelero E, Mannucci M, et al. The role of sonoelastography in the differential diagnosis of neck nodules. J Ultrasound. 2009 Sep;12(3):93–100.
34. Rago T, Santini F, Scutari M, Pinchera A, Vitti P. Elastography: new developments in ultrasound for predicting malignancy in thyroid nodules. J Clin Endocrinol Metab [Internet]. 2007 [cited 2024 Feb 4];92(8):2917–22.
35. Azizi G, Keller J, Lewis M, Puett D, Rivenbark K, Malchoff C. Performance of elastography for the evaluation of thyroid nodules: a prospective study. Thyroid. 2013 Jun 1;23(6):734–40.
36. Sun J, Cai J, Wang X. Real-time ultrasound elastography for differentiation of benign and malignant thyroid nodules: a meta-analysis. J Ultrasound Med. 2014 Mar 1;33(3):495–502.
37. Wang H, Brylka D, Sun LN, Lin YQ, Sui GQ, Gao J. Comparison of strain ratio with elastography score system in differentiating malignant from benign thyroid nodules. Clin Imaging. 2013 Jan;37(1):50–5.
38. Razavi SA, Hadduck TA, Sadigh G, Dwamena BA. Comparative effectiveness of elastographic and B-mode ultrasound criteria for diagnostic discrimination of thyroid nodules: a meta-analysis. AJR Am J Roentgenol. 2013 Jun;200(6):1317–26.
39. Cantisani V, De Silvestri A, Scotti V, Fresilli D, Tarsitano MG, Polti G, et al. US-Elastography With Different Techniques for Thyroid Nodule Characterization: Systematic Review and Meta-analysis. Front Oncol. 2022 Mar 16;12.
40. Garra BS. Elastography: current status, future prospects, and making it work for you. Ultrasound Q [Internet]. 2011 Sep [cited 2024 Feb 7];27(3):177–86.
41. Hegedüs L. Can elastography stretch our understanding of thyroid histomorphology? J Clin Endocrinol Metab [Internet]. 2010 [cited 2024 Feb 7];95(12):5213–5.

42. Szczepanek-Parulska E, Woliński K, Stangierski A, Gurgul E, Ruchała M. Biochemical and ultrasonographic parameters influencing thyroid nodules elasticity. Endocrine [Internet]. 2014 Oct 21 [cited 2024 Feb 7];47(2):519–27. Available from: https://pubmed.ncbi.nlm.nih.gov/24535467/
43. Dudea SM, Botar-Jid C. Ultrasound elastography in thyroid disease. Med Ultrason. 2015 17(1):74–96.
44. Wang HL, Zhang S, Xin XJ, Zhao LH, Li CX, Mu JL, et al. Application of Real-time Ultrasound Elastography in Diagnosing Benign and Malignant Thyroid Solid Nodules. Cancer Biol Med. 2012 Jun 9(2):124.
45. Luo S, Lim DJ, Kim Y. Objective ultrasound elastography scoring of thyroid nodules using spatiotemporal strain information. Med Phys. 2012 ;39(3):1182–9.
46. El-Hariri MA, Taha Ali TF, Tawab MA, Magid AMA, El-Shiekh AF. The clinical value of ultrasound elastography in predicting malignant thyroid nodules. Egyptian Journal of Radiology and Nuclear Medicine. 2014;45(2):353–9.
47. Cantisani V, Lodise P, Grazhdani H, Mancuso E, Maggini E, Di Rocco G, et al. Ultrasound elastography in the evaluation of thyroid pathology. Current status. Eur J Radiol. 2014 Mar 1;83(3):420–8.
48. Okasha HH, Mansor M, Sheriba N, Assem M, Abdelfattah Y, Ashoush OA, et al. Role of elastography strain ratio and TIRADS score in predicting malignant thyroid nodule. Arch Endocrinol Metab. 2021 Nov 1;64(6):735–42.
49. Stoian D, Timar B, Derban M, Pantea S, Varcus F, Craina M, et al. Thyroid Imaging Reporting and Data System (TI-RADS): the impact of Quantitative Strain Elastography for better stratification of cancer risks. Med Ultrason. 2015 Sep 1;17(3):327–32.
50. Wang J, Li P, Sun L, Sun Y, Fang S, Liu X. Diagnostic value of strain ratio measurement in differential diagnosis of thyroid nodules coexisted with Hashimoto thyroiditis. Int J Clin Exp Med. 2015;8(4):6420.
51. Chong Y, Shin JH, Ko ES, Han BK. Ultrasonographic elastography of thyroid nodules: Is adding strain ratio to colour mapping better? Clin Radiol. 2013 Dec 1;68(12):1241–6.
52. Dighe M, Luo S, Cuevas C, Kim Y. Efficacy of thyroid ultrasound elastography in differential diagnosis of small thyroid nodules. Eur J Radiol. 2013 Jun 1;82(6):e274–80.
53. Bae U, Dighe M, Dubinsky T, Minoshima S, Shamdasani V, Kim Y. Ultrasound thyroid elastography using carotid artery pulsation: preliminary study. J Ultrasound Med. 2007;26(6):797–805.
54. Zhang FJ, Han RL, Zhao XM. The value of virtual touch tissue image (VTI) and virtual touch tissue quantification (VTQ) in the differential diagnosis of thyroid nodules. Eur J Radiol. 2014 Nov 1;83(11):2033–40.
55. Sung HP, Soo JK, Kim EK, Min JK, Eun JS, Kwak JY. Interobserver agreement in assessing the sonographic and elastographic features of malignant thyroid nodules. AJR Am J Roentgenol. 2009 Nov ;193(5).
56. Bojunga J, Herrmann E, Meyer G, Weber S, Zeuzem S, Friedrich-Rust M. Real-time elastography for the differentiation of benign and malignant thyroid nodules: a meta-analysis. Thyroid. 2010 Oct 1;20(10):1145–50.
57. Casťera L, Foucher J, Bernard PH, Carvalho F, Allaix D, Merrouche W, et al. Pitfalls of liver stiffness measurement: a 5-year prospective study of 13,369 examinations. Hepatology. 2010 Mar;51(3):828–35.

58. Cantisani V, Grazhdani H, Ricci P, Mortele K, Di Segni M, D'Andrea V, et al. Q-elastosonography of solid thyroid nodules: Assessment of diagnostic efficacy and interobserver variability in a large patient cohort. Eur Radiol. 2014 Jan 27;24(1):143–50.
59. Song G, Jing L, Yan M, Cong S, Xuejiao W. Influence of various breast factors on the quality of strain elastograms. J Ultrasound Med. 2015 Mar 1;34(3):395–400.
60. Zou H, Xue Y, Ou Y, Li S, Zhao Y, Shao L, et al. Factors Affecting the Quality of Breast Quasistatic Ultrasound Elastograms. J Ultrasound Med. 2018 Jul 1;37(7):1701–12.
61. Luo S, Lim DJ, Kim Y. Objective ultrasound elastography scoring of thyroid nodules using spatiotemporal strain information. Med Phys. 2012;39(3):1182–9.
62. Hong YR, Wu YL, Luo ZY, Wu NB, Liu XM. Impact of nodular size on the predictive values of gray-scale, color-Doppler ultrasound, and sonoelastography for assessment of thyroid nodules. J Zhejiang Univ Sci B. 2012 Sep;13(9):707.
63. Xing P, Wu L, Zhang C, Li S, Liu C, Wu C. Differentiation of benign from malignant thyroid lesions: calculation of the strain ratio on thyroid sonoelastography. J Ultrasound Med [Internet]. 2011 May 1 [cited 2024 Feb 17];30(5):663–9.
64. Moon HJ, Sung JM, Kim EK, Yoon JH, Youk JH, Kwak JY. Diagnostic performance of gray-scale US and elastography in solid thyroid nodules. Radiology. 2012 Mar;262(3):1002–13.
65. Hong Y, Liu X, Li Z, Zhang X, Chen M, Luo Z. Real-time ultrasound elastography in the differential diagnosis of benign and malignant thyroid nodules. J Ultrasound Med. 2009 Jul 1;28(7):861–7.
66. Wang HL, Zhang S, Xin XJ, Zhao LH, Li CX, Mu JL, et al. Application of Real-time Ultrasound Elastography in Diagnosing Benign and Malignant Thyroid Solid Nodules. Cancer Biol Med. 2012 Jun;9(2):124.
67. Haugen BR, Alexander EK, Bible KC, Doherty GM, Mandel SJ, Nikiforov YE, et al. 2015 American Thyroid Association Management Guidelines for Adult Patients with Thyroid Nodules and Differentiated Thyroid Cancer: The American Thyroid Association Guidelines Task Force on Thyroid Nodules and Differentiated Thyroid Cancer. Thyroid. 2016 Jan 1;26(1):1–133.
68. Calcifications on thyroid ultrasound do not necessarily represent thyroid cancer. https://www.thyroid.org/patient-thyroid-information/ct-for-patients/may-2018/vol-11-issue-5-p-8-9.
69. Lu Z, Mu Y, Zhu H, Luo Y, Kong Q, Dou J, et al. Clinical value of using ultrasound to assess calcification patterns in thyroid nodules. World J Surg . 2011 Jan 2;35(1):122–7.
70. Cepeha CM, Paul C, Borlea A, Borcan F, Fofiu R, Dehelean CA, et al. The Value of Strain Elastography in Predicting Autoimmune Thyroiditis. Diagnostics. 2020 Oct 27;10(11).
71. Menzilcioglu MS, Duymus M, Gungor G, Citil S, Sahin T, Boysan SN, et al. The value of realtime ultrasound elastography in chronic autoimmune thyroiditis. British Journal of Radiology. 2014 Dec 1;87(1044).
72. Ruchala M, Szczepanek-Parulska E, Zybek A, Moczko J, Czarnywojtek A, Kaminski G, et al. The role of sonoelastography in acute, subacute and chronic thyroiditis: a novel application of the method. Eur J Endocrinol. 2012 Mar 1;166(3):425–32
73. Görgülü FF. Which Is the Best Reference Tissue for Strain Elastography in Predicting Malignancy in Thyroid Nodules, the Sternocleidomastoid Muscle or the Thyroid Parenchyma? J Ultrasound Med. 2019 Nov 1;38(11):3053–64.

74. Friedrich-Rust M, Romenski O, Meyer G, Dauth N, Holzer K, Grünwald F, et al. Acoustic Radiation Force Impulse-Imaging for the evaluation of the thyroid gland: A limited patient feasibility study. Ultrasonics. 2012 Jan;52(1):69–74.
75. Stoian D, Borcan F, Petre I, Mozos I, Varcus F, Ivan V, et al. Strain Elastography as a Valuable Diagnosis Tool in Intermediate Cytology (Bethesda III) Thyroid Nodules. Diagnostics. 2019 Sep 1;9(3).
76. Friedrich-Rust M, Vorlaender C, Dietrich CF, Kratzer W, Blank W, Schuler A, et al. Evaluation of Strain Elastography for Differentiation of Thyroid Nodules: Results of a Prospective DEGUM Multicenter Study Evaluation der Strain Elastografie für die Differenzierung von Schilddrüsenknoten: Ergebnisse einer prospektiven DEGUM Multizenter-Studie. 2016
77. Trimboli P, Guglielmi R, Monti S, Misischi I, Graziano F, Nasrollah N, et al. Ultrasound sensitivity for thyroid malignancy is increased by real-time elastography: a prospective multicenter study. J Clin Endocrinol Metab. 2012 Dec;97(12):4524–30.
78. Popa O, Barna RA, Borlea A, Cornianu M, Dema A, Stoian D. The impact of the COVID-19 pandemic on thyroid nodular disease: a retrospective study in a single center in the western part of Romania. Front Endocrinol (Lausanne). 2023 Jul 11;14:1221795.
79. Wang H, Zhao L, Xin X, Wei X, Zhang S, Li Y, et al. Diagnostic value of elastosonography for thyroid microcarcinoma. Ultrasonics. 2014;54(7):1945–9.
80. Wang Y, Dan HJ, Dan HY, Li T, Hu B. Differential diagnosis of small single solid thyroid nodules using real-time ultrasound elastography. J Int Med Res. 2010;38(2):466–72.
81. Andrioli M, Trimboli P, Amendola S, Valabrega S, Fukunari N, Moro •, et al. Elastographic presentation of medullary thyroid carcinoma.
82. Tatar IG, Kurt A, Yilmaz KB, Akinci M, Kulacoglu H, Hekimoglu B. The learning curve of real time elastosonography: a preliminary study conducted for the assessment of malignancy risk in thyroid nodules. Med Ultrason. 2013 Dec;15(4):278–84
83. Shiina T, Nightingale KR, Palmeri ML, Hall TJ, Bamber JC, Barr RG, et al. WFUMB guidelines and recommendations for clinical use of ultrasound elastography: Part 1: basic principles and terminology. Ultrasound Med Biol. 2015 May 1;41(5):1126–47.
84. Xu JM, Xu HX, Zhang YF, Guo LH, Liu LN, Bo XW, et al. Virtual Touch Tissue Imaging for Differential Diagnosis of Thyroid Nodules: Additional Value of the Area Ratio. J Ultrasound Med. 2016 May 1;35(5):917–26.
85. Fukuhara T, Matsuda E, Endo Y, Takenobu M, Izawa S, Fujiwara K, et al. Correlation between Quantitative Shear Wave Elastography and Pathologic Structures of Thyroid Lesions. Ultrasound Med Biol. 2015 Sep 1;41(9):2326–32.
86. Zhang FJ, Han RL, Zhao XM. The value of virtual touch tissue image (VTI) and virtual touch tissue quantification (VTQ) in the differential diagnosis of thyroid nodules. Eur J Radiol. 2014 Nov 1;83(11):2033–40.
87. Park AY, Son EJ, Han K, Youk JH, Kim JA, Park CS. Shear wave elastography of thyroid nodules for the prediction of malignancy in a large scale study. Eur J Radiol. 2015 Mar 1;84(3):407–12.
88. Zhang YX, Xue JP, Li HZ, Miao JW, Kang CS. Clinical Value of Shear Wave Elastography Color Scores in Classifying Thyroid Nodules . Int J Gen Med. 2021 Nov 10;14:8007–18.

89. Yi AJ, Yang WW, Cui XW, Dietrich CF, Wang B. The value of quantitative and a new qualitative color pattern shear wave elastography for the differentiation of ACR TI-RADS 4 or 5 category thyroid nodules measuring ≤10 mm. Front Endocrinol (Lausanne). 2023 Jan 8;14:1275256.
90. Tan S, Sun PF, Xue H, Fu S, Zhang ZP, Mei F, et al. Evaluation of thyroid micro-carcinoma using shear wave elastography: Initial experience with qualitative and quantitative analysis. Eur J Radiol. 2021 Apr 1;137:109571.
91. Zhang YX, Xue JP, Li HZ, Miao JW, Kang CS. Clinical Value of Shear Wave Elastography Color Scores in Classifying Thyroid Nodules. Int J Gen Med. 2021;14:8007.
92. Tozaki M, Fukuma E. Pattern classification of ShearWaveTM Elastography images for differential diagnosis between benign and malignant solid breast masses. http://dx.doi.org/101258/ar2011110276. 2011 Dec 1;52(10):1069–75.
93. Xue JP, Kang XY, Miao JW, Zhang YX, Li HZ, Yao FC, et al. Analysis of the Influence of Thyroid Nodule Characteristics on the Results of Shear Wave Elastography. Front Endocrinol (Lausanne). 2022 Jun 10;13:858565.
94. Zhao CK, Chen SG, Alizad A, He YP, Wang Q, Wang D, et al. Three-Dimensional Shear Wave Elastography for Differentiating Benign From Malignant Thyroid Nodules. J Ultrasound Med. 2018 Jul 1;37(7):1777–88.
95. Dobruch-Sobczak K, Zalewska EB, Gumińska A, Słapa RZ, Mlosek K, Wareluk P, et al. Diagnostic Performance of Shear Wave Elastography Parameters Alone and in Combination with Conventional B-Mode Ultrasound Parameters for the Characterization of Thyroid Nodules: A Prospective, Dual-Center Study. Ultrasound Med Biol. 2016 Dec 1;42(12):2803–11.
96. Li H, Kang C, Xue J, Jing L, Miao J. Influence of lesion size on shear wave elastography in the diagnosis of benign and malignant thyroid nodules. Sci Rep. 2021 Dec 1;11(1):21616.
97. Liu BX, Xie XY, Liang JY, Zheng YL, Huang GL, Zhou LY, et al. Shear wave elastography versus real-time elastography on evaluation thyroid nodules: a preliminary study. Eur J Radiol. 2014;83(7):1135–43.
98. Brandenstein M, Wiesinger I, Künzel J, Hornung M, Stroszczynski C, Jung EM. Multiparametric Sonographic Imaging of Thyroid Lesions: Chances of B-Mode, Elastography and CEUS in Relation to Preoperative Histopathology. Cancers 2022, Vol 14, Page 4745 . 2022 Sep 29;14(19):4745.
99. Borlea A, Sporea I, Popa A, Derban M, Taban L, Stoian D. Strain Versus 2D Shear-Wave Elastography Parameters—Which Score Better in Predicting Thyroid Cancer? Applied Sciences 2022, Vol 12, Page 11147. 2022 Nov 3;12(21):11147.
100. Shang H, Wu B, Liu Z, Liu Y, Cheng W. The effectiveness of shear wave elastography in the diagnosis of PTMC. Technol Health Care. 2020;28(2):221–6.
101. Wang F, Chang C, Chen M, Gao Y, Chen YL, Zhou SC, et al. Does Lesion Size Affect the Value of Shear Wave Elastography for Differentiating Between Benign and Malignant Thyroid Nodules? J Ultrasound Med. 2018 Mar 1;37(3):601–9.
102. Kim H, Kim JA, Son EJ, Youk JH. Quantitative assessment of shear-wave ultrasound elastography in thyroid nodules: diagnostic performance for predicting malignancy. Eur Radiol. 2013 Sep;23(9):2532–7.
103. Moon HJ, Sung JM, Kim EK, Yoon JH, Youk JH, Kwak JY. Diagnostic performance of gray-scale US and elastography in solid thyroid nodules. Radiology. 2012 Mar;262(3):1002–13.

104. Qi WH, Jin K, Cao LL, Peng M, He NA, Zhan XL, et al. Diagnostic performance of a new two-dimensional shear wave elastography expression using siemens ultrasound system combined with ACR TI-RADS for classification of benign and malignant thyroid nodules: A prospective multi-center study. Heliyon. 2023 Oct 1;9(10):e20472
105. Han DY, Sohn YM, Seo M, Yun SJ, Park WS, Jeon SH, et al. Shear-wave elastography in thyroid ultrasound: Can be a predictor of extrathyroidal extension and cervical lymph node metastasis in papillary thyroid carcinoma? Medicine. 2020 Dec 12 ;99(52).
106. Gao XQ, Ma Y, Peng XS, Wang LL, Li HX, Zheng XL, et al. Diagnostic performance of C-TIRADS combined with SWE for the diagnosis of thyroid nodules. Front Endocrinol (Lausanne). 2022 Sep 6;13:939303.
107. Chambara N, Lo X, Chow TCM, Lai CMS, Liu SYW, Ying M. Combined Shear Wave Elastography and EU TIRADS in Differentiating Malignant and Benign Thyroid Nodules. Cancers 2022, Vol 14, Page 5521. 2022 Nov 10;14(22):5521.
108. Li H, Xue J, Zhang Y, Miao J, Jing L, Kang C. Diagnostic efficacy of a combination of the Chinese thyroid imaging reporting and data system and shear wave elastography in detecting category 4a and 4b thyroid nodules. Front Endocrinol (Lausanne). 2023 Jun 12;14:1161424.
109. Filho RHC, Pereira FL, Iared W. Diagnostic Accuracy Evaluation of Two-Dimensional Shear Wave Elastography in the Differentiation Between Benign and Malignant Thyroid Nodules: Systematic Review and Meta-analysis. J Ultrasound Med. 2020 Sep 1;39(9):1729–41.
110. Nattabi HA, Sharif NM, Yahya N, Ahmad R, Mohamad M, Zaki FM, et al. Is Diagnostic Performance of Quantitative 2D-Shear Wave Elastography Optimal for Clinical Classification of Benign and Malignant Thyroid Nodules?: A Systematic Review and Meta-analysis. Acad Radiol. 2022 Mar 1;29:S114–21.
111. Cheng KL, Lai PH, Su CL, Baek JH, Lee HL. Impact of Region-of-Interest Size on the Diagnostic Performance of Shear Wave Elastography in Differentiating Thyroid Nodules. Cancers 2023, Vol 15, Page 5214. 2023 Oct 30;15(21):5214.
112. Liu Z, Jing H, Han X, Shao H, Sun YX, Wang QC, et al. Shear wave elastography combined with the thyroid imaging reporting and data system for malignancy risk stratification in thyroid nodules. Oncotarget. 2017 Feb 2;8(26):43406–16.
113. Monpeyssen H, Tramalloni J, Poirée S, Hélénon O, Correas JM. Elastography of the thyroid. Diagn Interv Imaging. 2013 May 1;94(5):535–44.
114. Chung J, Lee YJ, Choi YJ, Ha EJ, Suh CH, Choi M, et al. Clinical applications of Doppler ultrasonography for thyroid disease: consensus statement by the Korean Society of Thyroid Radiology. Ultrasonography. 2020 Oct 1;39(4):315.
115. Han RJ, Du J, Li FH, Zong HR, Wang JD, Shen YL, et al. Comparisons and Combined Application of Two-Dimensional and Three-Dimensional Real-time Shear Wave Elastography in Diagnosis of Thyroid Nodules. J Cancer. 2019;10(9):1975.
116. Bhatia KSS, Tong CSL, Cho CCM, Yuen EHY, Lee YYP, Ahuja AT. Shear wave elastography of thyroid nodules in routine clinical practice: Preliminary observations and utility for detecting malignancy. Eur Radiol. 2012 Nov 30;22(11):2397–406.
117. Barr RG. Breast Elastography: How to Perform and Integrate Into a “Best-Practice” Patient Treatment Algorithm. J Ultrasound Med. 2020 Jan 1 ;39(1):7–17.

118. Chen BD, Xu HX, Zhang YF, Liu BJ, Guo LH, Li DD, et al. Calcification of thyroid nodules increases shear-wave speed (SWS) measurement: using multiple calcification-specific SWS cutoff values outperforms a single uniform cutoff value in diagnosing malignant thyroid nodules. Oncotarget. 2016 Oct 10;7(40):66149.
119. Veyrieres JB, Albarel F, Lombard JV, Berbis J, Sebag F, Oliver C, et al. A threshold value in Shear Wave elastography to rule out malignant thyroid nodules: a reality? Eur J Radiol. 2012 Dec;81(12):3965–72.
120. SONG Y, XIE M, WANG J, XIANG F, YU C, ZHANG D, et al. Real-time shear wave elastography in differential diagnosis of benign and malignant thyroid nodules. Journal of Chinese Physician. 2019;324-326,330.
121. Bhatia KSS, Tong CSL, Cho CCM, Yuen EHY, Lee YYP, Ahuja AT. Shear wave elastography of thyroid nodules in routine clinical practice: preliminary observations and utility for detecting malignancy. Eur Radiol. 2012 Nov;22(11):2397–406.
122. Sebag F, Vaillant-Lombard J, Berbis J, Griset V, Henry JF, Petit P, et al. Shear wave elastography: a new ultrasound imaging mode for the differential diagnosis of benign and malignant thyroid nodules. J Clin Endocrinol Metab. 2010;95(12):5281–8.
123. Magri F, Chytiris S, Capelli V, Alessi S, Nalon E, Rotondi M, et al. Shear wave elastography in the diagnosis of thyroid nodules: feasibility in the case of coexistent chronic autoimmune Hashimoto's thyroiditis. Clin Endocrinol (Oxf). 2012 Jan;76(1):137–41.
124. Yoo MH, Kim HJ, Choi IH, Mok JO, Park HK, Won Byun D, et al. Differential Diagnosis of Thyroid Follicular Neoplasm from Nodular Hyperplasia by Shear Wave Elastography. 2019;
125. Yoo MH, Kim HJ, Choi IH, Park S, Yun S, Park HK, et al. Efficacy of Differential Diagnosis of Thyroid Nodules by Shear Wave Elastography—the Stiffness Map. J Endocr Soc. 2021 Nov 11;5(11):1–11.
126. Yi KH, Lee EK, Kang HC, Kim SW, Kim IJ, Park SY, et al. 2016 Revised Korean Thyroid Association Management Guidelines for Patients with Thyroid Nodules and Thyroid Cancer. International Journal of Thyroidology [Internet]. 2016 Nov 20 [cited 2024 Mar 1];9(2):59–126.
127. Dobruch-Sobczak K, Gumińska A, Bakuła-Zalewska E, Mlosek K, Słapa RZ, Wareluk P, et al. Shear wave elastography in medullary thyroid carcinoma diagnostics. J Ultrason. 2015;15(63):358–67.
128. Swan KZ;, Nielsen VE;, Bonnema SJ. Evaluation of thyroid nodules by shear wave elastography a review of current knowledge. https://doi.org/10.1007/s40618-021-01570-z
129. Duan SB, Yu J, Li X, Han ZY, Zhai HY, Liang P. Diagnostic value of two-dimensional shear wave elastography in papillary thyroid microcarcinoma. Onco Targets Ther. 2016 Mar 9;9:1311.
130. Slman R, Monpeyssen H, Desarnaud S, Haroche J, Fediaevsky LDP, Fabrice M, et al. Ultrasound, Elastography, and Fluorodeoxyglucose Positron Emission Tomography/Computed Tomography Imaging in Riedel's Thyroiditis: Report of Two Cases. https://home.liebertpub.com/thy. 2011 Jun 27;21(7):799–804.
131. Moraes PHDM, Sigrist R, Takahashi MS, Schelini M, Chammas MC. Ultrasound elastography in the evaluation of thyroid nodules: evolution of a promising diagnostic tool for predicting the risk of malignancy. Radiol Bras. 2019 Jul 1;52(4):247.

132. Chang N, Zhang X, Wan W, Zhang C, Zhang X. The Preciseness in Diagnosing Thyroid Malignant Nodules Using Shear-Wave Elastography. Med Sci Monit. 2018 Feb 2;24:671.
133. Cantisani V, D'Andrea V, Biancari F, Medvedyeva O, Di Segni M, Olive M, et al. Prospective evaluation of multiparametric ultrasound and quantitative elastosonography in the differential diagnosis of benign and malignant thyroid nodules: preliminary experience. Eur J Radiol. 2012 Oct;81(10):2678–83
134. Cantisani V, De Silvestri A, Scotti V, Fresilli D, Tarsitano MG, Polti G, et al. US-Elastography With Different Techniques for Thyroid Nodule Characterization: Systematic Review and Meta-analysis. Front Oncol. 2022 Mar 16;12:1.
135. Shao J, Shen Y, Lü J, Wang J. Ultrasound scoring in combination with ultrasound elastography for differentiating benign and malignant thyroid nodules. Clin Endocrinol (Oxf). 2015 Aug 1;83(2):254–60.
136. Borlea A, Borcan F, Sporea I, Dehelean CA, Negrea R, Cotoi L, et al. TI-RADS Diagnostic Performance: Which Algorithm is Superior and How Elastography and 4D Vascularity Improve the Malignancy Risk Assessment. Diagnostics. 2020 ;10(4).
137. Russ G, Royer B, Bigorgne C, Rouxel A, Bienvenu-Perrard M, Leenhardt L. Prospective evaluation of thyroid imaging reporting and data system on 4550 nodules with and without elastography. Eur J Endocrinol. 2013 May;168(5):649–55.
138. Moraes PHM, Takahashi MS, Vanderlei FAB, Schelini M V., Chacon DA, Tavares MR, et al. Multiparametric Ultrasound Evaluation of the Thyroid: Elastography as a Key Tool in the Risk Prediction of Undetermined Nodules (Bethesda III and IV)—Histopathological Correlation. Ultrasound Med Biol. 2021 May 1;47(5):1219–26.
139. Wickramaratne D, Wilkinson P, Rao JY, Ragavendra N, Sharma S, Gimzewski JK. Fine Needle Elastography (FNE) device for biomechanically determining local variations of tissue mechanical properties. J Biomech. 2015 Jan 2;48(1):81–8.
140. Borlea A, Stoian D, Cotoi L, Sporea I, Lazar F, Mozos I. Thyroid Multimodal Ultrasound Evaluation-Impact on Presurgical Diagnosis of Intermediate Cytology Cases. Appl Sci. 2020:3439.
141. Hairu L, Yulan P, Yan W, Hong A, Xiaodong Z, Lichun Y, et al. Elastography for the diagnosis of high-suspicion thyroid nodules based on the 2015 American Thyroid Association guidelines: A multicenter study. BMC Endocr Disord. 2020 Apr 3;20(1):1–10.
142. Potential value of elastosonography in the diagnosis of malignancy in thyroid nodules - ProQuest [Internet].
143. Samir AE, Dhyani M, Anvari A, Prescott J, Halpern EF, Faquin WC, et al. Shear-Wave Elastography for the Preoperative Risk Stratification of Follicular-patterned Lesions of the Thyroid: Diagnostic Accuracy and Optimal Measurement Plane. https://doi.org/101148/radiol2015141627. 2015 May 7; 277(2):565–73.
144. Tian W, Hao S, Gao B, Jiang Y, Zhang X, Zhang S, et al. Comparing the Diagnostic Accuracy of RTE and SWE in Differentiating Malignant Thyroid Nodules from Benign Ones: a Meta-Analysis. Cell Physiol Biochem. 2016;39(6):2451–63.
145. Liu BX, Xie XY, Liang JY, Zheng YL, Huang GL, Zhou LY, et al. Shear wave elastography versus real-time elastography on evaluation thyroid nodules: A preliminary study. Eur J Radiol. 2014 Jul 1;83(7):1135–43.
146. Borlea A, Sporea I, Popa A, Derban M, Taban L, Stoian D. Strain Versus 2D Shear-Wave Elastography Parameters—Which Score Better in Predicting Thyroid Cancer? Applied Sciences 2022, Vol 12, Page 11147. 2022 Nov 3 [cited 2024 Feb 19];12(21):11147.

147. Sigrist RMS, Liau J, Kaffas A El, Chammas MC, Willmann JK. Ultrasound Elastography: Review of Techniques and Clinical Applications. Theranostics. 2017;7(5):1303–29.
148. Shuzhen C. Comparison analysis between conventional ultrasonography and ultrasound elastography of thyroid nodules. Eur J Radiol. 2012 Aug;81(8):1806–11.
149. Zhao CK, Xu HX. Ultrasound elastography of the thyroid: principles and current status. Ultrasonography [Internet]. 2018/10/01. 2019 Apr;38(2):106–24.
150. Cosgrove D, Barr R, Bojunga J, Cantisani V, Chammas MC, Dighe M, et al. WFUMB Guidelines and Recommendations on the Clinical Use of Ultrasound Elastography: Part 4. Thyroid. Ultrasound Med Biol. 2017 Jan;43(1):4–26.
151. Bojunga J, Herrmann E, Meyer G, Weber S, Zeuzem S, Friedrich-Rust M. Real-time elastography for the differentiation of benign and malignant thyroid nodules: a meta-analysis. Thyroid. 2010 Oct;20(10):1145–50.
152. Li H, Kang C, Xue J, Jing L, Miao J. Influence of lesion size on shear wave elastography in the diagnosis of benign and malignant thyroid nodules. Sci Rep. 2021 Dec 1;11(1).
153. Oliver C, Vaillant-Lombard J, Albarel F, Berbis J, Veyrieres JB, Sebag F, et al. What is the contribution of elastography to thyroid nodules evaluation? Ann Endocrinol (Paris). 2011 Apr;72(2):120–4.
154. Moraes PHDM, Sigrist R, Takahashi MS, Schelini M, Chammas MC. Ultrasound elastography in the evaluation of thyroid nodules: evolution of a promising diagnostic tool for predicting the risk of malignancy. Radiol Bras. 2019 Jul 1;52(4):247.
155. Hong Y rong, Wu Y lian, Luo Z yan, Wu N bo, Liu X ming. Impact of nodular size on the predictive values of gray-scale, color-Doppler ultrasound, and sonoelastography for assessment of thyroid nodules. J Zhejiang Univ Sci B . 2012 Sep;13(9):707–16.
156. Stoian D, Bogdan T, Craina M, Craciunescu M, Timar R, Schiller A. Elastography: A New Ultrasound Technique in Nodular Thyroid Pathology. In: Thyroid Cancer - Advances in Diagnosis and Therapy. 2016.
157. Zhao HN, Liu JY, Lin QZ, He YS, Luo HH, Peng YL, et al. Partially cystic thyroid cancer on conventional and elastographic ultrasound: a retrospective study and a machine learning-assisted system. Ann Transl Med. 2020 Apr;8(7):495–495.
158. Dudea SM, Botar-Jid C. Ultrasound elastography in thyroid disease. Med Ultrason. 2015 Mar;17(1):74–96.
159. Kara T, Ateş F, Durmaz MS, Akyürek N, Durmaz FG, Özbakır B, et al. Assessment of thyroid gland elasticity with shear-wave elastography in Hashimoto's thyroiditis patients. J Ultrasound. 2020 Dec 1;23(4):543–51.
160. Stoian D, Borlea A, Sporea I, Popa A, Moisa-Luca L, Popescu A. Assessment of Thyroid Stiffness and Viscosity in Autoimmune Thyroiditis Using Novel Ultrasound-Based Techniques. Biomedicines 2023, Vol 11, Page 938. 2023 Mar 17;11(3):938.
161. Stoian D, Moisa L, Taban L, Sporea I, Popa A, Bende F, et al. Quantification of Thyroid Viscosity in Healthy Subjects Using Ultrasound Shear Wave Dispersion (Viscosity PLUS). Diagnostics 2022, Vol 12, Page 2194. 2022 Sep 9;12(9):2194.
162. Bakırtaş Palabıyık F, İnci E, Papatya Çakır ED, Hocaoğlu E. Evaluation of Normal Thyroid Tissue and Autoimmune Thyroiditis in Children Using Shear Wave Elastography. J Clin Res Pediatr Endocrinol . 2019 Jun 1;11(2):132.
163. Fukuhara T, Matsuda E, Izawa S, Fujiwara K, Kitano H. Utility of Shear Wave Elastography for Diagnosing Chronic Autoimmune Thyroiditis. J Thyroid Res . 2015;2015. pubmed.ncbi.nlm.nih.gov/26257979/

164. Ceyhan Bilgici M, Sağlam D, Delibalta S, Yücel S, Tomak L, Elmalı M. Shear wave velocity of the healthy thyroid gland in children with acoustic radiation force impulse elastography. J Med Ultrason (2001). 2018 Jan 1;45(1):75–80.
165. Bhatia K, Tong CSL, Cho CCM, Yuen EHY, Lee J, Ahuja AT. Reliability of shear wave ultrasound elastography for neck lesions identified in routine clinical practice. Ultraschall Med. 2012;33(5):463–8.
166. Vlad M, Golu I, Bota S, Vlad A, Timar B, Timar R, et al. Real-time shear wave elastography may predict autoimmune thyroid disease. Wien Klin Wochenschr. 2015 May 28;127(9–10):330–6.
167. Stoian D, Borlea A, Moisa-Luca L, Paul C. Multiparametric ultrasound-based assessment of overt hyperthyroid diffuse thyroid disease. Front Endocrinol (Lausanne). 2023 Dec 18;14:1300447.
168. Li S, Yao J, Hao S, Zhou X, Jiang N, Zhao X, et al. Multifactor analysis of thyroid stiffness in Graves disease: A preliminary study. American Journal of Roentgenology. 2019 May 1;212(5):950–7.
169. Menzilcioglu MS, Duymus M, Gungor G, Citil S, Sahin T, Boysan SN, et al. The value of realtime ultrasound elastography in chronic autoimmune thyroiditis. British Journal of Radiology. 2014 Dec 1;87(1044).
170. Cepeha CM, Paul C, Borlea A, Borcan F, Fofiu R, Dehelean CA, et al. The Value of Strain Elastography in Predicting Autoimmune Thyroiditis. Diagnostics (Basel). 2020 Oct 27;10(11).
171. I S, R S, S B, M V, A P, I Z. ARFI elastography for the evaluation of diffuse thyroid gland pathology: Preliminary results. World J Radiol. 2012;4(4):174.
172. Cepeha CM, Paul C, Borlea A, Fofiu R, Borcan F, Dehelean CA, et al. Shear-Wave Elastography-Diagnostic Value in Children with Chronic Autoimmune Thyroiditis. Diagnostics (Basel). 2021;11(2).
173. Kandemirli SG, Bayramoglu Z, Caliskan E, Sari ZNA, Adaletli I. Quantitative assessment of thyroid gland elasticity with shear-wave elastography in pediatric patients with Hashimoto's thyroiditis. Journal of Medical Ultrasonics. 2018 Jul 1 ;45(3):417–23.
174. Kamel SM, ElKhashab KM, Bhagat S, Elzayat WA. Shear wave elastography as a quantitative method for thyroid gland elasticity assessment in pediatrics patients with autoimmune-related thyroid disease, diagnostic utility and laboratory correlation. Egyptian Journal of Radiology and Nuclear Medicine 2022 53:1. 2022 Aug 24;53(1):1–8.
175. Cepeha CM, Paul C, Borlea A, Bende R, Mihuta MS, Stoian D. Is Strain Elastography Useful in Diagnosing Chronic Autoimmune Thyroiditis in Children? Applied Sciences 2022, Vol 12, Page 8881. 2022 Sep 4 ;12(17):8881.
176. Habibi HA, Durmaz ESM, Qarayeva V, Kandemirli SG, Kalyoncu Ucar A, Aslan M, et al. Quantitative Assessment of Thyroid, Submandibular, and Parotid Glands Elasticity With Shear-Wave Elastography in Children. Ultrasound Q. 2018 Jun 1;34(2):58–61.
177. Bandeira L, Bilezikian J. Primary Hyperparathyroidism. F1000Res . 2016;5:1–11.
178. Barr RG. Real-time ultrasound elasticity of the breast: initial clinical results. Ultrasound Q. 2010 Jun;26(2):61–6.
179. Hindié E, Ugur Ö, Fuster D, O'Doherty M, Grassetto G, Ureña P, et al. 2009 EANM parathyroid guidelines. Eur J Nucl Med Mol Imaging. 2009;36(7):1201–16.
180. Mizamtsidi M, Nastos C, Mastorakos G, Dina R, Vassiliou I, Gazouli M, et al. Diagnosis, management, histology and genetics of sporadic primary hyperparathyroidism: old knowledge with new tricks. Endocr Connect. 2018;7(2):R56–68.

181. Kebebew E, Clark OH. Parathyroid adenoma, hyperplasia, and carcinoma: localization, technical details of primary neck exploration, and treatment of hypercalcemic crisis. Surg Oncol Clin N Am. 1998 Oct;7(4):721–48.
182. Rahbari R, Holloway AK, He M, Khanafshar E, Clark OH, Kebebew E. Identification of differentially expressed microRNA in parathyroid tumors. Ann Surg Oncol. 2011;
183. Hedgeman E, Lipworth L, Lowe K, Saran R, Do T, Fryzek J. International burden of chronic kidney disease and secondary hyperparathyroidism: A systematic review of the literature and available data. Int J Nephrol. 2015;2015(April).
184. Jean G, Lafage-Proust MH, Souberbielle JC, Lechevallier S, Deleaval P, Lorriaux C, et al. Severe secondary hyperparathyroidism in patients on haemodialysis is associated with a high initial serum parathyroid hormone and beta-CrossLaps level: Results from an incident cohort. PLoS One. 2018;13(6):1–15.
185. Gokkaya N, Gungor A, Bilen A, Bilen H, Gviniashvili D, Karadeniz Y. Primary hyperparathyroidism in pregnancy: a case series and literature review. Gynecological Endocrinology. 2016;32(10):783–6.
186. Eufrazino C, Veras A, Bandeira F. Epidemiology of Primary Hyperparathyroidism and its Non-classical Manifestations in the City of Recife, Brazil. Clin Med Insights Endocrinol Diabetes. 2013 Dec 4;6:69–74.
187. Cotoi L, Amz D, Sporea I, Borlea A, Schiller O, Schiller A, et al. Parathyroid Elastography — Elastography Evaluation Algorithm. Cotoi, L; Amzăr, D; Sporea, I; Borlea, A; Schiller, O; Schiller, A; Pop, GN; Stoian, D Parathyroid Elastography—Elastography Evaluation Algorithm Timisoara Med 2020, 2020(1), 5; doi:1035995/tmj20200105. :1–16.
188. Arnold A, Staunton CE, Kim HG, Gaz RD, Kronenberg HM. Monoclonality and Abnormal Parathyroid Hormone Genes in Parathyroid Adenomas. New England Journal of Medicine. 1988;
189. Cotoi L, Stoian D, Borlea A, Varcus F. Ultrasonographic and Elastographic Diagnostic of Parathyroid Lesions – A Literature Review. 2019;6(2).
190. Allgrove J. Parathyroid disorders. 2001;249–57.
191. Arrangoiz R. Current Understanding and Management of Parathyroid Carcinoma. J Cancer Treat Res [Internet]. 2017;5(3):51.
192. Gasser RW. Clinical aspects of primary hyperparathyroidism: clinical manifestations, diagnosis, and therapy. Wien Med Wochenschr. 2013 Sep;163(17–18):397–402.
193. Bamber AJ, Cosgrove D, Dietrich CF, Fromageau J, Bojunga J, Calliada F, et al. EFSUMB Guidelines and Recommendations on the Clinical Use of Ultrasound Elastography. Part 1: Basic Principles and Technology. Ultraschall in Med [Internet]. 2013;34:169–84.
194. Russo D, Battaglia Y. Clinical Significance of FGF-23 in Patients with CKD. Int J Nephrol. 2011;2011:1–5.
195. Park AY, Son EJ, Han K, Youk JH, Kim JA, Park CS. Shear wave elastography of thyroid nodules for the prediction of malignancy in a large scale study. Eur J Radiol [Internet]. 2015;84(3):407–12.
196. Gennisson JL, Deffieux T, Fink M, Tanter M. Ultrasound elastography: Principles and techniques. Diagnostic and Interventional Imaging. 2013.
197. Cosgrove D, Barr R, Bojunga J, Cantisani V, Chammas MC, Dighe M, et al. WFUMB Guidelines and Recommendations on the Clinical Use of Ultrasound Elastography: Part 4. Thyroid. Ultrasound Med Biol. 2017;43(1):4–26.
198. Cotoi L, Stoian D, Borlea A, Varcus F. Ultrasonographic and Elastographic Diagnostic of Parathyroid Lesions – A Literature Review. 2019;6(2).

199. Sporea I. Is ARFI elastography reliable for predicting fibrosis severity in chronic HCV hepatitis? World J Radiol. 2011;
200. Sporea I. ARFI elastography for the evaluation of diffuse thyroid gland pathology: Preliminary results. World J Radiol [Internet]. 2012;4(4):174.
201. Sporea I, Lie I. Shear wave elastography. Ultraschall Med. 2012;
202. Stoian D, Timar B, Craina M, Bernad E, Petre I, Craciunescu M. Qualitative strain elastography-strain ratio evaluation-an important tool in breast cancer diagnostic. Med Ultrason. 2016;18(2):195–200.
203. Youk JH, Gweon HM, Son EJ. Shear-wave elastography in breast ultrasonography: the state of the art. Ultrasonography [Internet]. 2017;36(4):300–9.
204. Correas JM, Roumy J, Grenier N. Ultrasound elastography: A new modality in routine practice. Diagn Interv Imaging [Internet]. 2013;94(5):483–4.
205. Bhatia KSS, Rasalkar DP, Lee YP, Wong KT, King AD, Yuen HY, et al. Cystic change in thyroid nodules: A confounding factor for real-time qualitative thyroid ultrasound elastography. Clin Radiol [Internet]. 2011;66(9):799–807.
206. Franchi-Abella S, Elie C, Correas JM. Ultrasound elastography: Advantages, limitations and artefacts of the different techniques from a study on a phantom. Diagn Interv Imaging [Internet]. 2013;94(5):497–501.
207. Amzar D, Cotoi L, Borlea A, Adela C, Pop GN, Stoian D. Role of Elastography in the Evaluation of Parathyroid Disease. In: Stoian D, Popescu A, editors. Elastography [Internet]. Rijeka: IntechOpen; 2022.
208. Ruchała M, Szczepanek E. Endokrynologia polska. Endokrynol Pol [Internet]. 2010;61(3):330–44.
209. Stangierski A, Wolinski K, Ruchala M. Shear wave elastography in the diagnostics of parathyroid adenomas–new application of the method. Endocrine [Internet]. 2018;60(2):240–5.
210. Polat AV, Ozturk M, Akyuz B, Celenk C, Kefeli M, Polat C. The diagnostic value of shear wave elastography for parathyroid lesions and comparison with cervical lymph nodes. Med Ultrason. 2017;19(4):386–91.
211. Sung JY. Parathyroid ultrasonography: the evolving role of the radiologist. Ultrasonography. 2015;34(4):268–74.
212. Kunstman JW, Kirsch JD, Mahajan A, Udelsman R. Parathyroid localization and implications for clinical management. Journal of Clinical Endocrinology and Metabolism. 2013;98(3):902–12.
213. Geatti O, Shapiro B, Orsolon PG, Proto G, Guerra UP, Antonucci F, et al. Localization of parathyroid enlargement: experience with technetium-99m methoxyisobutylisonitrile and thallium-201 scintigraphy, ultrasonography and computed tomography. Eur J Nucl Med. 1994;
214. Casara D, Rubello D, Pelizzo M, Shapiro B. Clinical role of99mTcO4/MIBI scan, ultrasound and intra-operative gamma probe in the performance of unilateral and minimally invasive surgery in primary hyperparathyroidism. Eur J Nucl Med. 2001;28(9):1351–9.
215. Mariani LH, Berns JS. The renal manifestations of thyroid disease. Journal of the American Society of Nephrology. 2012;23(1):22–6.
216. Mariani G, Gulec S a, Rubello D, Boni G, Puccini M, Pelizzo MR, et al. Preoperative localization and radioguided parathyroid surgery. J Nucl Med. 2003;44(9):1443–58.

217. Rickes S, Sitzy J, Neye H, Ocran KW, Wermke W. High-resolution ultrasound in combination with colour-Doppler sonography for preoperative localization of parathyroid adenomas in patients with primary hyperparathyroidism. Ultraschall in der Medizin. 2003;
218. Lane MJ, Desser TS, Weigel RJ, Jeffrey RB. Use of color and power doppler sonography to identify feeding arteries associated with parathyroid adenomas. American Journal of Roentgenology. 1998;
219. Stoian D, Bogdan T, Craina M. Elastography : A New Ultrasound Technique in Nodular Thyroid Pathology Elastography : A New Ultrasound Technique in Nodular Thyroid Pathology. 2016;(September).
220. Dietrich. Introduction to Elastography. Strain Elastography -How … Ultrasound Int Open [Internet]. 2017;3:137–49.
221. G C, D M. Strain Elastosonography of Thyroid Nodules: A New Tool for Malignancy Prediction? Overview of Literature. Endocrinology & Metabolic Syndrome. 2016;
222. Rago T, Santini F, Scutari M, Pinchera A, Vitti P. Elastography: New developments in ultrasound for predicting malignancy in thyroid nodules. Journal of Clinical Endocrinology and Metabolism. 2007;92(8):2917–22.
223. Cotoi L, Amzar D, Sporea I, Borlea A, Navolan D, Varcus F, et al. Shear Wave Elastography versus Strain Elastography in Diagnosing Parathyroid Adenomas. Borretta G, editor. Int J Endocrinol [Internet]. 2020;2020:3801902.
224. Cotoi L, Borcan F, Sporea I, Amzar D, Schiller O, Schiller A, et al. Shear wave elastography in diagnosing secondary hyperparathyroidism. Diagnostics. 2019;9(4):1–16.
225. Amzar D, Cotoi L, Sporea I, Timar B, Schiller O, Schiller A, et al. Shear Wave Elastography in Patients with Primary and Secondary Hyperparathyroidism. J Clin Med. 2021 Feb;10(4):697.
226. Azizi G, Piper K, Keller JM, Mayo ML, Puett D, Earp KM, et al. Shear wave elastography and parathyroid adenoma: A new tool for diagnosing parathyroid adenomas. Eur J Radiol. 2016;
227. Batur A, Atmaca M, Yavuz A, Ozgokce M, Bora A, Bulut MD, et al. Ultrasound elastography for distinction between parathyroid adenomas and thyroid nodules. Journal of Ultrasound in Medicine. 2016;35(6):1277–82.
228. Gharib H, Papini E, Paschke R, Duick DS, Valcavi R, Heged??s L, et al. American Association of Clinical Endocrinologists, Associazione Medici Endocrinologi, and European Thyroid Association medical guidelines for clinical practice for the diagnosis and management of thyroid nodules. J Endocrinol Invest. 2010;33(5 SUPPL.):1–50.
229. Perros P, Boelaert K, Colley S, Evans C, Evans RM, Gerrard Ba G, et al. Guidelines for the management of thyroid cancer. Clin Endocrinol (Oxf). 2014 Jul;81 Suppl 1:1-122.

Chapter 11. Salivary Glands Elastography

Maria Bădărînză, Daniela Fodor

11.1. Introduction

The major salivary glands (parotid, submandibular, and sublingual) along with the minor glands (situated in the submucosa of the oral cavity) produce saliva, aiding in the formation of the food bolus and facilitating swallowing. The most common conditions affecting the salivary glands include inflammatory diseases (whether local or systemic, infectious, or obstructive) and tumoral pathology.

The location of the parotid and submandibular glands, at the preauricular level and in the submandibular area, respectively, makes them accessible to ultrasound evaluation. Currently, ultrasound is the first line investigation for the routine assessment of the major salivary glands after the physical examination. The main advantages of ultrasound include its ability to provide real-time results, its non-invasive nature, easy reproducibility, widespread use, and low costs. The limitations of ultrasound in the evaluation of the major salivary glands are due to the difficulty to visualize deep parts (especially in the parotid gland) or to character tumors extending into the retropharyngeal, parapharyngeal spaces, or under the mandibular ramus. In such cases, additional investigations using magnetic resonance imaging (MRI) or computed tomography (CT) are required.

11.2. Grey Scale and Doppler Mode Ultrasound of the Salivary Glands - Normal Aspect

The grey scale ultrasound aspect of the normal salivary glands is homogeneous, with an echogenicity similar to the thyroid gland (or more hyperechoic when compared to the surrounding muscles), regular contour, and visible posterior margin. The global hyperechogenicity is related to the infiltration of fatty tissue within the glandular parenchyma, causing significant attenuation that often makes it difficult to appreciate the deep glandular parenchyma and delineate the posterior margin. Inside the glandular parenchyma, lymph nodes can be present, especially in the superficial part of the parotid gland. In a cross-sectional view of the parotid gland, the retromandibular vein is observed dividing the gland into a superficial and a deep lobe. The mylohyoid muscle divides the submandibular gland into two lobes, which is best identified in the longitudinal section (2) (Fig. 11.1a, b). The vascularization of the parotid glands is supplied by the transverse facial artery and the superficial temporal artery, both branches of the external carotid artery. In the submandibular glands, vascularization is derived from branches of the facial and lingual arteries (Fig. 11.1c, d). Increased vascularization of the parenchyma occurs during acute or chronic inflammatory

processes. No significant ultrasonographic differences have been identified between the sexes or among different age categories (3).

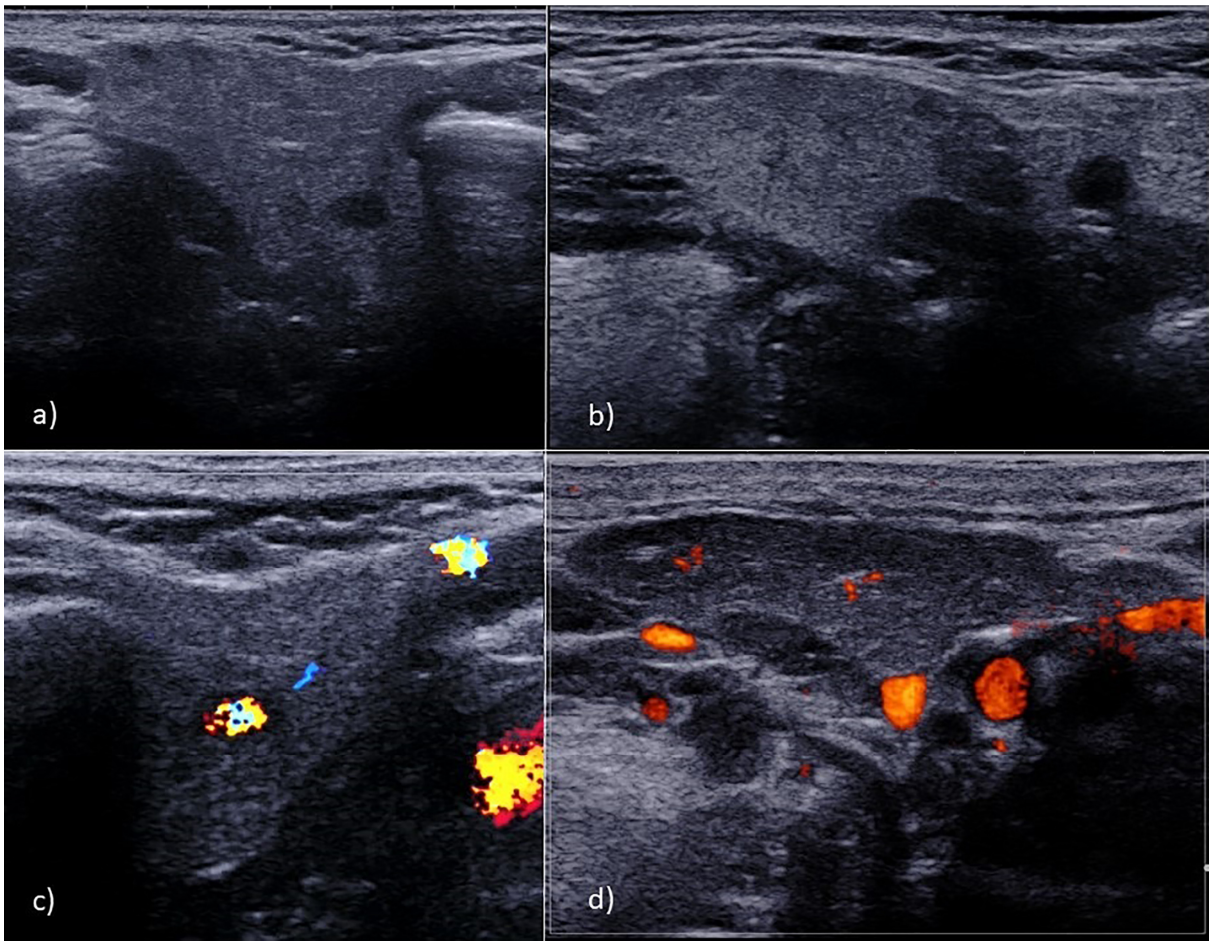

Fig. 11.1: The normal grey scale appearance of (a) the parotid gland in the transverse section and (b) the submandibular gland in the longitudinal section. In both images, the glandular parenchyma is isoechoic and homogeneous, with a regular contour and visible posterior margins. In the parotid gland, the retromandibular vein can be identified, dividing the gland into a superficial and a deep lobe. Normal vascularization in the (c) parotid gland and (d) submandibular gland.

In the pathology of the major salivary glands, grey scale ultrasonography is used to differentiate between inflammatory processes (infections, primary Sjogren's syndrome, sarcoidosis, IgG4-related disease, obstructive pathology, etc.) and non-inflammatory processes (sialoses), as well as benign tumors (Warthin tumor, pleomorphic adenoma, cysts) from malignant tumors (carcinomas, lymphomas, etc.). To achieve the highest diagnostic accuracy, the elastography technique is increasingly used to complement grey scale examination.

11.3. Sonoelastography of Normal Salivary Glands

The utility of elastography for salivary glands assessment is a relatively recent development and is not yet sufficiently standardized for routine clinical use. The difficulties arise from the variability of elastographic techniques used, the multiple values of the elasticity index across different ultrasound devices, and possible differences even between two versions of the same device. The initial studies on salivary glands focused on the use of strain elastography (SE), but more recently, there has been an increasing interest in the use of shear wave elastography (SWE).

For both elastographic techniques, the patient is placed in supine position with the head turned contralaterally for examining the parotid glands and with the head in slight hyperextension for evaluating the submandibular glands. The patient is instructed to breathe normally and to refrain from swallowing during image acquisition. A sufficient amount of gel is used to ensure good contact between the transducer and the area being examined. The parotid and submandibular glands are examined in both transverse and longitudinal sections. Once the highest quality grey scale image is obtained, the elastography button on the ultrasound machine (either SE or SWE) is activated to assess the elasticity of the glandular parenchyma.

Strain Elastography

SE is used to assess the degree of deformation of the glandular parenchyma under the pressure applied with the transducer. After activating the SE button, successive gentle compressions are applied, and once the desired image is obtained, the freeze button is pressed. In normal glandular parenchyma, the resulting images will display color-coded maps with a predominantly homogeneous distribution, featuring intermediate stiffness areas in green interspersed with soft areas coded in blue or red, depending on the color scale of the ultrasound device used, indicating relatively soft tissue elasticity (4) (Fig. 10.2a). Abnormal stiffness areas or heterogeneous patterns, which may indicate underlying pathology, are monitored. Using a region of interest (ROI) with a predefined diameter of 1-3 mm, the glandular parenchyma can be compared with surrounding tissues to obtain a strain ratio (SR) (Fig. 11.2b).

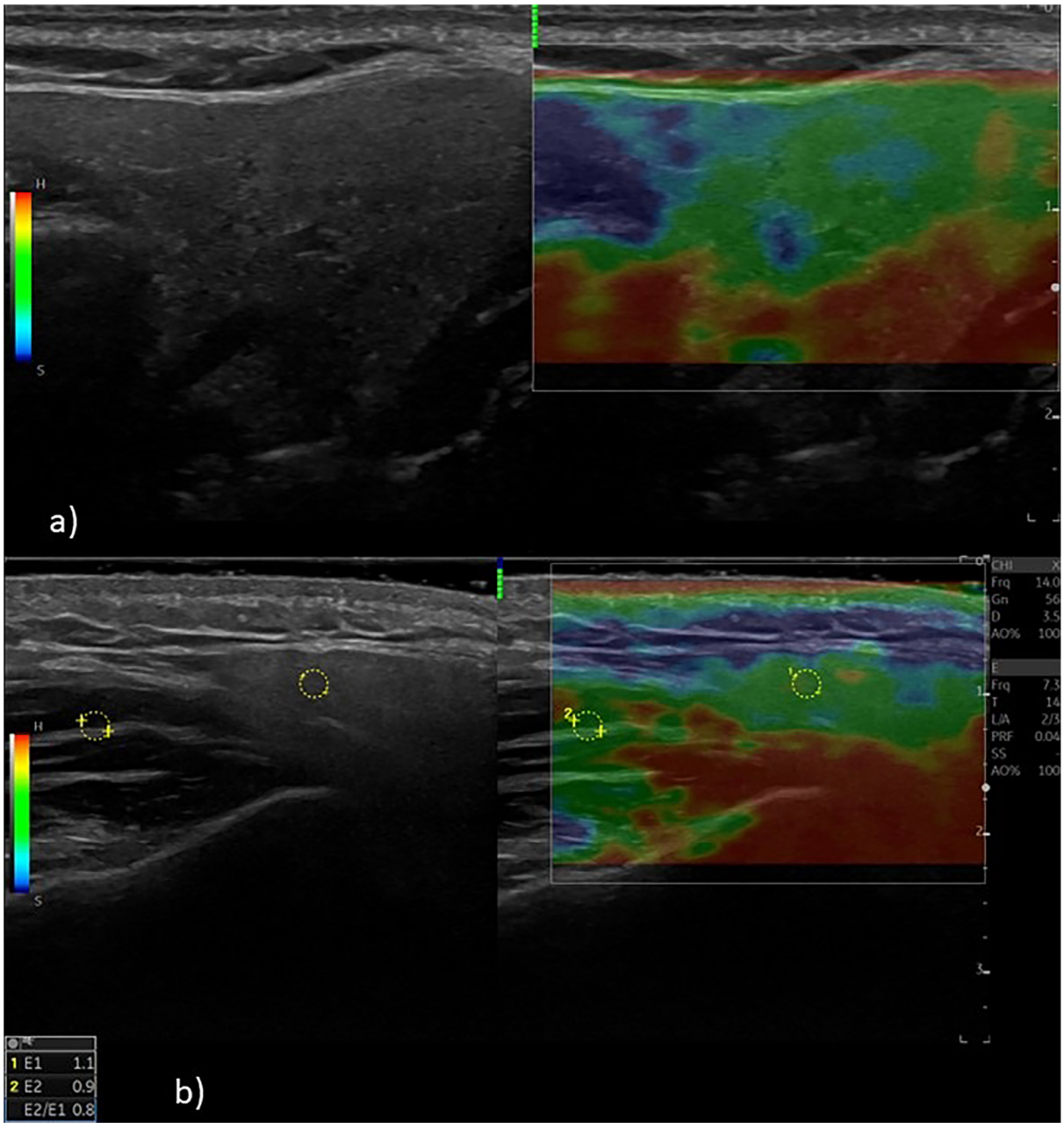

Fig. 11.2: Strain elastography of the parotid gland in the transverse section (a and b) showing predominantly blue and green shades corresponding to relatively soft tissue elasticity. In image (b), the method of obtaining the strain ratio is demonstrated by comparing the elasticity of the parotid gland tissue with that of the masseter muscle.

In studies measuring the elasticity of glandular tissue compared to an underlying area (the masseter muscle or subcutaneous tissue) in healthy subjects, SR values of 1.95 for the parotid glands and 1.75 for the submandibular glands were identified (4). Normal SR values (glandular tissue compared to subcutaneous tissue) have also been published for children for the parotid gland (1.24 ± 0.67), with no differences observed between sexes, body mass index, or age (5).

Shear Wave Elastography

The increased availability of SWE software on new ultrasound machines, as well as its advantage as an operator-independent method, have made SWE often preferred in the evaluation of both parotid and submandibular glands. Recently, Ferraioli et al. (6) have proposed several recommendations for using SWE in various organs, including salivary glands. Accordingly, it is recommended to use transducers with frequencies between 7-12 MHz, to place the ROI at a distance of 1-2 cm from the anterior glandular margin, in an area devoid of blood vessels, cysts, or fibrotic zones. To calculate the median elasticity index, between 3 and 10 measurements should be acquired (Fig. 10.3).

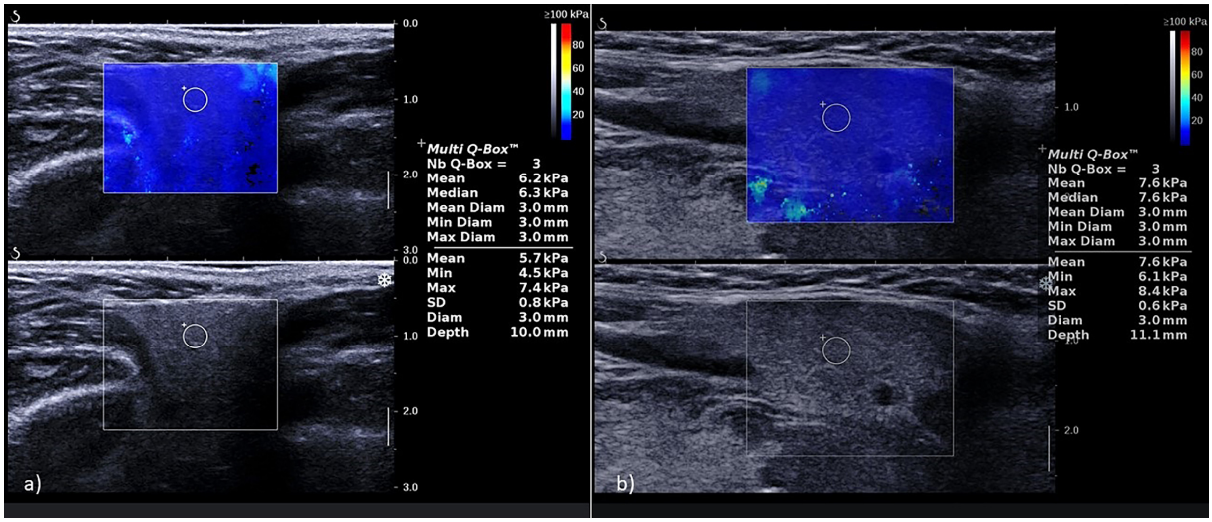

Fig. 10.3 Shear wave elastography of (a) normal parotid glands and (b) submandibular glands. The upper part highlights the elastographic image (homogeneous color box), while the lower part shows the corresponding grey scale image. On the right side, the average and median values of the elasticity index are displayed after performing 3 consecutive measurements. The values obtained are similar for both salivary glands.

Several values for the median elasticity index of normal glandular parenchyma have been determined between 5.46±1.57 kPa and 19.09±5.65 kPa depending on the ultrasound device used (3, 7). In children and adolescents, elasticity index values of 8.37±2.09 kPa and 8.33±2.04 kPa have been identified for both parotid glands (8). Using Acoustic Radiation Force Impulse Imaging (ARFI) technique, Badea et al. identified shear wave velocity (SWV) of 1.54±0.6 m/s in the parotid glands (9). The new techniques Viscosity PLUS and two-dimensional PLUS elastography appear to be effective in the functional assessment of major salivary glands (10).

Following the elastographic assessment of normal parenchyma in the parotid and submandibular glands, multiple studies have demonstrated its utility in diagnosing the primary conditions affecting salivary glands, as detailed in the subsequent paragraphs.

11.4. Elastography in the non-inflammatory Pathology of Salivary Glands

One of the non-inflammatory conditions is represented by sialosis or sialadenosis, where the replacement of glandular tissue with fibrosis or fatty tissue leads to painless progressive swelling of the salivary glands, most commonly affecting the parotids (11). Sialosis is found in patients with systemic diseases such as diabetes mellitus (DM), obesity, chronic alcoholism, and hyperlipidemia (12). The overall grey scale appearance highlights enlarged glands that are hyperechoic and homogeneous, with a posterior margin that is difficult to discern.

In the ultrasound assessment of the parotid and submandibular glands in patients with DM and obesity, differences compared to healthy subjects were observed only in grey scale imaging, while the elasticity index measured using SWE remained unchanged (3) (Fig. 11.4).

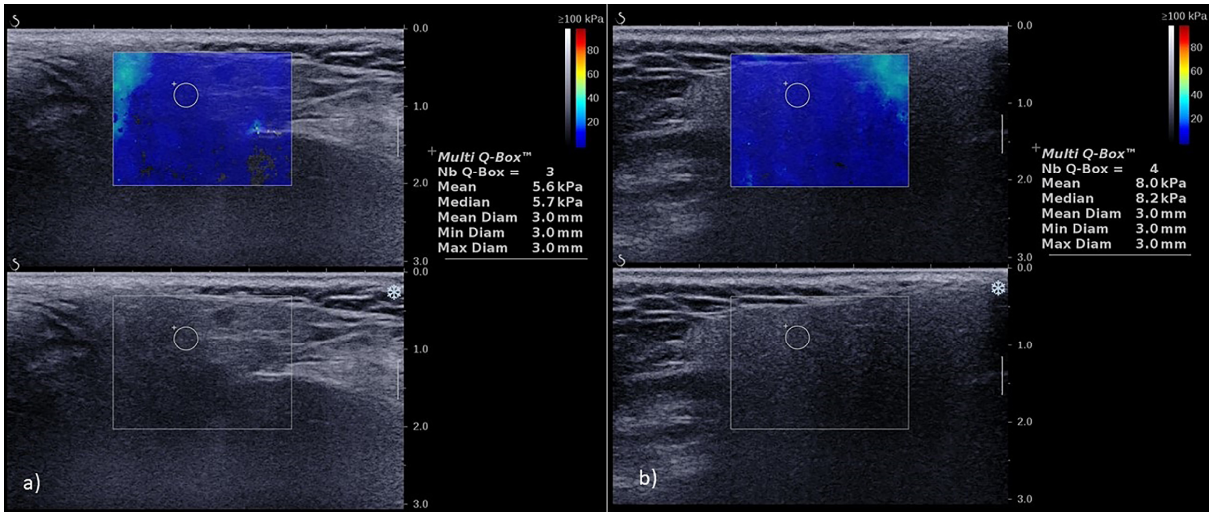

Fig. 11.4: Shear wave elastography appearance in an obese patient with sialosis in both (a) parotid gland and (b) submandibular gland.

11.5. Elastography in the Inflammatory Pathology of Salivary Glands

Acute inflammation can be caused by duct obstruction, viral or bacterial infections, or a combination of both. In cases of sialolithiasis, the parenchyma undergoes restructuring and becomes stiffer compared to the parenchyma of the contralateral gland (SWV of 2.66±0.89 in the healthy submandibular gland vs 2.98±0.4 m/s in the submandibular gland with stones) (13). Another study evaluating SWV before and after surgery observed a decrease in velocity in the affected gland following sialoendoscopy. This suggests that elastographic evaluation could serve as an objective method for monitoring treatment response (14).

Chronic inflammation of the salivary glands is largely attributed to systemic diseases such as primary Sjögren's syndrome (pSS), sarcoidosis, or IgG4-related disease. Over time, most studies have focused on elastographic evaluation of patients with pSS, a rare autoimmune disease characterized by lymphocytic infiltration of the salivary gland parenchyma leading to significant xerostomia. Based on the heterogeneous grey scale appearance of the parenchyma due to multiple hypoechoic areas, an OMERACT staging system was developed (15), and more recently, efforts have been made to identify the role of elastography.

Multiple studies have highlighted the diagnostic role of both SE and SWE in patients with pSS, where the glandular parenchyma is stiffer compared to healthy subjects. A recent meta-analysis of 15 articles reported a diagnostic sensitivity (Se) of elastography of 80% and specificity (Sp) of 87%, with no significant differences between SE and SWE (16). The highest diagnostic Sp (96%) is achieved when both parotid and submandibular glands are examined together because pSS affects all salivary glands (Fig. 11.5).

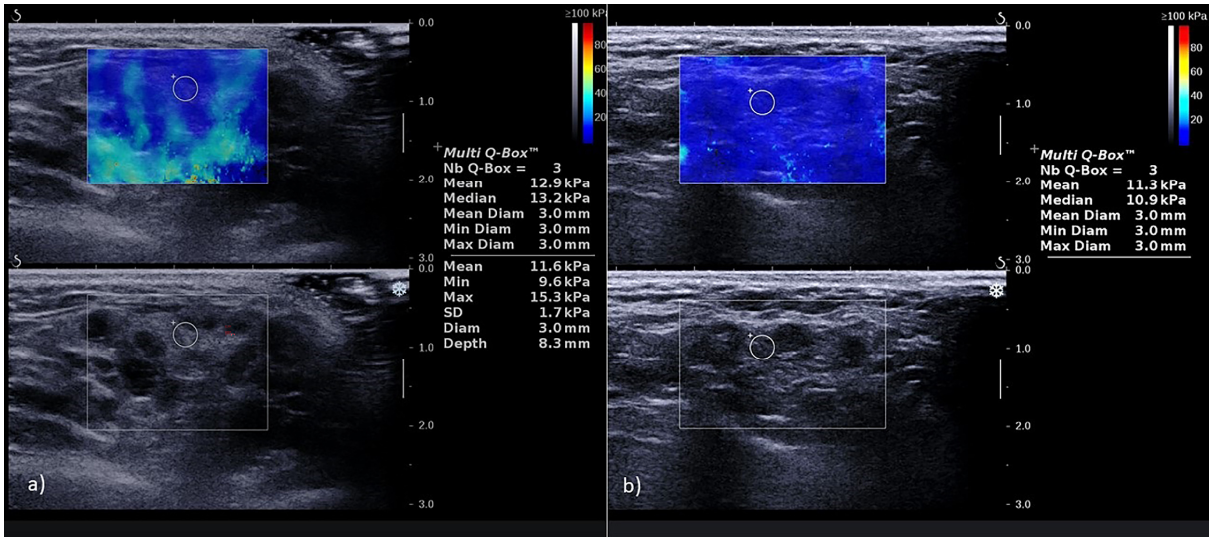

Fig. 11.5: Shear wave elastography of (a) parotid glands and (b) submandibular glands in a patient with primary Sjögren's syndrome. Similar median values of the elasticity index are observed between the two glands after 3 consecutive measurements.

In Table 11.I, several cutoff values for various elastographic indices used in studies for diagnosing pSS are presented (16). Elastography has also proven useful in distinguishing patients with pSS from those with sicca syndrome, showing increased stiffness of the salivary glands in pSS patients (17).

Table 11.I: Cutoff values of elastographic indices used for the diagnosis of pSS, adapted from Dai et al. (16)

Elastographic method	Index used	Minimum-maximum cutoff range (across various studies)
SWE	Young's modulus	6.45 kPa-18.5 kPa
ARFI	SWV	1.93 m/s-2.4 m/s
SE	VGS (grade 1-16)	7
SI	Strain ratio	1.1-2.45

pSS – primary Sjögren syndrome, SWE - shear wave elastography, ARFI - Acoustic Radiation Force Impulse, SE – strain elastography, SI - strain imaging, SWV - shear wave velocity, VGS – visual grading scale

Furthermore, ongoing research explores the potential of elastography as a prognostic tool in patients with pSS, providing insights into the risk of complications that may guide treatment strategies. Changes in glandular elasticity could correlate with the severity of inflammation or fibrosis, thus predicting overall prognosis (18). In another study, a strong correlation was found between SWV and grey scale ultrasound score, glandular and systemic activity assessed by unstimulated whole salivary flow (UWSF), EULAR Sjogren's Syndrome Disease Activity Index (ESSDAI), complement C4 levels, and certain pro-inflammatory chemokines in saliva (19). However, the same authors failed to establish a link between SWV and the degree of fibrosis, concluding that increased SWV may rather indicate chronic inflammation (19). Regarding the utility of elastography in quantifying changes in early or late stages of the disease, current studies remain contradictory (20, 21).

Differentiating between various pathologies causing chronic inflammation (such as chronic parotitis, pSS, or chronic sialolithiasis) using elastography is challenging, whether using SE or SWV (4). In chronic parotitis, Zengel et al. demonstrated that SWV is higher in the affected gland compared to the healthy contralateral gland (3.25±1.73 m/s vs 2.19±0.60 m/s) and decreases to 2.49±0.34 m/s with effective treatment (22).

11.6. Elastography in salivary gland tumor pathology

Salivary gland tumors encompass a variety of lesions, each with distinct clinical, histological, and prognostic characteristics. These tumors can arise in any minor or major salivary gland, although the parotid gland is most affected. Among the most common benign tumors are pleomorphic adenoma and Warthin tumor, while malignant tumors include mucoepidermoid carcinoma, acinic cell carcinoma, and lymphomas. Distinguishing between benign and malignant lesions using grey scale ultrasound imaging is often challenging because these formations lack characteristic features, frequently necessitating biopsy for definitive diagnosis (23, 24).

The utility of elastographic evaluation for distinguishing between benign and malignant tumors in salivary glands remains controversial. Most studies indicate that malignant tumors have higher stiffness compared to benign ones, with pleomorphic adenoma being stiffer than Warthin tumor (25). However, there is still insufficient data to draw a definitive conclusion, as demonstrated by two meta-analyses showing low diagnostic Se and Sp (26, 27). The greatest challenge lies in distinguishing pleomorphic adenoma from malignant tumors, as both can exhibit increased elasticity values (25). To improve diagnostic accuracy, Cantisani et al. demonstrated that using contrast-enhanced elastography increases diagnostic accuracy to 90.5% (28). Recently, it has been suggested that using SWE to guide biopsy site selection reduces the incidence of false-negative results (29).

Another benign tumor commonly found in the parotid glands is the parotid cyst, which appears hypoechoic on grey scale ultrasound, well-defined, and exhibits strong posterior enhancement. On SE evaluation, cysts produce a heterogeneous pattern characterized by varying levels of stiffness, often arranged in three layers of color, known as the "BGR sign" (blue/green/red) (30) (Fig.10.6).

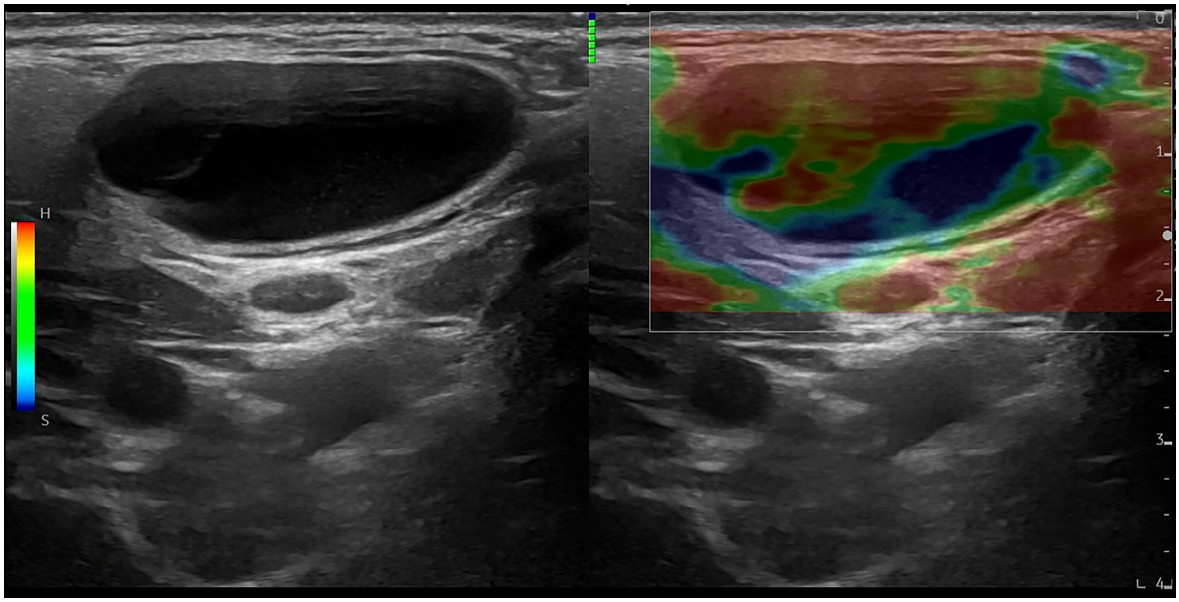

Fig. 11.6: Strain elastography of a parotid cyst demonstrating the presence of the BGR (blue/green/red) artifact.

In patients with pSS, periodic monitoring includes assessing the risk of parotid lymphoma, the most common complication in these patients. The predominant histological type is mucosa-associated lymphoid tissue (MALT) lymphoma, and suspicion arises when there are changes in clinical, biological, and/or ultrasound parameters. On grey scale ultrasound, it appears as a large hypoechoic mass with fine hyperechoic bands inside (31). On elastographic evaluation, these formations exhibit higher elasticity compared to the surrounding glandular tissue or the contralateral gland (32). Compared to other parotid tumors, parotid lymphoma shows an intermediate elastographic score (23) (Fig.11.7). In patients with pSS, combining grey scale ultrasound parameters with elasticity index can enable a diagnostic Se of 92.3% and Sp of 100% (32).

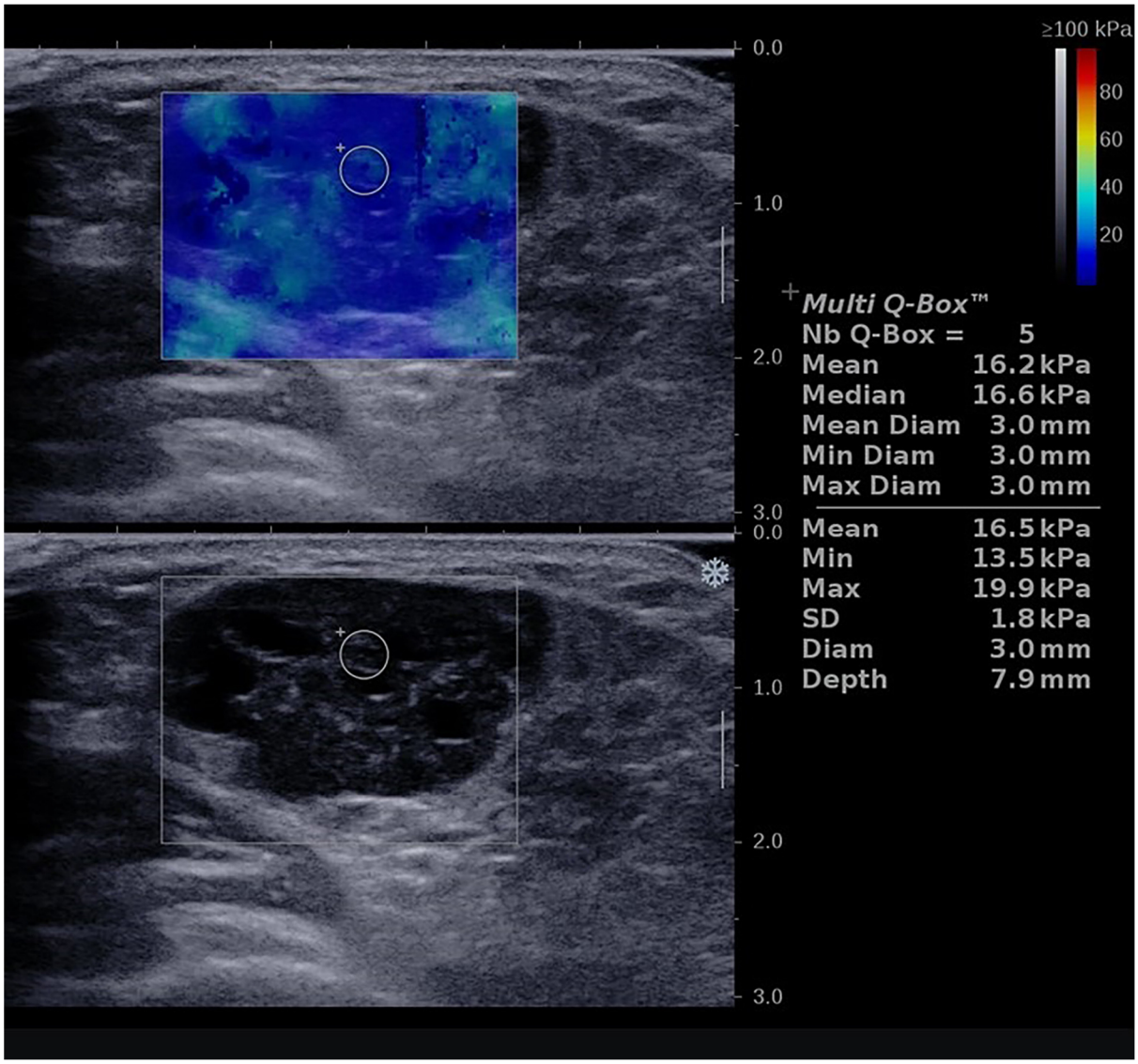

Fig.11.7: Shear wave elastography (top) and corresponding grey scale ultrasound image (bottom) of the parotid gland showing a hypoechoic, heterogeneous tumor mass. The image displays the mean and median values after 5 consecutive measurements taken at the site of the tumor mass, indicating increased stiffness in a patient with primary Sjögren's syndrome complicated by parotid non-Hodgkin lymphoma.

11.7. Elastography Evaluation Following Head and Neck Radiotherapy

Radiotherapy, although effective in treating head and neck cancers, often induces changes in the parenchyma of salivary glands such as fatty infiltration and/or fibrosis, frequently leading to xerostomia and affecting patients' quality of life. In grey scale imaging, acute phase changes reveal enlarged and hypoechoic salivary glands, while in the chronic phase, glandular volume decreases and echogenicity increases (33). Elastographic evaluation can provide benefits in quantifying the extent of fibrosis and identifying potentially reversible changes after irradiation of the head and neck region. Whether employing ARFI or SWE techniques, increased elasticity of the parenchyma post-irradiation compared to healthy control groups has been observed (9, 34, 35). Long-term monitoring after irradiation and oral administration of salivary products have shown a decrease in glandular parenchymal stiffness, suggesting a potential role for elastography in monitoring and guiding therapy for these patients (36).

11.8. Conclusions

The elastographic evaluation of salivary glands is useful as an extension of the grey scale assessment and, in some cases, it can enhance diagnostic accuracy. Although many studies have shown its usefulness, especially in chronic inflammatory conditions and tumors, widespread use continues to have difficulties in standardizing techniques and interpreting results. Ongoing research efforts are focused on refining elastographic methods, establishing protocols, and validating findings across various salivary gland conditions. These efforts aim to improve the reliability and reproducibility of elastography in diagnostic establishment, prognosis, and guiding treatment strategies.

References

1. Howlett DC, Kesse KW, Hughes DV, Sallomi DF. The role of imaging in the evaluation of parotid disease. Clin Radiol. 2002;57(8):692-701.
2. Nieto-González JC, Serrano Benavente B, Molina Collada J. Salivary gland ultrasound: Update. Med Clin (Barc). 2021;156(2):81-7.
3. Badarinza M, Serban O, Maghear L, Bocsa C, Micu M, Porojan MD, et al. Multimodal ultrasound investigation (grey scale, Doppler and 2D-SWE) of salivary and lacrimal glands in healthy people and patients with diabetes mellitus and/or obesity, with or without sialosis. Med Ultrason. 2019;21(3):257-64.
4. Elbeblawy YM, Eshaq Amer Mohamed M. Strain and shear wave ultrasound elastography in evaluation of chronic inflammatory disorders of major salivary glands. Dentomaxillofac Radiol. 2020;49(3):20190225.
5. Gungor G, Yurttutan N, Bilal N, Menzilcioglu MS, Duymus M, Avcu S, et al. Evaluation of Parotid Glands With Real-time Ultrasound Elastography in Children. J Ultrasound Med. 2016;35(3):611-5.

6. Ferraioli G, Barr RG, Farrokh A, Radzina M, Cui XW, Dong Y, et al. How to perform shear wave elastography. Part I. Med Ultrason. 2022;24(1):95-106.
7. Bedewi MA, Elsifey AA, Nassir EM, Elgazzar HM, Alfawaz AF, Hussein RS, et al. Shear wave elastography of the submandibular gland in healthy individuals. J Int Med Res. 2020;48(12):300060520979445.
8. Caliskan E, Ozturk M, Bayramoglu Z, Comert RG, Adaletli I. Evaluation of parotid glands in healthy children and adolescents using shear wave elastography and superb microvascular imaging. Radiol Med. 2018;123(9):710-8.
9. Badea I, Tamas-Szora A, Chiorean I, Crisan M, Ciuleanu E, Baciut G, et al. Acoustic Radiation Force Impulse quantitative elastography: a new noninvasive technique for the evaluation of parotid glands. A preliminary study in controls and in patients with irradiated nasopharyngeal carcinoma. Med Ultrason. 2015;17(3):308-14.
10. Muntean DD, Lenghel ML, Petea-Balea DR, Ciurea AI, Solomon C, Dudea SM. Functional Evaluation of Major Salivary Glands Using Viscosity PLUS and 2D Shear-Wave PLUS Elastography Techniques in Healthy Subjects-A Pilot Study. Diagnostics (Basel). 2022;12(8).
11. Bag AK, Curé JK, Chapman PR, Pettibon KD, Gaddamanugu S. Practical imaging of the parotid gland. Curr Probl Diagn Radiol. 2015;44(2):167-92.
12. Scully C, Bagán JV, Eveson JW, Barnard N, Turner FM. Sialosis: 35 cases of persistent parotid swelling from two countries. Br J Oral Maxillofac Surg. 2008;46(6):468-72.
13. Zengel P, Schrötzlmair F, Schwarz F, Paprottka P, Kramer M, Berghaus A, et al. Elastography: a new diagnostic tool for evaluation of obstructive diseases of the salivary glands; primary results. Clin Hemorheol Microcirc. 2012;50(1-2):91-9.
14. Chang CF, Wang HK. Ultrasound shear wave elastography for patients with sialolithiasis undergoing interventional sialendoscopy. Laryngoscope Investig Otolaryngol. 2023;8(1):76-81.
15. Jousse-Joulin S, D'Agostino MA, Nicolas C, Naredo E, Ohrndorf S, Backhaus M, et al. Video clip assessment of a salivary gland ultrasound scoring system in Sjögren's syndrome using consensual definitions: an OMERACT ultrasound working group reliability exercise. Ann Rheum Dis. 2019;78(7):967-73.
16. Dai X, Sui X, Chen S, Zhao B, Liu Z, Wang X. The diagnostic performance of salivary gland ultrasound elastography in Sjögren's syndrome and sicca symptoms: a systematic review and meta-analysis. Eur Radiol. 2023.
17. Chen S, Wang Y, Zhang G. Combination of Salivary Gland Ultrasonography and Virtual Touch Quantification for Diagnosis of Sjögren's Syndrome: A Preliminary Study. Biomed Res Int. 2016;2016:2793898.
18. Dejaco C, De Zordo T, Heber D, Hartung W, Lipp R, Lutfi A, et al. Real-time sonoelastography of salivary glands for diagnosis and functional assessment of primary Sjögren's syndrome. Ultrasound Med Biol. 2014;40(12):2759-67.
19. Kimura-Hayama E, Criales-Vera S, Azpeitia-Espinosa L, Pacheco-Molina C, Reyes E, Lima G, et al. Elastographic ultrasound: an additional image tool in Sjögren's syndrome. Int J Rheum Dis. 2018;21(6):1293-300.
20. Zhang X, Zhang S, Feng R, Yao H, Tang S, He J. Sonoelastography of salivary glands for diagnosis and clinical evaluation in primary Sjögren's syndrome. Clin Exp Rheumatol. 2021;39 Suppl 133(6):184-9.

21. Ma H, Liu L, Sun X, Liu M, Liu Z. The diagnostic value of shear-wave elastography in the salivary glands of patients with primary Sjögren syndrome. Int J Rheum Dis. 2023;26(7):1314-20.
22. Zengel P, Reichel CA, Vincek T, Clevert DA. Ultrasound elastography in diagnosis and follow-up for patients with chronic recurrent parotitis. Clin Hemorheol Microcirc. 2017;67(3-4):389-97.
23. Bhatia KS, Rasalkar DD, Lee YP, Wong KT, King AD, Yuen HY, et al. Evaluation of real-time qualitative sonoelastography of focal lesions in the parotid and submandibular glands: applications and limitations. Eur Radiol. 2010;20(8):1958-64.
24. Martino M, Fodor D, Fresilli D, Guiban O, Rubini A, Cassoni A, et al. Narrative review of multiparametric ultrasound in parotid gland evaluation. Gland Surg. 2020;9(6):2295-311.
25. Stoia S, Băciuț G, Lenghel M, Badea R, Băciuț M, Bran S, et al. Ultrasonography techniques in the preoperative diagnosis of parotid gland tumors - an updated review of the literature. Med Ultrason. 2021;23(2):194-202.
26. Li C, Zhang C, Li N, Li J. Compression Real-time Elastography for Evaluation of Salivary Gland Lesions: A Meta-analysis. J Ultrasound Med. 2016;35(5):999-1007.
27. Zhang YF, Li H, Wang XM, Cai YF. Sonoelastography for differential diagnosis between malignant and benign parotid lesions: a meta-analysis. Eur Radiol. 2019;29(2):725-35.
28. Cantisani V, David E, Sidhu PS, Sacconi B, Greco A, Pandolfi F, et al. Parotid Gland Lesions: Multiparametric Ultrasound and MRI Features. Ultraschall Med. 2016;37(5):454-71.
29. Abba M, Allon I, Markovich-Roth T, Abramson A, London D. Efficacy of Ultrasound Shear Wave Elastography in the Diagnosis of Salivary Gland Tumors. J Oral Maxillofac Surg. 2023;81(6):780-9.
30. Dietrich CF, Barr RG, Farrokh A, Dighe M, Hocke M, Jenssen C, et al. Strain Elastography - How To Do It? Ultrasound Int Open. 2017;3(4):E137-E49.
31. Orita Y, Sato Y, Kimura N, Marunaka H, Tachibana T, Yamashita Y, et al. Characteristic ultrasound features of mucosa-associated lymphoid tissue lymphoma of the salivary and thyroid gland. Acta Otolaryngol. 2014;134(1):93-9.
32. Bădărînză M, Serban O, Maghear L, Bocsa C, Micu M, Damian L, et al. Shear wave elastography as a new method to identify parotid lymphoma in primary Sjögren Syndrome patients: an observational study. Rheumatol Int. 2020;40(8):1275-81.
33. Katz P, Hartl DM, Guerre A. Clinical ultrasound of the salivary glands. Otolaryngol Clin North Am. 2009;42(6):973-1000, Table of Contents.
34. Rahatli FK, Turnaoglu H, Iyidir OT, Kirnap NG, Haberal KM, Aydın E, et al. Assessment of Parotid and Submandibular Glands With Shear Wave Elastography Following Radioactive Iodine Therapy for Papillary Thyroid Carcinoma. J Ultrasound Med. 2019;38(2):357-62.
35. Kałużny J, Kopeć T, Szczepanek-Parulska E, Stangierski A, Gurgul E, Ruchała M, et al. Shear wave elastography: a new noninvasive tool to assess the intensity of fibrosis of irradiated salivary glands in head and neck cancer patients. Biomed Res Int. 2014;2014:157809.
36. Hofauer B, Roth A, Heiser C, Schukraft J, Johnson F, Zhu Z, et al. Point Shear Wave Elastography in Diagnosis and Follow-Up of Salivary Gland Affection after Head and Neck Cancer Treatment. J Clin Med. 2022;11(21).

Chapter 12. Renal Elastography

Flaviu Bob

The use of imaging techniques in the assessment of the kidneys is of a certain importance, and therefore, kidneys ultrasound is a significant partof the activity of nephrologists, urologists and other connected specialties, as well. Despite this, imagistic methods are not the first line investigation in patients with chronic kidney disease (CKD), a potentially progressive disease associated with increased mortality, morbidity and an increasing incidence over the last years. For the diagnosis of CKD, according to the current definition, biochemical markers are used, such as glomerular filtration rate (estimated using a formula that contains serum creatinine as a biological variable) and urinary albumin creatinine ratio. (1). There is a constant search for the validation of additional biomarkers, both for diagnosis, as well as progression of CKD. On the other hand, for the assessment of CKD, besides the biological elements already mentioned, histology can be used, that is data obtained from renal biopsy specimens, this being the golden standard in the assessment of renal fibrosis (2).

As mentioned above, the use of imagistic non-invasive methods in the early diagnosis, or the assessment of progression of CKD, is extremely limited, especially in terms of the need for quantifiable methods. Conventional ultrasound is useful in the diagnosis of cystic renal diseases, but they represent only a small proportion of CKD causes. With regard to the main causes and risk factors of CKD (diabetes mellitus, arterial hypertension, glomerular disease or chronic tubulo-interstitial nephropathy), information provided by standard ultrasound are strictly indicative. We can quantify the size of the kidneys and the thickness of the renal parenchyma, both decreased in advanced stages of CKD. In these stages the decrease of the size of the kidneys is associated with an increase of the echogenicity of the cortex, due to the progression of fibrosis. (3). However, this increase of the echogenicity, observed by the investigator, is not quantifiable using conventional ultrasound, being therefore a subjective observation. Elastography represents an ultrasound-based method, that has proven its utility in the assessment of different organs, such as liver with diffuse or focal lesions (4), spleen, thyroid or prostate (5). Elastography determines the rigidity of the tissues, offering quantifiable results, thus it seems to be the right imagistic method to be added for a complete assessment of the kidney, even in CKD.

12.1. The Elastographic Assessment of the Kidneys - Techniques

12.1.1. Particularities of the Renal Tissue

In contrast to the situation of other tissues, elastographic assessment of the kidneys is confronted with some difficulties, that are due to the specific structure of the organ. Thus, renal architecture is complex, the kidneys being composed of cortex, medullary, adipous tissue at the central level, rich vasculature, collective system, surrounded by a renal capsule (6). The complexity of this structure leads to an increased degree of anisotropy, especially at the level of the medulla, composed of tubules that are aligned perpendicularly to the renal capsule (6). But even at the level of the cortex there is a degree of anisotropy, due to the spherical shape of the glomeruli, on one hand, and the convoluted aspect of the proximal and distal tubules, on the other hand (7).

The anisotropic structure of the renal structure has direct consequences on and influences the measurement of renal stiffness, irrespective of the elastographic method used (8). Thus, the obtained results will be influenced by the relationship between the ultrasound main axis and the axis of the renal pyramids. If measurements are performed in the parenchyma at mid-renal level the two axes are parallel, while if performed at the level of the renal poles (inferior or superior), the two axes are perpendicular, and the obtained result will be different (9). Therefore, in order to have a standardized approach, and also because the assessment at the level of the renal poles is sometimes difficult, renal elastographic measurements will be performed in the mid-renal parenchyma.

There is also the theory that renal tissue anisotropy can be used as a diagnostic aid, thus showing some benefits. An anisotropic ratio can be obtained, that shows variation of renal stiffness and can be used as a diagnostic element or marker for monitoring chronic kidney disease progression (10).

As already known, most elastographic methods use the so-called regions of interest (ROI), and it is at this level that the device performs the measurements. Another particularity regarding renal elastography is represented especially by these regions of interest, whose size is sometimes larger compared to the size of the measured region. It is well known that cortical stiffness is higher compared to medullary stiffness (11). We have mentioned above that measurements should ideally be performed at the level of the cortex, but the size of the cortex, especially in patients with CKD, can be smaller compared to the standard dimension of the ROI. Thus, in these situations, the measurement will contain not only cortex, but also medulla, and we can conclude that the measurement is performed at the level of the renal parenchyma (that contains both cortex and medulla).

Another problem that arises from the limited dimension of the renal parenchyma (compared to the liver), even in a normal-size kidney, is represented by the necessity of positioning the ROI near the renal capsule. This vicinity leads to the appearance of artifacts known as reverberation artifacts. This type of artifacts, known from standard ultrasound, represent the reverberation of acoustic waves between two strong reflectors. In

elastography, these artifacts lead to more increased values, and therefore it is recommended in the assessment of the liver to perform measurements 1.5-2 cm below the renal capsule. This recommendation cannot be respected in renal elastography (12).

All the mentioned difficulties lead to the necessity of standardization of renal elastography, and the use of a standardized method, even if it does not remove the difficulty of assessment, will lead to comparable intra- and interobserver results.

12.1.2. Elastographic Methods

As we know, there are many methods and techniques that can be used for the elastography of the tissues.

Strain elastography (SE) is a qualitative method, strain images being obtained by means of the displacement of tissues, through transducer pressure. The applicability at the renal level is reduced. Despite this, there is data in the literature, especially from experimental studies, using this method, particularly in transplanted kidneys, that are more superficial and can be assessed through this approach (13). Another difficulty of using this system is that in different studies there are different elastographic indices used (strain ratio between parenchyma and calices, mean tissue elasticity) (14, 15).

Shear Wave Elastography (SWE)

This is a quantitative method, which, unlike the one described above (SE), does not use transducer pressure, but is based on the generation of ultrasound pulses of high intensity, that produce shear waves in different tissues. The speed of these shear waves is expressed in m/s and is correlated with tissue stiffness, expressed by means of Young's modulus (kPa). By using this method, it has been observed that, in stiffer tissues, the obtained shear wave speed is higher. There are many elastography methods that use the measurement of shear wave speed.

a) Vibration Controlled Transient Elastography (VCTE) or Fibroscan is known for the assessment of hepatic stiffness. Shear waves are generated by a controlled external vibration, but the fact that the obtained image is not superposed on the elastography image makes the use of this method extremely difficult for the assessment of the kidneys. The results obtained using Fibroscan in the kidneys are influenced by the above-mentioned factors, especially the heterogeneity of the organ, responsible for the anisotropic aspect. Published studies using this type of approach induce the conclusion that the method cannot be used efficiently in practice, for the assessment of renal tissue stiffness (16, 17, 18).

b) Acoustic Radiation Force Impulse (ARFI) has the big advantage, in contrast to Fibroscan, of using the same transducer for the generation of shear waves and for capturing the image of their propagation. The system is integrated in an ultrasound device, and the ultrasound image is used in order to guide the exact location of the performance of elastographic measurements. Through this method, shear waves are generated inside the

organ due to strong impulses. Once generated, shear waves are propagated through the tissue with a certain speed and are attenuated through absorption in the soft tissue (19). There are two distinct ARFI methods available, that differ through the modality of generating and reporting information.

"Point shear wave elastography" (pSWE). The result obtained is the mean value of shear wave speed inside the region of interest (ROI). The types of systems that use this method are: Virtual Touch Quantification (VTQ) (Siemens S2000, S3000) (Fig. 12.1), Elastography Point Quantification (ElastPQ) (Phillips Affiniti) (Fig. 12.2).

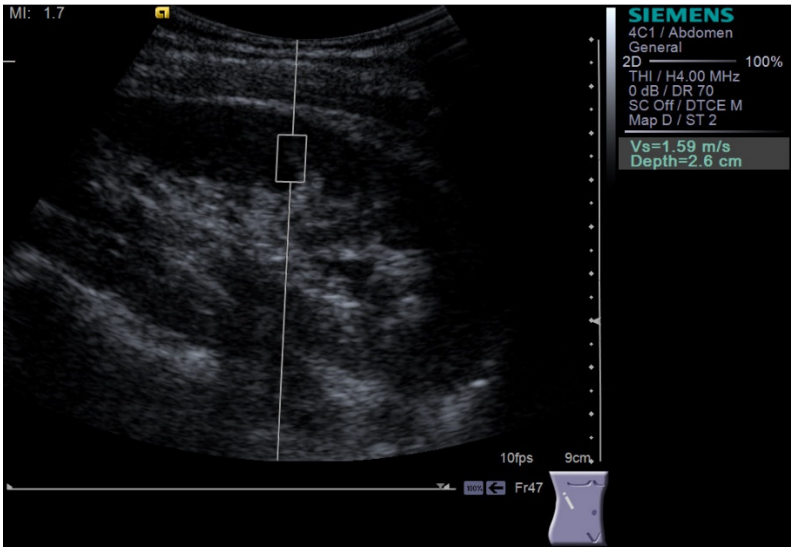

Figure 12.1. Shear wave speed (expressed in m/s) measured using the pSWE method: Virtual TouchTM Tissue Quantification (VTQ), software version 2.0, on an ultrasound system Siemens Acuson S2000TM (Siemens AG, Erlangen, Germany) with 4CI transducer.

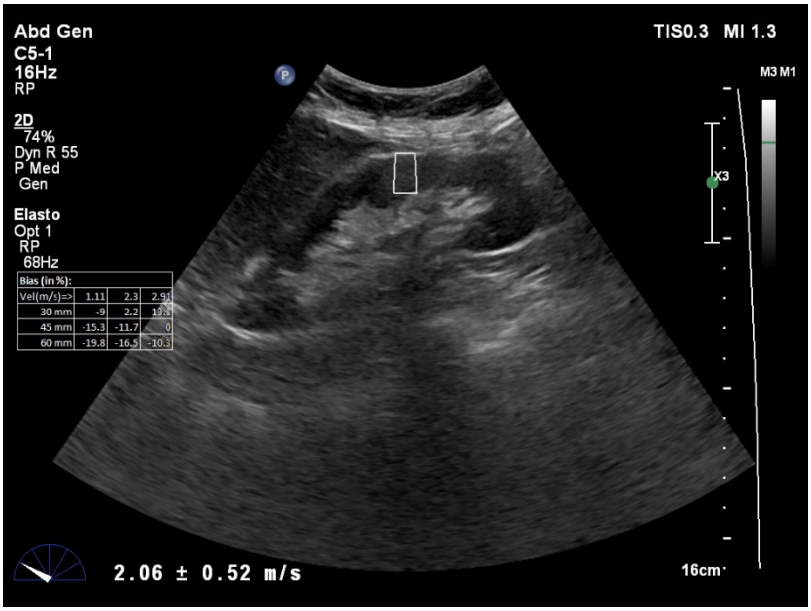

Figure 12.2: Shear wave speed (expressed in m/s) measured with pSWE method: Elastography Point Quantification system (ElastPQ) on a Phillips Affiniti system with 4CI transducer.

- *Shear wave speed imaging- 2D-SWE*. Instead of using a mean value inside the region of interest, this method uses a color coded map with different colors for different stiffness degrees, and the measurement is performed where the aspect has the highest homogenicity. Systems that use this method are: 2D SWE.SSI (Aixplorer) (Fig. 12.3), 2D SWE.GE (General Electric) (Fig. 12.4) or 2D-SWE PLUS (Aixplorer Hologic Mach30) (Fig. 12.7).

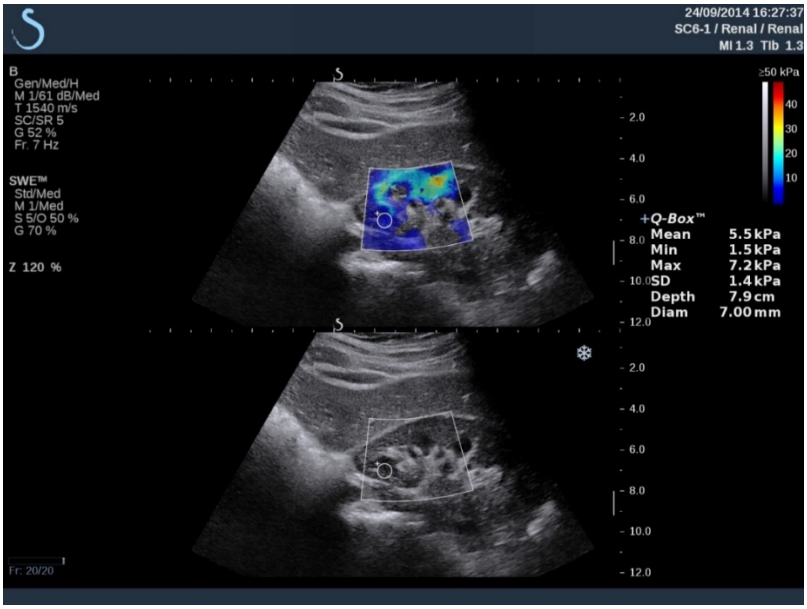

Figure 12.3: Renal stiffness (expressed in kPa) measured with the 2D-SWE.SSI method on a SuperSonic Imagine Aixplorer® ShearWave™ with a SuperCurved™ SC6-1 transducer.

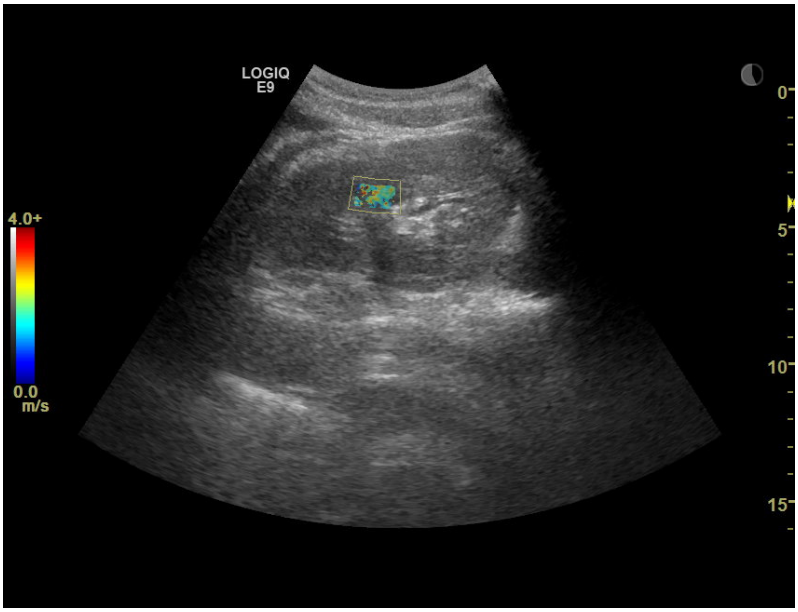

Figure 12.4: Shear wave speed measured with a 2D SWE.GE system on a Logiq E9 - General Electric ultrasound machine

The characteristics of the different elastographic systems, especially the fact that, for ARFI methods, elastography is integrated into the ultrasound machine and uses the same transducer, lead to the conclusion that, in practice, just the two methods based on ARFI can be used for the assessment of the kidneys. Therefore, we will refer strictly to these methods when we describe the method as well as the normal values corresponding to renal elastography.

12.1.3. Procedure of the Elastographic Assessment of the Kidney

As mentioned above, the two methods (pSWE and 2D-SWE) are ultrasound-based, being integrated into the ultrasound device. Therefore, in order toobtain a valid elastographic result, it is necessary to gain a good ultrasound image. The preparation of the patient before the investigation is similar to the one before ultrasound, the position being lateral, right or left decubitus, with the indication of breath holding during measurement (Fig. 12.5).

The correct ultrasound assessment of the kidney will always precede elastography. After this is obtained, the examiner can switch to the elastography mode. In this mode, the region of interest (ROI) will be superposed on the ultrasound image. In the ROI, shear wave speed will be obtained either as a mean value (in pSWE) or as a value in a selected homogenous area (in 2D-SWE). In both situations, the result will be displayed on the screen and can be expressed in m/s or in kPa.

Because the results are quantifiable and because, as mentioned before, the renal tissue is characterized by anisotropy, the standardization of the method is very important, and thus the ROI will always be positioned in the same way in all subjects, in the renal parenchyma in the mid-portion of the kidney.

In practice and taking into consideration the results of most published studies, although there is data that three valid measurements are sufficient, we consider that the value of renal shear wave speed should be reported as the median value of five valid measurements (20).

Data from the literature mention that a correct standardization leads to a good inter- and intraobserver reproducibility of the method, thus opening the path for the use of elastography in clinical practice (21,22).

Figure 12.5: For the elastographic assessment of the kidney, the patient should be examined in lateral decubitus, in order to obtain the best ultrasound image.

12.1.4. Normal Values for Renal Elastography

Regarding normal values of renal stiffness, we must take into account that there are different systems available, aspect that has been mentioned above. The values obtained using different types of elastography are different, they cannot be compared and there are no correlation tables ready to use in order to compare the results obtained with different systems from different providers.

For pSWE systems, normal values range between 2.15 and 2.54 m/s (for the VTQ system) and between 1.23 and 1.54 m/s (for the ElastPQ system) (5). For 2DSWE-GE, normal values are between 1.71 and 1.79 m/s. (23), while for 2D SWE PLUS, a normal value is considered 31.88+- 2.89 kPa. (24)

Renal stiffness and the values obtained using elastography are influenced by several factors. It has been shown that renal stiffness decreases with age, and there are significantly lower values in men compared to female subjects (25, 26).

Another factor that can influence the results is the measurement depth. Shear wave speed decreases with the increase of measurement depth (25, 27, 28). Moreover, it has to be mentioned that extreme depth makes the measurement impossible, because the maximum depth of the ROI is 8 cm.

Difficulties can occur in very superficial kidneys, because the results can be influenced by the degree of compression with the transducer, thus being operator dependent. A study

published by Correas et al. has shown that cortical stiffness increases with the increase of transducer compression (11). Thus, this could lead to different elastographic values in very superficial kidneys, such as in renal grafts. Therefore, the inter- and intraobserver reproducibility of renal transplant elastography is lower compared to the examination of the native kidney (29, 30).

The increase of urinary pressure, due to urinary obstruction, can also influence renal stiffness. There are published studies, particularly in pediatrics, that have assessed the influence of obstruction on elastography, although with contradictory results. In a study performed in 51 children with different degrees of hydronephrosis, compared to normal subjects, an increase of stiffness due to hydronephrosis has been observed (31). In another study performed in 88 children with vesico-uretheral reflux, the stiffness decreased with the increase of reflux (32), while in a smaller study (37 children), elastography could not differentiate between obstructive and non-obstructive hydronephrosis (33). Therefore, in order to avoid a potential influence of urinary pressure on the obtained results, it is routinely recommended to perform renal elastography after voiding.

12.1.5. Elastography in Renal Pathology

The main purpose of the use of renal elastography by the nephrologist is to assess diffuse renal lesions, and chronic kidney disease. Thus, the expected result from this type of investigation could be helpful in the early diagnosis, on one hand, and for the quantification of progression of CKD, on the other hand. That is why we need to assess renal stiffness in CKD.

There are published studies showing that shear wave speed is significantly increased in patients with chronic kidney disease compared to subjects without renal disease, underlining, as expected, that kidneys become more stiffer due to chronic disease (34-38). Despite this, such model of evolution is not confirmed by all published studies. There are studies showing a significantly lower value in patients with CKD (21, 39, 40). Some studies have shown a statistically significant relationship between shear wave speed and the renal function, expressed through estimated glomerular filtration rate (eGFR), showing that decreased renal stiffness was associated to a decrease in eGFR (41-43).

Despite the linear relationship between the decrease of shear wave speed and the decrease of renal function, mentioned in some studies, a differentiation between different stages of CKD was not possible, because no statistically significant difference was found between mean renal stiffness values in different CKD stages (21, 44).

In order to implement the use of elastography in clinical practice, for the diagnosis of CKD, it is important to find “cut-off” values. The attempts to establish such cut-off values that have been published until now mainly referto the diagnosis of advanced CKD and cannot be utilized in the early diagnosis.

Thus, the presence of diabetic kidney disease with an eGFR below 60 ml/min could be predicted using VTQ (pSWE) with a sensitivity of 67.4% and a specificity of 67.8%, if the value of shear wave speed was below 2.32 m/s (45). A better diagnostic predictive value (sensitivity - 89.2% and specificity - 76.9%) has been obtained using the 2D SWE- GE system. By this system, the presence of CKD has been predicted if shear wave speed was below 1.47 m/s (23).

In a meta-analysis comprising eleven studies, that included a total number of 1,241 patients with CKD and 781 subjects without renal disease, it has been shown that renal shear wave speed is decreased in patients with CKD. There is however the problem of the increased heterogeneity ($Q= 531.13$, $p<0.0001$), which means that results are extremely different in the included studies (46). Therefore, the question raises as to which factors influence the results obtained by means of elastography.

12.1.6. Fibrosis and Elastography

It is known from liver elastography studies that fibrosis, that appears due to the progression of liver disease, has as a consequence on the increased stiffness of the liver. The histological substrate of chronic kidney disease is renal fibrosis, particularly tubulo-interstitial fibrosis, thus we can raise the hypothesis that similar changes will occur at the renal level, with the progression of CKD leading to an increased renal stiffness. However, as shown in the previous chapter, studies published until now have revealed that elastography in patients with CKD shows sometimes higher values compared to normal subjects.

Therefore, it would be important to analyze those studies that also take into account, besides elastography, histological changes obtained through the assessment of renal biopsy specimens, in order to observe how histological changes influence renal stiffness. Thus it could be revealed whether fibrosis is the main factor that influences renal stiffness, and the question can be answered why in some cases renal stiffness is lower in advanced stages of CKD.

Chronologically, the first studies that compared elastography with histological parameters have been performed in renal transplant recipients. These studies used transient elastography and showed a positive correlation between stiffness and fibrosis (16-18, 47), however, as shown above, the use of Fibroscan for renal assessment is unsuitable, due to the special structure of the kidney, and to the fact that the image is not superposed on the ultrasound image. In more recent studies using pSWE or 2D-SWE on renal transplant patients, there was no correlation between fibrosis and renal stiffness (30, 48-50).

Assessments performed at the level of native kidneys show contradictory results. Some studies performed using different systems (VTQ, ElastPQ) have shown, as expected, that severe histological changes, at glomerular, as well as tubulo-interstitial level, are associated as expected, with a significant increase of kidney shear wave speed (34, 51). Moreover, a study performed using 2D-SWE-SSI has shown not only that the degree of glomerulosclerosis and tubulo-interstitial fibrosis is associated with higher levels of kidney shear wave speed, but there was also a correlation between decreased renal stiffness and the good response to

corticotherapy (52). This last observation could be explained by the fact that a high degree of fibrosis leads to a decreased response to treatment.

Despite this, again, not all studies are concordant with the mentioned results, in terms of the relationship between elastography and histology. In contrast to previous data,a study performed in 82 patients has shown that there is no correlation between histology and elastography, but subjects who did not respond to pathogenic treatment had significantly higher renal stiffness. This could be explained by the fact that patients with lower stiffness showed more severe inflammation, and therefore had a better response to treatment (53).

Similarly, to the previous situation, there is sometimes no correlation between histological changes and renal stiffness, as it has been shown in a small study performed in 45 patients with CKD (54). Similarly, there has been no correlation between stiffness and histology, neither in a study performed on donor kidneys for renal transplantation (27).

Even more surprising are the results of studies that show an association of fibrosis, not with the increase, but with the decrease of renal stiffness (42, 55).

Combining elastography with elements of conventional ultrasound (renal length, parenchyma thickness, resistivity index) can improve the predictive value and can offer a superior diagnostic performance in the assessment of pathological changes in CKD, as shown by a study performed in patients with IgA nephropathy, in whom stiffness has been significantly lower in more advanced disease (56).

An explanation of the different pattern of results, and for the non-linear and contradictory relationship shown in different studies between renal stiffness and elastography is that renal histological changes are heterogenous, with non-uniform involvement of different compartments (glomerular, vascular or tubulo-interstitial). Moreover, it is possible that, besides histological changes, there are other factors involved in influencing renal stiffness, such as vascularization.

12.2. The Vascular Hypothesis

Another important factor besides renal structure that could influence renal stiffness is renal blood flow, because the kidney is a very well vascularized organ, and thus every change in the blood flow could influence renal stiffness (57, 58).

The relationship between renal blood flow and elastography has first been shown in experimental studies. Such a study, that used *ex-vivo* animal kidneys perfused with increasing pressure of saline, has proven that stiffness (measured using 2D-SWE Aixplorer) increases with the increasing perfusion pressure (59). Similarly, in another study, renal elastography performed in an *in-vivo* animal kidney, showed that the ligation of the renal artery leads to a decrease in stiffness, while a ligation of the renal vein leads to increased stiffness (60,61).

These observations have been confirmed in men, initially in a case report of a patient with renal vein thrombosis, that was associated to increased stiffness values in the

thrombosed kidney, compared to the contralateral one (62). But there are also clinical studies available that sustain this vascular hypothesis. Asano et al. have shown, in over 300 patients with CKD, that an increase of arterial stiffness, measured using pulse wave velocity (PWV), is associated to a decrease of renal stiffness (57). These results have been confirmed in another study performed in patients with diabetic kidney disease, that has shown a statistically negative significant correlation between renal stiffness and PWV, but also with the aortic augmentation index (63). This data could suggest that in patients with increased arteriosclerosis in large vessels (increase of PWV and of the aortic augmentation index), a decrease of renal blood flow occurs, consequently associated to a decrease of renal stiffness.

There is also indirect proof of the validity of this hypothesis of the relationship between renal blood flow and renal stiffness. In patients with gestational hypertension, characterized by renal hypoperfusion, it has been shown that increased blood pressure values are associated to a decreased stiffness (64).

A study performed in renal transplant patients has shown that interstitial fibrosis and tubular atrophies do not influence renal stiffness, but adaptive glomerular hyperfiltration leads to an increase of shear wave speed. These observations are also in favor of the hypothesis that renal hemodynamics influences renal stiffness (49).

Considering the suggested relationship between renal blood flow and elastographic changes, it has even been proposed to use elastography before renal biopsy in order to predict the risk of post biopsy bleeding, however, although the specificity of the method was good, the sensitivity was low (65).

In a study performed in 20 renal transplant patients it has been found that renal stiffness is higher in a functional renal graft, compared to a non-functional one, this change being associated to a reduction of cortical microvascular blood flow (66).

A new experimental elastographic method that could explain the above-mentioned results could be the bi-dimensional ultrasound time-harmonic elastography. When using this method, the patient should be put on a special vibration bed, and the 2D-SWE elastogram obtained covers the whole kidney and is not limited to a special region (67). Using this type of elastography, Grossman et al. have shown that renal stiffness decreases significantly in CKD stage G1 in the glomerulonephritis patients studied, compared to the control group. Moreover, negative correlations have been found with the resistive index, which underlines that renal blood flow influences renal stiffness (68).

The decrease of renal blood flow may have a more important influence on renal stiffness compared to fibrosis, leading to a decrease of shear wave speed. The progression of fibrosis, especially at the interstitial level, that should lead to an increase of stiffness, leads to a decrease of intrarenal blood flow, counterbalancing the previously mentioned effect. This mechanism could explain why fibrosis is not always associated with an increase of renal stiffness (42, 55, 56).

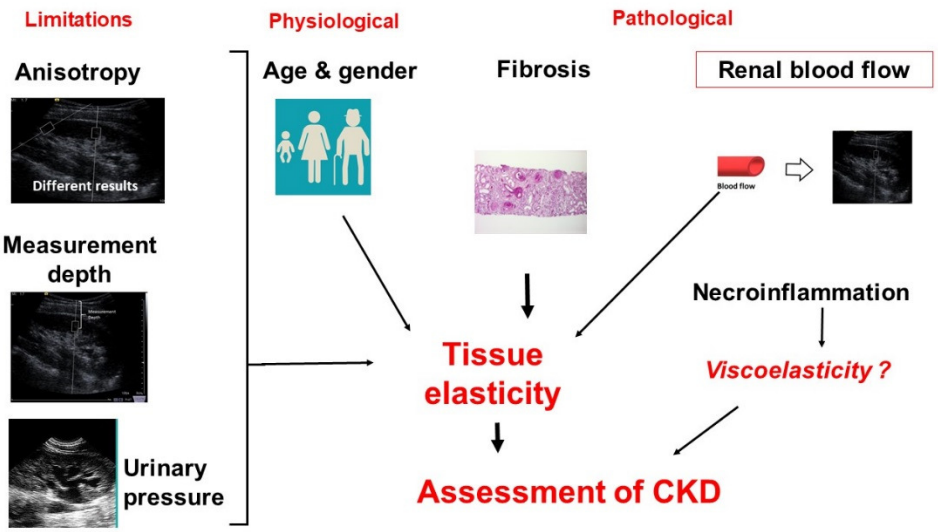

Figure 12.6: Factors that influence the use of elastography in the assessment of chronic kidney disease

12.3. Tissue viscosity

Alongside the elastic attribute of the tissues, viscosity also plays an important role in the propagation of shear waves. If a tissue were perfectly elastic, then shear wave speed would be constant, irrespective of the shear wave frequency. But the human tissues are viscoelastic, thus shear wave speed varies depending on the shear wave frequency. Consequently, the dispersion of shear waves can be utilized for the estimation of the change of tissue viscosity, which is useful for the assessment of the degree of necroinflammation (69).

Necroinflammation is described as a slope of autoamplification, stimulated by necrosis (cellular death that implies the rupture of cellular membranes) and inflammation (defined as the release of cytokines, the increase of vascular permeability and the recruiting of immune cells). This process is present in acute tubular necrosis, urosepsis, rapidly progressive glomerulonephritis or thrombotic microangiopathy (70).

In a study performed in children with glomerulonephritis, a significant increase of the dispersion slope has been observed, meaning a significantly higher viscoelasticity compared to normal subjects (13.5+-1.39 (m/s)/kHz vs. 12.4+-1.40 (m/s)/kHz, $p<0.001$). (71) Moreover, the level of viscosity is significantly higher in the transplanted kidney compared to the native kidney (72).

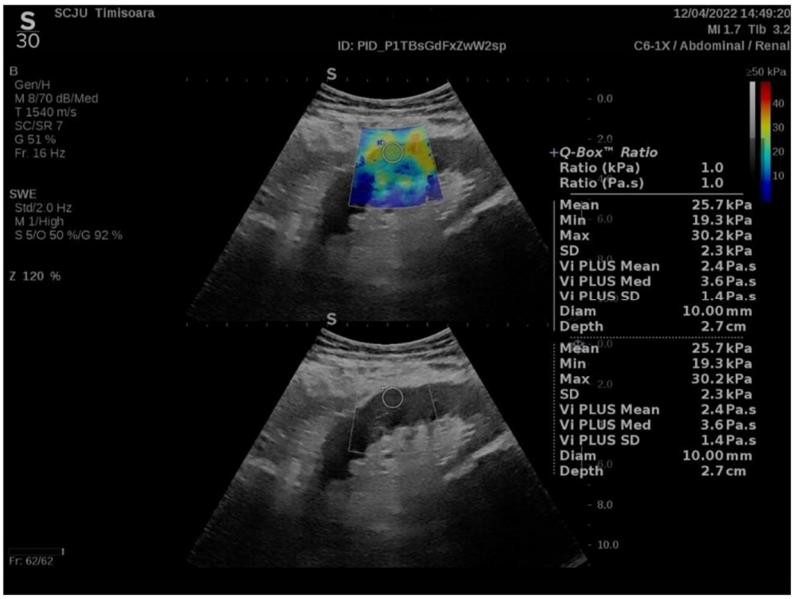

Figure 12.7 Viscoelasticity of tissue, expressed in Pa.s, obtained using the Hologic Aixplorer Mach 30 ultrasound system

12.4. Perspectives of Renal Elastography

Shear wave elastography could be the ideal imagistic procedure for the assessment of CKD, because it combines the already known advantages of ultrasound examination, such as its non-invasive nature, the real-time assessment and the low costs, with the fact that elastography yields quantifiable results. Nevertheless, the complexity of the renal architecture and the characteristics of the renal tissue may lead to sometimes contradictory results. Therefore, the use in clinical trials is difficult (73).

There are some aspects that can improve the use of renal elastography. The analysis of raw data originally generated by the system and an analysis by means of different processing algorithms lead to the final result displayed on the screen, which has underlined the importance of adapting such algorithms for the use in the kidneys. Such analysis, published by Richard Barr, has led to the conclusion that, by improving processing algorithms, we may obtain more accurate data regarding the assessment of renal stiffness. The use of systems with algorithms adapted for the renal assessment may render renal elastography more feasible (6, 74).

Therefore, the use of such a system with improved algorithms, as the Hologic Aixplorer Mach 30 system, leads to the increase of diagnostic accuracy. In a study performed on 40 patients, the presence of renal interstitial fibrosis could be predicted for a cut-off value of <20.77 kPa, AUC=0.860, $p < 0.001$, with a sensitivity of 88.89% and specificity of 75% (75).

Another improvement method of the diagnostic performances of renal elastography is the combination of the obtained results with other parameters, such as standard ultrasound or Color Doppler parameters. The resulting combined indices increase the prognostic value,

and thus the use of multiparametric ultrasound imaging represents a step forward for renal assessment as well.

Combining elastography with clinical parameters, such as albuminuria or the duration of diabetes mellitus, and the use of a logistic regression model, lead to an increased diagnostic accuracy, even in early stages, compared to the independent use of every parameter (76).

Moreover, the use of artificial intelligence in the processing of elastographic data may improve the diagnostic performance of the method. In a study performed in 208 patients with CKD, machine learning techniques have been used in order to combine the multiple characteristics obtained with elastography, Doppler and standard ultrasound. The result was an improvement of diagnostic performances of elastography, with an increased capacity to predict the degree of tubulo-interstitial fibrosis, and the ability to explain the lack of linear correlation between stiffness and CKD stages (77).

Considering all the presented aspects, there is not sufficient data yet to recommend the use of elastography in the diagnosis of chronic kidney disease (5). However, there are hopes that renal elastography will potentially be used as a screening method that draws attention to those subjects who might need further investigations. Therefore, new and more extensive studies are needed to establish the exact role and indication of renal elastography in practice.

References

1. Turner N, Lameire N, Goldsmith D et al. Oxford Textbook of Clinical Nephrology, 4th Ed; Oxford University Press, 2016
2. Jiang B, Liu F, Fu H, Mao J. Advances in imaging techniques to assess kidney fibrosis. Ren Fail. 2023 Dec;45(1):2171887.
3. Yu ASL, Chertow GM, Luyckx VA, et al.. Brenner & Rector's The Kidney 11th Edition, Elsevier Saunders, 2020
4. Ferraioli G, Filice C, Castera L, Choi BI, Sporea I, Wilson SR, et al. WFUMB guidelines and recommendations for clinical use of ultrasound elastography: Part 3: liver. Ultrasound Med Biol. 2015 May;41(5):1161-79.
5. Saftoiu A, Gilja OH, Sidhu PS, Dietrich CF, Cantisani V, Amy D, et al. The EFSUMB Guidelines and Recommendations for the Clinical Practice of Elastography in Non-Hepatic Applications: Update 2018. Ultraschall Med. 2019; 40(4):425-453.
6. Ferraioli G, Barr RG, Farrokh A, Radzina M, Cui XW, Dong Y, et al. How to perform shear wave elastography. Part II. Med Ultrason. 2021 Aug 3. doi: 10.11152/mu-3342. Epub ahead of print. PMID: 34379714.
7. Madsen K NSTC: Anatomy of the kidney. In: B B, ed. The Kidney. Philadelphia: Sanders Elsevier 2008;25-90.
8. Leong SS, Wong JHD, Md Shah MN, Vijayananthan A, Jalalonmuhali M, Mohd Sharif NH, Abas NK, Ng KH. Stiffness and Anisotropy Effect on Shear Wave Elastography: A Phantom and in Vivo Renal Study. Ultrasound Med Biol. 2020; 46(1):34-45.
9. Grenier N, Gennisson JL, Cornelis F, Le Bras Y, Couzi L. Renal ultrasound elastography. Diagn Interv Imaging. 2013, 94: 545 - 550.

10. Wang L. New insights on the role of anisotropy in renal ultrasonic elastography: From trash to treasure. Med Hypotheses. 2020 ;143:110146.
11. Correas JM, Anglicheau D, Joly D, Gennisson JL, Tanter M, Hélénon O. Ultrasound-based imaging methods of the kidney-recent developments. Kidney Int. 2016 ; 90(6):1199-1210.
12. Bruce M, Kolokythas O, Ferraioli G, Filice C, O'Donnell M. Limitations and artifacts in shear-wave elastography of the liver. Biomedical Engineering Letters. 2017;7(2):81-9.
13. Qi R, Yang C, Zhu T. Advances of Contrast-Enhanced Ultrasonography and Elastography in Kidney Transplantation: From Microscopic to Microcosmic. Ultrasound Med Biol. 2021; 47(2):177-184.
14. Kahn J, Slowinski T, Thomas A, Filimonow S, Fischer T. TSI ultrasound elastography for the diagnosis of chronic allograft nephropathy in kidney transplanted patients. J Ultrason. 2013 Sep;13(54):253-62.
15. Orlacchio A, Chegai F, Del Giudice C, Anselmo A, Iaria G, Palmieri G, et al. Kidney transplant: usefulness of real-time elastography (RTE) in the diagnosis of graft interstitial fibrosis. Ultrasound Med Biol. 2014 Nov;40(11):2564-72.
16. Arndt R, Schmidt S, Loddenkemper C, Grünbaum M, Zidek W,et al. Noninvasive evaluation of renal allograft fibrosis by transient elastography-a pilot study. Transpl Int. 2010; 23 : 871 -877.
17. Sommerer C, Scharf M, Seitz C, Millonig G, Seitz HK, et al. Assessment of renal allograft fibrosis by transient elastography. Transpl Int. 2013, 26: 545 - 551.
18. Lukenda V, Mikolasevic I, Racki S, Jelic I, Stimac D, Orlic L. Transient elastography: a new noninvasive diagnostic tool for assessment of chronic allograft nephropathy. Int Urol Nephrol. 2014; 46(7):1435-40.
19. Shiina T, Nightingale KR, Palmeri ML, Hall TJ, Bamber JC, Barr RG, et al. WFUMB guidelines and recommendations for clinical use of ultrasound elastography: Part 1: basic principles and terminology. Ultrasound Med Biol. 2015; 41(5):1126-47.
20. Bob F, Bota S, Sporea I, Gradinaru-Tascau O, Popescu M, Popescu A, Schiller A. How many measurements are needed for kidney stiffness assessment by acoustic radiation force impulse (ARFI) elastography? 26th Congress of the European Federation of Societies for Ultrasound in Medicine and Biology (EFSUMB) EUROSON, May 26-28 Tel Aviv, Israel.
21. Bob F, Bota S, Sporea I, Sirli R, Petrica L, Schiller A. Kidney Shear Wave Speed Values in Subjects with and without Renal Pathology and Inter-Operator Reproducibility of Acoustic Radiation Force Impulse Elastography (ARFI) - Preliminary Results. PLoS One. 2014, 26;9(11):e113761.
22. Hwang J, Kim HW, Kim PH, Suh CH, Yoon HM. Technical Performance of Acoustic Radiation Force Impulse Imaging for Measuring Renal Parenchymal Stiffness: A Systematic Review and Meta-Analysis. J Ultrasound Med. 2021 Feb 18. doi: 10.1002/jum.15654. Epub ahead of print.
23. Grosu I, Bob F, Sporea I, Popescu A, Sirli R, Schiller A. Two-Dimensional Shear-Wave Elastography for Kidney Stiffness Assessment. Ultrasound Q. 2019 30. doi: 10.1097/RUQ.0000000000000461. Epub ahead of print.
24. Maralescu FM, Bende F, Sporea I, Popescu A, Sirli R, Schiller A, et al. Non-Invasive Evaluation of Kidney Elasticity and Viscosity in a Healthy Cohort. Biomedicines. 2022 Nov 8;10(11):2859.

25. Bota S, Bob F, Sporea I, Sirli R, Popescu A. Factors that Influence Kidney Shear Wave Speed Assessed by Acoustic Radiation Force Impulse Elastography in Patients without Kidney Pathology. Ultrasound Med Biol. 2015; 41(1):1-6.
26. Guo LH, Xu HX, Fu HJ, Peng A, Zhang YF, et al. Acoustic radiation force impulse imaging for noninvasive evaluation of renal parenchyma elasticity: preliminary findings. PLoS One. 2013, 8: e68925.
27. Lee A, Joo DJ, Han WK, Jeong HJ, Oh MJ, Kim YS, Oh YT. Renal tissue elasticity by acoustic radiation force impulse: A prospective study of healthy kidney donors. Medicine (Baltimore). 2021, 22;100(3):e23561.
28. Zhao H, Song P, Urban MW, Kinnick RR, Yin M, Greenleaf JF, Chen S. Bias observed in time-offlight shear wave speed measurements using radiation force of a focused ultrasoundbeam. Ultrasound Med Biol. 2011; 370: 1884-92.
29. Ozkan F, Yavuz YC, Inci MF, Altunoluk B, Ozcan N, Yuksel M, Sayarlioglu H, Dogan E. Interobserver variability of ultrasound elastography in transplant kidneys: correlations with clinical-Doppler parameters. Ultrasound Med Biol. 2013 Jan;39(1):4-9.
30. Syversveen T, Brabrand K, Midtvedt K, Strøm EH, Hartmann A, et al. Assessment of renal allograft fibrosis by acoustic radiation force impulse quantification--a pilot study. Transpl Int. . 2011, 24: 100 - 105.
31. Sohn B, Kim MJ, Han SW, Im YJ, Lee MJ, Shear wave velocity measurements using acoustic radiation force impulse in young children with normal kidneys versus hydronephrotic kidneys. Ultrasonography. 2014 ;33(2):116-21.
32. Göya C, Hamidi C, Ece A, Okur MH, Taşdemir B, Çetinçakmak MG, Hattapoğlu S, Teke M, Şahin C. Acoustic radiation force impulse (ARFI) elastography for detection of renal damage in children. Pediatr Radiol. 2015;45(1):55-61.
33. Dillman JR, Smith EA, Davenport MS, DiPietro MA, Sanchez R, Kraft KH, Brown RK, Rubin JM. Can Shear-Wave Elastography be Used to Discriminate Obstructive Hydronephrosis from Nonobstructive Hydronephrosis in Children? Radiology. 2015; 277(1):259-67.
34. Cui G, Yang Z, Zhang W, et al. Evaluation of acoustic radiation force impulse imaging for the clinicopathological typing of renal fibrosis. Experimental and Therapeutic Medicine. 2014;7(1):233-235.
35. Yu N, Zhang Y, Xu Y. Value of virtual touch tissue quantification in stages of diabetic kidney disease. J Ultrasound Med. 2014 ;33(5):787-92.
36. Yang X, Yu N, Yu J, Wang H, Li X. Virtual Touch Tissue Quantification for Assessing Renal Pathology in Idiopathic Nephrotic Syndrome. Ultrasound Med Biol. 2018; 44(7):1318-1326.
37. Samir AE, Allegretti AS, Zhu Q, Dhyani M, Anvari A, Sullivan DA, Trottier CA, Dougherty S, Williams WW, Babitt JL, Wenger J, Thadhani RI, Lin HY. Shear wave elastography in chronic kidney disease: a pilot experience in native kidneys. BMC Nephrol. 2015 31;16:119.
38. Sumbul HE, Koc AS, Gülümsek E. Renal cortical stiffness is markedly increased in pre-diabetes mellitus and associated with albuminuria. Singapore Med J. 2020; 61(8):435-442.
39. Bilgici MC, Bekci T, Genc G, Tekcan D, Tomak L. Acoustic Radiation Force Impulse Quantification in the Evaluation of Renal Parenchyma Elasticity in Pediatric Patients With Chronic Kidney Disease: Preliminary Results. J Ultrasound Med. 2017;36(8):1555-1561.

40. Grosu I, Bob F, Sporea I, Popescu A, Şirli R, Schiller A. Correlation of Point Shear Wave Velocity and Kidney Function in Chronic Kidney Disease. J Ultrasound Med. 2018; 37(11):2613-2620.
41. Alan B, Göya C, Aktan A, Alan S. Renal acoustic radiation force impulse elastography in the evaluation of coronary artery disease. Acta Radiol. 2017;58(2):156-163.
42. Hu Q, Wang XY, He HG, Wei HM, Kang LK, Qin GC . Acoustic radiation force impulse imaging for non-invasive assessment of renal histopathology in chronic kidney disease. PLoS One. 2014, 29;9(12):e115051.
43. Bob F, Bota S, Sporea I, Sirli R, Popescu A, Schiller A. Relationship between the estimated glomerular filtration rate and kidney shear wave speed values assessed by acoustic radiation force impulse elastography: a pilot study. J Ultrasound Med. 2015;34(4):649-54
44. Sasaki Y, Hirooka Y, Kawashima H, Ishikawa T, Takeshita K, Goto H. Measurements of renal shear wave velocities in chronic kidney disease patients. Acta Radiol. 2018;59(7):884-890.
45. Bob F, Grosu I, Sporea I, Bota S, Popescu A, Sima A, Sirli R, Petrica L, Timar R, Schiller A. Ultrasound-Based Shear Wave Elastography in the Assessment of Patients with Diabetic Kidney Disease. Ultrasound Med Biol. 2017; 43(10):2159-2166.
46. Maralescu, F.-M.; Chiodan, M.; Sircuta, A.; Schiller, A.; Petrica, L.; Bob, F. Are the Currently Available Elastography Methods Useful in the Assessment of Chronic Kidney Disease? A Systematic Review and a Meta-Analysis. Appl. Sci. 2022, 12, 2359.
47. Nakao T, Ushigome H, Nakamura T, Harada S, Koshino K, Suzuki T, Ito T, Nobori S, Yoshimura N. Evaluation of renal allograft fibrosis by transient elastography (Fibro Scan). Transplant Proc. 2015;47(3):640-3.
48. Grenier N, Poulain S, Lepreux S, Gennisson JL, Dallaudière B, et al. Quantitative elastography of renal transplants using supersonic shear imaging: a pilot study. Eur Radiol. 2012; 22: 2138 - 2146.
49. Lee J, Oh YT, Joo DJ, Ma BG, Lee AL, Lee JG, Song SH, Kim SU, Jung DC, Chung YE, Kim YS. Acoustic Radiation Force Impulse Measurement in Renal Transplantation: A Prospective, Longitudinal Study With Protocol Biopsies. Medicine (Baltimore). 2015; 94(39):
50. Stock KF, Klein BS, Cong MT, Regenbogen C, Kemmner S, et al. ARFI-based tissue elasticity quantification and kidney graft dysfunction: first clinical experiences. Clin Hemorheol Microcirc. 2011; 49: 527 - 535.
51. Leong SS, Wong JHD, Md Shah MN, Vijayananthan A, Jalalonmuhali M, Chow TK, Sharif NHM, Ng KH. Shear wave elastography accurately detects chronic changes in renal histopathology. Nephrology (Carlton). 2021 ; 26(1):38-45.
52. Yang X, Hou FL, Zhao C, Jiang CY, Li XM, Yu N. The role of real-time shear wave elastography in the diagnosis of idiopathic nephrotic syndrome and evaluation of the curative effect. Abdom Radiol (NY). 2020; 45(8):2508-2517.
53. Mancianti N, Garosi G, Iadanza E, Tripodi SA, Guarnieri A, Belluardo M, La Porta E, Calatroni M, Mazzei MA, Sacco P. Using Renal Elastography to Predict the Therapeutic Response of Nephrological Patients. J Clin Med. 2023 Nov 29;12(23):7385.
54. Wang L., Xia P., Lv K. et al. Assessment of renal tissue elasticity by acoustic radiation force impulse quantification with histopathological correlation: preliminary experience in chronic kidney disease. Eur Radiol 2014; 24(7): 1694-9.

55. Bob F, Grosu I, Sporea I, Bota S, Popescu A, Sirli R, Petrica L, Schiller A. Is there a correlation between kidney shear wave velocity measured with VTQ and histological parameters in patients with chronic glomerulonephritis? A pilot study. Med Ultrason. 2018; 4;1(1):27-31.
56. Hu Q, Zhang WJ, Lin ZQ, Wang XY, Zheng HY, Wei HM, He HG. Combined Acoustic Radiation Force Impulse and Conventional Ultrasound in the Quantitative Assessment of Immunoglobulin A Nephropathy. Ultrasound Med Biol. 2019;45(9):2309-2316.
57. Asano K, Ogata A, Tanaka K, et al. Acoustic radiation force impulse elastography of the kidneys: is shear wave velocity affected by tissue fibrosis or renal blood flow? J Ultrasound Med. 2014;33(5):793-801.
58. Grenier N, Gennisson JL, Cornelis F, Le Bras Y, Couzi L. Renal ultrasound elastography. Diagn Interv Imaging. 2013, 94: 545 - 550.
59. Locke S. The effect of interstitial pressure on tumour stiffness. Thesis: Master of Science. Graduate Department of Medical Biophysics. University of Toronto, 2014 https://tspace.library.utoronto.ca>bitstream
60. Gennisson JL, Grenier N, Combe C, Tanter M. Supersonic shear wave elastography of in vivo pig kidney: influence of blood pressure, urinary pressure and tissue anisotropy. Ultrasound Med Biol. 2012; 38(9):1559-67.
61. Liu X, Li N, Xu T, Sun F, Li R, Gao Q, Chen L, Wen C. Effect of renal perfusion and structural heterogeneity on shear wave elastography of the kidney: an in vivo and ex vivo study. BMC Nephrol. 2017 8;18(1):265.
62. Grosu I, Bob F, Sporea I et al. Assessment of Renal Vein Thrombosis using Renal Acoustic Radiation Force Impulse (ARFI) Imaging in a Systemic Lupus Erythematosus (SLE) patient: a case report. [abstract] Medical Ultrasonography, The 17th National Conference of the Romanian Society of Ultrasound in Medicine and Biology, 2014, Timisoara, Romania.
63. Bob F, Grosu I, Sporea I, Timar R, Lighezan D, Popescu A, Sirli R, Buzas R, Petrica L, Munteanu M, Schiller A. Is Kidney Stiffness Measured Using Elastography Influenced Mainly by Vascular Factors in Patients with Diabetic Kidney Disease? Ultrason Imaging. 2018 Sep;40(5):300-309.
64. Wang Y, Feng Y, Yang X, Zhang L, Zhang T, Wang W. Clinical Values of Studying Kidney Elasticity with Virtual Touch Quantification in Gestational Hypertension Patients. Med Sci Monit. 2016 7;22:403-7.
65. Çildağ MB, Gök M, Abdullayev O. Pre-procedural shear wave elastography on prediction of hemorrhage after percutaneous real-time ultrasound-guided renal biopsy. Radiol Med. 2020;125(8):784-789..
66. Marticorena Garcia SR, Guo J, Dürr M, Denecke T, Hamm B, Sack I, Fischer T. Comparison of ultrasound shear wave elastography with magnetic resonance elastography and renal microvascular flow in the assessment of chronic renal allograft dysfunction. Acta Radiol. 2018 Sep;59(9):1139-1145
67. Marticorena Garcia SR, Grossmann M, Lang ST, Nguyen Trong M, Schultz M, Guo J, Hamm B, Braun J, Sack I, Tzschätzsch H. Full-Field-of-View Time-Harmonic Elastography of the Native Kidney. Ultrasound Med Biol. 2018 May;44(5):949-954.
68. Grossmann M, Tzschätzsch H, Lang ST, Guo J, Bruns A, Dürr M, Hoyer BF, Grittner U, Lerchbaumer M, Nguyen Trong M, Schultz M, Hamm B, Braun J, Sack I, Marticorena Garcia SR. US Time-Harmonic Elastography for the Early Detection of Glomerulonephritis. Radiology. 2019; 292(3):676-684.

69. Sugimoto K, Moriyasu F, Oshiro H, Takeuchi H, Yoshimasu Y, Kasai Y, Itoi T. Clinical utilization of shear wave dispersion imaging in diffuse liver disease. Ultrasonography. 2020 Jan;39(1):3-10.
70. Mulay SR, Linkermann A, Anders HJ. Necroinflammation in Kidney Disease. J Am Soc Nephrol. 2016 Jan;27(1):27-39.
71. Yao S, Cai Y, Hu S, Liu X, Gao X, Li G, Wang H, Yu H. The value of shear wave elasticity and shear wave dispersion imaging to evaluate the viscoelasticity of renal parenchyma in children with glomerular diseases. BMC Nephrol. 2023 Oct 19;24(1):306.
72. Maralescu FM, Bende F, Sporea I, Popescu A, Șirli R, Schiller A, et al. Assessment of Renal Allograft Stiffness and Viscosity Using 2D SWE PLUS and Vi PLUS Measures-A Pilot Study. J Clin Med. 2022 Jul 27;11(15):4370.
73. Lim WTH, Ooi EH, Foo JJ, Ng KH, Wong JHD, Leong SS. Shear Wave Elastography: A Review on the Confounding Factors and Their Potential Mitigation in Detecting Chronic Kidney Disease. Ultrasound Med Biol. 2021 Aug;47(8):2033-2047.
74. Barr RG. Can Accurate Shear Wave Velocities Be Obtained in Kidneys? J Ultrasound Med. 2020; 39(6):1097-1105.
75. Maralescu FM, Vaduva A, Schiller A, Petrica L, Sporea I, Popescu A, et al. Relationship between Novel Elastography Techniques and Renal Fibrosis—Preliminary Experience in Patients with Chronic Glomerulonephritis. Biomedicines 2023, 11, 365.
76. Liu QY, Duan Q, Fu XH, Fu LQ, Xia HW, Wan YL. Value of elastography point quantification in improving the diagnostic accuracy of early diabetic kidney disease. World J Clin Cases. 2019, 6;7(23):3945-3956.
77. Zhu M, Ma L, Yang W, Tang L, Li H, Zheng M, Mou S. Elastography ultrasound with machine learning improves the diagnostic performance of traditional ultrasound in predicting kidney fibrosis. J Formos Med Assoc. 2021 Aug 24:S0929-6646(21)00387-9.

Chapter 13. Elastography of the Prostate

Sorin M. Dudea, Carolina Solomon, Anca Ciurea

The sonoelastographic difference between normal and tumoral prostate tissue has been described since 1998 [1]. The description of the clinical use of elastography for the diagnosis of adenocarcinoma of the prostate (ADKP) dates back to 2000 [2]. Preliminary studies published as far back as 2002 have demonstrated that elastography can detect more cases of ADKP than other ultrasound techniques [3]. The principle of ADKP detection by elastography is based on the fact that the tumor tissue has a greater stiffness than the surrounding normal prostate. Based on this premise, the method is expected to compensate for the lack of sensitivity of the other ultrasonographic techniques in diagnosing ADKP.

13.1. Elastographic Examination Techniques of the Prostate

Almost all known elastographic techniques are used to evaluate the prostate.

a) ***Strain elastography (SE)*** uses a relative colorimetric scale on the image. The most frequently used is the colorimetric scale in which blue designates stiff tissue, red is assigned to elastic, soft components and green denotes intermediate hardness. To induce tissue dislocation, external mechanical force (vibration of the transducer) or acoustic force (impulse wave emitted by the transducer) are used. Stiffness quantification is carried out semi-quantitatively using one of the two classic methods:

- The colorimetric ***score*** or

- The strain ratio (***SR***), in which the relative displacement of two neighboring structures on the same image is compared.

b) ***Shear wave elastography (SWE).*** In this method, transverse shear waves (SW) appear after the tissue is exposed to a focused ultrasound pulse (US). The machine detects the SW and measures its propagation speed. Based on the measured SW speed, tissue stiffness can be calculated and expressed in specific units of measure – kilopascal (kPa). There are several measurement options:

- Elastography with unifocal or "punctiform" detection of the shear wave (***pSWE*** - point shear wave elastography), also named ARFI (Acoustic Radiation Force Impulse) by a manufacturer, measures the SW velocity in a single sample of the image; it only provides numerical information.

- Two-dimensional shear wave elastography produces instantaneous information about the shear waves in multiple samples in an examination plane on a single image.

• The two-dimensional shear wave elastography technique (***2DSWE***) produces a sequence of images with color representation of tissue stiffness and the possibility of measuring the hardness in kPa or the SW speed at any point of the image.

• The three-dimensional shear wave elastography technique (***3DSWE***) associates the 2DSWE technique with 3D volumetric acquisition with a dedicated transducer. It results in a volume where tissue consistency is represented in color and average hardness values of a volume can be measured.

The peculiarity of prostate elastography resides in the fact that an endorectal examination is necessary. Initially, manufacturers only developed SE for endocavitary transducers, with SWE becoming available on this type of transducer later and from a limited number of manufacturers. As such, initially, prostate elastography meant almost exclusively SE and knowledge about SWE has accumulated over the last decade.

13.2. Appearance and Normal Values that Define Prostate Stiffness

SE

Quite often, at the periphery of the prostate, a red border of elastic periprostatic adipose tissue is observed, producing the appearance of a "soft border" (figure 13. 1) [4, 5].

The appearance of the normal prostate depends on the patient's age and the gland size. The normal prostate in young men has a homogeneous consistency, the entire gland being uniformly colored in green (figure 13.1) [4].

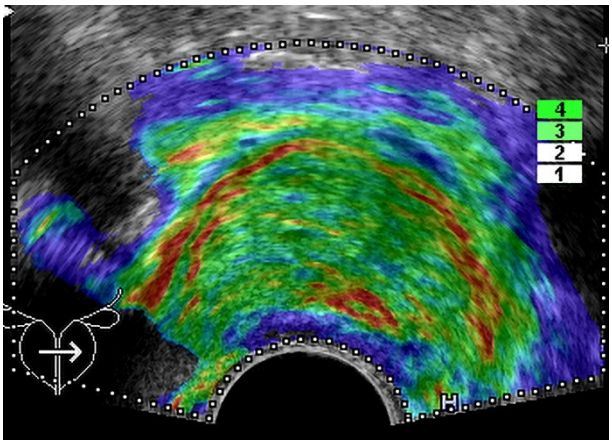

Figure 13.1. SE – normal prostate. The soft border (red) is visible on the periphery of the gland; the parenchyma of the gland has intermediate hardness (green); the apparent stiffness in the vicinity of the transducer (blue) is due to the axial compression exerted by the transducer.

The zonal structure of the prostate translates into different stiffnesses on the SE image.

The transitional zone and the periurethral fibromuscular stroma surrounding the sphincter may appear stiffer than the rest of the gland, inducing a central blue core (figure 13.2) [4, 5].

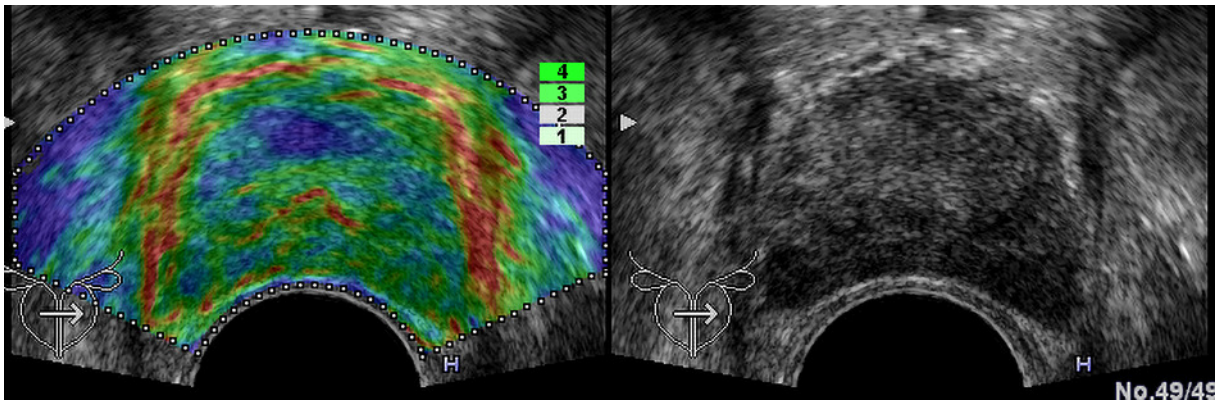

Figure 13.2. SE – normal prostate. The periurethral fibromuscular stroma produces a stiff core (blue) in the center of the prostate.

The appearance of the central area varies. The posterior portion is almost always elastic, while the lateral and basal portions are often harder [5].

The peripheral area is homogeneous, with intermediate hardness, with small focal areas that are harder in patients over forty [5].

Prostates larger than 45 ccs, usually with benign prostatic hyperplasia, may have a heterogeneous, symmetrical mosaic appearance or a striated pattern consisting of a mixture of green and blue (figure 13.3) [5]. The larger the prostate and the greater the distance from the transducer, the more pronounced the heterogeneity. The prostate's lack of elastographic signal (and color) denotes a complete lack of dislocation, induced either by too great a distance or by excessive stiffness.

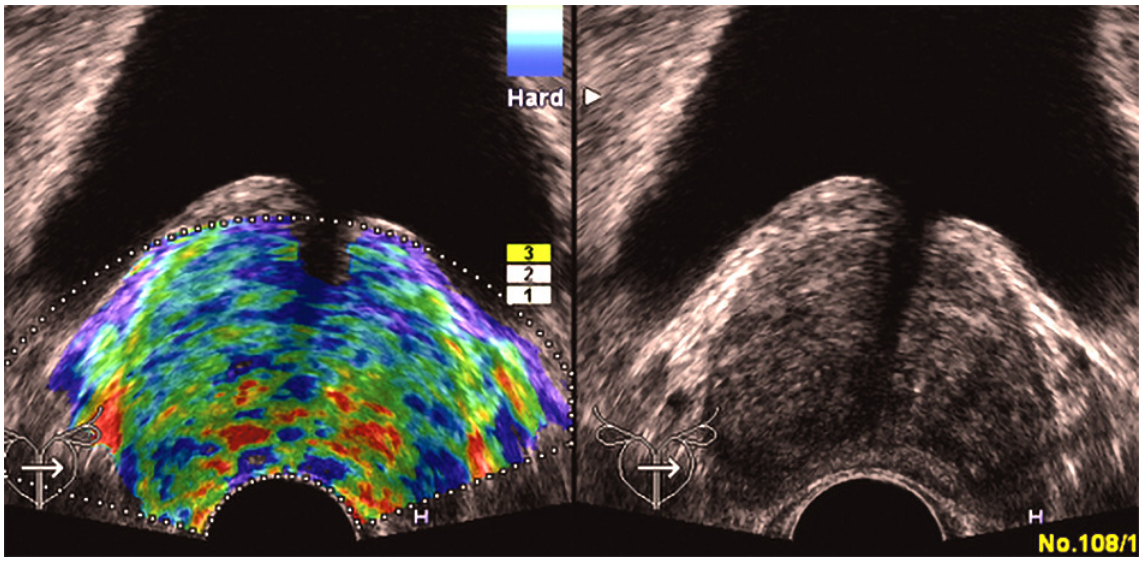

Figure 13.3. SE – hypertrophied prostate. The entire texture of the base of the gland has a mosaic appearance.

ARFI

An initial study, in vitro, demonstrated the ability of the ARFI technique, performed with experimental devices, to define prostate hardness on prostatectomy specimens [6]. Later, the method was applied transabdominally to analyze the variation of prostate consistency with age [7]. It was found that, with age, the SW speed increases as an expression of the increased hardness of the gland (Table 13.I).

Table 13.I. Average SW velocities in the normal prostate, measured by the ARFI technique [7]

Age group	Average SW speed in the internal prostate (m/s)	Average SW speed in the external prostate (m/s)
Young (< 30 years)	0.86 ± 0.21	0.85 ± 0.32
Adult (30-60 years)	1.17 ± 0.42	1.15 ± 0.49
Elderly (> 60 years)	1.82 ± 0.61	1.87 ± 0.75

There are no differences between the internal and external prostate, regardless of the age group. Prostate hardness is significantly higher in older people compared to the other two age groups [7]. Unfortunately, the method had no further applications, as the ARFI technique was not implemented on endocavitary transducers.

2DSWE

The method defines stiffness by colors similarly to SE. Its main advantage is the possibility of quantifying Young's modulus numerically.

The first studies evaluating the utility of SWE in the diagnosis of prostatic pathology defined normal prostate tissue as having a mean stiffness value of 33 kPa [8], with a threshold (cut-off) value of 35 kPa to differentiate benign from malignant prostatic sextants [9]. On the other hand, the usefulness of hardness, measured by SWE, as a criterion for distinguishing between benign and cancerous prostate tissue is challenged in studies published in the same period [10, 11]. A recent meta-analysis defines the mean hardness threshold value of 38kPa as the criterion for differentiating between benign and malignant [12].

Another criterion for evaluating normal prostate tissue is the ratio between the average hardness of a sector and the lowest value of the average hardness measured in a sector of the prostate. Typically, this ratio is 3.1 ± 2.1 [8].

It is noteworthy that cancerous tissue is harder than the benign peripheral area. All anatomic compartments and prostatic tissue classes appear harder on sagittal scans compared to the transverse plane. The transitional zone is harder than the peripheral prostate. The median peripheral prostate is harder than the lateral segments of the same area [13].

13.3. Elastography in the Diagnosis of Prostate Cancer

13.3.1. Diagnostic criteria

The use of elastography in the diagnosis of prostate cancer is based on the assumption that carcinoma is stiffer than the surrounding tissue.

SE

The original diagnostic criteria proposed [14] were:

– stiff lesion

– reproducible appearance after tilting the transducer

– diameter of the lesion of at least 5 mm.

These criteria were later refined [15] and another classification system, also in three steps, was proposed (table 13.II).

Table 13. II. Sonoelastographic three-score system for the diagnosis of prostate cancer [15].

Score	Description	% patients with cancer
1	Uniform stiffness (green)	2.3 - 11.9
2	In homogeneously increased stiffness, a mixture of blue and green areas, each blue area with a diameter less than 5mm, reproducible appearance after transducer tilting (indeterminate).	26.4 - 28.8
3	Focal increase of stiffness, an asymmetric stiff (blue) area almost homogenous, diameter larger than 5mm, reproducible appearance after transducer tilting (suspicious).	68 - 82.4

Inspired by the scores used for the elastographic evaluation of breast or thyroid lesions (the so-called Tsukuba scores), a subjective evaluation system was proposed that takes into account both the grayscale appearance and the stiffness displayed by elastography [16] (table 13.III) (figure 13.4). The key point in this scale is the relationship between a hypoechoic lesion and a stiff prostate focus. Lesions with a score of 3 or higher are highly suggestive of malignancy.

Table 13.III. Sonoelastographic five score system for the diagnosis of prostate cancer - Kamoi [16].

Score	Description	Significance
1	Homogenous texture: the whole gland is colored in green	normal
2	Symmetric heterogeneous texture, symmetric blue-green mosaic pattern	probably normal
3	Asymmetric focal stiff (blue) lesion, unrelated to any hypoechoic change in the parenchyma	undetermined
4	Hypoechoic lesion with stiff (blue) core and more elastic (green) periphery	probably carcinoma
5	Hypoechoic stiff (blue) lesion, occasionally associated with stiffness extension farther than the visible lesion borders	definitely carcinoma

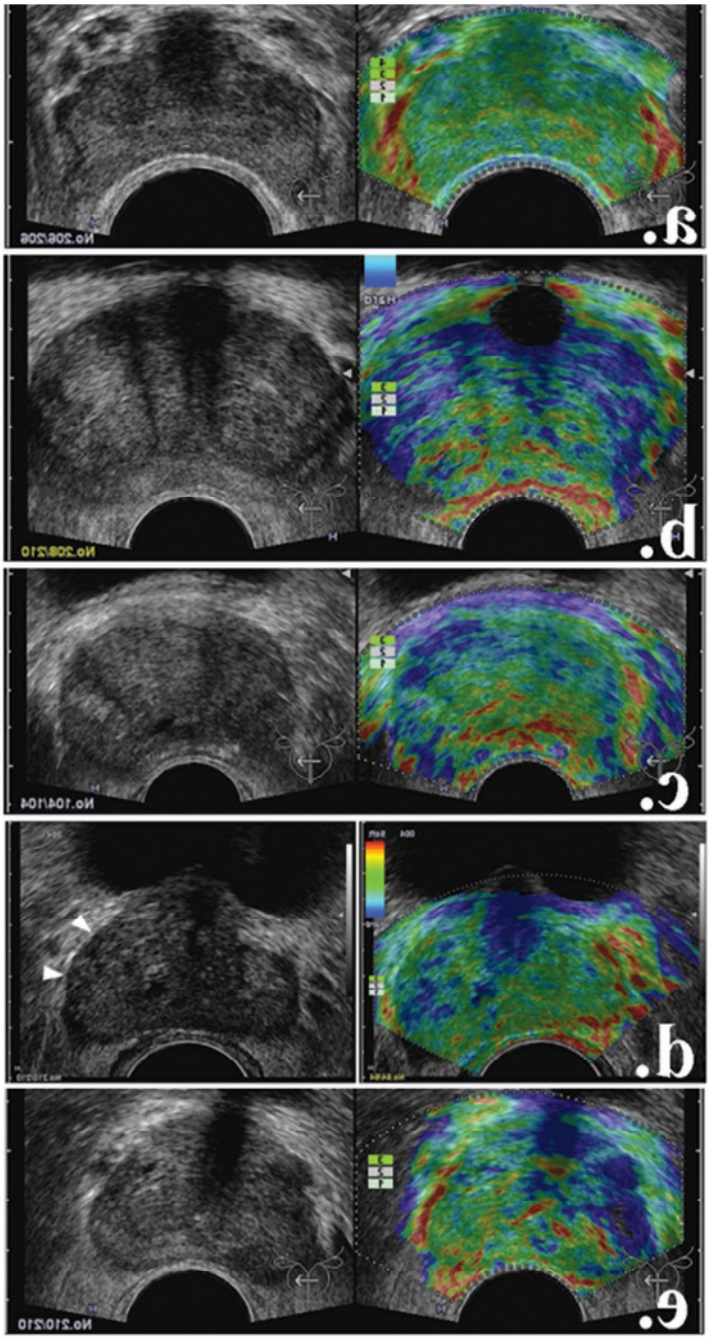

Figure 13.4. Sonoelastographic five score system [16]: a) score 1 – normal – homogeneous hardness, the entire gland has shades of green; b) score 2 – probably normal – inhomogeneous, symmetrical hardness, the gland appears as a symmetric green-blue mosaic; c) score 3 - undetermined - hard asymmetric focal lesion not associated with a hypoechoic nodule; the hard focal area is located in the left lobe; d) score 4 - probably carcinoma – hypoechoic lesion (deforms the contour of the left lobe, arrowheads) with hard core of the lesion and softer periphery; the peripheral area of the lesion is green and the central area, blue; e) score 5 - definitely carcinoma – hardness in the entire hypoechoic lesion in the right lobe and in the surrounding tissues, the entire lesion is blue. (Image reproduced from [4] with permission of the rightful holders).

Extracapsular spread of malignancy is suggested by the disruption of the periprostatic soft border (Fig. 7), while increased vesicular rigidity indicates seminal vesicle involvement [17] (Fig. 13.5).

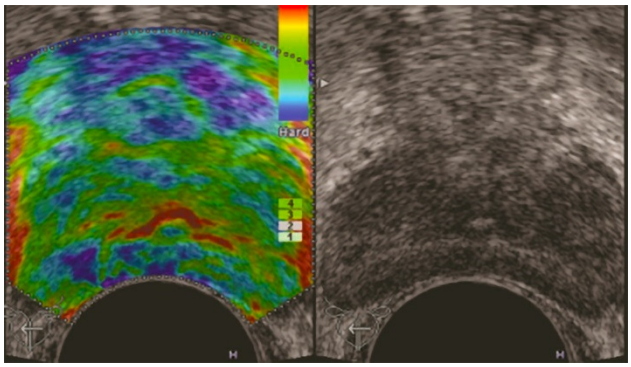

Figure 13.5. SE. Periprostatic tumor spread: the extension of the hardness in the periprostatic tissues on the anterior part of the gland is obvious.

Another approach of classifying SE images into five scores was proposed more recently [18] (table 13. IV).

Table 13.IV. Sonoelastographic scoring system in five stages for the diagnosis of prostate cancer - Xu [18].

Score	Description
1	No blue areas or stellate appearance of the peripheral zone
2	Mosaic pattern or symmetrical blue areas with a diameter of less than 5 mm in the peripheral zones
3	Small, symmetric blue area in the peripheral prostate bilaterally, diameter > 5mm
4	Asymmetric blue area in the peripheral prostate, diameter > 5mm
5	Asymmetric blue area in the peripheral prostate, covering > 50% of the peripheral zone of a lobe

In this scoring system, lesions with a score of 3 or higher also indicate malignancy.

SR

A study that measured SR by the ratio between a hard peripheral lesion and the neighboring intact peripheral prostate established the value of 5.97 as a threshold capable of indicating clinically relevant cancer - see also Table 13.V [19].

A recent publication analyzed the role of SR, calculated between the lesion in the peripheral prostate and the levator anal muscle, used as a reference structure, in the diagnosis of prostate cancer [20]. The SR value ≥ 4.6 enables the positive cancer diagnosis in lesions classified PIRADS 3 on magnetic resonance examination. The SR value ≥ 6.8 enables the diagnosis of clinically significant prostate cancer [20].

ARFI

An experimental device study in vivo, coupling ARFI information with two-dimensional images in a three-dimensional acquired volume, demonstrated the ability of the technique to highlight cancer as being harder than the neighboring prostate. At the same time, benign hyperplasia was observed as an area of consistency heterogeneity; the ejaculatory ducts and verumontanum appeared softer than the rest of the prostate and a rigid demarcation zone was observed between the transitional and peripheral zones [21]. The method has not been translated into commercially available devices.

2DSWE

In a meta-analysis of published works, cut-off values of the mean hardness of the lesion between 28.5 and 52 kPa are mentioned for the diagnosis of prostate cancer [22]. Another study established the diagnostic cut-off of mean hardness as 62.27 kPa [23]. Several studies have indicated close values, greater than 33 – 38 kPa to diagnose the presence of cancer [8, 9, 12] (figure 13.6). A summary of the threshold values, their diagnostic utility and the particularities of application is presented in Table 13.VI.

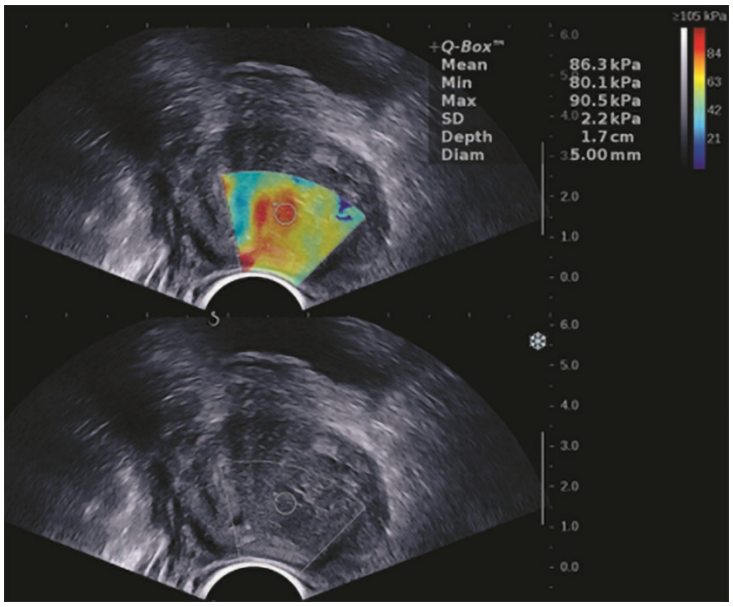

Figure 13.6. 2DSWE – malignant prostatic nodule. The color scale identifies the position of the lesion, and the measurement reveals very high hardness values for the lesion (86.3 kPa).

3DSWE

A comparative analysis between 3DSWE, magnetic resonance imaging (MRI) and prostate biopsy results have defined the average threshold value of 41kPa to diagnose the presence of clinically significant cancer [24].

13.3.2. Diagnostic value

SE

A number of studies have evaluated the value of SE in the diagnosis of ADKP, using either prostate needle biopsy or radical prostatectomy as the reference standard. The results of these studies are summarized in Table 13.V.

Table 13.V. The diagnostic value of SE

Author	SE %	SP %	PPV %	NPV %	AUC	Remarks	Reference standard
[25]	80					Preliminary experience	Needle biopsy
[16]	68	81				For score 3 of 5	Needle biopsy
	78					If power Doppler is associated	Needle biopsy
[17]	88					Pilot study	Needle biopsy
	86	72				For the whole gland	Needle biopsy
	79	85-93				For the peripheral gland, the greatest at the apex	Needle biopsy
[26]	75.4	76.6	87.8	59			Radical prostatectomy
[27]	72.6						Needle biopsy
	89.5					When combining SE with a greyscale image	Needle biopsy
[28]	51	75	64	64		Analysis per patient	Needle biopsy
	36	93	72	74		Analysis per core	Needle biopsy
	66	78	77	67		Analysis per core from the peripheral gland	Needle biopsy
[29]	89.8	78.5				Identify the existence of a tumor	Radical prostatectomy
	60.5	78.3				Identify the presence of a tumor in a specific quadrant	Radical prostatectomy
[30]	71.9	85.9				Manual vibration	Needle biopsy
	85.8	97.7				Automated balloon vibration	Needle biopsy
[31]	70.6	67.9	57	79		Pilot study	Needle biopsy
	82.3					Associating grey scale or Doppler	Needle biopsy
	88.2					Associating grey scale and Doppler	Needle biopsy
[32]	67.85	62.16	57.57	71.85			Needle biopsy
[33]	52	73	78	46			Radical prostatectomy
[19]	87,5	85,5			0,95	For SR ≥ 5,97	Needle biopsy
[34]	76	62			0.7417	Metanalysis per patient	Needle biopsy
	51	88			0.9246	Meta-analysis per biopsy core	Needle biopsy

SE=sensitivity, SP=specificity, PPV=positive predictive value, NPV=negative predictive value, AUC=area under the receiver operating characteristic (ROC) curve

All studies published to date find that SE increases the sensitivity and, depending on the study design, the specificity of ultrasound imaging diagnosis of prostate cancer.

2DSWE

Studies that evaluated the value of 2DSWE in diagnosing ADKP, using either prostate needle biopsy or radical prostatectomy as the reference standard, have their results summarized in Table 13.VI.

Table 13.VI. Diagnostic value of 2DSWE

Author	SE %	SP %	PPV %	NPV %	AUC	Remarks	Reference standard
[35]	84.4	86			0,91	Meta-analysis	Needle biopsy / Radical prostatectomy
[36]	77.88	85.33	83.02	77.06	0.855	For Emax = 128.48 kPa	Needle biopsy
	81.42	74.51	77.97	78.35	0.842	For Emed = 62.27 kPa	Needle biopsy
	60.18	63.73	64.15	58.72	0.588	For Emin = 20.03 kPa	Needle biopsy
[37]	86	89			0.94	Meta-analysis	Needle biopsy / Radical prostatectomy
[9]	96	85	48	99	0.95	For Emed = 35 kPa, sextant assessment	Needle biopsy
[38]	86	85			0.91	Meta-analysis, analysis per core	Needle biopsy
	87	69			0.89	Meta-analysis, analysis per patient	Needle biopsy
	71	74			0.78	Meta-analysis, analysis per patient	Radical prostatectomy
	82	79				Meta-analysis, analysis per core for detecting clinically significant cancer	Needle biopsy
	77	84				Meta-analysis, analysis per patient for detecting clinically significant cancer	Radical prostatectomy
[39]	81	82	69	89	0.84	Using 3DSWE, experimental device, for SW velocity 5,5 m/s, Emed = 94,1 kPa	Radical prostatectomy

[40]	61.6	91.6			0.88	Artificial intelligence using logistic regression	Needle biopsy
	84.9	43			0.78	Artificial intelligence using decision tree classifier	Needle biopsy
	87	85.5			0.94	Artificial intelligence using dense neural network	Needle biopsy
[41]	70.6	100			0.84	For Emed = 41,3 kPa, per patient, for detecting any type of cancer	Needle biopsy
	84.6	92			0.865	For Emax = 52,4 kPa, per patient, for detecting clinically significant cancer	Needle biopsy
	43.6	87.6			0.71	For Emed = 41,1 kPa, per sector, for detecting any type of cancer	Needle biopsy
	50	92.4			0.77	For Emed = 47 kPa, per sector, for detecting clinically significant cancer	Needle biopsy
[42]	96,8	67.8			0.976	For 82,6 kPa in differentiating benign–malignant, applied to index lesions	Radical prostatectomy
	88.6	97.3	86.3	97.3		To detect clinically significant cancer	Radical prostatectomy

SE = sensitivity, SP = specificity, PPV = positive predictive value, NPV = negative predictive value, AUC = area under the receiver operating characteristic (ROC) curve, Emax = maximum value of hardness in the measured sample, Emed = mean value of hardness in the measured sample, Emin = the minimum hardness value in the measured sample.

All studies published to date find that 2DSWE alone increases the sensitivity and specificity of ultrasound imaging diagnosis of prostate cancer and performs better than other ultrasound diagnostic techniques.

13.3.3. Artifacts, false results and limitations

SE

Artifacts and false results, both positive and negative, may occur during SE screening for prostate cancer, with considerable influence on sensitivity and specificity [4, 43].

***Transducer tilt*.** The main artifact in prostate elastography, although mentioned more as a technical prerequisite, is related to the tilt of the transducer.

Since most transducers used for prostate scanning are end-fire microconvex, the applied pressure is uneven. Most of it is oriented along the transducer's axis, towards the central part of the prostate, while the sides of the gland only receive a derivative of the motion vector. This results in less movement to the sides of the image and, consequently, less distortion and a stiffer appearance with more blue areas. This scanning peculiarity explains why a rigid lesion must be reproducible after changing the tilt of the transducer [4] (figure 13.7).

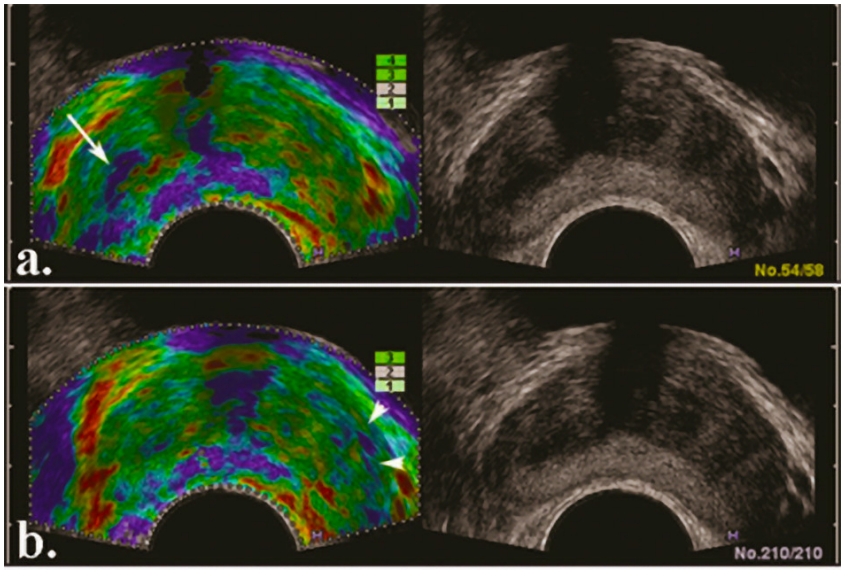

Figure 13.7. SE. Effect of transducer tilt. The apparent hard focal lesion indicated by the arrow in image a) disappears after tilting the transducer (image b)). A hard area appears in this image (arrowheads), which is not apparent in image a). (Image reproduced from [4] with permission of the rightful holders).

Slippage from the plane of examination is encountered in up to 32% of cases during manually induced vibration but only in 1% of cases when using automatic balloon inflation [44]

A prostate volume larger than 80 cm^3 or a large transition zone places part of the prostate outside the optimal range of SE exploration (Figure 13.8).

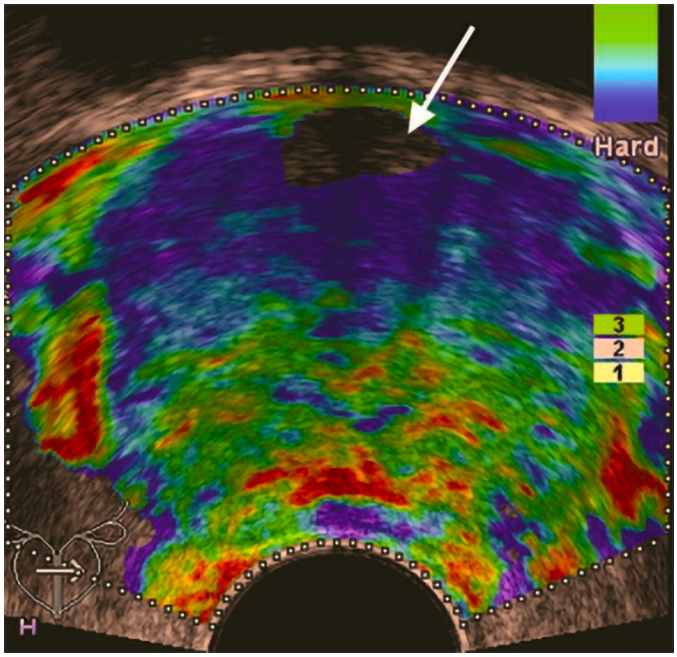

Figure 13.8. SE of a bulky prostate. At the base, the entire area away from the transducer is blue (apparently rigid) due to the considerable distance and low displacement. An area of signal loss (arrow) appears in the center of this zone.

Bulky calcifications in the peripheral gland secondary to prostatitis or ***focal stiffness changes secondary to transurethral resection*** induce hard areas in the parenchyma.

Multifocal tumors with the diameter of individual foci less than 3-5 mm are difficult to identify and describe.

Extensive tumors involving the entire gland do not produce rigid focal areas.

The exam is challenging for patients who ***cannot relax the pelvic floor***.

On the other hand, positive elastography with negative biopsy has been reported in patients with ***benign hypertrophy*** [27].

Well-differentiated adenocarcinoma resembles normal parenchyma, and SE cannot exclude its presence (figure 13.9).

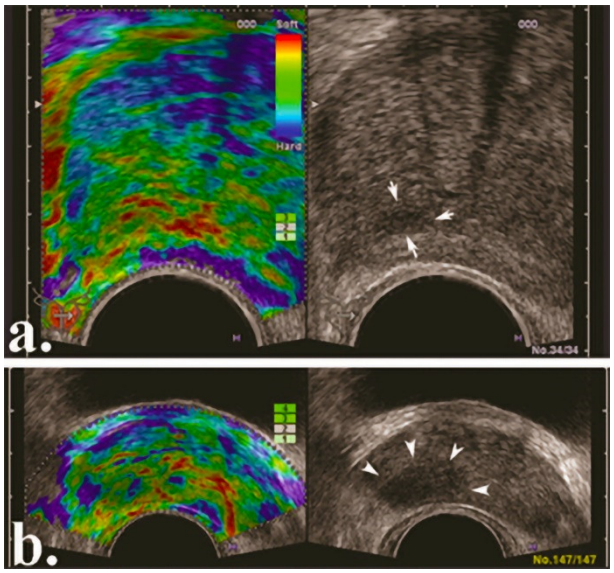

Figure 13.9. **SE. Cancerous nodules visible on the grayscale image but without elastographic expression: a) small nodule, diameter 6 mm (arrows); b) large nodule (arrowheads). In both cases, the Gleason score was 6. (Image reproduced from [4] with permission).**

Chronic prostatitis and ***BPH***, due to their inherent rigidity, can mimic carcinoma on SE examination. Hardness artifacts may also appear in BPH in the lateral parts of the gland. Repeating the examination after changing the tilt of the transducer can cancel lateral artifacts, but distance artifacts remain and ultimately alter the diagnostic value of the method [17].

Most false-positive results are associated with chronic inflammation and ***atrophy*** in the basal area of the gland [45].

Some of the causes of false results in SE examination of prostate cancer are summarized in Table 13.VII.

Table 13.VII. Causes of false results in prostate SE examination [4, 46]

False-positive	**False-negative**
Prostatitis	"Soft" cancer – predominantly Gleason 3 or 3 + 4
Fibrosis / calcification	Small cancer
Atrophy	Very large, diffuse tumor
Adenomyosis	Transducer tilt
Distance	Distance to the tumor
Attenuation	
Hard nodule in BPH	
Periurethral central zone	
Transducer tilt	
Striate base in elderly patients	

The main limitations of the method are related to the ***variability*** induced by the manual operation of the transducer and the examiner's experience. The effect of these limitations can be reduced by using automatic balloon pulsation and checking the accuracy of vibrations on the quality scale available on the ultrasound machine [17].

The ***learning curve effect*** of SE cannot be underestimated [25, 31]. At least 30 supervised examinations are needed to reach acceptable quality standards [46].

SWE

The causes of artifacts and false results presented for SE also apply to 2DSWE to varying degrees.

In the case of SWE, methodologically, in phantom studies, ***intraobserver variations*** were found to be lower for 2DSWE compared to ARFI. With both methods, ***interobserver variations*** are small. In the case of 2DSWE, ***the relative stiffness of the environment*** around the explored target influences the measurement result in the target. If the surrounding environment has lower stiffness than the target, the target hardness is underestimated. If the environment has greater stiffness than the target, the stiffness of the target is overestimated [47].

The measurement with the lowest degree of error is obtained if an ***ROI smaller than the surface of the target*** is used and the ROI is placed ***inside the target***, at least 3 mm from its edge [47].

Specifically, in the case of endorectal transducers, a very good inter- and intraobserver correlation was found [48]. The results of the measurements depend on the ***target size*** (the larger the target, the lower the variability), the ***distance*** between the transducer and the target (variability increases with distance), and the ***device*** used. Machines from different manufacturers produce measurements with different values (kPa) of the same object, especially if it is soft tissue with hardness < 50-60 kPa. For objects with stiffness > 100 kPa, the measurement differences among devices are minor. Also, the variability between measurements of the same object on the same device differs among manufacturers [48].

13.3.4. Gland volume, intraprostatic tumor volume, tumor location, and Gleason score

For both SE and 2DSWE, it is necessary to consider some essential factors that influence the examination result: gland volume, intraprostatic tumor volume, tumor location and Gleason score.

SE

Several studies have shown that the ***intraprostatic location*** of the tumor influences the detection rate by SE [17, 26, 44, 49]. For tumors located at the apex of the gland, sensitivities range from 79 to 89%, while at the base and the posterior parts of the gland, reported sensitivities range from 60 to 76%. Whether or not automatic balloon inflation is used, anterior tumors are detected to a greater extent than posterior ones. The specificity for detecting apical tumors varies between 68 and 93%.

Tumor volume. Small tumors with less than 1 ml volume are detected in 72.7% of the cases, while 100% of tumors larger than 5 ml are identified with SE [50]. Increasing tumor diameter and volume is linearly associated with increasing detection rate. Most tumors with diameter > 20 mm and volume > 0.5 cm^3 are detected [46, 51]. For tumors with a volume > 0.2 cm^3, the detection rate is not influenced by the ***total volume of the prostate*** or the intraglandular location [51].

There is also a linear relationship between the detection rate by SE and ***the Gleason score*** [50]. About 74% of tumors with a Gleason score of 9–10 are detected by SE, while for scores of 5–6, the detection rate drops to 60% [44]. One study detected 74% of tumors with Gleason < 7, 78% of those with Gleason 7 and 93% with Gleason > 7 [26]. For tumors with a volume > 0.2 cm^3, the only cause of a false negative detection result is the predominance of Gleason score 3 (3+3, 3+4)[51].

Studies by our group showed a higher sensitivity of SE in patients with PSA > 10 ng/ml, patients aged over 70 years and patients with fewer fragments (6 versus 10-12 biopsy fragments) [31, 32].

2DSWE

Gland volume and ***tumor location*** in the prostate also affect the performance of 2DSWE in the same way as SE.

The ***tumor size*** determines the detection sensitivity of the method: 30.9% for tumors < 5 mm, 68.5% for tumors with sizes of 5-10 mm and 92.4 % for tumors > 10 mm [42].

The increase in the ***Gleason score*** is associated with the increase in tumor hardness, expressed by the median values of the Emed indicator, in kPa: 58.3 for non-tumor prostate tissue, 91.6 for Gleason score 6, 102.3 for Gleason score 7 and 131.8 for Gleason ≥ 8 [42] (figure 13.10).

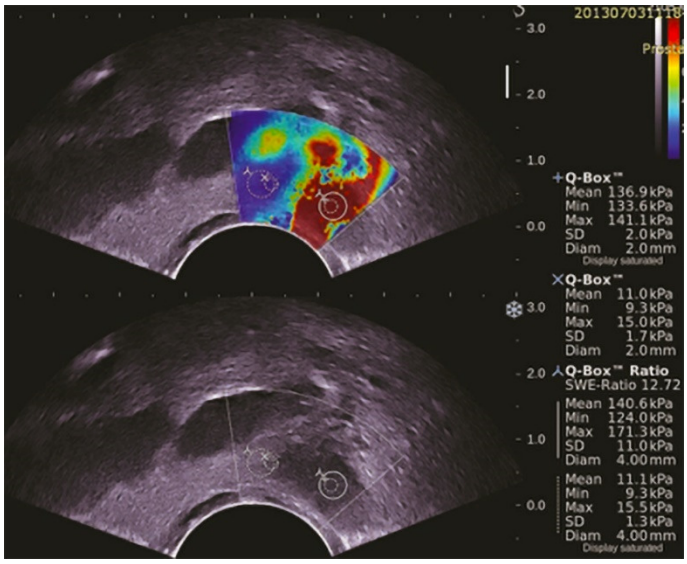

Figure 13.10. 2DSWE. The tumor highlighted in red has a hardness of 140 kPa. On biopsy, the Gleason score was 9.

13.3.5. Guide to biopsy

The main advantage of **SE** appears to be the improved results of biopsy guidance. While systematic biopsy detected 76.9% of cancers, SE-guided biopsy detected 88.8%, 91% or even 93% of cancers in preliminary studies [15, 52]. Puncture guidance with SE improves the detection of prostate cancer, as it has a detection rate of 2.9 to 4.7 times higher than systematic biopsy [17, 53, 54]. Elastography can reduce the number of biopsy fragments required to diagnose carcinoma because it detects more cancer foci than systematic biopsy, with less than half the number of fragments [17, 53].

SE-guided biopsy detects more cancers than grayscale US-guided biopsy or the power Doppler method [52]. Furthermore, the detection rate of SE-guided biopsy combined with power Doppler is higher than that of SE-guided biopsy alone or power Doppler alone [16]. Although guided biopsy (grayscale US, power Doppler, SE) is more likely to yield positive fragments, more than 50% of cancer-positive sites (on sextant biopsy) have no associated sonographically detectable changes [55].

Combining SE with systematic biopsy results in detecting of up to 18% more clinically significant cancers [26]. It is considered that positive SE is an independent marker for the detection of a clinically significant cancer and negative SE advocates against this diagnosis [56].

Using SR ≥ 5.97 to guide the puncture improves the detection of clinically significant cancer by 10%, resulting in the detection of most tumors with a Gleason score ≥ 7 [19].

A recently published meta-analysis shows that, at the patient level, SE guided biopsy does not perform better than systematic biopsy. However, biopsy fragment-level analysis indicates that SE-guided biopsy produces 2.1 times more positive fragments than systematic biopsy and combining the two leads to increased cancer detection rates [57].

The larger the volume of the prostate, the lower the sensitivity of tumor detection by SE-guided puncture. For prostates with volume < 30 cm^3, guided SE puncture is more sensitive than systematic biopsy puncture (91.7% vs. 62.5%) [58]. In all patient groups, the addition of guided SE puncture leads to increased cancer detection rates [58].

2DSWE-guided biopsy can improve the cancer detection rate using a threshold value of 47 kPa [59].

The 2DSWE method has higher sensitivity than conventional US or MRI examination in detecting potentially malignant focal lesions, produces fewer false-negative biopsy results, and has very good interoperator reproducibility [60].

Patients with suggestive focal changes on 2DSWE examination have a 6.4 times higher risk of clinically significant prostate cancer. The detection rate per fragment is not significantly higher in 2DSWE-guided punctures [61].

The best practice guidelines of the European Federation of Societies of Ultrasound in Medicine and Biology (EFSUMB) recommend using elastographic techniques during prostate biopsy to increase the detection rate [62].

13.3.6. Comparison with magnetic resonance imaging (MRI) evaluation of the prostate.

The sensitivity and specificity of **SE** are higher than T2-weighted images at 1.5T magnetic field for detecting morphological changes associated with carcinoma [63]. When using automatic balloon pulsation, SE and SP associated with SE examination are higher than those of T2-weighted and dynamic contrast-enhanced MRI sequences [30]. Another study found an equal diagnostic value for SE examination and 3T field MRI imaging of the prostate, with obviously higher costs and times associated with MRI [29]. SE better detects tumors located in the apical and middle areas of the prostate, while multiparametric MRI (MP-MRI) is more useful for tumors located in the base and transitional zone. Also, MRI-MP better detects tumors in large glands with a volume > 40 cm^3 [46]. The association of SE information may contribute to downgrading the PIRADS score established by MRI-MP [64].

Although hardness measured by **2DSWE** on the one hand and PIRADS score on the other hand correlate with Gleason score, and hardness > 100 kPa and high PIRADS scores detect most high-risk prostate cancers, a direct correlation between hardness measured by 2DSWE and the PIRADS score could not be established [65].

Recent studies have shown that 2DSWE has similar sensitivity and specificity to MRI-MP in prostate cancer detection and that 3DSWE further improves the identification of target lesions for biopsy, with performance criteria similar or superior to MRI-MP [66].

The best practice guidelines developed by the World Federation of Societies of Ultrasound in Medicine and Biology (WFUMB) recommend always performing 2DSWE alongside routine biopsy [67]. There are still no randomized trials comparing 2DSWE with MRI-

MP on the same groups of patients in view of possible recommendations to change the strategy of the imaging approach to prostate cancer.

There are no differences in sensitivity between 2DSWE and MRI in cancer diagnosis, but for clinically significant cancer, the sensitivity of 2DSWE is somewhat higher [68]. A recent study found that 2DSWE can detect 66% of clinically significant and MRI-negative cancers [69]. The 2DSWE examination takes much less time at a diagnostic sensitivity similar to that of MRI. The costs associated with 2DSWE recommend it as a competitive method for MRI [70].

13.3.7. Other applications of prostatic elastography

Analysis of collagen composition in the prostate. A study performed with SE demonstrated that stiff areas were associated with type I collagen, while type III collagen did not influence the hardness of the gland [71].

In the tumor tissue, the gene expression of collagen type Col1A1 is increased, and the orientation of the fibers is modified; these two characteristics present a linear correlation with the Gleason score and the hardness measured by 2DSWE. It appears that not only increased cell density, but also abnormal collagen content induces stiffness in prostate tumors [72]. The linear increase, with hardness measured by 2DSWE and Gleason score, of the proportion of fibroblasts associated with prostate cancer has also been proven [73].

Prediction of extracapsular extension and seminal vesicle invasion. On SE examination, extracapsular extension is suggested by the disruption of the periprostatic soft border and invasion of the seminal vesicles by the extension into the vesicles of the intraprostatic hardness [4, 17].

When performing 2DSWE, threshold values of the Emax stiffness indicator were identified that can signal extracapsular extension (60.45 kPa) or seminal vesicle invasion (81.55 kPa), and the association of 2DSWE information with MRI-MP data led to a substantial increase in diagnostic accuracy [74].

The prediction of biochemical recurrence after radical prostatectomy is possible for the threshold value of 144.85 kPa, measured with the 2DSWE method, with moderate sensitivity and specificity (77.4% and 61%) [75].

Guiding the intervention of radical prostatectomy is another proposed application for SE, considering that the method offers a way of intraoperative instrumental "palpation" that is more sensitive than manual or visual-instrumental classical palpation (SE=84%, SP=74% in tumor detection) [76].

Identification of HIFU lesions. Elastography has been used to highlight HIFU-induced lesions in the prostate as soft areas, with SE being useful in both localizing lesions and monitoring therapy effectiveness [77].

Determination of the severity of benign prostatic hypertrophy (BPH). By transabdominal application, the ARFI method was used to study the central prostate. BPH patients were found to have greater central gland stiffness than normal subjects, and severe BPH patients have greater stiffness than moderate BPH patients [78].

13.3.8. Remarks

Sonoelastography improves prostate cancer detection.

International best practice guidelines recommend the use of elastographic techniques during prostate biopsies, even if image fusion is used.

The prostate size, tumor size, location and cellularity influence the sonoelastographic appearance and detection rate.

Elastography is burdened by the dependence of the result on manually induced vibrations by the operator, the transducer tilt, and the different approaches manufacturers use to achieve elasticity imaging. It is impossible to state the superiority of one of the two methods: SE or 2DSWE.

There are positive correlations between tumor hardness and Gleason grade, an aspect that influences the diagnostic capacity of elastography. The method helps detect clinically significant cancer.

The reference standard used is, by itself, debatable, as needle biopsy of the prostate does not detect all tumors or tumor foci.

The association of elastographic techniques with grayscale ultrasound, Power Doppler, contrast ultrasound and microultrasonography, in what is called ***multiparametric ultrasonographic exploration of the prostate***, greatly improves the diagnostic value of the method.

The method is validated for clinical use. Sonoelastography represents a valuable addition to the arsenal of imaging diagnostic methods for the prostate, reviving the ultrasonography of this organ and opening the competition with MRI for the benefit of the patient.

References

1. Krouskop TA, Wheeler TM, Kallel F, Garra BS, Hall T - Elastic moduli of breast and prostate tissues under compression - Ultrason Imaging 1998, 20, 260-274.
2. Lorenz A, Ermert H, Sommerfeld HJ, Garcia-Schürmann M, Senge T, Philippou S - Ultrasound elastography of the prostate. A new technique for tumor detection - Ultraschall Med 2000, 21, 8-15.
3. Cochlin DL, Ganatra RH, Griffiths DF - Elastography in the detection of prostatic cancer - Clin Radiol 2002, 57, 1014- 1020.

4. Dudea SM, Giurgiu CR, Dumitriu D, Chiorean A, Ciurea A, Botar-Jid C, Coman I - Value of ultrasound elastography in the diagnosis and management of prostate carcinoma - Med Ultrason 2011, 13, 1, 45-53
5. Goddi A, Sacchi A, Magistretti G, Almolla J - Transrectal real-time elastography of the prostate: normal patterns - J Ultrasound 2011, 14, 220-232
6. Zhai L, Madden J, Foo WC, Mouraviev V, Polascik TJ, Palmeri ML, Nightingale KR - Characterizing the stiffness of Human Prostates using Acoustic Radiation Force - Ultrason Imaging 2010, 32, 4, 201–213
2. Zheng XZ, Ji P, Mao HW, Zhang XY, Xia EH, Gu X, Chen XF - A Novel Approach to Assessing Changes in Prostate Stiffness With Age Using Virtual Touch Tissue Quantification - J Ultrasound Med 2011, 30, 387–390
3. Woo S, Kim SY, Cho JY, Kim SH - Shear Wave Elastography for Detection of Prostate Cancer: A Preliminary Study - Korean J Radiol 2014, 15, 3, 346-355
4. Correas JM, Tissier AM, Khairoune A, Vassiliu V, Méjean A, Hélénon O, Memo R, Barr RG - Prostate cancer: Diagnostic Performance of Real-time Shear-Wave Elastography - Radiology 2015, 275, 1, 280–289
5. Porsch M, Wendler JJ, Liehr UB, Lux A, Schostak M, Pech M - New aspects in shear-wave elastography of prostate cancer - J Ultrason 2015, 15, 5–14
6. Porsch M, Görner C, Wendler JJ, Liehr UB, Lux A, Siedentopf S, Schostak M, Pech M - Inability of shear-wave elastography to distinguish malignant from benign tissue – a comparison of biopsy, whole-mount sectioning and shear-wave elastography - J Ultrason 2016, 16, 348–358
7. Yang Y, Zhao X, Shi J, Huang Y - Value of shear wave elastography for diagnosis of primary prostate cancer: a systematic review and meta-analysis - Med Ultrason 2019, 21, 4, 382-388
8. Rouvière O, Melodelima C, Hoang Dinh A, Bratan F, Pagnoux G, Sanzalone T, Crouzet S, Colombel M, Mege-Lechevallier M, Souchon R - Stiffness of benign and malignant prostate tissue measured by shear-wave elastography: a preliminary study. Eur Radiol, 2016, 27, 5, 1858–1866
9. Konig K, Scheipers U, Pesavento A, Lorenz A, Ermert H, Senge T - Initial experiences with real-time elastography guided biopsies of the prostate - J Urol 2005, 174, 115–117
10. Pallwein L, Aigner F, Pinggera G, Mitterberger M, Frauscher F, Bartsch G - Is real-time elastography targeted biopsy able to enhance prostate cancer detection? Value of an elasticity-scoring system, American Urological Association Annual Meeting, 2008, May 17–22, Orlando, USA.
11. Kamoi K, Okihara K, Ochiai A, Ukimura O, Mizutani Y, Kawauchi A, Miki T - The utility of transrectal real-time elastography in the diagnosis of prostate cancer - Ultrasound Med Biol 2008, 34, 7, 1025-1032.
12. Pallwein L, Aigner F, Faschingbauer R, Pallwein E, Pinggera G, Bartsch G, Schaefer G, Struve P, Frauscher F - Prostate cancer diagnosis: value of real-time elastography - Abdom Imaging 2008, 33, 729-735.
13. Xu G, Feng L, Yao M, Wu J, Guo L, Yao X, Zhao L, Xu H, Wu R - A new 5-grading score in the diagnosis of prostate cancer with real-time elastography - Int J Clin Exp Pathol 2014, 7, 7, 4128-4135
14. Ma Q, Yang DR, Xue BX, Wang C, Chen HB, Dong Y, Wang CS, Shan YX - Transrectal real-time tissue elastography targeted biopsy coupled with peak strain index improves the detection of clinically important prostate cancer - Oncology Letters 2017, 14, 210-216

15. Yoo JW, Koo KC, Chung BH, Lee KS - Role of the elastography strain ratio using transrectal ultrasonography in the diagnosis of prostate cancer and clinically significant prostate cancer - Scientific Reports 2022, 12, 21171
16. Zhai L, Polascik TJ, Foo WC, Rosenzweig S, Palmeri ML, Madden J, Nightingale KR - Acoustic Radiation Force Impulse Imaging of Human Prostates: Initial *in vivo* Demonstration - Ultrasound Med Biol 2012, 38, 1, 50–61
17. Sang L, Wang XL, Xu DY, Cai YF - Accuracy of shear wave elastography for the diagnosis of prostate cancer: A meta-analysis - Scientific Reports 2017, 7, 1949
18. Ji Y, Ruan L, Ren W, Dun G, Liu J, Zhang Y, Wan Q - Stiffness of prostate gland measured by transrectal real-time shear wave elastography for detection of prostate cancer: a feasibility study - Br J Radiol 2019, 92, 20180970.
19. Shoji S, Hashimoto A, Nakamura T, Hiraiwa S, Sato H, Sato Y, Tajiri T, Miyajima A - Novel application of three-dimensional shearwave elastography in the detection of clinically significant prostate cancer - Biomed Rep 2018, 8, 373-377
20. Pallwein L, Mitterberger M, Struve P, Pinggera G, Horninger W, Bartsch G, Aigner F, Lorenz A, Pedross F, Frauscher F - Real-time elastography for detecting prostate cancer: preliminary experience - BJU Int 2007, 100, 42-46
21. Salomon G, Köllerman J, Thederan I, Chun FKH, Budaus L, Schlomm T, Isbarn H, Heinzer H, Huland H, Graefen M - Evaluation of prostate cancer detection with ultrasound real-time elastography: a comparison with step section pathological analysis after radical prostatectomy - Eur Urol 2008, 54, 1354-1362
22. Miyagawa T, Tsutsumi M, Matsumura T, Kawazoe N, Ishikawa S, Shimokama T, Miyanaga N, Akaza H - Real-time elastography for the diagnosis of prostate cancer: evaluation of elastographic moving images - Jpn J Clin Oncol 2009, 39, 6, 394–398.
23. Ferrari FS, Scorzelli A, Megliola A, Drudi FM, Trovarelli S, Ponchietti R - Real-time elastography in the diagnosis of prostate tumor - J Ultrasound 2009, 12, 22-31
24. Pelzer A, Heinzelbecker J, Kirchner M, Schönberg S, Stroebel P, Dinter D et al. - Real-time elastography compared to 3.0T MRI findings in the localization and diagnosis of prostate cancer: preliminary results of a single centre study - J Urol 2010, 183 (Suppl), e832.
25. Sumura M, Mitsui Y, Arichi N, et al. - Real-time balloon inflation elastography of prostate might surpass MRI for detection of prostate cancer - J Urol 2010, 183(Suppl), e780.
26. Giurgiu CR, Dudea SM, Coman I - Elastography in the early detection of prostate cancer - J Radiother Med Oncol 2010, 16, 89-93.
27. Giurgiu CR, Manea C, Crişan N, Bungărdean C, Coman I, Dudea SM - Real-time sonoelastography in the diagnosis of prostate cancer - Med Ultrason 2011, 13, 1, 5-9
28. Rausch S, Alt W, Arps H, Alt B, Kälble T - The utility of transrectal sonoelastography in preoperative prostate cancer assessment - Med Ultrason 2012, 14, 3, 182-186
29. Zhang Y, Meng Z, Xu Y, Lu Q, Hou R, Cai X, Lin L, Luo Y, Wei F, Zheng Y, Hu B - Real-Time Elastography in the diagnosis of prostate cancer: a systematic review - Med Ultrason 2019, 21, 3, 327-335
30. Sang S, Wang XM, Xu DY, Cai YF - Accuracy of shear wave elastography for the diagnosis of prostate cancer: a meta-analysis - Scientific Reports 2017, 7, 1949
31. Ji Y, Ruan L, Ren W, Dun G, Liu J, Zhang Y, Wan Q - Stiffness of prostate gland measured by transrectal real-time shear wave elastography for detection of prostate cancer: a feasibility study - Br J Radiol 2019, 92, 20180970.

32. Yang Y, Zhao X, Shi J, Huang Y - Value of shear wave elastography for diagnosis of primary prostate cancer: a systematic review and meta-analysis - Med Ultrason 2019, 21, 4, 382-388
33. Anbarasan T, Wei C, Bamber JC, Barr RG, Nabi G - Characterisation of Prostate Lesions Using Transrectal ShearWave Elastography (SWE) Ultrasound Imaging: A Systematic Review - Cancers 2021, 13, 122
34. Cody Morris D, Chana DY, Palmeria ML, Polascik TJ, Foo WC, Nightingale KR - Prostate Cancer Detection Using 3D Shear Wave Elasticity Imaging - Ultrasound Med Biol 2021, 47, 7, 1670–1680
35. Secasan CC, Onchis D, Bardan R, Cumpanas A, Novacescu D, Botoca C, Dema A, Sporea I - Artificial Intelligence System for Predicting Prostate Cancer Lesions from ShearWave Elastography Measurements – Curr Oncol 2022, 29, 4212–4223
36. Jeon SS, Kim CK, Park SY, Chung JH, Kang M, Sung HH, et al. The utility of two-dimensional shear wave elastography for predicting prostate cancer: a preliminary study – Ultrasonography 2023, 42, 3, 400-409
37. Wei C, Li C, Szewczyk-Bieda M, Upreti D, Lang S, Huang Z, Nabi G - Performance Characteristics of Transrectal Shear Wave Elastography Imaging in the Evaluation of Clinically Localized Prostate Cancer: A Prospective Study - J Urol 2018, 200, 3, 549–558
38. Pelzer A, Heinzelbecker J, Kirchner M, Stroebel P, Michel SM - Limitations of real-time elastography in the detection of prostate cancer. Important facts for future studies - J Urol 2010, 183 (Suppl), e780
39. Tsutsumi M, Miyagawa T, Matsumura T, Endo T, Kandori S, Shimokama T, Ishikawa S - Real-time balloon inflation elastography for prostate cancer detection and initial evaluation of clinicopathologic analysis - AJR Am J Roentgenol 2010, 194, 6, W471-W476.
40. Pallwein L, Mitterberger M, Pelzer A, Bartsch G, Strasser H, Pinggera GM, Aigner F, Gradl J, zur Nedden D, Frauscher F - Ultrasound of prostate cancer: recent advances - Eur Radiol 2008, 18, 707- 715
41. Junker D, De Zordo T, Quentin M, Ladurner M, Bektic J, Horniger W, Jaschke W, Aigner F - Real-Time Elastography of the Prostate - BioMed Res Int 2014, ArtID 180804, 11 p
42. Seliger G, Chaoui K, Kunze C, Dridi Y, Jenderka KV, Wienke A, Tchirikov M - Intra- and inter-observer variation and accuracy using different shear wave elastography methods to assess circumscribed objects – a phantom study - Med Ultrason 2017, 19, 4, 357-365
43. Lee J, Yoon SK, Cho JH, Kwon HJ, Kim DW, Lee JW - Variability of Transrectal Shear Wave Elastography in a Phantom Model - J Korean Soc Radiol 2023, 84, 5, 1110-1122
44. Tsutsumi M, Miyagawa T, Matsumura T, Kawazoe N, Ishikawa S, Shimokama T, Shiina T, Miyanaga N, Akaza H - The impact of real-time tissue elasticity imaging (elastography) on the detection of prostate cancer: clinicopathological analysis - Int J Clin Oncol 2007, 12, 250–255.
45. Sumura M, Shigeno K, Hyuga T, Yoneda T, Shiina H, Igawa M - Initial evaluation of prostate cancer with real-time elastography based on step-section pathologic analysis after radical prostatectomy: a preliminary study - Int J Urol 2007, 14, 811–816.
46. Junker D, Schafer D, Aigner F, Schullian P, Pallwein-Prettner L, Bektic J, Horninger W, Halpern EJ, Frauscher F - Potentials and Limitations of Real-Time Elastography for Prostate Cancer Detection: A Whole-Mount Step Section Analysis – Sci World J, 2012, Art ID 193213, 6

47. Miyanaga N, Akaza H, Yamakawa M, Oikawa T, Sekido N, Hinotsu S, Kawai K, Shimazui T, Shiina T - Tissue elasticity imaging for diagnosis of prostate cancer: a preliminary report. Int J Urol 2006, 13, 12, 1514-1518
48. Pallwein L, Mitterberger M, Struve P, Horninger W, Aigner F, Bartsch G, Gradl J, Schurich M, Pedross F, Frauscher F - Comparison of sonoelastography guided biopsy with systematic biopsy: impact on prostate cancer detection - Eur Radiol. 2007, 17, 9, 2278-2285
49. Aigner F, Pallwein L, Junker D, Schäfer G, Mikuz G, Pedross F, Mitterberger MJ, Jaschke W, Halpern EJ, Frauscher F - Value of real-time elastography targeted biopsy for prostate cancer detection in men with prostate specific antigen 1.25 ng/ml or greater and 4.00 ng/ml or less - J Urol 2010, 184, 3, 913-917
50. Nelson ED, Slotoroff CB, Gomella LG, Halpern EJ - Targeted biopsy of the prostate: the impact of color Doppler imaging and elastography on prostate cancer detection and Gleason score - Urology 2007, 70, 1136-1140
51. Nygård Y, Haukaas SA, Halvorsen OJ, Gravdal K, Frugård J, Akslen LA, Beisland C - A positive real-time elastography is an independent marker for detection of high-risk prostate cancers in the primary biopsy setting - BJU Int 2014, 113, 5b, E90-97
52. Tu X, Qiu S, Chang T, Jin K, Bao Y, Yang L, Wei Q - The role of real-time elastography-targeted biopsy in the detection and diagnosis of prostate cancer: a systematic review and meta-analysis - Medicine 2018, 97, 12, e0220
53. Zhu YC, Shan J, Zhang Y, Jiang Q, Wang YB, Deng SH, Qu QH, Li Q - Strain Elastography-Targeted Biopsy: Does Prostate Volume Affect Prostate Cancer Detection? - Med Sci Monit, 2019, 25, 8836-8842
54. Sharen GW, Zhang J - Application of Shear Wave Elastography and Contrast-Enhanced Ultrasound in Transrectal Prostate Biopsy - Curr Med Sci 2022, 42, 2, 447-452
55. Gandhi J, Zaidi S, Shah J, Joshi G, Khan SA - The Evolving Role of Shear Wave Elastography in the Diagnosis and Treatment of Prostate Cancer - Ultrasound Q 2018, 34, 4, 245-249.
56. Boehm K, Budäus L, Tennstedt P, Beyer B, Schiffmann J, Larcher A, Simonis K, Graefen M, Beyersdorff D, Salomon G - Prediction of Significant Prostate Cancer at Prostate Biopsy and Per Core Detection Rate of Targeted and Systematic Biopsies Using Real-Time Shear Wave Elastography - Urol Int 2015, 95, 2, 189-196
57. Săftoiu A, Gilja OH, Sidhu PS, Dietrich CF, Cantisani V, Amy D, Bachmann-Nielsen M, Bob F, Bojunga J, Brock M, Calliada F, Clevert DA, Correas JM, D'Onofrio M, Ewertsen C, Farrokh A, Fodor D, Fusaroli P, Havre RF, Hocke M, Ignee A, Jenssen C, Klauser AS, Kollmann C, Radzina M, Ramnarine KV, Sconfienza LM, Solomon C, Sporea I, Ștefănescu H, Tanter M, Vilmann P - The EFSUMB Guidelines and Recommendations for the Clinical Practice of Elastography in Non-Hepatic Applications: Update 2018 - Ultraschall Med 2019, 40, 4, 425-453
58. Pallwein L, Aigner F, Horninger W, Schocke M, Frauscher F - Prostate cancer detection: biopsy findings based on tissue alterations in real-time elastography and T2 weighted endorectal magnetic resonance imaging - Focal Therapy and Imaging in Prostate and Kidney Cancer, 2009, June 10 – 13th, Amsterdam, The Netherlands

59. Tian H, Ding Z, Wu H, Yang K, Song D, Xu J, Dong F - Assessment of elastographic Q-analysis score combined with Prostate Imaging-Reporting and Data System (PI-RADS) based on transrectal ultrasound (TRUS)/multi-parameter magnetic resonance imaging (MP-MRI) fusion-guided biopsy in differentiating benign and malignant prostate - Quant Imaging Med Surg 2022, 12, 7, 3569-3579
60. Ageeli W, Wei C, Zhang X, Szewcyk‐Bieda M, Wilson J, Li C, Nabi G - Quantitative ultrasound shear wave elastography (USWE)‐measured tissue stiffness correlates with PIRADS scoring of MRI and Gleason score on whole‐mount histopathology of prostate cancer: implications for ultrasound image‐guided targeting approach - Insights Imaging 2021, 12, 96
61. Gurwin A, Kowalczyk K, Knecht-Gurwin K, Stelmach P, Nowak Ł, Krajewski W, Szydełko T, Małkiewicz B - Alternatives for MRI in Prostate Cancer Diagnostics - Review of Current Ultrasound-Based Techniques - Cancers (Basel) 2022, 14, 8, 1859
62. Barr, R.G.; Cosgrove, D.; Brock, M.; Cantisani, V.; Correas, J.M.; Postema, A.W.; Salomon, G.; Tsutsumi, M.; Xu, H.X.; Dietrich, C.F. - WFUMB Guidelines and Recommendations on the Clinical Use of Ultrasound Elastography: Part 5. Prostate. Ultrasound Med. Biol. 2016, 43, 27–48.
63. Fu S, Tang Y, Tan S, Zhao Y, Cui L - Diagnostic Value of Transrectal Shear Wave Elastography for Prostate Cancer Detection in Peripheral Zone: Comparison with Magnetic Resonance Imaging - J Endourol 2020, 34, 5, 558-566
64. 692. Xiang LH, Fang Y, Wan J, Xu G, Yao MH, Ding SS, Liu H, Wu R - Shear-wave elastography: role in clinically significant prostate cancer with false-negative magnetic resonance imaging - Eur Radiol 2019 29, 12, 6682-6689
65. Shiva M, Wei C, Molana H, Nabi G - Cost-Effectiveness of Prostate Cancer Detection in Biopsy-Naïve Men: Ultrasound Shear Wave Elastography vs. Multiparametric Diagnostic Magnetic Resonance Imaging - Healthcare 2022, 10, 254
66. Tang J, Zhang Y, Zhang MB, Li YM, Fei X, Song ZG - Tissue elasticity displayed by elastography and its correlation with the characteristics of collagen type I and type III in prostatic stroma - Asian J Androl 2014, 16, 305–308
67. Ageeli W, Zhang X, Ogbonnaya CN, Ling Y, Wilson J, Li C, Nabi G - Characterisation of Collagen Re-Modelling in Localised Prostate Cancer Using Second-Generation Harmonic Imaging and Transrectal Ultrasound ShearWave Elastography – 3. Cancers 2021, 13, 5553.
68. Ageeli W, Zhang X, Ogbonnaya CN, Bray SE, Kernohan NM, Wilson J, Li C, 4. d Nabi G – Multimodality Characterization of Cancer-Associated Fibroblasts in Tumor Microenvironment and Its Correlation With Ultrasound Shear Wave-Measured Tissue Stiffness in Localized Prostate Cancer - Front Oncol 2022, 12, 822476.
69. Sun YK, Yu Y, Xu G, Wu J, Liu YY, Wang S, Dong L, Xiang LX, Xu HX - Added value of shear-wave elastography in the prediction of extracapsular extension and seminal vesicle invasion before radical prostatectomy - Asian J Androl 2023, 25, 259–264
70. Wei C, Zhang Y, Malik H, Zhang X, Alqahtani S, Upreti D, Szewczyk-Bieda M, Lang S, Nabi G - Prediction of Postprostatectomy Biochemical Recurrence Using Quantitative Ultrasound Shear Wave Elastography Imaging - Front Oncol 2019, 9, 572.
71. Nicolaescu Fleming I, Kut C, Macura KJ, Su LM, Rivaz H, Schneider C, Hamper U, Lotan T, Taylor R, Hager G, Boctor E - Ultrasound elastography as a tool for imaging guidance during prostatectomy: initial experience - Med Sci Monit, 2012, 18, 11, CR635-642

72. Souchon R, Rouvière O, Gelet A, Detti V, Srinivasan S, Ophir J, Chapelon JY - Visualisation of HIFU lesions using elastography of the human prostate in vivo: preliminary results - Ultrasound Med Biol 2003, 29, 7, 1007-1015
73. Alan B, Utangaç M, Göya C, Dağgülli M - Role of Acoustic Radiation Force Impulse (ARFI) Elastography in Determination of Severity of Benign Prostate Hyperplasia - Med Sci Monit 2016, 22, 4523-4528

Chapter 14. Testicular Elastography

Sorin M. Dudea, Vasile Simon

The evaluation of the testicular parenchyma is one of the clinically relevant applications of elastography and is recognized as such in international guidelines [1]. Some recently published papers provide a synthetic overview of the main current applications of elastosonography in testicular pathology [2,3].

14.1. Testicular Elastographic Examination Techniques

All known elastographic techniques can be used to evaluate the testes and scrotal contents.

a) Strain elastography (SE) uses the relative colorimetric scale on the image, colors representing stiffer or more elastic structures depending on the equipment manufacturer. External mechanical force (vibration of the transducer), internal force (vascular pulsations), or acoustic force (impulse wave emitted by the transducer) can be used to induce tissue dislocation. Stiffness is quantified in a semi-quantitative way, using one of two already classic methods:

- ***The colorimetric score*** usually fits into a variant of the Tsukuba scale, described initially for breast pathology or

- ***The strain ratio (SR)***, where the relative dislocation of two neighboring structures is compared on the same image.

b) **Shear wave elastography (SWE)** is the method in which, following the exposure of tissues to a focused pulse of ultrasound (US), transverse shear waves (SW) appear. The device detects these waves and measures their propagation speed. Based on the measured speed, tissue stiffness can be calculated and expressed in specific units of measure – kilopascal (kPa). All existing techniques use the standard two-dimensional US image for orientation, however, there are several measurement variants:

- ***Point shear wave elastography (pSWE)***, also named ARFI (Acoustic Radiation Force Impulse) by one manufacturer, measures the SW velocity and, respectively, the stiffness in a single image sample, and only provides numerical information.

- ***Two-dimensional shear wave elastography*** yields instantaneous information about SW in multiple samples of an examination plane.

• One manufacturer's ***VTIQ (virtual touch tissue imaging and quantification)*** technique provides a single two-dimensional image where stiffness is represented in color and where multiple SW velocity measurements can be performed at any examiner-chosen point;

• The ***2DSWE technique (two-dimensional shear wave elastography)*** produces a sequence of up to 6 images / second, with the color representation of tissue stiffness and the possibility of measuring the hardness in kPa or the SW speed at any point of the image;

• The ***3DSWE technique (three-dimensional shear wave elastography)*** associates the 2DSWE technique with 3D volumetric acquisition with a dedicated transducer. It results in a volume where tissue consistency is represented in color, and average hardness values of a volume can be measured;

• ***Viscoelastography*** is based on shear wave dispersion, produces viscosity information in color and allows for the measurement of tissue viscosity in specific units: Pa.s

14.2. Appearance and Normal Values of the Measurements that Define the Testicles Consistency

SE

On strain elastography, the parenchyma of normal testes is homogeneous and appears in intermediate shades of hardness, usually green. The apparent hardness can be higher at the periphery and the poles due to the tunica albuginea's proximity (figure 14.1.a). The triple ring appearance can be identified [4]: the center has colors corresponding to an intermediate stiffness, while the periphery, under the albuginea, appears stiffer, and the peritesticular tissues of the scrotum appear very elastic (figure 14.1.b). The testicles have identical consistency, left-right; the SR has a unit value.

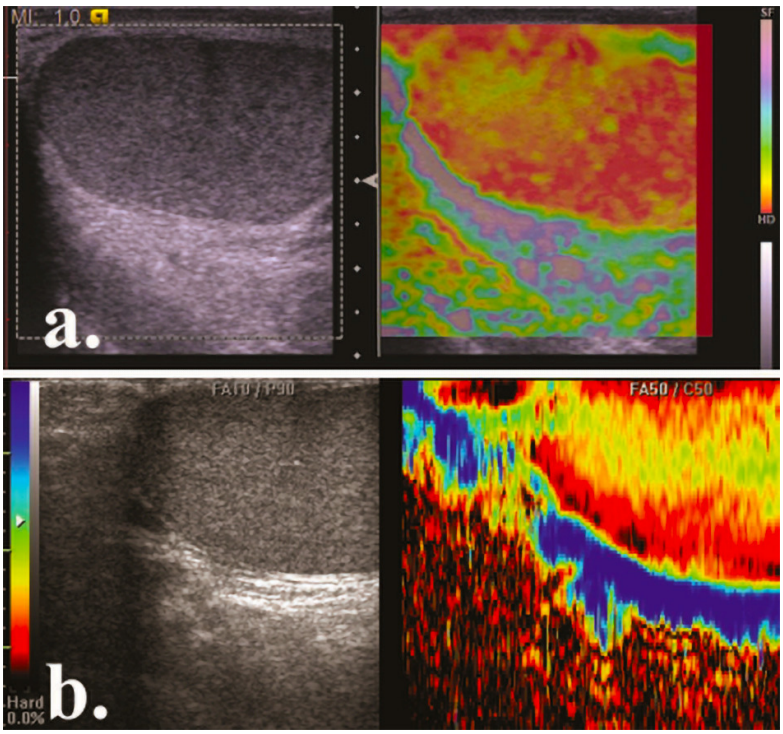

Figure 14.1. Normal testis: a) acoustic force displacement elastography. Homogeneous testicular parenchyma appears harder (red) than neighboring structures; b) strain elastography with external mechanical force. The center of the testicle shows intermediate hardness (yellow-green), the periphery appears hard (red), and the peritesticular tissues appear soft (blue) – triple ring appearance.

pSWE

The measurement is made in the center of the testicle (figure 14.2). The published studies have determined, for the normal testicle, average values of the SW speed between 0.62 and 1.01 m/s [5]. Most studies indicate that the normal SW velocity value is between 0.76 and 0.81 m/s [6-8]. A significant association was found between speed, subject age and testicular volume [5]. The speeds measured in normal subjects are statistically significantly lower than in patients with pathological changes such as microlithiasis or tumors [6].

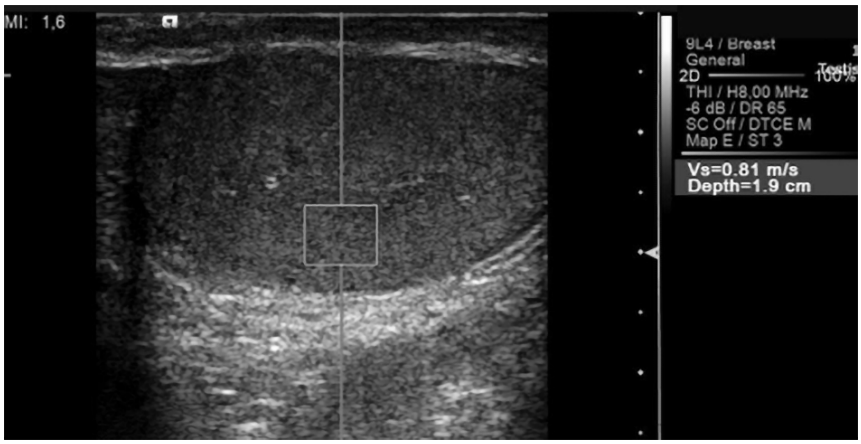

Figure 14.2. ARFI examination (pSWE) of the normal testis.

VTIQ

Measured by this method, the average velocity of the SW in the normal testis is between 1.07 and 1.17 m/s [8,9].

If VTIQ is used, significantly higher SW velocity values are obtained compared to ARFI for the same testis. Although the same machine is used, differences are of 0.22 – 0.29 m/sec higher for VTIQ [8].

2D SWE

a) The ***average velocity*** of the SW measured in several segments of the normal testis has values between 1.05 – 1.1 m/s, without differences between the segments [7,10].

The results obtained with two devices and two methods from different manufacturers agree almost perfectly. Moreover, the mean velocity measured by 2DSWE is higher than the mean velocity determined by ARFI in the same subjects [7].

In another study, mean SW velocity values were similar for the superior and inferior testicular poles (1.15 m/s) and lower for the center of the testis (0.9 m/s). The measured values are independent of age. Simultaneously with the increase in volume, significantly less stiffness is observed in the upper pole compared to the rest of the testicle [11].

b) ***Rigidity***. The central region of the testis, measured in sections on the longitudinal axis, has the lowest stiffness values (3.14 ± 0.35 kPa), followed by the upper and lower poles (3.94 ± 0.97 kPa) [12]. The measurement at the poles included the testicular capsules, thus explaining the increased stiffness. Central stiffness is significantly higher if measured in sections on the transverse axis of the testis (3.47 ± 0.32 kPa) [12] (figure 14.3)

Including fibrous peritesticular tissue in the measurement sample is irrelevant to the state of the testicular parenchyma, however, it expectedly leads to an increase in the measured stiffness.

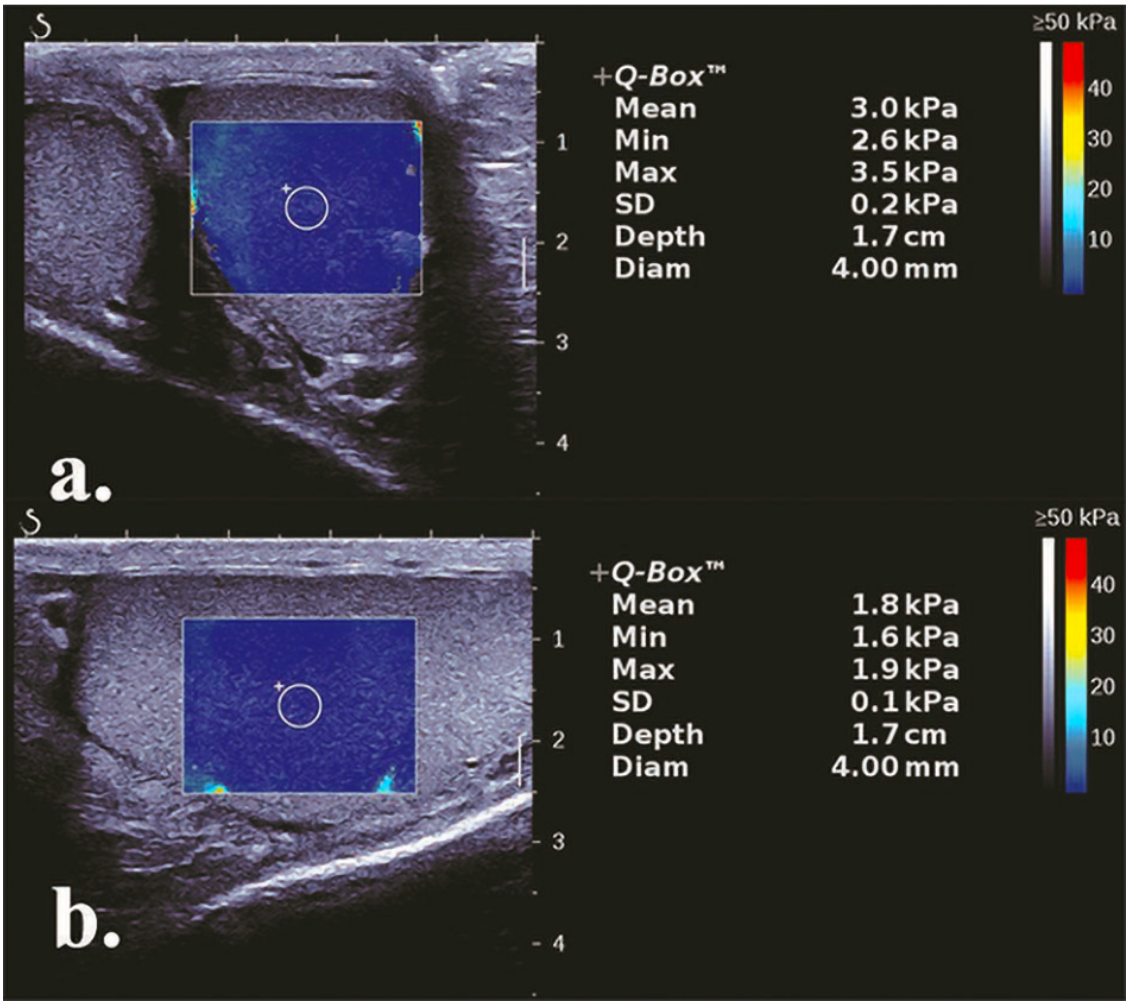

Figure 14.3. 2DSWE examination of the normal testis: a) cross section; b) longitudinal section through the same testis. The mean stiffness value is higher on the cross-section.

3D SWE

At 3DSWE, the average velocity in the normal adult testis is 1.12 m/sec, with no differences between regions [10].

Testicular stiffness values were negatively correlated with age and weight in a pediatric population of boys aged 1 to 92 months [13].

Viscoelastography

There are no published values for normal testicular viscosity.

Table 14. I summarizes the values that characterize the normal testicle.

Table 14. I. Normal values of testicular stiffness parameters

Year	Author	No. subjects	Method	Normal values	Unit	Remarks
2011	[5]	23	ARFI	0.62-1.02	m/s	
2016	[7]	58	ARFI	0.8	m/s	
2016	[8]	20	ARFI	0.81	m/s	
2017	[6]	300	ARFI	0.76	m/s	
2014	[9]	20	VTIQ	1.17	m/s	
2016	[8]	20	VTIQ	1.07	m/s	
2016	[10]	32	2DSWE	1.05	m/s	
2016	[7]	58	2DSWE	1.1	m/s	
2016	[11]	66	2DSWE	1.15	m/s	In testicular poles
2016	[11]	66	2DSWE	0.9	m/s	In the center of the testis
2021	[12]	110	2DSWE	3.14 ± 0.35	kPa	Longitudinal, in the center of the testis
2021	[12]	110	2DSWE	3.47 ± 0.32	kPa	Transverse, in the center of the testis
2021	[12]	110	2DSWE	3.94 ± 0.97	kPa	longitudinal, in the poles
2016	[10]	32	3DSWE	1.12	m/s	

Conclusions

There are few studies describing normal testicular stiffness.

The SW velocity value measured by the ARFI method in the normal adult testis is between 0.6 and 0.8 m/s. The SW velocity in the normal adult testis, measured by VTIQ, is 1.07 – 1.17 m/s. When examining with 2DSWE or 3DSWE, the SW velocity is 1-1.15 m/s.

To measure testicular stiffness reproducibly, it is necessary to consistently use the same method and the same scanning plane (longitudinal or transverse) in all patients. The stiffness of the testicle measured in its center has typical values between 3.1 and 3.5 kPa.

It is not advisable to assess testicular consistency by measuring velocity or stiffness at the poles or periphery of the organ, as higher and inconstant values may be obtained. Testicular stiffness in the pediatric population decreases with increasing age and weight. There are no studies on the age dependence of testicular stiffness in the adult population.

Methodological variations and those associated with the differences between machines and transducers must be considered in the elastographic evaluation of the testicles [14].

14.3. Elastography in Testicular Pathology

The published use of testicular elastography is summarized in Figure 14.4.

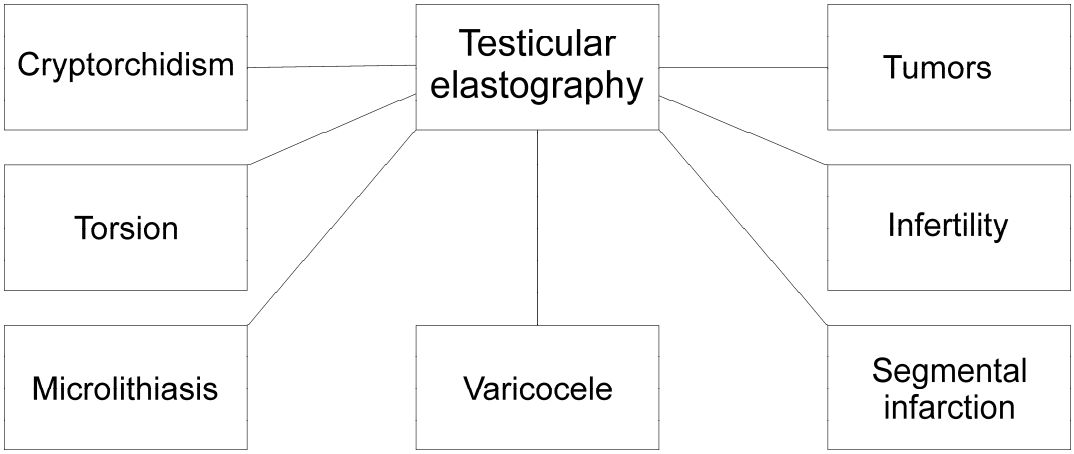

Figure 14.4. Known uses of testicular elastography (inspired from [14]).

14.3.1. Cryptorchidism

SE

SE may be used as a complement for gray-scale ultrasonography to confirm the presence of undescended testes located in the abdominal cavity or inguinal canal, to establish the persistence of areas of increased stiffness after orchidopexy, in post-traumatic regressive changes or ischemic foci after testicular torsion [14]. Using SR between the subcutaneous tissue and the undescended testicle, no signs of testicular fibrosis were observed in children under five years of age [16].

pSWE

pSWE was used to determine the SW velocity in the testes of pediatric patients after orchidopexy, with the operated testes significantly stiffer than the unaffected ones (table 14. II) [17].

2D SWE

A study of 29 patients with a mean age of 7.5 years observed a significant difference in stiffness values between undescended and contralateral descended testes, with the former being stiffer (Table 14. II) but with no difference in volume [18].

In a retrospective study in a pediatric population under 60 months of age, stiffness values expressed in kPa in the cryptorchidism group had a positive correlation with patient age and a negative correlation with testicular volume. The opposite was described in the group of

normal testes [19]. Another study found high stiffness and velocity values not only in cases of undescended testes but also for retractile testes compared to normal ones (table 14. II) [20].

Table 14. II. Values of testicular stiffness parameters in studies of pediatric patients with cryptorchidism.

Year	Author	No.	Metoda	Values	Meas. unit	Remarks
2016	[17]	47	pSWE	0.75 – 2.8 (median 1.1)	m/s	Operated testes, orchidopexy
2016	[17]	27	pSWE	0.62 – 1,2 (median 0.84)	m/s	Testes contralateral to the operated ones
2016	[17]	60	pSWE	0,65 – 1 (median 0.82)	m/s	Testes control group
2017	[18]	29	2DSWE	9.6 ± 3.15	kPa	Patients, undescended testes
2017	[18]	29	2DSWE	4.76 ± 1.5	kPa	Patients, descended testes
2019	[20]	37	2DSWE	13.80 ± 4.14 2.14 ± 0.29	kPa m/s	Undescended testes
2019	[20]	15	2DSWE	9.64 ± 3.71 1.75 ± 0.35	kPa m/s	Retractile testes
2019	[20]	56	2DSWE	7.44 ± 2.11 1.57 ± 0.21	kPa m/s	Normal testes

Conclusions

Current studies do not use RTE to evaluate cryptorchidism except as a complementary tool to two-dimensional ultrasonography.

Both pSWE and 2DSWE may be used to assess the elasticity of cryptorchid testes before and after surgery. 2DSWE has demonstrated the ability to differentiate between an orthotopic and a retractile testis independent of the examination time. Undescended, retractile and orchidopexy testicles are harder than orthotopic ones.

14.3.2. Torsion of the spermatic cord

SE and pSWE

To the best of our knowledge, there are no published papers on the use of pSWE and SE to assess spermatic cord torsion.

2D SWE

In a study with a limited number of patients, a clear statistically significant difference was found between the SWE values in testicular torsion and normal testicles, with the twisted testicles being harder, especially at the periphery [21] (Table 14. III).

Correctly differentiating between testicular torsion and acute orchitis has always been a clinical challenge in urological practice. Another study with limited patients reported higher SWE values for the testicular capsule and the twisted spermatic segment in the torsion group compared to the orchitis group. On the two-dimensional SWE image, the signs of the "hard ring", representing the periphery of the testicle affected by torsion, and that of the "hard knot", representing the area of torsion at the level of the funicle, were described. No statistically significant differences were observed between torsion and orchitis for the stiffness of the middle parenchyma of the testis [22] (table 14. III).

Table 14. III. Values of testicular stiffness parameters in studies for testicular torsion

Year	Author	No.	Method	Values	Meas. unit	Remarks*
2015	[21]	15	2DSWE	78.07 ± 9.01	kPa	Emed torsion
2015	[21]	15	2DSWE	22.0 ± 5.10	kPa	Emed normal
2015	[21]	15	2DSWE	94.07 ± 6.53	kPa	Emax torsion
2015	[21]	15	2DSWE	27.87 ± 5.78	kPa	Emax normal
2015	[21]	15	2DSWE	60.73 ± 7.84	kPa	Emin torsion
2015	[21]	15	2DSWE	18.90 ± 4.39	kPa	Emin normal
2020	[22]	14	2DSWE	138.76 ± 58.27	kPa	Emax torsion testicular capsule
2020	[22]	16	2DSWE	16.40 ± 4.71	kPa	Emax orchitis testicular capsule
2020	[22]	14	2DSWE	166.61 ± 60.07	kPa	Emax torsion spermatic cord
2020	[22]	16	2DSWE	14.14 ± 4.93	kPa	Emax orchitis spermatic cord

* Emed, Emax and Emin represent the mean, maximum and minimum stiffness values in the SWE sample

An inhomogeneous, Doppler avascular, stiff nodular mass on SE indicates torsion of the testicular appendix [23].

Conclusion

2DSWE elastography may be used to differentiate between testicular torsion, acute orchitis and normal testis.

Accessibility and time spent getting to an ultrasound machine and an examiner capable of adequately performing testicular elastography should be considered in testicular torsion, as delays in surgical exploration and detorsion of the spermatic cord may lead to testicular necrosis, atrophy or loss of the function [14].

14.3.3. Testicular microlithiasis

pSWE

Very few papers address the use of sonoelastography in evaluating testicular microlithiasis (MLT). A preliminary study on 12 patients found no difference between pSWE values in normal and microlithiasis testes [24]. In a subsequent study with more patients, the same researcher found a slight but statistically significant difference in SW velocity in men with MLT compared to normal testes, with higher velocities in the MLT group [25].

Another study described higher mean SW velocities when examining pSWE in the pediatric population in a small group of patients with MLT compared to a healthy control group of the same size and mean age [26].

When assembling this chapter, we found no published studies regarding the role of 2DSWE or RTE in evaluating testicular microlithiasis.

Conclusion

MLT-carrying testes are stiffer than normal, especially in the pediatric population. Due to the small number of published studies and the small number of examined patients, further exploration of the utility of pSWE in the assessment of MLT is needed.

14.3.4. Varicocele

SE

Strain elastography can be used to evaluate the varicocele-bearing testicle.

When comparing the varicocele-bearing testicle with the contralateral testicle, strain ratios with values above unity were obtained, indicating that testicular stiffness increases in patients affected by varicocele [27-29]. Significant inverse correlations were observed between strain elastography (SR and elasticity scores) and spermogram parameters such as total motile sperm count, sperm concentration and normal sperm morphology. Some groups have identified correlations between varicocele grade, SR and elasticity scores [28,29].

pSWE

A study using pSWE (ARFI) in infertile patients with varicocele revealed significantly different SW velocities between normal and varicocele carriers, with lower velocity in the varicocele group (Table 14. IV). A negative correlation was observed between FSH values and testicular elasticity. A negative correlation between the degree of varicocele and elasticity has also been described. The main limitation of this study was the enrollment of patients with only mild oligospermia and no patients with oligoasthenospermia or azoospermia [30].

2D SWE

A study on a small group of adolescents found a progressive increase in testicular hardness with the degree of varicocele without reaching significant differences (table 14. IV). The difference in SWE values between grade III varicocele and the contralateral testis was significant only if the difference in testicular volume was >20% [31].

Another study, in a large group of adults, observed that varicocele-bearing testicles were softer than normal testicles without statistical significance [32]. Two recent papers found no differences in mean SWE values between testes with varicocele, contralateral ones, or those of healthy subjects [33,34]. Even if, at rest, there are no differences between the mean stiffness values between the groups with different degrees of varicocele, during the Valsalva maneuver, testicular stiffness increases significantly for varicocele of degree II and III (table 14. IV) [35]. It should be noted that the groups of patients in this study were very small.

Monitoring patients with varicocele before and after surgery allowed for establishing the cut-off value of 4.5 kPa to predict postoperative improvement of spermogram parameters. SWE showed a significant negative correlation between SWE stiffness index and sperm count (millions/ml) and total motility but no statistically significant correlation between SWE stiffness values and the percentage of normal-shaped spermatozoa [36].

SWE was used to evaluate patients with left varicocele and compare mean stiffness values in subjects with normal spermogram parameters and those with oligospermia. Varicocele patients with oligospermia had values of SWE stiffness higher than normozoospermic patients. All patients with varicocele showed higher SWE values than the healthy control group, but no differences existed between the testes contralateral to the varicocele and those of healthy subjects [37]. Another study confirmed the observation of higher stiffness values and SW velocities in the varicocele-bearing testis compared to the contralateral testis and control groups. This study found no correlation between testicular volume and SWE values [38].

Table 14. IV. Values of testicular stiffness parameters in studies for varicocele

Year	Author	No.	Method	Values	Meas. unit	Remarks
2016	[30]	30	pSWE	0.82 ± 0.08	m/s	Patients with varicocele
2016	[30]	30	pSWE	0.87 ± 0.09	m/s	Normal subjects
2019	[31]	30	2DSWE	2.5 ± 0.49	kPa	Varicocele grade I
2019	[31]	30	2DSWE	2.59 ± 0.81	kPa	Varicocele grade II
2019	[31]	30	2DSWE	2.80 ± 0.72	kPa	Varicocele grade III
2019	[31]	30	2DSWE	2.39 – 2.42	kPa	Contralateral testes
2017	[32]	132	2DSWE	2.2 (1,8–2.6)	kPa	Testes with varicocele
2017	[32]	108	2DSWE	2.4 (2–2.9)	kPa	Normal testes
2022	[35]	27	2DSWE	2.7 ± 0.6 2.7 ± 0.6	kPa	Normal at rest Normal + Valsalva

2022	[35]	6	2DSWE	2.8 ± 0.5 2.8 ± 0.5	kPa	Varicocele gr. I at rest Varicocele gr. I +Valsalva
2022	[35]	8	2DSWE	2.5 ± 0.3 2.9 ± 0.9	kPa	Varicocele gr. II at rest Varicocel gr. II + Valsalva
2022	[35]	13	2DSWE	3.0 ± 1.0 3.8 ± 1.4	kPa	Varicocele gr. III at rest Varicocel gr. III + Valsalva
2020	[37]	29	2DSWE	4.77 ± 1.16 3.52 ± 0.41	kPa	Normospermic left testis with varicocele Contralateral testis
2020	[37]	29	2DSWE	6.15 ± 1.96 3.81 ± 0.71	kPa	Oligospermic left testis with varicocele Contralateral testis
2020	[37]	58	2DSWE	3.79 ± 0.94	kPa	Normal subjects

Conclusions

Studies with a broader variety of spermogram parameters are needed to confirm the utility of pSWE in evaluating varicocele.

The varicocele-bearing testicle is stiffer than the unaffected or normal contralateral testicle. There are negative correlations between testicular stiffness and sperm parameters. The Valsalva maneuver electively increases the stiffness of high-grade varicocele-bearing testes.

2DSWE appears to perform better when there is a significant difference in testicular volume and the high-grade varicocele is examined. Stiffness values at 2DSWE correlate negatively with sperm count. In certain situations, the method seems promising as an alternative to the spermogram. 2DSWE has the potential to predict postoperative improvement in spermogram parameters after the surgical cure of varicocele.

14.3.5. Segmental testicular infarction (STI)

Due to the rarity of this pathology, there are only two case reports on elastography of segmental testicular infarction and a small series reporting six patients [39–41].

SE (SR) and 2DSWE

Both SE, including SR, and 2DSWE revealed, in the acute phase, lower hardness of the infarcted area compared to the adjacent normal testis. In evolution, the hardness of the infarcted area increases, equaling the testicle, so that, after two weeks, it becomes stiffer than the rest of the parenchyma, associated with the fibrous transformation.

We found no studies using pSWE in segmental testicular infarction.

Figure 14.5. shows different stiffness values in the same testis with STI.

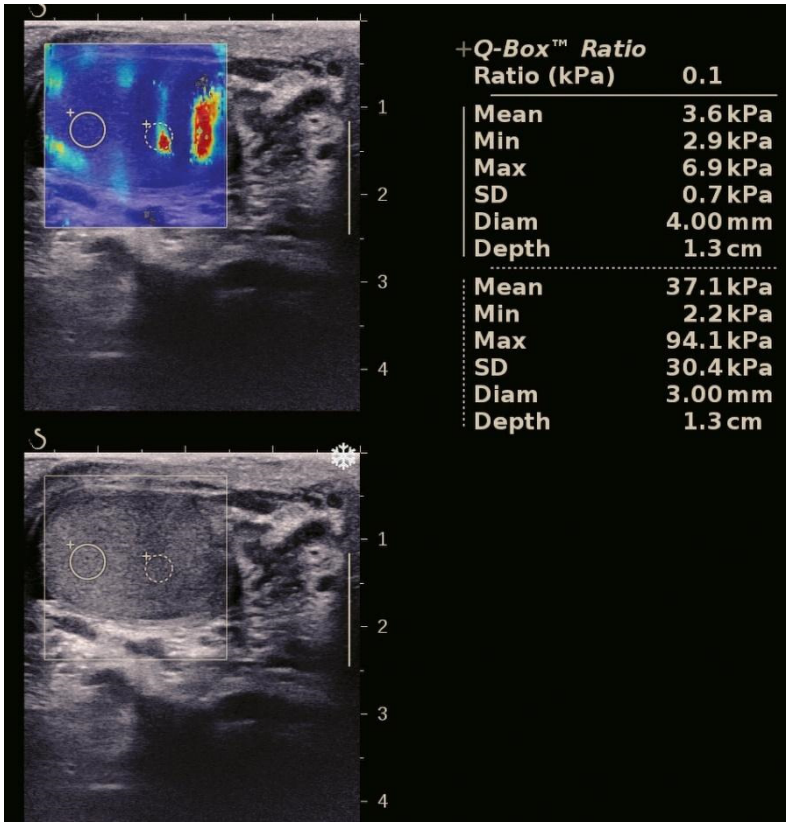

Figure 14.5. ITS, 2DSWE examination. The gray-scale image (bottom) shows the hypotrophic, inhomogeneous testis with slightly reduced echogenicity in the lower half. 2DSWE (top) reveals increased inhomogeneity and stiffness in the infarcted area compared with the normal upper pole. Contrast-enhanced Doppler and MRI examinations confirmed chronic STI.

Conclusion

Due to the rapidly evolving nature of this pathological entity, serial examinations are necessary to document the changes properly. The rarity of such cases makes extensive studies difficult to conduct.

14.3.6. Infertility

SE

When using strain elastography to assess infertility in patients and applying the SR between the testicular parenchyma and the hypodermic tissue of the scrotal wall, statistically significant differences were found between men with normal sperm analysis and those with abnormal analysis, the latter having a higher SR. Although FSH levels were statistically different in the two studied groups, there was no correlation between FSH and SR values [29].

When applying elastographic scores and SR to a large group of patients, it was found that patients with nonobstructive azoospermia have lower testicular consistency compared to those with obstructive azoospermia and compared to normal subjects [42].

VTIQ

Using the VTIQ technique to measure the SW velocity, cut-off values were obtained that allow for the separation between normal and azoospermia (1.465 m/s) or

oligozoospermia (1.328 m/s) as well as the differentiation of oligozoospermia from azoospermia (1.528 m/s). Unfortunately, the specificity and sensitivity of these values, located between 60 and 75%, do not allow the use of the method for diagnostic purposes. Significant negative correlations were described between patients' average testicular SW velocities and sperm count [43].

2DSWE

2DSWE has been used to analyze the correlation of various parameters in infertile men. The absolute values of testicular stiffness, as measured by 2DSWE, varied according to the cause of infertility, the total sperm count and the machine used to perform the examination.

An initial study reported no clear differences in SWE values between patients with varicocele, oligoasthenoteratozoospermia (OAT), obstructive azoospermia, non-Klinefelter nonobstructive azoospermia, or Klinefelter nonobstructive azoospermia due to a substantial overlap of value ranges [32]. In men with OAT, a higher mean stiffness value was observed in both testes compared to men with normal sperm parameters (table 14. V). The same study showed negative correlations between testicular stiffness and total sperm count, concentration and progressive motility [44].

In patients with azoospermia, the cut-off value of 1.55 kPa could discriminate between the groups with normal spermatogenesis and hypospermatogenesis versus those with the arrest of spermatogenesis and Sertoli-only cells syndrome [45].

The mean values of SW velocity and testicular stiffness, measured by 2DSWE, are significantly higher in infertile men compared to the control group (Table 14. V). Positive correlations were found between testicular volume and SWE values in the infertile men group [46].

Table 14.V. Values of testicular stiffness parameters in infertility studies

Year	Author	No.	Method	Values	Meas. unit	Remarks
2021	[44]	50	2DSWE	21.4 ± 5.4	kPa	OAT patients, left testicle
2021	[44]	50	2DSWE	9.9 ± 1.6	kPa	Subjects, left testicle
2021	[44]	50	2DSWE	22.9 ± 4.8	kPa	OAT patients, right testicle
2021	[44]	50	2DSWE	9.5 ± 1.6	kPa	Subjects, right testicle
2020	[46]	50	2DSWE	12.82 ± 5.19 1.85 ± 0.31	kPa m/s	Infertile patients
2020	[46]	50	2DSWE	8.01 ± 3.02 1.53 ± 0.25	kPa m/s	Normal subjects
2021	[47]	8	2DSWE	3.65 ± 1.24	kPa	Positive TESE retrieval
2021	[47]	42	2DSWE	9.59 ± 6.68	kPa	Negative TESE retrieval

In a group of 50 patients with nonobstructive azoospermia, significant differences in stiffness values measured by 2DSWE were observed between patients with successful sperm retrieval and those with negative retrieval using testicular sperm extraction (TESE) (Table 14. V). The cut-off value of ≤ 4.125 kPa can predict successful sperm retrieval with 84% accuracy [47].

A recently published study on a large number of patients managed to propose cut-off values for the differentiation between obstructive and nonobstructive azoospermia (Emax = 3.525) as well as for the differentiation between nonobstructive azoospermia grouped with severe oligozoospermia from normal and other groups with spermatogenesis problems ((Emax= 3.275), with good sensitivity and specificity (>80%) [48].

Conclusions

RTE can differentiate between patients with normal and abnormal sperm counts. In addition, it may play a role in the selection of patients who would benefit from deobstructive surgery or sperm retrieval procedures.

Due to its low specificity and sensitivity, pSWE cannot be considered as an alternative to semen analysis. The method could be helpful as a screening and follow-up tool in men with infertility.

2DSWE can be used to predict infertility but cannot differentiate between its causes due to overlapping values. Patients with infertility, OAT or azoospermia have significantly stiffer testes compared to normal subjects. 2DSWE can also predict successful sperm retrieval using TESE in men with nonobstructive azoospermia.

14.3.7. Testicular tumors

RTE and 2DSWE

The use of elastography in the differential diagnosis of testicular masses shows promising results in differentiating benign from malignant testicular masses, with similar results for RTE and 2D SWE. Benign lesions (tumorous or not) are more elastic compared to malignant tumors (fig. 14.6.) [4].

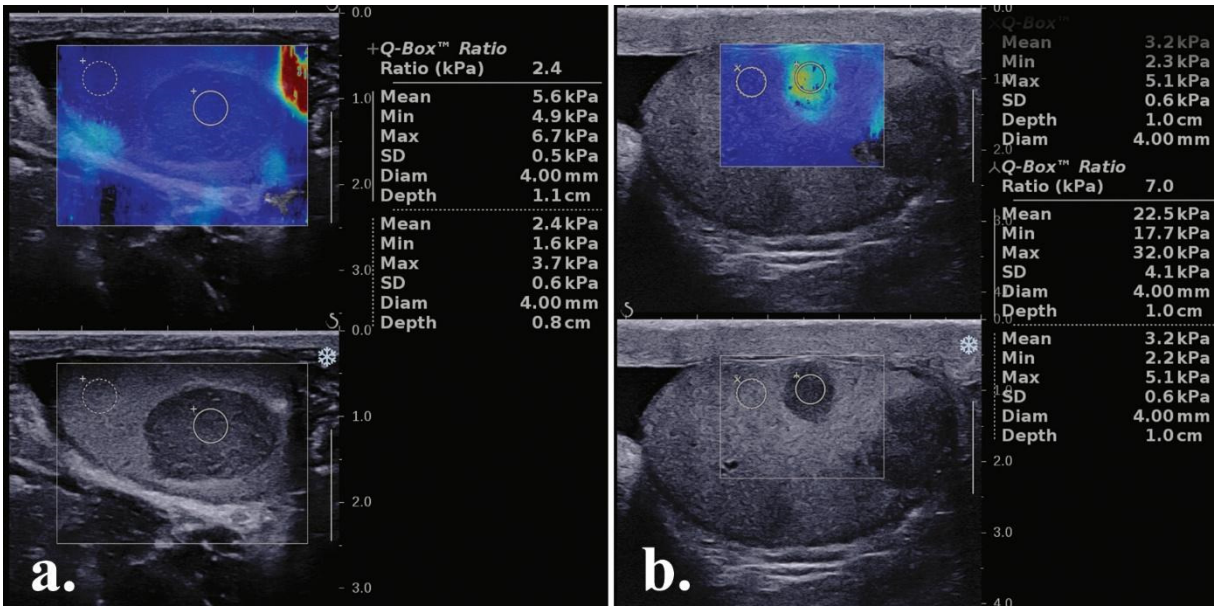

Figure 14.6. 2DSWE elastography of testicular tumors: a) Leydig cell tumor – discretely higher stiffness than the testicular parenchyma; b) seminoma - greater rigidity than the neighboring testicle.

A meta-analysis showed that malignant lesions were "stiffer" with both methods. However, overlapping results in these pathologies were reported. The main causes of overlapping results were the presence of calcifications in benign lesions and necrosis/liquefaction in advanced malignant testicular masses (49).

In large testicular tumors, areas with varied stiffnesses can be observed, an aspect illustrated by Figure 14.7.

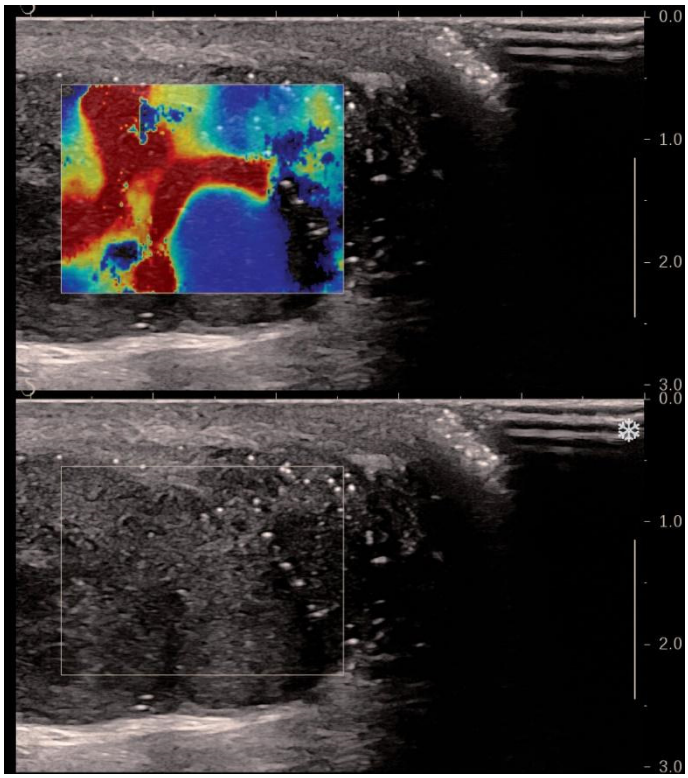

Figure 14.7. 2DSWE elastography. Voluminous testicular seminoma. Significant variations in the hardness of the tumor are evident, translated by the alternation of colors between red and blue.

Several authors have attempted to differentiate seminomatous from nonseminomatous tumors using elastography. Preliminary results indicate that nonseminomatous tumors are significantly stiffer than seminomas (figure 14.8). Still, there is heterogeneity between results, and the studies have been performed in small series of patients, so that no clear conclusions can be drawn [50,51].

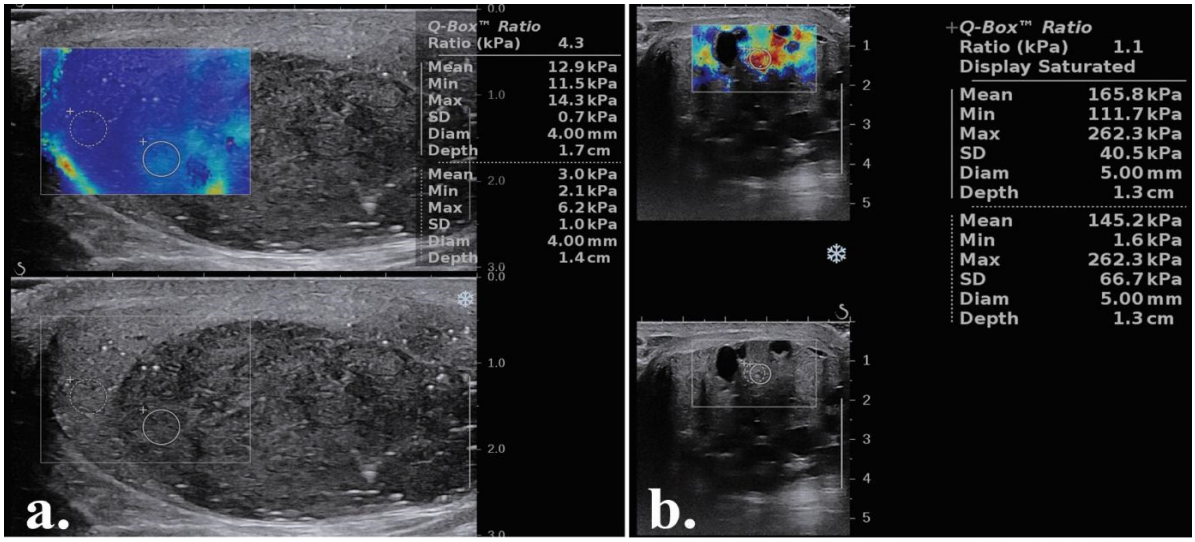

Figure 14.8. 2DSWE elastography. Malignant testicular tumors: a) testicular seminoma; b) teratocarcinoma.

It was proven that there is an inverse correlation between SR and the tumor vascularization index, measured immunohistochemically[52].

In evaluating the nature of a focal testicular lesion, elastography is only a complementary imaging element to the classic ultrasound diagnostic criteria: morphological, Doppler and clinical-evolutionary aspects. A possible approach to the main intratesticular hypoechoic focal lesions by multiparametric clinical-sonographic exploration is presented in Table 14. VI [4,49,50,53].

Table 14. VI. "First aid kit" in the multiparametric clinical-sonographic approach to the main intratesticular hypoechoic focal lesions.

Diagnosis	**Clinical presentation**	**Hypoechoic nodule**	**Homogenous**	**Doppler vascularization**	**CEUS**	**Elastographic stiffness**	**Stiffness evolution**
Focal orchitis	Celsian signs	++	++	++	++	+	decrease
Hematoma	Trauma history	++	+/-	-	-	+	decrease
Focal infarction	Pain, no celsian signs	++	++	-	-	+	increase
Benign tumor (Leydig)	Asymptomatic / mass	++	++	+/-	++	+/-	unchanged
Seminoma	Asymptomatic / mass	+++	+	+++	++	++	unchanged
Malignant nonseminomatous tumor	Asymptomatic / mass	+++	-	++	++	+++	unchanged

Particular types of tumors

Non-palpable and small testicular tumors (< 1.5 cm) benefit from SE by semi-quantitative scoring. A system of three colorimetric scores was defined: 1= uniformly soft, elastic lesion (green); 2 = lesion with mixed consistency (mixture of green and blue areas); and 3 = lesion with nodular hardness (blue) regardless of the surface occupied by the hardness compared to the 2D surface of the nodule. A score of 3 is associated with malignancy, while scores of 1 and 2 predict the benignity of a lesion, regardless of whether it is a tumor or a focal non-tumoral change. SR did not improve the quality of diagnosis by scores in these patients [54,55].

Regressive tumors (burned-out) appear at 2DSWE as nodules with greater stiffness than the neighboring parenchyma without correlations with the pathological substrate, vasculature or degree of regression. Differentiating from a nonregressive tumor by using elastography alone is impossible [56].

Although benign, an ***adenomatoid tumor*** appears very rigid on SE, regardless of whether it is classically located in the epididymis or intratesticularly, where it mimics seminoma [57,58].

On SE, the ***Leydig cell tumor*** may appear either elastic, similar to the testicular parenchyma (see figure 14.6.a), or stiff, similar to malignant tumors. As such, SE is not practical for differentiation [59].

2SWE, on the other hand, can discriminate between Leydig cell tumors and malignant ones and against non-tumorous lesions, as Leydig tumors appear softer (mean stiffness 6kPa, range 4-10 kPa) [60,61].

Capillary hemangioma appears in SE as an elastic lesion with intermediate hardness but is delimited by a more rigid border than the rest of the testicle [62].

We observed a similar stiff shell of the tumor in the ***epidermoid cyst***. However, epidermoid cysts may also appear uniformly stiff (Figure 14.9).

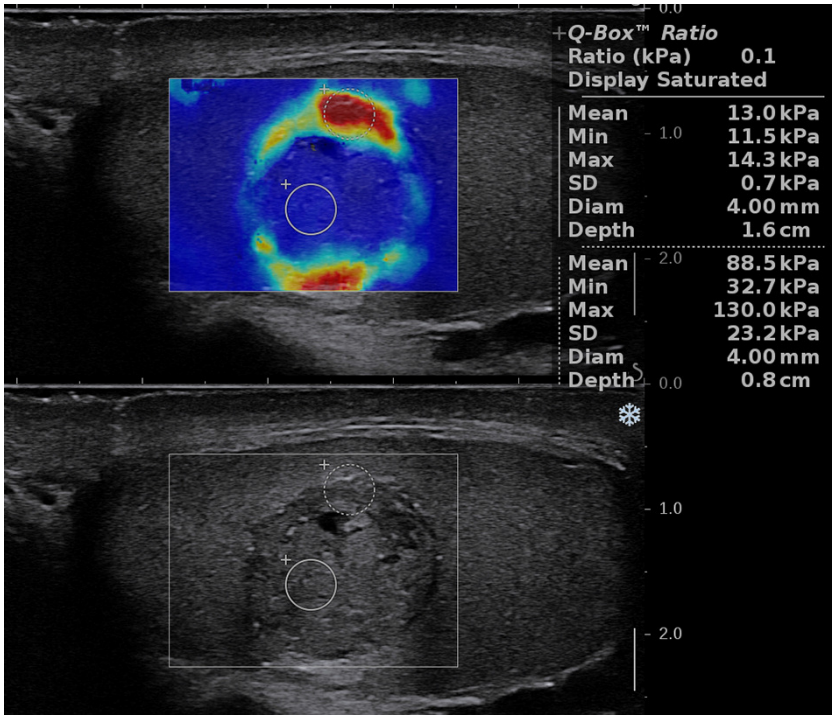

Figure 14.9. 2DSWE elastography. Epidermoid cyst in the testis. A stiff shell is visible at the periphery of the lesion.

Testicular involvement in ***hematological malignancies*** (leukemias, lymphomas) results in the appearance of focal lesions or diffuse damage, both with greater stiffness than normal ipsi- or contralateral testicular parenchyma [63].

Conclusions

Elastography may play a role in differentiating tumoral from non-tumorous focal testicular lesions.

In the evaluation of testicular tumor pathology by elastography, technical problems induce the variability of studies and results: how to achieve compression at SE, qualitative evaluation based on non-standardized color codes, localization of regions of interest, choice of reference for comparison, how SWE was implemented in the machine etc. [64].

Although the published information is promising, there are still no definite criteria to differentiate, by elastography, between benign and malignant tumors or between seminomas and nonseminomatous tumors. In-depth studies are needed using the anatomopathological appearance, T stage, and tumor size stratification [14].

14.3.8. Other Pathological Entities and Applications

COVID 19 infection

In unvaccinated SARS-CoV 2-infected patients, VTIQ demonstrated significantly higher testicular SW velocities than normal subjects [65]. The same method also observed greater testicular stiffness in patients with COVID-19 infection during recovery [66].

Tuberculous orchitis

Testicular tuberculosis appears as a hypoechoic mass, hard on SE, located intratesticularly [67].

Chronic hemodialysis

2DSWE observed greater hardness of the testes in patients with chronic hemodialysis compared to normal subjects. The appearance was attributed to fibrosis [68].

Inguinal hernia surgery

When examined by 2DSWE, testes on the operated side for inguinal hernia had significantly greater stiffness compared to the contralateral ones or normal subjects. A positive correlation was observed between stiffness and the severity and duration of the hernia before surgery [69].

Estimation of the postmortem interval

A cadaveric 2DSWE study found that, unlike the liver, although testicular stiffness is significantly greater than in live subjects, the method does not help determine the postmortem interval more than 24 hours after death [70].

Complex cases

As a defining biological parameter, tissue stiffness evaluation can contribute to the diagnosis in complex cases. We illustrate with the case of a 38-year-old patient, clinically presenting with acute scrotal pain syndrome, in which gray-scale ultrasound showed an enlarged, hypoechoic, inhomogeneous testicle without a focal tumor mass; the absence of intratesticular vascular signal was found during the Doppler examination, thus establishing the diagnosis of acute testicular torsion. Surprisingly, abdominal ultrasound revealed bulky retroperitoneal adenopathic masses. 2DSWE evaluation of the twisted testis revealed very high hardness of the upper half, raising the suspicion of torsion of a tumor-bearing testis. The diagnosis was confirmed at surgery (figure 14.10).

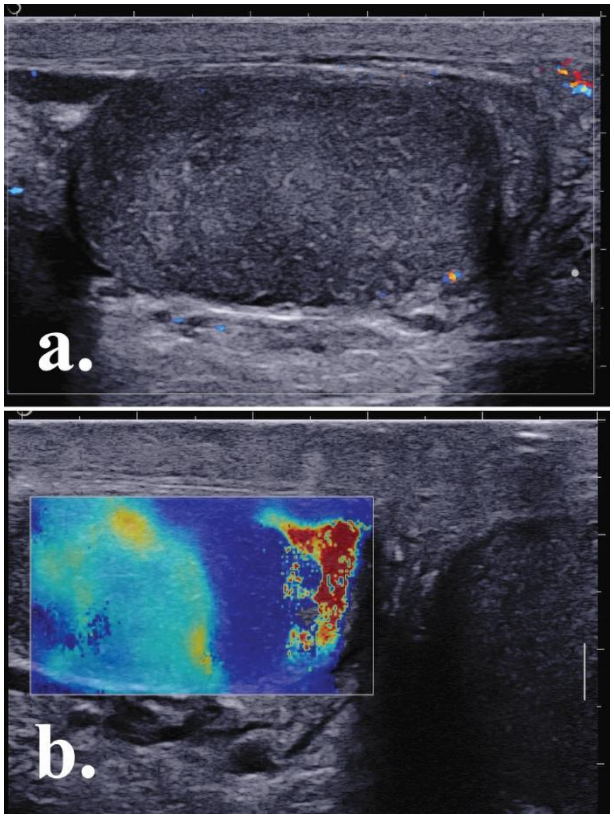

Figure 14.10. a) color Doppler examination: hypoechoic testicle, discretely inhomogeneous, without focal mass, without vascular signal; b) 2DSWE - high stiffness of the upper half of the twisted testicle. Pathology – testicular torsion and embryonal cell carcinoma in the upper half of the testicle.

14.3.9. Remarks

In evaluating the results of elastography, especially in the case of SWE techniques, it must be taken into account that, due to differences in the technical way of implementing the method and the production of transducers, different results can be obtained on the same type of pathology. One study demonstrated statistically significant differences between three devices used to measure SWE stiffness values on the same phantom device [71].

The observed differences between the hardness of the testis in normal subjects, noticeable even in the content of this chapter, are explained by the use of devices from different manufacturers. Standard values for the hardness of normal testes, measured with Aixplorer (Supersonic) devices, are lower than those measured with Canon (Toshiba) devices. No published studies use two types of machines to study the same set of normal subjects and to allow them to compare the results directly.

Although extremely promising and applicable in varied pathologies and domains, elastography alone is not a "panacea." The observations and results of the method must always be integrated into the patient's broad clinical and ultrasound context. Elastography is only one of the components of multiparametric ultrasonography.

References

1. Saftoiu A, Gilja OH, Sidhu PS, Dietrich CD, Cantisani V, Amy D, Bachmann-Nielsen M, Bob F, Bojunga J, Brock M, Calliada F, Clevert DA, Correas JM, D'Onofrio M, Ewertsen C, Farrokh A, Fodor D, Fusaroli P, Havre RF, Hocke M, Ignee A, Jenssen C, Klauser AS, Kollmann C, Radzina M, Ramnarine KV, Sconfienza LM, Solomon C, Sporea I, Ștefanescu H, Tanter M, Vilmann P - The EFSUMB Guidelines and Recommendations for the Clinical Practice of Elastography in Non-Hepatic Applications: Update 2018 – Ultraschall in Med 2019, 40, 425–453
2. Cantisani V, Di Leo N, BertolottoM, Fresilli D, Granata A, Polti G, Polito E, Pacini P, Guiban O, Del Gaudio G, Dolcetti V, D'Andrea V, Di Pierro GB, Verrengia M, Drudi FM, Catalano C - Role of multiparametric ultrasound in testicular focal lesions and diffuse pathology evaluation, with particular regard to elastography: Review of literature - Andrology 2021, 9, 1356–1368.
3. Muršic M, Sjekavica I, Šimunovic M, Ježek D - The role of ultrasound elastography In the diagnosis of pathologic conditions of testicles and scrotum - Acta Clin Croat 2021, 60, 41-49
4. Fang C, Huang DY, Sidhu PS - Elastography of focal testicular lesions: current concepts and utility. Ultrasonography 2019, 38, (4), 302–310.
5. D'Anastasi M, Schneevoigt BS, Trottmann M, Crispin A, Stief CG, Reiser MF, Clevert DA - Acoustic radiation force impulse imaging of the testes: a preliminary experience - Clin. Hemorheol. Microcirc. 2011, 49, 1-4, 105-114
6. Pedersen MR, Møller H, Osther PJS, Vedsted P, Holst R, Rafaelsen SR - Comparison of Tissue Stiffness Using Shear Wave Elastography in Men with Normal Testicular Tissue, Testicular Microlithiasis and Testicular Cancer - Ultrasound Int. Open 2017,3, E150–E155.
2. Trottmann M, Rübenthaler J, Marcon J, Stief CG, Reiser MF, Clevert DA - Differences of standard values of Supersonic shear imaging and ARFI technique - in vivo study of testicular tissue - Clin. Hemorheol. Microcirc. 2016, 64,(4), 729-733
3. Marcon J, Trottmann M, Rübenthaler J, Stief CG, Reiser MF, Clevert DA - Shear wave elastography of the testes in a healthy study collective - differences in standard values between ARFI and VTIQ techniques - Clin. Hemorheol. Microcirc. 2016, 64,(4), 721-728
4. Trottmann M, Marcon J, D'Anastasi M, Karl A, Stief CG, Reiser MF, Clevert DA - The role of VTIQ as a new tissue strain analytics measurement technique in testicular lesions - Clin. Hemorheol. Microcirc. 2014, 58,(1), 195-209
5. Marcon J, Trottmann M, Rübenthaler J, D'Anastasi M, Stief CG, Reiser MF, Clevert DA - Three-dimensional vs. two-dimensional shear-wave elastography of the testes - preliminary study on a healthy collective - Clin. Hemorheol. Microcirc. 2016, 64,(3), 447-456
6. Trottmann M, Marcon J, D'Anastasi M, Bruce MF, Stief CG, Reiser MF, Buchner A, Clevert DA - Shear-wave elastography of the testis in the healthy man - determination of standard values - Clin. Hemorheol. Microcirc. 2016, 62,(3), 273–281
7. Chen F, Mao L, Zhou X, Qiao X, Luo Y, Zhu Z, Chen R, Qiu S, Zeng B - Application of Shear Wave Elastography to Evaluate the Stiffness of Normal Testes and Inflammatory Epididymal Tail Masses - Ultrasound Q. 2021, 37, (2), 161–167.
8. Shin HJ, Yoon H, Lee YS, Kim MJ, Han SW, Roh YH, Lee MJ - Normal Changes and Ranges of Pediatric Testicular Volume and Shear Wave Elasticity - Ultrasound Med. Biol. 2019, 45,(7), 1638–1643.

9. Simon V, Dudea SM, Crisan N, Stanca VD, Dudea-Simon M, Andras I, Mihaly ZA, Coman I - Elastography in the Urological Practice: Urinary and Male Genital Tract, Prostate Excluded—Review - Diagnostics 2022, 12, 1727
10. Jędrzejewski G, Wieczorek A - Multiparametric ultrasonography of the pediatric scrotum and in boys with undescended testes - J. Ultrason. 2013, 13, 425–430.
11. Cildag NB - Evaluation of Pediatric Undescended Testes with Elastosonography - J Med Ultrasound 2017, 25, 157-160
12. Hattapoğlu S, Göya C, Arslan S, Alan B, Ekici F, Tekbaş G, Yildiz I, Hamidi C - Evaluation of postoperative undescended testicles using point shear wave elastography in children - Ultrasonics 2016, 72, 191–194.
13. Ucar A, Alis D, Samanci C, Aslan M, Habibi H, Dikici A, Namdar Y, Gultekin MH, Onal B, Adaletli I - A preliminary study of shear wave elastography for the evaluation of unilateral palpable undescended testes - Eur. J. Radiol. 2017, 86, 248–251.
14. Shin H, Lee Y, Yoon H, Kim M, Han S, Kim H, Lee J, Lee M - Testicular volume and elasticity changes in young children with undescended testes - Med. Ultrason. 2017, 19, (4), 380 - 385.
15. Turna O, Alis D - A comparative study of shear wave elastography in the evaluation of undescended and retractile testes in a pediatric population - J. Med. Ultrason. 2019, 46, 231–237.
16. Sun Z, Xie M, Xiang F, Song Y, Yu C, Zhang Y, Ramdhany S, Wang J - Utility of Real-Time Shear Wave Elastography in the Assessment of Testicular Torsion - PLoS ONE 2015, 10, e0138523.
17. Xue E, Yu Y, Lin L, Li Z, Su H - Application value of real-time shear wave elastography in differential diagnosis of testicular torsion - Med. Ultrason. 2020, 22, (1), 43-48
18. Laimer G, Müller R, Radmayr C, Lindner AK, Lebovici A, Aigner F - Multiparametric ultrasound in torsion of the testicular appendages: a reliable diagnostic tool? Med Ultrason 2022, 24, 1, 33-37
19. Pedersen M, Osther P, Rafaelsen S - Testicular microlithiasis and preliminary experience of acoustic radiation force impulse imaging - Acta Radiol. Open 2016, 5, (7), 1-4
20. 25 Pedersen M, Møller H, Osther P, Vedsted P, Holst R, Rafaelsen S - Comparison of Tissue Stiffness Using Shear Wave Elastography in Men with Normal Testicular Tissue, Testicular Microlithiasis and Testicular Cancer - Ultrasound Int. Open 2017, 3, E150–E155
21. Aslan S, Bilgici MC, Saglam D, Ozturk M - The role of ARFI elastography to evaluate microstructural changes of patients with testicular microlithiasis - Acta Radiol. 2018, 59, 1517–1522.
22. Camoglio F, Bruno C, Peretti M, Bianchi F, Bucci A, Scirè G, Patane S, Zampieri N - The Role of Sonoelastography in the Evaluation of Testes with Varicocele - Urology 2017, 100, 203–206.
23. Salama N, Samir M, Blgozah S - Evaluation of Normal and Varicocele-Bearing Testes Using Real-time Strain Elastography - J. Ultrasound Med. 2018, 38, 621–627.
24. Kucukdurmaz F, Sarica M, Emre O, Baykara M, Kizildag B, Resim S - Evaluation of the diagnostic efficacy of strain elastography in infertile population with normal and abnormal semen parameters - Turk. J. Urol. 2017, 43, 261–267.
25. Dede O, Teke M, Daggulli M, Utangaç M, Baş O, Penbegül N - Elastography to assess the effect of varicoceles on testes: a prospective controlled study - Andrologia 2016, 48, (3), 257–261.

26. Jedrzejewski G, Osemlak P, Wieczorek A, Nachulewicz P - Prognostic values of shear wave elastography in adolescent boys with varicocele - J. Pediatric Urol. 2019, 15, 223.e1–223.e5.
27. Rocher L, Criton A, Gennisson J, Izard V, Ferlicot S, Tanter M, Benoit G, Belin MF, Correas JM - Testicular Shear Wave Elastography in Normal and Infertile Men: A Prospective Study on 601 Patients - Ultrasound Med. Biol. 2017, 43, (4), 782–789.
28. Yüzkan S, Çilengir AH. Shear wave elastography for assessment of testicular stiffness in patients with varicocele: a prospective comparative study - J Med Ultrasound 2022, 30, 277-281.
29. Baleato-Gonzalez S, Osorio-Vazquez I, Flores-Ríos E, Santiago-Pérez MI, Laguna-Reyes JP, Garcia-Figueiras R - Testicular Evaluation Using Shear Wave Elastography (SWE) in Patients with Varicocele - J. Imaging 2023, 9, 166.
30. Ryu YJ, Choi YH, Kim JY, Cheon JE, Kim WS, Kim IO, Park JE, Im YJ, Park K - A preliminary study of shear-wave elastography for the evaluation of varicoceles in adolescents and young adults – Ultrasonography, 2022, 41, (1), 131 -139.
31. Abdelwahab K, Eliwa A, Seleem M, El Galaly H, Ragab A, Desoky E, Naguib M, Ali MM, Saber S, Kamel H - Role of Preoperative Testicular Shear Wave Elastography in Predicting Improvement of Semen Parameters after Varicocelectomy for Male Patients with Primary Infertility - Urology 2017, 107, 103–106.
32. Turna O, Aybar MD - Testicular stiffness in varicocele: evaluation with shear wave elastography – Ultrasonography, 2020, 39, (4), 350– 355.
33. Erdogan H, Durmaz M, Arslan S, Durmaz FG, Cebeci H, Ergun O, Karaagac SS - Shear Wave Elastography Evaluation of Testes in Patients with Varicocele - Ultrasound Q., 2020, 36, (1), 64–68.
34. Ernst S, Saar M, Brenneis H, Kubale R, Ueberdiek S, Ohlmann C, Stoeckle M, Heinzelbecker J - Segmental Testicular Infarction: Case Series and Literature Review of a Rare Diagnosis in Men with Acute Testicular Pain - Urol. Int. 2018, 101, (1), 114– 116.
35. Kantarci F, Olgun DC, Mihmanli I - Shear-Wave Elastography of Segmental Infarction of the Testis - Korean J. Radiol. 2012, 13, (6), 820 - 822.
36. Patel K, Huang D, Sidhu P - Metachronous bilateral segmental testicular infarction: multiparametric ultrasound imaging with grey-scale ultrasound, Doppler ultrasound, contrast-enhanced ultrasound (CEUS) and real-time tissue elastography (RTE) - J. Ultrasound 2014, 17, 233–238.
37. Li M, Du J, Wang Z, Li F - The Value of Sonoelastography Scores and the Strain Ratio in Differential Diagnosis of Azoospermia - J. Urol., 2012, 188, 1861–1866.
38. Yavuz A, Yokus A, Taken K, Batur A, Ozgokce M, Arslan H - Reliability of testicular stiffness quantification using shear wave elastography in predicting male fertility: a preliminary prospective study - Med. Ultrason. 2018, 20, (2), 141 - 147.
39. 4436. Illiano E, Trama F, Ruffo A, Romeo G, Riccardo F, Crocetto F, Iacono F, Costantini E - Testicular shear wave elastography in oligo-astheno-teratozoospermic individuals: a prospective case–control study - Int. Urol. Nephrol. 2021, 53, (9),1773 - 1783.
40. Hu JY, Huang WL, Gao Y, Yang Z, Ding L, Xie Y, Xie XY, Hu HT, Wang Z - Preliminary investigation of the diagnostic value of shear wave elastography in evaluating the testicular spermatogenic function in patients with azoospermia - Andrologia 2021, 53, (5), e14039.

41. Erdoğan H, Durmaz MS, Özbakır B, Cebeci H, Özkan D, Gökmen İE - Experience of using shear wave elastography in evaluation of testicular stiffness in cases of male infertility - J. Ultrasound 2020, 23, 529–534.
42. Abdelaal AMA, El-Azizi HM, GamalEl Din SF, Azzazi OAM, Mohamed MS - Evaluation of the potential role of shear wave elastography as a promising predictor of sperm retrieval in nonobstructive azoospermic patients: a prospective study - Andrology 2021, 9, 1481–1489.
43. Cui J, Du Q, Fu W - Application of real-time shear wave elastography in the assessment of male infertility - Quant Imaging Med Surg 2022, 12, (2), 1505-1516
44. Lin Z, Lin R, Wu H, Wu L, Zeng J, Xu J, Dong F - Elastography for the differential diagnosis of malignant versus benign testicular lesions: a meta-analysis - Ultrasonography 2021, 40, (4), 465–473.
45. Roy C, de Marini P, Labani A, Leyendecker P, Ohana M - Shear-wave elastography of the testicle: potential role of the stiffness value in various common testicular diseases - Clin. Radiol. 2020, 75, (7), 560.e9–560.e17.
46. Dikici AS, Er ME, Alis D, Samanci C, Ustabasioglu FE, Demirag C, Durak H, Kantarci F, Mihmanli I - Is there any difference between seminomas and nonseminomatous germ cell tumors on shear wave elastography? A preliminary study - J.Ultrasound Med. 2016, 35, (12), 2575–2580.
47. PastoreAL, Palleschi G, Maceroni P, Manfredonia G, Autieri D, Cacciotti J, Sardella B, Porta N, Petrozza V, Carbone A – Correlation between semi-quantitative sonoelastography and immunohistochemistry in the evaluation of testicular focal lesions – Cancer Imaging 2014, 14, 29
48. Tenuta M, Sesti F, Bonaventura I, Mazzotta P, Pofi R, Gianfrilli D, Pozza C – Use of contrast enhanced ultrasound in testicular diseases: a comprehensive review – Andrology, 2021, 9, 1369-1382
49. Pozza C, Gianfrilli D, Fattorini G, Giannetta E, Barbagallo F, Nicolai E, Cristini C, Di Pierro GB, Franco G, Lenzi A, Sidhu PS, Cantisani V, Isidori AM - Diagnostic value of qualitative and strain ratio elastography in the differential diagnosis of non-palpable testicular lesions - Andrology, 2016, 4, 1193–1203
50. Reginelli A, D'Andrea A, Clemente A, Izzo A, Urraro F, Scala F, Nardone V, Guida C, Scialpi M, Cappabianca S - Does multiparametric US improve diagnostic accuracy in the characterization of small testicular masses? - Gland Surg 2019, 8, (Suppl 3), S136-S141
51. Desmousseaux T, Arama E, Maxwell F, Ferlicot S, Hani C, Fizazi K, Lebacle C, Loriot Y, Boumerzoug M, Cohen J, Garrouche N, Rocher L - Ultrasound and Magnetic Resonance Imaging of Burned-Out Testicular Tumours: The Diagnostic Keys Based on 48 Cases - Cancers 2022, 14, 4013.
52. Phatak SV, Manoj M, Bhansali PJ, Ghanta P - Adenomatoid tumor of epididymis associated with tubular ectasia of rete testis: Sonographic evaluation - J Med Ultrasound 2023, 31, 157-159.
53. Pichler R, Tulchiner G, Steinkohl F, Soleiman A, Horninger W, Heidegger IM, Aigner F - Adenomatoid tumor of the testis mimicking malignant testicular cancer on multiparametric ultrasound - Eur J Med Res 2018, 23, 3
54. Corcioni B, Brandi N, Marasco G, Gaudiano C, De Cinque A, Ciccarese F, Ercolino A, Schiavina R, Brunocilla R, Renzulli M, Golfieri R - Multiparametric ultrasound for the diagnosis of Leydig cell tumours in non-palpable testicular lesions - Andrology 2022, 10, 1387–1397.

55. Rocher L, Criton A, Gennisson JL, Creze M, Albiges L, Ferlicot S, Bellin MF, Izard V, Correas JM - Characterization of Testicular Masses in Adults: Performance of Combined Quantitative Shear Wave Elastography and Conventional Ultrasound - Ultrasound Med. Biol. 2019, 45, 720–731.
56. Maxwell F, SavignacA, Bekdache O, Calvez S, Lebacle C, Arama E, Garrouche N, Rocher L - Leydig Cell Tumors of the Testis: An Update of the Imaging Characteristics of a Not So Rare Lesion - Cancers 2022, 14, 3652.
57. Bernardo s, Konstantatou E, Huang DY, Deganello A, Philippidou M, Brown C, Sellars ME, Sidhu PS - Multiparametric sonographic imaging of a capillary hemangioma of the testis: appearances on gray-scale, color Doppler, contrast-enhanced ultrasound and strain elastography - J Ultrasound (2016) 19:35–39
58. Koh SY, Lee S, Lee SB, Cho YJ, Choi YH,Cheon JE, Kim WS - Shear-wave elastography for the assessment of testicular involvement of hematologic malignancies in children and young adults: a feasibility study - Ultrasonography 2022, 41 ,(2), 325-334
59. Lai DKH, Cheng ESW, Mao YJ, Zheng Y, Yao KY, Ni M, Zhang YQ, Wong DWC, Cheung JCW - Sonoelastography for Testicular Tumor Identification: A Systematic Review and Meta-Analysis of Diagnostic Test Accuracy - Cancers 2023, 15, 3770
60. Ertaș K, Eryilmaz R, Yokuș A, Körpe K, Gedük N, Özkan M, Aslan R - Examining changes on testicular structure and sperm analysis of COVID-19 patients - Andrologia, 2022, e14609
61. Dogan F, Dere O - Evaluation of testicles by sonoelastography in men recovering after Covid-19 disease - Radiography 2023, 29, 675 - 679
62. Ahmed R, Wolfe K, Acher P, Liyanage S - Multiparametric ultrasound findings of tuberculous orchitis following bacillus Calmette-Guérin therapy - Radiology Case Reports 2017, 12, 746–751
63. Hekimoglu A, Tatar IG, Ergun O, Turan A, Ayli MD, Hekimoglu B - Shear Wave Sonoelastography Findings of Testicles in Chronic Kidney Disease Patients Who Undergo Hemodialysis - Eurasian J Med 2017, 49, 12-15
64. Durmaz MS, Ateș F, Arslan S, Kara T, Durmaz FG, Eryilmaz MA, Arslan K - Assessment of testes with two-dimensional Shear Wave Elastography in patients with operated inguinal hernia - Med Ultrason 2021, Vol. 23, no. 2, 181-187
65. Mosadegh M, Khazaei M, Abdollahpour ZD, Alahyari S, Moharamzad Y, Emamhadi M, Aram S, Abolbaghaei M, Taheri MS - Ultrasound shear-wave elastography applicability in estimation of postmortem time - Ultrasound 2022, 30, 2, 134 –140
66. Shin, H.; Kim, M.; Kim, H.; Roh, Y.; Lee, M. Comparison of shear wave velocities on ultrasound elastography between different machines, transducers, and acquisition depths: A phantom study. Eur. Radiol. 2016, 26, 3361–3367.

Chapter 15. Elastography in Musculoskeletal Diseases

Michael Pelea, Oana Șerban, Daniela Fodor

Elastography has emerged as a valuable complement to traditional imaging modalities in the evaluation of musculoskeletal pathology. By providing information about tissue elasticity, elastography offers clinicians a non-invasive means of assessing various structures of the musculoskeletal system. This technique is based on the principle that abnormal tissues often exhibit altered mechanical properties compared to healthy tissues. In the context of musculoskeletal imaging, elastography allows for characterization of soft tissue lesions, assessment of tendon and ligament integrity, evaluation of muscle stiffness, and detection of joint pathology. Furthermore, elastography complements existing imaging modalities such as ultrasound and magnetic resonance imaging (MRI), providing additional information that enhances diagnostic accuracy and guides therapeutic decisions. As we delve deeper into the applications and nuances of elastography in musculoskeletal imaging, it becomes evident that this technique promises to advance our understanding and management of various musculoskeletal disorders.

15.1. Musculoskeletal Elastography Examination Techniques

15.1.1. Normal Gray Scale Appearance

Muscles

For a better understanding of the elastographic appearance of muscles, it is essential to first know their gray scale appearance. The ultrasound examination is initially performed at rest, keeping the transducer perpendicular to the muscle fibers to avoid anisotropy. Longitudinal and transverse scans are made, and the transducer is moved over the entire surface of the muscle being examined. Afterward, ultrasound examination can be performed during isometric contraction. For paired muscles, examining the contralateral muscle can be useful for interpreting changes (1).

The gray scale ultrasound appearance of muscles is closely related to their anatomical structure, starting from muscle fibers encased in endomysium, which are grouped into fascicles surrounded by perimysium. These fascicles collectively form the muscle body, which is encased in epimysium. During ultrasound examination, muscle fascicles appear as hypoechoic areas, while the perimysium appears as hyperechoic lines that separate them. In a longitudinal scan, the muscle displays an alternating pattern of linear hypoechoic areas and parallel hyperechoic lines, creating a “comb” or “leaf” like appearance (Fig.15.1a). In a transverse plane, the muscle appears as a hypoechoic background with multiple hyperechoic dots and lines, creating a “starry sky” appearance (Fig 15.1b). Examination of the muscle during isometric contraction (Fig.15.1c,d) reveals an increase in the thickness of the muscle

fascicles and, consequently, the entire muscle. This is accompanied by a decrease in overall echogenicity and an accentuation of the obliquity of the fibers (1,2).

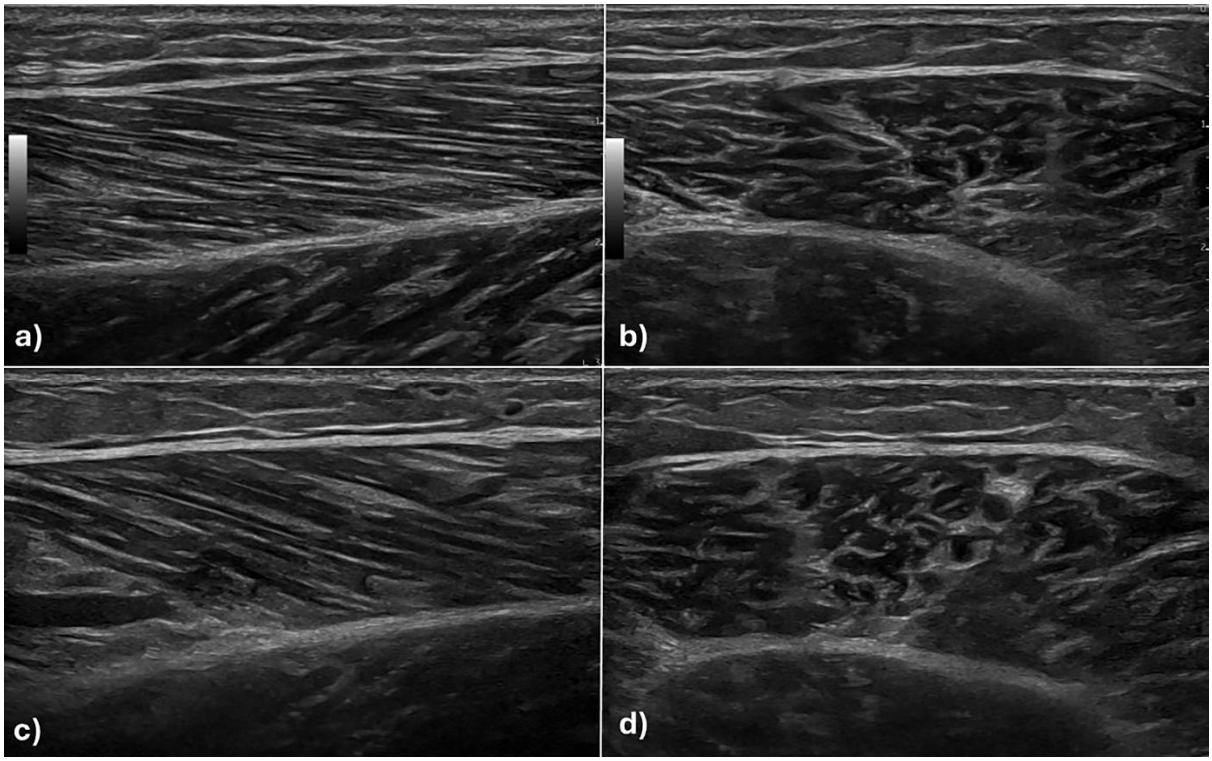

Fig.15.1. The gray scale ultrasound appearance of muscles at rest or in a relaxed state (a) in a longitudinal plane has a "comb" appearance due to the alternation of hypoechoic linear zones corresponding to muscle fascicles and parallel hyperechoic lines, and (b) in a transverse plane, it has a "starry" appearance due to multiple hyperechoic dots and lines on a hypoechoic background. The ultrasound appearance of muscles during isometric contraction (c) in a longitudinal plane (d) in a transverse plane, an increase in muscle size can be observed, a decrease in overall echogenicity, and an accentuation of the obliquity of muscle fibers

Tendons

Tendons are composed of connective fibrous tissue primarily made up of water, proteoglycans, and collagen fibers arranged in parallel bundles. This unique composition provides tendons with the ability to resist tension, absorb energy, and facilitate movement (3,4). Their function is to form a mechanical "bridge" between muscles and bones, while some tendons connect two muscle bodies (4).

Ultrasonography has become one of the most important techniques for evaluating tendons due to its high spatial resolution, the ability to perform multiplanar scanning, and the advantage of both static and dynamic examinations (5). The gray scale appearance of normal and pathological tendons is fundamental for understanding and identifying elastographic changes. In a longitudinal scan, tendons exhibit an echogenic, fibrillar pattern reflecting the parallel arrangement of collagen fibers. In a transverse view, tendons typically appear as round or oval structures with an alternating pattern of hyperechoic and hypoechoic dots (Fig.15.2) resulting from the arrangement of collagen bundles and surrounding connective

tissue (5,6). Anisotropy is a sonographic artifact where tendons show variations in echogenicity depending on the insonation angle. When the ultrasound beam is perpendicular to the tendon fibers, it receives all the emitted echoes, and the structure appears hyperechoic. If the insonation angle is changed, only a portion of the echoes are reflected to the transducer, causing the structure to appear hypoechoic (7,8). Correction of this artifact can be achieved by simply angling the transducer or tensioning the tendon, but recognizing anisotropy is essential for accurate examination in both gray scale imaging and elastography image acquisition.

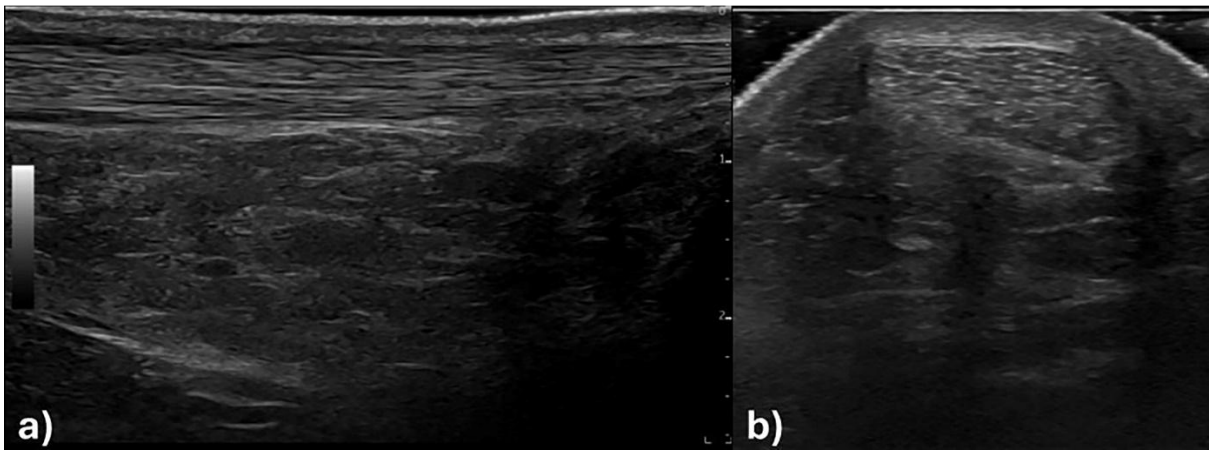

Fig.15.2. The normal gray scale appearance of the Achilles tendon (a) in a longitudinal plane (b) in a transverse plane.

Understanding the normal ultrasound appearance is fundamental in distinguishing healthy tissues from pathological ones and forms the basis for interpreting elastographic changes.

15.1.2. Normal Elastography Appearance

Muscles

Elastography uses innovative principles to assess the elastic properties in musculoskeletal imaging, offering a unique perspective on the pathological state of various structures. Its use in muscle evaluation has significantly expanded in recent years, and there is now a wide range of elastographic characteristics of both normal and pathological muscles documented in the literature, however, well-established reference values are still lacking (9). For paired muscles, examining the contralateral muscle and making left-right comparisons is always useful in interpreting images and values obtained (9). The main elastographic techniques used for muscle evaluation are strain elastography (SE) and shear-wave elastography (SWE).

For applying elastographic techniques to muscle, the patient is positioned similarly to a gray scale examination, comfortably, and with the muscle of interest relaxed (10). Linear transducers with a high frequency of at least 12 MHz, or adaptable frequency transducers ranging from 3 to 12 MHz for deeper structures are used for muscle examinations (11), taking into account that spatial resolution decreases and ultrasound attenuation increases as the

transducer frequency rises (10). The transducer is placed on the skin along the muscle fibers (9,12), and strictly perpendicular to them to avoid anisotropy (9,12-15). A sufficient amount of gel is used to ensure full contact between the transducer and the skin, but excessive gel should be avoided as it can affect measurements when included in the elastogram (13,14,16). First, a high-quality gray scale image is obtained, as this influences the elastogram's quality (10,16,17), and then the button for the desired elastography technique is activated.

Strain elastography

Strain elastography, also known as compression elastography, evaluates deformation changes in muscle during the application of a controlled external force, typically through manual compression with the transducer (16). This manually applied compression does not easily transmit to deeper structures (18), however, for most superficial structures, including muscles and tendons, this method is very useful. Strain elastography allows for the evaluation of muscle structures and their lesions, as well as monitoring their progression over time.

After activating the SE button, the size and position of the elastography box is set to encompass the muscle structure of interest and enough adjacent normal or reference tissue (since SE displays the relative elasticity of tissues) (16). Afterwards, gradual, uniform, repetitive compression at a low frequency is applied with the transducer on the examined muscle, keeping the transducer as perpendicular as possible to avoid lateral movement on the skin surface (outside the plane perpendicular to the muscle). This generates the elastogram (a color-coded map of elasticity distribution – the color scale may vary by manufacturer or can be selected by the user, as indicated by the color bar attached to the elastogram) superimposed on the gray scale image (9,13,14,16,19,20). The "Freeze" button is then activated, and to ensure a good quality and reproducibility of the elastographic image, the temporarily stored cineloop frames are analyzed. Consistent elastographic images across multiple consecutive frames indicate good reliability (16) and can therefore be interpreted.

Compression along the longitudinal axis of the structure of interest has proven optimal because the primary tissue deformation occurs longitudinally (20). Transverse compression can generate artifacts at the medial and lateral edges of the muscle, and moving the transducer out of the perpendicular plane can also create similar artifacts (21). Because the applied force is unknown, quantitative measurements cannot be made. Only qualitative assessments or semi-quantitative evaluations can be performed by calculating the ratio between the region of interest and an adjacent structure, such as subcutaneous fat tissue (21).

In SE, a normal resting muscle exhibits a heterogenous appearance, often described as a mosaic of colors. This heterogeneity is characterized by regions of intermediate stiffness, usually represented by shades of green and yellow, interspersed with areas of higher stiffness, which may appear blue or red depending on the color scale used (Fig.15.3a). Notably, the periphery of the muscle may show more pronounced variability in stiffness, with both low and high stiffness areas being more dispersed (12,13,22).

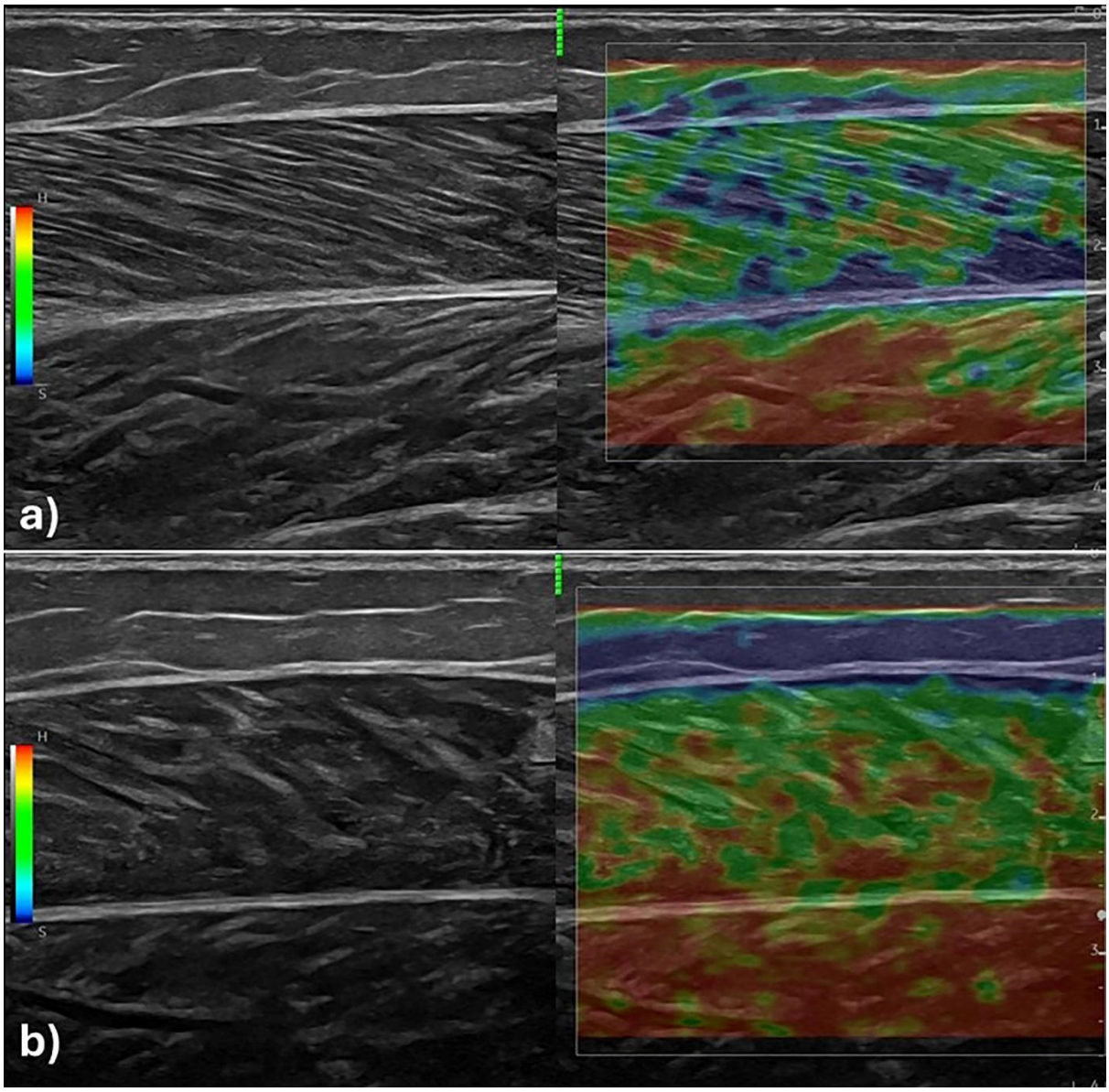

Fig.15.3. (a) Strain elastogram of the lateral gastrocnemius muscle at rest, in a longitudinal plane, showing a mosaic of colors characterized by regions of intermediate stiffness (shades of green and yellow), interspersed with areas of increased stiffness (red) and reduced stiffness (blue). (b) Strain elastogram of the lateral gastrocnemius muscle during isometric contraction with zones of intermediate stiffness (green) interspersed with areas of increased stiffness (red) or a predominance of increased stiffness areas; quality indicators in green signal demonstrating adequate compression with the transducer.

The heterogeneity observed in muscle elastograms is a phenomenon that has not been fully elucidated, with specific causes remaining unknown. Although elastography has clinical applications in evaluating muscle pathology and guiding interventions, the correlation between the color-coded patterns in muscle elastograms and underlying histopathological changes has not been established through comparative studies. The absence of such studies leaves a gap in understanding the precise histopathological basis for the observed patterns. Current knowledge is based on the assumption that tissue injuries and structural abnormalities lead to changes in physical properties, including elasticity, which should be

reflected in the elastographic image. Nonetheless, without direct histopathological comparisons, the exact causes of heterogeneity in muscle elastograms remain speculative and require further investigation (22).

Shear-Wave Elastography

Shear-Wave elastography uses acoustic waves to evaluate the propagation speed of shear waves through muscle. This method provides both a qualitative color-coded elastogram and a quantitative measurement of tissue stiffness by calculating Young's modulus (in kPa) or the shear wave propagation speed (in cm/s), and is used in the evaluation of muscle pathology and other musculoskeletal conditions (9,14,18). By integrating these elastographic techniques into the musculoskeletal imaging arsenal, we can achieve a more comprehensive and accurate assessment of muscle tissue. There are, however, concerns about using this method for very superficial structures, as shear waves require ultrasound to travel a certain depth to be generated effectively (14).

After activating the SWE button, the size and position of the SWE box are set over the region of interest, which results in a color-coded map (elastogram) that is obtained by calculating the shear-wave propagation speed for each pixel. Since shear wave reflection at the interfaces between structures can generate artifacts, it is useful to exclude the edges of visible structures in B-mode from the measurement region (18). For SWE evaluation of musculoskeletal structures, it is recommended to apply minimal and constant compression with the transducer, similar to that used for breast tissues (<1% or <0.3 mm in a 3 cm thick breast). Although minimal compression can help improve measurement reproducibility, it is important to avoid applying excessive compression to ensure an accurate assessment of muscle elasticity. This is based on the observation that increased transducer compression during measurements correlates with an increase in shear wave propagation speed (11,18) (Fig.15.4). After setting the elastography box, the transducer is held stable in the same position for a few seconds (approximately 5 seconds) to allow the color map to stabilize and homogenize (10), then the Freeze button is pressed. Subsequently, measurements can be performed by placing one or more regions of interest (ROI), usually small circles (9-11), within the elastography box in an area with the most homogenous color on the elastogram. This should be where shear wave propagation is parallel on the shear wave propagation map and/or where the shear wave quality is highest on the color-coded confidence/quality map, if available. The elasticity values generated within the ROI include the minimum, maximum, and mean of all measurements taken inside it. Reporting the elasticity is preferred using the mean value of the measurements (10). The size of the ROI is chosen on the dimensions of the structure or lesion being examined and does not influence the mean elasticity values (10,12). Similar to other organs where a minimum of 3, 5 or 10 measurements is recommended (11,23), multiple measurements should also be performed within the region of interest in the musculoskeletal system. However, there are currently no clear recommendations regarding the exact number of measurements needed for accuracy in this context.

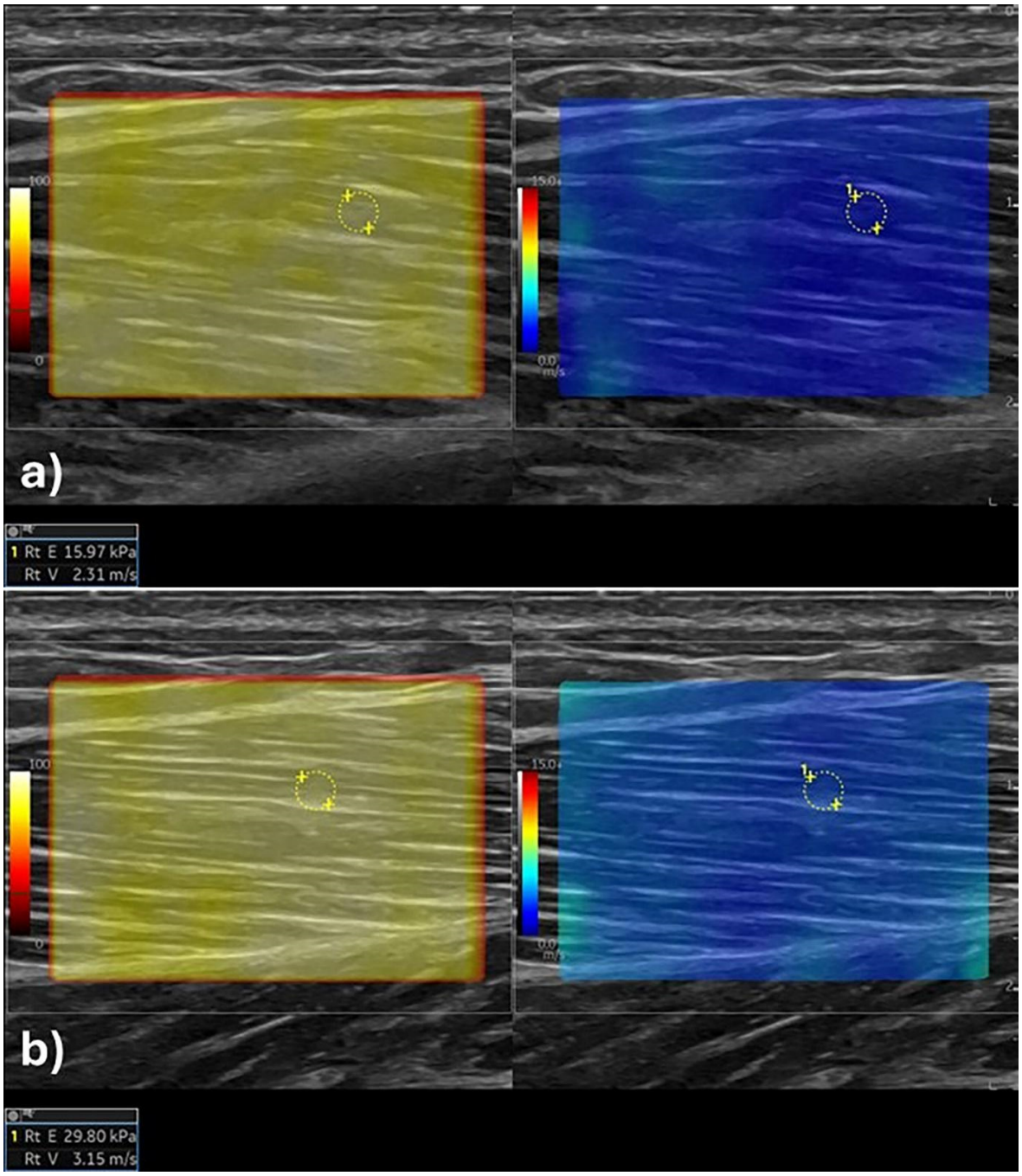

Fig.15.4. SWE of the relaxed medial gastrocnemius muscle, in a longitudinal plane (a) during minimal and constant compression with the transducer and (b) during exaggerated compression with the transducer, which increases the shear wave propagation speed compared to the correctly performed initial image; the left side of the images represent color-coded confidence/quality maps, with maximum quality coded in white.

SWE provides a color-coded elastogram recorded alongside the standard gray-scale image, offering anatomical specificity and allowing detailed spatial evaluation of absolute muscle stiffness. Normal muscle shows characteristic shear wave propagation patterns, with waves traveling slower through relaxed ("softer") tissue (Fig.15.5a) and faster through contracted (stiffer) tissue (Fig.15.5b), along the long axis of the muscle fibers (9,12,15). Aponeuroses and muscle fascia exhibit an intermediate speed of shear wave propagation (12). Anisotropy is crucial for accurately interpreting SWE images. Due to varying architecture of

muscles (unipennate, bipennate, multipennate), aligning the transducer along all individual muscle fibers is challenging, sometimes impossible (24). The orientation of muscle fibers relative to the ultrasound transducer, and the refraction effect that attenuates shear wave, can significantly impact the accuracy of elasticity measurements (11,15).

In clinical practice, SWE can be used to establish reference values for muscle stiffness, which can then be compared to pathological states or used to monitor changes over time, such as during the rehabilitation process or after interventions (15). Several studies have reported normal and abnormal SWE value ranges for different muscle groups, however, reference values for SWE in muscles have not yet been established (12).

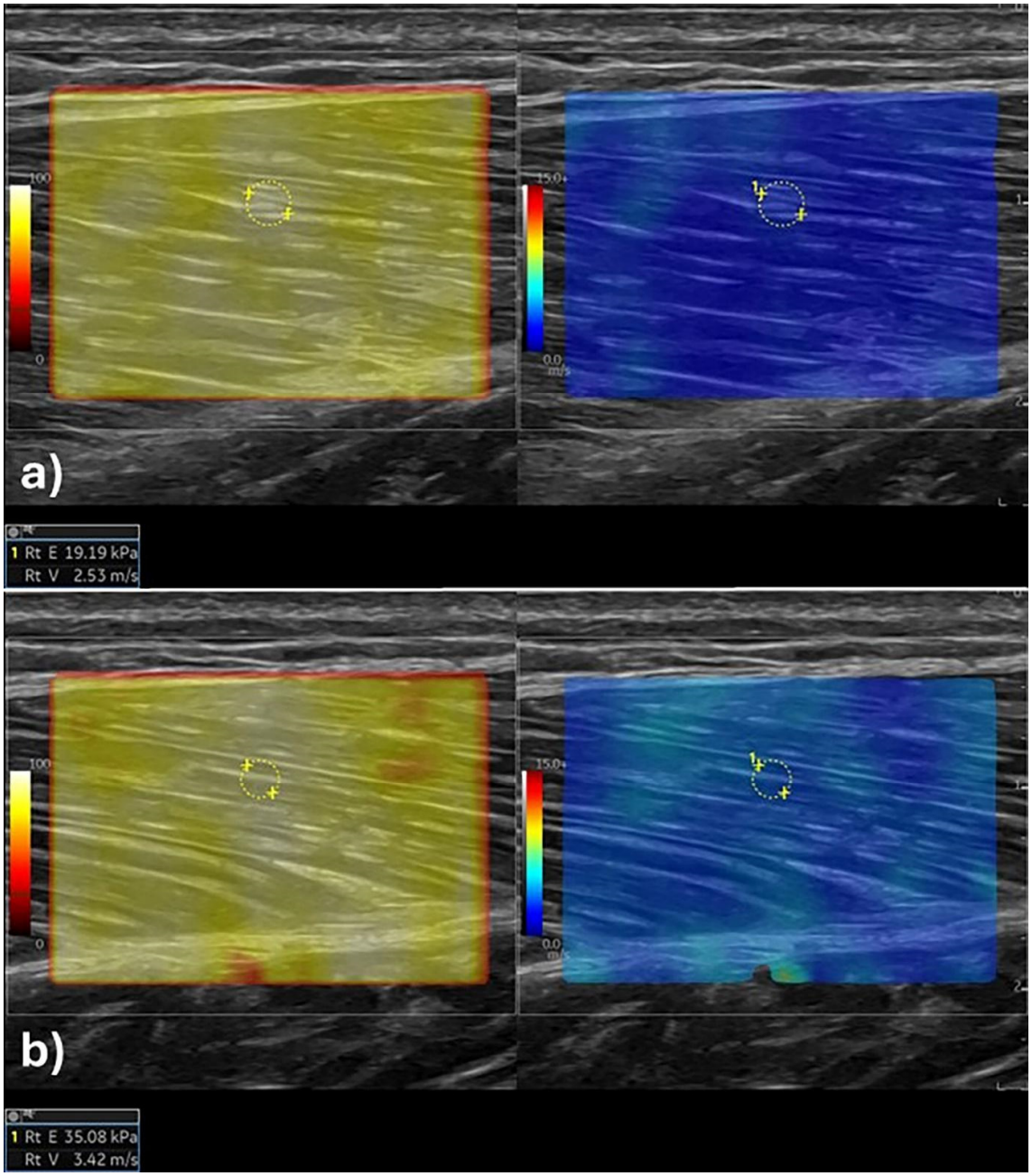

Fig.15.5. SWE performed on the medial gastrocnemius muscle in a longitudinal plane (a) at rest or relaxed with lower shear wave speeds and (b) during isometric contraction with higher shear wave speeds; the left side of the images represents color-coded confidence/quality maps, with maximum quality coded in white.

Tendons

Although conventional ultrasound is essential for tendon evaluation, its limitations in detecting only morphological changes have led to the adoption of new techniques like elastography. Elastography can detect microstructural changes and evaluate mechanical properties, which are critical indicators of early stages of tendinopathies. In tendon pathologies, collagen degeneration is a major factor, resulting over time in decreased elasticity (25,26). During the healing process, the inflammatory response can lead to development of regions of pathological fibrosis, thereby increasing elasticity values (27). Elastography is essential for detecting these changes, providing dynamic information about the mechanical properties of tendons during both degenerative and healing phases.

In the evaluation of tendons, most applications have focused on degenerative and traumatic tendinopathies, as well as monitoring their healing process. In recent years, both strain and shear wave elastography have been the subject of numerous studies, highlighting their importance and interest in this field (13,28).

Strain Elastography

Strain elastography uses manual compression applied to the tendon via the transducer to measure its degree of deformation. This technique illustrates how tissues with varying degrees of stiffness respond differently to the same applied force. Superficial tendons are most accessible to this technique as they allow efficient application of manual compression. Relevant examples include the Achilles tendon, patellar tendon, and the common extensor tendon of the elbow.

For optimal examination, the patient should be positioned to allow easy access to the evaluated tendon, similar to standard gray scale ultrasound practices for the examined regions. Ensuring the tendon is properly relaxed during the examination is essential for accurately assessing its response to applied pressure, as muscle tension can significantly alter the results. High-frequency linear transducers, ideally with a wider footprint, should be used to encompass the entire tendon or as much of it as possible. A mandatory condition for elastographic examination is obtaining a high-quality gray scale image. This step ensures clear visualization of the examined structure and surrounding tissues, facilitating precise application and accurate interpretation of elastographic data. The elastography map should be adjusted to a size large enough to include both the tendon and the surrounding reference tissue, usually adipose tissue (16). A sufficient amount of gel should be used to ensure proper contact with the skin, and the pressure applied with the transducer should be constant and gentle, enough to induce tissue deformation without causing excessive compression. The purpose is to create a subtle and measurable tension in the tendon to allow optimal evaluation of its elasticity, with the optimal pressure varying depending on the specific characteristics of the tendon and the patient (16,29). The transducer should be positioned so that the ultrasound beam aligns with the longitudinal axis of the tendon fibers to avoid anisotropy, as

this artifact negatively impacts the elastograms (12). It is recommended to record at least three cycles of compression-relaxation using the device's cineloop function and to verify the quality of compressions using the specific quality indicator for each device (12,29). This semi-quantitative technique involves comparing the elasticity of the examined tissue with that of a reference tissue.

Under normal conditions, the Achilles tendon evaluated by SE shows a predominantly uniform "hard" pattern, or and intermediate-"hard" mosaic (30-32). The patellar tendon exhibits a predominantly "hard" elasticity pattern (Fig.15.6). This specific elastography profile has been attributed to the anatomical characteristics of the tendon, which acts as a bridge between two bony structures, in contrast to other tendons that connect tissue and bone (33,34).

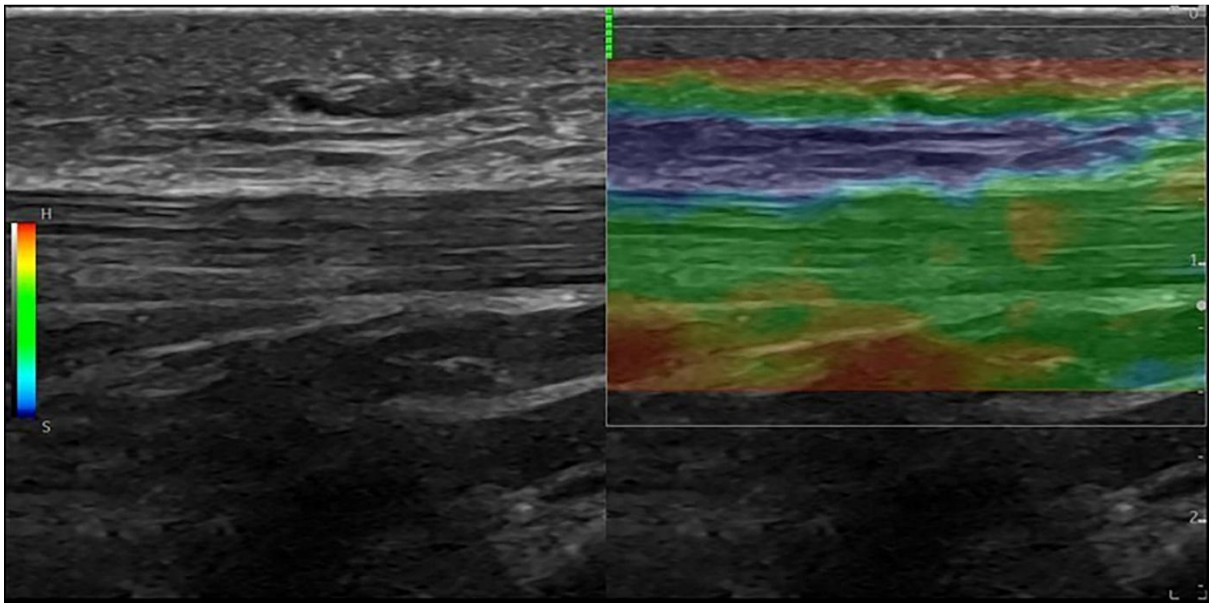

Fig.15.6. Strain elastography of the normal patellar tendon in the middle portion, demonstrating an elasticity pattern with an intermediate to "hard" appearance.

Shear-Wave Elastography

Although SE is a useful and accessible technique, it has certain limitations, particularly regarding objectivity and reproducibility. SWE addresses these constraints by providing a more objective and reproducible measurement of tissue elasticity, leveraging the quantifiable nature of shear waves to offer precise and reliable assessments of tissue stiffness. Despite the increasing attention and numerous publications on SWE in recent years, uncertainties remain about the optimal approach for tendon examination. Currently, the lack of standardization is the main obstacle to the uniform application of this method.

For the examination, general recommendations for performing elastography should be followed, but specific considerations for tendons must also be considered. The patient should be positioned similarly to SE, ensuring easy access to the tendon, followed by a relaxation of

at least 10 minutes to ensure complete muscle relaxation. Preferably, a high-frequency linear transducer with a footprint suitable for the examined tendon should be used. The transducer should be placed on the patient's skin with a sufficient amount of gel and minimal pressure should be applied. The elastography map should be adjusted to an appropriate size to fully encompass the tendon and surrounding tissue, and the ROI can be set to a variable size, provided it does not exceed the tendon's boundaries, as its size does not appear to influence the examination (35). Similar to SE, obtaining a gray scale image is an essential preliminary step, preferably in the longitudinal section of the tendon (Fig.15.7-9). This orientation is preferred due to the more efficient transmission of shear waves along its long axis (12,15). Anisotropy in this case is also an artifact that can significantly affect the quality of the obtained elastography map, therefore, the transducer positioning should be adjusted to minimize the occurrence of this artifact (12). It is recommended to perform at least three acquisitions to ensure the reliability of the results, however, the exact number is variable, and ideally, acquisitions should be repeated until a homogenous elastography map is obtained (15). Some equipment offers the ability to evaluate acquisition quality by overlaying a qualitative map on the gray scale image. Measurements taken near highly reflective structures, such as bones, should be interpreted with caution, as these regions are susceptible to the "bone proximity" artifact, recognized as a potential source of measurement errors (36).

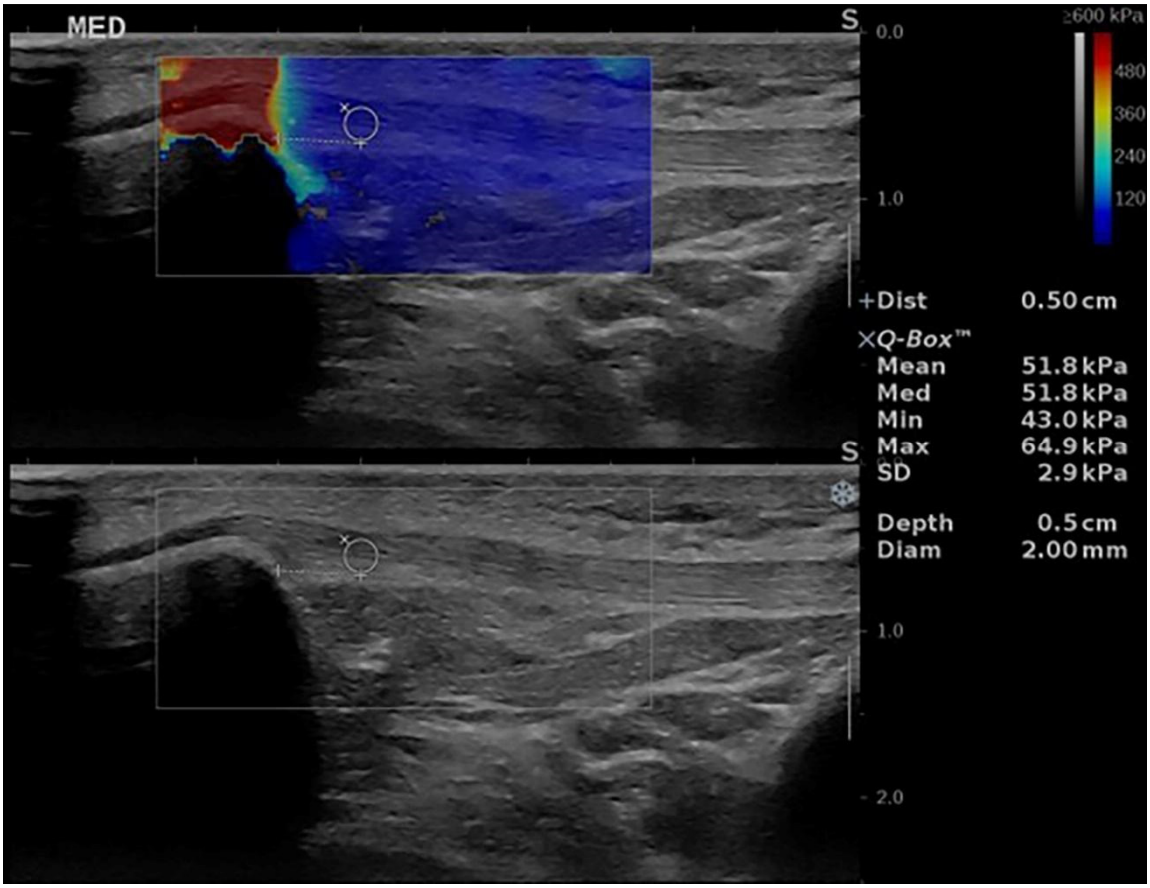

Fig.15.7. The normal SWE appearance of the patellar tendon at its proximal insertion, using a standardized distance from the patella.

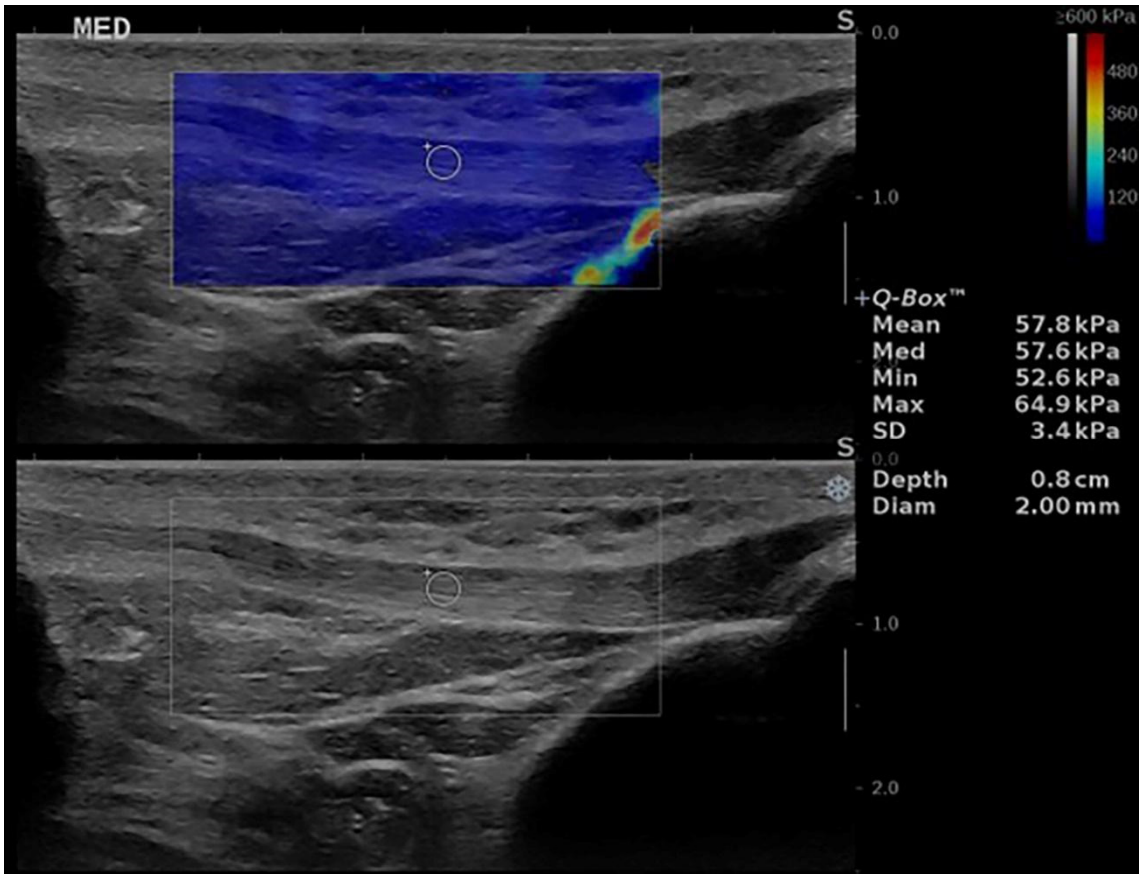

Fig.15.8. The normal SWE appearance of the patellar tendon in its middle third portion.

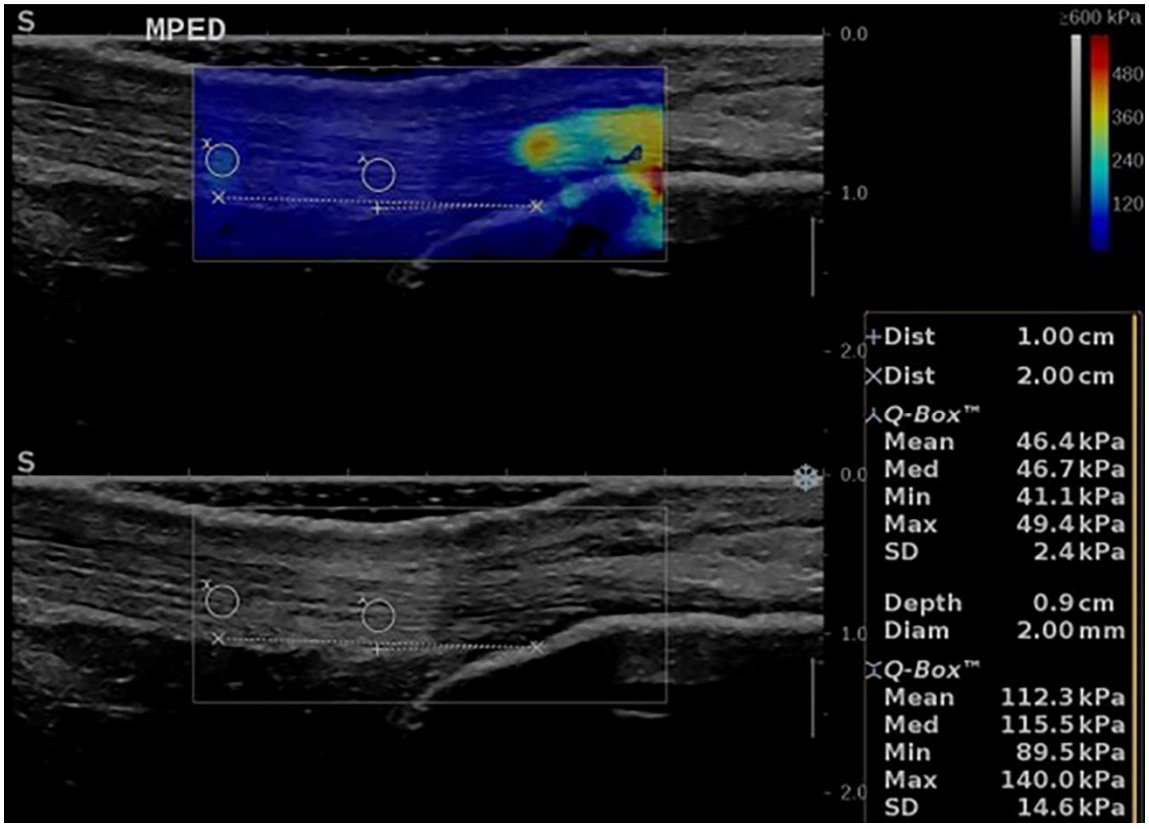

Fig.15.9. Evaluation of the normal Achilles tendon at its distal insertion using SWE, with measurements taken at a standardized distance from the calcaneus.

Although SWE does not have many of the limitations of SE and is considered to be more reliable, inconsistencies have been reported in the literature, especially for lower limb tendons (37). Additionally, establishing normal tendon elasticity values is challenging due to significant variability between studies, resulting from differences in equipment and methodologies. Due to their deformable nature, tendons show considerable variability in elasticity values, influenced by joint position and the degree of muscle contraction (35,38,39).

15.1.3. Reliability, Limitations and Artifacts

Strain Elastography

The reliability and reproducibility of SE are challenging due to the use of manual compression, which can influence tissue deformation based on the level of applied compression, the depth of different tissues, correct perpendicular alignment of the transducer with the structure of interest, and its movement outside the perpendicular plane. This results in a considerable operator dependency for this method. For the Achilles tendon, the reproducibility and validity of this method have been evaluated as moderate, the effectiveness of the procedure being influenced by the operator's experience, showing increased reliability in the hands of more experienced examiners (40).

Uneven, too gentle (Fig.15.10a), or too strong (Fig.15.10b) compression can distort elastograms, leading to incorrect elasticity calculations since tissue elasticity changes are nonlinear. Most manufacturers provide a visual compression indicator on the screen, offering real-time feedback on the compression level. This indicator must be maintained above a certain value (e.g. a "quality factor"> 60) or in a specific color (e.g. green) to ensure accurate measurements (9,13,14,16). Another issue with using SE in the musculoskeletal system is the presence of bony surfaces near the structures of interest or protuberant masses on the skin, which make compression with the transducer difficult or uneven (13,14).

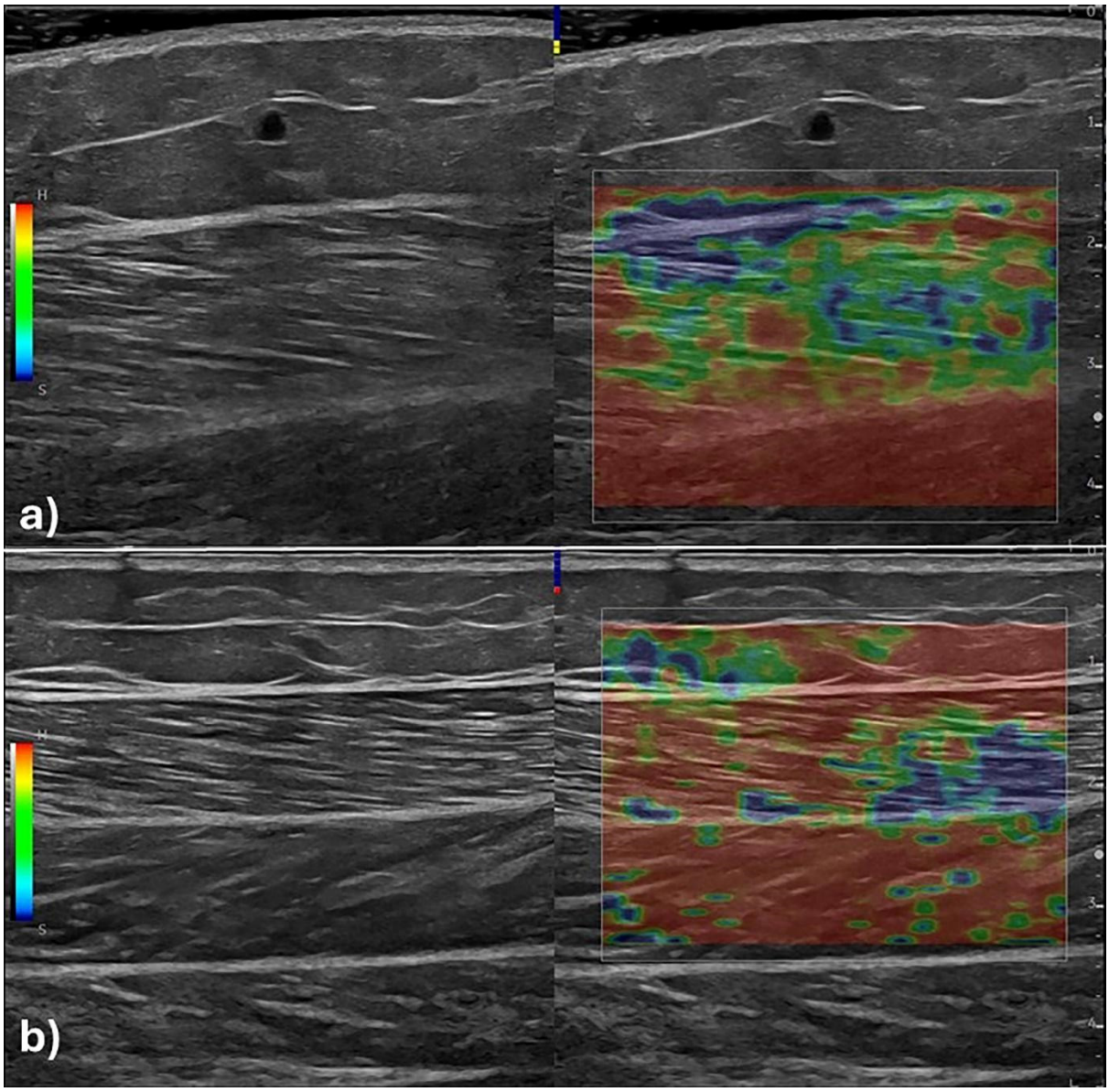

Fig.15.10. Strain elastograms of the relaxed lateral gastrocnemius muscle, in a longitudinal plane, showing altered appearances due to transducer compression that is (a) too gentle or (b) too strong. Quality indicators in red or yellow signal inadequate compression.

When comparing elastograms, the size of the elastogram and the tissues included must be considered. An elastogram is a relative image where the elasticity of each tissue is displayed in comparison to the average elasticity of all tissues in the examination. In musculoskeletal imaging, where tissues with different elasticities (bones, tendons, muscles, fat) are included in the same image, there is a greater variation in recorded elasticity values (13,14).

In some cases, musculoskeletal structures are positioned superficially, and certain ultrasound equipment requires a minimum distance, typically around 1-1.2 mm, between the transducer and the elastogram. To achieve this distance, gel pads or transducer adaptors can be used to increase the space between the transducer and the skin. In conventional musculo-skeletal ultrasound, a large amount of gel is commonly used. However, in elastography, special

care is needed because including a layer of gel in the elastogram can distort the results, and structures may appear much stiffer compared to the gel layer (Fig.15.11), potentially masking subtle changes in the elasticity of the structure of interest (12-14,17).

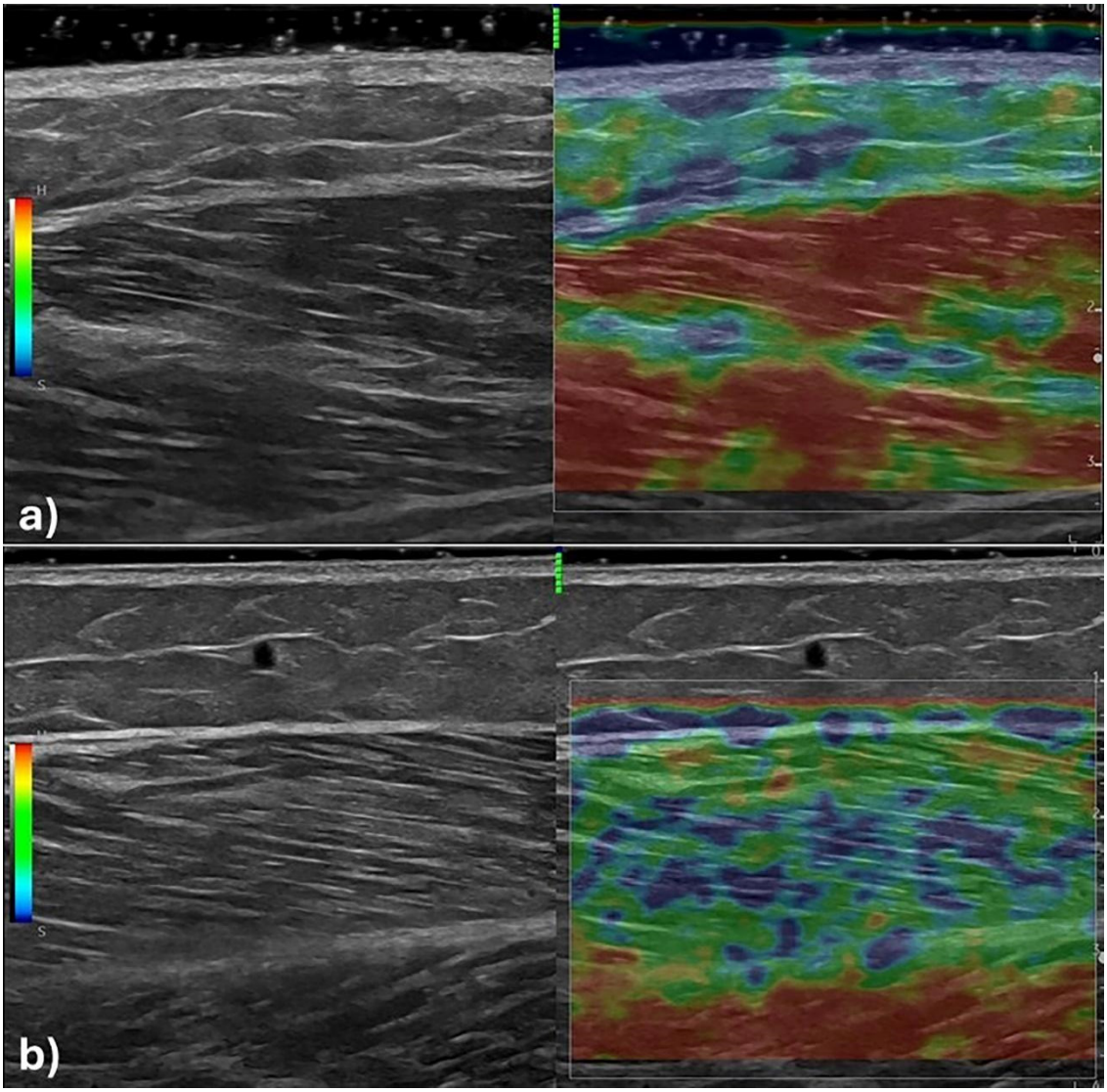

Fig.15.11. Strain elastogram of the relaxed lateral gastrocnemius muscle, in a longitudinal plane, showing (a) an altered appearance due to excessive ultrasound gel, with the gel included in the elastogram, resulting in the muscle appearance predominantly red and much stiffer compared to the included gel vs (b) a strain elastogram without the gel layer included, showing a normal muscle appearance. Green quality indicators signal adequate compression with the transducer.

There are several artifacts to consider when interpreting SE images in the musculoskeletal system: fluctuating values at the edges of elastograms or the medial and lateral margins of structures (Fig.15.12a,b), values indicating reduced rigidity (corresponding to a “soft” structure) around calcifications, bone structures (Fig.15.12c), the superficial edge of homogenous structures (e.g. lipomas), and at tissue interfaces (e.g. between adjacent muscles – Fig.15.12a). Other characteristic artifacts include those found in cystic masses, where a mosaic of colors corresponding to all levels of stiffness is created (often appearing as the BRG sign – Fig.15.12d – three layers of color: blue/green/red – or the “bull’s eye” artifact),

while artifacts can also occur in structures adjacent to large vessels, whose pulsations can influence elasticity measurements (12-14,16). When examining a rigid lesion within soft tissue, the soft tissue located above the rigid lesion will appear stiffer than the rest of the tissue adjacent to the lesion (16).

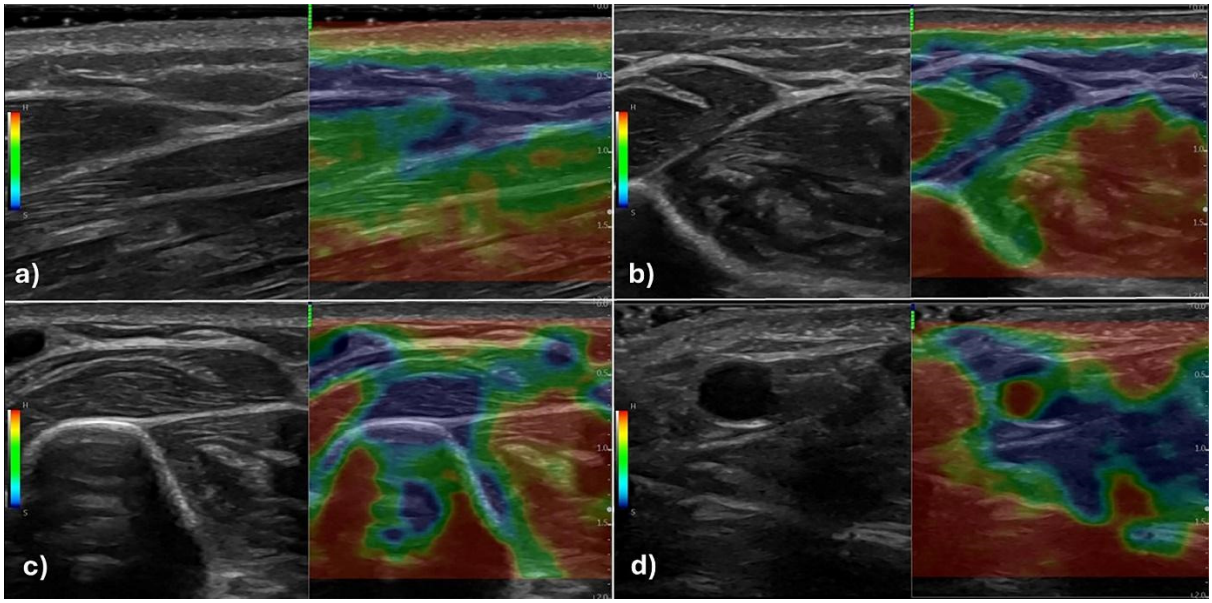

Fig.15.12. Artifacts in SE: (a) strain elastogram of the dorsal forearm in a longitudinal plane with areas of reduced stiffness (blue) at the interfaces between the two extensor muscles; (b) strain elastogram of the dorsal forearm in a transverse plane with areas of reduced stiffness (blue) at the medial and lateral edges of the extensor muscles; (c) strain elastogram of the dorsal forearm in a transverse plane with areas of reduced stiffness (blue) around the radius located on the left sides of the image; (d) strain elastogram reveals the BRG artifact at a superficial vein in transverse plane.

Shear-Wave Elastography

SWE operates under the assumption that tissues are elastic, incompressible, homogenous, and isotropic. However, soft tissues are generally viscoelastic, inhomogeneous, and anisotropic, possessing both elastic solid properties and viscous fluid properties, which can affect elasticity measurements. In reality, the elasticity of soft tissues is nonlinear and influenced by factors such as tissue density, deformation magnitude, and excitation frequency, a phenomenon known as dispersion (18,41).

When calculating Young's modulus to obtain elasticity measurements in kPa, it is assumed that the tissue density is constant (which is true for tissues such as the liver or thyroid). However, in the musculoskeletal system, tissues are heterogeneous and anisotropic, therefore, it is more accurate to report SWE measurements as the shear wave propagation speed in cm/s rather than Young's modulus in kPa (9,24). Ignoring the assumption of tissue homogeneity in the region of interest can generate artifacts and erroneous estimates of shear wave speed. These artifacts stem from wave reflections at the interfaces between structures, often resulting in a "soft center" artifact within very stiff lesions (18).

In addition to the heterogeneity of musculoskeletal tissues, the tissue of interest is often located above a bone structure, which poses another challenge for obtaining SWE measurements due to the artifacts produced by wave reflection at the bone interface (24), which some authors refer to as "bone proximity" artifacts (36). These artifacts appear as an inhomogeneity in SWE measurements on the elastogram within the same structure, with the alternating arrangement of linear zones of colors, almost parallel to each other, indicating low and high elasticity values. Moreover, areas indicating high rigidity are located above convex bony prominences, which some authors call "reflective corridors" (24). Since measurements can be influenced even in the areas between these "corridors", it is ideally preferred to change the patient's and/or the transducer's position as much as possible to minimize these artifacts (24).

In SWE, there is a trade-off between precision and spatial resolution in estimating shear wave propagation speed, such that using larger propagation distances ensures greater precision and accuracy but reduces spatial resolution. The reported resolution for SWE systems is 1-2 mm (18). This trade-off can impact the use of SWE in the musculoskeletal system, especially for superficial structures. While shorter distances may provide better spatial resolution for detecting changes in superficial musculoskeletal tissues, this can increase the variance in estimates at each pixel, affecting the precision of measurements. Moreover, when larger propagation distances are used for greater precision, the spatial resolution can be reduced, which may be insufficient for detecting subtle changes in deeper musculoskeletal structures (18). Studies have shown that variance within the ROI increases with depth, making measurements unreliable at depths of at least 4 cm (especially in structures comparable to contracted muscles and medium-sized tendons, and less so in structures comparable to relaxed muscles) (24) (Fig.15.13). Therefore, it is important to consider this balance and adapt the SWE technique according to the specific needs of each patient.

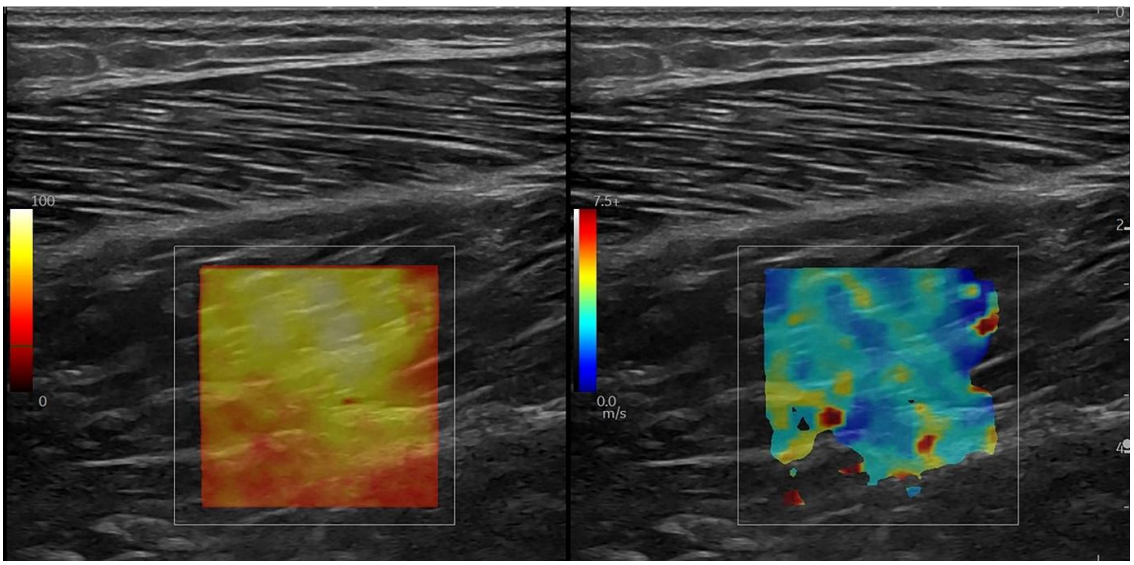

Fig.15.13. SWE of the relaxed medial gastrocnemius muscle in a longitudinal plane, with the elastography box positioned between 2 and 5 cm from the transducer surface. The elastogram shows a heterogeneous appearance and the absence of color with the box starting at approximately 4 cm depth. Additionally, the lower confidence/quality map (left side of the image) displays shades of red in the lower half, indicating reduced confidence of the elastographic measurements.

Like SE, artifacts can also occur in SWE. The “signal void area” artifact appears on the elastogram as a region where no elasticity measurements are recorded, and it appears black. Causes of this artifact include incorrect gray scale and SWE acquisition settings, the presence of fluid (which prevents shear wave propagation), a lesion that is too rigid (where propagation speed is too high to be measured), acoustic shadowing artifact, excessive depth of the structure being analyzed, or too low echogenicity (pseudo-cystic lesion) (10).

SWE is a reliable tool for assessing muscle stiffness, provided that the muscle examined in a relaxed state, and the force applied with the transducer is constant and minimal to avoid compromising the repeatability of measurements (18,42). Unlike SE, this method appears to be less operator-dependent and more dependent on the equipment used (43), in this case, reproducibility being ensured by using a standardized protocol and the same equipment for conducting measurements. The reproducibility and objectivity of SWE measurements make it a valuable tool for longitudinal studies and comparing muscle properties between different populations or within the same individual over time. As SWE technology becomes more widely available and integrated into clinical ultrasound system, its role in evaluating and managing muscle disorders is expected to grow, providing clinicians with a powerful tool to improve patient management (15,42).

15.2. Elastography in Musculoskeletal Diseases

15.2.1. Muscles

Muscle elasticity is influenced by a range of physiological factors (age, gender, muscle contraction, fatigue, physical exercise) and pathological factors (trauma, degenerative diseases, inflammatory conditions or neuromuscular disorders) (12).

Elastography detects even the smallest variations in elasticity from the onset of muscle contraction. Muscles in a relaxed/resting state show the lowest elasticity parameter values, with stiffness increasing as the degree of contraction increases (44) (Fig.15.3b). The elastogram during muscle contraction shows a heterogeneous pattern of colors, as the contraction of motor units is not synchronous. A similar effect of increased stiffness is also observed with passive stretching and twisting of the muscle (44). Muscle stiffness increases immediately after exertion, likely due to increased blood flow and capillary permeability (21,45), however, prolonged and intense exercise can lead to a reduction in muscle elasticity 48 hours post-exertion, most likely due to the onset of an inflammatory process and swelling within the muscle (41,46).

There is no consensus in the literature regarding the influence of age, gender, or sarcopenia on muscle elasticity, with studies providing contradictory results (9,47,48). This inconsistency may be partly due to the lack of standardization in examination techniques.

Examination of inflamed muscles (Fig.15.14) revealed a reduction in elasticity parameters in the presence of fatty infiltration (“softer” muscles) and an increase in these

parameters in the presence of fibrosis (“stiffer” muscles) (12,19,22,49). The existence of a positive correlation between quantitative elasticity parameters and the degree of histopathological changes, along with an association with serum muscle enzymes, demonstrates the utility of elastography in evaluating and monitoring the progression of inflammatory myopathies (12,19,49). The utility of elastography has also been suggested for guiding muscle biopsies (19). The heterogeneity of elastographic results in the literature, the variability of protocols used, the limited number of studies, and the lack of standardized examination make it impossible to draw a clear conclusion about the use of elastography as a measurement tool in inflammatory myopathies (50).

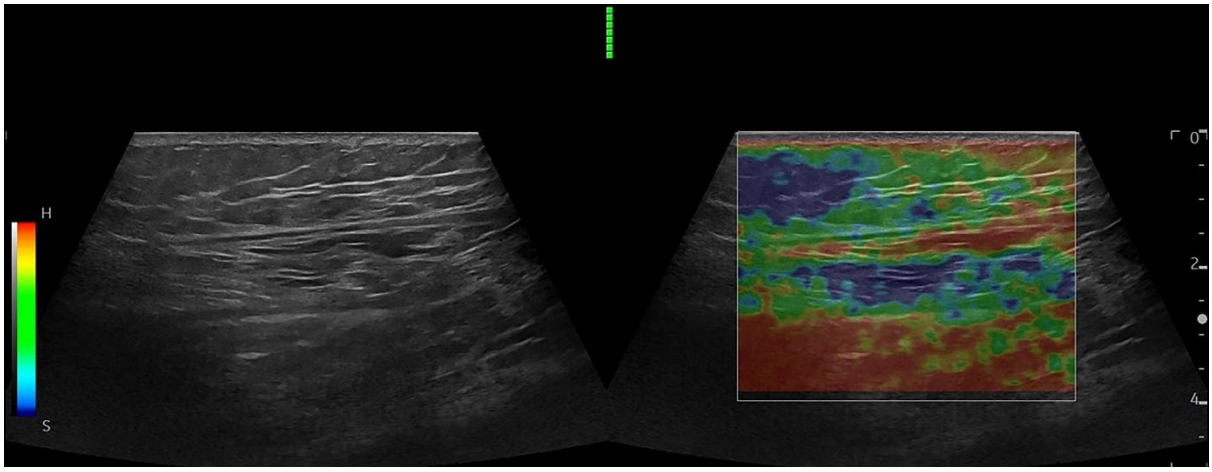

Fig.15.14. Strain elastogram of the relaxed rectus femoris muscle in a longitudinal plane, in a 21-year-old patient with dermatomyositis, demonstrates an altered mosaic appearance with extensive areas of increased stiffness (red) and areas of reduced stiffness (blue).

Muscle tears involve areas of hemorrhage within the examined muscle, which appear as very “soft”, homogeneous zones on SE. Over time, as healing occurs and fibrosis develops, these areas appear as rigid zones on SE (51).

The elastographic appearance of muscles has also been studied in neuromuscular diseases. Changes in muscle elasticity have been reported in congenital myopathies, for example, increased stiffness in Duchenne muscular dystrophy and reduced stiffness in GNE myopathy (44,52). The stiffness of spastic muscles in post-stroke patients, with multiple sclerosis, spinal cord injuries or cerebral palsy (neurological conditions causing contractures) is significantly higher than that of normal muscles, suggesting the utility of elastography in diagnosing, monitoring disease progression, and selecting appropriate therapies (e.g. choosing injection sites for botulinum toxin) (9,13,14,21,52,53). Increased muscle stiffness has also been detected in Parkinson’s disease compared to control groups (52).

15.2.2. Tendons

Tendon pathology alters their normal, fibrillar appearance and induces changes in their mechanical properties, resulting in variations of elasticity. Tendon pathology can arise from repetitive overuse or acute events where mechanical forces exceed the tendons' resistance to deformation (54).

In Achilles tendinopathy, the normal SE pattern is altered, with the appearance of "soft" areas (Fig.15.15) corresponding to degenerated regions visible on gray scale imaging (55-57). Elastography adds value by identifying "soft" areas in symptomatic patients, before these areas become visible on gray scale ultrasound. The strain ratio analysis using the pre-Achilles fat pad as reference has been proposed as a method for estimating the likelihood of tendinopathy in patients, even in the absence of detectable changes of gray scale ultrasound. A strain ratio value greater than 1, in an appropriate clinical context, suggests a higher probability of the presence of tendinopathy (58). However, it is not recommended to use this ratio as an absolute measure of deformation, but rather as a comparative index (40). The strain ratio values do not account for changes in pre-Achilles fat that can occur in patients with tendinopathy, a factor that can significantly influence the accuracy of this estimation (59).

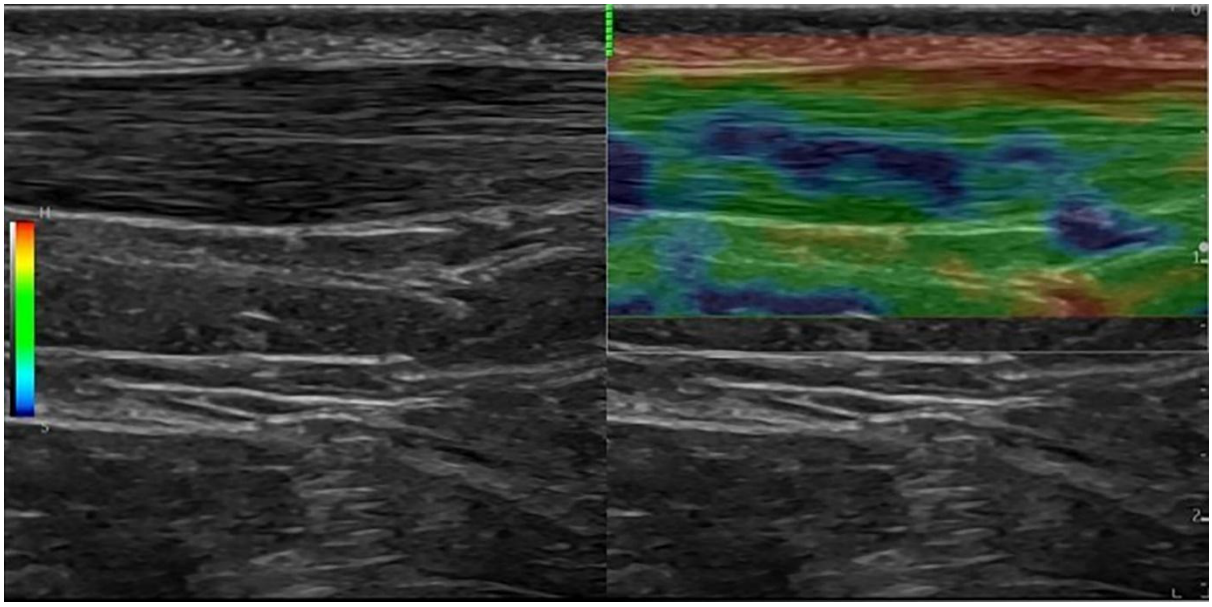

Fig.15.15. Strain elastography in a patient with mid-portion Achilles tendinopathy. The gray scale image reveals tendon thickening and the appearance of focal hypoechoic areas. The elastogram corresponds to these changes, highlighting focal "soft" areas.

The SE technique has also been used to monitor the healing process after surgical repair of Achilles tendon ruptures, but the benefits in this regard remain uncertain. It has been found that, in the initial phase after surgical repair, the tendon shows reduced elasticity; however, over time, it becomes stiffer compared to the contralateral side (60-62). Although SE allows for tracking changes in elasticity during the healing process, it has been observed that these changes do not correlate with the clinical evaluation scores of these patients (63).

In the evaluation of Achilles tendon pathologies, the combined use of SWE and gray scale ultrasonography has demonstrated a significant improvement in diagnostic accuracy (64,65). In the case of this technique, a reduction in shear wave propagation speed has been demonstrated in symptomatic tendons or those affected by tendinosis (65,66). Various studies have shown that tendon ruptures accompanied by hematomas or fluid collections lead to absence of signal on the elastography map, due to rapid dissipation of shear wave energy in the liquid medium (64,67,68). This makes evaluation using the SWE technique difficult, if not impossible. In a study by Coombes et al (65) on patients with tendinosis showed an increase in Achilles tendon thickness in the mid-portion compared to the insertion region (mid portion tendinopathy). Despite these morphological differences, the elasticity values measured by SWE in the mid-portion were comparable to those in the control group. In contrast, the insertion region showed a reduction in shear wave propagation speeds. These observations highlight the capability of this technique to identify patients at an early stage, who are at increased risk of tendon pathology.

Studies on the applicability of SE in patients with patellar tendinopathy have revealed that the tendon exhibits reduced stiffness. This elastographic aspect correlates better with the clinical evaluation scores of patients compared to identifying hypoechoic areas in gray scale ultrasound images (69,70). However, data regarding changes in this region are conflicting, as other authors have reported increased stiffness in studies using SWE elastography (65,71,72). Evaluation of patients with patellar tendinopathy using SWE has yielded conflicting results. Three studies demonstrated increased tendon stiffness, particularly in the proximal region, correlating with both clinical scores and gray scale changes, and reported high reproducibility (65,71,72). Another study using the same technique reported a decrease in stiffness in symptomatic patients (66). The origin of these discrepancies remains unclear, but methodological differences between studies might offer an explanation. It has been demonstrated that elasticity values are influenced by numerous factors, one of the most significant being the degree of flexion (35).

In the evaluation of epicondylitis, SE has been successfully used. The main pathogenic mechanism behind its development is repetitive microtrauma, which over time leads to the progressive degeneration of the tendon (73). Although gray scale ultrasound can identify changes as focal hypoechoic areas, these changes are not always detectable with this method (68). SE can detect affected areas by highlighting “soft” regions on the elastography map and decreasing strain ratio values, even when changes are not visible on gray scale ultrasound (28,56,74-76). Combining SE with traditional ultrasound significantly improves diagnostic accuracy (68,77). SWE has proven effective in evaluating both lateral and medial epicondylitis, offering a high sensitivity and specificity in diagnosing these conditions. Studies have shown a reduction in elasticity values in affected tendons compared to asymptomatic tendons or control groups, and the method has demonstrated good to excellent reproducibility (66,78,79).

Among the rotator cuff tendons, the supraspinatus tendon has garnered the most interest for elastographic evaluation, and the observed changes appear to correlate well with those obtained through MRI (80-82). The changes observed in SE for tendinopathies and ruptures in the supraspinatus tendon are similar to those in other regions discussed. These changes are manifested on the elastogram as a globally heterogeneous profile, characterized by the presence of focal “soft” areas (81-83). This technique has also been proposed for preoperative screening, aiding in patient selection, assessing the necessity of surgical intervention, and evaluating the degree of fatty infiltration and muscle atrophy, these factors being crucial in predicting postoperative outcomes (68). Lastly, elastography has been successfully used in patients with calcific tendinitis to predict symptomatic improvement after aspiration treatment (84). For the evaluation of the shoulder using SWE, a study (85) revealed that elasticity values did not significantly correlate with the symptoms of patients affected by rotator cuff tendon degeneration. However, the same study found a connection between decreased elasticity of the deltoid muscle and the severity of tendinopathy as seen on gray scale imaging. Studies on patients with idiopathic adhesive capsulitis have shown an increase in the elasticity of the rotator cuff tendons compared to the unaffected side and healthy subjects (86,87). In these studies, it was proposed that measuring elasticity could be useful not only for diagnostic purposes but also for predicting the development of this pathology.

In summary, advancements in elastography for evaluating muscles and tendons are significant, but notable limitations persist. SWE is more quantifiable, reproducible, and objective compared to SE, yet it suffers from a lack of standardization and an unclear role in diagnosing musculoskeletal conditions. Effective integration into clinical practice requires focused research efforts to develop standardized protocols, which would significantly enhance the applicability of the musculoskeletal system.

References

1. Fodor D. Semiologia normala si patologica (leziuni de baza) a structurilor musculoscheletale. Muschii. In: Fodor D, editor. Ecografie musculoscheletala - Volum I - Semiologia normală si patologica a structurilor musculoscheletale. I. Bucuresti: Librex Publishing; 2017. p. 25 - 36.
2. Ashir A, Jerban S, Barrere V, et al. Skeletal Muscle Assessment Using Quantitative Ultrasound: A Narrative Review. Sensors (Basel). 2023;23.
3. Thorpe CT, Screen HR. Tendon Structure and Composition. Adv Exp Med Biol. 2016;920:3-10.
4. Benjamin M, Kaiser E, Milz S. Structure-function relationships in tendons: a review. J Anat. 2008;212:211-28.
5. Hodgson RJ, O'Connor PJ, Grainger AJ. Tendon and ligament imaging. Br J Radiol. 2012;85:1157-72.
6. Tadros AS, Huang BK, Pathria MN. Muscle-Tendon-Enthesis Unit. Semin Musculoskelet Radiol. 2018;22:263-74.

7. Connolly DJ, Berman L, McNally EG. The use of beam angulation to overcome anisotropy when viewing human tendon with high frequency linear array ultrasound. Br J Radiol. 2001;74:183-5.
8. Lin DC, Nazarian LN, O'Kane PL, et al. Advantages of Real-Time Spatial Compound Sonography of the Musculoskeletal System Versus Conventional Sonography. American Journal of Roentgenology. 2002;179:1629-31.
9. Snoj Z, Wu CH, Taljanovic MS, et al. Ultrasound Elastography in Musculoskeletal Radiology: Past, Present, and Future. Semin Musculoskelet Radiol. 2020;24:156-66.
10. Bouchet P, Gennisson JL, Podda A, et al. Artifacts and Technical Restrictions in 2D Shear Wave Elastography. Ultraschall Med. 2020;41:267-77.
11. Ferraioli G, Barr RG, Farrokh A, et al. How to perform shear wave elastography. Part II. Med Ultrason. 2022;24:196-210.
12. Săftoiu A, Gilja OH, Sidhu PS, et al. The EFSUMB Guidelines and Recommendations for the Clinical Practice of Elastography in Non-Hepatic Applications: Update 2018. Ultraschall Med. 2019;40:425-53.
13. Drakonaki E. Ultrasound elastography for imaging tendons and muscles. J Ultrason. 2012;12:214-25.
14. Drakonaki EE, Allen GM, Wilson DJ. Ultrasound elastography for musculoskeletal applications. Br J Radiol. 2012;85:1435-45.
15. Taljanovic MS, Gimber LH, Becker GW, et al. Shear-Wave Elastography: Basic Physics and Musculoskeletal Applications. Radiographics. 2017;37:855-70.
16. Dietrich CF, Barr RG, Farrokh A, et al. Strain Elastography - How To Do It? Ultrasound Int Open. 2017;3:E137-E49.
17. Cosgrove D, Piscaglia F, Bamber J, et al. EFSUMB guidelines and recommendations on the clinical use of ultrasound elastography. Part 2: Clinical applications. Ultraschall Med. 2013;34:238-53.
18. Shiina T, Nightingale KR, Palmeri ML, et al. WFUMB guidelines and recommendations for clinical use of ultrasound elastography: Part 1: basic principles and terminology. Ultrasound Med Biol. 2015;41:1126-47.
19. Botar-Jid C, Damian L, Dudea SM, et al. The contribution of ultrasonography and sonoelastography in assessment of myositis. Med Ultrason. 2010;12:120-6.
20. Park GY, Kwon DR. Application of real-time sonoelastography in musculoskeletal diseases related to physical medicine and rehabilitation. Am J Phys Med Rehabil. 2011;90:875-86.
21. Winn N, Lalam R, Cassar-Pullicino V. Sonoelastography in the musculoskeletal system: Current role and future directions. World J Radiol. 2016;8:868-79.
22. Paluch L, Nawrocka-Laskus E, Wieczorek J, et al. Use of Ultrasound Elastography in the Assessment of the Musculoskeletal System. Pol J Radiol. 2016;81:240-6.
23. Ferraioli G, Barr RG, Farrokh A, et al. How to perform shear wave elastography. Part I. Med Ultrason. 2022;24:95-106.
24. Davis LC, Baumer TG, Bey MJ, et al. Clinical utilization of shear wave elastography in the musculoskeletal system. Ultrasonography. 2019;38:2-12.
25. Kader D, Saxena A, Movin T, et al. Achilles tendinopathy: some aspects of basic science and clinical management. Br J Sports Med. 2002;36:239-49.
26. Sharma P, Maffulli N. Biology of tendon injury: healing, modeling and remodeling. J Musculoskelet Neuronal Interact. 2006;6:181-90.

27. Nichols AEC, Best KT, Loiselle AE. The cellular basis of fibrotic tendon healing: challenges and opportunities. Transl Res. 2019;209:156-68.
28. Rossetto G, Scalona E, Comotti P, et al. Ultrasound Elastography in the Evaluations of Tendon-Related Disorders—A Systematic Review. Applied Sciences. 2023;13:4920.
29. Klauser AS, Faschingbauer R, Jaschke WR. Is sonoelastography of value in assessing tendons? Semin Musculoskelet Radiol. 2010;14:323-33.
30. Drakonaki EE, Allen GM, Wilson DJ. Real-time ultrasound elastography of the normal Achilles tendon: reproducibility and pattern description. Clin Radiol. 2009;64:1196-202.
31. De Zordo T, Chhem R, Smekal V, et al. Real-time sonoelastography: findings in patients with symptomatic achilles tendons and comparison to healthy volunteers. Ultraschall Med. 2010;31:394-400.
32. Dilip D, Khaladkar SM, Chanabasanavar V, et al. REAL-TIME strain elastography: Applications in musculoskeletal system. J Clin Orthop Trauma. 2022;26:101784.
33. Porta F, Damjanov N, Galluccio F, et al. Ultrasound elastography is a reproducible and feasible tool for the evaluation of the patellar tendon in healthy subjects. Int J Rheum Dis. 2014;17:762-6.
34. Ozcan AN, Tan S, Tangal NG, et al. Real-time sonoelastography of the patellar and quadriceps tendons: pattern description in professional athletes and healthy volunteers. Med Ultrason. 2016;18:299-304.
35. Pelea MA, Serban O, Badarinza M, et al. Factors influencing the Shear Wave Elastography evaluation of the patellar tendon. Med Ultrason. 2023;25:145-52.
36. Bortolotto C, Turpini E, Felisaz P, et al. Median nerve evaluation by shear wave elastosonography: impact of "bone-proximity" hardening artifacts and inter-observer agreement. J Ultrasound. 2017;20:293-9.
37. Schneebeli A, Folli A, Falla D, et al. Reliability of Sonoelastography Measurements of Lower Limb Tendon Properties: A Systematic Review. Ultrasound Med Biol. 2021;47:1131-50.
38. Pearson SJ, Mohammed ASA, Hussain SR. Patellar tendon in vivo regional strain with varying knee angle. J Biomech. 2017;61:45-50.
39. Schneebeli A, Fiorina I, Bortolotto C, et al. Shear wave and strain sonoelastography for the evaluation of the Achilles tendon during isometric contractions. Insights Imaging. 2021;12:26.
40. Mifsud T, Gatt A, Micallef-Stafrace K, et al. Elastography in the assessment of the Achilles tendon: a systematic review of measurement properties. J Foot Ankle Res. 2023;16:23.
41. Ryu J, Jeong WK. Current status of musculoskeletal application of shear wave elastography. Ultrasonography. 2017;36:185-97.
42. Sarabon N, Kozinc Z, Podrekar N. Using shear-wave elastography in skeletal muscle: A repeatability and reproducibility study on biceps femoris muscle. PLoS One. 2019;14:e0222008.
43. Vuorenmaa AS, Siitama EMK, Makela KS. Inter-operator and inter-device reproducibility of shear wave elastography in healthy muscle tissues. J Appl Clin Med Phys. 2022;23:e13717.
44. Creze M, Nordez A, Soubeyrand M, et al. Shear wave sonoelastography of skeletal muscle: basic principles, biomechanical concepts, clinical applications, and future perspectives. Skeletal Radiol. 2018;47:457-71.

45. Dankel SJ, Razzano BM. The impact of acute and chronic resistance exercise on muscle stiffness: a systematic review and meta-analysis. J Ultrasound. 2020;23:473-80.
46. Andonian P, Viallon M, Le Goff C, et al. Shear-Wave Elastography Assessments of Quadriceps Stiffness Changes prior to, during and after Prolonged Exercise: A Longitudinal Study during an Extreme Mountain Ultra-Marathon. PLoS One. 2016;11:e0161855.
47. Janczyk EM, Champigny N, Michel E, et al. Sonoelastography to Assess Muscular Stiffness Among Older Adults and its Use for the Diagnosis of Sarcopenia: A Systematic Review. Ultraschall Med. 2021;42:634-42.
48. Stiver ML, Mirjalili SA, Agur AMR. Measuring Shear Wave Velocity in Adult Skeletal Muscle with Ultrasound 2-D Shear Wave Elastography: A Scoping Review. Ultrasound Med Biol. 2023;49:1353-62.
49. Song Y, Lee S, Yoo DH, et al. Strain sonoelastography of inflammatory myopathies: comparison with clinical examination, magnetic resonance imaging and pathologic findings. Br J Radiol. 2016;89:20160283.
50. Paramalingam S, Morgan K, Becce F, et al. Conventional ultrasound and elastography as imaging outcome tools in autoimmune myositis: A systematic review by the OMERACT ultrasound group. Semin Arthritis Rheum. 2021;51:661-76.
51. Botar Jid C, Vasilescu D, Damian L, et al. Musculoskeletal sonoelastography. Pictorial essay. Med Ultrason. 2012;14:239-45.
52. Miller T, Ying M, Sau Lan Tsang C, et al. Reliability and Validity of Ultrasound Elastography for Evaluating Muscle Stiffness in Neurological Populations: A Systematic Review and Meta-Analysis. Phys Ther. 2021;101.
53. Bilston LE, Tan K. Measurement of passive skeletal muscle mechanical properties in vivo: recent progress, clinical applications, and remaining challenges. Ann Biomed Eng. 2015;43:261-73.
54. Wu F, Nerlich M, Docheva D. Tendon injuries: Basic science and new repair proposals. EFORT Open Rev. 2017;2:332-42.
55. Klauser AS, Miyamoto H, Tamegger M, et al. Achilles tendon assessed with sonoelastography: histologic agreement. Radiology. 2013;267:837-42.
56. Galletti S, Oliva F, Masiero S, et al. Sonoelastography in the diagnosis of tendinopathies: an added value. Muscles Ligaments Tendons J. 2015;5:325-30.
57. Kandil NM, Abdelkarim MA, Abdelwahab NM, et al. In Achilles Tendon Disorders, Will Sonoelastography Add to Grey-Scale Ultrasound? Using MRI as Gold Standard. Indian J Radiol Imaging. 2021;31:350-9.
58. Ooi CC, Schneider ME, Malliaras P, et al. Diagnostic performance of axial-strain sonoelastography in confirming clinically diagnosed Achilles tendinopathy: comparison with B-mode ultrasound and color Doppler imaging. Ultrasound Med Biol. 2015;41:15-25.
59. Pingel J, Petersen MC, Fredberg U, et al. Inflammatory and Metabolic Alterations of Kager's Fat Pad in Chronic Achilles Tendinopathy. PLoS One. 2015;10:e0127811.
60. Busilacchi A, Olivieri M, Ulisse S, et al. Real-time sonoelastography as novel follow-up method in Achilles tendon surgery. Knee Surg Sports Traumatol Arthrosc. 2016;24:2124-32.
61. Tan S, Kudaş S, Özcan AS, et al. Real-time sonoelastography of the Achilles tendon: pattern description in healthy subjects and patients with surgically repaired complete ruptures. Skeletal Radiol. 2012;41:1067-72.

62. Ciloglu O, Görgülü FF. Evaluation of a Torn Achilles Tendon After Surgical Repair: An Ultrasound and Elastographic Study With 1-Year Follow-up. J Ultrasound Med. 2020;39:1263-9.
63. Çetin M, Sökmen BK, Fidan F, et al. HOW USEFUL IS ELASTOGRAPHY IN THE FOLLOW-UP OF ACHILLES TENDON REPAIR? Acta Ortop Bras. 2022;30:e246613.
64. Aubry S, Nueffer JP, Tanter M, et al. Viscoelasticity in Achilles tendonopathy: quantitative assessment by using real-time shear-wave elastography. Radiology. 2015;274:821-9.
65. Coombes BK, Tucker K, Vicenzino B, et al. Achilles and patellar tendinopathy display opposite changes in elastic properties: A shear wave elastography study. Scand J Med Sci Sports. 2018;28:1201-8.
66. Dirrichs T, Quack V, Gatz M, et al. Shear Wave Elastography (SWE) for the Evaluation of Patients with Tendinopathies. Acad Radiol. 2016;23:1204-13.
67. Chen XM, Cui LG, He P, et al. Shear wave elastographic characterization of normal and torn achilles tendons: a pilot study. J Ultrasound Med. 2013;32:449-55.
68. Prado-Costa R, Rebelo J, Monteiro-Barroso J, et al. Ultrasound elastography: compression elastography and shear-wave elastography in the assessment of tendon injury. Insights Imaging. 2018;9:791-814.
69. Ooi CC, Richards PJ, Maffulli N, et al. A soft patellar tendon on ultrasound elastography is associated with pain and functional deficit in volleyball players. J Sci Med Sport. 2016;19:373-8.
70. Rist HJ, Mauch M. [Quantified TDI elastography of the patellar tendon in athletes]. Sportverletz Sportschaden. 2012;26:27-32.
71. Breda SJ, van der Vlist A, de Vos RJ, et al. The association between patellar tendon stiffness measured with shear-wave elastography and patellar tendinopathy-a case-control study. Eur Radiol. 2020;30:5942-51.
72. Zhang ZJ, Ng GY, Lee WC, et al. Changes in morphological and elastic properties of patellar tendon in athletes with unilateral patellar tendinopathy and their relationships with pain and functional disability. PLoS One. 2014;9:e108337.
73. Vaquero-Picado A, Barco R, Antuña SA. Lateral epicondylitis of the elbow. EFORT Open Rev. 2016;1:391-7.
74. De Zordo T, Lill SR, Fink C, et al. Real-time sonoelastography of lateral epicondylitis: comparison of findings between patients and healthy volunteers. AJR Am J Roentgenol. 2009;193:180-5.
75. Shin M, Hahn S, Yi J, et al. Clinical Application of Real-Time Sonoelastography for Evaluation of Medial Epicondylitis: A Pilot Study. Ultrasound Med Biol. 2019;45:246-54.
76. Arslan S, Karahan AY, Oncu F, et al. Diagnostic Performance of Superb Microvascular Imaging and Other Sonographic Modalities in the Assessment of Lateral Epicondylosis. J Ultrasound Med. 2018;37:585-93.
77. Park G, Kwon D, Park J. Diagnostic confidence of sonoelastography as adjunct to greyscale ultrasonography in lateral elbow tendinopathy. Chin Med J (Engl). 2014;127:3110-5.
78. Zhu B, You Y, Xiang X, et al. Assessment of common extensor tendon elasticity in patients with lateral epicondylitis using shear wave elastography. Quant Imaging Med Surg. 2020;10:211-9.
79. Bang JY, Hahn S, Yi J, et al. Clinical applicability of shear wave elastography for the evaluation of medial epicondylitis. Eur Radiol. 2021;31:6726-35.

80. Seo JB, Yoo JS, Ryu JW. Sonoelastography findings of supraspinatus tendon in rotator cuff tendinopathy without tear: comparison with magnetic resonance images and conventional ultrasonography. J Ultrasound. 2015;18:143-9.
81. Vasishta A, Kelkar A, Joshi P, et al. The value of sonoelastography in the diagnosis of supraspinatus tendinopathy-a comparison study. Br J Radiol. 2019;92:20180951.
82. Frere R, Libda I, Tantawy F, et al. Sonoelastography, conventional ultrasound and magnetic resonance imaging in detection of rotator cuff lesions in patients with chronic shoulder pain. The Egyptian Rheumatologist. 2021;43:17-21.
83. Tudisco C, Bisicchia S, Stefanini M, et al. Tendon quality in small unilateral supraspinatus tendon tears. Real-time sonoelastography correlates with clinical findings. Knee Surg Sports Traumatol Arthrosc. 2015;23:393-8.
84. Lin Y-H, Chiou H-J, Wang H-K, et al. Management of rotator cuff calcific tendinosis guided by ultrasound elastography. Journal of the Chinese Medical Association. 2015;78:603-9.
85. Hou SW, Merkle AN, Babb JS, et al. Shear Wave Ultrasound Elastographic Evaluation of the Rotator Cuff Tendon. J Ultrasound Med. 2017;36:95-106.
86. Yun SJ, Jin W, Cho NS, et al. Shear-Wave and Strain Ultrasound Elastography of the Supraspinatus and Infraspinatus Tendons in Patients with Idiopathic Adhesive Capsulitis of the Shoulder: A Prospective Case-Control Study. kjr. 2019;20:1176-85.
87. Wada T, Itoigawa Y, Yoshida K, et al. Increased Stiffness of Rotator Cuff Tendons in Frozen Shoulder on Shear Wave Elastography. J Ultrasound Med. 2020;39:89-97.

Chapter 16. Magnetic Resonance Elastography of the Liver

Nuran Seneviratne, Cheng Fang, Paul S. Sidhu

Introduction

Magnetic resonance elastography (MRE) was first described by Muthupillai et. al. in gel materials in 1995[1], it has undergone various technical refinements into a clinically applicable modality which provides a robust, large field-of-view elastography method which has been used to assess liver stiffness (Liver Stiffness Measurement – LSM). We will discuss the physics underpinning the technique, the practical element of performing the liver MRE examination, how to interpret MRE study including its performance and its clinical utility. Ultrasound based quantitative elastography is an established method for assessing the degree of liver fibrosis in patients with chronic liver disease. Therefore, comparisons with ultrasound-based techniques are frequently commented on in this chapter.

Physics

Elastography is fundamentally the study of the ability of a material to return to its original shape after an external force is transiently applied. In essence, it is an extension of clinical palpation, which determines how 'stiff' a tissue by the subjective feedback felt by the clinician after application of force from their hand. Stiffness is one of the characteristics used to differentiate normal and pathological tissue. However, this material property cannot be measured directly in vivo, and therefore shear wave velocity are measured as a surrogate marker of stiffness. Shear waves oscillate perpendicular to the direction of the applied force (i.e. side to side), in contrast to the parallel movement of pressure waves (i.e. back and forward). Pressure waves travel significantly faster than shear waves (approximately 1500m/s compared to 1-10m/s respectively). Shear wave velocities are higher in stiffer tissues, and this relationship underpins modern elastography techniques.

Several parameters can be determined, including shear wave speed (in m/s), the complex shear modulus, G^* (in kilopascals) and Young elastic modulus, E (in kilopascals, also referred to as 'elasticity'). Complex shear modulus depicts the tissue behaviour when under shear (side to side) stress, whereas Young modulus describes behaviour in relation to the longitudinal pressure wave. Biological tissue is viscoelastic, in that it not only stores energy to returns to its original shape (like a spring), but also absorbs energy and may even irreversibly deform (like honey or wax), termed viscosity. Therefore, G* is a function of the elastic component, the storage modulus, G', and the viscous component, the loss modulus, G''. Therefore, in combination with another derived parameters, namely the damping ratio ζ, which corresponds to the viscosity to elasticity ratio, viscosity assessment can be undertaken. This has potential clinical utility as a way of discriminating raised tissue stiffness due to irreversible fibrosis, from more dynamic processes such as inflammation and haemodynamic

changes in tissue (such as portal and hepatic venous hypertension), however this remains a pre-clinical tool currently[2].

Ultrasound elastography measures shear wave velocity or *E* by tracking the motion of shear waves from an insonated region of interest, however MR techniques generally report the magnitude of *G**, termed shear stiffness. Young modulus is approximately three times the shear modulus, assuming incompressibility[3,4]. This difference in measured parameters means ultrasound and MRE derived stiffness measurements are not interchangeable.

Whichever modality is used, the fundamental sequence of elastography is as follows; imaging of areas of interest, produce shear waves, track shear waves and measure the tissue response from external forces.

Imaging area of interest

In MRE, raw data is obtained by magnitude and phase images commonly using a two-dimensional gradient recalled-echo MR elastography sequence (2D GRE MRE), however spin-echo echo-planar imaging-based MRE (SE- EPI-MRE) is also commonly used, which is less sensitive to liver iron content and may have shorted acquisition times [5]. Anatomical information is provided by the magnitude images, with phase images producing information on shear wave motion. Conventionally, four slices of 5-10mm thick are placed in the widest part of the liver to obtain four elastograms (Figure 1).

Production of Shear Waves

Shear wave production in MRE requires applying a continuous mechanical force to tissue, which is unique to this modality. Transient elastography (e.g. Fibroscan™, Echosens, Paris) also uses an external mechanical force, however, is transient (a short 'thump'). Ultrasound based elastography focuses ultrasonic waves on an area of interest (acoustic radiation force impulse, ARFI) on a single small region of interest (point shear wave elastography), or a limited area of interest (shear wave imaging, or two-dimensional shear wave elastography), again in a temporary fashion. Oscillations of the external mechanical force produces a pressure wave which passes rapidly through the tissue and dissipates energy, some of which is released in the form of shear waves. The fixed external oscillation frequency allows the produced shear wave frequency to be more accurately controlled. This is important, as stiffness measurements are frequency dependant, with higher frequencies giving higher readings[6]. Field strength does not impact stiffness measurements, therefore 1.5T and 3T systems can produce interchangeable results[7]. In MRE, there is a requirement for continuous vibration as shear wave spacial encoding is undertaken over multiple wave cycles, so MR cannot measure transient shear waves unlike ultrasound (echo-return of echo sequence).

Practically, several methods can be used to produce this external continuous mechanical force. Pneumatic actuators are used in commercial MRE systems, where an active

driver (Figure 2) outside of the scan room produces generates waves like a 'sub-woofer' and transmits this compression wave via tubing to a MR compatible passive actuator which is secured on the patient's body[8] (Figure 3). An electromechanical device outside of the field of view can oscillate based on the alternating current that can be produced by the B0 field, the static magnetic field (conventionally 1.5 or 3T) and was used by the prototypical MRE system generating waves in agar gel[1]. As in ultrasound wave generation, a piezoelectric actuator oscillates when current is applied, and is used in animal model research.

The frequency of the shear waves in commercial MRE systems is 60 Hz, which gives sufficient penetration whilst still producing measurable shear waves, however 20-100 Hz systems are available[9]. Transient elastography uses 50 Hz, and ARFI uses higher frequencies (50-100 Hz). Whilst an exclusively elastic material will have the same shear waves at different frequencies, a viscoelastic biological tissues shows different wave speeds at different frequencies, therefore changes of the complex shear modulus at various frequencies can yield novel biomarkers[3]. Therefore, multi-frequency actuation with a broadband motion sensitive MRE techniques are being investigated, including in improving differentiation of normal and fibrotic livers[10].

Tracking Shear Waves

To perceive the micron level tissue displacement (wave amplitude), the external driver frequency, and a phase contrast pulse sequence with motion encoding gradients (MEGs) are synchronised using a trigger pulse. Continuous driver motion allows tissues to reach a steady state. A single acquisition in the z-axis encodes wave motion in the axial (x-y direction) is required for two dimensional MRE, common in commercial systems, however successive x, y and z axis motion encoding gradient application can allow three dimensional wave displacement data to be obtained, currently in the experimental stage, but allows the derivation of the viscous and elastic components of complex shear modulus, as potential biomarkers for clinical use[3,11]. Both a positive and negative motion encoding gradient is required to produce phase difference images of a displacement. Multiple acquisitions with varied time (phase) offsets between mechanical excitation and motion-sensitizing gradients are performed. Each acquisition is at a different time in the wave cycle. A Fourier transform is then applied over time to isolate the motion at the external driver frequency, resulting in a complex number for each pixel that represents the amplitude and phase of the harmonic motion in a specific direction[3]. From this, a magnitude image and a phase image are produced.

Measure Parameters of Interest

Firstly, the phase maps are converted into a wave image showing propagation through tissue. Compression and shear waves are separated by a mathematical function, and additional phase offsets are interpolated from the measured offsets to produce a cinematic

loop of multiple wave images (Figure 4). These are colorized with red and blue being opposite directions, and the intensity of the colour representing amplitude.

Further post-processing of wave images creates maps of the complex shear modulus magnitude, termed elastogram, in greyscale and colour (Figure 5). Wave propagation is inherently three-dimensional. Transforming shear-wave displacement images into parametric maps involves solving an inverse problem to deduce the stiffness distribution or related parameters that account for the observed wave patterns. Two-dimensional inversion algorithms analyse wave components in only two directions within a slice, whereas three-dimensional inversion algorithms enable a comprehensive analysis of the entire wave motion. These algorithms rely on the assumptions that tissues have a uniform density of 1 g/cm³ and exhibit pure viscoelasticity with uniform, isotropic (i.e. direction independent), and linear mechanical properties[4]. On top of these elastograms, a 95% confidence map (Figure 6) can be applied to depict areas where the data is considered reliable, and unreliable areas are masked by a cross-hatch pattern[12].

A scale of 0-8kPa is frequently used, or for more stiff tissues, a 0-20 kPa scale. The colour elastograms allow the heterogeneity of stiffness to be appreciated by 'eye-balling' the map, with greyscale maps traditionally used for quantitative measurement, however measurements can also be done on colour maps.

Technique

MRE is available from several vendors, including Siemens (Erlangen, Germany, Table 1), General Electric (GE, Waukesha, Wisconson, USA, Table 2, called MR Touch ™.) and Philips (Best, Netherlands, Table 3). MRE is available on new machines but can also be an add on to older machines as a hardware and software package. The vendor engineers set up the active driver in the equipment room, to prevent imaging artefacts and due to additional noise produced by the driver, which is attached by tubing to a passive driver on the patient's body. A passive driver is a flat pad that transmits the vibrations generated by the active driver onto the patients abdomen, and can be rigid or flexible. It is secured to the patient by an adjustable belt.

Patient Preparation

The patient is required to fast for 4 to 6 hours before the study, as the post prandial state increases liver stiffness both in ultrasound and MRI elastography. The increase in splanchnic blood flow to the liver following a meal is thought to have negligible impact on MRE-derived liver stiffness measurements in healthy individuals, despite the rise in superior mesenteric venous flow[13]. However, in F3 and F4 fibrosis, approximately 20% and 28% increases in stiffness are observed[14]. Therefore, for meaningful longitudinal comparisons, follow up scans should also be in a fasted state.

Driver Placement

The passive driver is placed on the right upper quadrant of the patient, using anatomical landmarks to approximate maximal coverage of the right lobe of liver. The right lobe is the preferred placed for ultrasound elastography, where readings are more accurate[15] (higher values are found in the left lobe) and have higher technical success rate[16]. This is thought to be due to cardiac pulsations, and pressure effects from stomach. This convention continues in MRE, with magnetic resonance artefacts being seen from cardiac pulsations.

The craniocaudal positioning is determined by placement in the axial plane at the xiphoid process. The medial-lateral positioning is determined by the mid-axillary line. If there is colon or lung interposed between driver and liver, positioning in the mid-clavicular line can be used instead, and if the liver is not in the expected position, placement of the driver should be as close as possible to the liver (e.g. surgical resections, abnormal situs).

Ideally, a flexible driver should wrap around from anterior to posterior, to maximise coverage of the right lobe. Flexible drivers have been found be more comfortable to patients than rigid drivers, produce more parallel waves, and have fewer wave interferences, which have the potential to artificially 'hot spots' of raised liver stiffness[17], however no significant difference is stiffness measurements is found[18].

Breathing requirements

Four breath holds, each lasting approximately 15s, is required for typical MRE sequences with few seconds of free breathing in between.

The passive driver is secured using a belt, the tightness of which must allow constant contact with the abdomen for wave generation throughout the respiratory cycle. For larger patients, contact may be lost during end expiration[19], which is problematic as this is the optimum time for a breath hold for image. Inspiratory phase imaging increases liver stiffness values in MRE[18], again this effect is more pronounced in higher fibrosis grades[20]. Breath holding at end expiration is recommended as it has shown it allows more reproducible liver position[21],. The scout and localiser images should also be undertaken in end expiration.

Certain patient population, including children, are unable to maintain these breath-holds, therefore, respiratory triggering in the free breathing patient has been investigated for MRE and found to have similar performance to the breath hold method, as free breathing without triggering shows poor performance[22]. Advanced signal processing methods are also being investigated to reduce breath hold times, such as compressed sensitivity encoding (C-SENSE) allows image reconstruction from less sampled data, and show early promise[23]. Being a phase-based technique even small changes in the protons position alters the local magnetic field experiences by them, thus alters the phase of the signal they emit.

Pulse Sequence Parameters

Liver MRE can be obtained in less than two minutes, and can be undertaken before or any time after gadolinium-based contrast agent administration including hepatobiliary specific agents, with no impact on liver stiffness measurements[24,25]. If undertaken beforehand, it allows for repetition if the sequence fail, and the technologist can post process the images whilst awaiting post contrast images. If undertaken afterwards, there is an increase in returned signal intensity which may allow a greater areas of high confidence for liver stiffness measurements[7]. Field strength does not impact stiffness values[26].

Various sequences can be used, with the most established being Gradient-Recalled Echo MR Elastography (GRE MRE). This sequence is prone to artefacts from paramagnetic substances, in particular iron, giving a short T2* relaxation time, particularly at high field strengths (3.0 T). This is a common cause of failure, as whilst shear waves continue to propagate in livers with iron overloaded, signal to noise ratio is poor, so far as to lead to uninterpretable elastograms[19]. This is most pronounced at longer time to echo (TE) and therefore an alternative low TE sequence, SE- EPI-MRE, is being more commonly used and shows an improved technical success rate (98% vs 94.2%)[5]. This also has the benefit of having shorter acquisition times while achieving similar accuracy to the conventional GRE MRE[5]. However, lower agreement and reproducibility has been shown [27]. Therefore, SE-EPI-MRE can be used for 3T systems to mitigate T2* effects.

Exact parameters for each sequence depend on the manufacturer and field strength, and can be found on the Radiological Society of North America (RSNA), Quantitative Imaging Biomarkers Alliance (QIBA) Profile on MRE[12]. This document recommends a TE that is in-phase, to reduce the impact of signal loss due to hepatic steatosis[7], which may not be the default protocol TE. However, the motion-encoding gradient (MEG) and MEG direction, the number of phase offsets, and the fractional encoding should be kept constant.

Passive Driver Frequency and Amplitude

For evaluating liver, a low frequency mechanical waves vibration, typically at of 60 Hz is used and the vibrations generated are well tolerated by the patient. Established cut-offs are reported at 60Hz, and for comparisons of MRE at different time points, this frequency should be kept constant[6] as the shear wave speed is inversely related to frequency.

Passive driver amplitude determines the intensity of the passive driver waves delivered to the abdomen, and must be set to reflect the body habitus, size of patient and diver used (rigid or flexible) while maintaining the same driver frequency. Higher amplitudes are needed in larger patients, to penetrate a greater skin-to-capsule distance containing adipose tissue. If the amplitude is too high, it will lead to excessive liver motion, particularly near the driver, can lead to a poor-quality exam and areas of artefactually high stiffness[7]. This may also lead to patient discomfort. If the amplitude is too low, the propagation of shear waves is poor leading to suboptimal examination. A standard 50% setting using a large flexible driver is suitable for

patients with BMI of 20 to 25, however 40% may be used in BMI less than 20 and 70% in high BMI patients. Lower amplitudes are needed for smaller flexible and rigid drivers. These can be adjusted approximately 10% higher or lower if needed [19], and lower amplitudes are used in paediatric patients[28].

Imaging analysis and interpretation

Quality Control

Firstly, a review of the magnitude images is needed to ensure there is a signal void underlying the passive driver (Figure 7), to ensure there is delivery of waves. If not present, then the active and passive driver function must be checked, including ensuring the connections between them are working[19]. The belt securing the passive driver to the abdomen should maintain contact throughout the breathing cycle, in particular end expiration, as mentioned above.

If there is a flow void in the abdominal wall, wave propagation into the liver is confirmed by reviewing the phase images. Here, wave propagation is demonstrated by alternating layers paralleling the right liver edge. A disorganised pattern of black and white suggest lack of wave propagation, and a non-diagnostic study.

Then, the wave images are reviewed to appreciate areas of poor wave propagation, low wave amplitude or wave distortion. Good quality waves should pass undisturbed through the liver, although in less stiff livers one expects their amplitude to reduce as they pass centrally due to attenuation by soft parenchyma, in contrast with stiff livers where the waves are thicker and penetrate deeper (Figure 8). Poor wave propagation is represented by lack of parallel orientation and therefore areas of low signal. Low amplitude waves will also show low signal, leading to low stiffness measurements[7]. Wave distortion (Figure 9), caused by reflecting waves passing in different directions than the intended waves, can lead to interfering waves, either constructively or destructively, and therefore can increase or decrease the wave amplitude and can artefactually increase or decrease stiffness measurements[7]. These are expected at the liver edge, fissures, and large blood vessels[12].

Finally, a review of the elastograms with 95% confidence maps is required to assess the proportion of liver that is not masked by the confidence map and therefore can be used for region of interest (ROI) placement. In order to draw an appropriate sized ROI, 500 pixels per slice should be uncovered by the confidence map[12], however 2000 is used as a minimum at our centre, therefore a poor quality elastograms will have a greater proportion of liver uncovered by the confidence map (Figure 10).

It is important to note that less stiff livers have intrinsically lower wave propagation depths, so may have smaller areas uncovered by the confidence map, however other technical and biological factors may impact elastograms quality. Technical issues include incorrect driver amplitude and incorrect placement. Implanted paramagnetic materials, such as

embolization coils, surgical clips and portosystemic shunt stent-grafts can interfere with signal acquisition. Liver parenchymal issues include iron overload, and significant steatosis without an in-phase TE, and are discussed in the Technique section.

Liver Stiffness Measurement

An overall assessment of a good quality study allows a qualitative assessment of whether the study appears normal or of high stiffness. Normal studies have waves that attenuate as they pass centrally, are thinner and exhibit colours representing low stiffness on the colour scale (blue/purple)[7]. The confidence map may only uncover a small area of liver, at the periphery and towards the passive driver. In contrast, a stiff liver will propagate waves much better than a soft one, leading to larger areas uncovered by the confidence map without central liver wave attenuation, and will show colours representing higher stiffness on the colour scale (orange/red) (Figure 11).

For quantitative assessment, a ROI is drawn over the right lobe of liver for each of the individual slices. This can be automated or manually obtained. The specific sequence of the freehand drawing of ROIs depends on the PACS system and workflow. The largest geographic area of liver is drawn which fulfils the following criteria ; i) it is uncovered by the elastograms with confidence map and avoids areas of focal high liver stiffness (so-called 'hot spots', Figure 12), ii) on anatomical magnitude images, it is 1cm from the liver edge, its borders ideally parallel the liver edge, avoids fissures and large vessels, iii) on wave images, it is in an area of good wave propagation. This is repeated for the 4 slices giving 4 mean liver stiffness measurements and 4 areas. The liver stiffness measurements and areas are used to calculate a weighted mean, where the LSM is multiplied by the ROI area, summed, and divided by the total ROI area[19].

Due to the mean stiffness being used, then 'hot spots' can be increasing the reported liver stiffness value. They are not always excluded on the 95% confidence map, and so should be actively searched for, by visual assessment of colour maps. This effect is more significant in less stiff livers, as stiffer livers propagate waves more effectively and have a higher background stiffness value. Focal liver lesions may show areas of high stiffness, and so should be looked for on magnitude images (or other imaging if available) when a hot spot is identified (Figure 13). Excess vibrations near the passive driver may produce a 'hot spot' in the anterior liver, and, due to the shape of the liver, the dome may also show an area of raised stiffness[7].

Confounders of liver stiffness measurement

MRE is a useful tool for assessing liver fibrosis in chronic liver disease. LSM tends to increase with fibrosis but can also be affected by inflammation (see physics for detailed explanation), which is common in early chronic liver disease. This inflammation effect is most pronounced at lower stages of fibrosis[29]. However, certain conditions, like acute hepatitis,

biliary obstruction, and venous congestion, can also raise liver stiffness and should be considered when interpreting results, as is the case with ultrasound elastography. Diffuse liver diseases such as amyloidosis or Gaucher's disease can also increase liver stiffness and should be distinguished from fibrosis[19]. Liver fat content, generally, does not impact LSM significantly[7,30].

Changes in liver stiffness observed over time can reflect treatment responses, with inflammation improving faster than fibrosis. A change of over 19% in LSM is considered significant according to QIBA guidelines[12].

Diagnostic performance and Clinical Applications

MRE has a high technical success rate of 94.4% at 1.5T, with the leading cause of failure being increased hepatic iron (3% of all examinations)[29]. Failure rates are higher at 3T using GRE MRE sequences, at 15.3%[31], however this is reduced to 2% when SE-EPI sequences are used, as recommended for 3T field strengths[32]. Failure rates are increased in patients with massive ascites[31], however small volumes still exhibit good performance[19]. The effect of BMI is likely small, with some studies showing no impact on failure rates[29] and others showing a small increase in likelihood of failure (Odds Ratio 1.09)[31]. It has a low failure rate in children (4%).[33] This failure rate is lower than ultrasound based methods[34].

MRE shows excellent interobserver reliability (ICC 0.96)[35]. Its repeatability using the same examination settings is excellent in multiple vendors and field strengths (ICC 0.77-0.94), however there is some variability across vendors and field strengths (ICC 0.68)[27], suggesting care should be taken comparing LSMs obtained in different examination conditions.

With histology from liver biopsy as the reference standard, MRE correlates strongly with fibrosis stage[36]. In classifying fibrosis, a good performance has been found in detecting any fibrosis (F>0, AUROC 0.84) and significant fibrosis (F>1, AUROC 0.88) and excellent performance at detecting advanced fibrosis (F>2, AUROC 0.92) at an individual patient data meta-analysis, with high a sensitivity and specificity (both being 85%) of advanced fibrosis[37]. Good to excellent performance for significant fibrosis and excellent performance for advanced fibrosis seen in multiple other studies[21], which is superior to ultrasound based techniques[34,38]. This performance is more impressive given the traditional reference standard for fibrosis is histology from liver biopsies, which suffers sampling error assessing only a tiny proportion of whole liver parenchyma, and interobserver reproducibility of pathologists is a factor (κ 0.4-0.9)[39]. However, liver biopsy remains an essential clinical tool in assessing for the various non fibrotic causes of increased liver stiffness measurement.

Novel MR based techniques for assessing liver fibrosis have been investigated, such as diffusion weighted imaging (DWI), which relies on fibrosis leading to reduced diffusion of water and therefore a negative correlation between with apparent diffusion coefficients (ADC) and fibrosis grades[40]. However, performance is inferior with DWI in fibrosis assessment with

AUROC of 0.86 and 0.83 in significant and advanced fibrosis compared to greater than 0.95 in both GRE MRE and SE-EPI-MRE in the same tasks[41].

Normal liver parenchyma has a MRE LSM of less than 2.5kPa[7], with LSMs greater than 3.0 kPa highly sensitive and specific for fibrosis[36]. Cut-offs are variable in the literature; however Pepin et al.[19] recommend the following simplified interpretation of values (METAVIR fibrosis scale used). Less than 2.5kPa is considered normal. As the stiffness increases, it suggests the presence of liver inflammation or early-stage fibrosis between 2.5 to 3.0 kPa. A measurement between 3.0 to 3.5 kPa is associated with Stage 2 to 3 fibrosis, signifying moderate liver fibrosis. Readings in the 3.5 to 4.0 kPa range, suggest Stage 3 to 4 fibrosis. Severe liver conditions, such as Stage 4 fibrosis or cirrhosis is seen with stiffness value ranging from 4.0 to 5.0 kP, while readings above 5.0 kPa are strongly indicative of cirrhosis.

Diffuse Liver Disease

MR proton-derived fat fraction, the current imaging modality of choice for fat quantification, demonstrates high reproducibility, high diagnostic accuracy for all stages of steatosis, with good sensitivity and specificity[42,43]. Therefore, MRE is combination with MR PDFF allows for comprehensive steatosis and fibrosis assessment. In MASLD (Metabolic Dysfunction Associated Steatotic Liver Disease), MRE shows superior performance and a lower rate of failure than ultrasound based methods[44,45]. MRE shows high reproducibility in MASLD patients[46]. An individual patient data meta-analysis recommended the follow cut offs: greater than 3.14 kPa for significant steatosis, greater than 3.53 kPa for advanced steatosis, and showed inflammation (steatohepatitis grade) increased LSMs at low fibrosis grades [47].

The inflammation caused by viral hepatitis, and the response to antiviral treatment are potential co-founders in interpreting stiffness measurements. The advent of three dimensional MRE allows the derivation of viscous components of the complex shear modulus, such as loss modulus and damping ratio, which are currently being investigated for its use in discriminating inflammation from fibrosis both in viral hepatitis[11,48] and MASLD[49].

Predictor of negative outcomes

Higher LSMs in MASLD patients have, expectedly, been found to correlate with the risk of decompensation, hepatic encephalopathy, variceal bleeding and death, with a cut-off of 6.48 kPa (AUROC 0.71) associated with decompensation[50]. This correlation of LSMs with negative outcomes is also seen in viral hepatitis, where raised LSM predicted progression from Childs Pugh A to B in hepatitis C[51]. A LSM of 4.8kPa or more was associated with decompensation in viral hepatitis[52], and in primary sclerosing cholangitis, a LSM of greater than 6kPa was high risk for decompensation[53]. Patients with chronic liver disease (CLD) have a significantly increased risk of developing hepatocellular carcinoma (HCC). LSM through MRE serves as an independent predictor for HCC in these patients. Studies have identified various

LSM thresholds associated with higher HCC risk, ranging from >3.75 kPa to >5.5 kPa[54–56] and even recurrence after HCC treatment[57]. Increased MRE LSM are associated with portal hypertension and resultant gastroesophageal varices[58].

Conclusion

MRE) has demonstrated substantial clinical utility as a non-invasive technique to measure liver stiffness, reliably indicating the presence and stage of fibrosis, as well as predicting adverse outcomes in liver diseases.

The quantitative nature of MRE allows for the detection of changes in liver stiffness over time, aiding in the assessment of disease progression or regression in response to therapeutic interventions. Liver pathologies like inflammation, congestion, and biliary obstruction can confound measurements, so LSM must be interpreted within the clinical context. In assessing the whole liver, the heterogeneity of fibrosis is observed, and overcomes the potential sampling error of ultrasound based elastography methods and liver biopsy. Whilst limited by cost and availability, MRE outperforms ultrasound in technical success rates and diagnostic performance.

Emerging advancements in MRE technology, such as three-dimensional wave displacement data and multi-frequency elastography, are promising in refining the assessment of liver stiffness and in differentiating fibrotic changes from inflammatory processes. Furthermore, MRE, in conjunction with MR proton-derived fat fraction (PDFF) imaging, offers a comprehensive evaluation of liver disease, notably in conditions like MASLD. In the context of chronic liver diseases, MRE has proven to be a predictor of negative clinical outcomes such as decompensation and risk assessment for hepatocellular carcinoma.

MRE offers a combination of diagnostic precision, non-invasiveness, and prognostic ability. As MRE technology develops, its integration into routine clinical practice is likely to escalate, potentially reducing the need for invasive procedures and allow accurate information to be gathered, upon which clinical decision making will rely.

Table 1 – Siemens MRE protocols, taken from QIBA 2022[12]

		Siemens 1.5T		Siemens 3T	
Scanners and Sequences	**Scanner**	MAGNETOM Tim 3G or Tim 4G		MAGNETOM Tim 3G or Tim 4G	
	Software versions	N4 VE11C SP01 and above		N4 VE11C SP01 and above	
	Pulse sequence	greMRE	epseMRE (WIP)	greMRE	epseMRE
	Mode	2D			
Coil		Torso			

Imaging Parameters	**Imaging Plane**	Axial			
	No. of slices	4			
	Slice thickness (mm)/dist. Factor	10 mm / 0% (0)	8 mm / 25% (2mm)	10 mm / 0% (0)	8 mm / 25% (2mm)
	Matrix (Base × Phase)	256 × 25% (64)	98 × 100% (128)	256 × 25%(64)	98 × 100%(128)
	TE (msec)	min (about ~20 with flow comp off)	min (about 40 with flow comp on)	min (about 20 with flow comp off)	min (about 40 with flow comp on)
	TR (msec)	50	1000	50	1000
	No. of breath holds	4 (each 17sec) (note 2)	1 (each 11 sec)	4 (each ~17sec)	1 (each ~11 sec)
	scan time	4 × 17 sec	11 sec	4 × 17 sec	11 sec
Driver Parameters (Generic)	**Driver Power (%)**	50 (default)			
	Driver frequency (Hz)	60 (default)		60	60
Motion Encoding Gradients (Generic)	**MEG fractional encoding**	85%	80%		
	MEG frequency (Hz)	60 Hz (Hard Coded)			
	MEG Amplitude	(Hard coded)	30 mT/m (Hard coded)		
	Axis of MEG	Slice (Hard Coded)	Slice		
	Number of phase	4 (Hard coded)	3		

Table 2 – GE MRE Protocols, taken from QIBA MRE 2022[12]

		GE 1.5T			GE 3T		
Scanners and Sequences	**Scanner**	Artist, Creator, Explorer, HDx, Optima MR450w, Voyager			Architect, Discovery MR750w, PET/MR, Pioneer, Premier		
	Software versions	HD16 and ≥DV22.1	HD16 and ≥DV22.1	≥DV22.1	HD16 and ≥DV22.1	HD16 and ≥DV22.1	≥DV22.1
	Pulse sequence	fgremre (Resoundant-GE)	epimre (Resoundant-GE)	MR-Touch (GRE)	fgremre (Resoundant-GE)	epimre (Resoundant-GE)	MR-Touch (EPI)
Coil		Torso					
Imaging Parameters	**Imaging Plane**	Axial					
	No. of slices	4					
	Slice thickness (mm)/gap	10 mm / 0 mm	8 mm / 2 mm	10 mm / 0 mm	10 mm / 0 mm	8 mm / 2 mm	8 mm / 2 mm
	FOV (mm) / Phase FOV (100%)	420(required)x420(or less)					
	Matrix	256 × 64	80 × 80	256 × 64	256 × 64	96 x 96	96 x 96
	TE (msec)	in-phase TE	min full	min TE	min full (around 15.9, this is close to in-phase TE)	min full (around 55.4)	min full (around 55.4)
	TR (msec)	50	1000	50	50	1000	1000
	No. of breath holds	4	1	4	4	1	1
	Scan time	55 s	11 s	55 s	about 55 s	about 11 sec	about 16 sec
Driver Parameters	**Driver Power (%)**	50				50	50
	Driver frequency (Hz)	60					
	Driver cycles/ trigger (Duration)	3 (auto-calculated)	Auto-calculated	Auto-calculated	3 (auto-calculated)	Auto-calculated	Auto-calculated

Motion Encoding Gradients	**MEG frequency (Hz) (or Period Mismatch)**	75 Hz (0.8)	80	75	80 Hz (0.75)	80	80
	MENC (1/motion sensitivity)	~30 µm / (π radian)					
	Axis of MEG	4 (Z)					

Table 3 – Philips MRE Protocols, taken from QIBA MRE 2022[12]

		Philips 1.5T		**Philips 3T**	
Scanners and Sequences	**Scanner**	Achieva, Ambition, Ingenia		Achieva, Elition, Ingenia	
	Software versions	MR R5.1.7 SP2 (or later)		MR R5.1.7 SP2	
	Pulse sequence	FFE MRE	SE-EPI MRE	FFE MRE	SE-EPI MRE
Coil		Torso			
Imaging Parameters	**Imaging Plane**	Transverse			
	No. of slices	4			
	Slice thickness (mm)/gap	10 mm / 1 mm			
	FOV (mm) / Phase FOV (mm)	450(required) x403(or less)	400(required) x400(or less)	450(required) x403(or less)	400(required) x400 (or
	Matrix	300 × 86	100 x 100	300 × 86	100 x 100
	TE (msec)	20	58	20 “shortest”	58 “shortest”
	TR (msec)	50	1000	50	1000
	No. of breath holds	4	1	4	1
	Scan time	71 s (~17 s breathholds)	~13 s	71 s (~17 s breathholds)	9 sec
Driver Parameters	**Driver Power**	Moderate (50%)	Low (25%)	Moderate (50%)	Low (25%)
	Driver frequency (Hz)	60			
Motion Encoding Gradients	**MEG frequency (Hz)**	60 Hz			
	Axis of MEG	FH	FH		

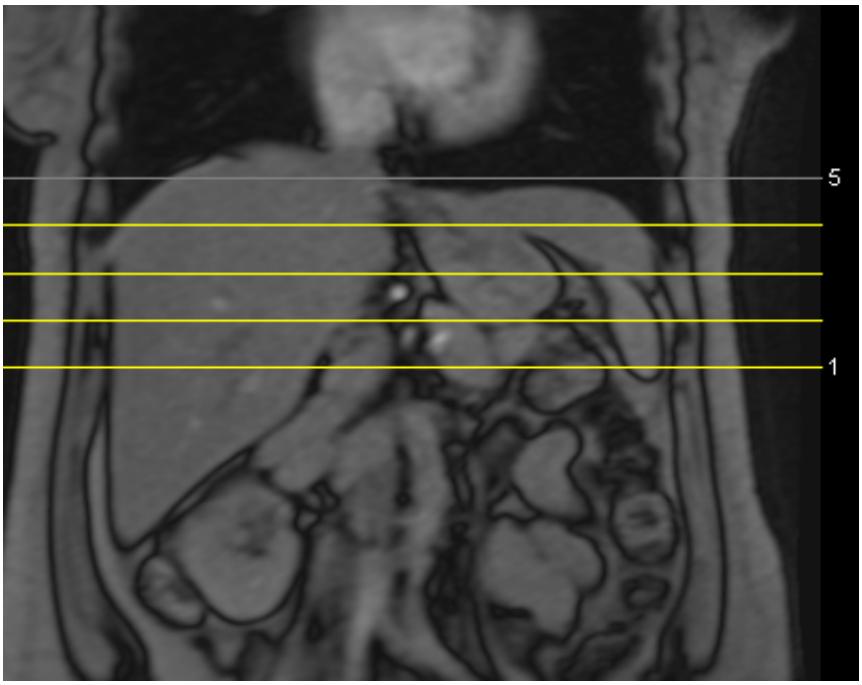

Figure 1 - Four slices (yellow lines) on a coronal localiser used for two- dimensional elastography measurements, including large cross sections of the liver and avoiding the dome and inferior liver.

Figure 2 – Active Driver, by Resoundant (Rochester, MN, USA), which is placed outside of the scanning room, which produces waves by pneumatic action

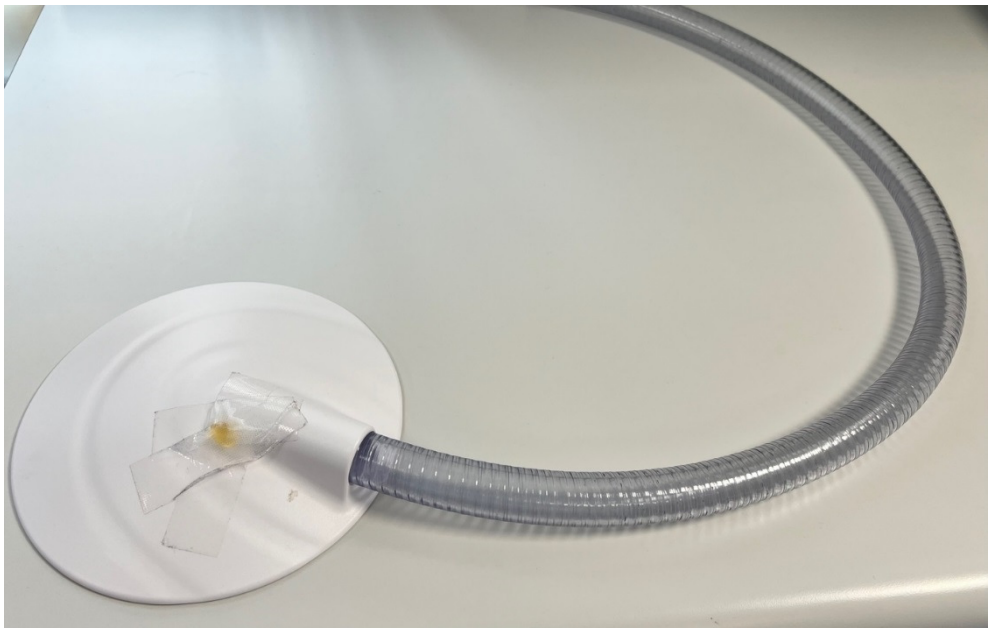

Figure 3 – Passive driver and tubing, by Resoundant (Rochester, MN, USA), which is secured to the patient by a belt to transmit vibrations to the abdomen

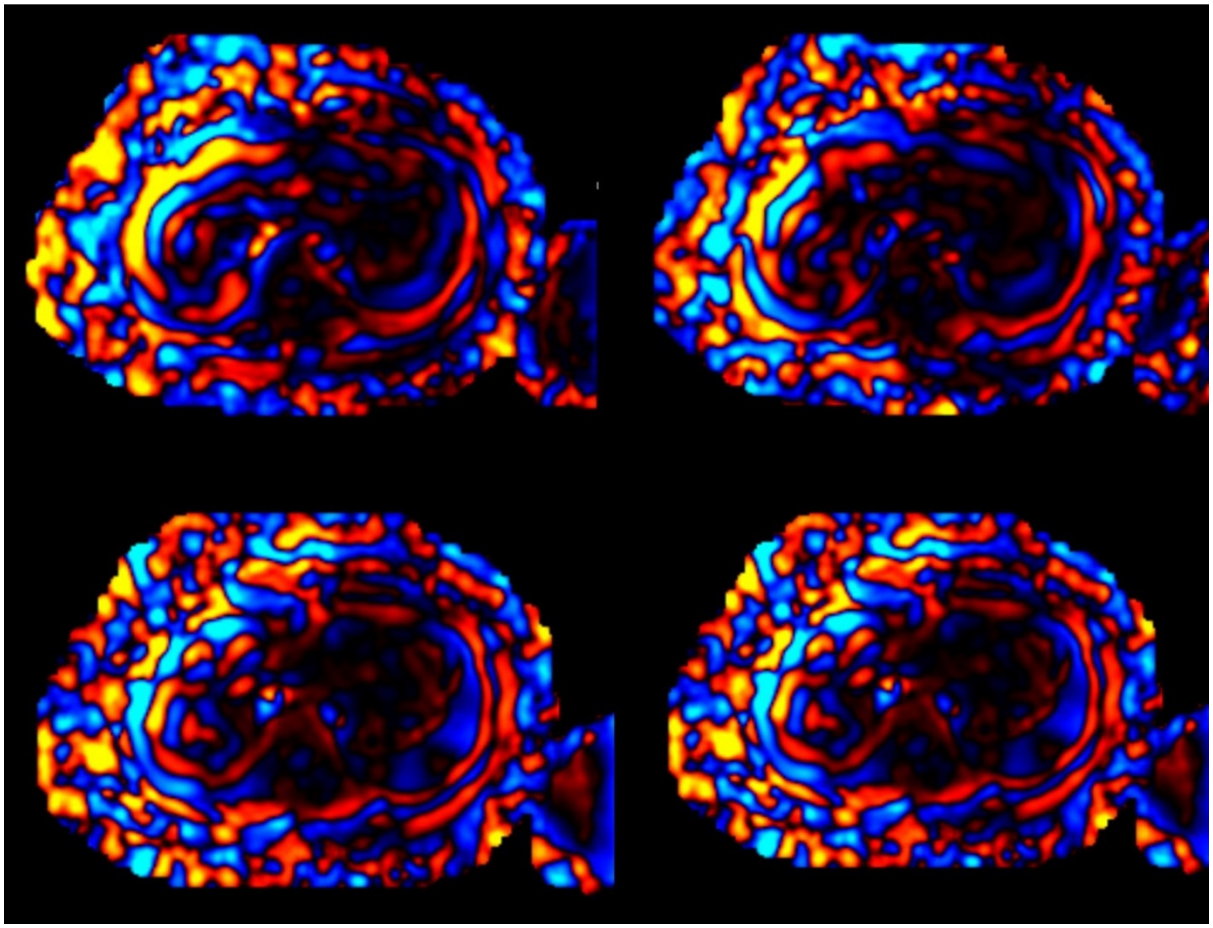

Figure 4 – Wave images which can be combined into a cine loop to represent wave propagation into the right liver. In this normal examination with good propagation, waves run parallel to the liver surface and there is expected attenuation of waves centrally due to the soft liver it passes through

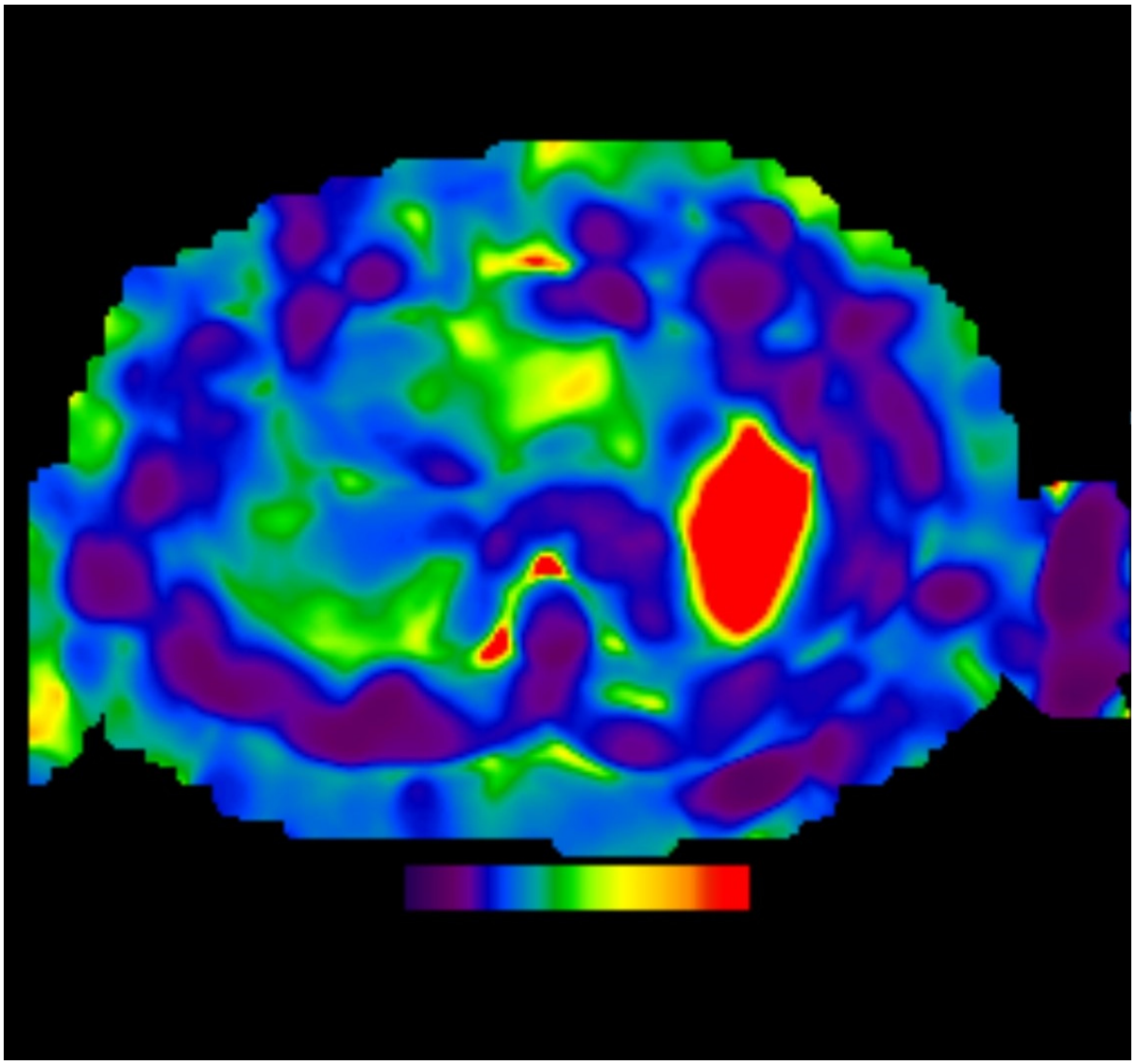

Figure 5 – Colour Elastogram showing Stage 1-2 fibrosis, with the liver parenchyma showing colours in the middle of the colour scale (blue/green/yellow).

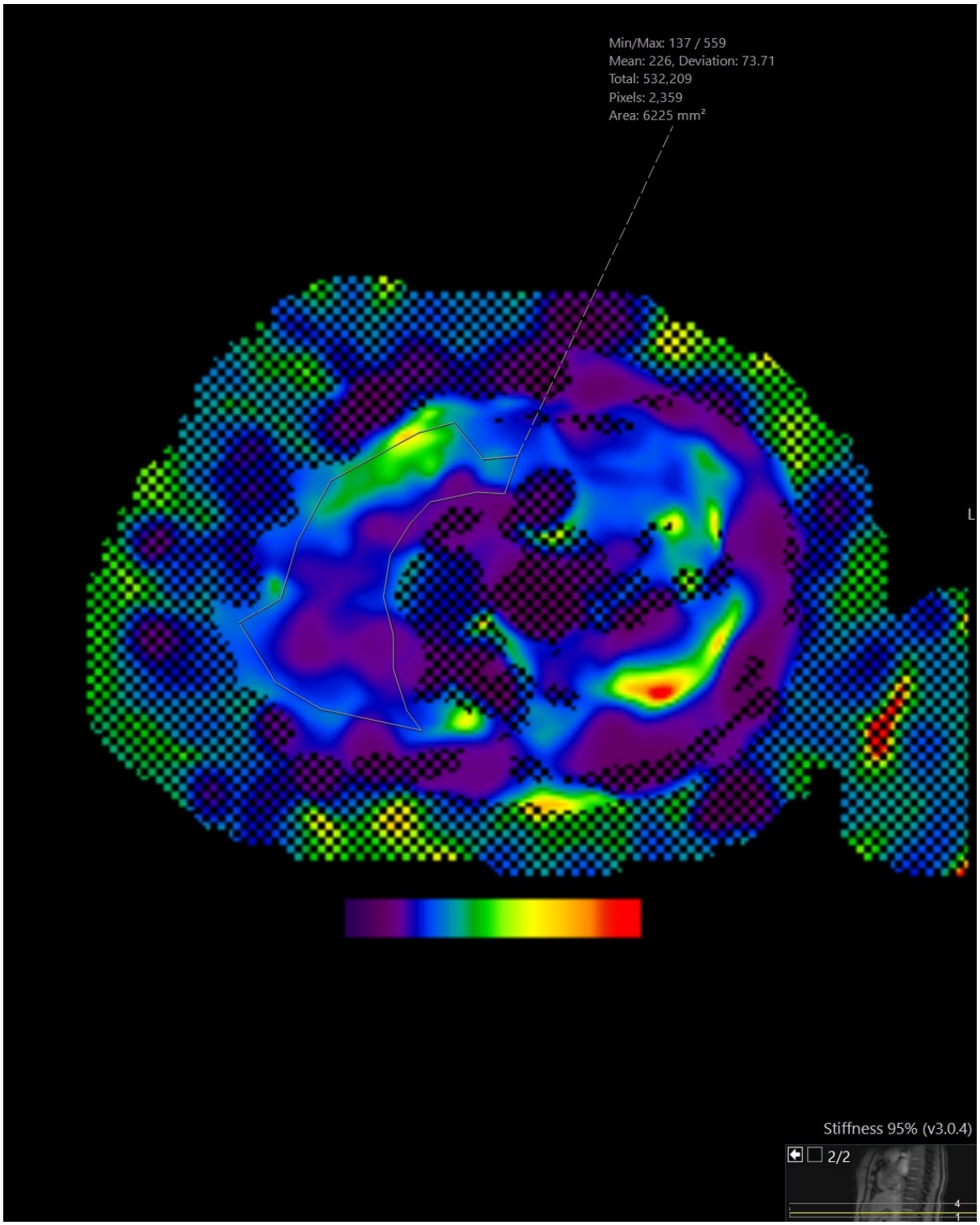

Figure 6 – Colour elastograms with overlying 95% confidence map, with unhatched regions deemed unreliable for selection. Liver stiffness measures are normal (low stiffness colours predominate, purple/blue). A freehand region of interest is present, with 2,359 pixels covered.

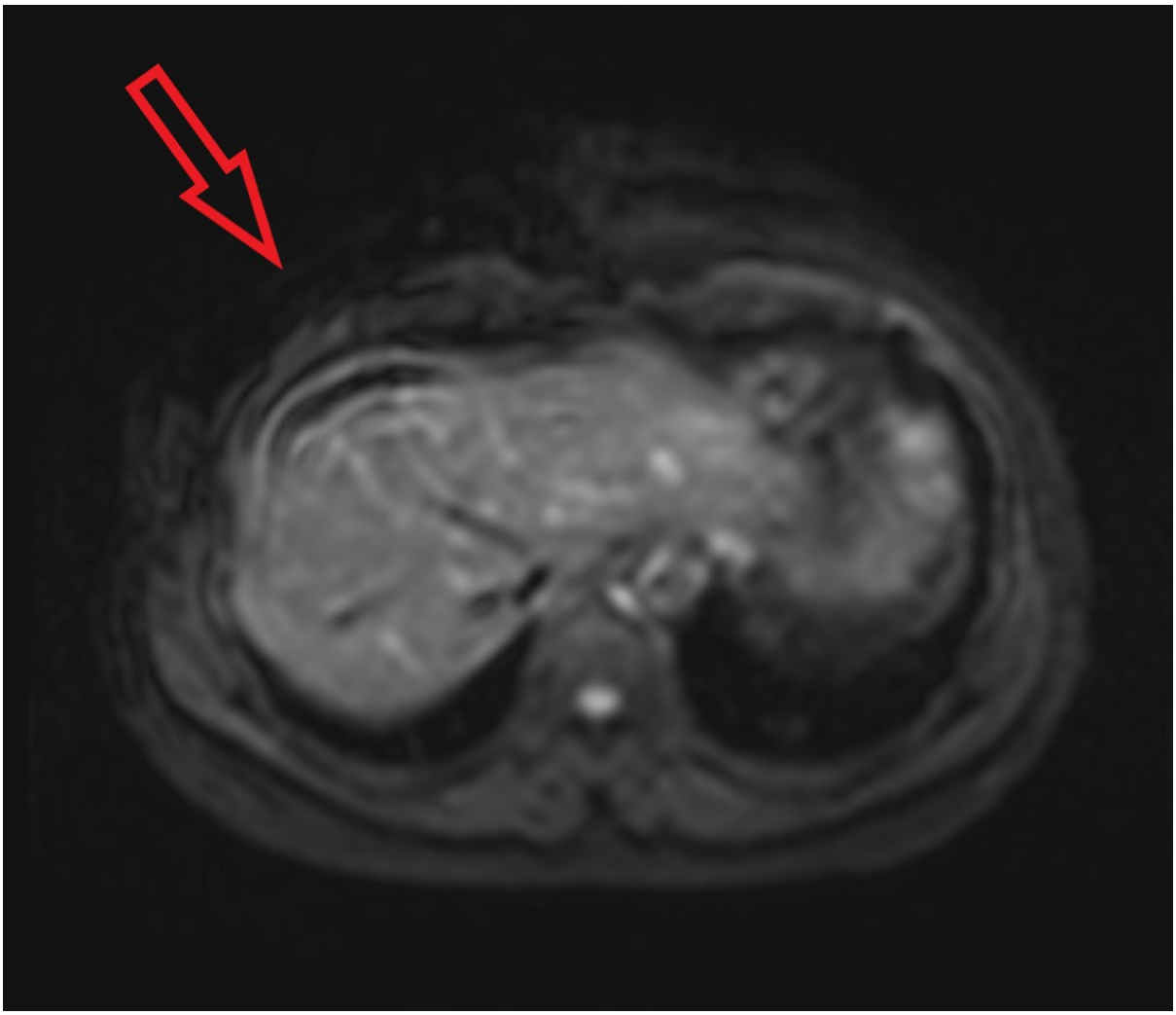

Figure 7 – Magnitude images showing the passive driver signal void (red arrow) in the subcutaneous tissue underlying the passive driver

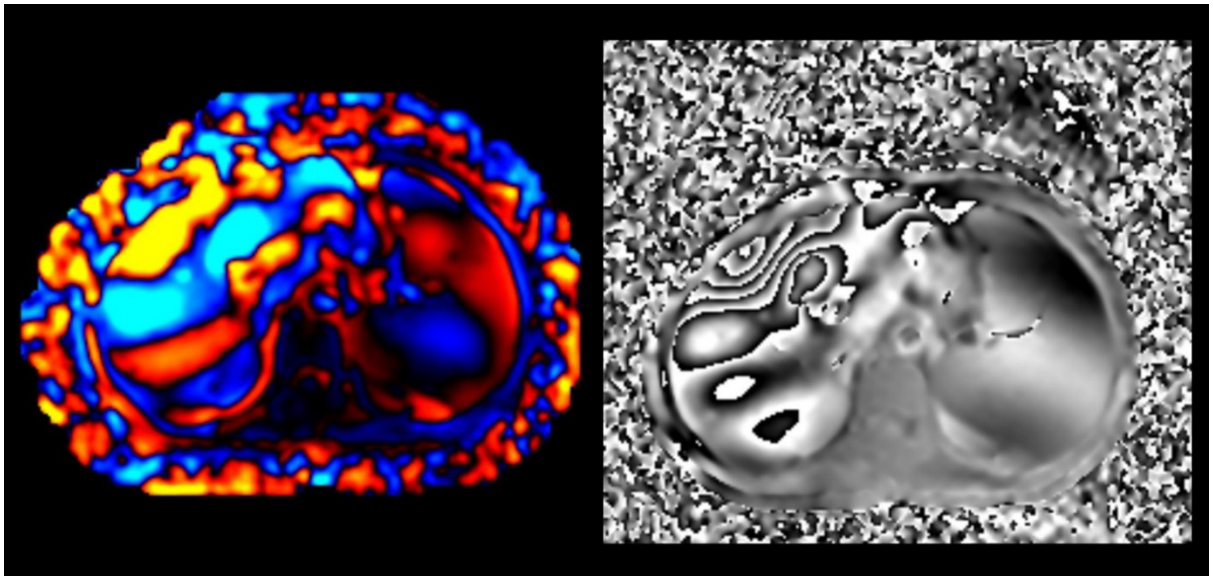

Figure 8 – Wave image (left) showing thick waves penetrating into the central liver in this stiff liver (6.9 kPa). Corresponding phase image (right) shows widespread wave propogation throughout the whole liver

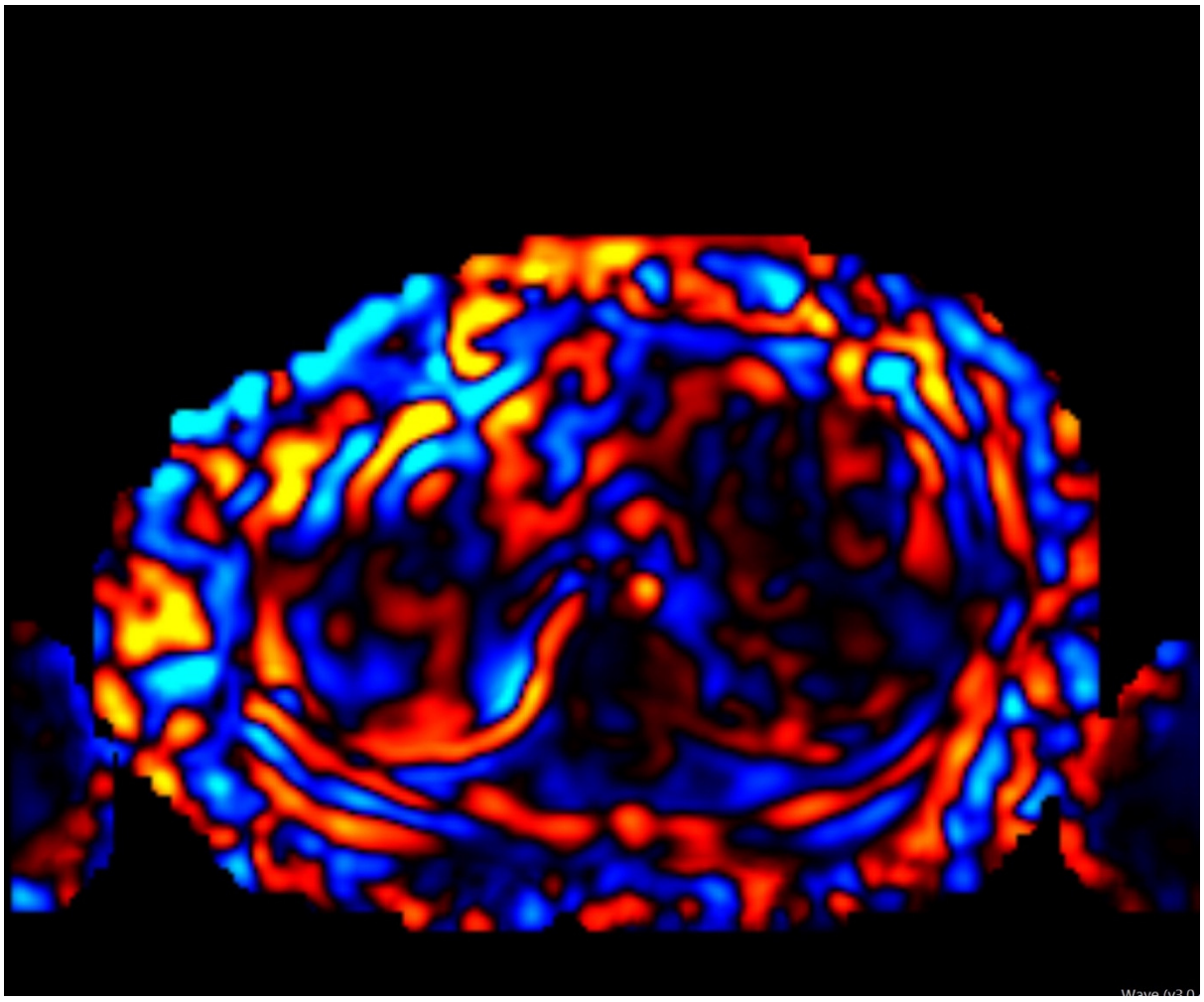

Figure 9 – Relatively low quality wave image with wave distortion where the normal parallel arrangement of waves is lost

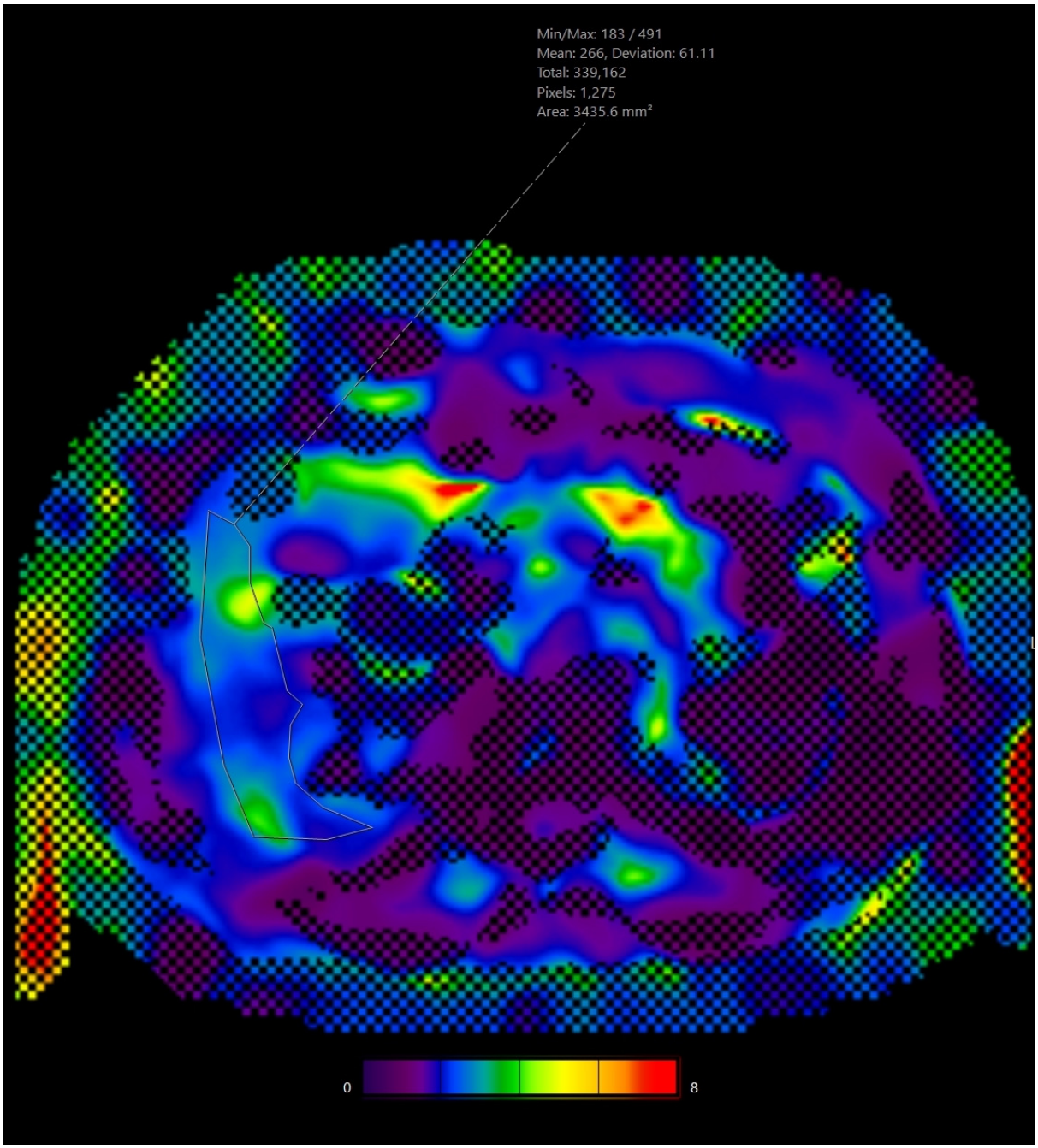

Figure 10 – Relatively small uncovered area in the colour elastograms with 95% confidence map, the background liver stiffness is low and therefore smaller uncovered areas as expected compared to stiffer livers

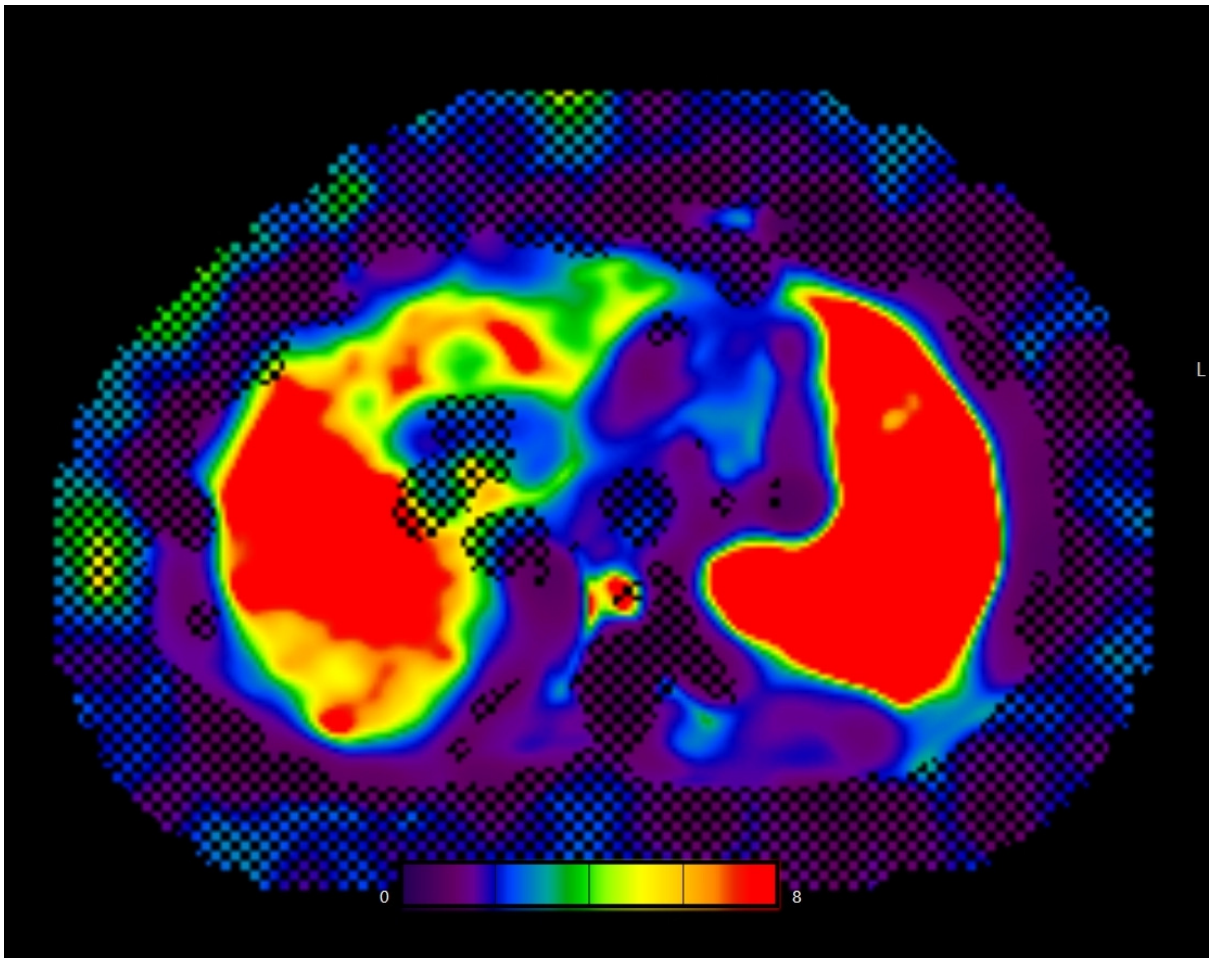

Figure 11 – Stiff liver (6.9kPa) showing large area of uncovered liver on this colour elastograms with 95% confidence map and higher colours on the scale present

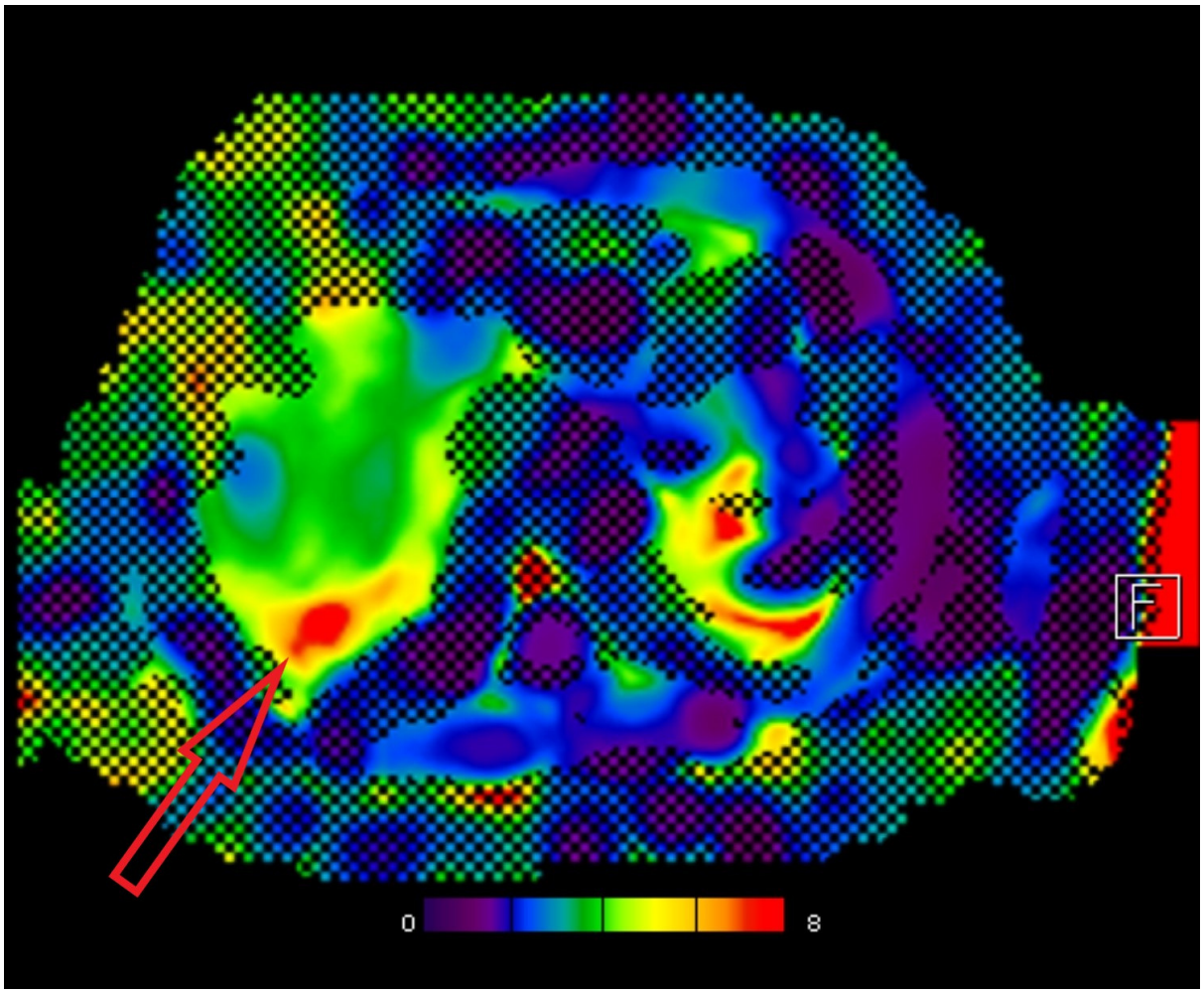

Figure 12 – Focal hot spot on colour elastogram (red arrow), which remains uncovered by the 95% confidence map. These should be excluded as when the mean is calculated, it can artificially increase stiffness values

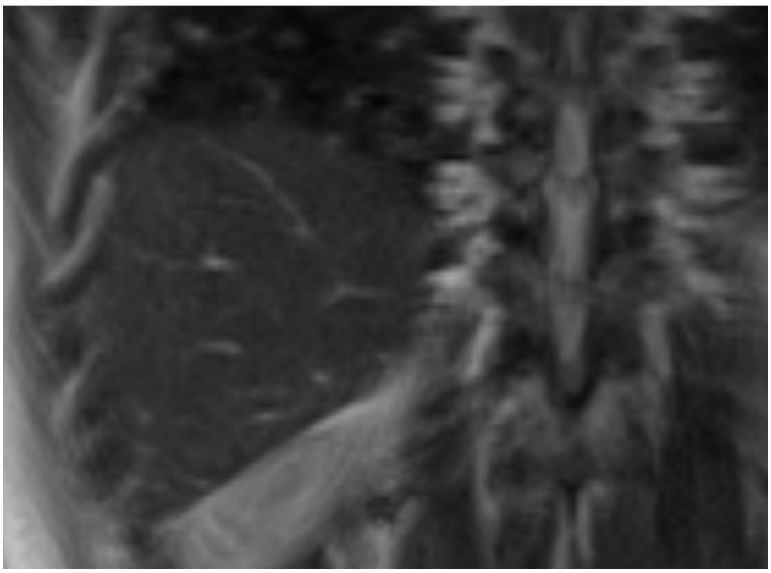

Figure 13 –Coronal T2 MRI region of the area of raised stiffness in Figure 12, showing no focal lesion, as this is sometimes a cause of elastogram 'hot spots'

References

1. Muthupillai R, Lomas DJ, Rossman PJ, Greenleaf JF, Manduca A, Ehman RL. Magnetic resonance elastography by direct visualization of propagating acoustic strain waves. *Science*. 1995;269(5232):1854-1857. doi:10.1126/science.7569924
2. Yin M, Glaser KJ, Manduca A, et al. Distinguishing between hepatic inflammation and fibrosis with MR elastography. *Radiology*. 2017;284(3):694-705. doi:10.1148/radiol.2017160622
3. Manduca A, Bayly PJ, Ehman RL, et al. MR elastography: Principles, guidelines, and terminology. 2021;85(5):2377-2390. doi:10.1002/mrm.28627.MR
4. Tang A, Cloutier G, Szeverenyi NM, Sirlin CB. Ultrasound elastography and MR elastography for assessing liver fibrosis: Part 1, principles and techniques. *Am J Roentgenol*. 2015;205(1):22-32. doi:10.2214/AJR.15.14552
5. Kim YS, Jang YN, Song JS. Comparison of gradient-recalled echo and spin-echo echo-planar imaging MR elastography in staging liver fibrosis: a meta-analysis. *Eur Radiol*. 2018;28(4):1709-1718. doi:10.1007/s00330-017-5149-5
6. Tang A, Cloutier G, Szeverenyi NM, Sirlin CB. Ultrasound elastography and MR elastography for assessing liver fibrosis: Part 2, diagnostic performance, confounders, and future directions. *Am J Roentgenol*. 2015;205(1):33-40. doi:10.2214/AJR.15.14553
7. Guglielmo FF, Venkatesh SK, Mitchell DG. Liver MR elastography technique and image interpretation: Pearls and pitfalls. *Radiographics*. 2019;39(7):1983-2002. doi:10.1148/rg.2019190034
8. Bayly P V, Garbow JR. Pre-clinical MR elastography: Principles, techniques, and applications. *J Magn Reson*. 2018;291:73-83. doi:10.1016/j.jmr.2018.01.004
9. Glaser KJ, Manduca A, Ehman RL. Review of MR elastography applications and recent developments. *J Magn Reson Imaging*. 2012;36(4):757-774. doi:10.1002/jmri.23597
10. Asbach P, Klatt D, Hamhaber U, et al. Assessment of liver viscoelasticity using multifrequency MR elastography. *Magn Reson Med*. 2008;60(2):373-379. doi:10.1002/mrm.21636
11. Shi Y, Qi YF, Lan GY, et al. Three-dimensional MR elastography depicts liver inflammation, fibrosis, and portal hypertension in chronic hepatitis B or C. *Radiology*. 2021;301(1):154-162. doi:10.1148/radiol.2021202804
12. Biomarkers QI. 2022 - QIBA - MRE-QIBAProfile-2022-02-14-TECHNICALLY-CONFIRMED. 2022.
13. Hines CDG, Lindstrom MJ, Varma AK, Reeder SB. Effects of postprandial state and mesenteric blood flow on the repeatability of MR elastography in asymptomatic subjects. *J Magn Reson Imaging*. 2011;33(1):239-244. doi:https://doi.org/10.1002/jmri.22354
14. Yin M, Talwalkar JA, Glaser KJ, et al. Dynamic postprandial hepatic stiffness augmentation assessed with MR elastography in patients with chronic liver disease. *AJR Am J Roentgenol*. 2011;197(1):64-70. doi:10.2214/AJR.10.5989
15. Toshima T, Shirabe K, Takeishi K, et al. New method for assessing liver fibrosis based on acoustic radiation force impulse: a special reference to the difference between right and left liver. *J Gastroenterol*. 2011;46(5):705-711. doi:10.1007/s00535-010-0365-7

16. Goertz Y.; Jugl, V.; Heide, R.; Janson, C.; Strobel, D.; Bernatik, T.; Haendl, T. RS. Z. Measurement of Liver Elasticity with Acoustic Radiation Force Impulse (ARFI) Technology: An Alternative Noninvasive Method for Staging Liver Fibrosis in Viral Hepatitis TT - Acoustic Radiation Force Impulse (ARFI) zur Messung der Leberelastizität: Eine a. *Ultraschall Med*. 2010;31(02):151-155. doi:10.1055/s-0029-1245244
17. Chen J, Stanley D, Glaser K, Yin M, Rossman P, Ehman R. Ergonomic Flexible Drivers for Hepatic MR Elastography.
18. Wang K, Manning P, Szeverenyi N, et al. Repeatability and reproducibility of 2D and 3D hepatic MR elastography with rigid and flexible drivers at end-expiration and end-inspiration in healthy volunteers. *Abdom Radiol (New York)*. 2017;42(12):2843-2854. doi:10.1007/s00261-017-1206-4
19. Pepin KM, Welle CL, Guglielmo FF, Dillman JR, Venkatesh SK. Magnetic resonance elastography of the liver: everything you need to know to get started. *Abdom Radiol (New York)*. 2022;47(1):94-114. doi:10.1007/s00261-021-03324-0
20. Ren H, Yang D, Xu H, et al. Effect of breath holding at the end of the inspiration and expiration phases on liver stiffness measured by 2D-MR elastography. *Abdom Radiol*. 2021;46(6):2516-2526. doi:10.1007/s00261-020-02893-w
21. Kennedy P, Wagner M, Castéra L, et al. Quantitative elastography methods in liver disease: Current evidence and future directions. *Radiology*. 2018;286(3):738-763. doi:10.1148/radiol.2018170601
22. Murphy IG, Graves MJ, Reid S, et al. Comparison of breath-hold, respiratory navigated and free-breathing MR elastography of the liver. *Magn Reson Imaging*. 2017;37:46-50. doi:https://doi.org/10.1016/j.mri.2016.10.011
23. Boyarko AC, Dillman JR, Tkach JA, Pednekar AS, Trout AT. Comparison of compressed SENSE and SENSE for quantitative liver MRI in children and young adults. *Abdom Radiol*. 2021;46(10):4567-4575. doi:10.1007/s00261-021-03092-x
24. Hallinan JTPD, Alsaif HS, Wee A, Venkatesh SK. Magnetic resonance elastography of liver: influence of intravenous gadolinium administration on measured liver stiffness. *Abdom Imaging*. 2015;40(4):783-788. doi:10.1007/s00261-014-0275-x
25. Plaikner M, Kremser C, Zoller H, et al. Does gadoxetate disodium affect MRE measurements in the delayed hepatobiliary phase? *Eur Radiol*. 2019;29(2):829-837. doi:10.1007/s00330-018-5616-7
26. Venkatesh SK, Ehman RL. Magnetic resonance elastography of liver. *Magn Reson Imaging Clin N Am*. 2014;22(3):433-446. doi:10.1016/j.mric.2014.05.001
27. Trout AT, Serai S, Mahley AD, et al. Liver Stiffness Measurements with MR Elastography: Agreement and Repeatability across Imaging Systems, Field Strengths, and Pulse Sequences. *Radiology*. 2016;281(3):793-804. doi:10.1148/radiol.2016160209
28. Kim D-K, Yoon H, Han K, et al. Effect of different driver power amplitudes on liver stiffness measurement in pediatric liver MR elastography. *Abdom Radiol (New York)*. 2021;46(10):4729-4735. doi:10.1007/s00261-021-03197-3
29. Yin M, Glaser KJ, Talwalkar JA, Chen J, Manduca A, Ehman RL. Hepatic MR elastography: Clinical performance in a series of 1377 consecutive examinations1. *Radiology*. 2016;278(1):114-124. doi:10.1148/radiol.2015142141
30. Lee DH, Lee JM, Han JK, Choi BI. MR elastography of healthy liver parenchyma: Normal value and reliability of the liver stiffness value measurement. *J Magn Reson Imaging*. 2013;38(5):1215-1223. doi:10.1002/jmri.23958

31. Wagner M, Corcuera-Solano I, Lo G, et al. Technical failure of MR elastography examinations of the liver: Experience from a large single-center study. *Radiology*. 2017;284(2):401-412. doi:10.1148/radiol.2016160863
32. Choi SL, Lee ES, Ko A, et al. Technical success rates and reliability of spin-echo echo-planar imaging (SE-EPI) MR elastography in patients with chronic liver disease or liver cirrhosis. *Eur Radiol*. 2020;30(3):1730-1737. doi:10.1007/s00330-019-06496-y
33. Joshi M, Dillman JR, Towbin AJ, Serai SD, Trout AT. MR elastography: high rate of technical success in pediatric and young adult patients. *Pediatr Radiol*. 2017;47(7):838-843. doi:10.1007/s00247-017-3831-z
34. Yin M, Venkatesh SK. Ultrasound or MR elastography of liver: which one shall I use? *Abdom Radiol*. 2018;43(7):1546-1551. doi:10.1007/s00261-017-1340-z
35. Lee Y ji, Lee JM, Lee JE, et al. MR elastography for noninvasive assessment of hepatic fibrosis: Reproducibility of the examination and reproducibility and repeatability of the liver stiffness value measurement. *J Magn Reson Imaging*. 2014;39(2):326-331. doi:https://doi.org/10.1002/jmri.24147
36. Venkatesh SK, Yin M, Ehman RL. Magnetic resonance elastography of liver: Technique, analysis, and clinical applications. *J Magn Reson Imaging*. 2013;37(3):544-555. doi:https://doi.org/10.1002/jmri.23731
37. Singh S, Venkatesh SK, Wang Z, et al. Diagnostic performance of magnetic resonance elastography in staging liver fibrosis: A systematic review and meta-analysis of individual participant data. *Clin Gastroenterol Hepatol*. 2015;13(3):440-451.e6. doi:10.1016/j.cgh.2014.09.046
38. Barr RG, Ferraioli G, Palmeri ML, et al. Elastography Assessment of Liver Fibrosis: Society of Radiologists in Ultrasound Consensus Conference Statement. *Radiology*. 2015;276(3):845-861. doi:10.1148/radiol.2015150619
39. Goodman ZD. Grading and staging systems for inflammation and fibrosis in chronic liver diseases. *J Hepatol*. 2007;47(4):598-607. doi:10.1016/j.jhep.2007.07.006
40. Taouli B, Tolia AJ, Losada M, et al. Diffusion-Weighted MRI for Quantification of Liver Fibrosis: Preliminary Experience. *Am J Roentgenol*. 2007;189(4):799-806. doi:10.2214/AJR.07.2086
41. Jang W, Jo S, Song JS, Hwang HP, Kim SH. Comparison of diffusion-weighted imaging and MR elastography in staging liver fibrosis: a meta-analysis. *Abdom Radiol*. 2021;46(8):3889-3907. doi:10.1007/s00261-021-03055-2
42. Qu Y, Li M, Hamilton G, Zhang YN, Song B. Diagnostic accuracy of hepatic proton density fat fraction measured by magnetic resonance imaging for the evaluation of liver steatosis with histology as reference standard: a meta-analysis. *Eur Radiol*. 2019;29(10):5180-5189. doi:10.1007/s00330-019-06071-5
43. Bohte AE, van Werven JR, Bipat S, Stoker J. The diagnostic accuracy of US, CT, MRI and 1H-MRS for the evaluation of hepatic steatosis compared with liver biopsy: a meta-analysis. *Eur Radiol*. 2011;21(1):87-97. doi:10.1007/s00330-010-1905-5
44. Imajo K, Kessoku T, Honda Y, et al. Magnetic Resonance Imaging More Accurately Classifies Steatosis and Fibrosis in Patients With Nonalcoholic Fatty Liver Disease Than Transient Elastography. *Gastroenterology*. 2016;150(3):626-637.e7. doi:https://doi.org/10.1053/j.gastro.2015.11.048

45. Park CC, Nguyen P, Hernandez C, et al. Magnetic Resonance Elastography vs Transient Elastography in Detection of Fibrosis and Noninvasive Measurement of Steatosis in Patients With Biopsy-Proven Nonalcoholic Fatty Liver Disease. *Gastroenterology*. 2017;152(3):598-607.e2. doi:https://doi.org/10.1053/j.gastro.2016.10.026
46. Tang A, Dzyubak B, Yin M, et al. MR elastography in nonalcoholic fatty liver disease: inter-center and inter-analysis-method measurement reproducibility and accuracy at 3T. *Eur Radiol*. 2022;32(5):2937-2948. doi:10.1007/s00330-021-08381-z
47. Liang J xu, Ampuero J, Niu H, et al. An individual patient data meta-analysis to determine cut-offs for and confounders of NAFLD-fibrosis staging with magnetic resonance elastography. *J Hepatol*. 2023;79(3):592-604. doi:10.1016/j.jhep.2023.04.025
48. Garteiser P, Pagé G, d'Assignies G, et al. Necro-inflammatory activity grading in chronic viral hepatitis with three-dimensional multifrequency MR elastography. *Sci Rep*. 2021;11(1):1-11. doi:10.1038/s41598-021-98726-x
49. Allen AM, Shah VH, Therneau TM, et al. The Role of Three-Dimensional Magnetic Resonance Elastography in the Diagnosis of Nonalcoholic Steatohepatitis in Obese Patients Undergoing Bariatric Surgery. *Hepatology*. 2020;71(2):510-521. doi:10.1002/hep.30483
50. Han MAT, Vipani A, Noureddin N, et al. MR elastography-based liver fibrosis correlates with liver events in nonalcoholic fatty liver patients: A multicenter study. *Liver Int*. 2020;40(9):2242-2251. doi:10.1111/liv.14593
51. Takamura T, Motosugi U, Ichikawa S, et al. Usefulness of MR elastography for detecting clinical progression of cirrhosis from child-pugh class A to B in patients with type C viral hepatitis. *J Magn Reson Imaging*. 2016;44(3):715-722. doi:https://doi.org/10.1002/jmri.25182
52. Asrani SK, Talwalkar JA, Kamath PS, et al. Role of magnetic resonance elastography in compensated and decompensated liver disease. *J Hepatol*. 2014;60(5):934-939. doi:10.1016/j.jhep.2013.12.016
53. Eaton JE, Dzyubak B, Venkatesh SK, et al. Performance of magnetic resonance elastography in primary sclerosing cholangitis. *J Gastroenterol Hepatol*. 2016;31(6):1184-1190. doi:10.1111/jgh.13263
54. Ichikawa S, Motosugi U, Enomoto N, Onishi H. Magnetic resonance elastography can predict development of hepatocellular carcinoma with longitudinally acquired two-point data. *Eur Radiol*. 2019;29(2):1013-1021. doi:10.1007/s00330-018-5640-7
55. Lee DH, Lee JM, Chang W, et al. Prognostic Role of Liver Stiffness Measurements Using Magnetic Resonance Elastography in Patients with Compensated Chronic Liver Disease. *Eur Radiol*. 2018;28(8):3513-3521. doi:10.1007/s00330-017-5278-x
56. Yasui Y, Abe T, Kurosaki M, et al. Non-invasive liver fibrosis assessment correlates with collagen and elastic fiber quantity in patients with hepatitis C virus infection. *Hepatol Res*. 2019;49(1):33-41. doi:10.1111/hepr.13286
57. Cho HJ, Kim B, Kim HJ, et al. Liver stiffness measured by MR elastography is a predictor of early HCC recurrence after treatment. *Eur Radiol*. 2020;30(8):4182-4192. doi:10.1007/s00330-020-06792-y
58. Morisaka H, Motosugi U, Ichikawa S, Sano K, Ichikawa T, Enomoto N. Association of splenic MR elastographic findings with gastroesophageal varices in patients with chronic liver disease. *J Magn Reson Imaging*. 2015;41(1):117-124. doi:10.1002/jmri.24505

The publication of this Textbook Elastography responded to a need in the medical community. The development of elastography, especially in the last decade, has led to more and more practitioners using it, and information related to the latest developments in the method is indispensable to correct medical practice.

We hope that reading this book will be useful to as many doctors as possible, for the benefit of patients.

For those who do not yet practice elastography, we hope that reading this book will attract them to this field.

Editura „VICTOR BABEȘ”
Timișoara, 2024

ISBN 978-606-786-416-8 E-Book